Computer Aided Dynamic Analysis And Optimal Design of Suspension Systems for Off-Road Tractors

Subhash Rakeja

A Thesis

in

The Faculty

of

Engineering

and

Computer Science

Presented in Partial Fulfillment of the Requirements
for the degree of Doctor of Philosophy at
Concordia University
Montreal, Quebec, Canada

October 1983

TC 61845

ISBN 0-315-13936-6

ABSTRACT

COMPUTER AIDED DYNAMIC ANALYSIS AND OPTIMAL DESIGN OF SUSPENSION SYSTEMS FOR OFF-ROAD TRACTORS

Subhash Rakheja
Concordia University, 1983

Low frequency terrain induced vibrations transmitted to the off-road vehicle operator are quite severe and exceed International Standards Organization (ISO) recommended *fatigue decreased proficiency* limits. Prolonged exposure to such low frequency and large amplitude vibration cause health hazards and inefficient performance. In this thesis, the ride improvement of an agricultural tractor is investigated through passive suspensions at the seat and at the cab, and semi-active seat suspension employing "on-off" damping. The investigation has been carried out in four phases, *namely*: passive seat suspension incorporating bounce, longitudinal, lateral, roll, and pitch modes on a rigidly mounted cab; cab suspension with rigidly mounted seat; bounce, bounce-lateral, and bounce-roll seat suspensions mounted on a suspended cab; semi-active bounce seat suspension using "on-off" damping.

A seat suspension configuration for longitudinal and lateral modes and a gimbal supported arrangement for rotational modes is proposed. Mathematical models incorporating non-linearities arising from suspension elements are developed for passive seat suspensions. The mathematical models are also developed for linear cab and cab-seat suspensions. The input vibrations for simulation of the suspension models are taken from the artificial track constructed at National Institute of Engineers, Silsoe, England.

A frequency dependent linearization technique, based on dissipation of energy, is developed. The non-linear seat suspension models are represented by their linear equivalent using the frequency dependent

linearization approach. The sensitivity of response characteristics of suspension models to variations in suspension parameters is investigated to establish an understanding of the suspension behaviour and to establish the base for formulating an optimization problem.

Objective functions are formulated for each suspension model, such that the ride performance of suspension models is maintained within the ISO recommended *fatigue decreased proficiency* limits corresponding to at least 4 hours exposure time. The relative displacement response is constrained to certain maximum permissible value. The objective functions are minimized using non-linear programming techniques. The ride performance characteristics of optimal suspensions in terms of acceleration PSD and ISO weighted rms acceleration at the driver's location are presented.

Finally, the concept of semi-active "on-off" damping is developed. The "on-off" damper utilizes a simple 2-position on-off valve, which operates with the command signal manipulated from the directly measurable variables. The response characteristics of bounce seat suspension using "on-off" damping are evaluated and compared to that of a passive bounce seat suspension.

ACKNOWLEDGEMENTS

The author is deeply indebted to his supervisor, Dr. S. Sankar for his encouragement and continued guidance during the course of this investigation. The author wishes to express his sincere thanks to the colleagues, faculty and staff of Mechanical Engineering Department, specifically to Dr. T.S. Sankar for valuable discussions.

The author wishes to acknowledge the support provided by NSERC post graduate scholarship, FCAC fellowship, Concordia University graduate fellowship, and NSERC grant No. A3685 during the course of this research.

Finally, the author wishes to express his appreciation to Mrs. Madeleine Klein for typing this thesis.

TABLE OF CONTENTS

		Page
ABSTRACT		1
ACKNOWLEDGEMENTS		iii
LIST OF FIGURES		ix
LIST OF TABLES		xx
NOMENCLATURE		xxii
CHAPTER 1		
INTRODUCTION AND LITERATURE REVIEW		
1.1	General	1
1.2	Review of Previous Investigations	2
1.2.1	Effects of Off-Road Vehicles Vibration	2
1.2.2	Ride Quality Evaluation Criteria	10
1.2.3	Modeling of Human Body	16
1.2.4	Approaches to Ride Improvement	19
1.2.5	Seat Suspension	20
1.2.6	Cab Suspension	23
1.3	Scope of the Present Investigation	24
CHAPTER 2		
DEVELOPMENT OF SUSPENSION MODELS		
2.1	Introduction	28
2.2	Design Specifications of Commercially Available Suspension Seats	29
2.3	Schematic Configurations of Passive Seat Suspension	38
2.4	Development of Mathematical Models for Passive Seat Suspension	41
2.4.1	Translational Seat Suspension Model	42
2.4.2	Rotational Seat Suspension Model	49
2.5	Formulation of Cab Suspension Model	56
2.6	Development of Mathematical Models	58
2.6.1	Cab Suspension Model	59
2.6.2	Cab and Seat Suspension Models	59
2.6.3	Equations of Motion for Passive Cab Suspension Models	62

		Page
2.7	Summary	67
	CHAPTER 3	
	REPRESENTATION OF INPUT EXCITATION FROM THE AGRICULTURAL TERRAINS	
3.1	Introduction	68
3.2	ISO Input Data	69
3.3	Silsoe Track Data	72
3.4	Summary	82
	CHAPTER 4	
	RESPONSE EVALUATION OF SUSPENSION MODELS	
4.1	Introduction	84
4.2	Analytical Techniques	84
	4.2.1 Time-Domain Analysis	85
	4.2.2 Frequency Domain Analysis	86
4.3	Response Evaluation of Non-Linear Suspension Models	89
	4.3.1 Review of Existing Techniques	90
	4.3.2 Linearization Based on Dissipation of Energy	92
	4.3.3 Frequency Dependent Linearization	95
4.4	Applications of Frequency Dependent Linearization	99
	4.4.1 Bounce Seat Suspension	99
	4.4.2 Longitudinal and Lateral Seat Suspension	101
	4.4.3 Rotational Seat Suspension Model	101
4.5	Verification of Frequency Dependent Linearization	105
	4.5.1 Non-Linear Seat Suspension Subject to Harmonic Excitations	105
	4.5.2 Stochastically Described Excitations	120
4.6	Summary	128
	CHAPTER 5	
	PARAMETRIC STUDY OF SUSPENSION MODELS	
5.1	Introduction	129
5.2	Objectives	130
5.3	Parametric Study of the Suspension Models	130

		Page
5.3.1	Influence of Variations in Suspension Parameters on the Performance of Passive Translational Seat Suspension Model	130
5.3.2	Influence of Variations in Suspension Parameters on the Performance of Passive Rotational Seat Suspension Model.	136
5.3.3	Influence of Suspension Parameters on the Performance of Cab Suspension Model.	158
5.3.4	Influence of Suspension Parameters on the Performance of Cab and Seat Suspension Models.	182
5.4	Conclusions	189
5.4.1	Translational Seat Suspension Model	189
5.4.2	Rotational Seat Isolator	197
5.4.3	Cab Suspension Model	198
5.4.4	Cab and Seat Suspension Models	199
5.5	Summary	200

CHAPTER 6

OPTIMIZATION OF SUSPENSION MODELS

6.1	Introduction	201
6.2	Selection of Performance Criterion	201
6.2.1	Performance Criteria for Translational Seat Suspension Model	203
6.2.2	Performance Criteria for Optimization of Rotational Seat Isolator	207
6.2.3	Performance Criteria for Optimizing 5 DOF Cab-Suspension Model	209
6.2.4	Performance Criterion for Optimizing 6 DOF Cab-Suspension Model	212
6.3	The Optimization Algorithm	213
6.4	Optimization Results and Discussion	217
6.4.1	Ride Performance of Optimum Seat Suspension	217
6.4.2	Ride Performance Characteristics of Optimum Cab Suspension Model	239
6.4.3	Ride Performance Characteristics of Optimum Cab and Seat Suspension Model (6 DOF)	258
6.5	Summary	264

Page

CHAPTER 7

PERFORMANCE CHARACTERISTICS OF SEAT SUSPENSION USING A SEMI-ACTIVE "ON-OFF" DAMPER

7.1 Introduction 272

7.2 The Concept 273

7.3 "ON-OFF" Damper Control Schemes 277

7.4 Development of the Seat Suspension Model Using "ON-OFF" Damping 280

7.5 Performance Characteristics of Bounce Seat Suspension with "ON-OFF" Damping 281

7.5.1 Harmonic Excitation 282
7.5.2 Ride Performance Characteristics of Suspension Seat with "ON-OFF" Damping when Subjected to Stochastically Described Terrain Excitations. 298

7.6 Summary 301

CHAPTER 8

CONCLUSIONS AND RECOMMENDATIONS FOR FUTURE WORK

8.1 General 302

8.2 Major Highlights of the Investigation 303

8.3 Conclusions 308

8.4 Recommendations for Further Work 312

REFERENCES 313

APPENDIX I

EXPERIMENTAL VERIFICATION OF THE PASSIVE SEAT SUSPENSION MODEL 322

APPENDIX II

MATRICES DESCRIBING EQUATIONS OF MOTION OF CAB, AND CAB-SEAT SUSPENSION MODELS 332

APPENDIX III

GENERATION OF EQUIVALENT ACCELERATION PSD LIMITS FROM RMS ACCELERATION LIMITS 343

APPENDIX IV

TIME SERIES REPRESENTATION OF INPUT SPECTRAL DENSITIES 348

LIST OF FIGURES

Figure

1.1 Compensatory tracking error caused by vertical and horizontal vibrations.

1.2 Error in maintaining constant foot pressure due to exposure to vibrations.

1.3 Effects of vibration on performance rate.

1.4 Effects of vertical vibration on visual acuity.

1.5 *Fatigue decreased proficiency* limits for exposure to vertical vibration.

1.6 *Fatigue decreased proficiency* limits for exposure to horizontal vibration.

1.7 k-factor and corresponding RMS acceleration limits as a function of input frequency.

1.8 Average absorbed power (P) and Janeway's ride vibration limits.

1.9 Mechanical impedance of subjects exposed to vertical vibration.

2.1 Levelair II, bounce suspension seat with pneumatic levelling system [Bostrom].

2.2 Pneumatic seat suspension [Anchorlok].

2.3 Viking, Bounce suspension seat [Bostrom].

2.4 Schematic of a Viking T-bar bounce suspension seat [Bostrom].

2.5 Force-displacement characteristics of the bounce suspension linkage mechanism.

2.6 Force-displacement characteristics of Marshall cushion.

2.7 Transmissibility characteristics of Marshall cushion.

2.8 Typical force-displacement characteristics of elastic limit stops.

2.9 Schematic configurations of longitudinal and lateral seat isolators.

2.10 Schematic configuration of the rotational seat isolator.

Figure

2.11 Model representation of bounce seat suspension.

2.12 Model representation of bounce and longitudinal seat suspension, in the longitudinal plane.

2.13 Model representation of translational seat suspension in the lateral plane.

2.14 Model representation of rotational seat isolator in longitudinal-bounce, lateral-bounce, and longitudinal-lateral planes.

2.15 Schematic configuration of a tractor cab mounted on four corner mounts.

2.16 Plane models representation of the corner mounted cab.

2.17 Plane models representation of 5 DOF cab suspension with rigidly mounted seat.

2.18 Plane models representation of cab and bounce seat suspension (Model I).

2.19 Plane models representation of Bounce and lateral seat suspension with a sprung cab (Model II).

2.20 Plane models representation of bounce and roll seat suspensions with a sprung cab (Model III).

3.1 Approximate function for the bounce acceleration PSD at the seat attachment point of Class 1 tractors.

3.2 Approximate function for the bounce-acceleration PSD at the seat attachment point of Class 2 tractors.

3.3 Bounce acceleration PSD measured at the cab floor.

3.4 Longitudinal acceleration PSD measured at the cab floor.

3.5 Lateral acceleration PSD measured at the cab floor.

3.6 Pitch acceleration PSD measured at the cab cg.

3.7 Roll acceleration PSD measured at the cab cg.

3.8 ISO weighting factors for bounce and horizontal accelerations.

3.9 Bounce rms acceleration measured at the cab.

3.10 Lateral and longitudinal rms acceleration at the cab floor.

Figure

3.11 Roll and pitch rms accelerations measured at the cab.

4.1 Absolute transmissibility response of SDOF longitudinal isolator subject to constant amplitude harmonic excitation.

4.2 Relative transmissibility response of SDOF longitudinal seat isolator subject to constant amplitude harmonic excitation.

4.3 Absolute transmissibility characteristics of SDOF longitudinal isolator for various magnitudes of Coulomb friction.

4.4 Relative transmissibility characteristics of longitudinal seat isolator for various magnitudes of Coulomb friction.

4.5 Absolute transmissibility characteristics of longitudinal seat isolator for various values of velocity squared damping coefficient.

4.6 Relative transmissibility characteristics of the linearized longitudinal seat isolator for various values of velocity squared damping coefficient.

4.7 Absolute transmissibility characteristics of the bounce seat suspension for various amplitudes of harmonic excitation.

4.8 Absolute transmissibility characteristics of bounce suspension seat for various amplitudes of harmonic excitation.

4.9 Relative transmissibility characteristics of bounce suspension seat for various amplitudes of harmonic excitation.

4.10 Relative transmissibility characteristics of bounce suspension seat for various amplitude of harmonic excitation.

4.11 Absolute transmissibility characteristics of bounce suspension seat for various magnitudes of Coulomb friction.

4.12 Absolute transmissibility characteristics of bounce suspension seat for various magnitudes of Coulomb friction.

4.13 Relative transmissibility characteristics of bounce suspension seat for various magnitude of Coulomb friction.

Figure

4.14 Absolute bounce transmissibility characteristics of rotational seat isolator subject to constant amplitude harmonic excitation.

4.15 Absolute pitch transmissibility characteristics of rotational seat isolator subject to constant amplitude harmonic excitation.

4.16 Absolute roll transmissibility characteristics of rotational seat isolator subject to harmonic excitation.

4.17 Relative roll transmissibility characteristics of the rotational seat isolator subject to constant amplitude harmonic excitation.

4.18 Response PSD evaluation of non-linear seat suspension models using frequency dependent linearization (Scheme A), and numerical integration (Scheme B) techniques.

4.19 Acceleration PSD response of longitudinal seat isolator.

4.20 Acceleration PSD response of bounce seat isolator.

5.1 Influence of cushion stiffness on the performance of bounce suspension seat.

5.2 Bounce seat suspension performance sensitivity to variations in suspension stiffness.

5.3 Influence of variations in the shock absorber damping coefficient on bounce acceleration response.

5.4 Influence of magnitude of Coulomb damping on the bounce performance of bounce suspension seat.

5.5 Sensitivity of longitudinal seat suspension performance to variations in suspension stiffness.

5.6 Influence of variations in suspension stiffness (K_x) on the relative displacement response of longitudinal seat isolator.

5.7 Influence of shock absorber damping on the performance of longitudinal seat suspension.

5.8 Influence of Coulomb damping on the performance of longitudinal seat suspension.

5.9 Influence of variations in suspension stiffness on the acceleration response of the lateral seat isolator.

5.10 Influence of variations in suspension stiffness (K_y) on the relative displacement response of the lateral seat isolator.

Figure

5.11 The influence of lateral damping coefficient on the lateral performance of translational seat suspension model.

5.12 Influence of Coulomb damping force on the performance of the lateral seat isolator.

5.13 Influence of variations in bounce suspension stiffness (K_z) on the bounce performance of rotational isolator.

5.14 The influence of variations in bounce suspension stiffness (K_z) on the pitch performance of rotational isolator.

5.15 Sensitivity of rorational isolator's bounce performance to variations in bounce suspension damping coefficient.

5.16 Sensitivity of rotational isolator's pitch performance to variations in bounce suspension damping coefficient.

5.17 Influence of Coulomb damping force on the bounce performance of rotational isolator.

5.18 Influence of Coulomb friction force on the pitch performance of the rotational seat isolator.

5.19 Sensitivity of bounce performance of the rotational seat isolator due to variations in support's stiffness.

5.20 Pitch performance of the rotational seat isolator with variations in the stiffness of end supports.

5.21 Influence of end supports stiffness on the roll response of rotational seat suspension.

5.22 Influence of variations in torsional stiffness (K_ϕ) on the roll acceleration response of rotational seat isolator.

5.23 Influence of variations in the stiffness of pitching suspension (K_θ) on the bounce acceleration response of the rotational seat isolator.

5.24 Pitch acceleration response of rotational seat isolators with variations in the stiffness of pitching suspension (K_θ).

5.25 Bounce acceleration response of rotational seat isolator with variations in pitch suspension damping coefficient (C_θ).

5.26 Influence of variations in the pitch suspension damping coefficient (C_θ) on the pitch acceleration response of rotational seat isolator.

Figure

5.27 Bounce acceleration response of 5 DOF cab suspension model.

5.28 Roll acceleration response of the 5 DOF cab suspension model.

5.29 Pitch acceleration response of 5 DOF cab suspension model.

5.30 Influence of variations in the stiffness of corner mounts on the bounce relative displacement response of the 5 DOF cab suspension.

5.31 Influence of variations in the stiffness of corner mounts on the pitch relative motion response of 5 DOF cab suspension.

5.32 Influence of variations in the stiffness of corner mounts on the roll relative motion response of 5 DOF cab suspension.

5.33 Sensitivity of bounce acceleration response to variations in corner mounts damping coefficient.

5.34 Influence of corner mounts damping on the pitch acceleration response of 5 DOF cab suspension model.

5.35 Influence of corner mounts damping on the roll acceleration response of 5 DOF cab suspension model.

5.36 Lateral acceleration PSD response at the cab floor with variations in corner mounts damping.

5.37 Influence of corner mounts damping on the cab cg lateral acceleration PSD response of the 5 DOF cab suspension model.

5.38 Influence of variations in lateral isolator stiffness on the lateral acceleration response of the 5 DOF cab suspension.

5.39 Influence of variations in lateral isolator stiffness on the roll acceleration response of 5 DOF cab suspension model.

5.40 Influence of variations in lateral isolator stiffness on the lateral acceleration response at cab cg.

5.41 Influence of variations in the stiffness of lateral isolator (K_s) on the roll relative displacement response of 5 DOF cab suspension.

Figure

5.42 Influence of variations in the stiffness of lateral isolator (K_8) on the lateral relative displacement response of 5 DOF cab suspension.

5.43 Influence of variations in lateral isolator damping coefficient on the lateral acceleration response of 5 DOF cab suspension model.

5.44 Influence of variations in lateral isolator damping coefficient on the roll acceleration PSD response of the 5 DOF cab suspension.

5.45 Influence of variations in lateral isolator damping coefficient on the lateral acceleration response at cab cg.

5.46 Sensitivity of the bounce acceleration response of the 6 DOF cab-seat suspension model to variations in bounce seat suspension stiffness (K_7).

5.47 Sensitivity of bounce acceleration response of 6 DOF cab-seat suspension model to variations in the seat suspension damping.

5.48 Influence of seat height on lateral acceleration response at the seat.

5.49 Influence of cab cg height on the lateral response of seat mass.

5.50 Influence of cab cg height on the roll acceleration response of cab and bounce seat suspension model.

5.51 Lateral acceleration response at the cab floor of the cab with bounce and lateral seat suspensions.

5.52 Influence of variations in the lateral seat isolator damping coefficient on the lateral acceleration of the cab.

5.[illegible] Sensitivity of seat lateral acceleration response to variations in stiffness of lateral seat isolator.

5.54 Sensitivity of the seat lateral acceleration response to variations in the damping coefficient of lateral seat isolator.

5.55 Sensitivity of seat roll acceleration PSD to variations in the torsional stiffness of the roll seat isolator.

5.56 Influence of variations in roll isolator's damping coefficient on the roll acceleration response at the seat.

Figure

5.57 Sensitivity of the lateral acceleration response at the seat to variations in the torsional stiffness of the roll seat isolator.

5.58 Lateral acceleration PSD response at the seat due to variations in roll isolator damping coefficient.

6.1 Bounce acceleration PSD response of the optimum bounce suspension seat.

6.2 Relative displacement PSD of an optimum bounce seat suspension.

6.3 ISO weighted bounce rms acceleration response of an optimal bounce seat suspension.

6.4 Longitudinal acceleration PSD response of the optimum longitudinal seat suspension.

6.5 Relative displacement PSD response of the optimum longitudinal seat suspension.

6.6 Longitudinal rms acceleration response of optimal longitudinal seat isolator.

6.7 Lateral acceleration response of the optimum lateral seat suspension.

6.8 Lateral relative displacement response of the lateral seat suspension.

6.9 Lateral acceleration PSD response of the optimum seat suspension.

6.10 Lateral relative displacement PSD response of the lateral seat suspension.

6.11 rms acceleration response of the lateral seat suspension.

6.12 Roll acceleration PSD response of the optimum rotational isolator.

6.13 Roll relative displacement PSD response of optimum rotational seat suspension.

6.14 rms roll acceleration response of optimum rotational seat suspension.

6.15 Bounce acceleration PSD response at the frames of optimum rotational seat suspension.

6.16 Bounce acceleration response at the seat mass of the optimum rotational seat suspension.

Figure

6.17 Bounce acceleration response (rms) at the seat mass of the optimum rotational seat suspension.

6.18 Roll acceleration PSD response of the optimum rotational seat suspension.

6.19 Pitch relative displacement PSD response of the optimum rotational seat suspension.

6.20 Pitch acceleration (rms) response of the rotational seat suspension.

6.21 Bounce acceleration PSD response of the optimum 5 DOF cab suspension model.

6.22 ISO weighted rms bounce acceleration response of 5 DOF cab suspension.

6.23 Bounce relative displacement PSD response of the optimum 5 DOF cab suspension model.

6.24 PSD of the pitch acceleration response of the optimum 5 DOF cab suspension model.

6.25 Pitch acceleration (rms) response of optimum 5 DOF cab suspension model.

6.26 Pitch relative displacement PSD response of the optimum 5 DOF cab suspension model.

6.27 PSD of the roll acceleration response of 5 DOF optimum cab suspension.

6.28 Roll acceleration (rms) response of optimum 5 DOF cab suspension model.

6.29 Roll relative motion response PSD of the optimum 5 DOF cab suspension model.

6.30 Lateral acceleration PSD response of the optimum 5 DOF cab suspension model.

6.31 Lateral acceleration (rms) response of 5 DOF optimum cab suspension.

6.32 Lateral relative displacement PSD response of 5 DOF optimum cab suspension model.

6.33 Lateral acceleration PSD response at the cab cg.

6.34 Longitudinal acceleration PSD response of optimum 5 DOF cab suspension.

Figure

6.35 Longitudinal acceleration (rms) response of the optimum 5 DOF cab suspension.

6.36 Longitudinal relative displacement PSD response of optimum 5 DOF cab suspension model.

6.37 PSD of the bounce acceleration response at the seat of 6 DOF cab-seat suspension model.

6.38 PSD of the lateral acceleration response at the seat of 6 DOF cab-seat suspension model.

6.39 PSD of the longitudinal acceleration at the seat of optimum 6 DOF cab-seat suspension model.

6.40 Bounce acceleration (rms) response at the seat of 6 DOF cab-seat suspension (Model I).

6.41 Lateral acceleration (rms) response at the seat of 6 DOF cab-seat suspension (MOdel I).

6.42 Longitudinal acceleration (rms) response at the seat of 6 DOF cab-seat suspension (Model I).

7.1 Conventional spring-mass-damper system.

7.2 Steady state spring, damper and inertial forces of harmonically excited SDOF system.

7.3 Semi-active skyhook damper system.

7.4 Inertia, spring, and damper forces of a SDOF passive bounce seat suspension ($f/f_n = 0.5$).

7.5 Inertia, spring and damper forces of harmonically excited SDOF passive system ($f/f_n = 0.75$).

7.6 Inertia, spring and damper forces of semi-active seat suspension using control scheme I ($f/f_n = 0.5$).

7.7 Inertia, spring and damper forces of semi-active seat suspension using control scheme I ($f/f_n = 0.75$).

7.8 Spring, damper and inertia forces of semi-active seat suspension operating with scheme I ($f/f_n = 1$).

7.9 Inertia, spring and damper forces of semi-active seat suspension using scheme I ($f/f_n = 1.4$).

7.10 Inertia, spring and damper forces of semi-active seat suspension using control scheme I ($f/f_n = 2$).

7.11 Inertia, spring and damper force plots of semi-active seat suspension using control scheme II ($f/f_n = 0.5$).

Figure

7.12 Inertia, spring and damper force plots of semi-active seat suspension using control scheme II ($f/f_n = 0.75$).

7.13 Inertia, spring and damper force plots of semi-active seat suspension using control scheme II ($f/f_n = 1$).

7.14 Inertia, spring and damper force plots of semi-active seat suspension using control scheme II ($f/f_n = 1.4$).

7.15 Inertia, spring and damper force plots of the semi-active seat suspension using scheme II ($f/f_n = 2$).

7.16 Acceleration PSD response of passive and semi-active seat suspension.

7.17 Relative displacement PSD response of the passive and semi-active seat suspension.

I.1 Schematic of the cross linkage mechanism.

I.2 Static characteristics of the cross-linkage mechanism.

I.3 Schematic of the shock absorber.

I.4 Static characteristics of the seat cushion.

I.5 Force-displacement characteristics of seat cushion.

I.6 Transmissibility characteristics of bounce seat suspension.

I.7 Transmissibility characteristics of bounce seat suspension.

III.1 Equivalent acceleration PSD *fatigue decreased proficiency* boundaries, for exposure to bounce vibrations.

III.2 Equivalent acceleration PSD *fatigue decreased proficiency* boundaries, for exposure to horizontal vibrations.

IV.1 Bounce acceleration PSD.

IV.2 Longitudinal acceleration PSD.

IV.3 Lateral acceleration PSD.

IV.4 Pitch acceleration PSD.

IV.5 Roll acceleration PSD.

LIST OF TABLES

TABLE	DESCRIPTION
1.1	Deductions from Stomach X-Ray Examination.
1.2	Pathological Spine Deformations in Different Occupations.
1.3	Summary of Spinal Defficiencies Diagnosed among Tractor Drivers.
1.4	Subjective Assessment of Tractor Ride in Relation to Various Tasks.
1.5	Power Utilization of Tractors on Various Farmlands.
1.6	Comparison of Human Body Models.
2.1	Specifications of Commercially Available Bounce Seat Suspensions.
2.2	Physical Parameters of the Rotational Seat Isolator Geometry.
2.3	Nomenclature to Describe Motion of the Rotational Seat Suspension Model.
2.4	Physical Parameters of the Representative Cab Geometry.
2.5	Nomenclature Describing Cab Motion.
3.1	Technical Data of References Tractors.
5.1	Parametric Sensitivity of Translational Seat Suspension Performance
5.2	Parametric Sensitivity of Rotational Seat Suspension Performance
5.3	Parametric Sensitivity of Cab Suspension Performance
6.1	Design Variables and Parametric Constraints selected for Optimization of Passive Seat Suspension Models.
6.2	Design Variables and Parametric Constraints Selected for Optimizing Cab Suspension Models.
6.3	Optimal Seat Suspension Parameters
6.4	Optimal Cab Suspension Parameters
6.5	Comparison of Peak Acceleration PSD response with ISO-FDP-4 Hours Exposure Limits.
7.1	Acceleration Transmissibilities of Bounce Suspension Seat with Passive and "On-Off" Damping.

I.1 Static Characteristics of Suspension Linkage Mechanism.

I.2 Geometric Parameters of the Bostrom Shock Absorber.

II.1 Absolute Translational motion of the seated Operator.

III.1 Slopes and Intercepts of rms and equivalent PSD limits (Fatigue decreased proficiency boundaries).

NOMENCLATURE

a_1, a_2	location of cab cg along the longitudinal axis
a_3	location of the seat along the longitudinal axis
$\bar{a}$	rms acceleration
$\bar{a}_i$	rms acceleration corresponding to i^{th} frequency
$\bar{a}(\bar{f})$	rms acceleration corresponding to center frequency
a_i	coefficient of harmonic component
AF	acceleration factor
A_p	piston area
A_R	piston rod area
A_{r_1}, A_{r_2}	orifice areas
b_1, b_2	location of the cab cg along the lateral axis
b_3	location of the seat along the lateral axis
b_i	intercept of the i^{th} segment
C_1, C_2, C_3, C_4	linear damping coefficient due to corner mounts
C_5, C_6	damping coefficient of the lateral and longitudinal cab suspensions, respectively
C_7, C_8, C_9	linear damping coefficient of the bounce, lateral, and roll seat suspensions, respectively
[C], [C_f]	damping coefficient matrices
C_c	linear damping coefficient due to the seat cushion
C_v', C_z'	coefficient of velocity square damping corresponding to maximum orifice opening.
C_x, C_y, C_z	coefficient of velocity squared damping due to shock absorbers in the longitudinal, lateral and bounce planes, respectively
cg	center of gravity
C_{eq}	equivalent viscous damping coefficient
C_{eq}^c, C_{eq}^d	equivalent viscous damping coefficient due to coulomb friction, and shock absorber damping, respectively.

$C_{eq}^{i}(\omega,u)$	equivalent viscous damping coefficient as a function of excitation frequency and relative displacement, corresponding to i^{th} iteration.
$C_{eq}^{z}, C_{eq}^{\theta}, C_{eq}^{\phi}$	equivalent viscous damping coefficients in the bounce, pitch, and roll modes, respectively.
CSD	cross spectral density
C_{θ}, C_{ϕ}	velocity squared damping coefficient of the shock absorbers in the pitch, and roll modes, respectively
D	dissipation function
DOF	degree of freedom
d_x, d_y, d_z	suspension travel in the longitudinal, lateral, and bounce modes, respectively.
ΔE^{c}	energy dissipated by the coulomb damper
ΔE^{d}	energy dissipated by the velocity squared damper
f	frequency - Hz
f_n	natural frequency - Hz
$\bar{f}$	center frequency of the third octave band
f_{ℓ}, f_u	lower and upper frequency limits of the third octave band, respectively
f_i	i^{th} frequency
f_m	frequency corresponding to the peak acceleration PSD at the seat attachment point of class 1 and class 2 tractors
F	magnitude of coulomb friction
[F]	forcing function matrix
FDP	*fatigue decreased proficiency*
F(t)	acceleration time history
F_c	coulomb friction force
F_d	damping force
F_k	spring force
F_x, F_y, F_z	magnitudes of coulomb friction force in the longitudinal, lateral, and bounce modes, respectively
F_c^x, F_c^y, F_c^z	damping force in the longitudinal, lateral, and bounce modes, respectively

F_d^θ, F_d^ϕ	damping forces in the pitch and roll modes, respectively
$g_j(\bar{x})$	inequality constraint equations
G_j	function of constraint equations
h_0	operator height with respect to the frames
h_1	operator height with respect to the cab floor
h_2	cab cg height
h_3	roll seat isolator height
h_4	operator height with respect to the roll seat isolator
h_5	bounce suspension height with respect to the frames
$h_{pk}(j\omega)$	complex frequency response function of the p^{th} response variables with reference to the k^{th} input
$[H(j\omega)]$	frequency response function matrix
i	index
$I_{\theta\theta}^c, I_{\phi\phi}^c$	pitch and roll moments of inertia of the cab, respectively
$I_{\phi\theta}$	product of inertia
j	index
J_f	roll moment of inertia of the outer frame
$J_{\theta\theta}, J_{\phi\phi}$	pitch and roll moments of inertia of the operator, respectively
$J_{\theta\theta}^I, J_{\theta\theta}^O$	pitch moments of inertia due to inner and outer frames, respectively
$J_{\theta\theta}^z, J_{\theta\theta}^z$	pitch and roll moments of inertia due to bounce suspension
$J_{\phi\phi}^I, J_{\phi\phi}^O$	roll moments of inertia due to inner and outer frames, respectively
k	factor to assess the ride
k_1	absorbed power constant of the human body at i^{th} frequency
K	constant stiffness coefficient
$[K], [K_e]$	stiffness matrices
K_1, K_2, K_3, K_4	constant stiffness of the corner mounts

K_s, K_t	constant stiffness of the lateral and longitudinal cab suspension, respectively
K_y, K_s, K_ϕ	constant stiffness of the bounce, lateral, and roll seat suspensions, respectively
K_c	spring rate of the seat cushion
K_x, K_y, K_z	spring rates of the translational seat isolator in the longitudinal, lateral, and bounce modes, respectively
K_e	stiffness due to end supports
K_e^*	optimal value of the stiffness due to end supports
K_s^*	stiffness of the limit stops
K_s^x, K_s^y, K_s^y	spring rates of the elastic limit stops in the longitudinal, lateral, and bounce modes, respectively
K_θ, K_ϕ	stiffness in the pitch and roll modes of the rotational seat isolator, respectively
ℓ	power of the penalty function
m_i	slope of the i^{th} segment
M	mass
M_o	mass of the operator
M_c	mass of the cab
M_x	mass due to the operator and bounce suspension
M_y	mass due to the operator, bounce suspension, and longitudinal isolator
M_s^x, M_s^z	mass of the longitudinal and bounce seat suspensions, respectively
[M]	mass matrix
M'	operator and bounce suspension mass
n	index
N	number of discrete frequencies
P	average absorbed power
[P]	coefficient matrix

P_1, P_2, P_3	pressure in the chambers 1, 2, and 3 of the shock absorber, respectively
P_0	initial absolute pressure of the inert gas
V_0	initial volume of the inert gas
P_A	atmospheric pressure
PSD	power spectral density
$q(u, \dot{u}, t)$	non linear damping function
q	number of inequality constraints
$[Q]$	coefficient matrix
r_k	penalty parameter
Re	designates real part
S_x, S_y, S_z, S^*	non-linear functions describing stiffness of the elastic limit stops
$S_1(f)$	input power spectral density corresponding to frequency f.
$S_0^p(\omega)$	output power spectral density of the p^{th} variable
$\bar{S}(\bar{f})$	average PSD corresponding to the center frequency
$[S_1(\omega)]$	input spectral density matrix
$[S_0(\omega)]$	output spectral density matrix
$[S_0^r(\omega)]$	spectral density of the response coordinates, other than the generalized coordinates
$S_{\ddot{x}}(f), S_{\ddot{y}}(f), S_{\ddot{z}}(f)$	longitudinal, lateral, and bounce acceleration PSD, respectively
$S_{\ddot{\theta}}(f), S_{\ddot{\phi}}(f)$	pitch, and roll acceleration PSD, respectively
$S_{\ddot{y}_2}(f), S_{\ddot{z}_2}(f)$	PSD of the lateral, and bounce accelerations of the cab corresponding to frequency f, respectively
$(S_{\ddot{z}_2})_{max}$	maximum permissible cab bounce acceleration PSD
$(S_{\ddot{\theta}_2})_{max}$	maximum permissible cab pitch acceleration PSD

$S_u^x(f), S_u^y(f), S_u^z(f)$	relative displacement PSD in the longitudinal, lateral and bounce modes, respectively
$S_u^\theta(f), S_u^\phi(f)$	pitch, and roll relative displacement
$(S_u^x)_{max}, (S_u^z)_{max}$	maximum permissible relative displacement PSD's in the longitudinal and bounce modes, respectively
$(S_u^y)_{max}$	maximum permissible lateral relative displacement PSD
$(S_u^\theta)_{max}, (S_u^\phi)_{max}$	maximum permissible relative displacement PSD's in the pitch, and roll modes, respectively
s	stage index
$S_d^x(f), S_d^z(f)$	acceleration PSD's from the ISO specified limits
t	time
t_o	initial time
T	kinetic energy function
[T]	transformation matrix
u	relative displacement
u^i	relative motion corresponding to i^{th} iteration
u_s	relative motion of the bounce suspension mass with respect to the floor
u_z	relative motion of the bounce suspension mass with respect to the frames
u_θ, u_ϕ	relative displacement across the pitch and roll dampers, respectively
U_m	modified objective function
U	objective function
v	rms velocity
V	potential energy function
V_o	initial volume of the inert gas
V_s	volume of the inert gas
v_z	bounce relative motion of the frames with respect to the cab floor

v_ϕ	roll relative motion of the outer frame with respect to the cab floor
w_z	bounce relative motion of the operator with respect to the bounce suspension mass
WF	the weighting factor
x_1, x_2, x_c	longitudinal motion of the operator, cab floor, and cab cg, respectively
x_0	input longitudinal motion
$\tilde{X}, \hat{X}$	vectors of design variables
y_1, y_2, y_c	lateral motion of the operator, cab floor, and cab cg, respectively
y_0	input lateral motion
z_1, z_s, z_g, z_2	bounce motion of the opertor, bounce suspension mass, frames mass, and cab mass, respectively
z_0	input bounce motion
$\{Z(j\omega)\}, \{Z_0(j\omega)\}$	Fourier transform of the vectors containing output, and input variables, respectively
α_1, α_2	cg location of the gimbal mounted frames along the longitudinal axis
β	cg location of the gimbal mounted frames along the lateral axis
$\gamma_1, \gamma_2, \gamma_3$	constant to determine k - factor
θ_1 θ_2	pitch rotation of the operator and the cab, respectively
θ_0	input pitch rotation
ϕ_1, ϕ_f, ϕ_2	roll motion of the operator, outer frame, and the cab, respectively
ϕ_0	input roll motion
$\phi_z^{(1)}$	bounce acceleration PSD at the seat attachment point of class 1 tractors
$\phi_z^{(2)}$	bounce acceleration PSD at the seat attachment point of class 2 tractors
$\phi_{max}^{(1)}, \phi_{max}^{(2)}$	maximum values of bounce acceleration PSD's at the seat attachment point of class 1, and class 2 tractors, respectively

$\{\Phi\},\{\Phi_0\}$	vectors of output and input variables, respectively
ϵ	error parameter
ζ	rms displacement
ω	frequency - rad/s
ω_n	natural frequency - rad/s
ω_j	frequency of j^{th} harmonic - rad/s
ζ_{eq}	equivalent damping ratio
τ	period of oscillation
ρ	density of the shock absorber oil
ψ	a constant
$(\dot{})$	denotes derivative with respect to time
$\lvert\ \rvert$	denotes the magnitude

CHAPTER 1

INTRODUCTION AND LITERATURE REVIEW

1.1 GENERAL

Modern agricultural industry is inclined towards high power, high speed, and efficient agricultural machinery for the reasons of economy. Consequently, the machinery operator is exposed to a comprehensive magnitude of noise and vibrational environment introduced by various sources. With a constant need to maintain operator comfort and safety, progress has been made in subsiding noise levels, and emphasis is being diverted to the reduction of vibration levels. The intensified concern over ride comfort, safety, and efficient performance of the operator has lead to the proposal of numerous ride comfort criteria, established from subjective and objective human body response analyses.

Large and significantly soft tires of the agricultural tractors offer very light damping. Consequently, the ride vibration of agricultural tractors is characterized by lightly damped system resonance occurring at low frequencies. The vehicle vibrations, mainly originating from irregular terrains, are directly transmitted to the seat-pan through unsprung chassis and the cab. The amplitude of vibration encountered by seated operators surpasses the entire ensemble of ride criteria proposed by various researchers, thus imposing health hazards and limited speeds of operation during various farming tasks.

Effective low natural frequency passive suspension seats have been developed by John Deere, Bostrom and Anchorlok. These low natural frequency, passive seat suspensions have been employed to isolate operators from terrain induced bounce vibrations only. Longitudinal, lateral, pitch and roll modes of tractor vibration have also been found either as

severe or more severe than the bounce mode, and thus require vibration isolation. Over the past few years, intensified efforts have been made to develop design concepts of off-road vehicle suspensions to provide satisfactory ride. These studies have focused on modeling of the human body to characterize human body dynamics, analytical solutions, and computer simulations to predict suspension performance associated with health hazards and the driver's performance ability.

In this investigation, the suspension models are developed that would isolate the tractor drivers from the ride vibrations in the bounce, longitudinal, lateral, pitch, and roll modes. Analytical techniques are employed to predict the ride improvement via suspensions at the seat and the cab. The parameters of suspension models are selected through multivariable optimization techniques and ride performance of suspension models is assessed with reference to the ISO specified *fatigue decreased proficiency* limits.

1.2 REVIEW OF PREVIOUS INVESTIGATIONS

Previous investigations in tractor dynamics and vehicle ride quality improvement encompass a diversity of subjects concerning the development of satisfactory ride criteria, appropriate human body model, seat and cab suspension designs. A review of relevant literature is presented in the following subsections, grouped in a sequence so as to develop the scope of the thesis.

1.2.1 EFFECTS OF OFF-ROAD VEHICLE VIBRATION

Vibration is a prevalent characteristic of modern man-machine environment. Prolonged exposure to low frequency, large amplitude and whole-body vibration causes degenerative physiological symptoms, and degradibility in responding to certain stimuli prominent to human safety and efficiency.

Physiological Damage

Two forms of degenerative health effects due to long periods of tractor operation have clearly been demonstrated; namely stomach sickness and spinal disorders. X-ray examinations of a sample of 322 tractor drivers reflect the poor state of spinal and stomach health of tractor drivers in relation to other population of workers [1]. The results of X-ray examinations are summarized in Table 1.1 and a comparison of spinal disorders of population of workers associated with various occupations is presented in Table 1.2. Pathological studies conducted by Reason [2] reflect a risk of motion sickness under prolonged exposure to low frequency bounce vibrations. A number of subjective surveys conducted by Orthopaedic surgeons in the U.S.A. have also established that truck and tractor driving can either cause or aggravate a number of disorders of the spine and supporting structures [3,4]. Numerous surveys pursued on a sample of tractor drivers over a period of five years support the above mentioned X-ray findings and establish the rate of degeneration of spinal deformation [5]. A comparison of results is summarized in Table 1.3.

TABLE 1.1

DEDUCTIONS FROM STOMACH X-RAY EXAMINATION [1]

	Sample Size	% of Total
without X-ray examination	77	23.9
with X-ray examination	245	76.1
Acute	182	74.3
with gastroptosis	113	62.1
without gastroptosis	69	37.9
Chronic	63	25.7

TABLE 1.2

PATHOLOGICAL SPINE DEFORMATIONS IN DIFFERENT OCCUPATIONS [1]

OCCUPATION	SAMPLE SIZE	SPINE DEFORMATIONS %
Carrying heavy loads	97	98
TRACTOR DRIVERS	310	71.3
Miners	116	70
Farmers	31	55
Pneumatic drill operators	500	46
Factory workers	100	43
Construction workers	113	37
Craftsman	51	29

TABLE 1.3

SUMMARY OF SPINAL DEFICIENCIES DIAGNOSED AMONG TRACTOR DRIVERS

RESEARCHERS	ROSEGGER *ET AL* [1]	DUPUIS *ET AL* [5]	
		1960	1966
Sample Size	310	211	137
Percentage with total symptoms	71.3	72.5	78.9
Definite Abnormality	--	50.2	68.7
Limited Abnormality	--	22.3	10.2

Impaired Performance Ability

Excessive low frequency vibration transmitted to the agricultural tractor drivers causes bodily discomfort as indicated by the subjective survey conducted at the National Institute of Agricultural Engineers (N.I.A.E) [6]. The results of the survey are presented in Table 1.4. Consequently, the performance ability of tractor drivers is highly impaired in an environment of discomfort. The reduced working efficiency has been attributed to several factors influenced by tractor vibrations. Schmitz *et al* [7] and Hornick [8] presented experimental evidences to establish deterioration of performance ability of human subjected to vibrations, which are also supported by the experimental investigations of Matthews [9] and Müller [10]. Their findings concluded the following:

i) The compensatory tracking ability is impaired under vertical as well as horizontal vibrations as shown in Figure 1.1.

ii) The ability to maintain constant foot pressure is deteriorated as a function of frequency and intensity of vibration as shown in Figure 1.2.

iii) The reaction time immediately following the exposure to transverse vibration was found to be relatively slow as presented in Figure 1.3.

iv) Significant deterioration of visual acuity is presented in Figure 1.4.

Under-utilization of available power of the agricultural tractor is evidenced from tests conducted at N.I.A.E. (Table 1.5), which has been attributed to impairment of performance abilities of tractor drivers [11].

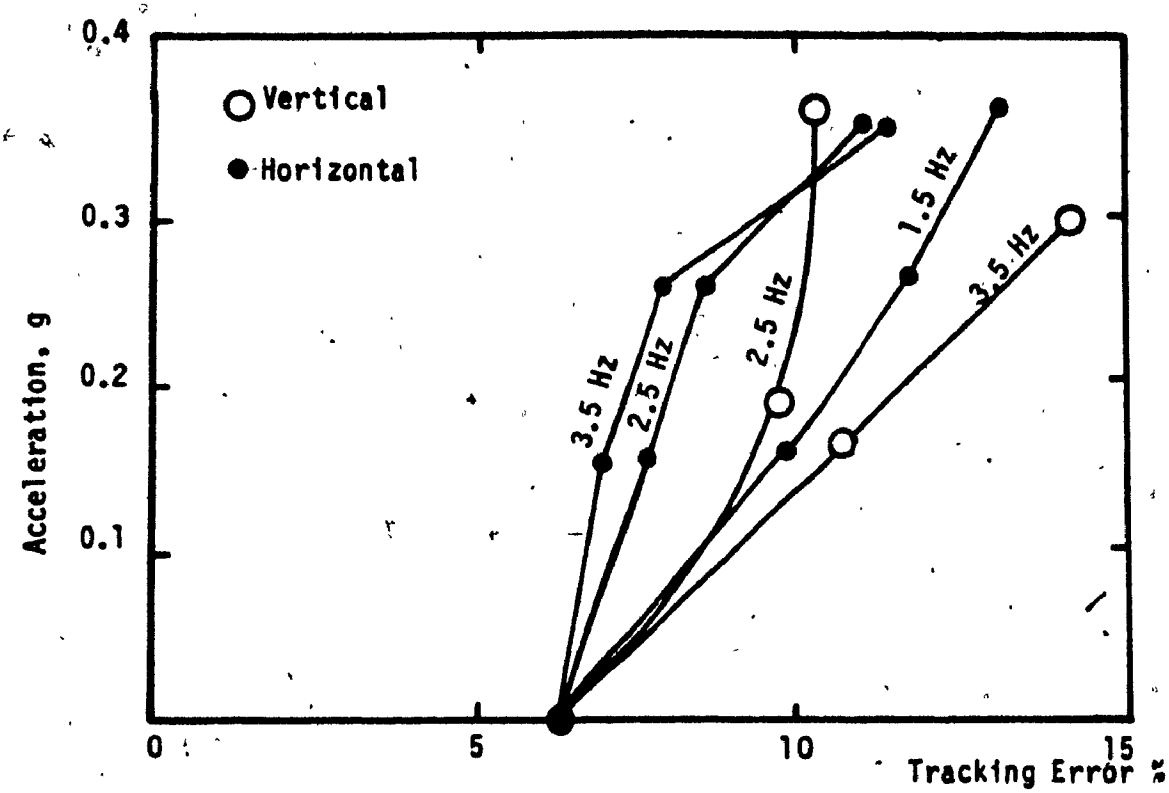

FIGURE 1.1: Compensatory tracking error caused by vertical and horizontal vibrations [9].

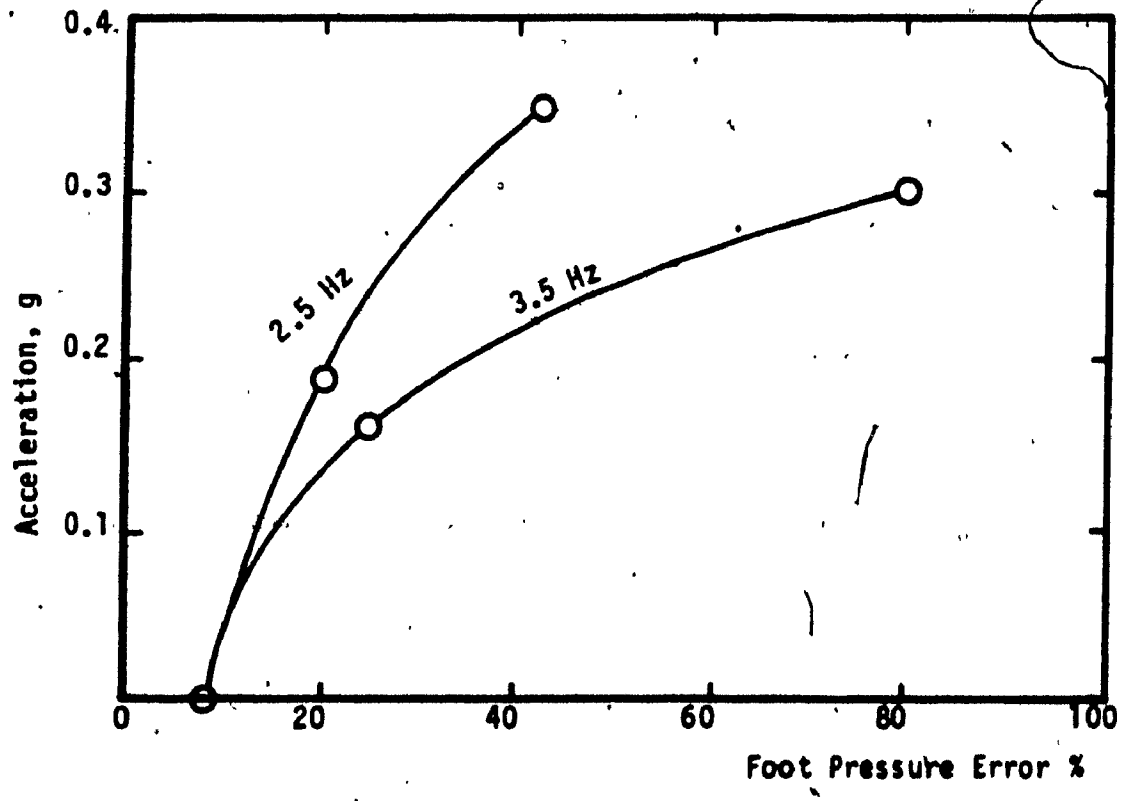

FIGURE 1.2: Error in maintaining constant foot pressure due to exposure to vibrations [9].

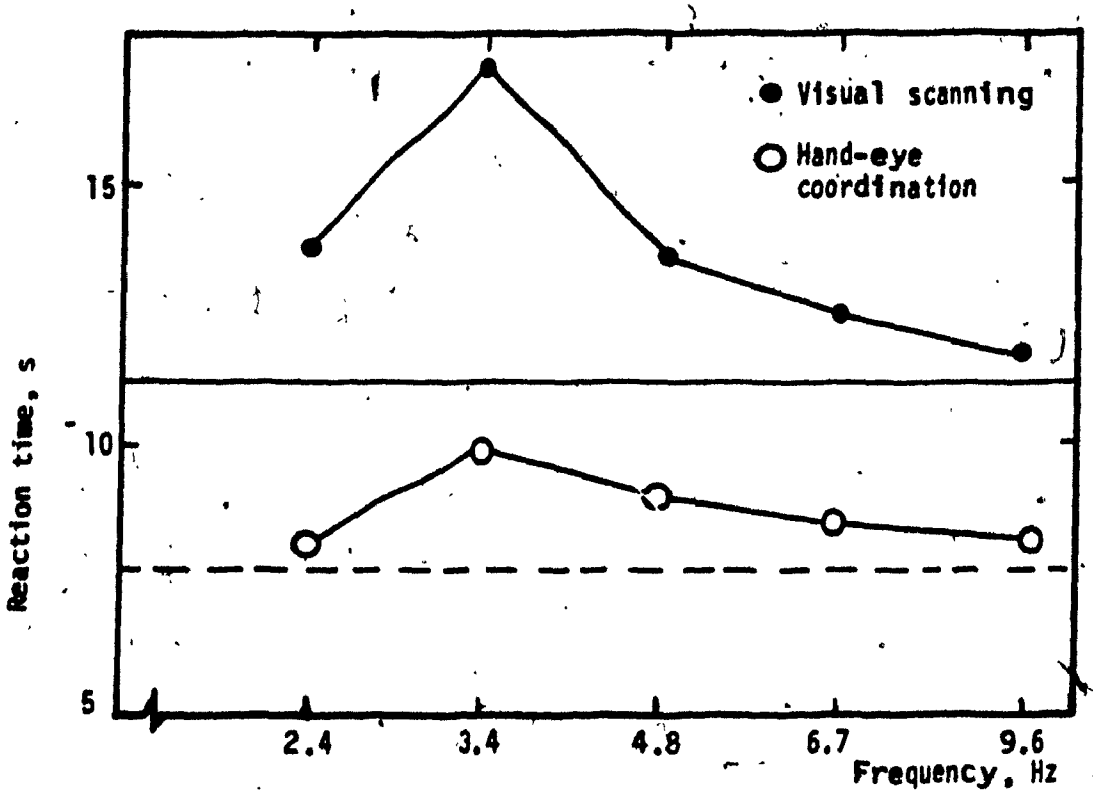

FIGURE 1.3: Effects of vibration on performance rate [8].

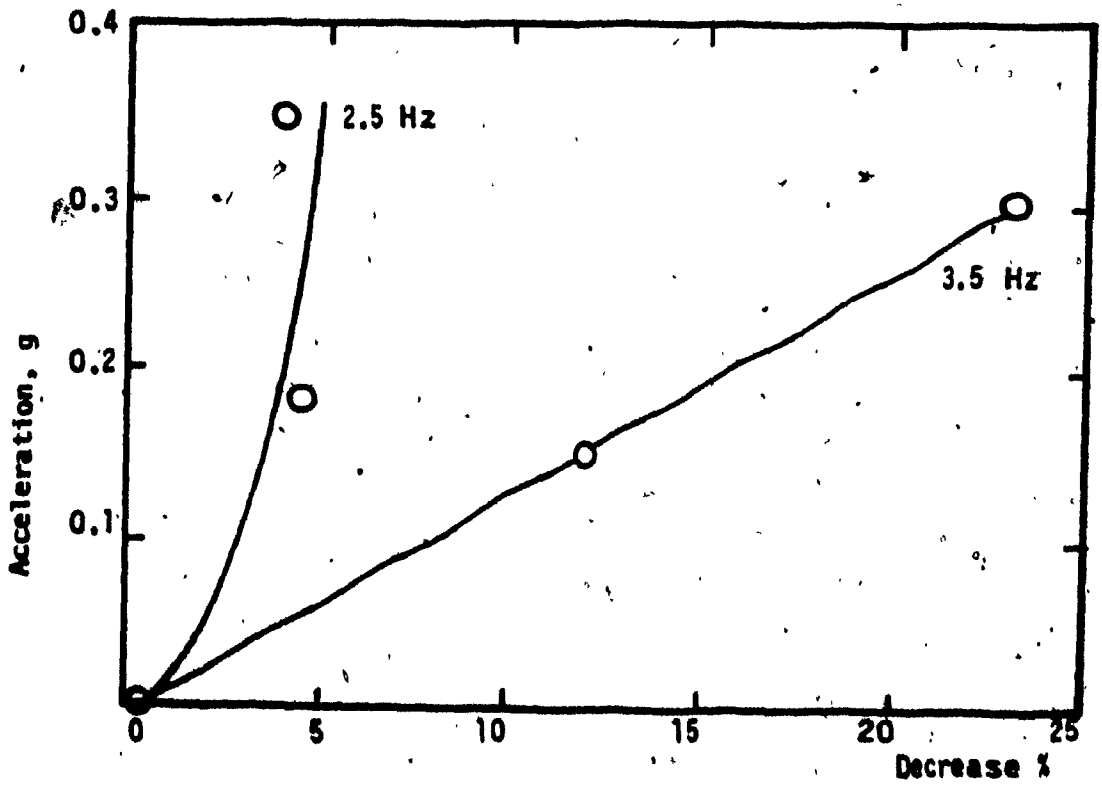

FIGURE 1.4: Effects of Vertical Vibrations on Visual acuity [10].

TABLE 1.4

SUBJECTIVE ASSESSMENT OF TRACTOR RIDE IN RELATION TO VARIOUS TASKS [6]

TRACTOR TASK	SAMPLE SIZE	PERCENT OF DRIVERS CONSIDERED RIDE COMFORT UNSATISFACTORY
Mouldboard Ploughing	176	19.9
Disc Harrowing	50	50
Rigid tine cultivating	40	10
Spring tine cultivating	95	24.2
Rotary cultivating	34	29.4
Cereal Drilling	54	37
Fertilizer Distribution	22	27.3
Rolling	54	24.1
Hoeing	31	29
Mowing	65	33.8
Hay Turning/Raking	17	52.9
Bailing	27	25.9
Front Loading	35	57.1
Transport	126	26.2
Spraying	36	41.7

TABLE 1.5

POWER UTILIZATION OF TRACTORS ON VARIOUS FARMLANDS [11]

Tractor and farm description		Power Utilization* %		
Tractor type	Soil type	Farming Tasks		
		Mouldboard Ploughing	Heavy Cultivation	Light Cultivation
90hp-2WD	Light	65	71	68
	Heavy	67	63	67
90hp-4WD	Light	56	54	60
	Heavy	58	61	58
70hp-track layer	Light	76	71	71
	Heavy	77	78	79
70hp-2WD	Light	43	39	47

* 100% is taken to be the use of 90% of the engine power established by official tests of the particular tractor model. The remaining 10% is considered as a necessary contingency.

1.2.2 RIDE QUALITY EVALUATION CRITERIA

Investigations carried out on various aspects of human response to vibration have provided the data base to establish ride criteria for preservation of health, comfort, and performance. A number of vibration tolerance criteria have been established based on subjective response, relative ride quality ranking of a group of vehicles, tolerance related to machine productivity, vibration interference with normal operator control tasks, health aspects due to vocational exposure, competitive significance, and cost/benefit ratio of potential ride-improvement [12]. Although reasonable similarity in the proposed comfort criteria has been shown with respect to input frequency, the subjective response data has been insufficient and inconsistent to derive a generally acceptable comfort criterion with respect to intensity of vibration. The inconsistencies inherent to the proposed criteria have a multitude of explanations, namely semantic problems, age and moods of subjects at the time of experiments, etc.

Alternatively, objective methods propose direct measure of physical quantities such as velocity, acceleration, jerk, and absorbed power as ride evaluation criteria. At the present time, although many objective methods have been suggested, a generally acceptable measure is yet to be established. However, objective measures of mean square jerk and acceleration have good correlation with subjective human response [13]. In general, a considerable similarity exists among the ride evaluation criteria, regardless of the types of subjective or objective measures. Some of the ride criteria are summarized in the following sections.

Dieckman constant and Janeway limits [14], based on experimental subjective response, imply that human is most sensitive to vertical vibrations below 20 Hz, and were proposed as comfort criteria for automotive passengers. Goldmann [15] also established three vibration levels in the vertical mode, *viz*, perceptible, unpleasant and intolerable, as a function of frequency and peak acceleration response. The validity of these subjective tests has been questioned by researchers [16,17] due to their inconsistent conclusions. However, the most obvious phenomenon occurring consistently in the equal discomfort contours was a dip in the frequency range 5 to 7 Hz.

The International Organization for Standardization (ISO) [18] has setforth three exposure criteria as a function of exposure time in the frequency range 1 - 80 Hz, under horizontal and vertical vibrations. The proposed exposure limits are *health and safety* limits for occupational exposure, *fatigue decreased proficiency* limits associated with preservation of working efficiency, and *comfort* limits (ISO-2631). Figures 1.5 and 1.6 present the *fatigue decreased profiency* rms accleration limits for exposure to vertical and horizontal vibrations.

k-factor, as a measure of vibration intensity, function of frequency and rms acceleration, velocity or displacement amplitude has been proposed in Germany [19]. Figure 1.7 shows acceleration limits associated with *k*-factor. Suspension seats characterizing a *k*-factor of 25 or less, which is equivalent to rms acceleration 1.25 m/s^2 or approximately 1 hour exposure time ISO *fatigue decreased proficiency criteria*, have been proposed to be acceptable.

The *k*-factor for suspension seats is evaluated in the following manner:

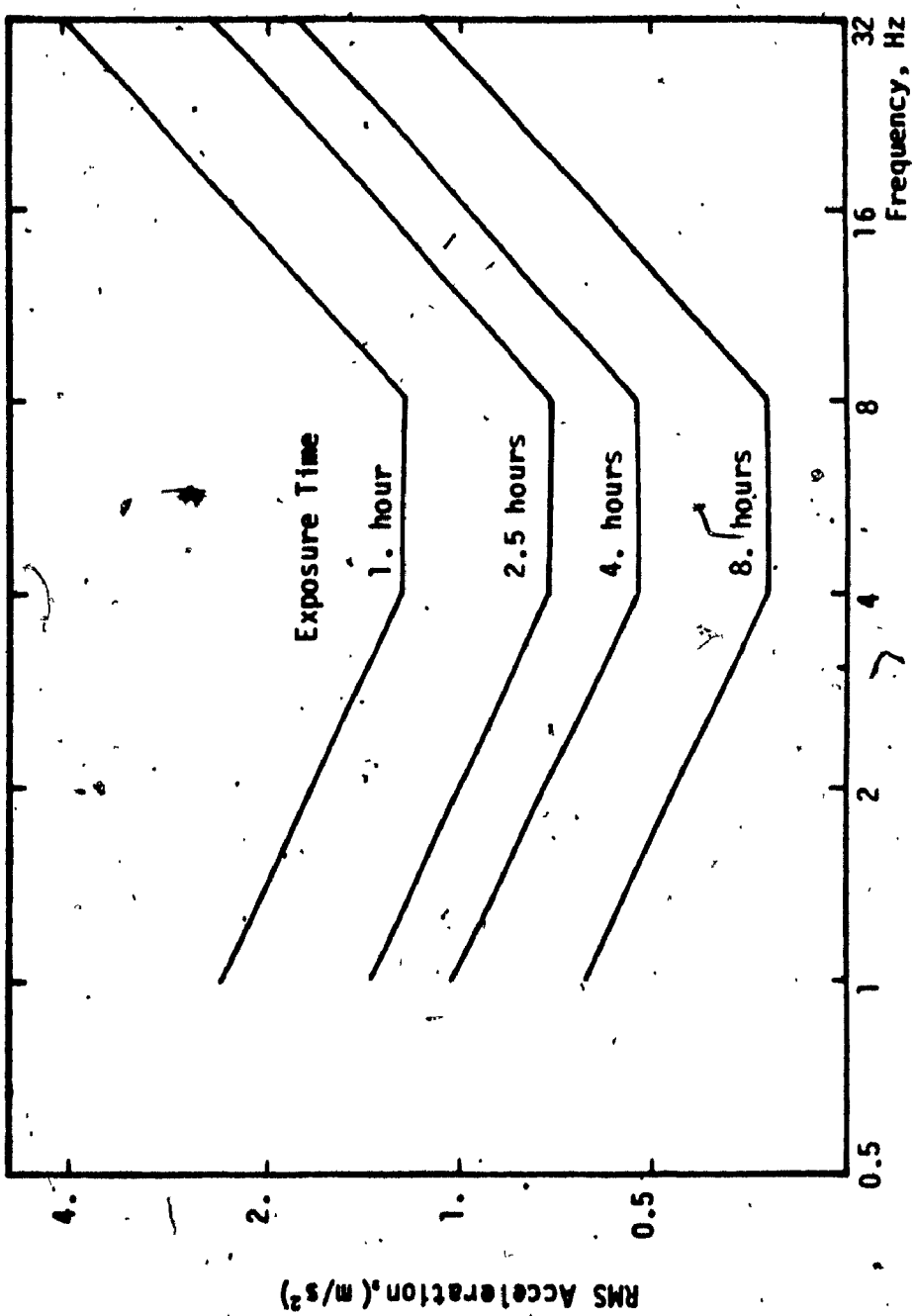

FIGURE 1.5: *Fatigue decreased proficiency* limits, for exposure to vertical vibration [18].

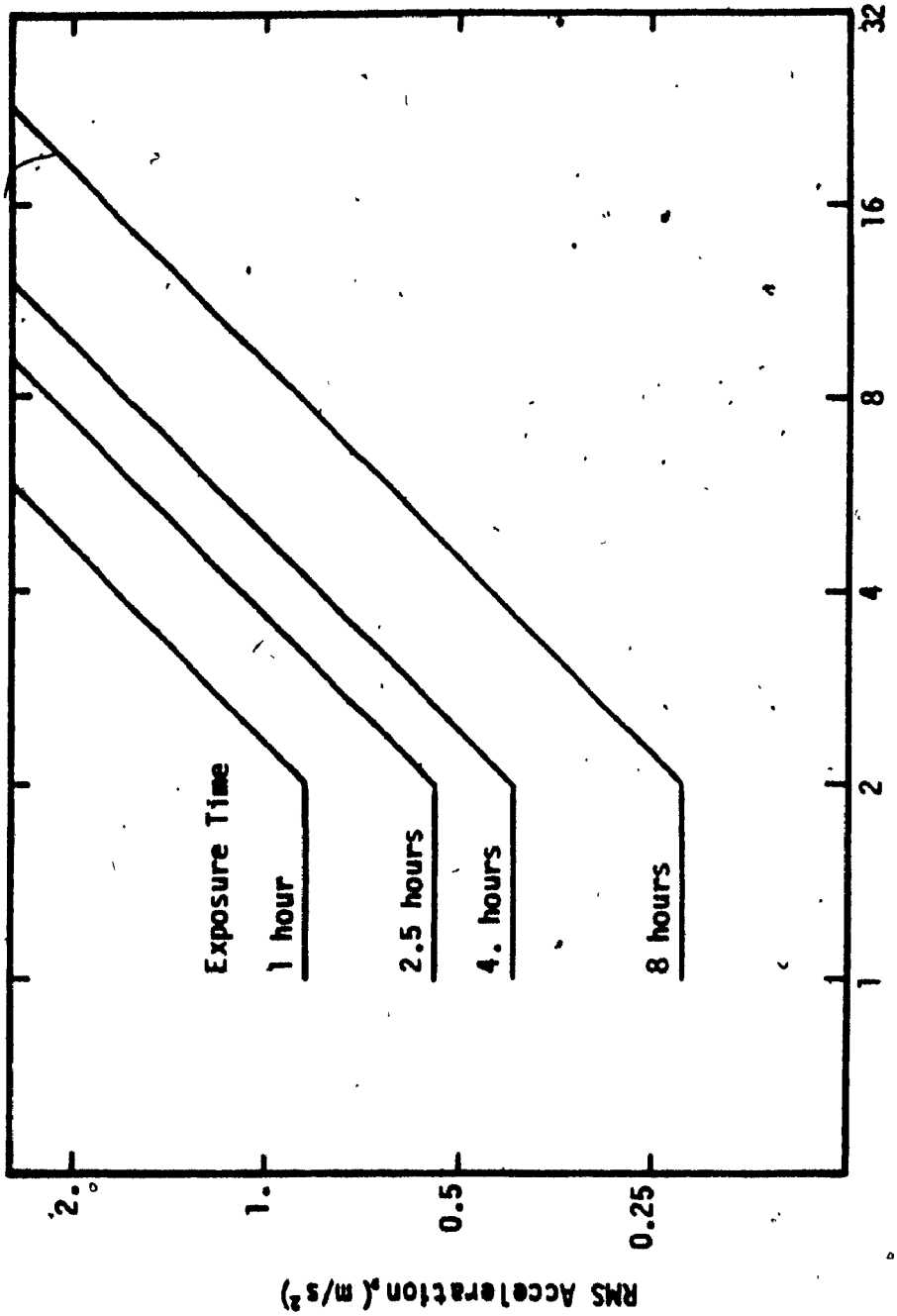

FIGURE 1.6: *Fatigue decreased proficiency* limits for exposure to horizontal vibration [18].

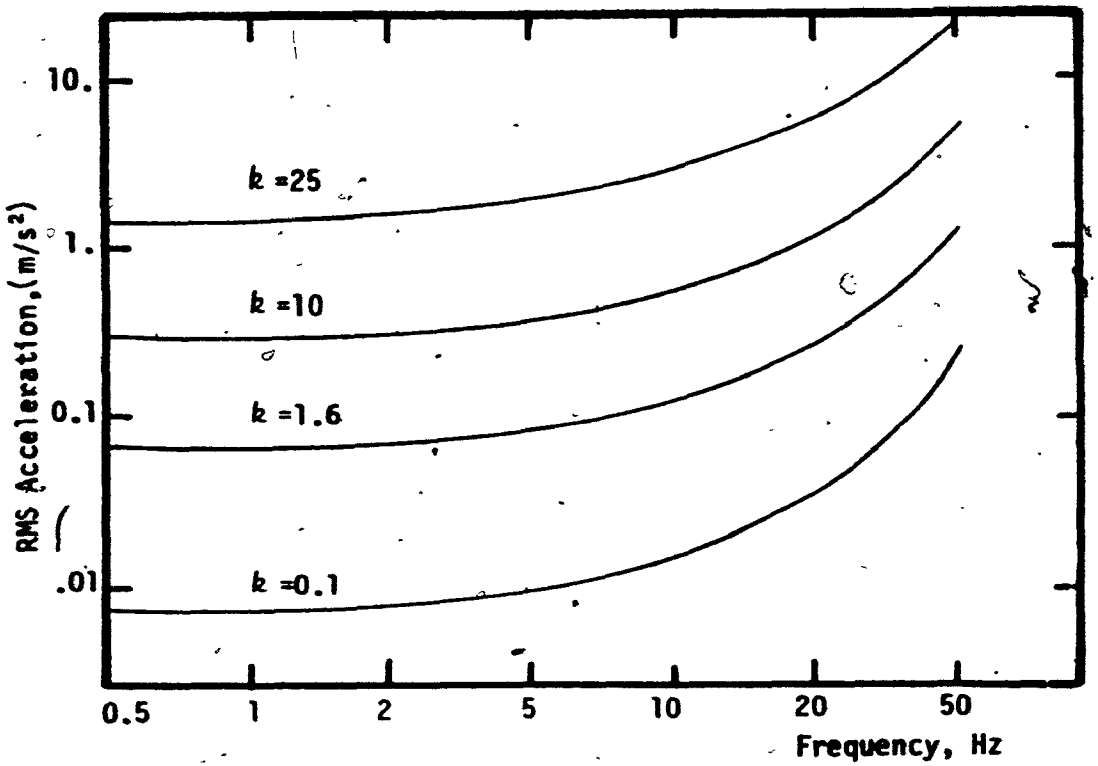

FIGURE 1.7: k factor and corresponding RMS acceleration limits as a function of input frequency.

$$k = \bar{a} \frac{\gamma_1}{\sqrt{1+(f/f_0)^2}} \quad (1.1)$$

$$k = v \frac{\gamma_2 f}{\sqrt{1+(f/f_0)^2}} \quad (1.2)$$

$$k = \xi \frac{\gamma_3 f^2}{\sqrt{1+(f/f_0)^2}} \quad (1.3)$$

where:

$\bar{a}$ = rms acceleration in m/s^2.

v = rms velocity in mm/s.

ξ = rms displacement in mm.

and the constants are given by,

$f_0 = 10$ Hz. $\qquad \gamma_1 = 18 \frac{k}{m/s^2}$

$\gamma_2 = 0.112 \frac{k}{mm/s^2} \qquad \gamma_3 = 0.71 \frac{k}{mm/s^2}$

/Lee and Pradko [20] proposed a comfort parameter named "Average Absorbed Power", as the rate of energy flow dissipated by the complex damped elastic properties of human anatomy. Average absorbed power is determined by the intensity and frequency of the input vibration.

$$P = \sum_{i=1}^{n} k_i \bar{a}_i^2 \quad (1.4)$$

where:

P = Average absorbed power in N.m/s.

$\bar{a}_i$ = rms acceleration at frequency i in m/s^2.

k_i = Absorbed power constant of the body at frequency i, in $\frac{N.m/s}{(m/s^2)^2}$.

The absorbed power criteria is also supported by Janeway [14] limits as shown in Figure 1.8. A number of objective criteria have been put into practice in recent years. In Austria, absolute displacement of tractor seat loaded with 50 kg inert mass must not exceed 10 mm in the frequency range 0.5 to 4 Hz. In Sweden, vibration level at the driver's shoulder must be less than 0.8g for all frequencies, which is roughly equivalent to 1.25 g at the human body-seat interface in the frequency range 5 to 7 Hz [21].

Stikeleather [22] has recommended three ride comfort criteria, namely International Standard ISO-2631, total integrated absorbed power, and overall weighted rms acceleration. Of all these, only International Standard specifies rms acceleration limits as a function of exposure time under vertical as well as horizontal vibration, and is most widely accepted. The standard is applicable to whole-body vibration as percepted by the drivers of agricultural tractors and industrial off-road vehicles. However, the standard fails to quantify ride criteria under rotational modes of vibration.

1.2.3 MODELING OF HUMAN BODY

The human body possesses a set of physical properties responding to input vibration in a highly complex manner. There have been continuous efforts in modeling the human body in order to understand its behaviour in vibrational environment. In order to evaluate vehicle suspension performance characteristics, it is essential to develop an acceptable human body model. Quantitative information on human body dynamics have been obtained from impedance and transmissibility characteristics of human

body. Coermann *et al* [23] established impedance characteristics of standing and seated subjects as shown in Figure 1.9. The impedance characteristics exhibit two resonance peaks corresponding to 5 Hz and 11 Hz. Their findings have been supported by various other experimental investigations as summarized in Table 1.6 [24]. Consequently, a human body simulator of two damped spring masses suspended from a common frame has been proposed by Suggs *et al* [25] and Park *et al* [26]. Although the proposed simulator duplicated the low frequency characteristics accurately, the models have been questioned due to the lack of resemblance of the human anatomy. However, the low frequency impedance characteristics of human body correspond to that of a rigid mass up to 4.5 Hz [23].

TABLE 1.6

COMPARISON OF HUMAN BODY MODELS [24]

DEVELOPER	POSTURE	FIRST TWO RESONANCE FREQUENCIES	DEGREES OF FREEDOM
Coermann *et al* [23]	sitting	5 Hz - Upper Torso 11 Hz - Pelvis	2
	standing	3-4 Hz - Abdomen 7 Hz - Chest	7
Suggs *et al* [25]	sitting	4-5 Hz - Lower body 8 Hz - Upper body	2
Payne *et al*	sitting	4-6 Hz - Torso 30 Hz	4
Muksian and Nash	sitting	3 Hz 6-7 Hz	7

Many degrees of freedom human body model comprising of linear and non-linear lumped stiffness and damping elements have been developed to match the experimental transfer functions [27]. These models describe anatomical path between the pelvis and head more closely. However, there are many

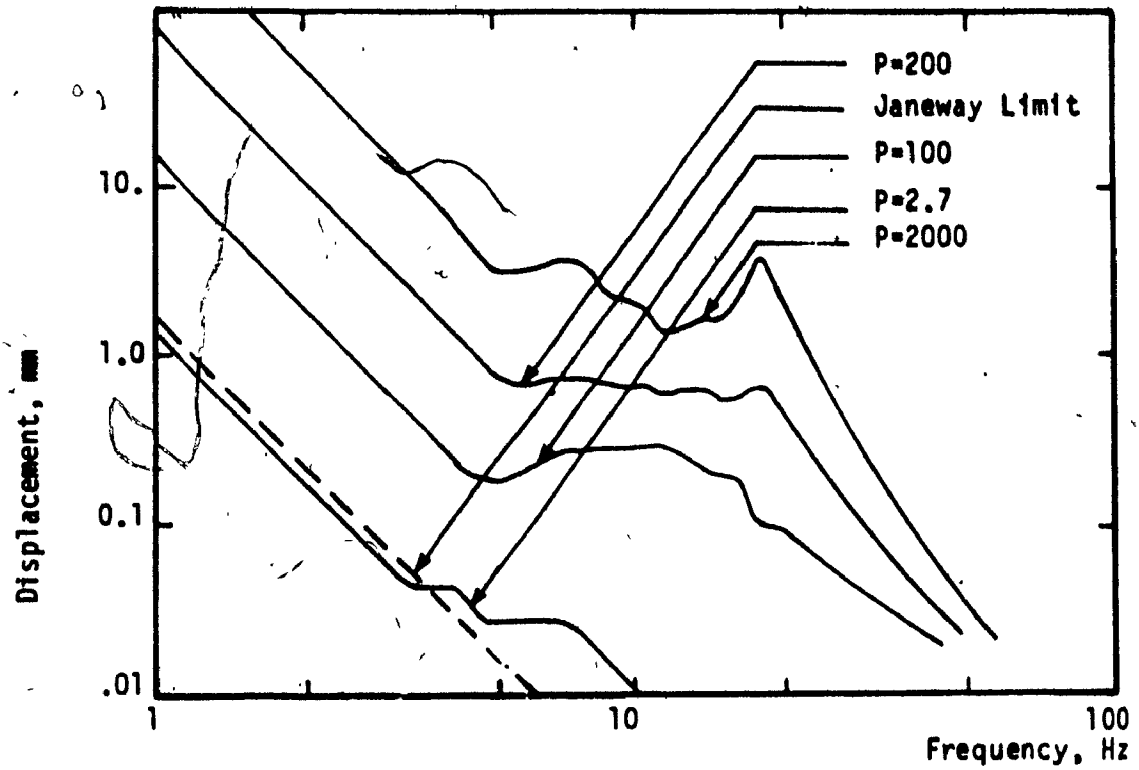

FIGURE 1.8: Average absorbed power (P) and Janeways ride vibration limits [20].

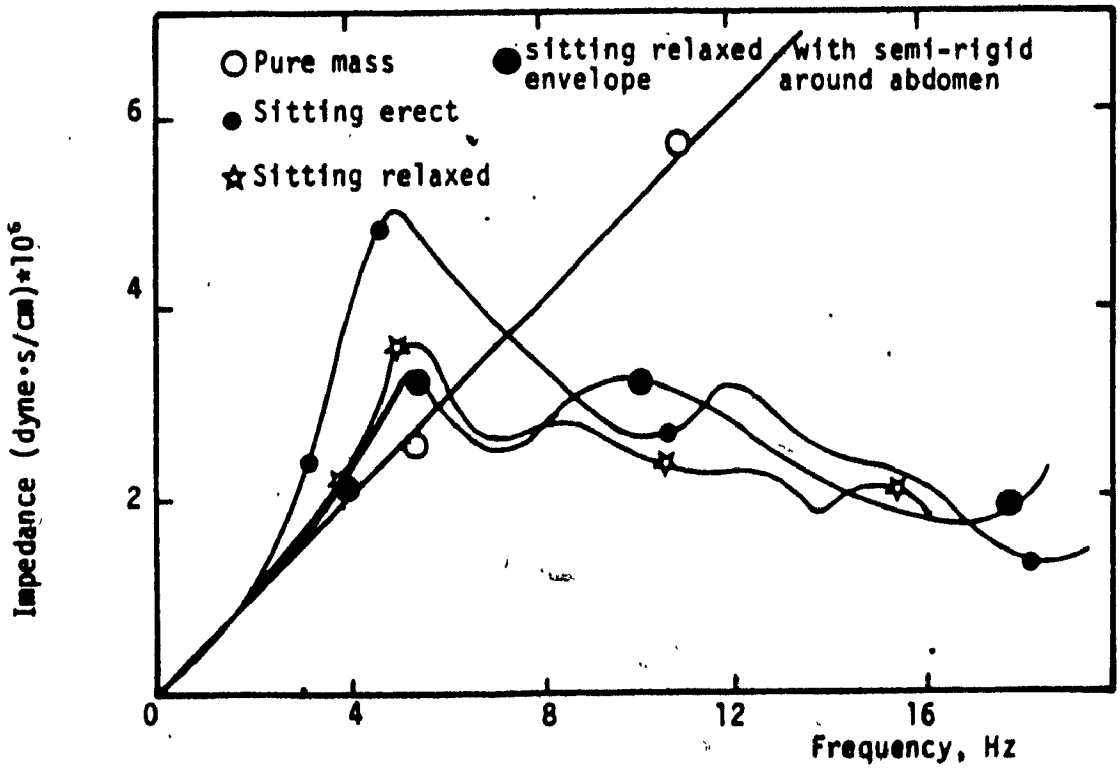

FIGURE 1.9: Mechanical impedance of subjects exposed to vertical vibration [23].

unanswered questions concerning the nature and process associated with determination of various lumped parameters representing human anatomy.

1.2.4 APPROACH TO RIDE IMPROVEMENT

Ride vibration, imposed by large diameter and soft tires, are directly transmitted to the seated operator through unsprung vehicle structure. The amplitude of vibration encountered by the seated operator, measured during numerous investigations, surpass the 1 hour exposure time *fatigue decreased proficiency* limits specified by ISO, in all the translational coordinates. The ride vibrations encountered in the roll and pitch coordinates are also found to be as severe. A need to reduce vibration levels perceived by the operators has been identified and various ride improvement approaches have been proposed, namely suitable tires, primary suspension at front and rear axles, cab suspension, and seat suspension. Improvement in ride may also be contributed by factors like, location of cab-mounts, seat-location, and cab-geometry.

Each of the ride improvement approaches offer respective advantages, limitations, and performance characteristics. Large diameter, soft tires subside the forces transmitted in the bounce and pitch modes with an amplification of roll and lateral vibrations due to higher location of the driver and cab [28, 29]. Terrain induced tractor ride vibration predominate in the frequency range 1 - 5 Hz, implying that even softer and consequently larger tires are required, such that vehicle would not resonate during the ride frequencies. Thus, the ride improvement via tires alone have been found infeasible due to size limitations on tires [30].

Alternatively, a primary suspension at the axles can significantly improve ride by increasing the proportion of sprung mass to unsprung mass of the vehicle. Plane model of a tractor idealized by a suspended seat

and suspended chassis have been analysed by Matthew [31] and Patil *et al* [32]. The concept of primary suspension, however, would require complex alterations in vehicle design and would be impractical to implement to vehicles carrying frame mounted equipment. Suspension at the cab can provide for the drivers: a stable floor, isolation from forces introduced by implemented loads, and isolation from noise and chassis vibrations. A cab suspension helps to protect the cab and cab mounted equipment from frame vibrations and shock loads. Moreover, a cab-suspension can be readily implemented to the existing vehicle design.

Suspension at the seat is the simplistic alternative for vibration isolation. Effective low natural frequency bounce seat suspensions have been commercially employed. However, effectiveness of seat suspension is achieved at the expense of excessive relative motion between the driver and tractor controls.

Of the possible approaches to ride improvement, the concepts of seat suspension and cab suspension merit initial considerations in attempting to improve ride comfort and safety, due to their easier adaptability to an existing vehicle design configuration.

1.2.5 SEAT SUSPENSION

A driver seat, being a link between the driver and the controls, has a peculiar prominence on off-the-road vehicles. The seat, therefore, must be a steady platform for the actions of the driver. Since, most off-road vehicles are unsuspended and directly supported by tires with little inherent damping, the vehicle vibrations are directly transmitted to the driver. The seat, therefore, must attenuate vibrations for operator's ride comfort.

Passive, active, and semi-active suspension systems may be considered for potential use in attenuating vehicle vibrations. Passive systems are

the simplistic suspensions consisting of passive energy dissipators. Requirements of extremely low natural frequency suspensions may limit the application of passive isolators in certain modes due to associated large static and dynamic deflections [33]. Active suspensions overcome the performance limitations of passive isolators. Active systems require a continuous power source, and a power actuator controlled by a manipulated command signal from the instrumentation implemented on the vehicle. Extremely low natural frequency active suspensions can be designed to provide superior performance. However, the superior performance of active vibration isolators is obtained for increased cost, complex control techniques, and poor reliability.

A compromise between the excellent performance of active suspension and the mechanical simplicity of passive system is achieved by a semi-active system. Semi-active system consists of sensors, control package, and suspension element with variable parameters [34, 35]. The control system provides feedback signal to vary suspension parameters and needs only a small electrical power. All three concepts have been employed to develop seat suspension and cab suspension models. They offer their respective advantages, limitations and performance characteristics.

Passive Seat Suspension

Bounce seat suspensions with natural frequencies 1.5 to 4 Hz have been commercially developed [36, 37]. A number of recommendations concerning geometrical configurations, levelling mechanisms, and seat location have been made by De Longchamp [21] and Rosso [38]. Configurations of passive bounce seat suspensions possessing variable stiffness characteristics have been developed [39, 40] and experimentally evaluated [41, 42].

The experimental results reflect that a good bounce seat suspension has natural frequency in the range 0.4 to 0.5 of the natural frequency of the tires.

Ordinarily, vibration encountered by the tractor operators are characterized by the relatively high frequency vibration arising from engine and drive trains, and relatively low frequency vibration caused by irregular terrains. Latter being in the frequency range 1 to 5 Hz is quite complex to be isolated by passive means. Matthews [43] suggested 1.5 Hz or less as the natural frequency and 76.2 mm as the maximum vertical travel for bounce seat suspensions. Various configurations of pneumatic bounce seat suspensions with flexible natural frequencies, using diaphragms and constant air supply have been developed for highway vehicles. Such suspensions are infeasible for off-road applications due to limited diaphragm displacement and inavailability of air supply. A longitudinal seat isolator consisting of mechanical linkages, springs and dampers has also been proposed to John Deere [44].

Active and Semi-Active Seat Isolators

In recent years, active seat suspensions have been developed to control low frequency vibrations. Suggs *et al* [45, 46] developed a bounce active seat suspension employing linear potentiometer, electro-hydraulic servo valve, and hydraulic actuator. The suspension system provided 65 to 70% of acceleration attenuation in the frequency range 1.5 to 8 Hz. Grimm [47] analyzed bounce seat relative motion with respect to the tractor frame using a seat accelerometer signal to control hydraulic actuator through a proportional servovalve. Suggs *et al* [48] developed roll and pitch active seat isolator using rotary potentiometer at the seat, and a

vibrometer at the chassis to provide the necessary control signal to the electro-hydraulic isolation system. Kim [49] presented a computer model for active bounce isolator using acceleration, relative position, and relative velocity feedback signals to an electro-hydraulic system through a control package.

Models of semi-active suspensions employing local absolute and relative velocity signals to produce on-off skyhook damping have been developed [34, 35, 50]. Such suspensions do not require continuous power source but associate a complex instrumentation and control strategy. Computer model for a semi-active bounce seat-isolator with skyhook damping has been developed by Kim [49]. While many studies on active suspensions have been carried out, relatively few active suspensions have been put in service. In fact, the only common type of active suspension is a "Load Leveler" in which the average suspension deflection is maintained at zero through the use of a slow feedback system [51]. A system of this type cannot be speeded up, however, without encountering both stability problems and high power requirements.

1.2.6 CAB SUSPENSION

Stayner [52] found that vibration in horizontal coordinates are as hazardous as vertical vibration, and listed the order of priority of vibration isolation as vertical, lateral, pitch, and roll. Consequently, multimode cab-suspension models have been proposed to isolate the operators from the terrain induced vibrations in bounce, lateral, pitch, and roll modes.

A scale model for one degree of freedom cab has been simulated by Suggs *et al* [53]. The resulting system consisted of two torsion type springs mounted at the rear of cab and showed a natural frequency of

2.5 Hz. The scaled model offered ride improvement at high frequencies alone. Hilton [54] conducted experiments on tractor cab suspension with natural frequencies 0.8 and 1.0 Hz in vertical, 0.6, 0.85 and 1.2 Hz in pitch, and 0.5 Hz in roll. Using computer models for a linear four degrees of freedom agricultural tractor cab, performance characteristics of cab suspension have been developed with passive, active, and semi-active suspension elements [55].

Numerous cab-suspensions have been developed for highway vehicles over the past decade, namely Ford's CL-9000, Easy-rider I, Easy-rider II, etc. Easy rider I, a completely pneumatic cab suspension for highway tractor-trailer vehicles, provided low and variable natural frequency along with static position compensation [56]. Wallace [57] proposed front and rear cab isolators consisting of accumulators containing pressurized air and ethylene glycol separated by diaphragm and a diaplacer unit. Crosby [58] presented the analysis of highway vehicle cab associated with cab geometry, cg location, and the ratio of sprung to unsprung mass. The analysis showed that such factors influence highway vehicle ride significantly.

1.3 SCOPE OF THE PRESENT INVESTIGATION

Objective of this investigation is to develop suspension models that would isolate the tractor drivers from the ride vibrations in bounce, longitudinal, lateral, roll, and pitch modes. The ride improvement is sought via suspensions at the seat and at the cab for the reasons of simpler adaptability to an existing agricultural vehicle. The objectives of the study are:

1) To develop a mathematical model for commercially available passive bounce seat suspension, and to predict the suspension performance through computer simulation.

2) To verify the bounce suspension model through laboratory experimentation.

3) To propose configurations of longitudinal, lateral, roll, and pitch passive seat suspensions, which can be attached to an existing bounce seat suspension.

4) To develop mathematical models corresponding to suspension systems in translational and rotational modes, and to evaluate their ride performance characteristics.

5) To study the sensitivity of the seat suspension response to variations in the values of suspension parameters.

6) To select optimal suspension parameters to ensure ride performance with 4 hours exposure time *fatigue decreased proficiency* limits, using multivariable optimization techniques.

7) To develop mathematical models for linear passive cab suspensions with rigidly and suspension mounted seat.

8) To carry out a parametric study to establish the sensitivity of suspension performance to variations in suspension parameters.

9) To determine optimal suspension parameters with an objective to maintain the acceleration response at the seat within ISO specified 4 hours exposure time *fatigue decreased proficiency* limits.

10) To assess the ride quality of cab-suspension models with reference to the ISO proposed limits.

11) To develop the concept of semi-active "ON-OFF" damping.

12) To develop and to simulate the bounce seat suspension model with "ON-OFF" damping.

13) To evaluate the performance characteristics of bounce seat suspension model using "ON-OFF" damping.

In Chapter 2, configurations for passive longitudinal, lateral, pitch, and roll seat suspensions are proposed. The mathematical models of passive seat suspension are formulated including non-linearities arising from Coulomb friction, shock absorbers, and elastic limit stops. The major assumptions associated with the model formulation are discussed. The mathematical models for the cab suspension with rigidly and suspension mounted seat are formulated with linear suspension elements.

In Chapter 3, the bounce acceleration excitations at the seat attachment point as proposed by ISO are discussed. The acceleration PSD measured at the cab floor at the Silsoe track are presented in bounce, longitudinal, lateral, roll, and pitch modes. The terrain induced acceleration levels at the cab floor are compared to the ISO proposed *fatigue decreased proficiency* limits in order to assess the ride behaviour of an unsprung agricultural vehicle. The acceleration PSD's are represented by the summation of harmonic components corresponding to discrete frequencies, that would represent a replica of the terrain measured acceleration spectral densities.

In Chapter 4, the analytical techniques for solving the differential equations characterizing the dynamics of suspension models are discussed. Various techniques for solving the non-linear equations of motion are briefly summarized, followed by the development of a simpler analytical technique based on dissipation of energy. The non-

linear equations of motion are represented by their linear equivalents using the technique based on dissipation of energy. The transmissibility characteristics of the linear equivalent system are obtained and compared to the transmissibility characteristics of the non-linear system, obtained through numerical integration technique. The accuracy of the linearization technique is also tested for the stochastically described agricultural terrain excitations.

In Chapter 5, the sensitivity of the passive seat and cab suspension response to variations in suspension parameters is investigated. The response acceleration and relative displacement are selected as the performance indices to represent the performance of passive suspension systems.

In Chapter 6, a performance criterion for each suspension model is formulated alongwith the constraints on the suspension parameters. Optimal suspension parameters, that would minimize the performance criterion, are obtained using non-linear programming technique. The suspension systems are optimized using a direct search method based on Hooke and Jeeves algorithm. The ride performance of optimum suspension models is assessed with reference to the ISO proposed *fatigue decreased proficiency* limits.

Chapter 7 presents the development of the concept of semi-active "on-off" damping, that operates as a conventional passive damper for part of the vibration cycle and assumes negligible damping for the remaining part of the vibration cycle. Bounce suspension seat is modeled with "on-off" damping and its performance is investigated for harmonic as well as stochastically described excitations.

Finally, the conclusions and recommendations for future work are presented in Chapter 8.

CHAPTER 2

DEVELOPMENT OF SUSPENSION MODELS

2.1 INTRODUCTION

Passive seat suspension is the simplest option to ride improvement of agricultural and industrial off-road vehicles. A seat suspension can readily be implemented to an existing vehicle configuration. Passive bounce suspension seats have been commercially developed and successfully employed to highway and off-highway vehicles, over past few years. These passive seat suspensions invariably include fixed or variable stiffness element, shock absorber as the dissipative element, and a mechanism to vary the load carrying capacity of the suspension system. Since it has been established that agricultural terrain induced vibrations in the longitudinal, lateral, roll, and pitch modes are as severe as that in the bounce mode, it is essential to develop a seat suspension capable of isolating the tractor operators in these modes of tractor vibrations.

Improvement in tractor ride can be accomplished through the simplistic low natural frequency and lightly damped passive suspension seats. However, the low natural frequency and light damping requirements limit the performance of passive suspension seats due to excessively large relative motion of the operator with reference to the vehicle controls. Consequently, the performance ability of the vehicle operator is highly impaired. Alternatively, the relative displacement between the operator and the controls may be eliminated by a sprung cab. A suspension at the cab can be implemented to an existing vehicle configuration. Moreover, a cab suspension can isolate the driver not only from the terrain induced vibrations but also from the vibrations introduced by the articulated equipment.

In this chapter, the design specifications of commercially available bounce seat suspensions are summarized. The geometric configurations of longitudinal, lateral, roll, and pitch passive seat isolators are proposed. The proposed configurations in various planes of motion are attachable to an existing bounce seat suspension, such that a multimode passive seat-isolator is formulated. Mathematical models for multimode translational and rotational passive seat-isolation systems are formulated. The translational model is formulated by combining three translational isolators, *viz*, bounce, longitudinal, and lateral. The rotational seat suspension model incorporates roll and pitch seat isolators to an existing bounce seat suspension.

A passive cab suspension model based on existing cab geometry is presented. The mathematical models are formulated for the cab suspension with rigidly and suspension mounted seat. The differential equations characterizing the motion of passive seat and cab suspension models are formulated to investigate the suspension performance characteristics.

2.2 DESIGN SPECIFICATIONS OF COMMERCIALLY AVAILABLE SUSPENSION SEATS

Bounce suspension seats have been employed to off-road vehicles for past few years. Such seats can attenuate the vertical component of vehicle vibration by 50% or more, when properly tuned. Figures 2.1 to 2.4 present some of the suspension seats developed by Bostrom, and Anchorlok. These suspension seats consist of either a kinematic linkage mechanism or a pneumatic cylinder to compensate for static deflection, shock absorber, and elastic limit stops.

The suspension seats are generally designed as single degree of freedom isolators, neglecting cushion dynamics, and assuming the seated human body mass to be either 75% [21] or 5/7 of total body mass [22].

FIGURE 2.1: Levelair II, bounce suspension seat with pneumatic levelling system [Bostrom].

FIGURE 2.2: Pneumatic seat suspension [Anchorlok]

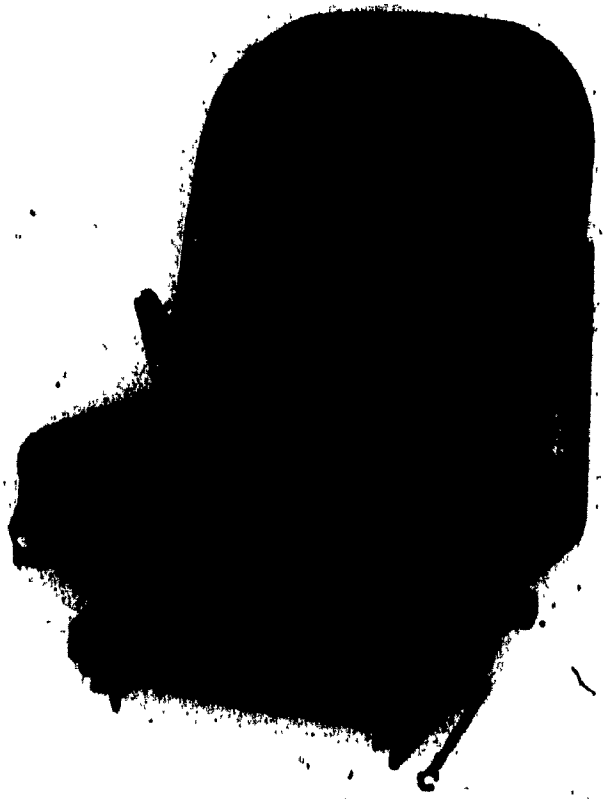

FIGURE 2.3: Viking, Bounce suspension seat [Bostrom]

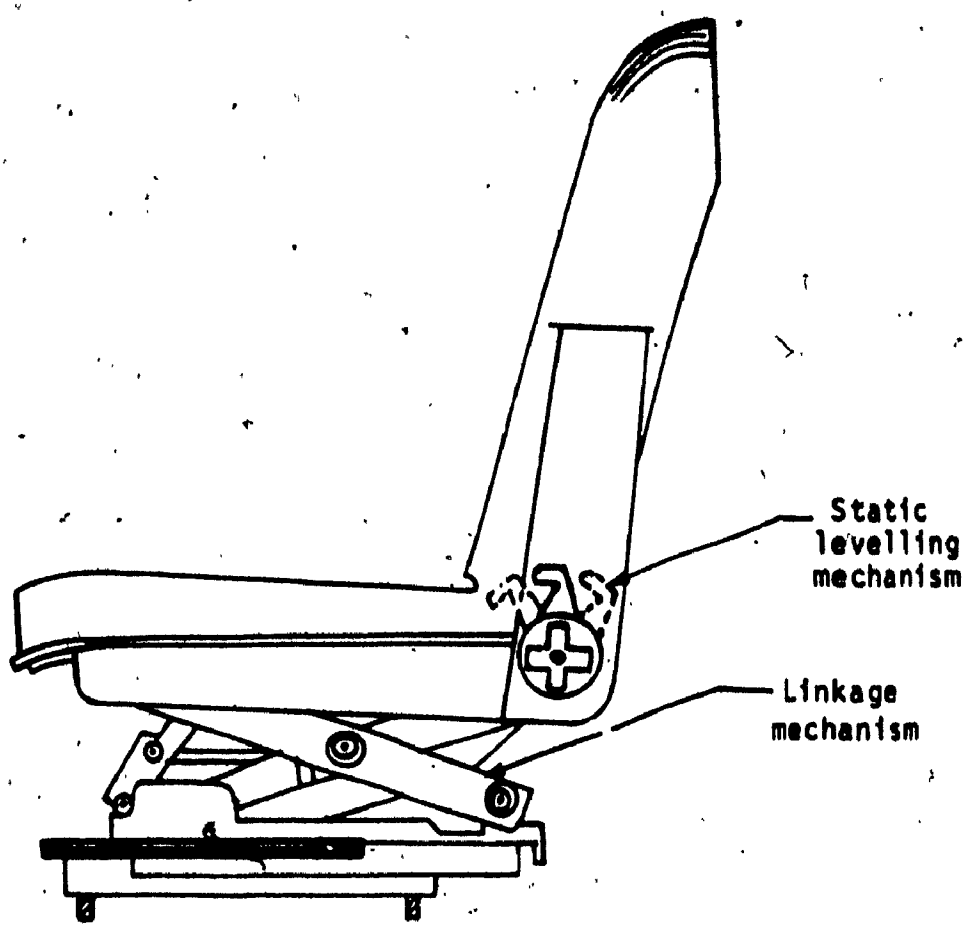

FIGURE 2.4: Schematic of a Viking T-bar bounce suspension seat [Bostrom].

The influence of suspension characteristics on the vehicle is assumed negligible due to extremely small ratio of operator mass to vehicle mass. The natural frequency of suspension seats ranges from 1.5 to 3. Hz with operators weight 588N to 1180N. An adjustable preload is incorporated by means of torsion springs or manually controlled pneumatic cylinders to offset the static deflection caused by operator's weight. Soft elastic stops, limit the excessive relative displacements associated with relatively low natural frequency suspension designs. Total travel of seat suspensions ranges from 60 mm for highway articulated vehicles to 130 mm for off road vehicles on extremely rough terrains. In general, suspension seats implemented to agricultural tractors provide a total travel of 100 mm. The specifications of passive bounce suspension seats are summarized in Table 2.1.

Ride performance of passive bounce suspension seats have been evaluated through transmissibility characteristics obtained in the laboratory. Alternatively, computer simulation techniques may be used to predict the ride performance of a suspension system. However, computer simulation technique requires identification of suspension components, mathematical model of the suspension system, and the discretized terrain description or road input to suspension system.

Various suspension components are identified through static or dynamic characteristics. Force-displacement characteristics of suspension linkage mechanism invariably exhibit linear stiffness and hysteresis as a measure of static friction as shown in Figure 2.5. Force-displacement, and transmissibility characteristics of Marshall cushions indicate very low damping and linear stiffness properties within practical limits, as shown in Figures 2.6 and 2.7. Typical force-displacement characteristics of elastic limit stops can be presented as shown in Figure 2.8. The

TABLE 2.1

SPECIFICATIONS OF COMMERCIALLY AVAILABLE BOUNCE SEAT SUSPENSION

Manufacturer	Model	Construction	Natural Frequency	Pre-Load Mechanism	Suspension Travel	Application
Bostrom	Air-Viking	Cross linkage mechanism and inclined shock absorber	1.5 to 3Hz	Push-pull valve with pneumatic cylinder	102mm	Highway and off-highway vehicles
	Westcoaster	Kinematic linkage and selective shock absorber designed to engage automatically over a rough bump	1.5 to 3Hz	Rubber torsion spring	95mm	Highway Vehicles
	Levelair II	Linkage, selective shock absorber and air spring	1.5 - 2Hz	Pneumatic cylinder	75mm	Highway vehicles
	Viking T-bar	Cross linkage and inclined shock absorber	1.5 - 2.5Hz	Torsion spring	75-100mm	Highway and off-highway vehicles
Anchorlok	Monarch	Diaphragm and shock tube. Requires continuous air supply	1.5 - 2Hz	Manually controlled valve	60-100mm	Highway vehicles

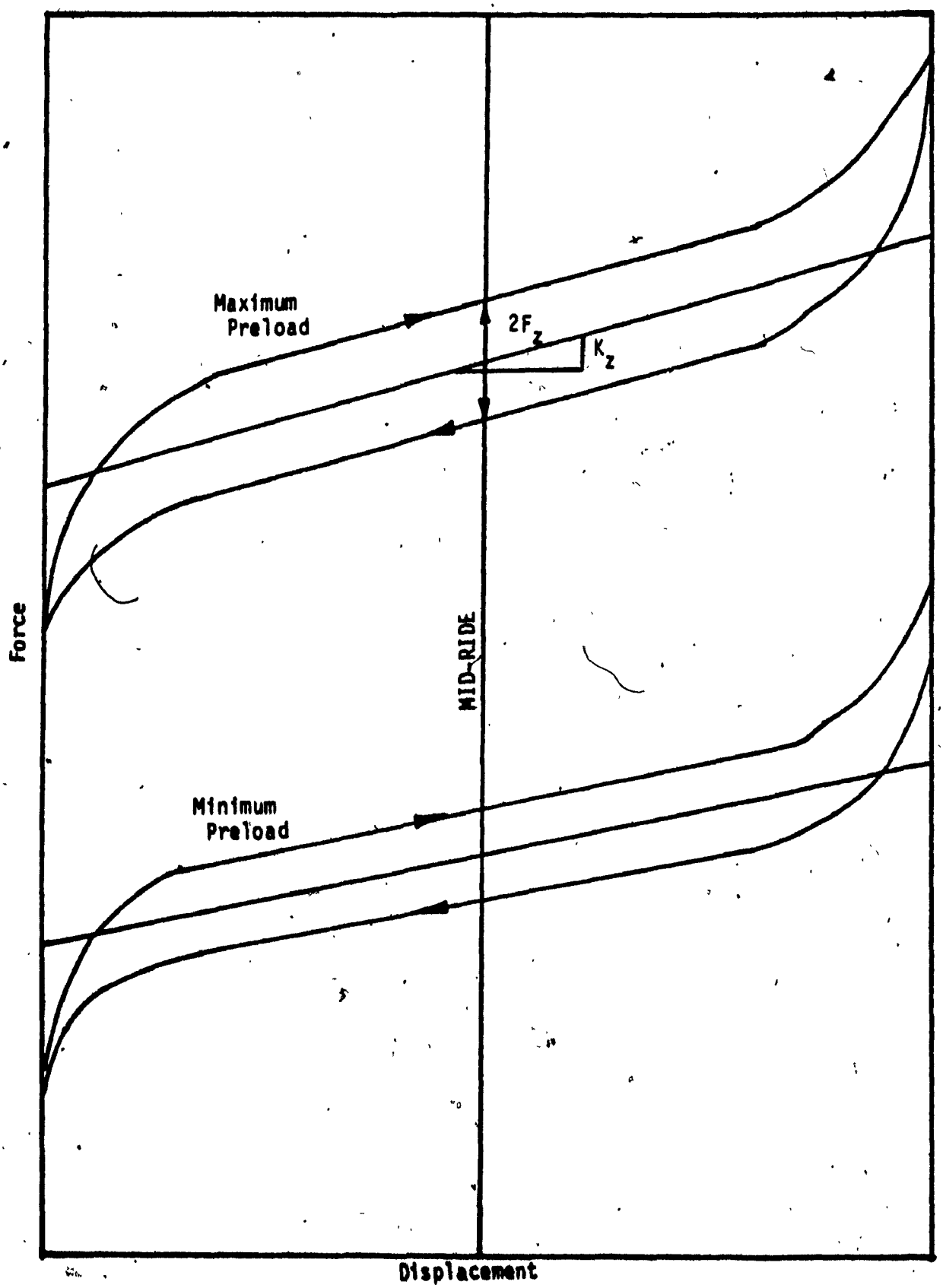

FIGURE 2.5: Force-displacement characteristics of the bounce suspension linkage mechanism [36].

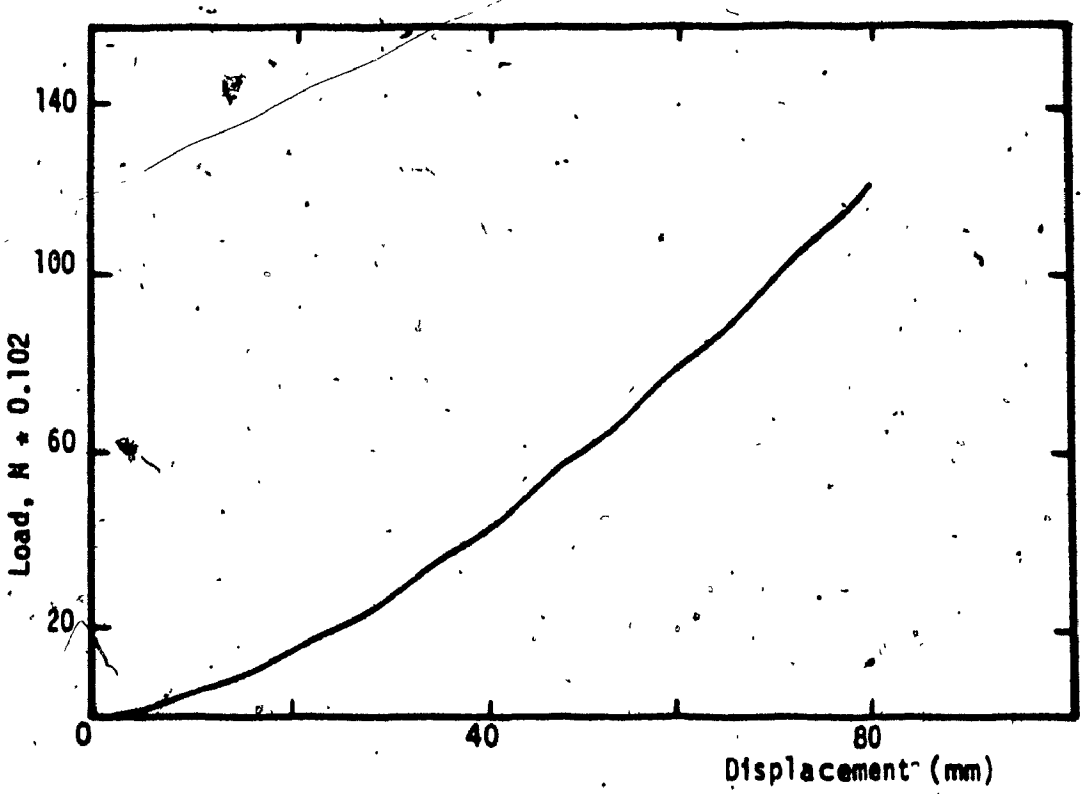

FIGURE 2.6: Force-displacement characteristics of Marshall Cushion [36].

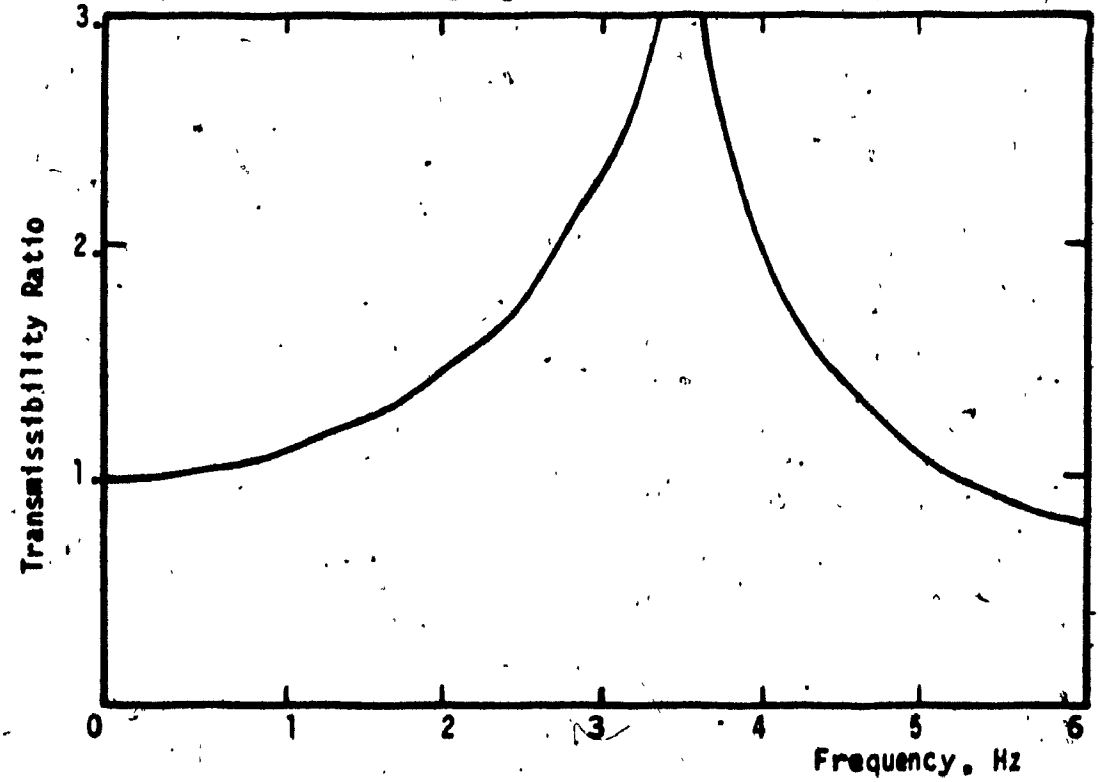

FIGURE 2.7: Transmissibility characteristics of Marshall Cushion [36].

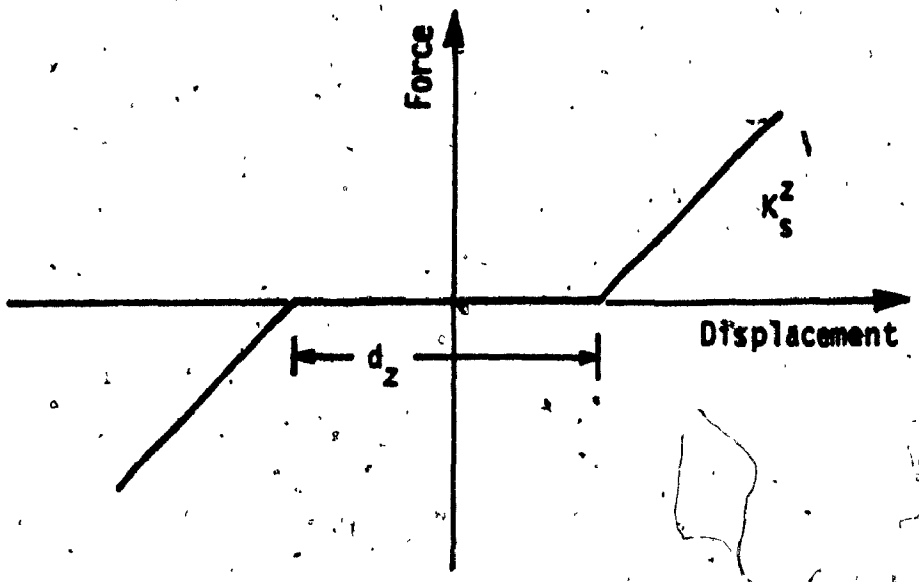

FIGURE 2.8: Typical force-displacement characteristics of elastic limit stops.

damping characteristics of shock absorber is a synthesis of velocity squared damping associated with orifice flows, linear viscous damping due to leakage flows, and seal friction. Identification of component characteristics form the basis for development of mathematical models of the suspension systems.

2.3 SCHEMATIC CONFIGURATIONS OF PASSIVE SEAT SUSPENSIONS

A horizontal isolator that can provide vibration isolation in the longitudinal and lateral modes is configured as shown in Figure 2.9. The isolator consists of a sprung platform supported on a set of linear bearings, and a shock absorber to provide the necessary dissipation of energy. Bounce suspension seat can be mounted on the sprung platform to form a suspension system capable of isolating the driver along three translational coordinates. A four degrees of freedom translational seat suspension is formulated, assuming transverse stiffness of the cushion to be very high.

Terrain induced roll, and pitch vibrations are attenuated by a rotational isolator, which consists of two gimbal mounted, concentric frames as shown in Figure 2.10. The two frames are separated by a torsion shaft, and a torsional damper. The outer frame is supported by a spring and shock absorber at one of the ends, and the two rear ends of the outer frame may have rigid or flexible supports. Bounce suspension seat may also be mounted on to the inner frame to form a rotational seat suspension capable of attenuating bounce, roll, and pitch vibrations. The horizontal isolators can be inserted between the bounce suspension and gimbal supported frames to formulate multimode seat isolation system. However, a multimode seat suspension would lead to higher location of the driver, thus requires modifications in the cab design. In the following section, separate mathematical models are developed for translational and rotational

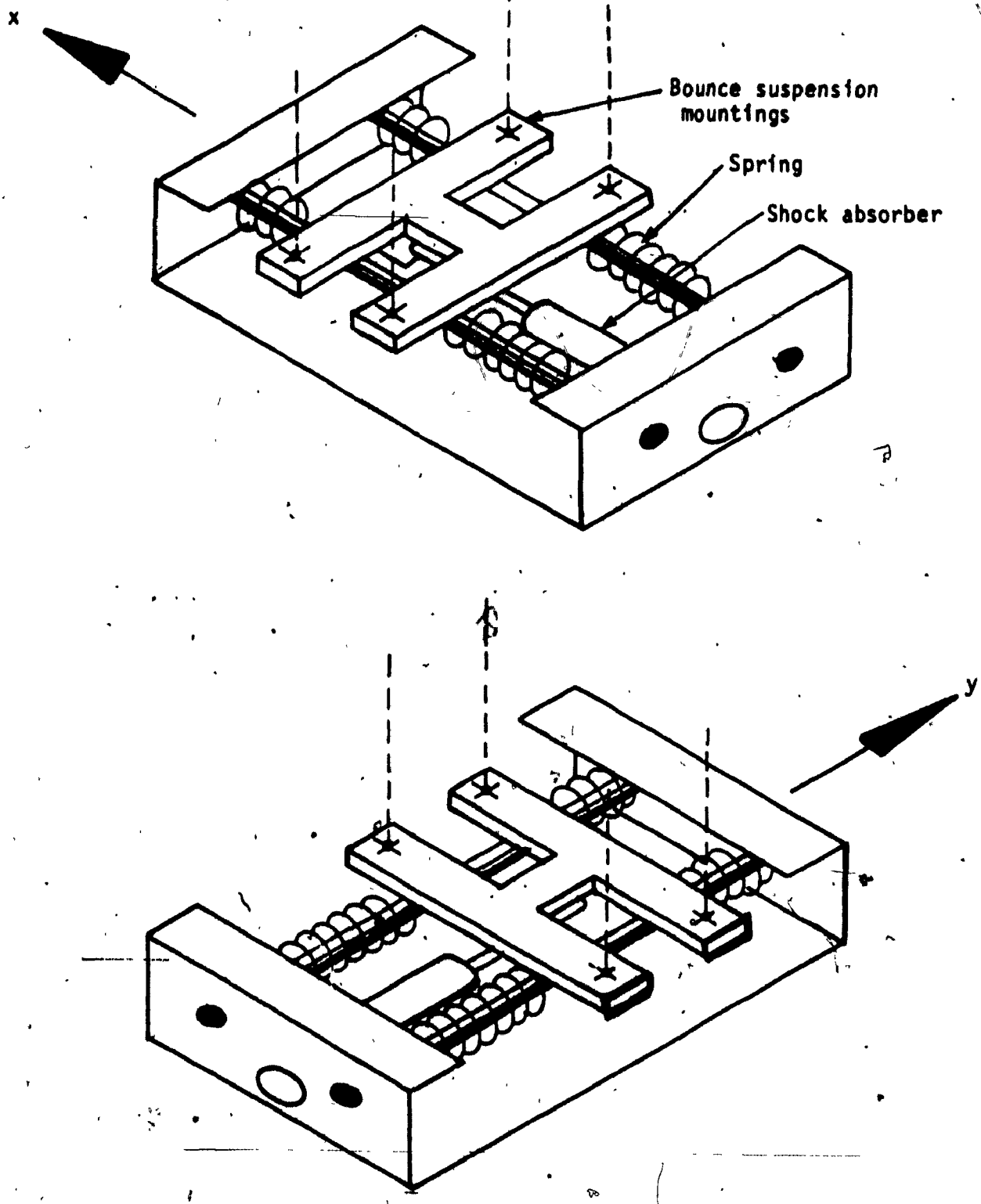

FIGURE 2.9 : Schematic configurations of longitudinal and lateral seat isolators.

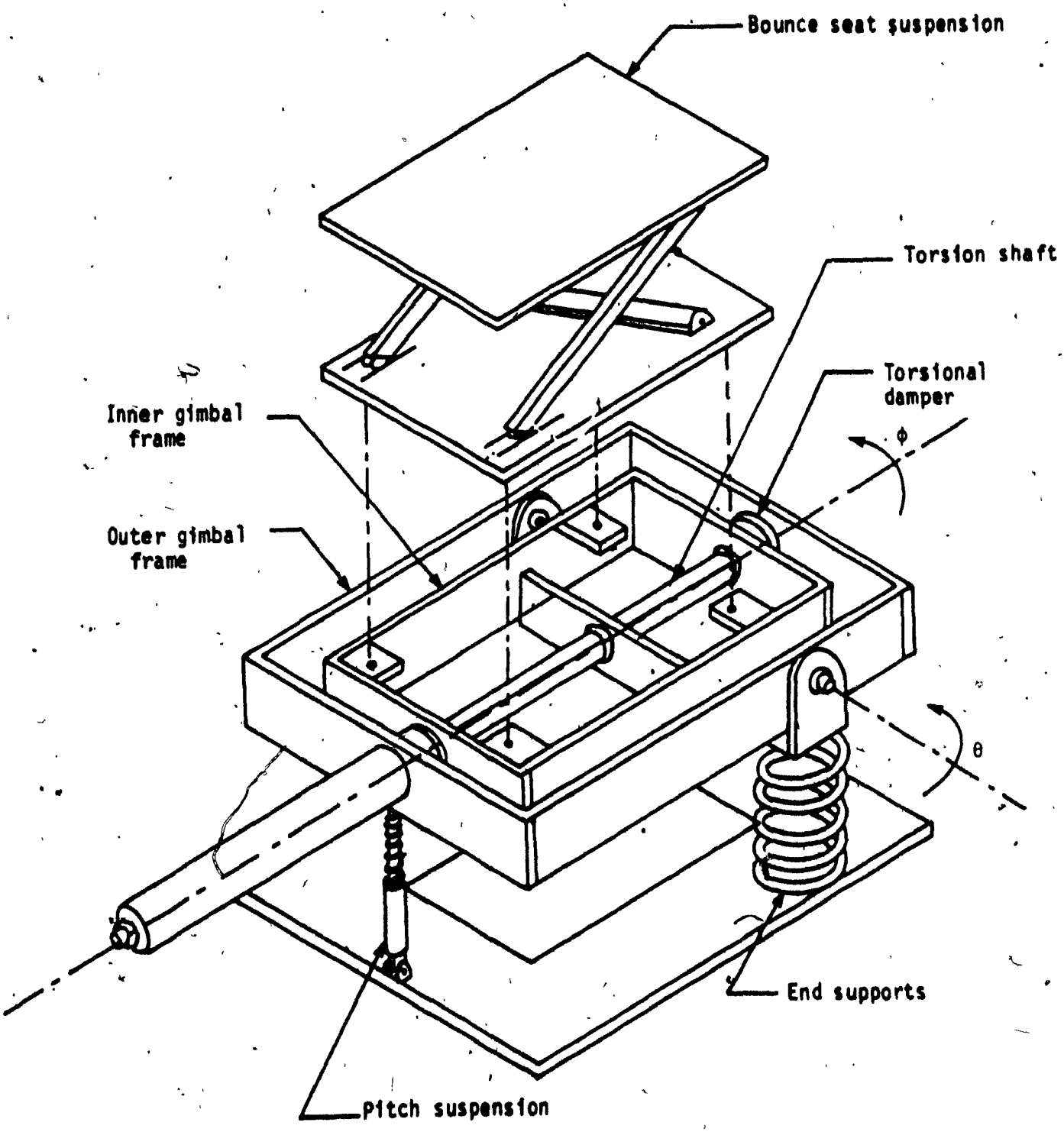

FIGURE 2.10: Schematic conftguration of the rotational seat isolator.

seat isolation systems.

2.4 DEVELOPMENT OF MATHEMATICAL MODELS FOR PASSIVE SEAT SUSPENSION

Mathematical models for the configured seat suspensions are formulated incorporating non-linearities arising from coulomb friction, orifice damping, and elastic limit stops. Mathematical models are developed for translational and rotational seat suspensions. A translational seat suspension is a synthesis of bounce, longitudinal and lateral isolators, and the rotational model incorporates bounce, roll, and pitch isolators. The main assumptions implied in the modeling process may be stated in the following manner:

(i) Transverse stiffness due to cushion is assumed to be very high, thus, a four degrees of freedom model may be formulated to represent the translational seat suspension. The equations of motion developed along three translational coordinates are uncoupled in nature, and may be treated independently.

(ii) The human body is represented by a rigid mass for the sake of simplicity. This assumption is attributed to the fact that the impedance, and transmissibility characteristics of seated human body correspond to that of a rigid mass in extremely low frequencies (up to 4.5Hz) [23]. Since tractor vibrations predominate in the frequency range 1 to 5Hz, a rigid body representation of seated operator is feasible in this frequency range. However, the human body may be represented by a multi degree of freedom simulator to evaluate human body response beyond 4.5Hz [25, 26, 27].

(iii) Operator's mass is assumed to be 5/7 of the total human body mass [21, 22].

(iv) The bounce stiffness due to cushion is assumed to be linear within operating limits.

(v) The shock absorber is represented by velocity squared damping while neglecting leakage flows and seal friction.

(vi) Motions along the generalized coordinates are assumed to be small relative to overall dimensions of the suspension.

(vii) The operator mass together with bounce suspension mass and frames experience rigid body rotation, when subject to pitching motion. The operator and bounce suspension mass moves rigidly with inner frame alone under roll motion.

(viii) Supports to the frames are located in equidistant manner such that a decoupled roll mode is obtained.

(ix) The excitations are assumed to be acting at the C.G. location of the seat.

2.4.1 TRANSLATIONAL SEAT SUSPENSION MODEL

The mathematical models and associated equations of motion along three translational coordinates are formulated subject to the assumptions, described in previous subsections. Translational seat suspension is represented by three independent models for the bounce, longitudinal and lateral planes as shown in Figures 2.11, 2.12 and 2.13. The bounce suspension seat is represented by a two degrees of freedom model, incorporating human body mass, cushion stiffness, suspension mass, suspension stiffness, coulomb friction, velocity squared damping, and elastic limit stops. The model representation of bounce seat suspension is shown in Figure 2.11. The parameters for various suspension elements are determined from static and dynamic characteristics obtained in the laboratory. Appendix I lists the characteristics of Bostrom seat suspension followed by the experimental verification, of the mathematical model.

Mathematical models in lateral and longitudinal planes are developed

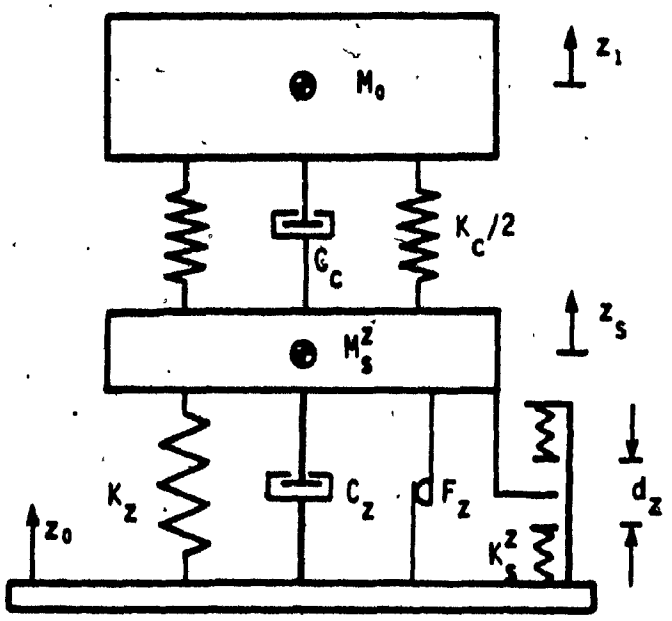

FIGURE 2.11: Model representation of bounce seat suspension.

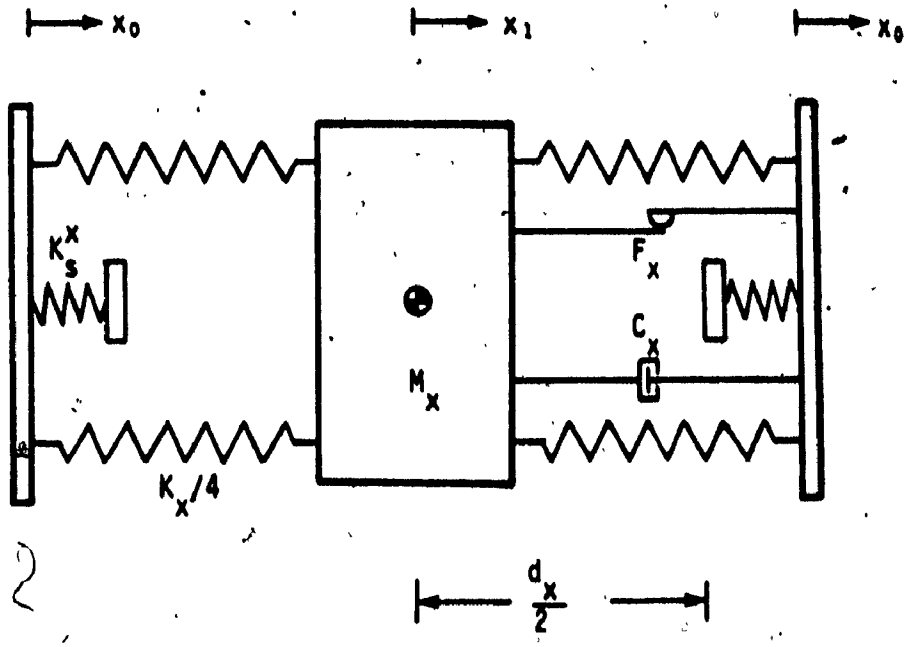

FIGURE 2.12: Model representation of bounce and longitudinal seat suspension, in the longitudinal plane.

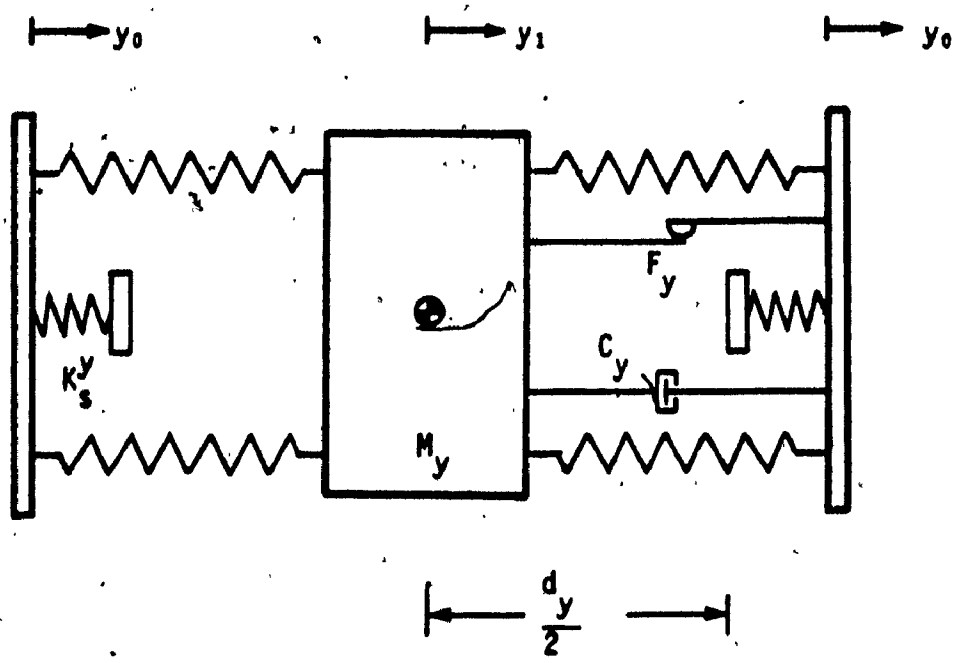

FIGURE 2.13: Model representation of translational seat suspension in the lateral plane

in a similar manner and corresponding uncoupled equations of motion are formulated.

EQUATIONS OF MOTION

Bounce Motion:

$$M_o \ddot{z}_1 + K_c(z_1 - z_s) + C_c(\dot{z}_1 - \dot{z}_s) = 0 \qquad (2.1)$$

$$M_s^z \ddot{z}_s - C_c(\dot{z}_1 - \dot{z}_s) - K_c(z_1 - z_s) + K_z(z_s - z_0) + F_c^z + F_d^z + F_s^z = 0 \qquad (2.2)$$

Longitudinal motion:

$$M_x \ddot{x}_1 + K_x(x_1 - x_0) + F_c^x + F_d^x + F_s^x = 0 \qquad (2.3)$$

Lateral motion:

$$M_y \ddot{y}_1 + K_y(y_1 - y_0) + F_c^y + F_d^y + F_s^y = 0 \qquad (2.4)$$

$$\left.\begin{aligned} M_x &= M_o + M_s^z \\ M_y &= M_o + M_s^z + M_s^x \end{aligned}\right\} \qquad (2.5)$$

where,

M_o = Mass of the operator (kg)

M_s^z, M_s^x = mass due to bounce and longitudinal isolators, respectively (kg).

K_c = Constant stiffness coefficient due to cushion (N/m)

C_c = Viscous damping coefficient due to cushion (N.s/m)

K_x, K_y, K_z = Constant stiffness coefficients of the longitudinal, lateral, and bounce seat isolators, respectively (N/m).

F_c^x, F_c^y, F_c^z = Suspension forces due to coulomb friction in the longitudinal, lateral and bounce modes, respectively (N).

F_d^x, F_d^y, F_d^z = Suspension forces arising from shock absorbers in longitudinal, lateral and bounce planes, respectively (N).

F_s^x, F_s^y, F_s^z = Suspension forces due to elastic limit stops in the longitudinal, lateral, and bounce planes, respectively (N).

x_1, y_1, z_1 = Generalized coordinates characterizing displacements of the operator mass in longitudinal, lateral, and bounce planes, respectively (m).

z_s = Displacement coordinate of bounce suspension mass (m).

x_0, y_0, z_0 = Displacement of cab floor in longitudinal, lateral, and bounce planes, respectively (m).

$(\dot{\ }), (\ddot{\ })$ = First and second order time derivatives of position coordinates characterizing velocities and accelerations.

The suspension forces due to coulomb friction, shock absorber, and elastic limit stops in the three translational planes are given in the following manner.

Coulomb friction:

$$\left.\begin{aligned} F_C^x &= F_x \text{ sgn } (\dot{x}_1 - \dot{x}_0) \\ F_C^y &= F_y \text{ sgn } (\dot{y}_1 - \dot{y}_0) \\ F_C^z &= F_z \text{ sgn } (\dot{z}_s - \dot{z}_0) \end{aligned}\right\} \qquad (2.6)$$

where,

$$\text{sgn } (\dot{\ }) = \begin{cases} -1 & \text{for } (\dot{\ }) < 0 \\ +1 & \text{for } (\dot{\ }) > 0 \end{cases} \qquad (2.7)$$

and

F_x, F_y, F_z = Magnitude of friction force in longitudinal, lateral, and bounce modes, respectively (N).

Shock Absorber:

$$F_d^x = C_x |\dot{x}_1 - \dot{x}_0|^2 \ \text{sgn}(\dot{x}_1 - \dot{x}_0)$$

$$F_d^y = C_y |\dot{y}_1 - \dot{y}_0|^2 \ \text{sgn}(\dot{y}_1 - \dot{y}_0) \qquad (2.8)$$

$$F_d^z = C_z |\dot{z}_s - \dot{z}_0|^2 \ \text{sgn}(\dot{z}_s - \dot{z}_0)$$

where,

C_x, C_y, C_z = Coefficients of velocity squared damping arising from shock absorbers in longitudinal, lateral, and bounce planes, respectively (Ns^2/m^2).

Elastic Limit Stops:

$$\left.\begin{aligned} F_s^x &= K_s^x \cdot S^x \cdot \left[x_1 - x_0 - \frac{d_x}{2} \text{sgn}(x_1 - x_0)\right] \\ F_s^y &= K_s^y \cdot S^y \cdot \left[y_1 - y_0 - \frac{d_y}{2} \text{sgn}(y_1 - y_0)\right] \\ F_s^z &= K_s^z \cdot S^z \cdot \left[z_s - z_0 - \frac{d_z}{2} \text{sgn}(z_s - z_0)\right] \end{aligned}\right\} \qquad (2.9)$$

where,

K_s^x, K_s^y, K_s^z = Stiffness coefficients due to elastic stops in x, y, and z planes, respectively (N/m).

d_x, d_y, d_z = Total suspension travel within elastic stops in x, y, and z planes, respectively (m).

and

S^x, S^y, S^z = Non-linear functions describing characteristics of elastic limit stops given by:

$$S^x = \begin{cases} 0 & \text{for } |x_1 - x_0| < \frac{d_x}{2} \\ 1 & \text{for } |x_1 - x_0| > \frac{d_x}{2} \end{cases}$$

$$S^y = \begin{cases} 0 & \text{for } |y_1 - y_0| < \frac{d_y}{2} \\ 1 & \text{for } |y_1 - y_0| > \frac{d_y}{2} \end{cases} \qquad (2.10)$$

$$S^z = \begin{cases} 0 & \text{for } |z_s - z_0| < \frac{d_z}{2} \\ 1 & \text{for } |z_s - z_0| > \frac{d_z}{2} \end{cases}$$

Subscripts ^{1} and ^{0} refer to motion of the mass constrained within stops and the base motion.

2.4.2 ROTATIONAL SEAT SUSPENSION MODEL

The rotational seat isolator consists of pitch and roll seat isolators in addition to a bounce seat suspension. The mathematical models in the longitudinal-bounce, lateral-bounce, and longitudinal-lateral planes are presented in Figure 2.14. The nomenclature and geometric parameters of the model are presented in Tables 2.2 and 2.3. The differential equations of motion for the rotational seat suspension are formulated, while neglecting elastic limit stops.

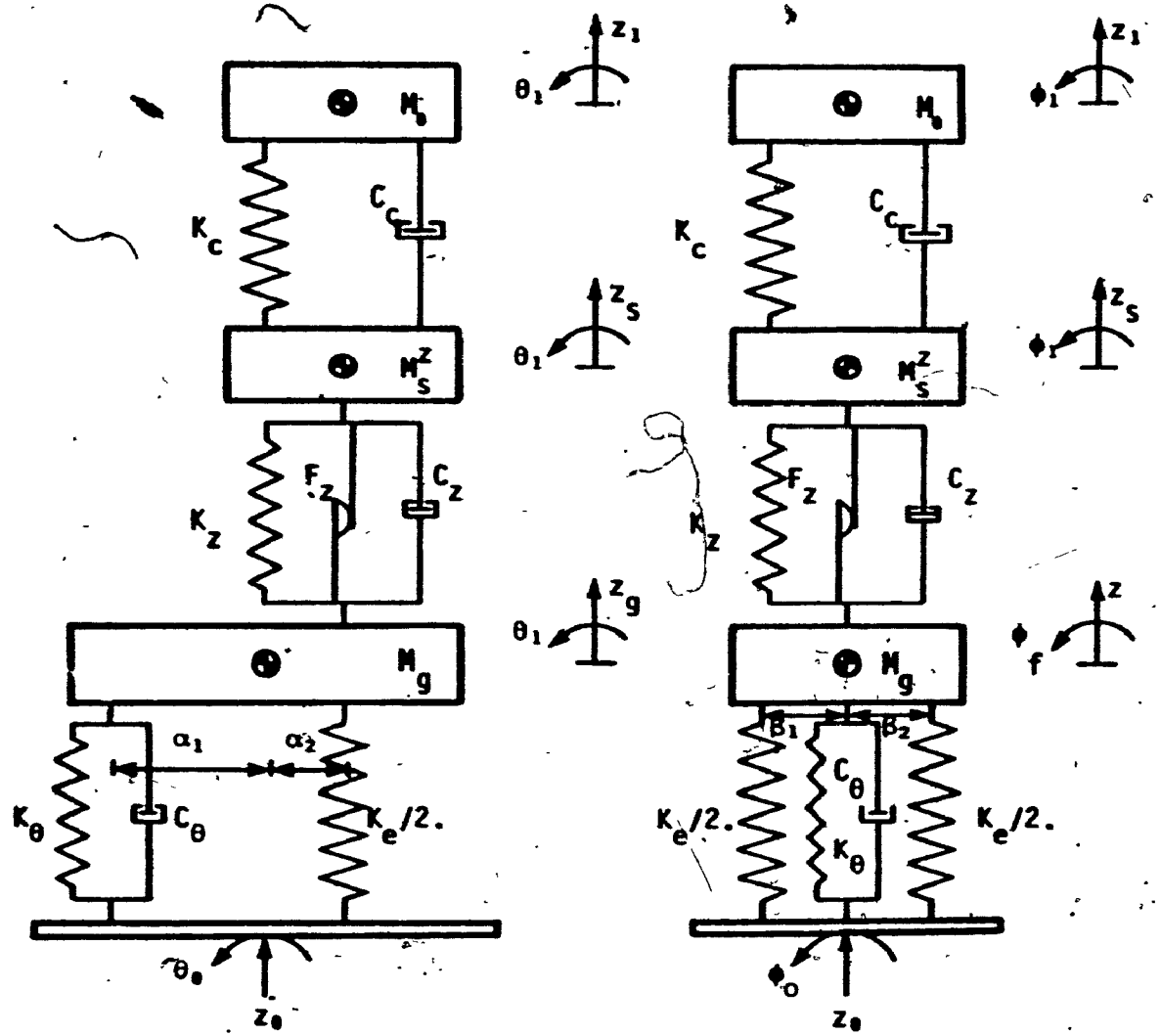

(a) Longitudinal-bounce plane

(b) Lateral-bounce plane

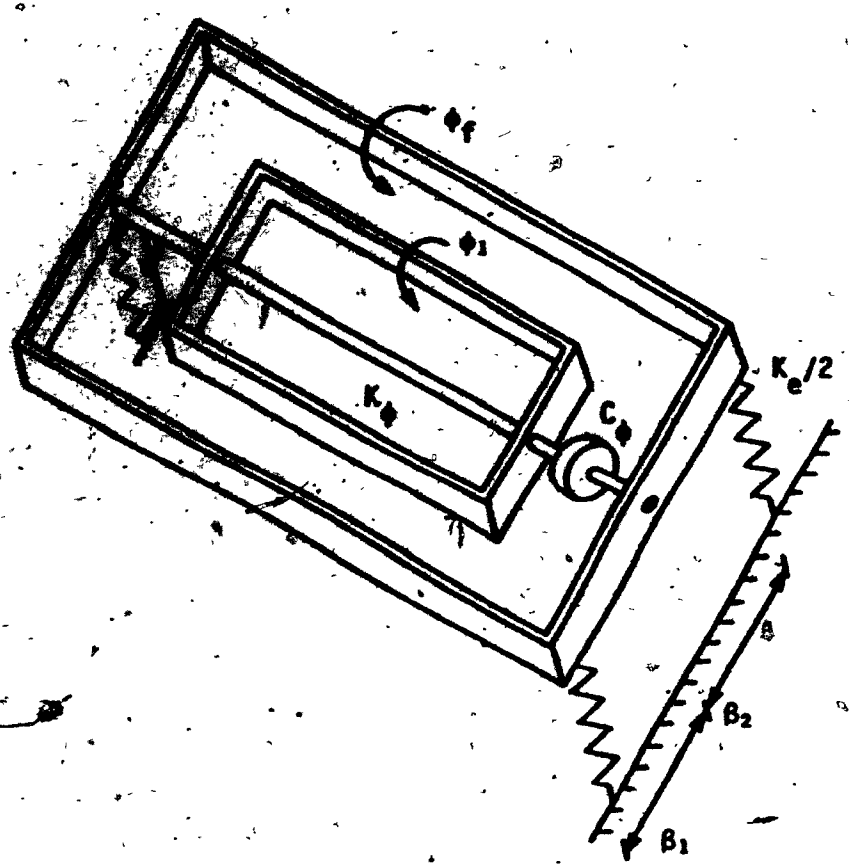

(c) Longitudinal-lateral plane

FIGURE 2.14: Model representation of rotational seat isolator in longitudinal bounce, lateral-bounce, and longitudinal-lateral planes.

TABLE 2.2

PHYSICAL PARAMETERS OF THE

ROTATIONAL SEAT ISOLATOR MODEL

Symbol	Description	Parameter value
M_o	Operator mass	85 kg
M_s^z	Bounce suspension mass	4.5 kg
$J_{\theta\theta}$	Pitch moment of inertia of the operator	9.36 kg.m^2
$J_{\phi\phi}$	Roll moment of inertia of the operator	6.41 kg.m^2
$J_{\theta\theta}^z$, $J_{\phi\phi}^z$	Pitch and roll moment of inertia of the suspension mass	0.12, 0.08 kg.m^2
$J_{\theta\theta}^o$, $J_{\theta\theta}^I$	Pitch moment of inertia of outer and inner frames	0.06, 0.04 kg.m^2
$J_{\phi\phi}^o$, $J_{\phi\phi}^I$	Roll moment of inertia of outer and inner frames	.04, .025 kg.m^2
α_1	Location of pitching suspension from cg of the frames	0.15 m
α_2	Location of end supports with reference to cg of the frames	0.09 m
β	Lateral location of end supports	0.10 m
h_o, h_s	Operator and bounce suspension height from the cg of frames	0.335, 0.15

TABLE 2,3

NOMENCLATURE TO DESCRIBE MOTION OF THE ROTATIONAL SEAT SUSPENSION MODEL

MODE	SYMBOL	DESCRIPTION OF MOTION OF.
Bounce	z_1	Operator
	z_s	Bounce suspension mass
	z_g	Gimbal mounted frames
	z_o	Cab
Pitch	θ_1	Operator and gimbal mounted frames
	θ_0	Cab
Roll	ϕ_1	Operator and bounce suspension
	ϕ_f	Outer frame
	ϕ_1	Inner frame
	ϕ_0	Cab

Bounce Motion:

$$M_0\ddot{z}_1 + K_c(z_1-z_s) + C_c(\dot{z}_1-\dot{z}_s) = 0 \tag{2.11}$$

$$M_s^z\ddot{z}_s - C_c(\dot{z}_1-\dot{z}_s) - K_c(z_1-z_s) + K_z(z_s-z_g-\alpha_2\theta_1) + F_c^z + F_d^z = 0 \tag{2.12}$$

$$M_g\ddot{z}_g - K_z(z_s-z_g-\alpha_2\theta_1) - F_c^z - F_d^z + K_\theta[z_g-z_0-\alpha_1(\theta_1-\theta_0)]$$

$$+K_e[z_g-z_0+\alpha_2(\theta_1-\theta_0)] + F_d^\theta = 0 \tag{2.13}$$

Pitch Motion:

$$J_\theta\ddot{\theta}_1 + \alpha_2 K_z(z_s-z_g-\alpha_2\theta_1) - \alpha_2(F_c^z+F_d^z)$$

$$-\alpha_1 K_\theta[z_g-z_0-\alpha_1(\theta_1-\theta_0)] + \alpha_2 K_e[z_g-z_0+\alpha_2(\theta_1-\theta_0)]$$

$$-\alpha_1 F_d^\theta = 0 \tag{2.14}$$

where,

$$J_\theta = J_{\theta\theta} + J_{\theta\theta}^0 + J_{\theta\theta}^I + J_{\theta\theta}^z + M_0h_0^2 + m_s^zh_s^2 \tag{2.15}$$

Roll Motion:

$$J_\phi\ddot{\phi}_1 + K_\phi(\phi_1-\phi_f) + F_d^\phi = 0 \tag{2.16}$$

$$J_f\ddot{\phi}_f - K_\phi(\phi_1-\phi_f) - F_d^\phi + K_e\beta^2(\phi_f-\phi_0) = 0 \tag{2.17}$$

where,

$$J_\phi = J_{\phi\phi} + J_{\phi\phi}^I + J_{\phi\phi}^z + M_0h_0^2 + M_s^zh_s^2 \tag{2.18}$$

$$J_f = J_{\phi\phi}^0 \tag{2.19}$$

M_g = Mass of the gimbal mounted frames (kg)

K_c = Constant cushion stiffness coefficient (N/m)

K_z = Constant stiffness coefficient due to bounce suspension (N/m)

K_θ, K_e = Constant stiffness coefficient due to pitching suspension and end supports (N/m)

K_ϕ = Torsional stiffness coefficient due to torsion shaft (N·m/rad)

F_d^θ, F_d^ϕ = Suspension forces due to pitching and roll dampers, given by:

$$F_d^\theta = C_\theta |\dot{z}_g - \dot{z}_0 - \alpha_1(\dot{\theta}_1 - \dot{\theta}_0)|^2 \ \mathrm{sgn}[\dot{z}_g - \dot{z}_0 - \alpha_1(\dot{\theta}_1 - \dot{\theta}_0)]$$
$$F_d^\phi = C_\phi |\dot{\phi}_1 - \dot{\phi}_f|^2 \ \mathrm{sgn}(\dot{\phi}_1 - \dot{\phi}_f) \qquad (2.20)$$

C_θ, C_ϕ = Coefficients of velocity squared damping pitch and roll modes, respectively $(\frac{Ns^2}{m^2}, \frac{Nms^2}{rad^2})$

F_d^z = Suspension force due to bounce suspension shock absorber, given by:

$$F_d^z = C_z |\dot{z}_s - \dot{z}_g - \alpha_2 \dot{\theta}_1|^2 \mathrm{sgn}(\dot{z}_s - \dot{z}_g - \alpha_2 \dot{\theta}_1) \qquad (2.21)$$

By locating the end supports in a equi-distant manner, completely decoupled equations (2.16) and (2.17) describing roll motion of the isolator are obtained.

2.5 FORMULATION OF CAB SUSPENSION MODELS

The investigation is initiated with the selection of geometric configuration of a cab that would be compatible with present cab designs and mounting locations. Figure 2.15 presents the geometric configuration of an agricultural tractor cab suspended on four corner mounts. Longitudinal-bounce and lateral-bounce plane models are presented in Figure 2.16. The geometric parameters of chosen cab models are presented in Table 2.4.

TABLE 2.4

PHYSICAL PARAMETERS OF A REPRESENTATIVE CAB GEOMETRY

Symbol	Description	Parameter value
M_c	Cab mass	681.82 kg.
M_o	Seat mass	85 kg.
$I^c_{\phi\phi}$	Roll moment of inertia about cab cg.	306.82 kg·m^2
$I^c_{\theta\theta}$	Pitch moment of inertia about cab cg.	340.77 kg m^2
$I^c_{\phi\theta}$	Product of inertia	0.
h_2	Vertical location of cab cg.	0.762 m
a_1, a_2	Longitudinal location of cab mounts	0.457 m
b_1, b_2	Lateral location of cab mounts	0.457 m

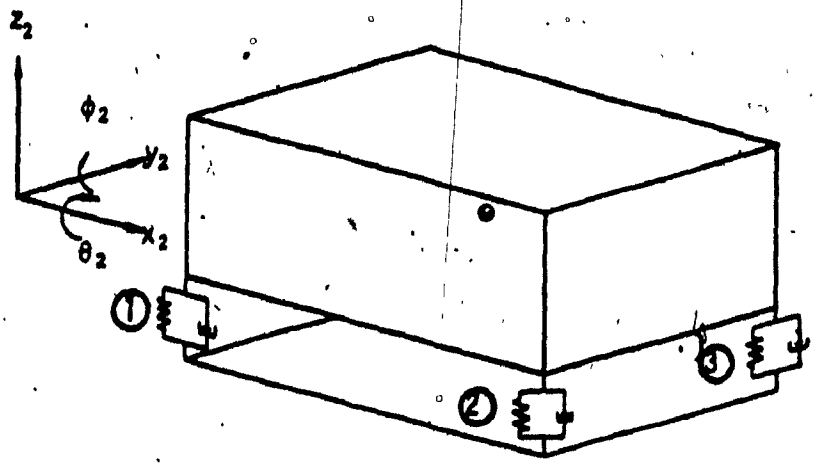

FIGURE 2.15: Schematic configuration of a tractor cab mounted on four corner mounts.

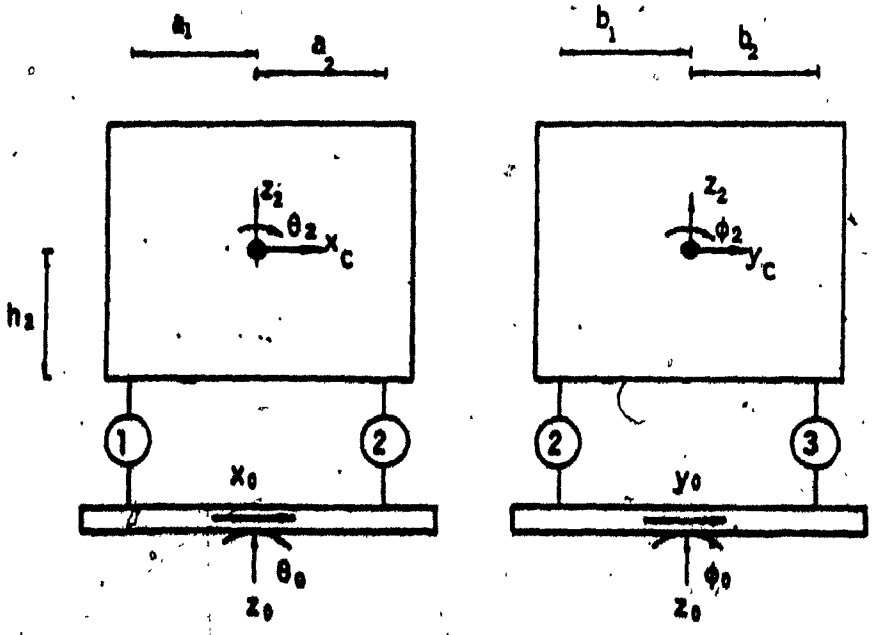

FIGURE 2.16: Plane model representation of the corner mounted cab.

2.6 DEVELOPMENT OF MATHEMATICAL MODELS

Multi-degrees of freedom models are developed for the following combinations of seat and cab suspensions.

(i) Cab suspension with rigidly mounted seat.

(ii) Cab suspension with bounce suspension seat.

(iii) Cab suspension with bounce and lateral seat isolators.

(iv) Cab suspension with bounce and roll seat isolators.

The cab suspension includes four corner mounted passive suspension units, and two suspension units implemented parallel to cab base plate to provide isolation in longitudinal and lateral modes. The assumptions implied in the modeling process can be described in the following manner.

(i) The dynamics of cab and cab suspension only, is considered in the modeling process. Alternatively, the cab suspension dynamics may be incorporated to a larger vehicle dynamic model. However, for this study, the goals can be accomplished without tackling the problems of working with a complete vehicle dynamic model. Thus, the mathematical models assume that the ratio of cab mass to the vehicle mass is small.

(ii) All the suspension units are constrained to translate in the longitudinal, lateral, and vertical directions with small motions.

(iii) Each suspension unit is represented by a linear spring and a viscous damper.

2.6.1 CAB-SUSPENSION MODEL (5 DOF)

The cab suspension model incorporates four suspension units at four corner mount locations, and two suspension units mounted parallel to the cab floor along the longitudinal and lateral coordinates. The operator seat is mounted rigidly to the cab floor. The plane representation of five degrees of freedom mathematical model of the cab suspension is presented in Figure 2.17. The generalized coordinates are chosen to be bounce motion of the cab, longitudinal and, lateral motion of cab floor, roll and pitch motion of the cab.

Although the cab suspension model consists of linear elements, many fundamental effects of vehicle-terrain dynamic interactions may be realistically studied. Considerable insight into the cab suspension characteristics may be gained, and motions at the driver's location may be studied in details. The linear analysis allows computations of results in the frequency domain, using frequency response function, which provides the designer with a clear and concise description of the system behaviour.

2.6.2 CAB AND SEAT SUSPENSION MODELS

Although passive suspension seats provide significant improvement in tractor ride, the levels of vibration in the bounce, and lateral modes require further vibration attenuation in order to meet ISO specified *fatigue decreased proficiency* limits. The passive suspension seats in these modes may be implemented to a suspended cab to accomplish a satisfactory ride. A number of cab and seat suspension models are formulated to investigate the ride performance characteristics.

Model I: CAB SUSPENSION WITH BOUNCE SUSPENSION SEAT

A single degree of freedom bounce suspension seat is added to the five degrees of freedom sprung cab. Figure 2.18 presents a model repre-

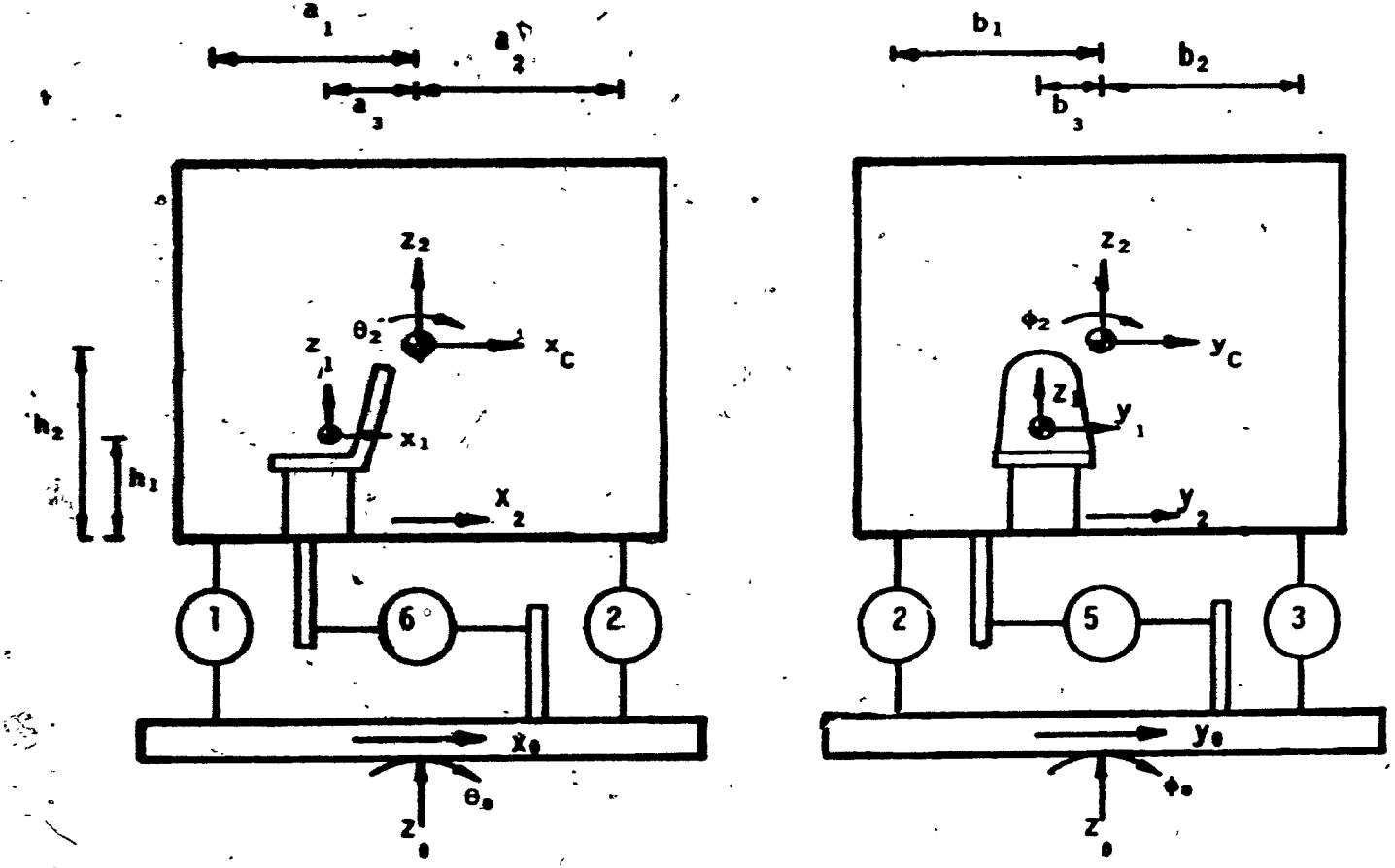

(a) Longitudinal - bounce plane (b) Lateral - bounce plane

① ② ③ ④ corner mounted suspension units

⑤ - Lateral suspension

⑥ - Longitudinal suspension

FIGURE 2.17: Plane model representation of 5 DOF cab suspension model.

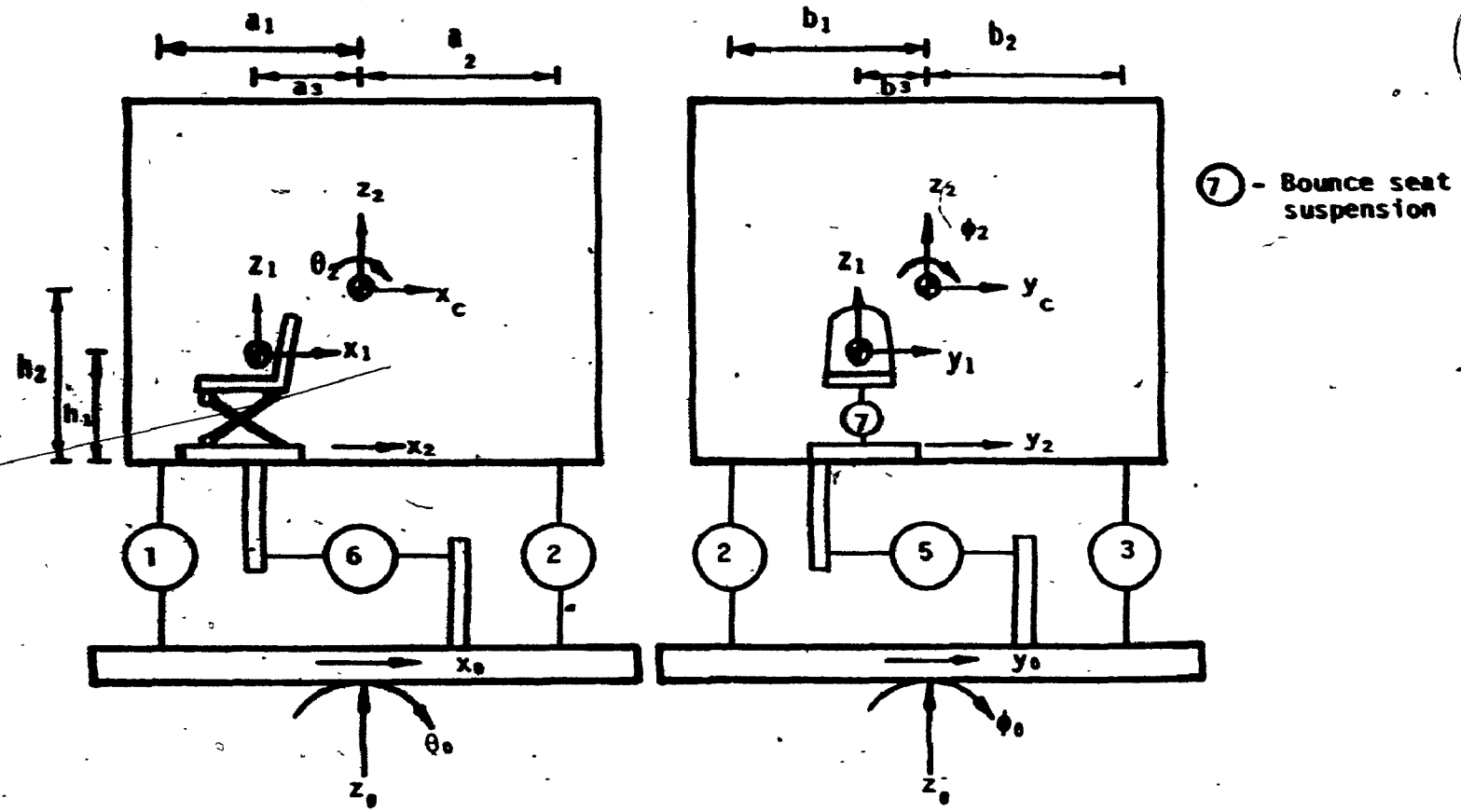

(a) Longitudinal - bounce plane (b) Lateral - bounce plane

FIGURE 2.18: Plane model representation of cab and bounce seat suspension (Model I).

sentation of cab and bounce seat suspension. The model does not include the seat cushion characteristics.

Model II: CAB SUSPENSION WITH BOUNCE AND LATERAL SEAT ISOLATORS

Ride performance characteristics of bounce and lateral seat suspensions with a sprung cab are investigated through the seven degrees of freedom model shown in Figure 2.19. The model incorporates bounce and lateral suspensions at the seat.

Model III: CAB SUSPENSION WITH BOUNCE AND ROLL SEAT SUSPENSIONS

A seven degrees of freedom model incorporating bounce and roll seat suspensions in addition to the cab suspension is formulated. Plane representation of the formulated model are presented in Figure 2.20.

2.6.3 EQUATIONS OF MOTION FOR PASSIVE CAB SUSPENSION MODELS

Assuming small perturbations relative to the overall dimensions of the cab, the kinetic, potential, and dissipative energy functions are developed from physical and geometric characteristics of each model. The energy functions are given by the following expressions [61].

Kinetic energy function;

$$T = \frac{1}{2} \{\dot{\phi}\}^T [M] \{\dot{\phi}\} \qquad (2.22)$$

Potential energy function;

$$V = \frac{1}{2} \{\phi\}^T [K] \{\phi\} \qquad (2.23)$$

Dissipation energy function;

$$D = \frac{1}{2} \{\dot{\phi}\}^T [C] \{\dot{\phi}\} \qquad (2.24)$$

where [M] is the mass matrix or equally well a combination of masses and moments of inertia.

[K] is the stiffness matrix

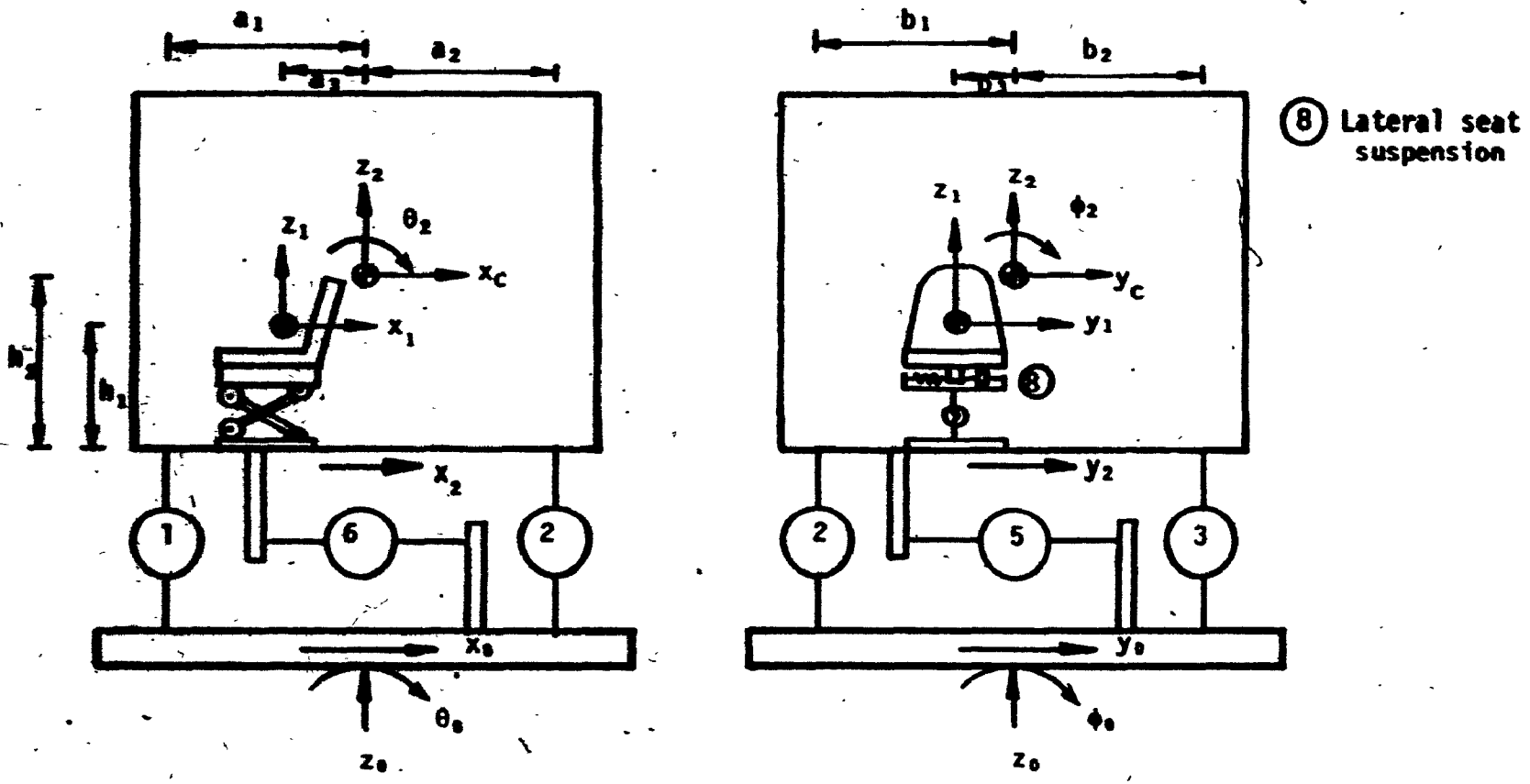

(a) Longitudinal - bounce plane (b) Lateral - bounce plane

FIGURE 2.19: Plane model representation of Bounce and lateral seat suspension with a sprung cab (model II)

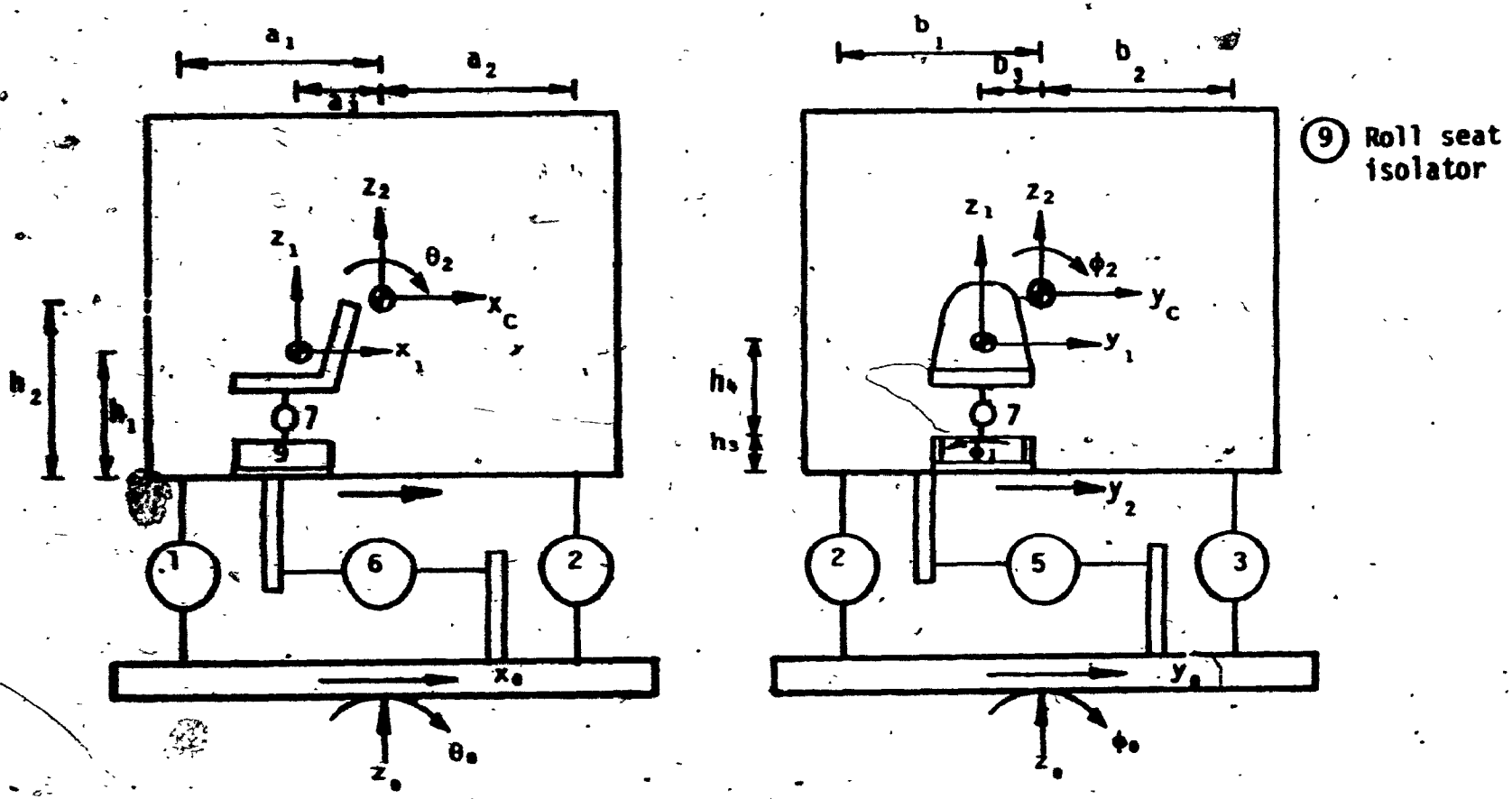

(a) Longitudinal - bounce plane (b) Lateral - bounce plane

FIGURE 2.20: Plane model representation of bounce and roll seat suspensions with a sprung cab (Model III).

[C] is the linear or viscous damping matrix

{ϕ} is the set of independent generalized coordinates which completely specify the configuration of the system and is measured from the equilibrium condition. Table 2.5 lists the generalized coordinates chosen for the cab-suspension model.

{$\dot{\phi}$} is the time derivative of generalized coordinate vector

Using the Lagrange's energy method,

$$\frac{d}{dt}\left(\frac{\partial T}{\partial \dot{\phi}_i}\right) + \frac{\partial D}{\partial \dot{\phi}_i} + \left(\frac{\partial V}{\partial \phi_i}\right) = 0 \qquad (2.25)$$

set of simultaneous, non-homogeneous, second order differential equations with constant coefficients is obtained. The differential equations of motion are presented in the following form.

$$[M]\{\ddot{\phi}\} + [C]\{\dot{\phi}\} + [K]\{\phi\} = [C_f]\{\dot{\phi}_0\} + [K_f]\{\phi_0\} \qquad (2.26)$$

where,

$[C_f]$ and $[K_f]$ are the forced damping and stiffness matrices, respectively.

$\{\phi_0\}$, $\{\dot{\phi}_0\}$ are the column vectors of excitation displacements, and velocities, respectively.

A complete description of matrices representing equations of motion of cab, and cab-seat suspension models is presented in Appendix II.

TABLE 2.5

NOMENCLATURE DESCRIBING CAB MOTION

MODE	DESCRIPTION OF MOTION AT	SYMBOL
Bounce	Seat	z_1
	Cab	z_2
	Input	z_0
Longitudinal	Seat	x_1
	Cab floor	x_2
	Cab cg.	x_c
	Input	x_0
Lateral	Seat	y_1
	Cab floor	y_2
	Cab cg.	y_c
	Input	y_0
Roll	Seat	ϕ_1
	Cab	ϕ_2
	Input	ϕ_0
Pitch	Seat	θ_1
	Cab	θ_2
	Input	θ_0

2.7 SUMMARY

In this chapter, schematic configurations of passive seat suspensions and cab suspension are presented. Mathematical models of passive seat suspensions incorporating non-linearities arising from shock absorbers, coulomb friction, and elastic limit stops, and five degrees of freedom cab suspension are formulated. Suspension seats in the bounce, lateral and roll modes are added to the sprung cab and models are formulated to investigate their respective ride performance. The differential equations characterizing the motion of suspension models are developed. In the following chapter, terrain irregularities transmitted to the cab floor are discussed, which will form the input forcing function to the suspension models.

CHAPTER 3

REPRESENTATION OF INPUT EXCITATION FROM THE AGRICULTURAL TERRAINS

3.1 INTRODUCTION

The prediction of ride performance characteristics of suspension models require tractor vibration input data. The input excitation data must be representative of typical agricultural terrains and be concise to minimize computation costs. Linear suspension models require acceleration power spectral densities (PDS's) and cross spectral densities (CSD's). Real time displacements and velocities are needed to simulate non-linear suspension models.

Tractor vibration data on various types of agricultural terrains have been reported in the literature. The random data gathered during field measurements have been characterized by PSD's [43,55]. The consistency of the measured data has lead to a rather standardized terrain description. International Organization for Standardization has proposed approximate expressions describing bounce acceleration PSD required for tractor seat testing [18]. Matthews [43] constructed a test track at National Institute of Agricultural Engineers (NIAE), Silsoe, England to represent the agricultural terrains, based on measurement of various agricultural surfaces. The test track has been widely accepted as the representation of agricultural terrains.

In this chapter, the input acceleration PSD's established by ISO and Silsoe track data are presented. A comparison of the input acceleration PSD's with ISO specified *fatigue decreased proficiency* limits is presented to assess the ride of an unsprung vehicle.

3.2 ISO INPUT DATA

The agricultural tractors are classified in two classes based on vehicle load, tire pressure, and wheelbase as presented in Table 3.1. The power spectral density of vertical acceleration are computed at the point of seat attachment of the tractor during a run at a speed 12 ± 0.5 km/h. The spectral densities of acceleration are approximately expressed by the following equations.

Class 1: The power spectral density of the vertical acceleration ($\phi_z^{(1)}$) at the seat attachment point

$$\phi_z^{(1)} = \phi_{max}^{(1)} \exp\left[-\frac{(f-f_m)^2}{2B^2}\right] \qquad (3.1)$$

where the constants are

$$\phi_{max}^{(1)} = 6.0\ (m/s^2)^2/Hz$$

$$f_m = 3.25\ Hz$$

$$B = 0.33\ Hz$$

Class 2: The power spectral density of the vertical acceleration ($\phi_z^{(2)}$) at the seat attachment point

$$\phi_z^{(2)} = \phi_{max}^{(2)} \exp\left[-\frac{(f-f_m)^2}{2B^2}\right] \qquad (3.2)$$

where the constants are

$$\phi_{max}^{(2)} = 5.5\ (m/s^2)^2/Hz$$

$$f_m = 2.65\ Hz$$

$$B = 0.3\ Hz$$

Figure 3.1 and 3.2 present a comparison of equations (3.1) and (3.2) with the acceleration PSD equivalent of ISO specified rms acceleration

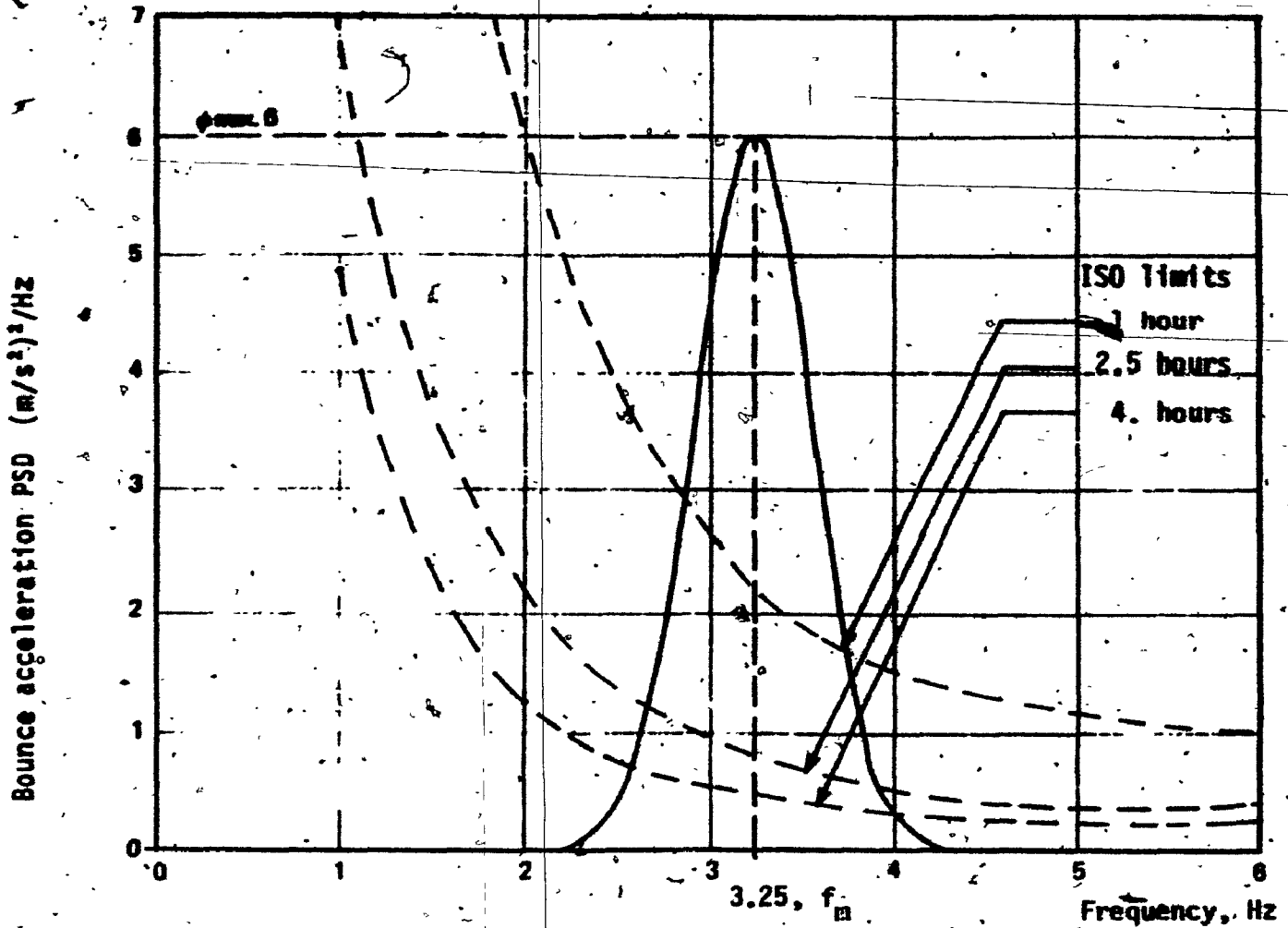

FIGURE 3.1: Approximate function for the bounce acceleration PSD at the seat attachment point of class 1 tractors [18].

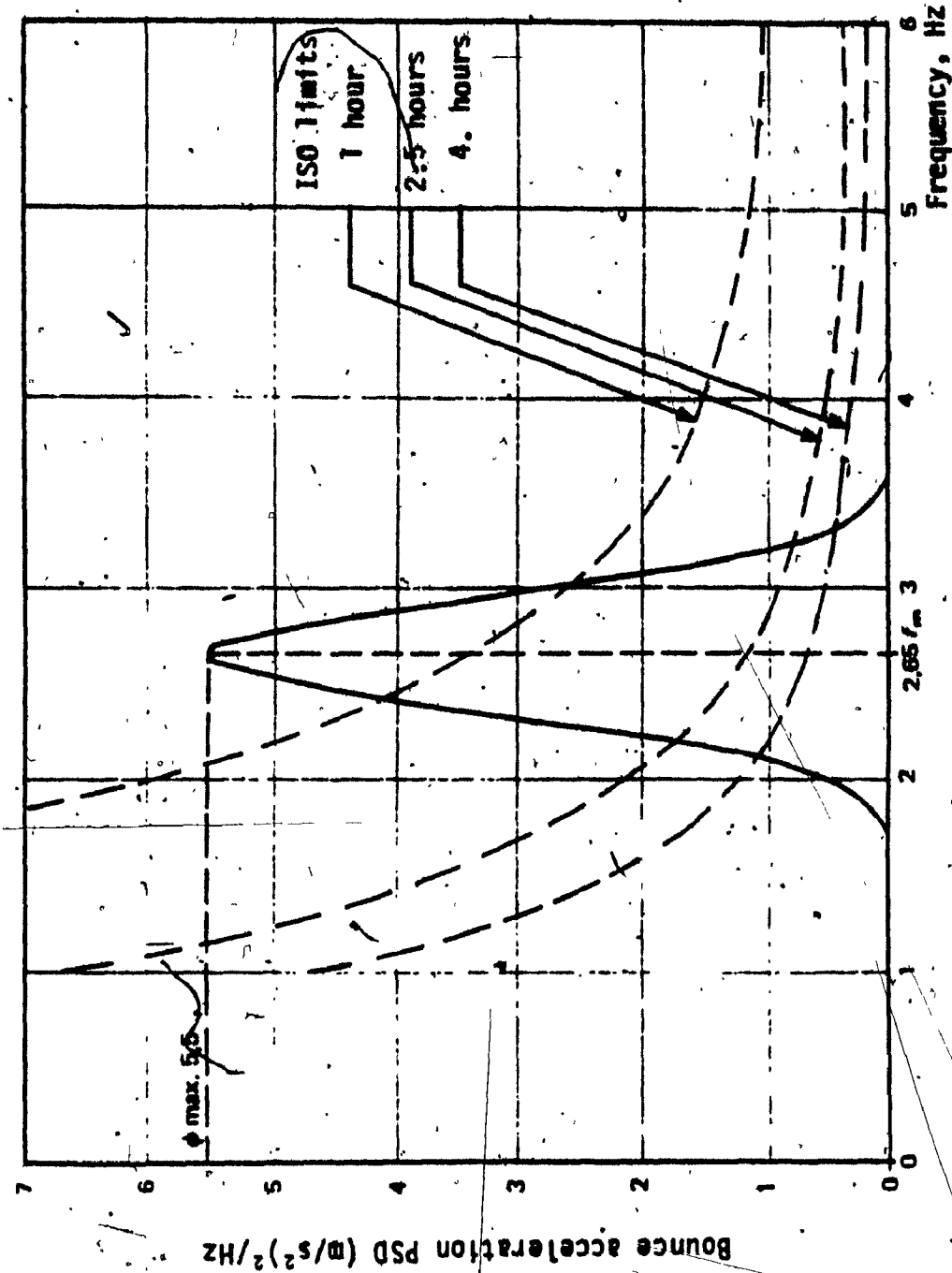

FIGURE 3.2: Approximate function for the bounce acceleration PSD at the seat attachment point of class 2 tractors [18].

fatigue decreased proficiency limits. Appendix III lists the procedure to generate equivalent acceleration PSD limits from the given rms acceleration limits. The ISO input data limits itself to the bounce excitation alone. Acceleration PSD's in bounce, longitudinal, lateral, pitch and roll have been described through measurements conducted at the Silsoe track.

TABLE 3.1

TECHNICAL DATA OF REFERENCE TRACTORS [62]

TECHNICAL DATA	CLASS 1	CLASS 2
Unladen mass, kg.	3040	4750
Front axle load, kg.	1300	1830
Rear axle load, kg.	1740	2920
Front tires	7.5-18	12.4/11-28
Rear tires	16.9/14-34	16.9/14-38
Front tire pressure, kPa.	200	150
Rear tire pressure, kPa.	110	130
Wheelbase, m	2.125	2.590

3.3 SILSOE TRACK DATA

The Silsoe track has been constructed at NIAE, Silsoe, England for standardization of vibration inputs to agricultural vehicles, based on measured agricultural terrain conditions. Matthews [43] consolidated terrain measured acceleration PSD's and constructed a 35m fixed track to represent the inputs from rough agricultural fields. The test track consists of wooden slats 0.076 x 0.762m of height ranging from 0 to 0.30m, fitted in the appropriate order on metal frames to produce the contours of left and right-hand wheel tracks over the surfaces. The Silsoe track

has been widely accepted as a standard for representation of agricultural terrains. An instrumentation package consisting of five accelerometers mounted on a T-bar, amplifiers, low pass filters, FM tape recorders, and a summing circuit has been developed at NIAE for measurement of tractor vibrations. The summing circuit enables one to determine bounce, lateral, longitudinal, roll and pitch accelerations from the five accelerometers mounted on the T-shaped bar.

The acceleration levels at the floor of a class 2 tractor's cab have been measured by Roley [55], using the above package. The acceleration power spectral densities are developed using fast Fourier transform algorithms. Figures 3.3 to 3.7 present PSD's of bounce, longitudinal, lateral, roll and pitch accelerations encountered at the centre of the cab floor. The measured acceleration PSD's are compared with the *fatigue decreased proficiency* acceleration PSD limits to assess the ride performance of the unsprung tractor. The cross correlation between the pair of tracks in which the left and right-hand wheels of the vehicle travel has been neglected.

In order to evaluate terrain induced vibration with reference to ISO *fatigue decreased proficiency* rms acceleration limits, the root mean square acceleration values filtered by the ISO frequency weighting curve are obtained. Figure 3.8 presents ISO frequency weighting curves for horizontal and bounce accelerations. The ISO frequency weighted rms accelerations are obtained in the following manner.

$$\bar{a}(\bar{f}) = WF(\bar{f}) \left[\int_{f_\ell}^{f_u} S_1(f)\,df \right]^{1/2} \qquad (3.3)$$

where

$\bar{a}(\bar{f})$ = ISO frequency weighted rms acceleration at the third octave band with center frequency $\bar{f}$.

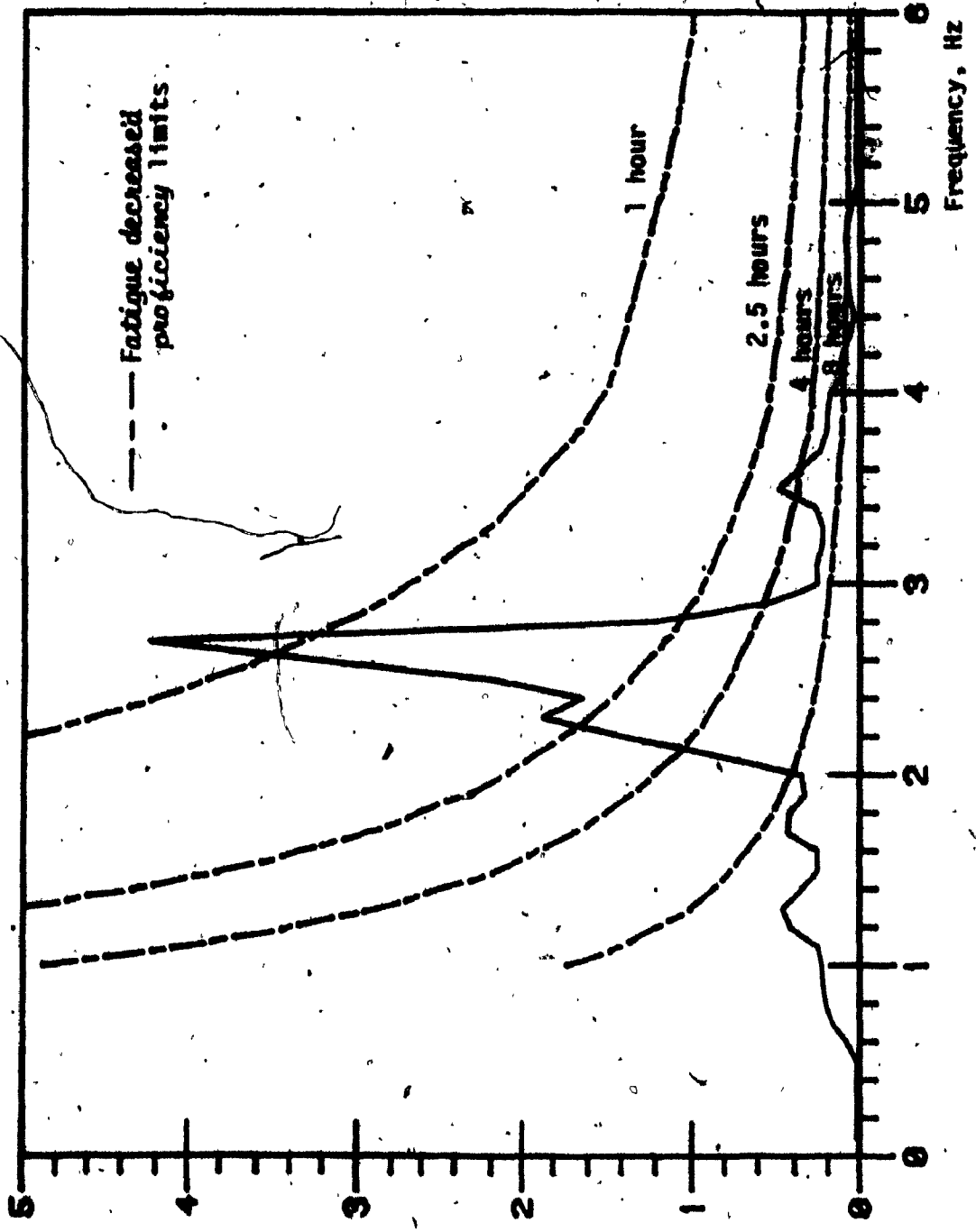

FIGURE 3.3: Bounce acceleration PSD measured at the cab floor [55].

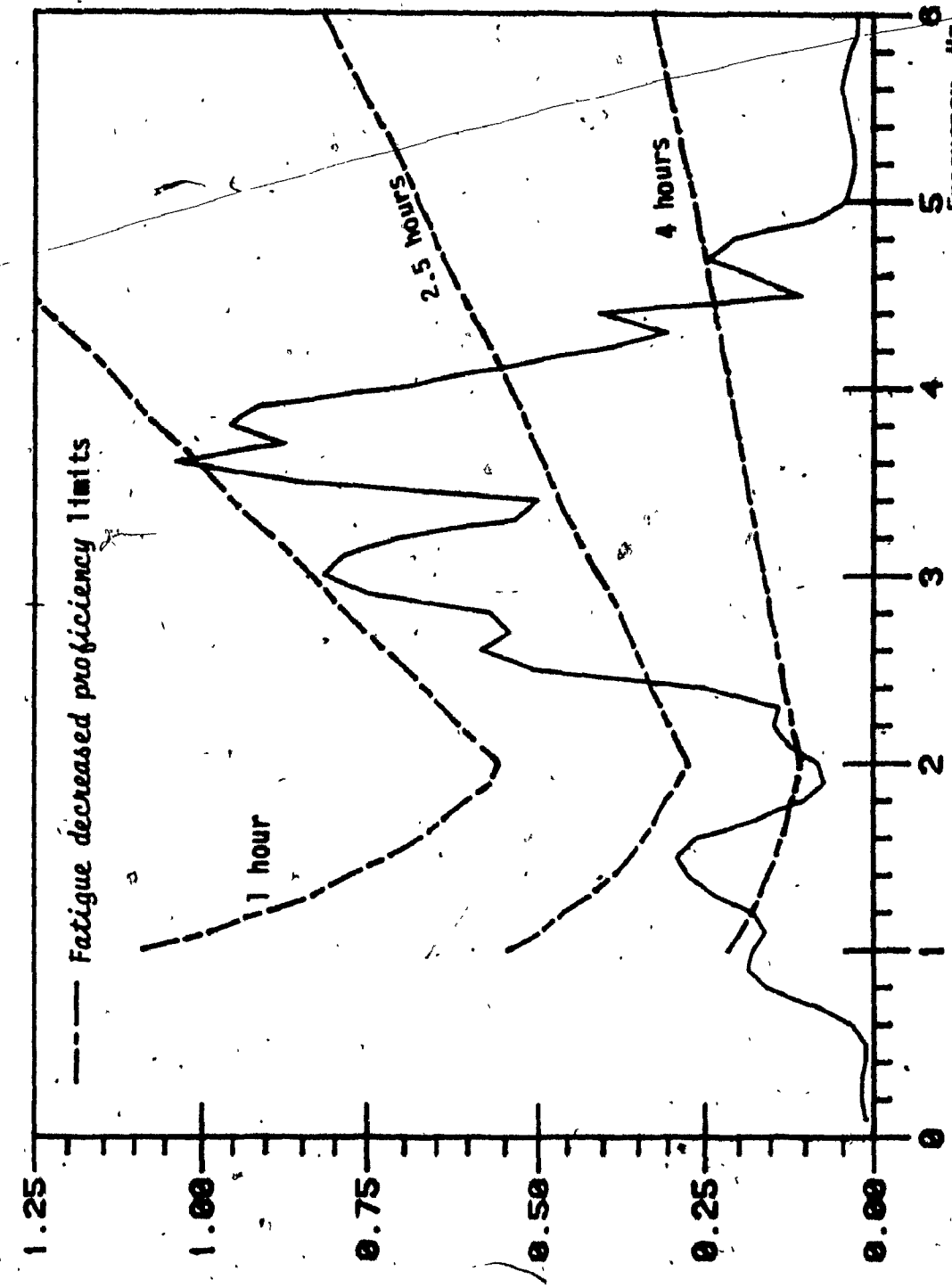

FIGURE 3.4: Longitudinal acceleration PSD measured at the cab floor [55].

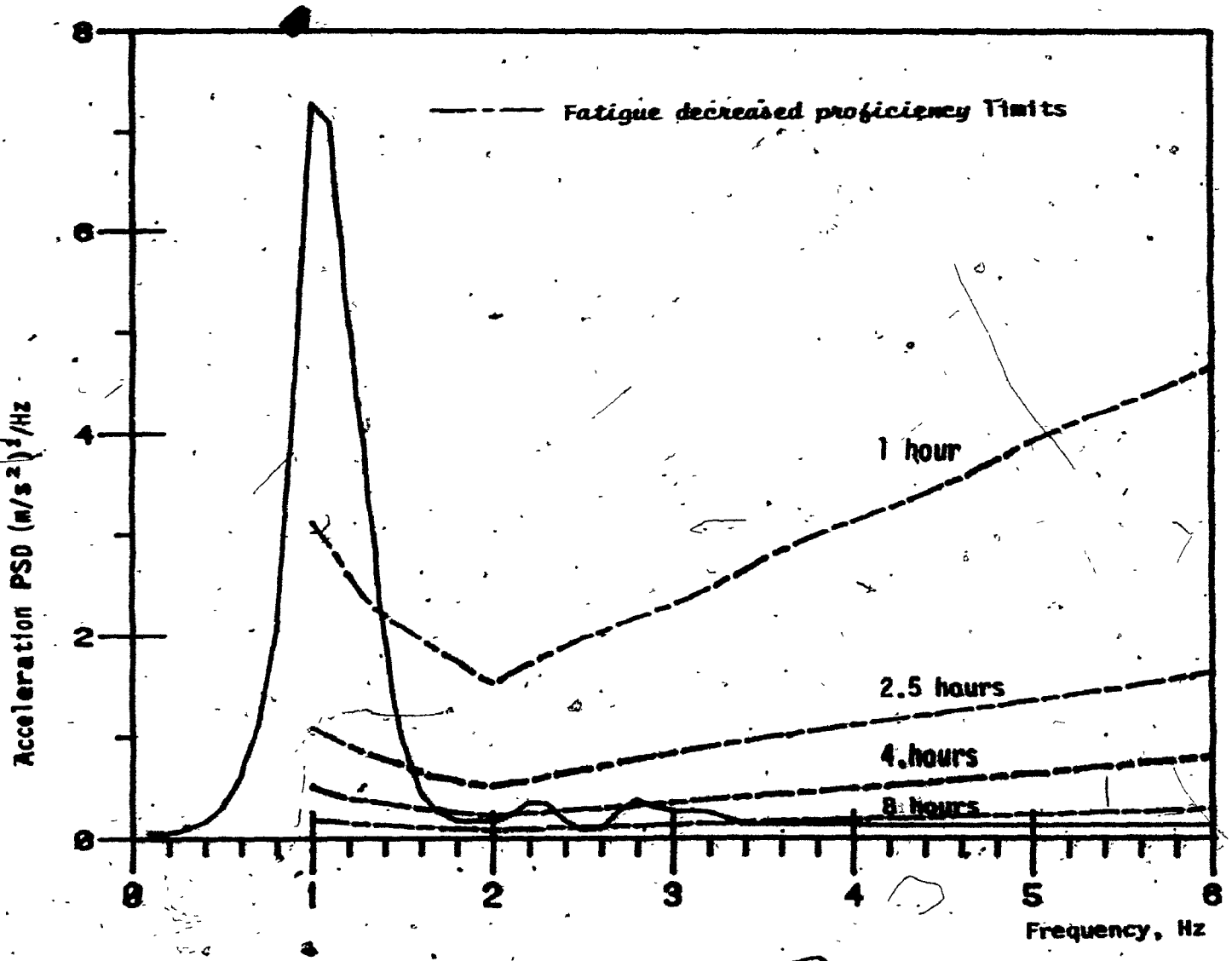

FIGURE 3.5: Lateral acceleration PSD measured at cab floor [55].

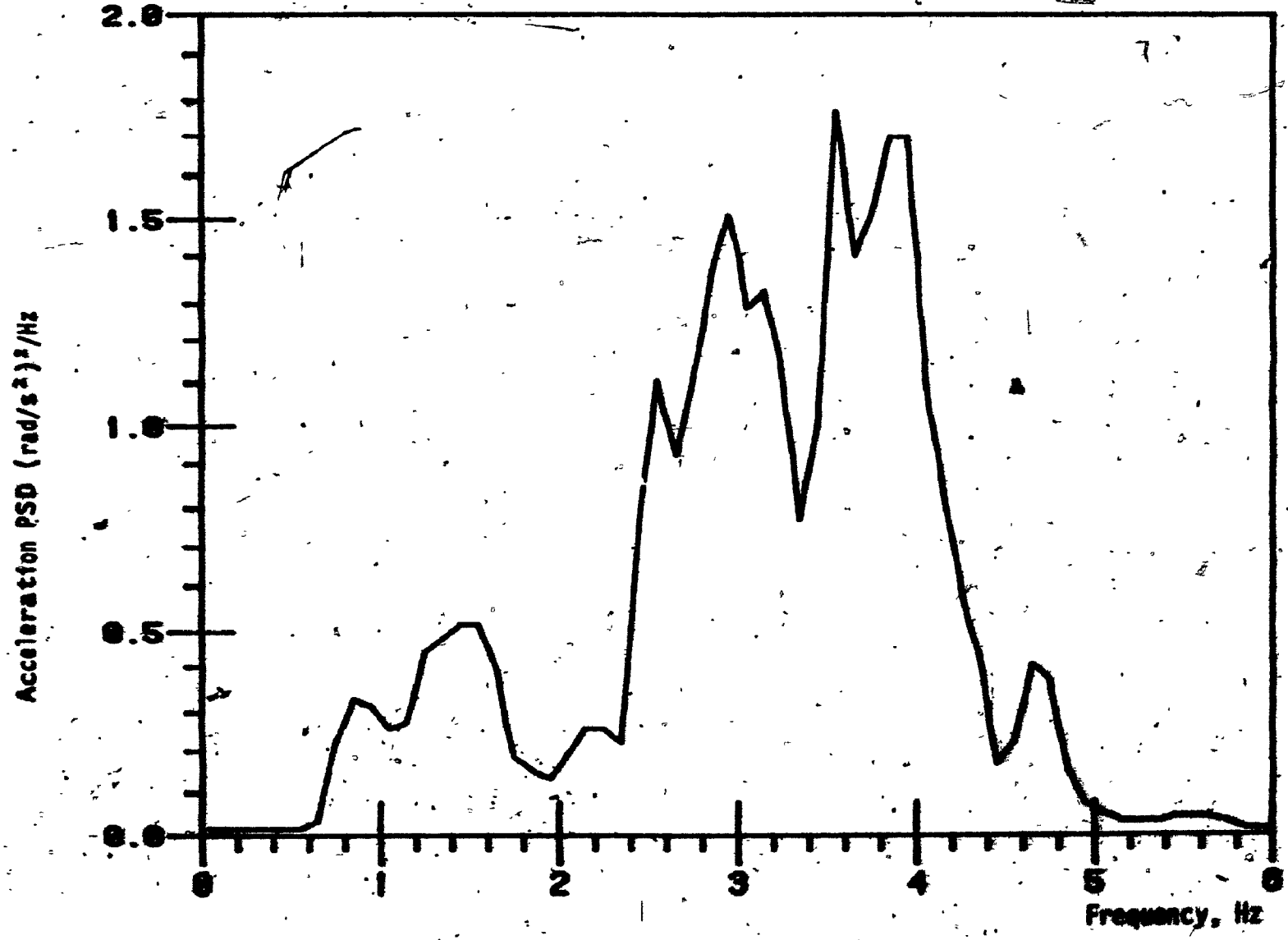

FIGURE 3.6: Pitch acceleration PSD measured at cab cg [55].

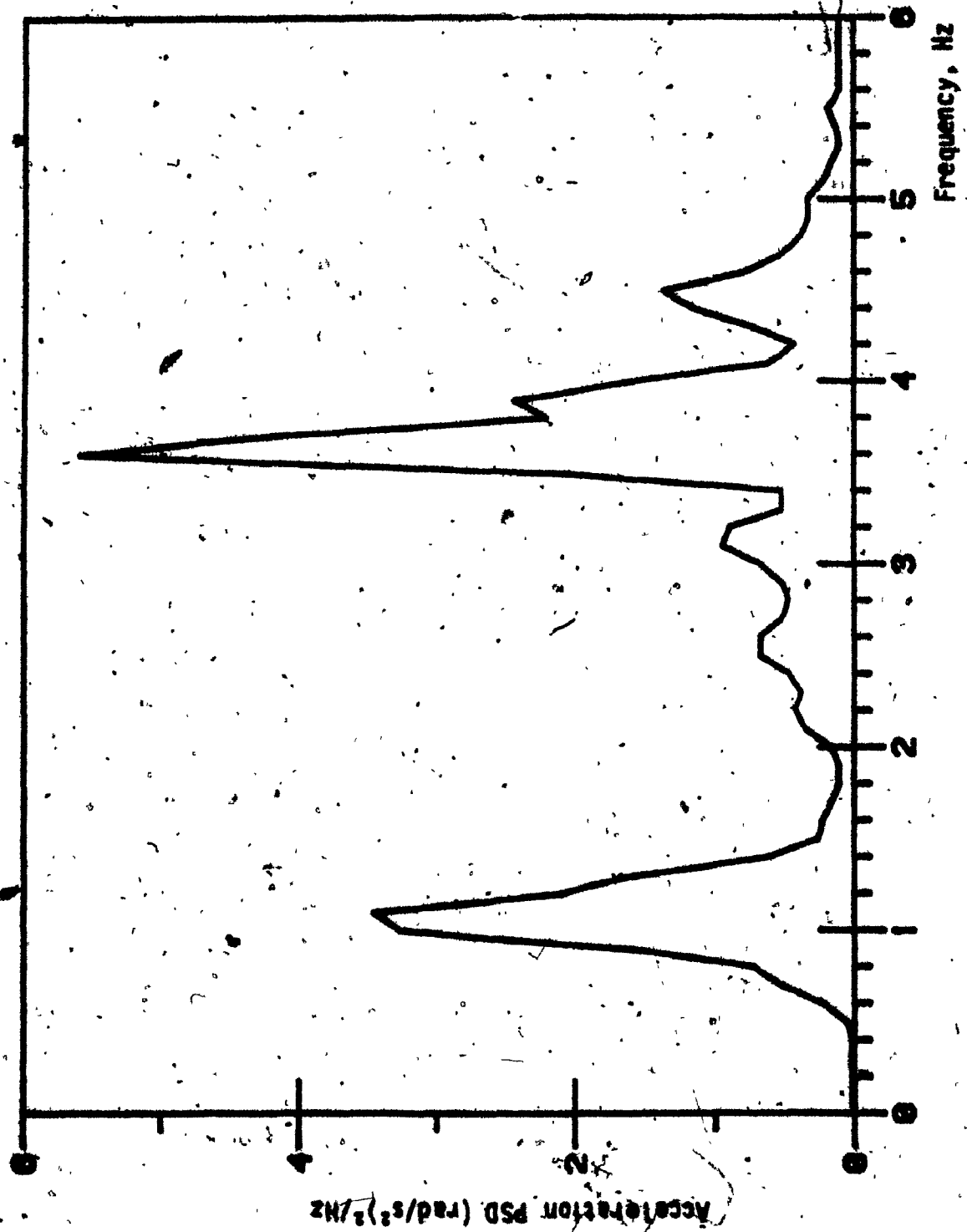

FIGURE 3.7: Roll acceleration PSD measured at the cab cg [55].

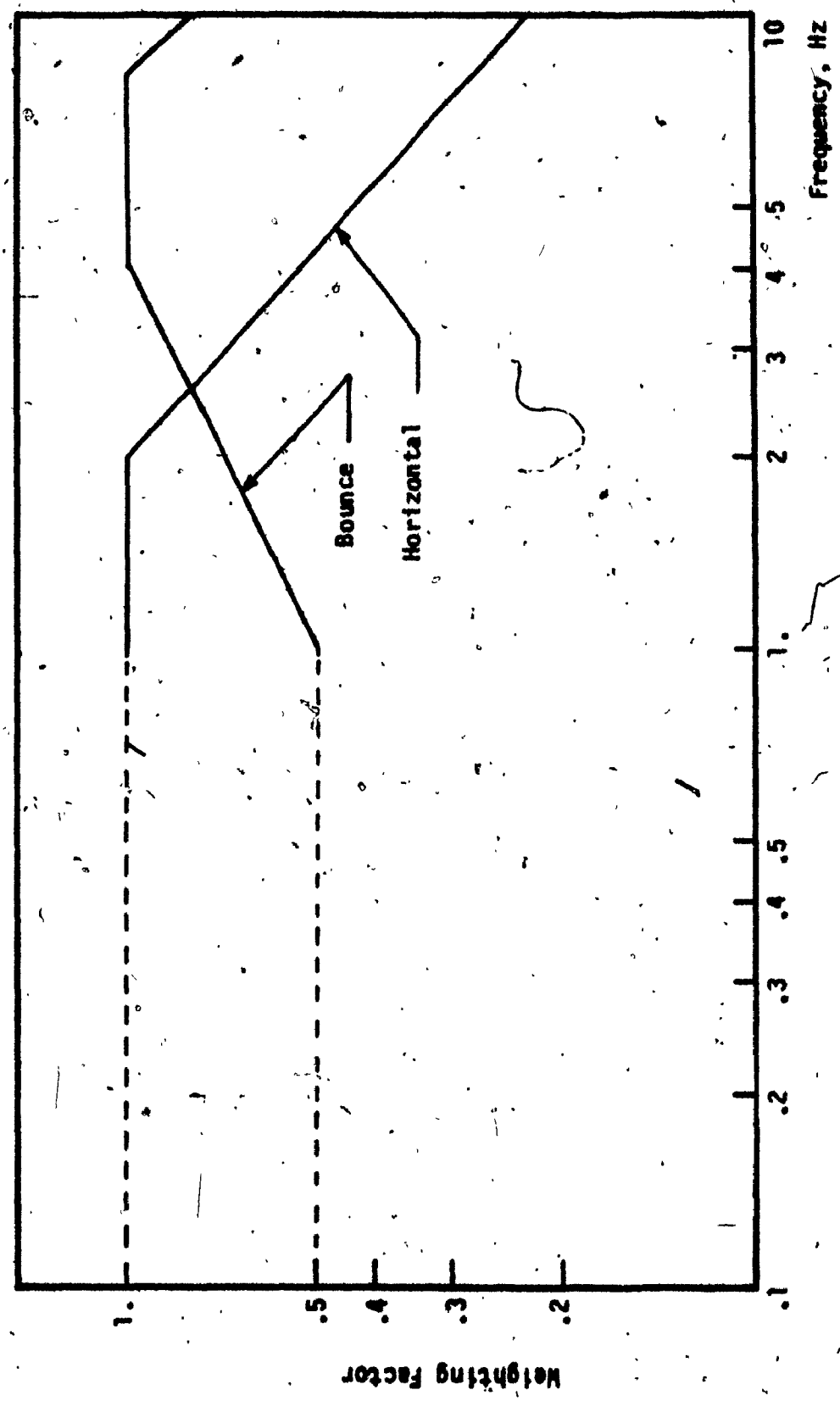

FIGURE 3.8: ISO weighting factors for bounce and horizontal accelerations [18].

$WF(\bar{f})$ = ISO frequency weighting factor at the third octave center frequency $\bar{f}$.

$S_1(f)$ = Acceleration PSD at frequency f.

f_ℓ, f_u = The lower and upper frequency limits of the third octave band, respectively.

Figures 3.9 and 3.10 present the comparison of ISO frequency weighted rms accelerations to ISO *fatigue decreased proficiency* limits in the bounce, longitudinal and lateral modes, respectively. Assuming the frequency weighting factor for roll and pitch vibrations to be unity, the rms roll and pitch accelerations are obtained as shown in Figure 3.11.

The acceleration at the seat attachment point or at the cab cg can be evaluated from the geometry of the cab [63]. The roll, pitch and bounce accelerations at the cab cg remain unchanged whereas the lateral and longitudinal accelerations at the cab cg are obtained by combining translational and rotational accelerations of the floor.

Although random terrain excitations characterized by PSD's are of the most convenient form for simulating linear systems, the simulation of non-linear systems require real time displacement and velocity excitations. The real time displacements and velocities can be achieved by representing the spectral densities or RMS acceleration spectrum as the summation of several sine waves. A number of methods have been devised for generating time histories whose spectra are replicas of some given spectra [64,65,66]. Most conveniently, the frequency spectrum can be represented by summation of several harmonics corresponding to discrete frequencies [65], that would represent a replica of the terrain measured acceleration spectral densities. The acceleration time history of the terrain excitations is then expressed by

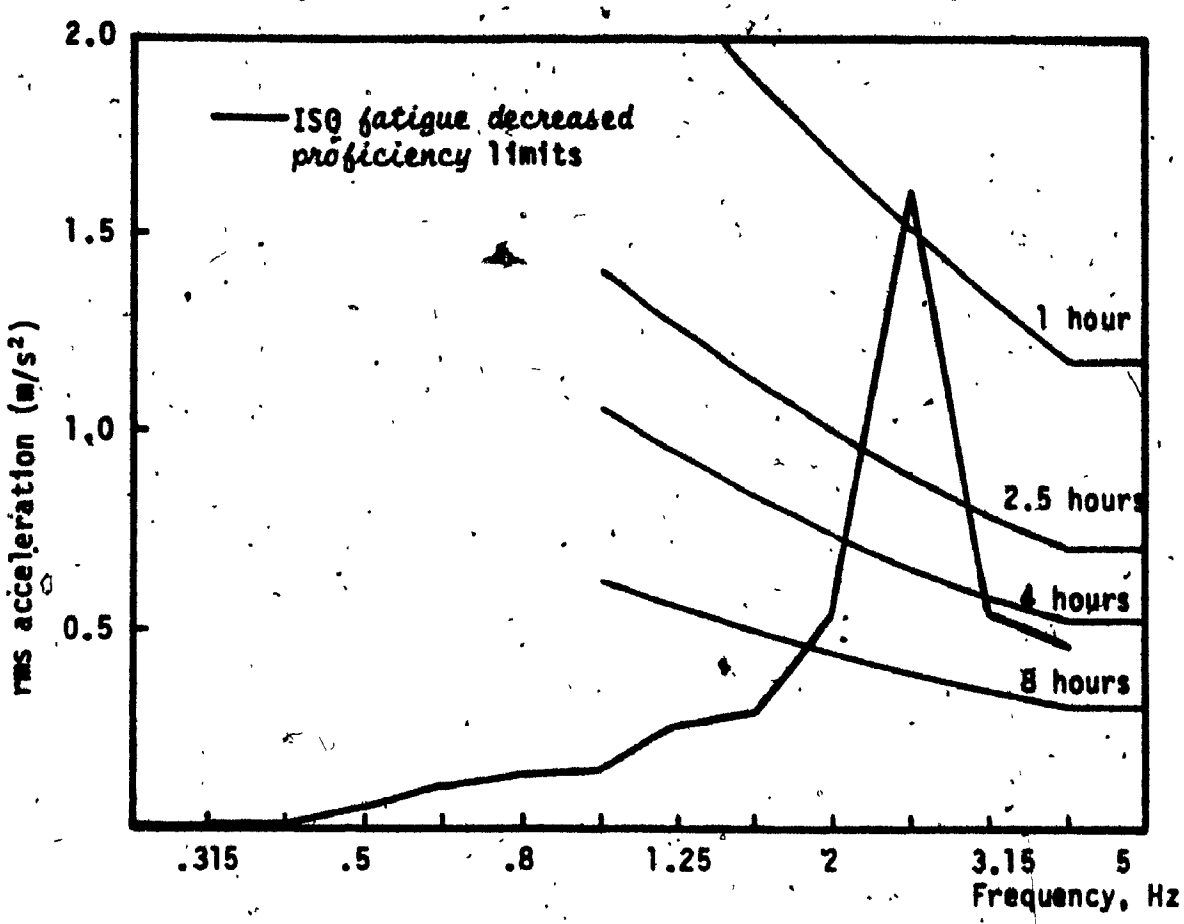

FIGURE 3.9: Bounce rms acceleration measured at the cab floor.

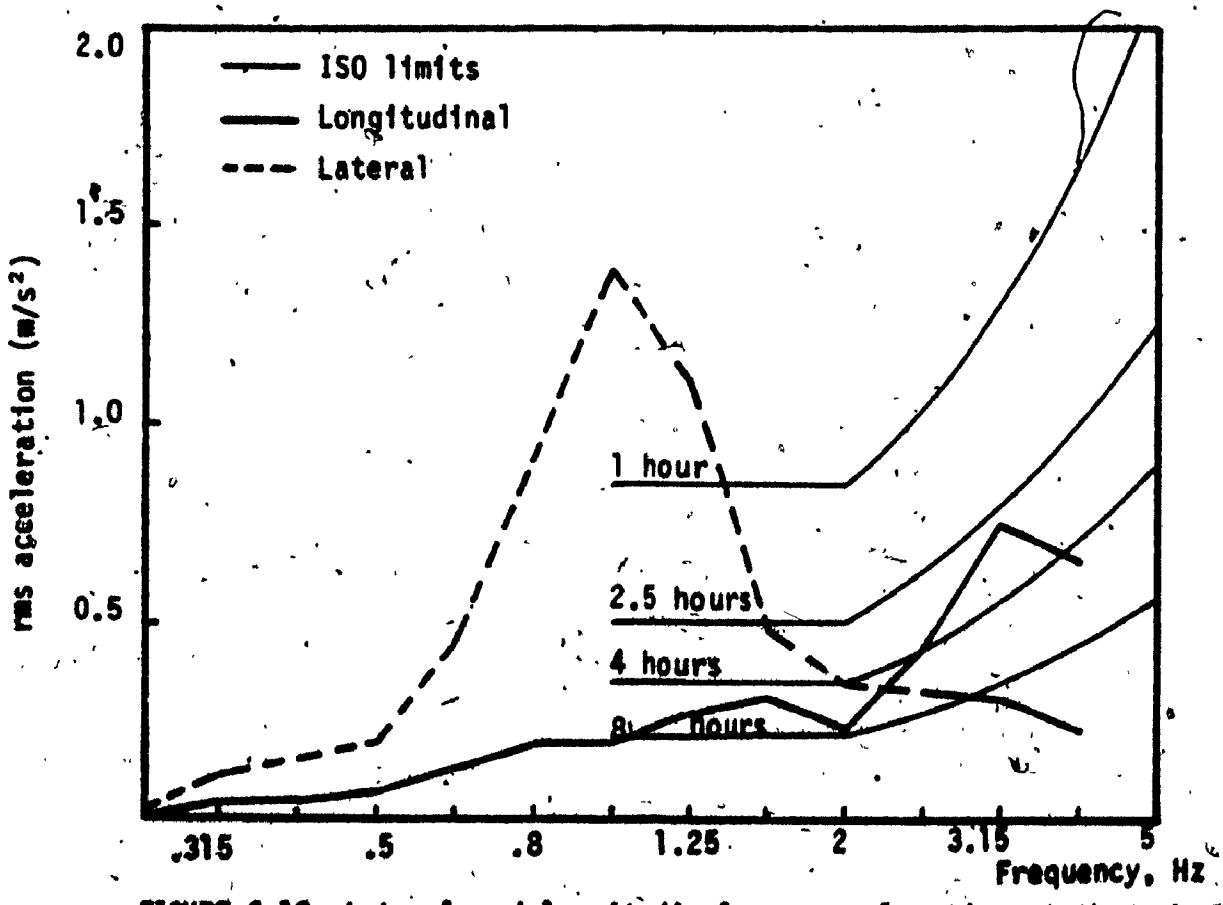

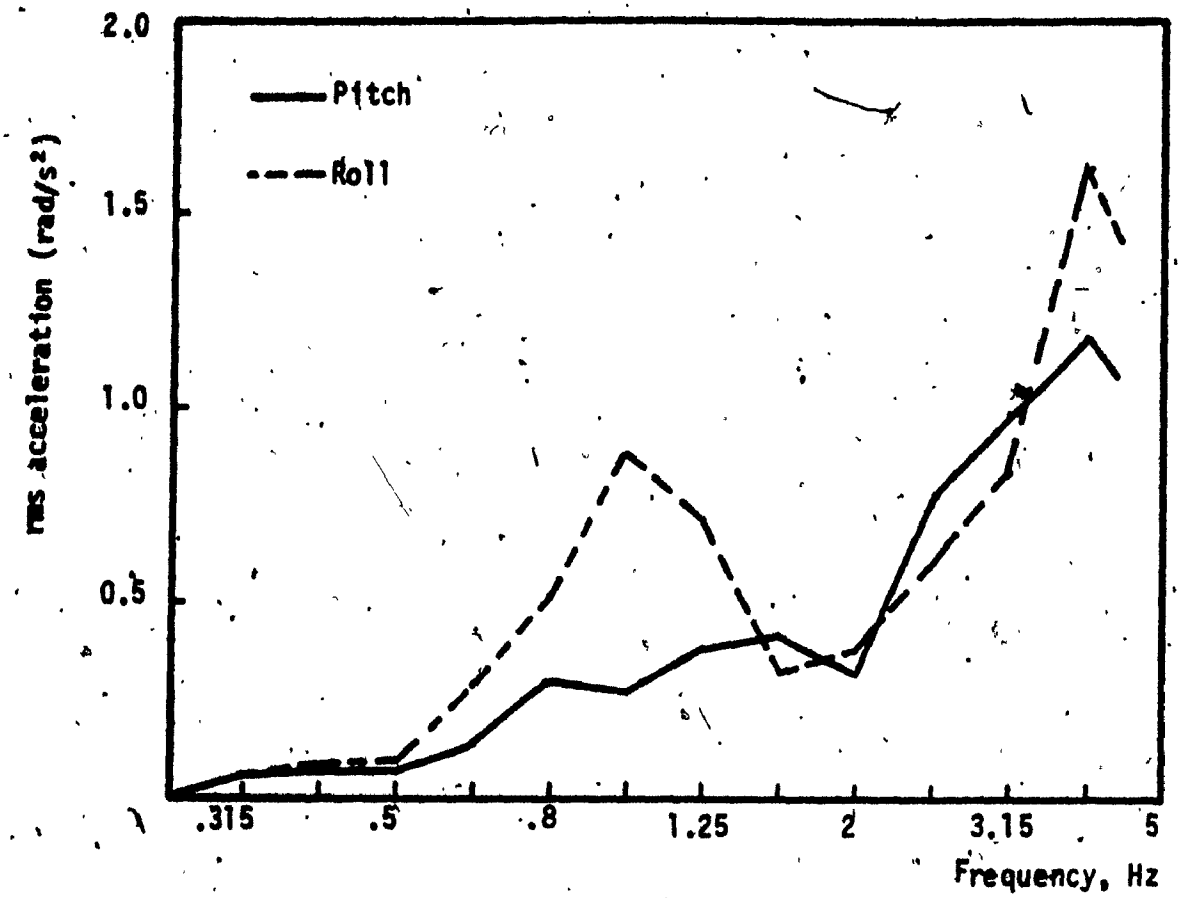

FIGURE 3.11: Roll and pitch rms acceleration measured at the cab.

$$F(t) = \sum_{i=1}^{N} a_i \sin(2\pi f_i t) \qquad (3.4)$$

where F(t) = Acceleration time history, whose spectra is a replica of terrain measured PSD's.

a_i = The coefficient determined from the frequency spectrum corresponding to frequency f_i.

N = The total number of discrete frequencies required to describe the frequency range of interest.

Appendix IV lists the detailed procedure of representing acceleration PSD's by the summation of sine waves.

3.4 SUMMARY

The random agricultural terrain excitations, characterized by acceleration PSD's and RMS accelerations are presented. The input spectras are compared with ISO specified rms and equivalent PSD acceleration limits to establish an understanding of the ride of an unsprung vehicle. The acceleration PSD's are represented by sine series to obtain real-time excitations as required for the simulation of non-linear seat-suspension models.

CHAPTER 4

RESPONSE EVALUATION OF SUSPENSION MODELS

4.1 INTRODUCTION

A number of mathematical options are available for solving the differential equations characterizing the dynamics of suspension models. The usual approach taken is to obtain the dynamic response of suspension systems with the vehicle traversing non-deformable off-road terrain as a function of time. This method, referred to as time-domain analysis, computes the translational and rotational motion of the driver as a function of time. Alternatively, the equations of motion are reduced to a frequency response function or algebraic expressions with frequency as the independent variable. The forcing function is then described statistically in the form of power spectral density (PSD) estimate. This method, referred to as frequency-domain analysis, is limited to the linear equations of motion only.

In this section, the two methods for solving differential equations of motion of the suspension models are described. A brief outline of the algorithm associated with the numerical integration of differential equations of motion, in the time-domain, is presented. Various techniques for solving the non-linear equations of motion are summarized, followed by the development of a simpler analytical technique based on dissipation of energy. Non-linear equations of motion characterizing seat-suspension models are represented by their linear equivalent using the linearization technique based on the dissipation of energy.

4.2 ANALYTICAL TECHNIQUES

Two options are available for solving the differential equations representing suspension models, namely time-domain and frequency-domain techniques. Frequency-domain analysis is more suitable for linear or linear

equivalent equations, whereas the time-domain technique can simulate both linear and non-linear equations.

4.2.1 TIME-DOMAIN ANALYSIS

Time-domain analysis utilizes variables as function of time and uses numerical integration techniques to solve differential equations of motion. The parameters of the physical system are represented as the coefficients of the time dependent variables. The time-domain analysis is carried out through a series of integrations. The integrations are performed electronically with analog computers or numerically using digital computers. The resulting information is obtained in the form of a time trace. Differential equations of motion for physical systems are commonly second order differential equations. A set of n second order differential equations are reduced to 2n first order differential equations using the following substitutions.

$$\dot{z}_i = z_{i+n}, \qquad i = 1,2,\ldots,n$$

$$\ddot{z}_i = \dot{z}_{i+n}, \qquad i = 1,2,\ldots,n \qquad (4.1)$$

The resulting first order differential equations are of the following format.

$$[P]\{\dot{Z}\} + [Q]\{Z\} = [F] \qquad (4.2)$$

where

$\{Z\}$ = Vector containing output variables

$\{\dot{Z}\}$ = Time derivative of $\{Z\}$

$[P]$ = Coefficient matrix of $\{\dot{Z}\}$

$[Q]$ = Coefficient matrix of $\{Z\}$

$[F]$ = Forcing function matrix

The prescribed numerical integration format is obtained by premultiplying equation (4.2) by the inverse of matrix [P].

$$\{\dot{Z}\} = -[P]^{-1}[Q]\{Z\} + [P]^{-1}[F] \qquad (4.3)$$

Numerous standard numerical integration algorithms are available for solving differential equations with the format of equation (4.3). The procedure for evaluating the time response of the suspension models can be summarized in the following manner.

i) The equations of motion for the suspension models are manipulated to obtain expressions for the accelerations in the explicit form.

ii) The set of n second order equations are then reduced to 2n first order equations using the substitution of equation (4.1).

iii) The first order expressions are integrated to evaluate velocities and displacements by employing fourth order Runge-Kutta technique for a set of successive time instant t_i's. The velocities and displacements previously obtained at t_{i-1} are used as the intial conditions associated with integrations at instant t_i.

The procedure described is repeated for successive t_i's and the process is terminated when t_i reaches a certain predetermined final time t_f. The value t_f is selected to exhibit a description of some of the aspects of response that illustrate the dynamic phenomena associated with the steady state response in the time domain.

4.2.2 FREQUENCY DOMAIN ANALYSIS

The frequency-domain approach for solving differential equations utilizes Fourier Transforms of the time dependent variables to frequency dependent variables. Differential equations, such as equation (2.26) representing the equations of motion for a linear system, are Fourier transformed to:

$$\{Z(j\omega)\} = [H(j\omega)]\{Z_0(j\omega)\} \tag{4.4}$$

where

$\{Z(j\omega)\}$ = Fourier transform of vector containing output variables.

$\{Z_0(j\omega)\}$ = Fourier transform of vector containing input variables.

$[H(j\omega)]$ = Complex matrix representing the frequency response function of the system.

In the frequency domain analysis, power spectral densities (PSD's) and cross spectral densities (CSD's) are used to characterize input and output variables. For a single input, single output system, the input and output PSD's are given by the following relationship [63]:

$$S_0(\omega) = h(j\omega)\cdot h^*(j\omega)\cdot S_1(\omega) \tag{4.5}$$

where

$S_0(\omega)$ = PSD of the response variable.

$S_1(\omega)$ = PSD of the input variable.

$h(j\omega)$ = Frequency response function of the system.

$h^*(j\omega)$ = Complex conjugate of $h(j\omega)$.

For a system of multiple inputs and outputs the PSD of an output variable is determined by:

$$S_0^p(\omega) = \mathrm{Re}\left[\sum_{k=1}^{n}\sum_{\ell=1}^{n} h_{pk}(j\omega)\cdot h^*_{p\ell}(j\omega)\cdot CSD_{k\ell}\right] \tag{4.6}$$

$$\text{for } p = 1,2,\ldots,N$$

where,

$S_0^p(\omega)$ = PSD of the p^{th} response variable.

$h_{pk}(j\omega)$ = Complex frequency response function between p^{th} output and k^{th} input variable.

$h^{*}_{p\ell}(j\omega)$ = Complex conjugate of $h_{p\ell}(j\omega)$.

$CSD_{k\ell}$ = Spectral density matrix of input variables (cross spectral density for $k \neq \ell$, Power spectral density for $k = \ell$).

n = Number of input variables.

Re = Designates real part.

N = Total number of response variables.

Equation (4.6) can be rewritten in the matrix form as [63]:

$$[S_0(\omega)] = [H^*(j\omega)][S_1(\omega)][H(j\omega)]' \tag{4.7}$$

where,

$[S_0(\omega)]$ = Spectral density matrix of the response variables.

$[S_1(\omega)]$ = Spectral density of the input variables.

$[H(j\omega)]'$ = Transpose of $[H(j\omega)]$

Equations (4.6) and (4.7) provide response spectral densities for the prescribed variables only, usually the generalized coordinates of the system. The response spectral densities at coordinates other than the generalized coordinates are obtained by using a transformation matrix [T], and is given by:

$$[S^r_0(\omega)] = [T]\ [S_0(\omega)][T]' \tag{4.8}$$

where

$[S^r_0(\omega)]$ = Response spectral density at coordinates other than generalized coordinates.

The procedure for evaluating the response in frequency domain can be summarized in the following manner.

1) The linear equations of motion of the suspension model are Fourier transformed to obtain frequency response function, $[H(j\omega)]$.

ii) The spectral density response at the generalized coordinates is evaluated from equations (4.5), (4.6) or (4.7) with known input spectral densities.

iii) The spectral density response at the coordinates other than the generalized coordinates is evaluated using equation (4.8).

The frequency-domain solution technique reduces simulation time considerably, as compared to the time-domain analysis. However, the method is limited to only linear equations. The non-linear differential equations characterizing the dynamics of seat suspensions must be linearized to be solved in the frequency-domain.

4.3 RESPONSE EVALUATION OF NON-LINEAR SUSPENSION MODELS

Equations of motion characterizing linear suspension models are easily analyzed through the eigenvalue/vector and frequency domain computations. The most straight forward numerical approaches to solution of non-linear equations of motion are numerical integration techniques. However, the simulation of suspension models subject to random terrain inputs, using numerical integration techniques, is extremely demanding on computer and human resources. Since linear systems are so much easier and economical to analyze than the non-linear ones, a convenient alternative is to replace the non-linear element with a linear element whose gain is a function of the properties of non-linearity. Such processes are referred to as linearization techniques.

Mathematical models developed for suspension seats include non-linearities arising due to shock absorber damping, coulomb friction, and elastic limit stops. A brief summary of the available analytical techniques developed to solve non-linear systems is discussed. A systematic technique based on frequency dependent linearization is developed and presented for harmonically and stochastically excited non-linear

seat suspension models.

4.3.1 REVIEW OF EXISTING TECHNIQUES

A number of techniques have been developed to study the stochastically excited non-linear systems. They are: Fokker-Planck equation approach, normal mode approach, perturbation technique and statistical linearization technique. A brief review of these techniques is presented as follows:

i) Fokker-Planck Equation technique: Trapsitional probability density of the response process of a system subject to Gaussian white noise excitation is governed by the Fokker-Planck equation [67,68]. The required statistics of the response process are completely defined by this transitional probability density. The Fokker-Planck equation provides an exact solution, however, the complete solution of the equation is available only for limited cases. The stationary form of the Fokker-Planck equation is inapplicable to systems with non-linearities involving velocities and/or with non-white excitations [67,71].

ii) Normal Mode Approach: The normal mode technique has been developed for obtainihg stationary random response of non-linear systems. A given set of coupled non-linear equations are reduced to a set of equations containing coupling only in the non-linear terms and having statistically uncorrelated excitations [71]. The reduced equations then can be solved using techniques such as equivalent linearization. The approach is applicable to dynamical systems which are excited at only a few points in the space, provided that the linear

system which is obtained by neglecting all non-linearities possesses normal modes [72].

iii) Perturbation Technique: The perturbation approach assumes the solution as an expansion in powers of some small parameters, which corresponds to the magnitude of the non-linearity. Substituting the power series solution in the original equation and equating the coefficients of like powers of the non-linearity parameter, a set of linear differential equations can be obtained for the terms in the expansion of the solution [69,70]. This leads to a first order approximation which can be obtained by solving two sets of linear differential equations. The first set of differential equations is obtained by assuming zero non-linearities and the second set of equations is formulated with the excitation as a function of the solution of first set of equations. The calculations are usually lengthy and become progressively tedious as the order of expansion parameter increases. This method can be effectively used with systems possessing sufficiently small non-linearities.

iv) Statistical Linearization Techniques: Statistical linearization technique is widely used for studying the stationary random response of non-linear systems. The technique is based on the concept of replacing the non-linear system by a related linear system such that the difference in the behaviour of two systems is a minimum possible. Usually, the mean square of the response error between the two systems is minimized [69,71]. This approach can be applied to a broad class of problems and is not limited by the restrictions on excitation and dissipation often encountered in other approximation approaches. However,

difficulties are encountered when the non-linear characteristics are discontinuous, as in Coulomb friction.

4.3.2 LINEARIZATION BASED ON DISSIPATION OF ENERGY

The linearization processes compute an equivalent viscous parameter to represent the non-linear dissipative elements of a system. The coefficient of equivalent viscous damping is a function of the magnitude of non-linearity and the excitation. The coefficient of viscous damping is computed such that the response behaviour of the linear system does not deviate significantly from the response behaviour of the original non-linear system.

One way to determine viscous damping coefficient is to find the percent of critical damping coefficient using logarithmic decrement of the free vibration decay response of the actual damped system. The non-linear effects of the damping element are completely ignored, using this technique. Alternatively, an equivalent viscous damping coefficient due to a non-linear dissipative device may be computed by equating the energy dissipated per cycle of the non-linear damper solution in steady state vibration to the energy dissipated per cycle of an equivalent viscous damper.

In case of the Coulomb damping, the force resisting motion is assumed to be proportional to the normal force between the sliding surfaces and independent of velocity except for the sign. The damping force is thus:

$$F_c = F \operatorname{sgn}(\dot{z}) \qquad (4.9)$$

Velocity squared damping characterizes the damping provided by a shock absorber when the fluid is forced through an orifice. The damping force is thus:

$$F_d = C_v |\dot{z}| \dot{z}$$

or

$$F_d = C_v \dot{z}^2 \, sgn(\dot{z}) \tag{4.10}$$

The energy dissipated by the dissipative elements, assuming harmonic solution is given in the following manner,

Coulomb damping:

$$\Delta E^c = 4 F \cdot u \tag{4.11}$$

Velocity squared damping:

$$\Delta E^d = \frac{8}{3} C_v u^3 \omega^2 \tag{4.12}$$

where, u is the steady state relative displacement across the damping element, and ω is the frequency of excitation. The equivalent viscous damping coefficient is obtained by equating equations (4.11) and (4.12) to the energy dissipated by the equivalent viscous damper. The equivalent viscous damping coefficients due to Coulomb friction and the velocity squared damping are given by [73].

Coulomb damping:

$$C_{eq}^c = \frac{4F}{\pi \omega u} \tag{4.13}$$

Velocity squared damping:

$$C_{eq}^d = \frac{8}{3\pi} C_v \omega u \tag{4.14}$$

The mathematical development of the procedure for computing the equivalent viscous damping coefficient is described in the following manner. For a single degree of freedom base excited system, the equation of motion is:

$$M\ddot{u} + q(u,\dot{u},t) + Ku = -M\ddot{z}_0 \tag{4.15}$$

where $q(u,\dot{u},t)$ represent the non-linear damping force. A change of variable can result in two simultaneous first order equations.

Let,

$$\dot{p} = \dot{u} = f_1(t,u,p) \tag{4.16}$$

Rearrange equation (4.15) to obtain

$$\ddot{u} = -\ddot{z}_o - \frac{1}{M} q(u,p,t) - \frac{K}{M} u$$

or

$$\dot{p} = -\ddot{z}_o - \frac{1}{M} q(u,p,t) - \frac{K}{M} u = f_2(t,u,p) \tag{4.17}$$

The expressions for $f_2(t,u,p)$ are derived from equation (4.17), depending on the nature of damping present in the system.

For Coulomb damping:

$$f_2(t,u,p) = -\ddot{z}_o - \frac{F}{M} \operatorname{sgn}(\dot{p}) - \frac{K}{M} u \tag{4.18}$$

For velocity squared damping:

$$f_2(t,u,p) = -\ddot{z}_o - \frac{C_v}{M} p^2 \operatorname{sgn}(p) - \frac{K}{M} u \tag{4.19}$$

Equations (4.18) and (4.19) are solved using numerical integration techniques to compute energy dissipated per cycle as follows.

$$\oint F_d \frac{du}{dt} dt$$

or

$$\oint F_c \frac{du}{dt} dt \tag{4.20}$$

The damping coefficient due to equivalent viscous damping is computed by equating equation (4.20) to the energy dissipated by a viscous damper. Hence, the non-linear equation of motion (4.15) may be replaced by an equivalent linear system given by:

$$M\ddot{u} + C_{eq} \dot{u} + Ku = -M\ddot{z}_o$$

or

$$M\ddot{z} + C_{eq}(\dot{z}-\dot{z}_o) + K(z-z_o) = 0 \tag{4.21}$$

This technique of replacing the non-linear damping by an equivalent viscous damping parameter, as a function of non-linearity and excitation amplitude, is extremely simple and economical. However, the approach assumes small damping and nearly linear response of the non-linear systems. Many non-linear damping mechanisms are not accurately represented by viscous damping, except for small damping [74]. Moreover, linear model with constant damping coefficient has their most correct application in a restricted frequency range only [75]. Specifically, non-linearities like Coulomb friction are not correctly represented by a constant damping coefficient.

4.3.3 FREQUENCY DEPENDENT LINEARIZATION

Frequency dependent linearization approach establishes equivalent viscous damping coefficient as a function of excitation frequency and amplitude. The equivalent linear single degree of freedom (SDOF) system may be represented as:

$$M\ddot{u} + C_{eq}(\omega,u)\dot{u} + Ku = - M\ddot{z}_0 \qquad (4.22)$$

where $C_{eq}(\omega,u)$ is the equivalent viscous damping coefficient as a function of excitation frequency and relative position response across the dissipative element. The equivalent viscous damping coefficient is obtained by equating the energy dissipated by non-linear damping to that of a viscous damper, at each excitation frequency. However, in order to evaluate the energy dissipated by non-linear damping, the relative position response of the system is required. For harmonically excited single degree-of-freedom system, the relative displacement response is given by :

$$|u| = \frac{\ddot{z}_o}{[(\omega_n^2-\omega^2)^2 + (2\zeta_{eq}(\omega,u)\omega\cdot\omega_n)^2]^{1/2}} \qquad (4.23)$$

where

ω_n = undamped natural frequency of the system $(K/M)^{1/2}$.

$\zeta_{eq}(\omega,u) = \frac{C_{eq}(\omega,u)}{2M\cdot\omega_n}$ the equivalent damping ratio.

$\ddot{z}_o$ = Amplitude of acceleration excitation.

For the non-linear suspension system with Coulomb and velocity squared damping elements, the equivalent linear viscous damping coefficients over the frequency range of interest are computed using the following algorithm.

1) Assume an initial value for $C_{eq}^1(\omega,u)$ for a given excitation frequency.

2) Determine the absolute relative position response corresponding to the given frequency from equation (4.23)

$$|u^1| = \frac{\ddot{z}_o}{\sqrt{[(\omega_n^2-\omega^2)^2+(2\zeta_{eq}^1(\omega,u)\omega\omega_n)^2]}} \qquad (4.24)$$

where

$$\zeta_{eq}^1(\omega,u) = C_{eq}^1(\omega,u)/2M\omega_n$$

3) Compute the equivalent damping coefficient from energy dissipation expressions of equations (4.13) and (4.14),

$$C_{eq}^{i+1}(\omega,u) = \frac{4F}{\pi\omega u^1} + \frac{8}{3\pi} C_v \omega u^{1} \qquad (4.25)$$

4) Compute the error between the assumed coefficient and the one computed from equation (4.25).

$$\epsilon = |C_{eq}^{i+1}(\omega,u) - C_{eq}^1(\omega,u)| \qquad (4.26)$$

If the absolute error is within the specified tolerance, the assumed coefficient is the linear equivalent corresponding to the chosen excitation frequency. The iterative procedure must be repeated if the absolute error exceeds the specified tolerance by assigning

$$C_{eq}^{i}(\omega,u) = C_{eq}^{i+1}(\omega,u) \tag{4.27}$$

5) At extremely low frequencies, when a lock up condition is experienced due to Coulomb friction, the coefficient of viscous damping is very large. If the relative motion is observed to be extremely small, compute the absolute acceleration response of the system

$$|\ddot{z}^{i}| = \left[\frac{(\omega_n^2)^2 + (2\zeta_{eq}^{i}(\omega,u)\omega\cdot\omega_n)^2}{(\omega_n^2-\omega^2)^2+(2\zeta_{eq}^{i}(\omega,u)\omega\cdot\omega_n)^2}\right]^{1/2} \ddot{y}_o \tag{4.28}$$

and check for lock up condition,

$$M|\ddot{z}^{i}| < F \tag{4.29}$$

If the inertial force is less than the friction force, lock up is experienced. Hence,

$$\ddot{y}^{i} = \ddot{y}_o$$

$$u^{i} = o \tag{4.30}$$

6) Non-linearity due to elastic limit stops can also be treated in this algorithm. The suspension force due to elastic limit stops is given by:

$$|F_s| = K_s^{*}\cdot S^{*}\cdot[|u^{i}| - \tfrac{d}{2}] \tag{4.31}$$

where

$S^{*} = 0.$ for $|u_1| \leq d/2$

$S^{*} = 1$ for $|u_1| > d/2$

d = Total travel between the two limit stops.

K_s^{*} = Stiffness due to elastic stops.

7) The iterative procedure is repeated for the entire frequency range to establish the linear equivalent coefficient over the range of interest.

The energy dissipation approach can correctly represent the non-linear damping mechanism over the frequency range of interest. The technique can also be extended to stochastically described excitations (stationary random excitations measured from the Silsoe track) by representing them as a summation of various harmonics as presented in Chapter 3. Such that the equations (4.24), (4.25), and (4.28) are re-written in the following manner.

$$|u^i| = \frac{\ddot{z}_o(\omega_j)}{[(\omega_n^2-\omega_j^2)+(2\zeta_{eq}^i(\omega_j,u)\omega_j\omega_n)^2]^{1/2}}$$

$$j = 1,2,\ldots,n \qquad (4.32)$$

where n is the number of harmonics considered to represent the track excitations.

$$c_{eq}^{i+1} = \frac{4F}{\pi\omega_j|u^i|} + \frac{8}{3\pi} c_v\omega_j|u^i| \qquad (4.33)$$

and

$$|\ddot{z}_j^i| = \left[\frac{(\omega_n^2)^2+(2\zeta_{eq}^i(\omega_j,u)\omega_j\omega_n)^2}{(\omega_n^2-\omega_j^2)^2+(2\,\zeta_{eq}^i(\omega_j,u)\omega_j\omega_n)^2}\right]^{1/2} \ddot{z}_o(\omega_j) \qquad (4.34)$$

where

$|u^i|$ = Absolute position response corresponding to i^{th} iteration.

$\ddot{z}_o(\omega_j)$ = Amplitude of excitation of the j^{th} harmonic.

ω_j = Frequency of the j^{th} harmonic, $j = 1,2,\ldots,n$.

$\ddot{z}_j^i$ = Response acceleration amplitude corresponding to j^{th} frequency and i^{th} iteration.

$\zeta_{eq}^i(\omega_j,u)$ = Equivalent damping ratio corresponding to j^{th} frequency and i^{th} iteration.

4.4 APPLICATIONS OF FREQUENCY DEPENDENT LINEARIZATION

Seat suspension models formulated in Chapter 2 include non-linearities due to Coulomb friction, shock absorber damping and elastic limit stops. Statistical linearization technique can be employed to evaluate the random response of the non-linear suspension models. However, in this section, the non-linear suspension models are represented by their equivalent linear models, using the frequency dependent linearization. Since translational seat suspension can be represented by three uncoupled seat isolators, the analysis is carried out for independent seat suspensions.

4.4.1 BOUNCE SEAT-SUSPENSION

Rewrite the equations of motion of bounce-seat suspension

$$M_0 \ddot{z}_1 + K_c(z_1 - z_s) + C_c(\dot{z}_1 - \dot{z}_s) = 0$$

$$M_s^z \ddot{z}_s - K_c(z_1 - z_s) - C_c(\dot{z}_1 - \dot{z}_s) + K_z(z_s - z_0)$$

$$+\{F_z + C_z|\dot{z}_s - \dot{z}_0|^2\}\operatorname{sgn}(\dot{z}_s - \dot{z}_0) + K_s^z \cdot S^z\left[z_s - z_0 - \frac{d_z}{2}\operatorname{sgn}(z_s - z_0)\right] = 0 \quad (4.35)$$

Non-linear damping in equation (4.35) is represented by a linear equivalent damping coefficient.

$$M_0 \ddot{z}_1 + K_c(z_1 - z_s) + C_c(\dot{z}_1 - \dot{z}_s) = 0$$

$$M_s^z \ddot{z}_s - K_c(z_1 - z_s) - C_c(\dot{z}_1 - \dot{z}_s) + K_z(z_s - z_0)$$

$$+ C_{eq}(\omega, u_s)[\dot{z}_s - \dot{z}_0] + K_s^z \cdot S^z\left[z_s - z_0 - \frac{d_z}{2}\operatorname{sgn}(z_s - z_0)\right] = 0 \quad (4.36)$$

Define

$$u_1 = z_1 - z_s$$

$$u_s = z_s - z_0$$

Substitute in equation (4.36), and rewrite in the matrix form.

$$\begin{bmatrix} M_o & M_o \\ 0 & M_s^z \end{bmatrix} \begin{bmatrix} \ddot{u}_1 \\ \ddot{u}_s \end{bmatrix} + \begin{bmatrix} C_c & 0 \\ -C_c & C_{eq}(\omega,u_s) \end{bmatrix} \begin{bmatrix} \dot{u}_1 \\ \dot{u}_s \end{bmatrix} + \begin{bmatrix} K_c & 0 \\ -K_c & K_s^z \cdot S^z + K_z \end{bmatrix} \begin{bmatrix} u_1 \\ u_s \end{bmatrix}$$

$$- \begin{bmatrix} 0 \\ K_s^z \cdot S^z \cdot \frac{d_z}{2} \end{bmatrix} = - \begin{bmatrix} M_o \\ M_s^z \end{bmatrix} \ddot{z}_o \qquad (4.37)$$

or

$$\begin{bmatrix} K_c - M_o\omega^2 + j\omega C_c & -M_o\omega^2 \\ -K_c - j\omega C_c & K_s^z \cdot S^z + K_z - \omega^2 M_s^z + jC_{eq}(\omega,u_s)\omega \end{bmatrix} \begin{bmatrix} u_1(j\omega) \\ u_s(j\omega) \end{bmatrix}$$

$$= \omega^2 \begin{bmatrix} M_o \\ M_s^z \end{bmatrix} Z_o(j\omega) + \begin{bmatrix} 0 \\ K_s^z \cdot S^z \cdot \frac{d_z}{2Z_o} \end{bmatrix} Z_o(j\omega) \qquad (4.38)$$

where C_{eq} is the equivalent viscous damping coefficient as a function of excitation frequency and relative position amplitude given by:

$$C_{eq} = \frac{4F_z}{\pi \omega u_s} + \frac{8}{3\pi} C_z \omega u_s \qquad (4.39)$$

and S^z, the non-linear function characterizing the elastic limit stops stiffness, given by:

$$S^z = \begin{cases} 0 & |u_s| \leq \frac{d_z}{2} \\ 1 & |u_s| > \frac{d_z}{2} \end{cases} \qquad (1.40)$$

An equivalent viscous damping coefficient corresponding to each excitation frequency is computed using the algorithm described in section 4.3.

4.4.2 LONGITUDINAL AND LATERAL SEAT SUSPENSIONS

Since the longitudinal and lateral seat isolators are characterized by similar equations of motion, the frequency dependent linearization is illustrated for the longitudinal isolator alone. The equation of motion for the longitudinal seat suspension model is given by

$$M_x \ddot{x}_1 + K_x(x_1 - x_0) + \{F_x + C_x(\dot{x}_1 - \dot{x}_0)^2\} \operatorname{sgn}(\dot{x}_1 - \dot{x}_0)$$

$$+ K_s^x \cdot S^x \cdot \{x_1 - x_0 - \frac{d_x}{2} \operatorname{sgn}(x_1 - x_0)\} = 0 \qquad (4.41)$$

Define, $u_x = x_1 - x_0$

Substitute in the linear representation of equation (4.41).

$$M_x \ddot{u}_x + K_x u_x + C_{eq}(\omega, u_x)\dot{u}_x + K_s^x \cdot S^x \{u_x - \frac{d_x}{2} \operatorname{sgn}(u_x)\} = M_x \ddot{x}_0 \qquad (4.42)$$

The equivalent viscous damping coefficient is computed from the energy dissipated by Coulomb, and velocity squared damping:

$$C_{eq}(\omega, u_x) = \frac{4F_x}{\pi \omega u_x} + \frac{8}{3\pi} C_x \omega u_x \qquad (4.43)$$

4.4.3 ROTATIONAL SEAT SUSPENSION MODEL

The rotational seat isolator consists of bounce seat suspension, pitch, and roll seat isolators. Non-linearities in the suspension model arise due to shock absorbers and Coulomb damping. As discussed in Chapter 2, the roll mode can be entirely decoupled from the rotational seat model by choosing the gimbal support springs equidistant. Hence, the roll mode can be treated independently.

Bounce and Pitch Modes

The equations of motion, formulated in Chapter 2 (Equations 2.11 to 2.14), are represented in the matrix form for the linearized system. Let the non-linear damping be represented by C_{eq}^{z} in the bounce mode and C_{eq}^{θ} in the pitch mode. Then

$$\begin{bmatrix} M_o & 0 & 0 & 0 \\ 0 & M_s^z & 0 & 0 \\ 0 & 0 & M_g & 0 \\ 0 & 0 & 0 & J_\theta \end{bmatrix} \begin{Bmatrix} \ddot{z}_1 \\ \ddot{z}_s \\ \ddot{z}_g \\ \ddot{\theta}_1 \end{Bmatrix}$$

$$+ \begin{bmatrix} K_c & -K_c & 0 & 0 \\ -K_c & K_z+K_c & -K_z & -\alpha_2 K_z \\ 0 & -K_z & K_e+K_\theta+K_z & -\alpha_1 K_\theta+\alpha_2 K_z+\alpha_2 K_e \\ 0 & -\alpha_2 K_z & \alpha_2 K_z-\alpha_1 K_\theta+\alpha_2 K_e & \alpha_2^2 K_z+\alpha_1^2 K_\theta+\alpha_2^2 K_e \end{bmatrix} \begin{Bmatrix} z_1 \\ z_s \\ z_g \\ \theta_1 \end{Bmatrix}$$

$$+ \begin{bmatrix} C_c & -C_c & 0 & 0 \\ -C_c & C_c+C_{eq}^{z} & -C_{eq}^{z} & -\alpha_2 C_{eq}^{z} \\ 0 & -C_{eq}^{z} & C_{eq}^{z}+C_{eq}^{\theta} & \alpha_2 C_{eq}^{z}-\alpha_1 C_{eq}^{\theta} \\ 0 & -\alpha_2 C_{eq}^{z} & \alpha_2 C_{eq}^{z}-\alpha_1 C_{eq}^{\theta} & \alpha_2^2 C_{eq}^{z}+\alpha_1^2 C_{eq}^{\theta} \end{bmatrix} \begin{Bmatrix} \dot{z}_1 \\ \dot{z}_s \\ \dot{z}_g \\ \dot{\theta}_1 \end{Bmatrix}$$

$$= \begin{bmatrix} 0 & 0 \\ 0 & 0 \\ K_\theta + K_e & -\alpha_1 K_\theta + \alpha_2 K_e \\ -\alpha_1 K_\theta + \alpha_2 K_e & \alpha_1^2 K_\theta + \alpha_2^2 K_e \end{bmatrix} \begin{Bmatrix} z_o \\ \theta_o \end{Bmatrix} + \begin{bmatrix} 0 & 0 \\ 0 & 0 \\ C_{eq}^{\theta} & -\alpha_1 C_{eq}^{\theta} \\ -\alpha_1 C_{eq}^{\theta} & \alpha_1^2 C_{eq}^{\theta} \end{bmatrix} \begin{Bmatrix} \dot{z}_o \\ \dot{\theta}_o \end{Bmatrix} \quad (4.44)$$

Define,

$$w_z = z_1 - z_s$$

$$u_z = z_s - z_g - \alpha_2 \theta_1$$

$$v_z = z_g - z_o$$

$$u_\theta = \theta_1 - \theta_o$$

Substitute in equation (4.44) to obtain

$$\begin{bmatrix} M_0 & M_0 & M_0 & \alpha_2 M_0 \\ 0 & M_s^z & M_s^z & \alpha_2 M_s^z \\ 0 & 0 & M_g & 0 \\ 0 & 0 & 0 & J_\theta \end{bmatrix} \begin{Bmatrix} \ddot{w}_z \\ \ddot{u}_z \\ \ddot{v}_z \\ \ddot{u}_\theta \end{Bmatrix}$$

$$+ \begin{bmatrix} K_c & 0 & 0 & 0 \\ -K_c & K_z & 0 & 0 \\ 0 & -K_z & K_\theta + K_e & -\alpha_1 K_\theta + \alpha_2 K_e \\ 0 & -\alpha_2 K_z & \alpha_2 K_e - \alpha_1 K_\theta & \alpha_1^2 K_\theta + \alpha_2^2 K_e \end{bmatrix} \begin{Bmatrix} w_z \\ u_z \\ v_z \\ u_\theta \end{Bmatrix}$$

$$+ \begin{bmatrix} C_c & 0 & 0 & 0 \\ -C_c & C_{eq}^z & 0 & 0 \\ 0 & -C_{eq}^z & C_{eq}^{\theta} & -\alpha_1 C_{eq}^{\theta} \\ 0 & -\alpha_2 C_{eq}^z & -\alpha_1 C_{eq}^{\theta} & \alpha_1^2 C_{eq}^{\theta} \end{bmatrix} \begin{Bmatrix} \dot{w}_z \\ \dot{u}_z \\ \dot{v}_z \\ \dot{u}_\theta \end{Bmatrix}$$

$$= \begin{bmatrix} -M_0 & -\alpha_2 M_\theta \\ -M_s^z & -\alpha_2 M_s^z \\ -M_g & 0 \\ 0 & -J_\theta \end{bmatrix} \begin{Bmatrix} \ddot{z}_0 \\ \ddot{\theta} \end{Bmatrix} \tag{4.45}$$

The relative displacements across the damping elements are computed from the equations of motion, and the equivalent viscous damping coefficient may be computed from the dissipation of energy expressions:

$$C_{eq}^{z} = \frac{4F_z}{\pi\omega u_z} + \frac{8}{3\pi} C_z \omega u_z \tag{4.46}$$

and

$$C_{eq}^{\theta} = \frac{8}{3\pi} C_\theta \omega u_\theta \tag{4.47}$$

Simultaneous solution of equations (4.45), (4.46) and (4.47) for given bounce and pitch excitation amplitudes and excitation frequencies results in the equivalent viscous damping coefficients for the non-linear damping.

Roll Mode

The equations of motion of the roll motion are given in Chapter 2. (Equations (2.16) and (2.17)).

Define,

$$u_\phi = \phi_1 - \phi_f$$
$$v_\phi = \phi_f - \phi_0 \tag{4.48}$$

and replace velocity squared damping terms by their linear equivalent. The equations (2.16) and (2.17) are reduced to:

$$J_\phi(\ddot{u}_\phi + \ddot{v}_\phi) + K_\phi u_\phi + C_{eq}^{\phi} \dot{u}_\phi = - J_\phi \ddot{\phi}_0 \tag{4.49}$$

$$J_f \ddot{v}_\phi - K_\phi u_\phi - C_{eq}^{\phi} \dot{u}_\phi + K_e \beta^2 v_\phi = - J_f \ddot{\phi}_0 \tag{4.50}$$

In the matrix form,

$$\begin{bmatrix} J_\phi & J_\phi \\ 0 & J_f \end{bmatrix} \begin{Bmatrix} \ddot{u}_\phi \\ \ddot{v}_\phi \end{Bmatrix} + \begin{bmatrix} K_\phi & 0 \\ -K_\phi & K_e\beta^2 \end{bmatrix} \begin{Bmatrix} u_\phi \\ v_\phi \end{Bmatrix}$$

$$+ \begin{bmatrix} C_{eq}^{\phi} & 0 \\ -C_{eq}^{\phi} & 0 \end{bmatrix} \begin{Bmatrix} \dot{u}_\phi \\ \dot{v}_\phi \end{Bmatrix} = \begin{bmatrix} -J_\phi \\ -J_f \end{bmatrix} \{\ddot{\phi}_0\} \qquad (4.51)$$

The relative displacements across the damper are computed from Equation (4.51) and the equivalent viscous damping coefficient is computed from the dissipation of energy as:

$$C_{eq}^{\phi}(\omega, u_\phi) = \frac{8}{3\pi} C_\phi \omega u_\phi \qquad (4.52)$$

Simultaneous solution of equation (4.51) and (4.52) results in the frequency dependent linear equivalent of the non-linear system.

4.5 VERIFICATION OF FREQUENCY DEPENDENT LINEARIZATION

The transmissibility characteristics obtained for the linear equivalent system (using frequency dependent linearization) are compared to the steady state transmissibility response computed through numerical integration techniques. The effectiveness of the frequency dependent linearization technique is verified for harmonic as well as stochastically described excitations.

4.5.1 NON-LINEAR SEAT SUSPENSIONS SUBJECT TO HARMONIC EXCITATIONS

Absolute and relative transmissibility responses are evaluated for the non-linear and the linear equivalent seat suspension models in the frequency range of interest. Influence of excitation amplitudes, magnitude of Coulomb friction force and the magnitude of velocity squared damping on the effectiveness of frequency dependent linearization is demonstrated

in the following sections.

1. SDOF LONGITUDINAL/LATERAL SEAT ISOLATOR

Figures 4.1 and 4.2 present the influence of excitation amplitude on the lock up behaviour of the linear equivalent system. An increase in excitation amplitude causes the breakaway at relatively lower frequency. Non-linear system solution in the time domain verifies the transmissibility response of the linear equivalent system. Transmissibility characteristics of the linear equivalent system with varying magnitude of Coulomb friction are shown in Figures 4.3 and 4.4 . Figures 4.5 and 4.6 show the linear equivalent system response for various coefficients of velocity squared damping.

2. 2-DOF BOUNCE SEAT SUSPENSION MODEL

Transmissibility characteristics of the bounce suspension seat for different excitation amplitudes are presented in Figures 4.7 to 4.10 . Figures 4.7 and 4.8 present a comparison of transmissibility response of the linear equivalent system to that of the non-linear system. Figure 4.9 shows the break-away frequency of the suspension mass corresponding to excitation amplitude. Influence of Coulomb friction magnitude is demonstrated in the transmissibility characteristics of Figures 4.11 to 4.13 . An increase in magnitude of Coulomb friction indicates a larger breakaway frequency of the suspension mass.

3. ROTATIONAL SEAT SUSPENSION MODEL

Bounce, pitch, and roll response transmissibility characteristics of the rotational seat suspension model are obtained using the energy dissipation approach and compared with the response obtained

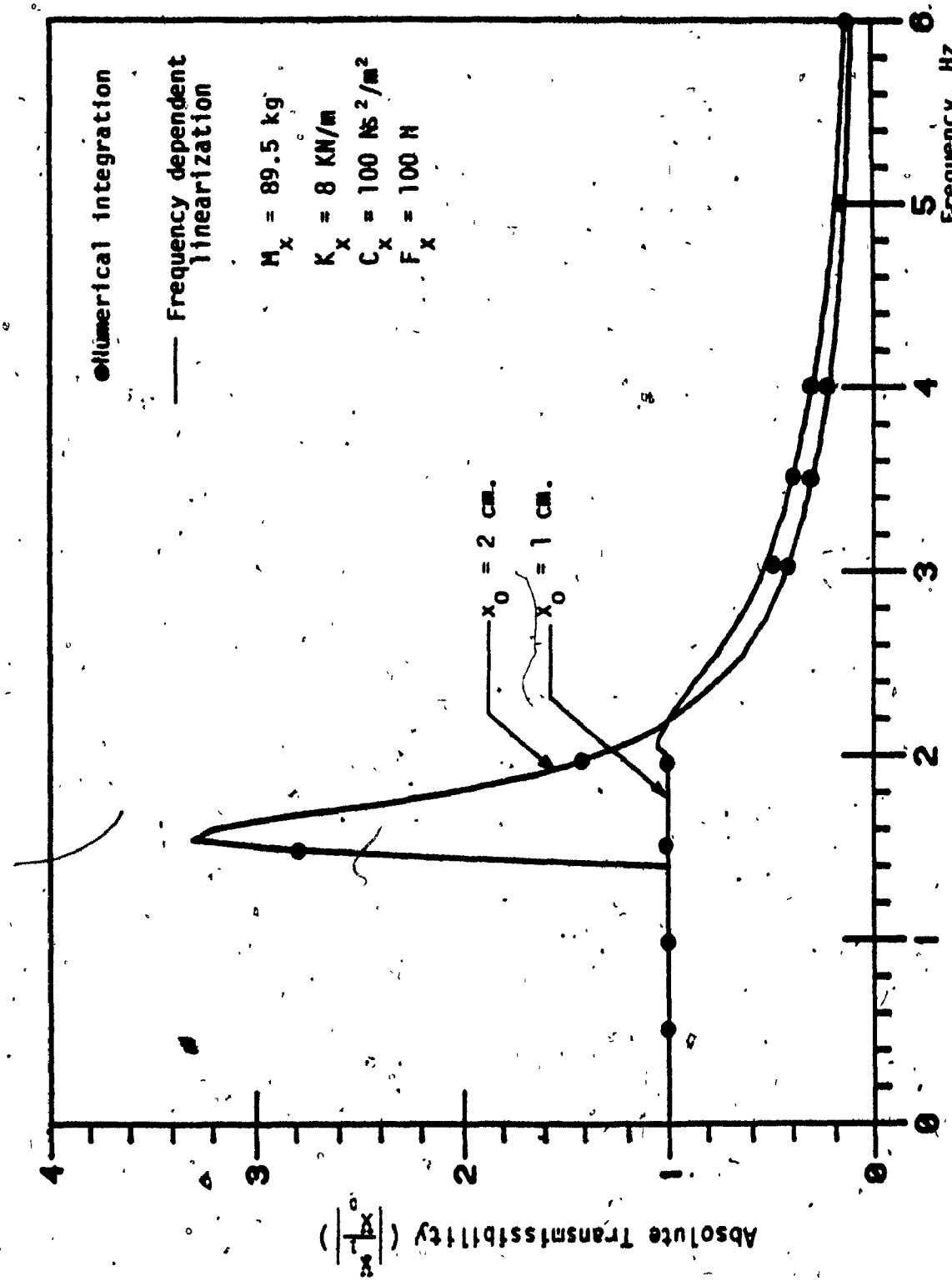

FIGURE 4.1: Absolute transmissibility response of SDOF longitudinal isolator subject to constant amplitude harmonic excitation.

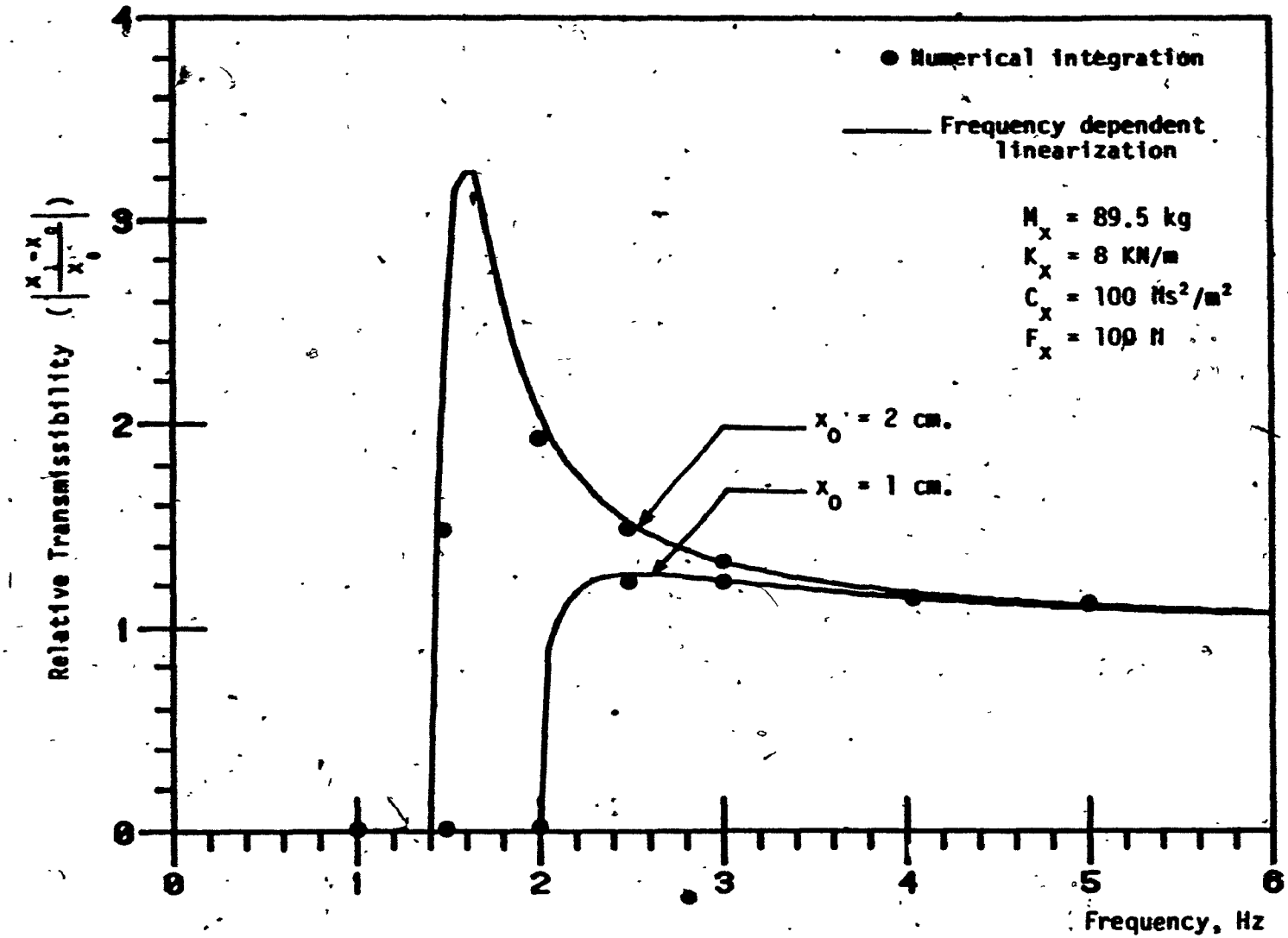

FIGURE 4.2: Relative transmissibility response of SDOF longitudinal seat isolator subject to constant amplitude harmonic excitation.

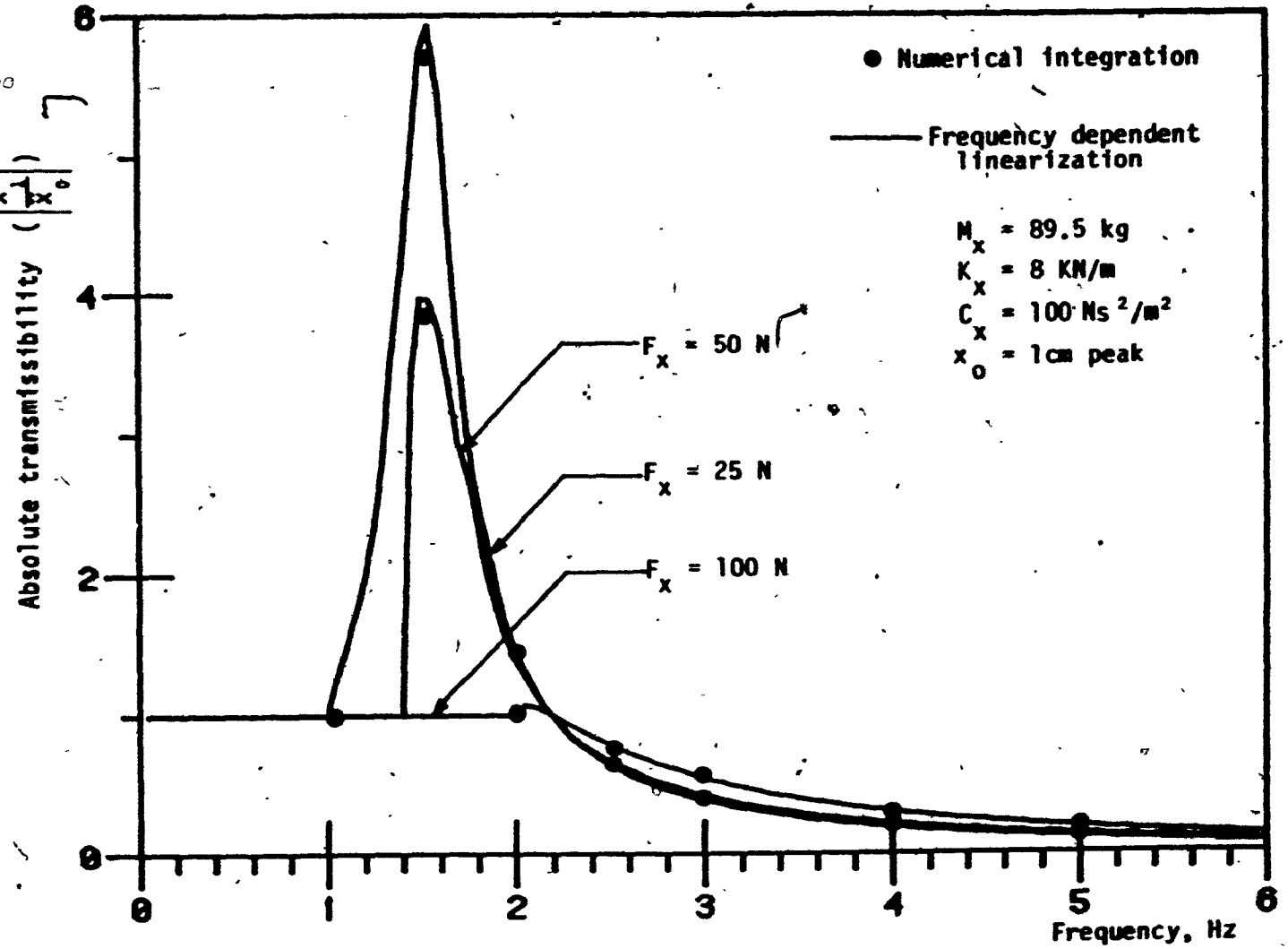

FIGURE 4.3: Absolute transmissibility characteristics of SDOF longitudinal isolator for various magnitudes of Coulomb friction.

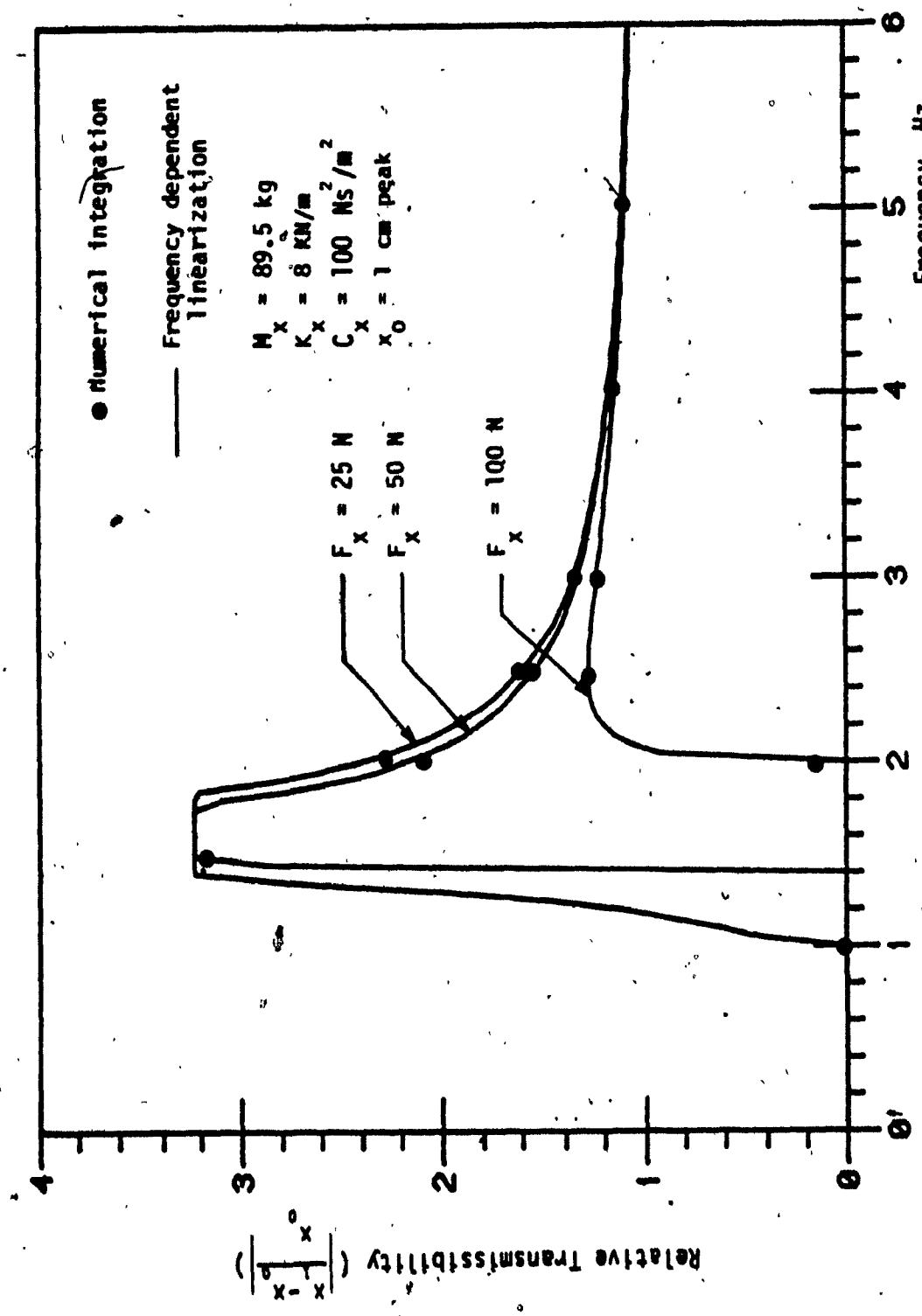

FIGURE 4.4: Relative transmissibility characteristics of longitudinal seat isolator for various magnitudes of Coulomb friction.

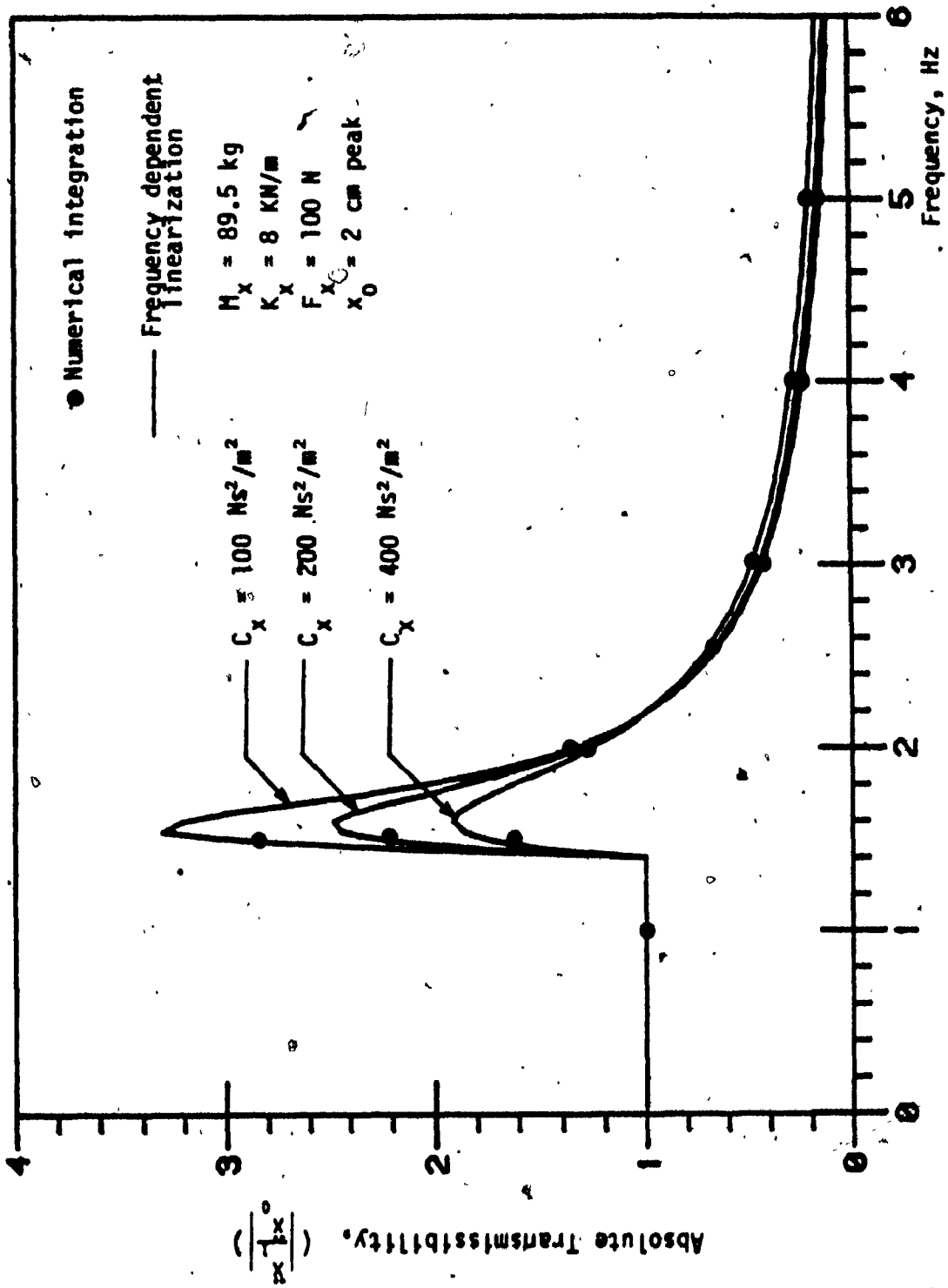

FIGURE 4.5: Absolute transmissibility characteristics of longitudinal seat isolator for various values of the velocity squared damping coefficient.

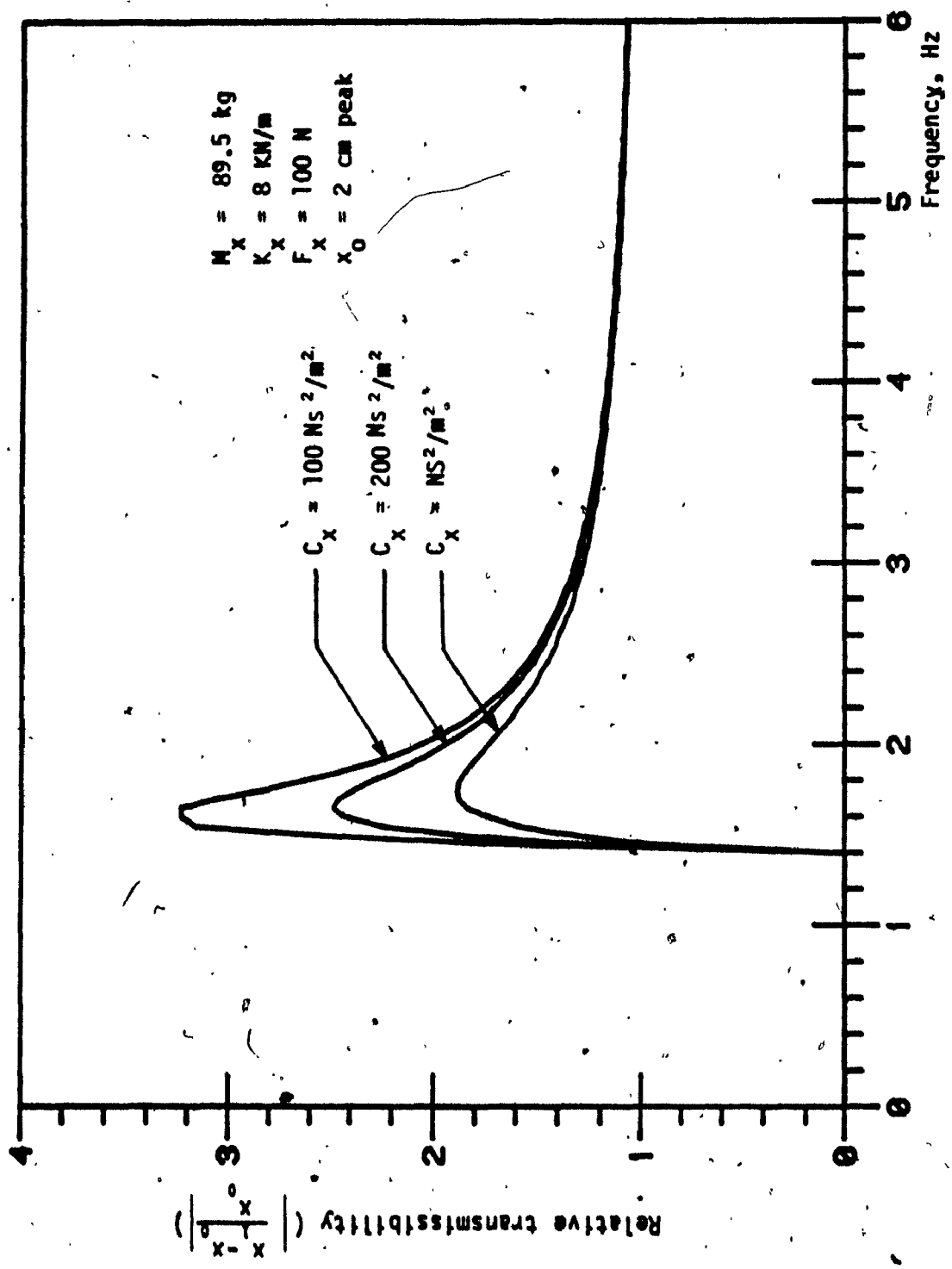

FIGURE 4.6: Relative transmissibility characteristics of the linearized longitudinal seat isolator for various values of velocity squared damping coefficient.

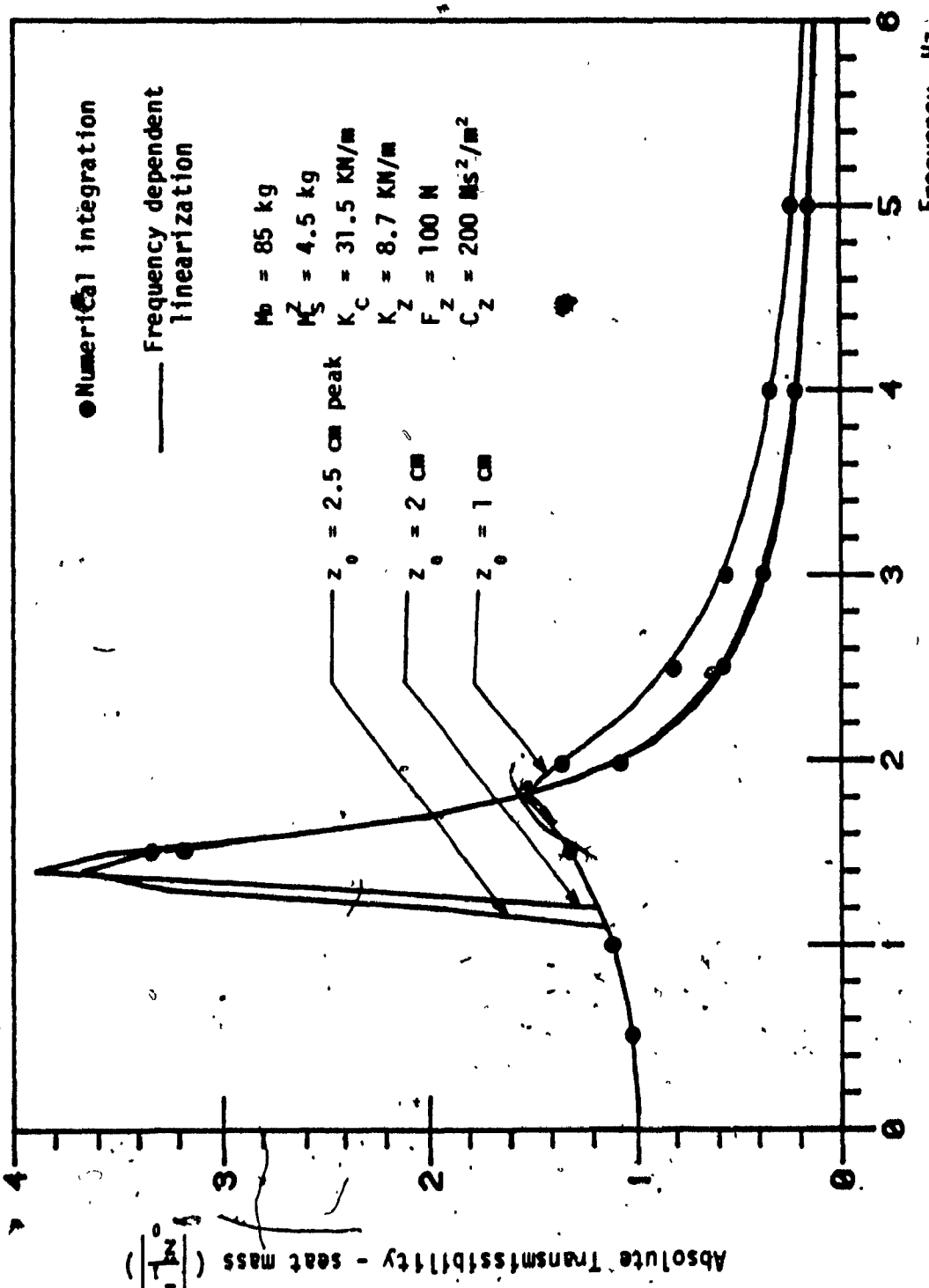

FIGURE 4.7: Absolute transmissibility characteristics of the bounce seat suspension for various amplitudes of harmonic excitation.

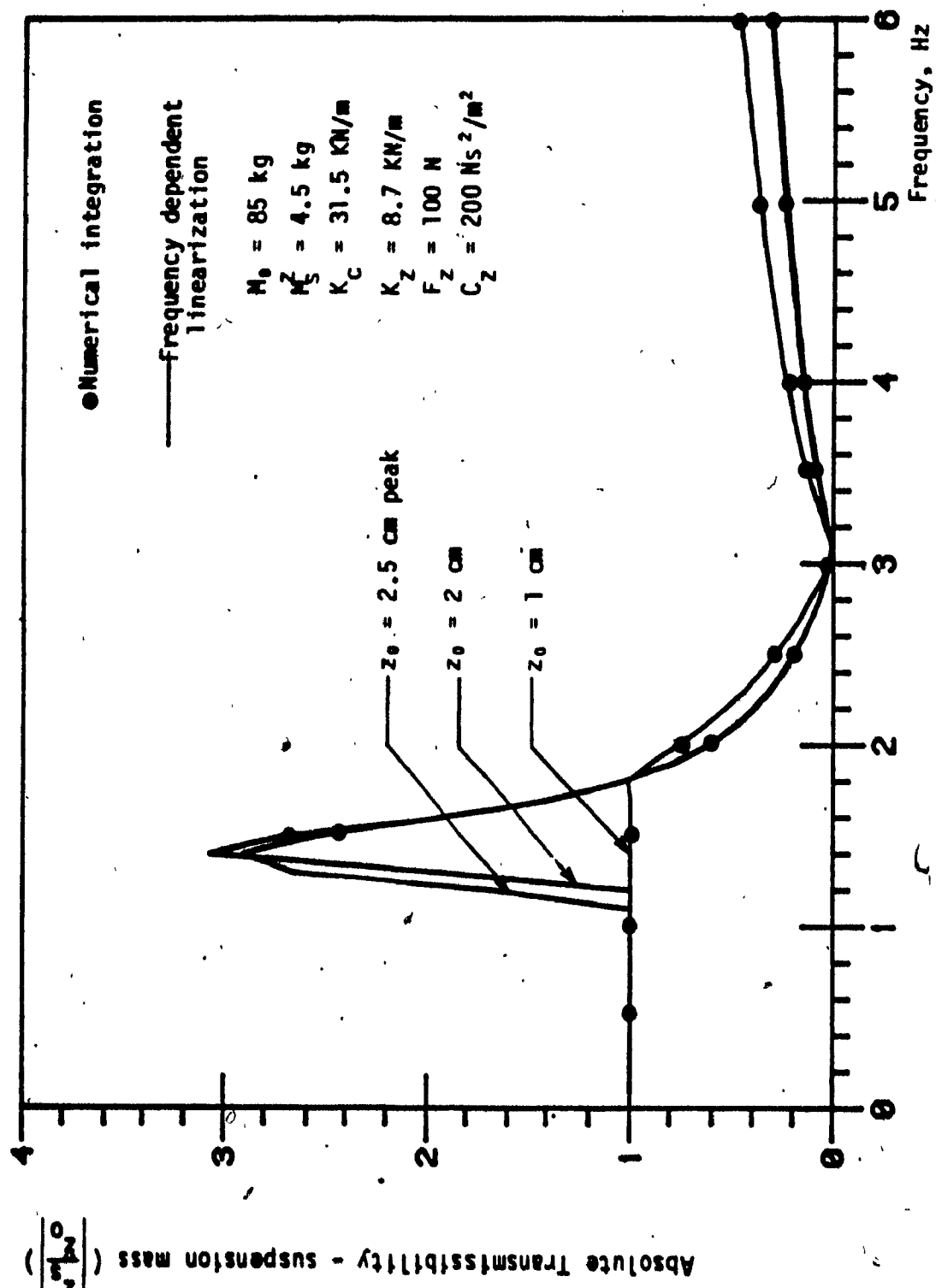

FIGURE 4.8: Absolute transmissibility characteristics of bounce suspension seat for various amplitudes of harmonic excitation.

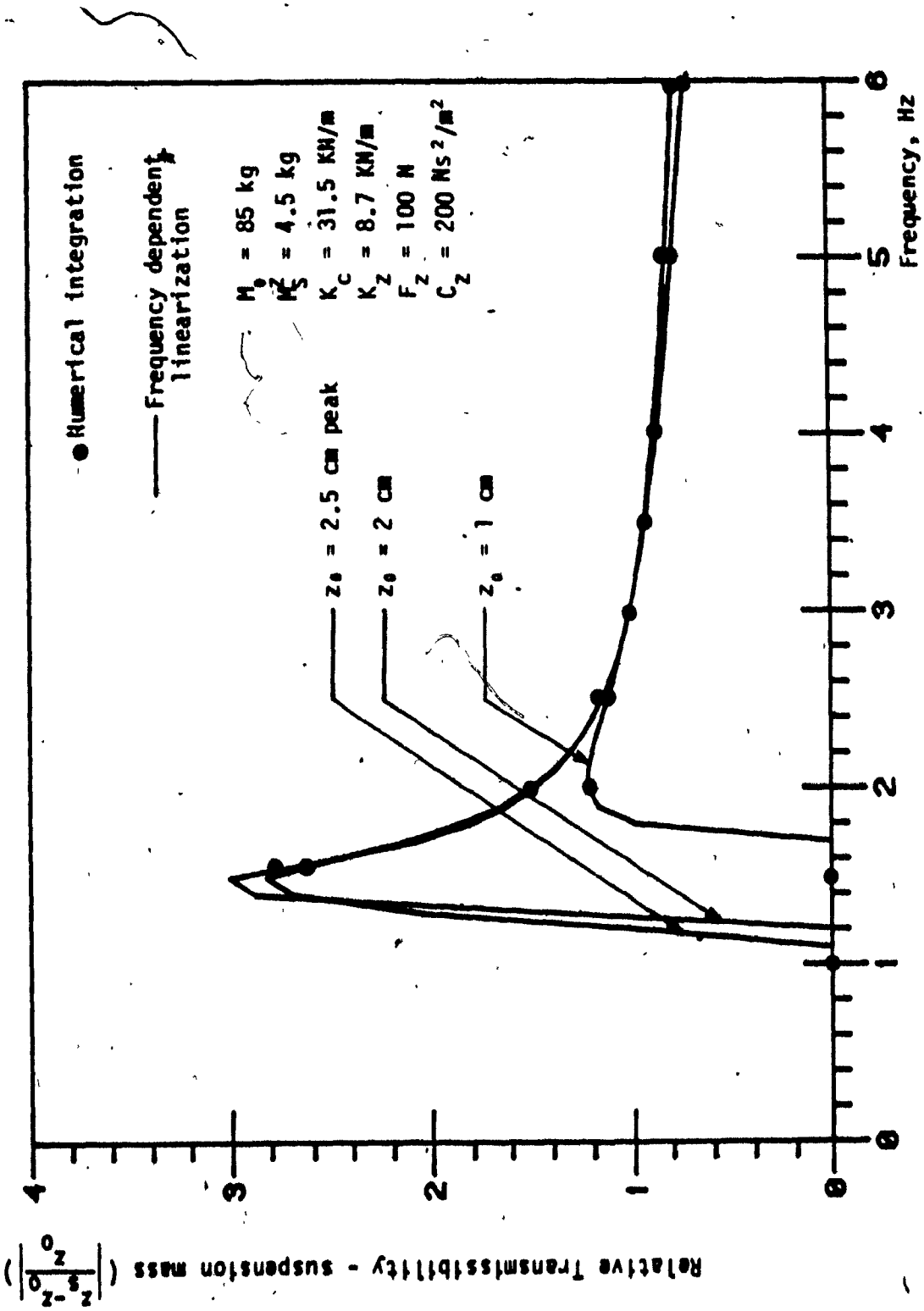

FIGURE 4.9: Relative transmissibility characteristics of bounce suspension seat for various amplitudes of harmonic excitation.

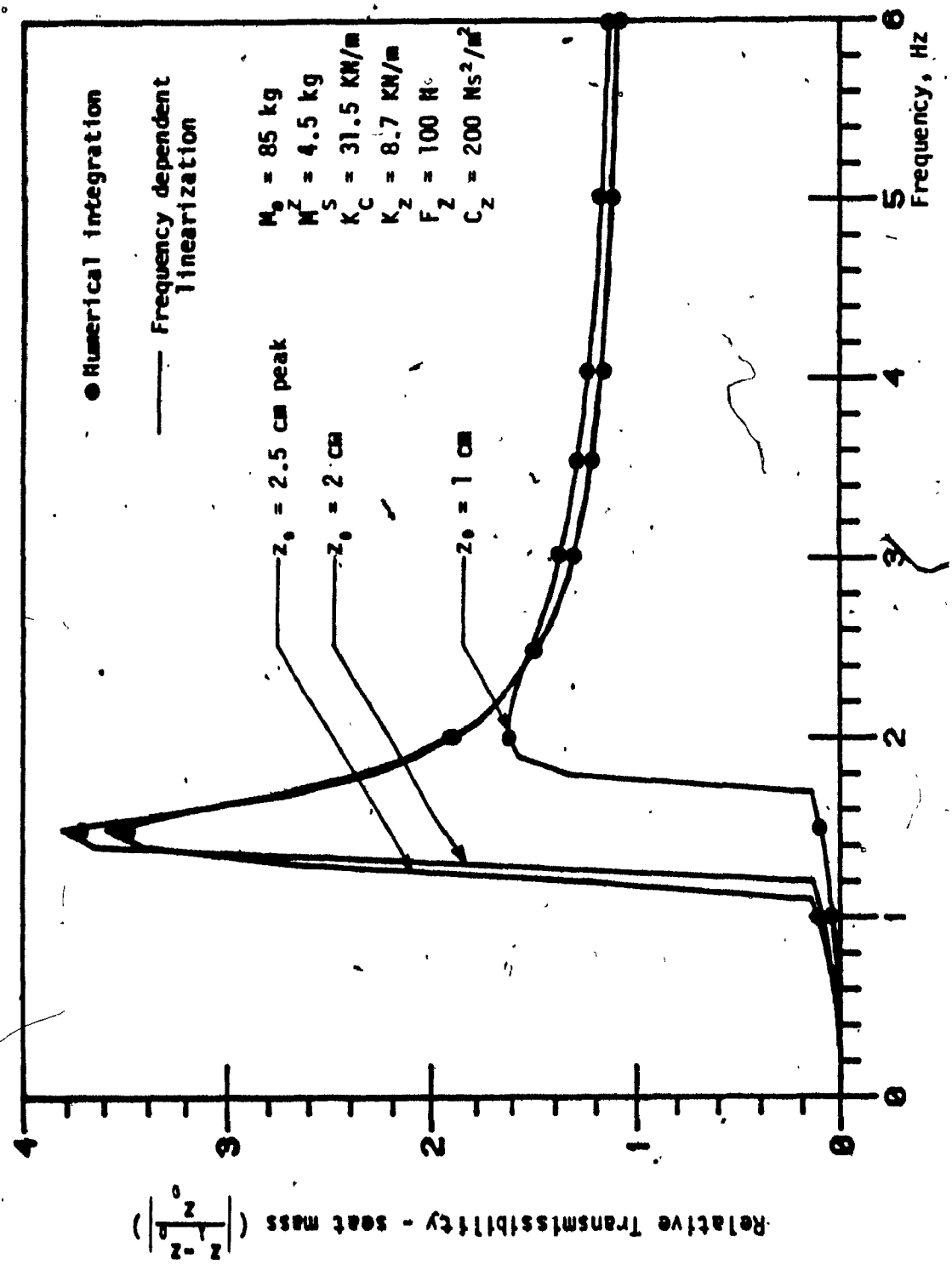

FIGURE 4.10: Relative transmissibility characteristics of bounce suspension seat for various amplitudes of harmonic excitation.

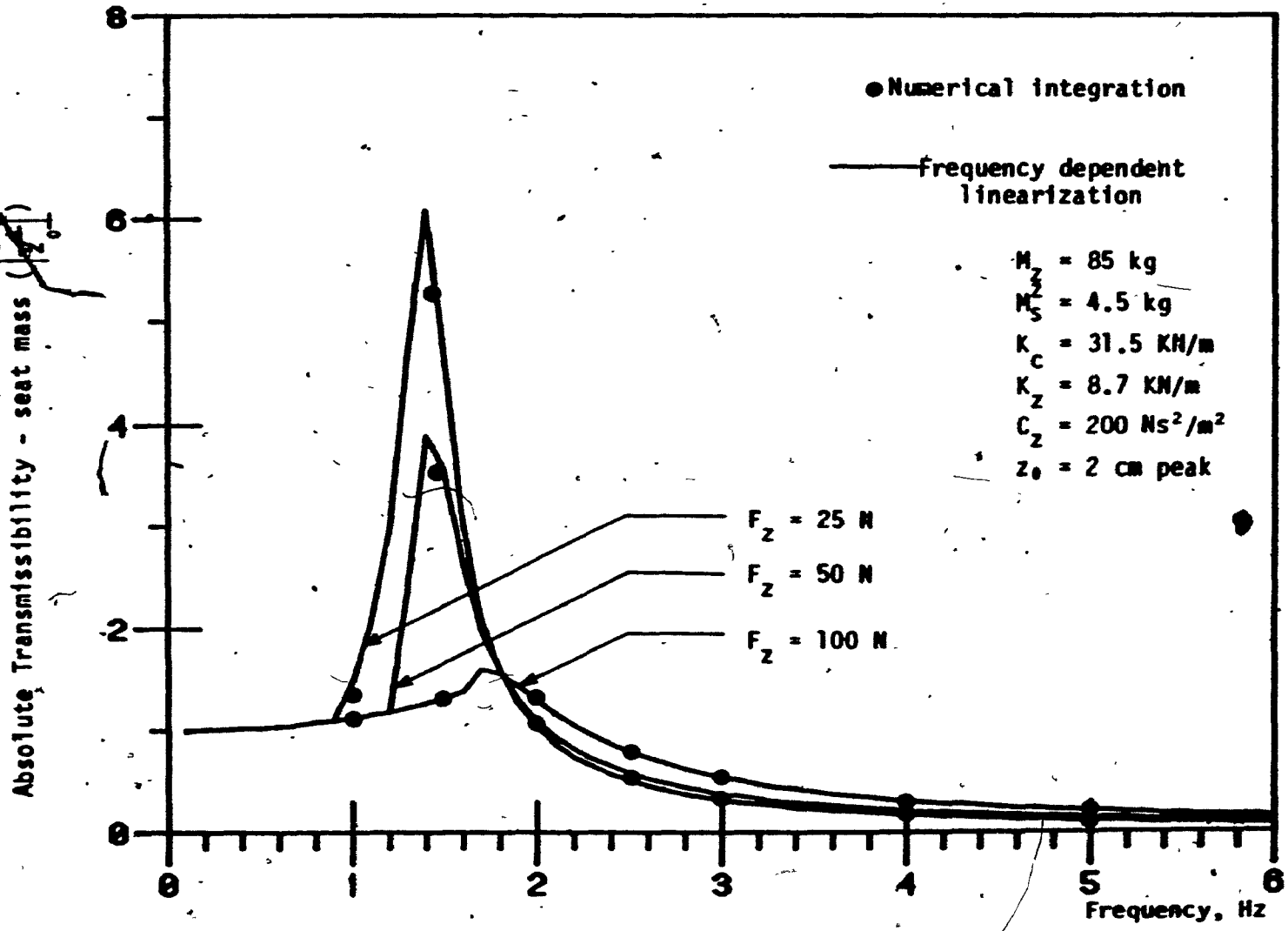

FIGURE 4.11: Absolute transmissibility characteristics of bounce suspension seat for various magnitudes of Coulomb friction.

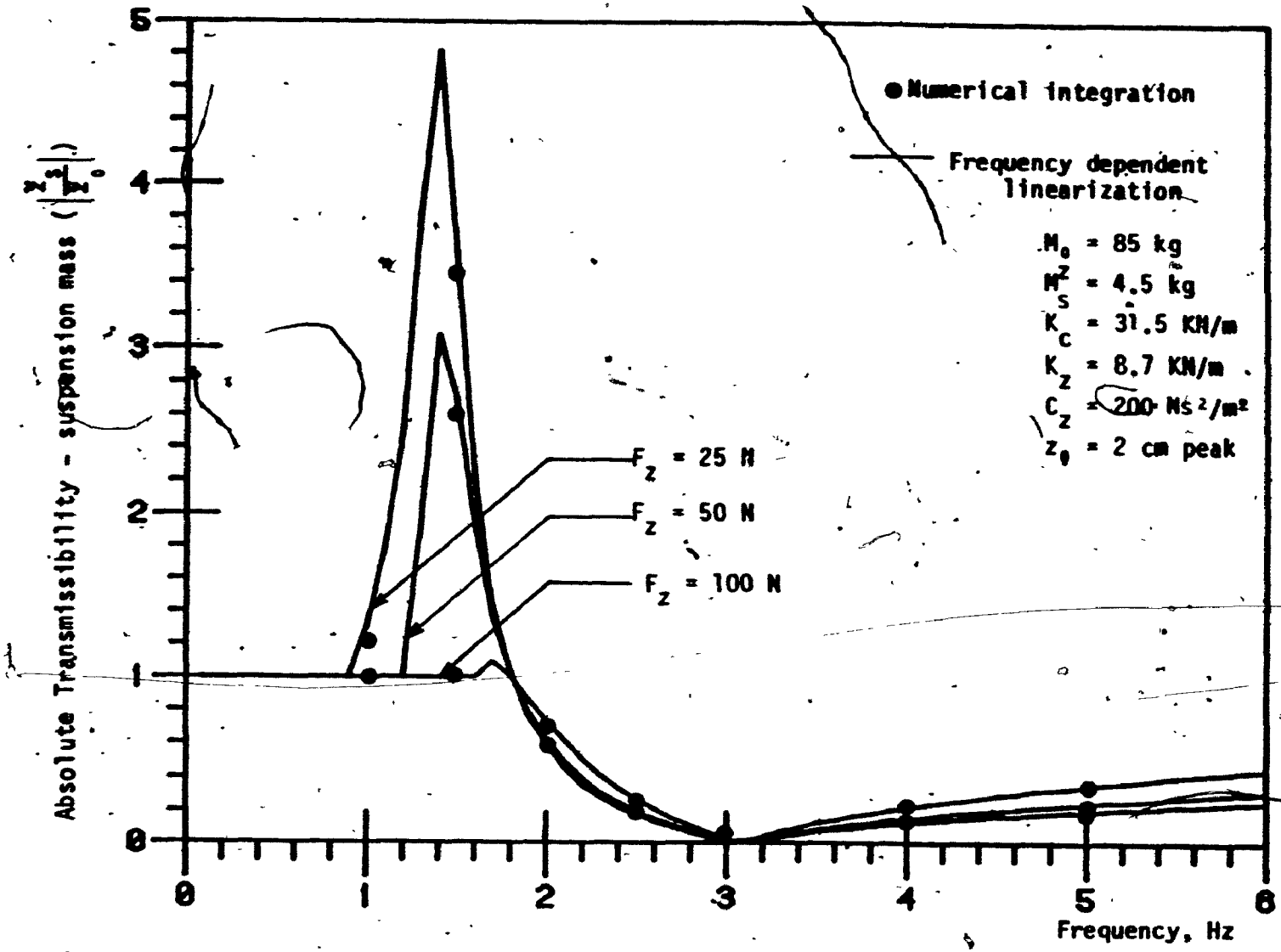

FIGURE 4.12: Absolute transmissibility characteristics of bounce suspension seat for various magnitudes of Coulomb friction.

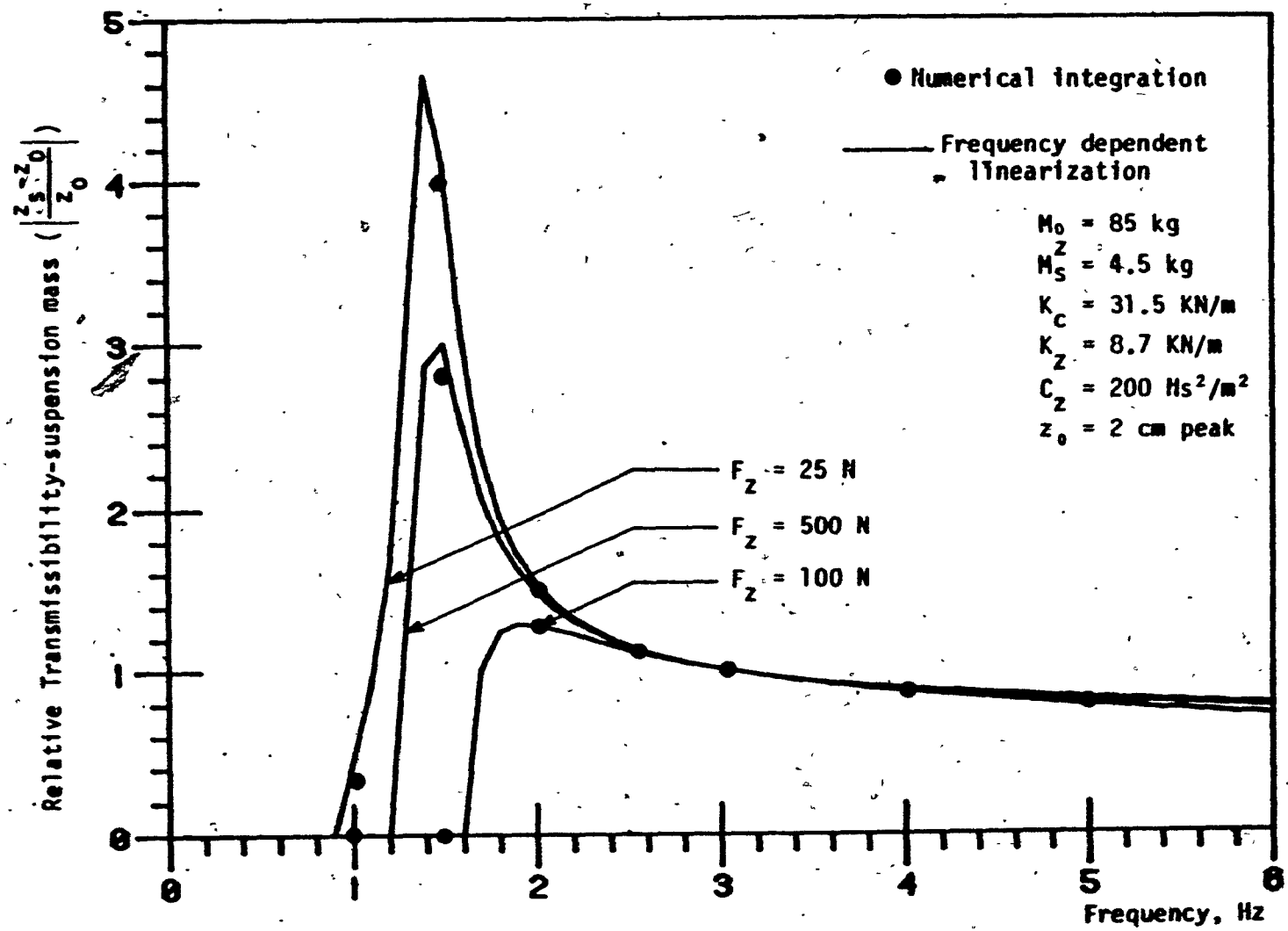

FIGURE 4.13: Relative transmissibility characteristics of bounce suspension seat for various magnitudes of Coulomb friction.

through the numerical integration of the equations of motion characterizing the non-linear system. Figures 4.14 and 4.15 present a comparison of the bounce and pitch responses obtained via the two techniques, respectively. The roll response of the rotational seat isolator is presented in Figures 4.16 and 4.17. Figure 4.16 shows the comparison between the two responses obtained via numerical integration and by frequency dependent linearization of the non-linear system.

4.5.2 STOCHASTICALLY DESCRIBED EXCITATIONS

The frequency dependent linearization technique is verified for the stochastically described excitations, using equations (4.32), (4.33), and (4.34). The power spectral density response of the linearized system is generated using frequency domain analytical techniques described in section 4.2.2. The PSD response of the linearized system is compared with the PSD response of the non-linear system, which is computed using the Fast Fourier transform of the numerical integration results. The two computation schemes are outlined in Figure 4.18 . Figures 4.19 and 4.20 present the acceleration power spectral density response of longitudinal and bounce seat suspensions obtained via schemes A and B of Figure 4.18 . The scheme A utilizes frequency dependent linearization techniques described in section 4.3, the scheme B is associated with numerical integration of non-linear equations of motion. The scheme B required a computation time of 170 s on Cyber 170 for evaluating the PSD response of SDOF longitudinal isolator compared to 1.1s required by scheme A. The results obtained by two schemes show a reasonable agreement.

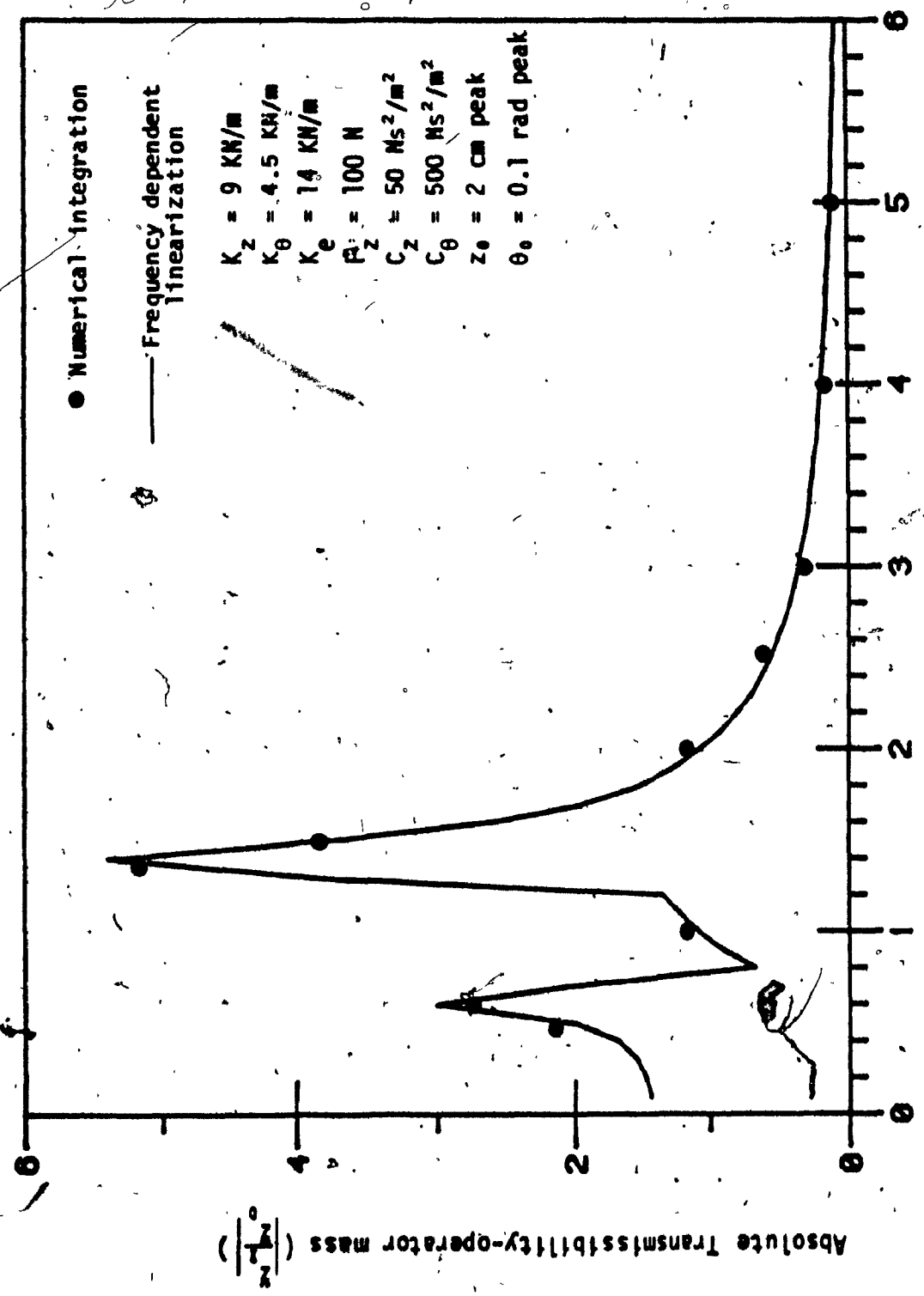

FIGURE 4.14: Absolute bounce transmissibility characteristics of rotational seat subject to constant amplitude harmonic excitation.

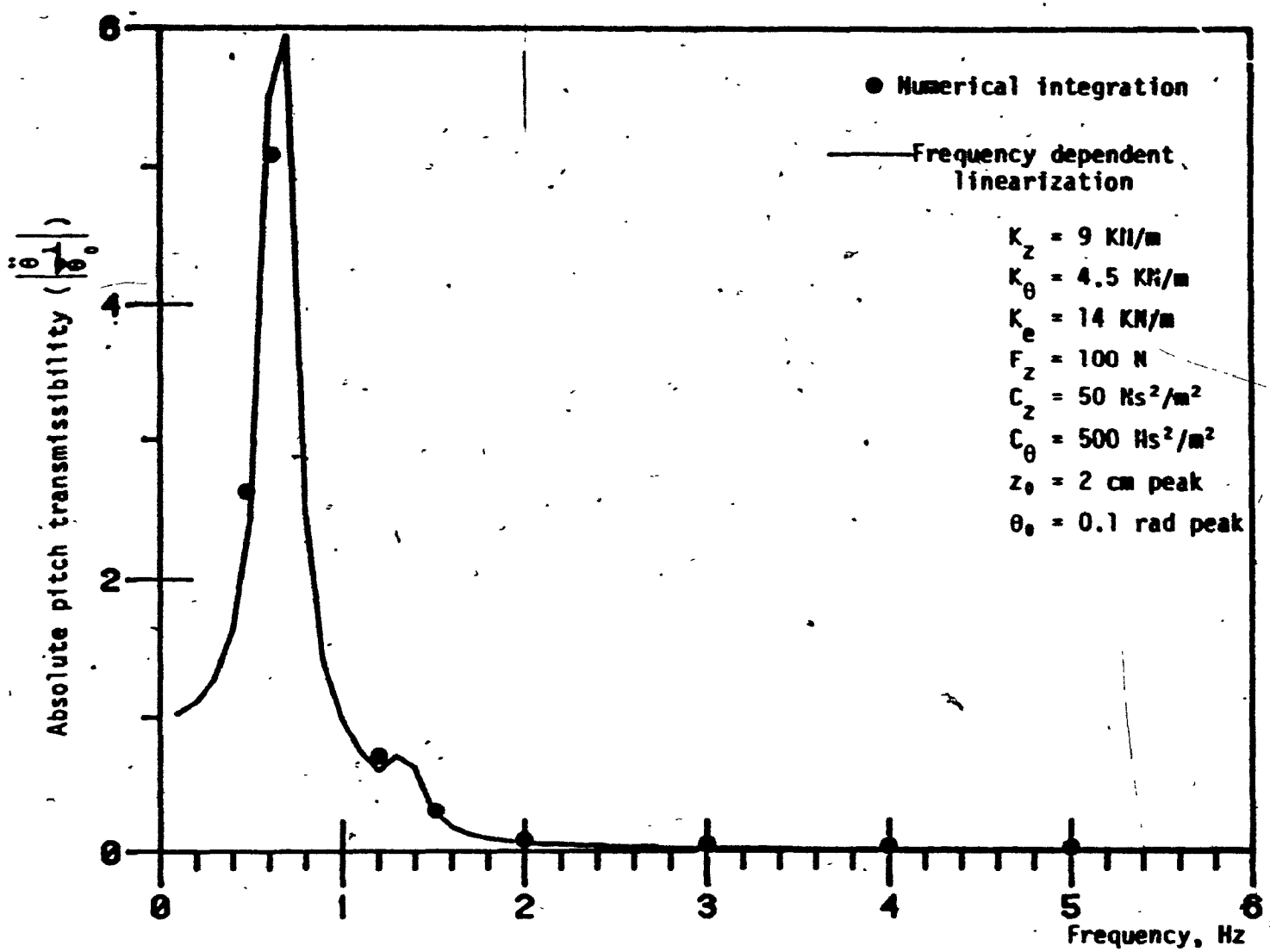

FIGURE 4.15: Absolute pitch transmissibility characteristics of rotational seat isolator subject to constant amplitude harmonic excitation.

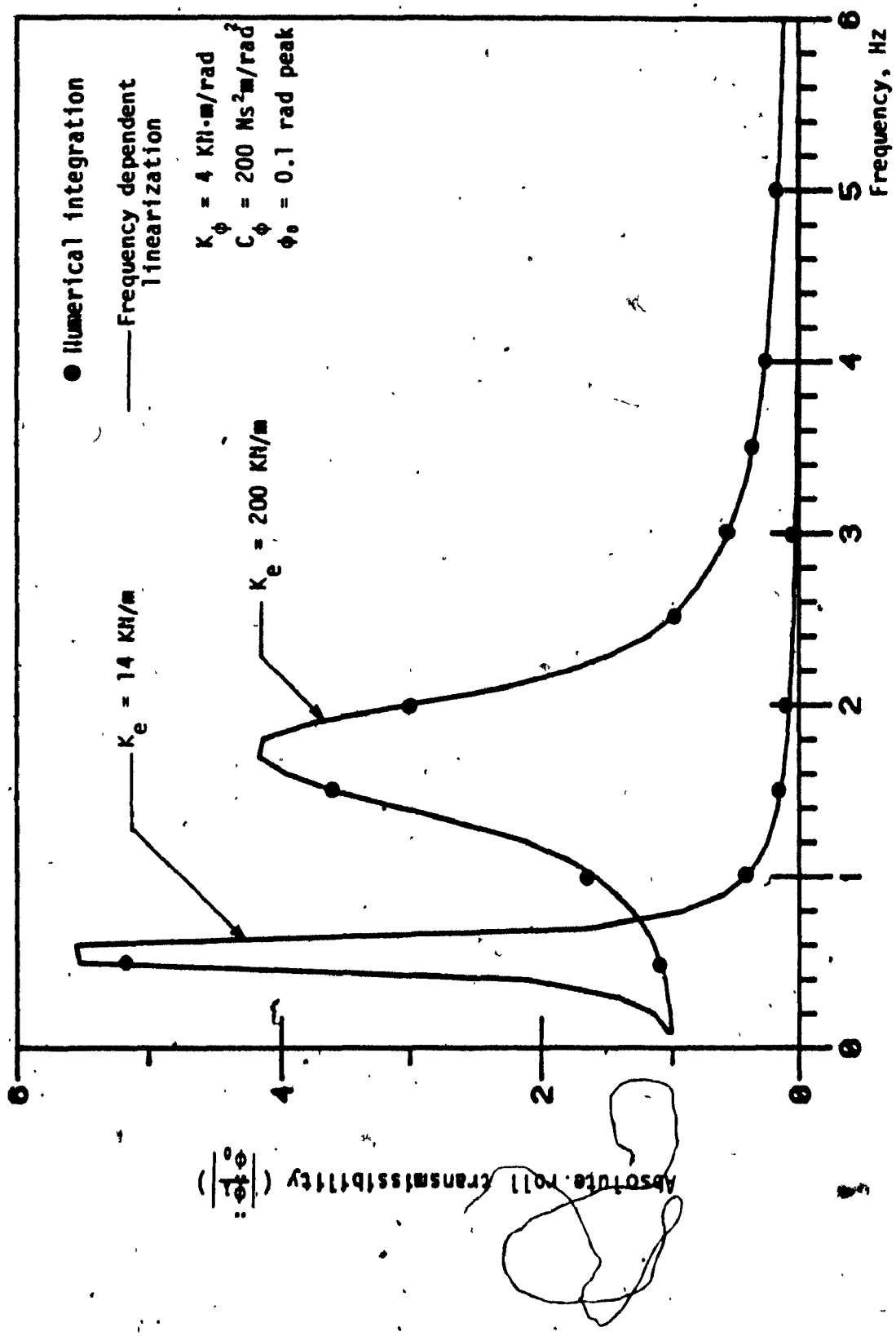

FIGURE 4.16: Absolute roll transmissibility characteristics of rotational seat isolator subject to harmonic excitation.

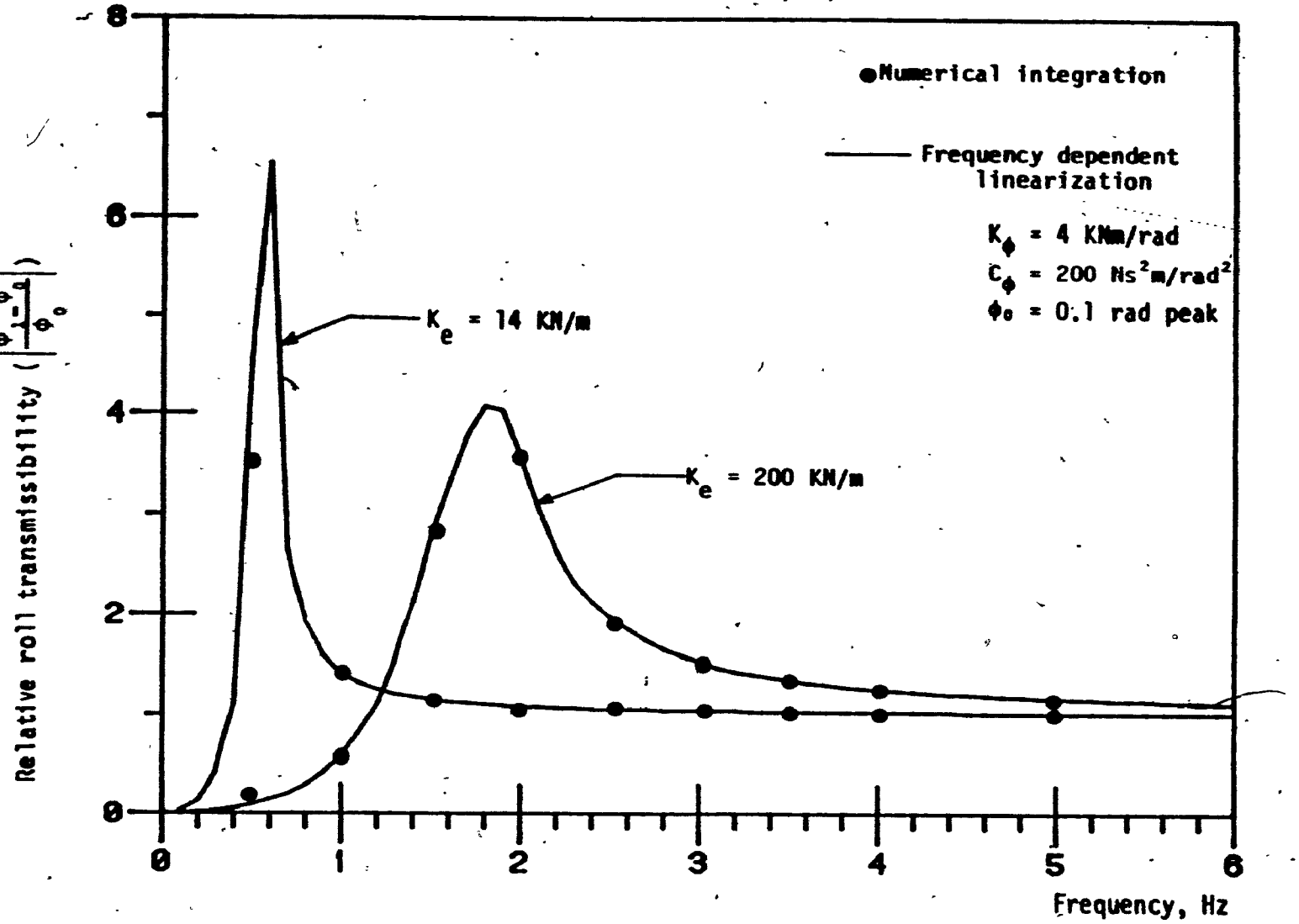

FIGURE 4.17: Relative roll transmissibility characteristics of the rotational seat isolator subject to constant amplitude harmonic excitation.

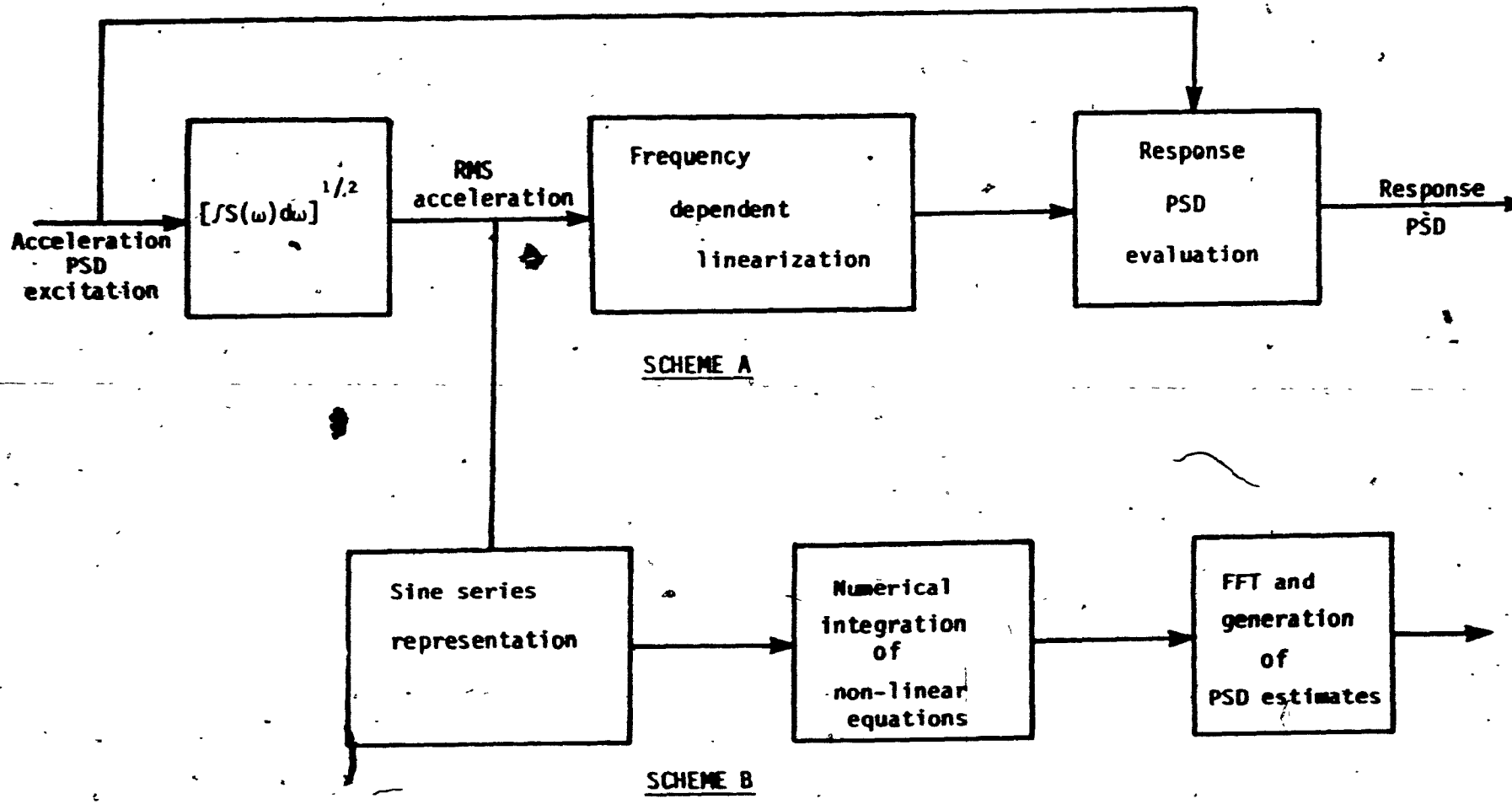

FIGURE 4.18: Response PSD evaluation of non-linear seat suspension models using frequency dependent linearization (Scheme A), and numerical integration (Scheme B) techniques.

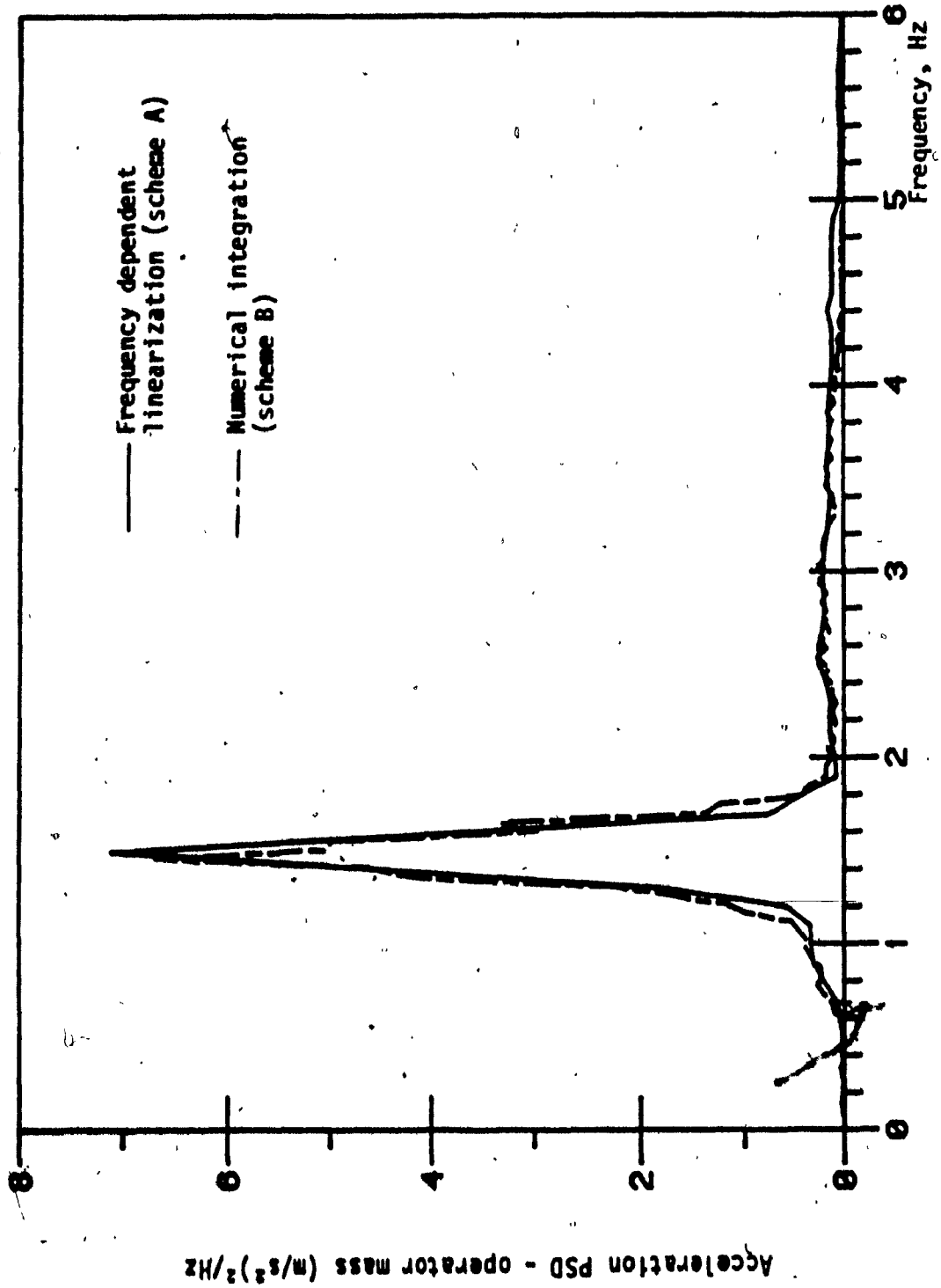

FIGURE 4.19: Acceleration PSD response of longitudinal seat isolator.

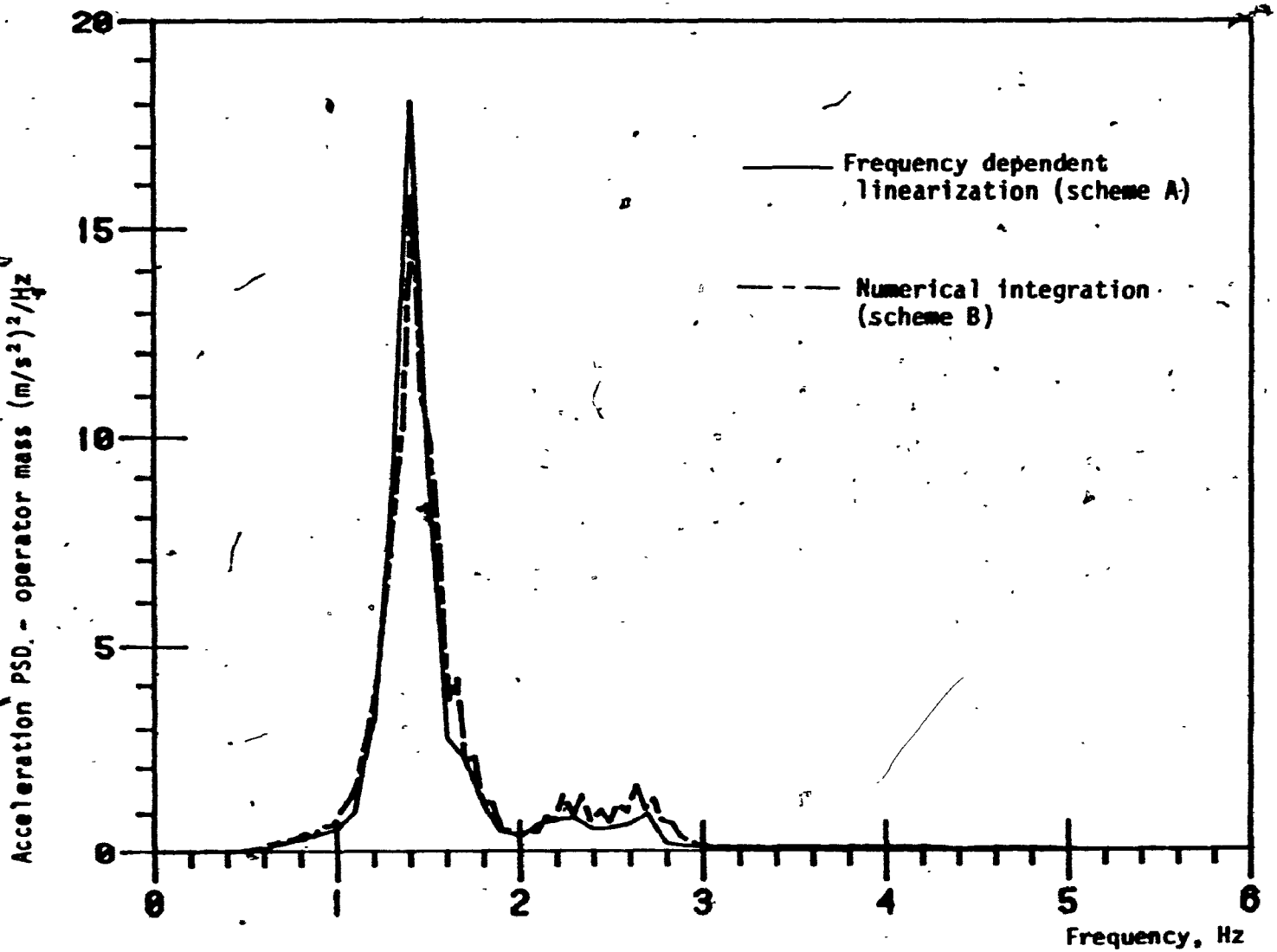

FIGURE 4.20: Acceleration PSD response of bounce seat isolator.

4.6 SUMMARY

In this chapter, the analytical technique used to predict the ride performance of suspension models are discussed. A frequency dependent linearization technique based on dissipation of energy from the non-linear dissipative elements is developed to solve the non-linear seat-suspension models. Simulation results are obtained for the non-linear suspension models using numerical integration techniques and frequency dependent linearization techniques. The results obtained using the two techniques are compared to demonstrate the effectiveness of frequency dependent linearization technique.

CHAPTER 5

PARAMETRIC STUDY OF SUSPENSION MODELS

5.1 INTRODUCTION

The agricultural terrain irregularities characterized by power spectral densities indicate severe vibrations of the vehicle at low frequencies. The vehicle resonance occurs at frequencies as low as 2.6 Hz in the bounce mode, 1.5 to 3.5 Hz in the longitudinal and pitch modes, 1 Hz in the roll and lateral modes. The severe vibrations at such low frequencies can be isolated by introducing low natural frequency suspension systems. However, soft suspensions provide excellent vibration isolation at the expense of excessive static and dynamic motion of the driver with reference to the controls. A better understanding of the suspension performance under such conditions can be accomplished only through parameter sensitivity studies of the suspension. The parametric study would describe the sensitivity of suspension performance, *viz*, acceleration and relative displacement responses to changes in various suspension parameters.

In order to investigate the parameter sensitivity, a performance index as a function of acceleration or relative motion response should be selected to represent truly the performance of the suspension systems. The performance index may be chosen either as the peak value of the steady state response or as the response spectra over the frequency range of interest. The response PSD over a frequency range provides a better basis for comparing the suspension performance with respect to the ISO specified *fatigue decreased proficiency* limits. In this chapter the performance index for the passive seat and cab suspensions is selected to be the acceleration PSD of the driver mass in order to evaluate the parameter sensitivity of the ride quality in comparison with ISO specified limits.

5.2 OBJECTIVES

A detailed parametric study is presented in this chapter utilizing the response power spectral densities obtained from the solution of passive seat suspension and cab suspension models. The study involves finding the effects of variation of each suspension parameter independently when subject to the Silsoe track input acceleration PSD's. The parametric study results indicate a trend in the behaviour of various suspension parameters on the response and provide a basis for further investigations involving multivariable optimization techniques. Through such optimization procedures, it would be possible to find the optimum combination of the suspension elements that would maintain the acceleration PSD of the human mass within the ISO specified limits, while constraining the relative displacement of the driver mass with respect to the cab floor to a minimum possible.

5.3 PARAMETRIC STUDY OF THE SUSPENSION MODELS

Sensitivity of the suspension performance index to variations in a single parameter at a time is studied in order to determine the near optimum suspension parameters which would maintain the acceleration response of the human mass in accordance with the ISO specified *fatigue decreased proficiency* limits. Specifically, the influence of the damping coefficients, Coulomb damping forces, and the stiffness of the springs on the suspension performance index are studied in detail.

5.3.1 INFLUENCE OF VARIATIONS IN SUSPENSION PARAMETERS ON THE PERFORMANCE OF PASSIVE TRANSLATIONAL SEAT SUSPENSION MODEL

Sensitivity of the suspension performance index to variations in parameters like cushion stiffness, suspension stiffness, Coulomb damping and shock absorber damping is investigated in this section. Various conclusions are drawn to form a basis for formulating a multivariable

optimization problem. Due to the uncoupled nature of the translational seat-suspension model, the parameter sensitivity of bounce, longitudinal, and lateral seat suspension performance is presented, independently.

1) Passive Bounce Seat Suspension

The sensitivity of the performance of bounce seat suspension to variations in cushion stiffness, suspension stiffness, Coulomb damping force and coefficient of velocity squared damping is investigated. The sensitivity of the acceleration response to variations in cushionstiffness is demonstrated in Figure 5.1. The acceleration PSD response reveals that a softer cushion tends to lower the seat resonant frequency with a significantly large acceleration of the human mass. A softer cushion also leads to large relative displacements of the human mass with respect to the cab floor.

The influence of suspension stiffness, coefficient of damping and Coulomb damping force on bounce suspension performance is presented in Figures 5.2 to 5.4. A stiffer suspension tends to increase natural frequency of the isolator with significantly lower resonance response. However, increased stiffness shows slight deterioration of suspension performance in the isolation region. An increase in coefficient of velocity squared damping suppresses the resonance peak significantly as shown in Figure 5.3. A further decrease in magnitude of resonance peak is observed with increased Coulomb damping force as presented in Figure 5.4. However large Coulomb friction reveals a deterioration in suspension performance in the isolation region.

2) Longitudinal Seat Suspension

Sensitivity of suspension performance index to variations in suspension parameters is demonstrated by the response plots in Figures 5.5 to 5.7. Since the vehicle resonance in the longitudinal mode occurs

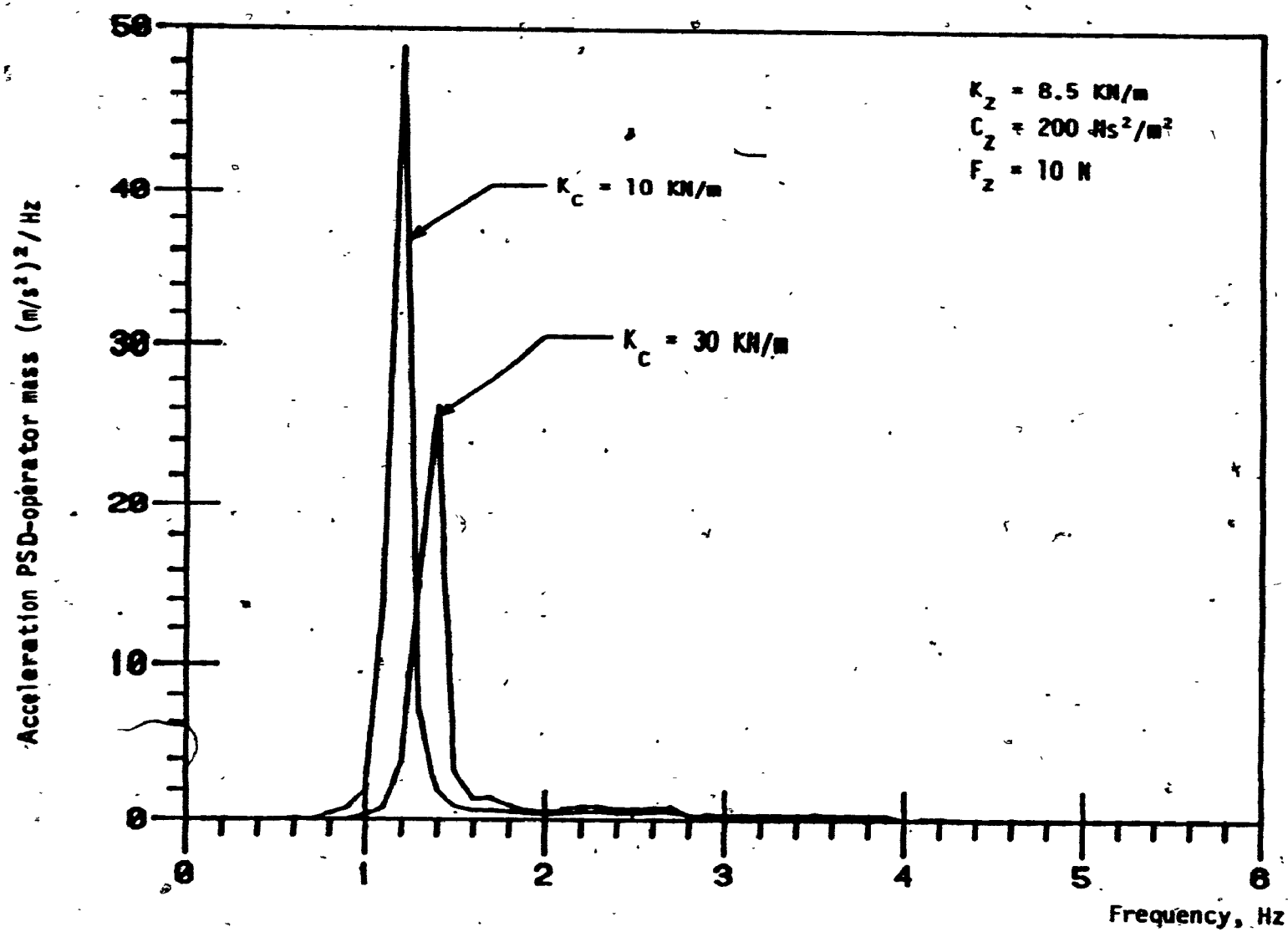

FIGURE 5.1: Influence of cushion stiffness on the performance of bounce suspension seat.

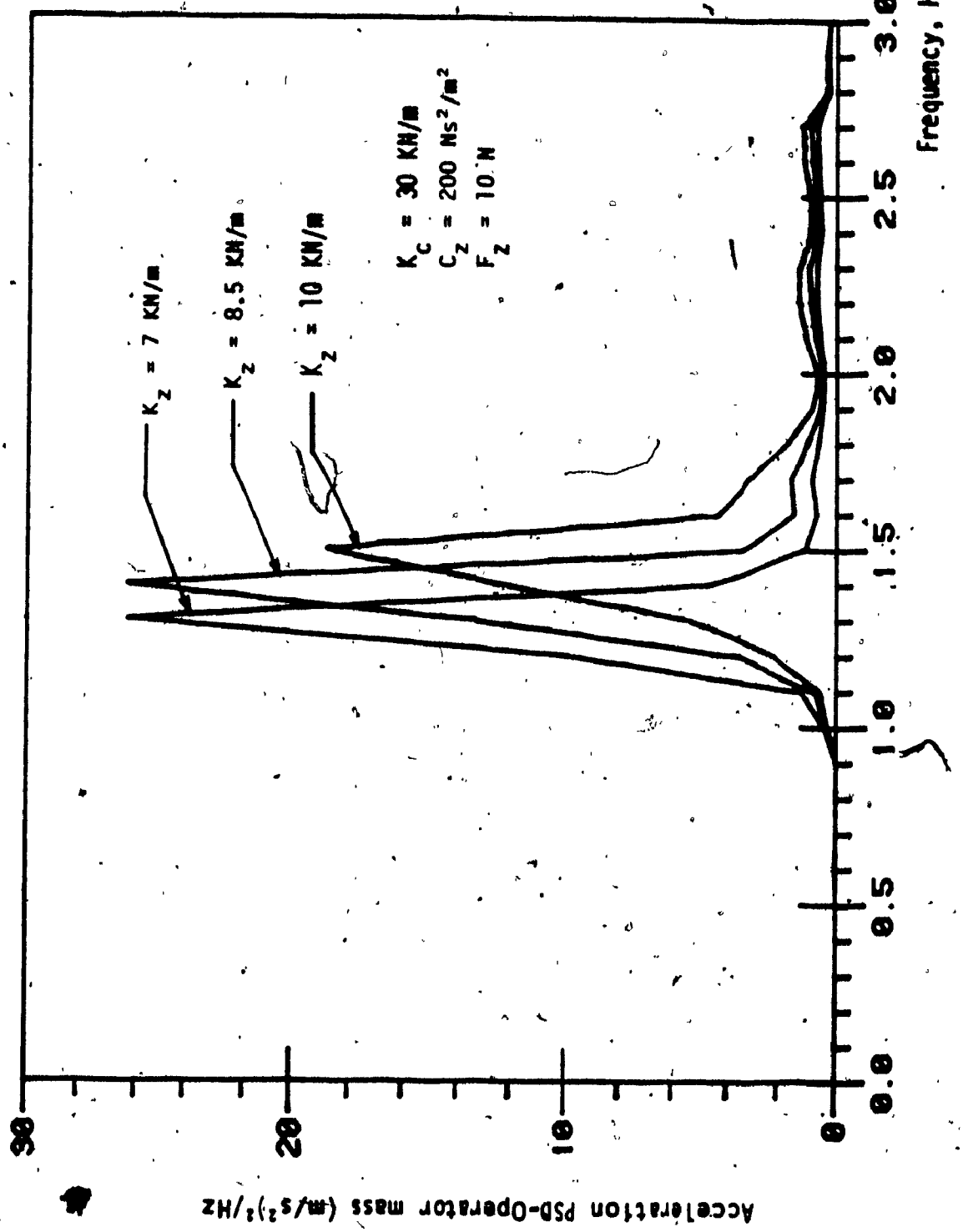

FIGURE 5.2: Bounce seat suspension performance sensitivity to variations in suspension stiffness.

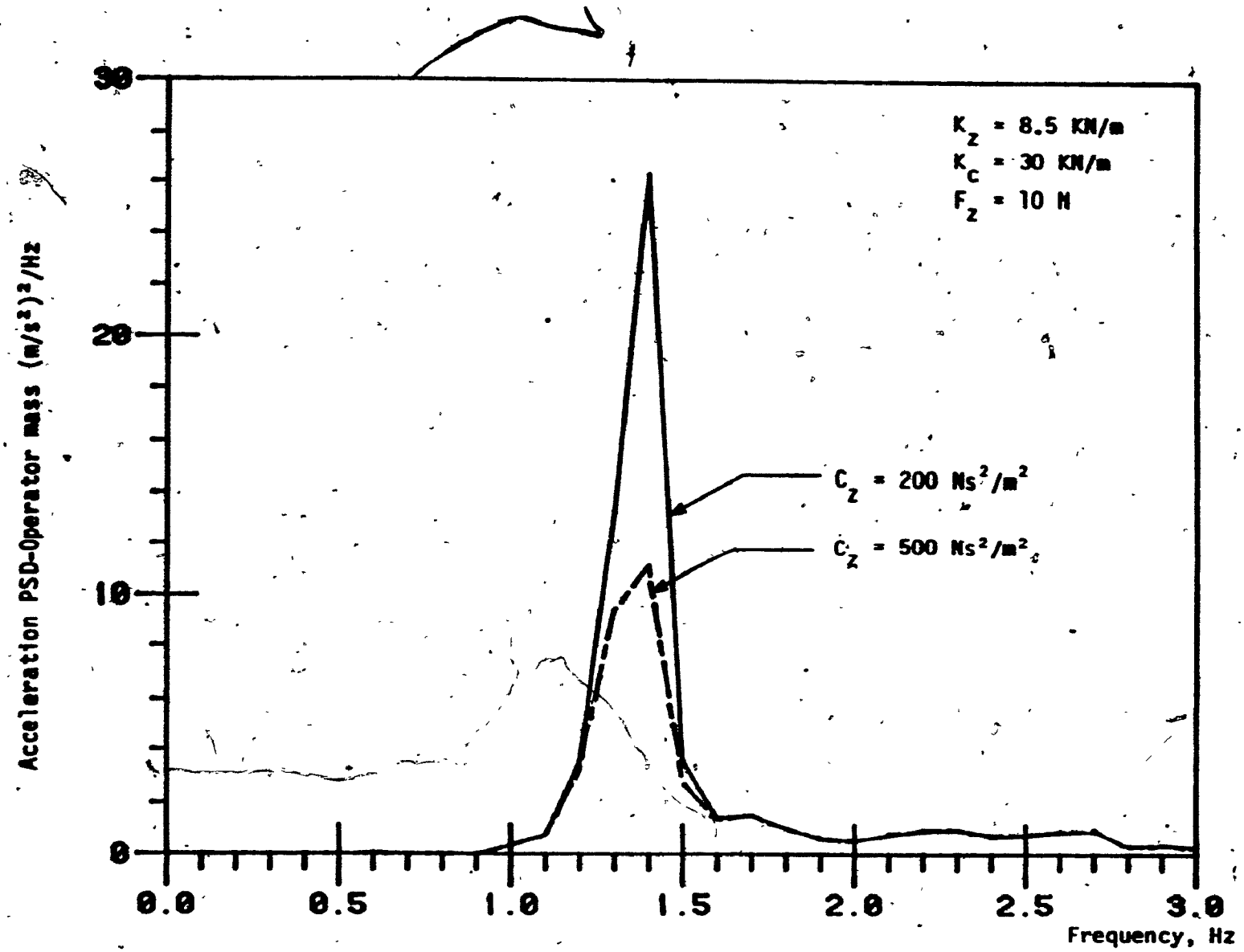

FIGURE 5.3: Influence of variations in the shock absorber damping coefficient on bounce acceleration response.

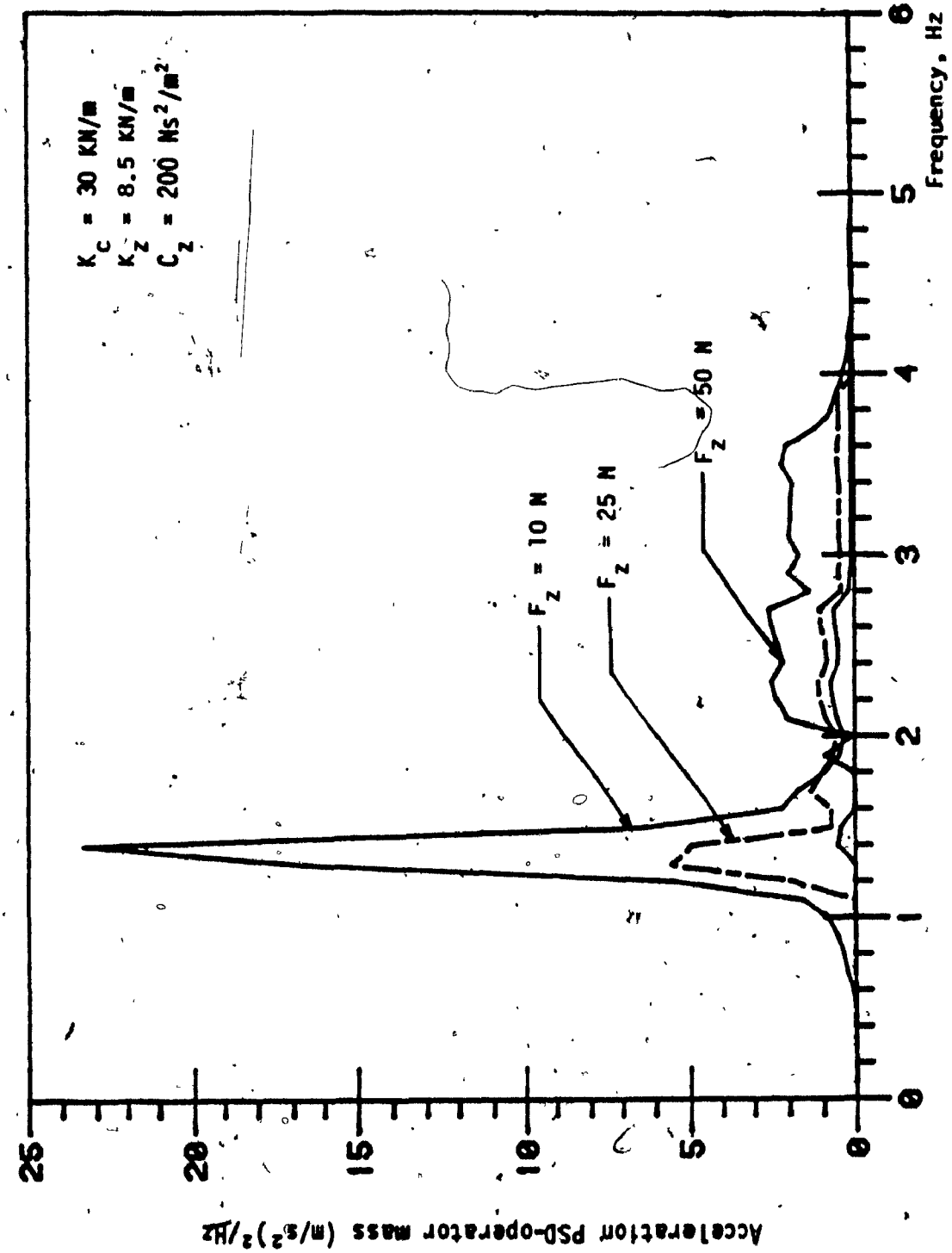

FIGURE 5.4: Influence of magnitude of Coulomb damping on the bounce performance of bounce suspension seat.

in the frequency range 1.5 to 3.5 Hz, a softer suspension exhibits superior performance as shown in Figure 5.5. However, the relative displacement response is deteriorated with soft suspension as shown in Figure 5.6. The relative displacement and acceleration PSD response show significant improvement with an increase in coefficient of velocity squared damping and Coulomb damping force as presented in Figures 5.7 and 5.8 respectively.

3) Lateral Seat Suspension

Since the lateral resonance of agricultural vehicle occurs around 1 Hz, it is necessary to design the passive lateral seat isolator with extremely low natural frequency. However, the low natural frequency isolator provides excellent acceleration response but poor relative displacement response as shown in Figure 5.9 and 5.10. Large values of Coulomb friction and velocity squared damping coefficient aid to suppress the lateral acceleration response corresponding to the lateral resonant frequency of the vehicle (1.1Hz) as shown in Figures 5.11 and 5.12, respectively.

5.3.2 INFLUENCE OF VARIATIONS IN SUSPENSION PARAMETERS ON THE PERFORMANCE OF PASSIVE ROTATIONAL SEAT SUSPENSION MODEL

Parameter sensitivity study of the performance of rotational seat isolator includes the following suspension parameters.

(i) Bounce seat stiffness, K_z.

(ii) Bounce shock absorber damping coefficient, C_z.

(iii) Coulomb damping force, F_z

(iv) Stiffness of the end supports, K_e.

(v) Stiffness of the pitching suspension, K_θ

(vi) Damping coefficient due to pitching shock absorber, C_θ.

(vii) Torsional stiffness of the shaft, K_ϕ.

(viii) Coefficient of torsional damping due to roll damper, C_ϕ.

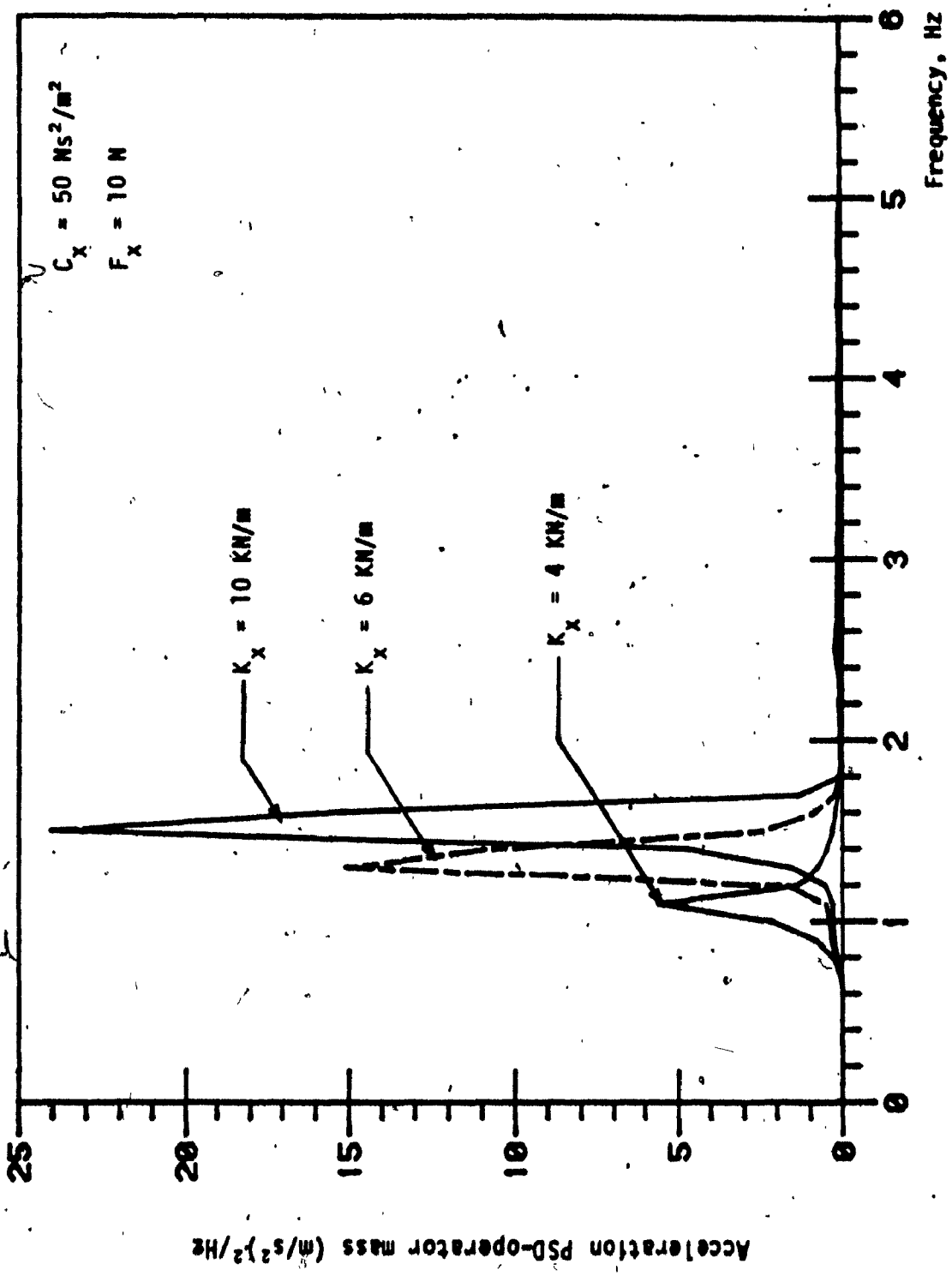

FIGURE 5.5: Sensitivity of longitudinal seat suspension performance to variations in suspension stiffness.

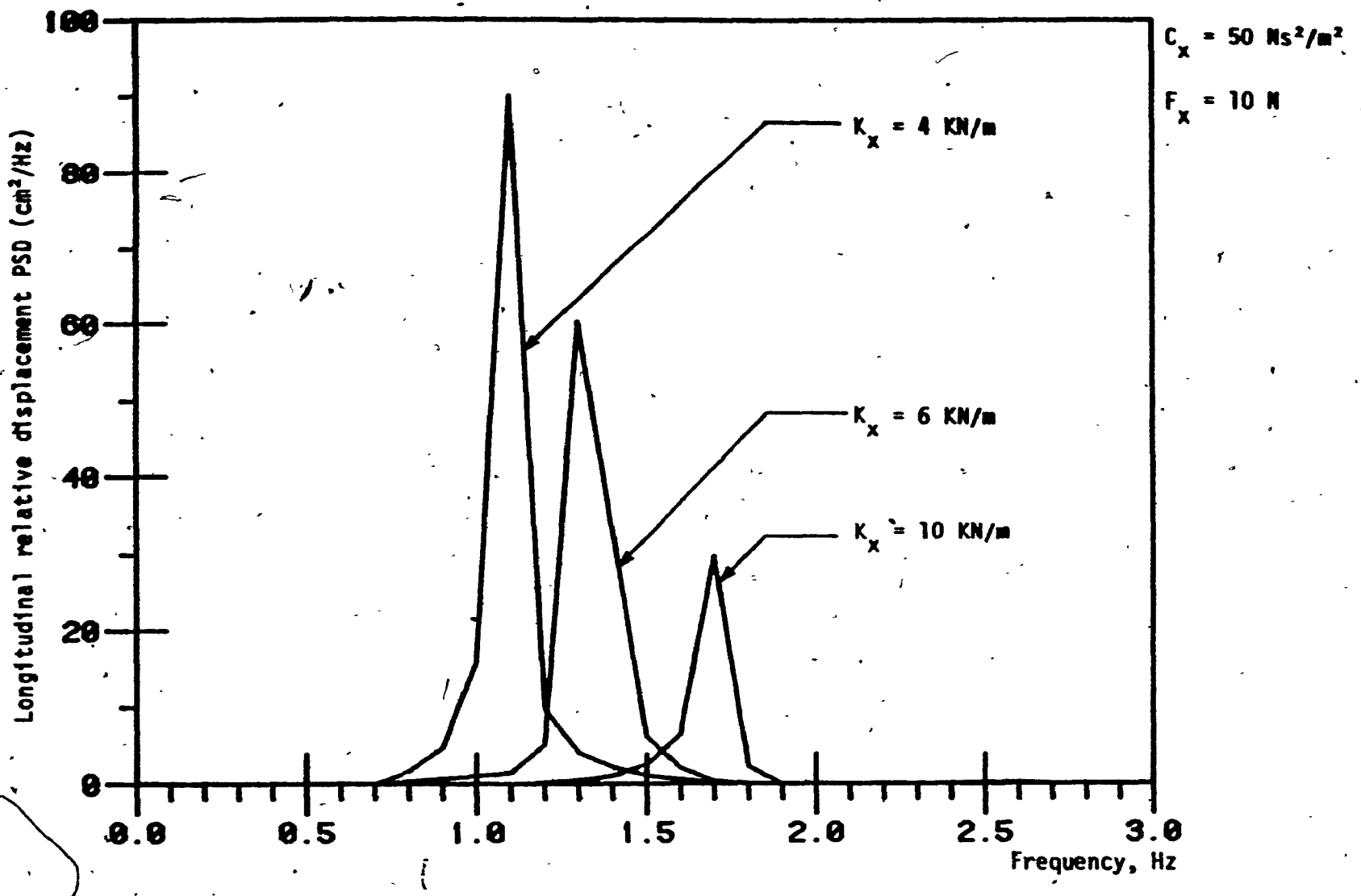

FIGURE 5.6: Influence of variations in suspension stiffness (K_x) on the relative displacement response of longitudinal seat isolator.

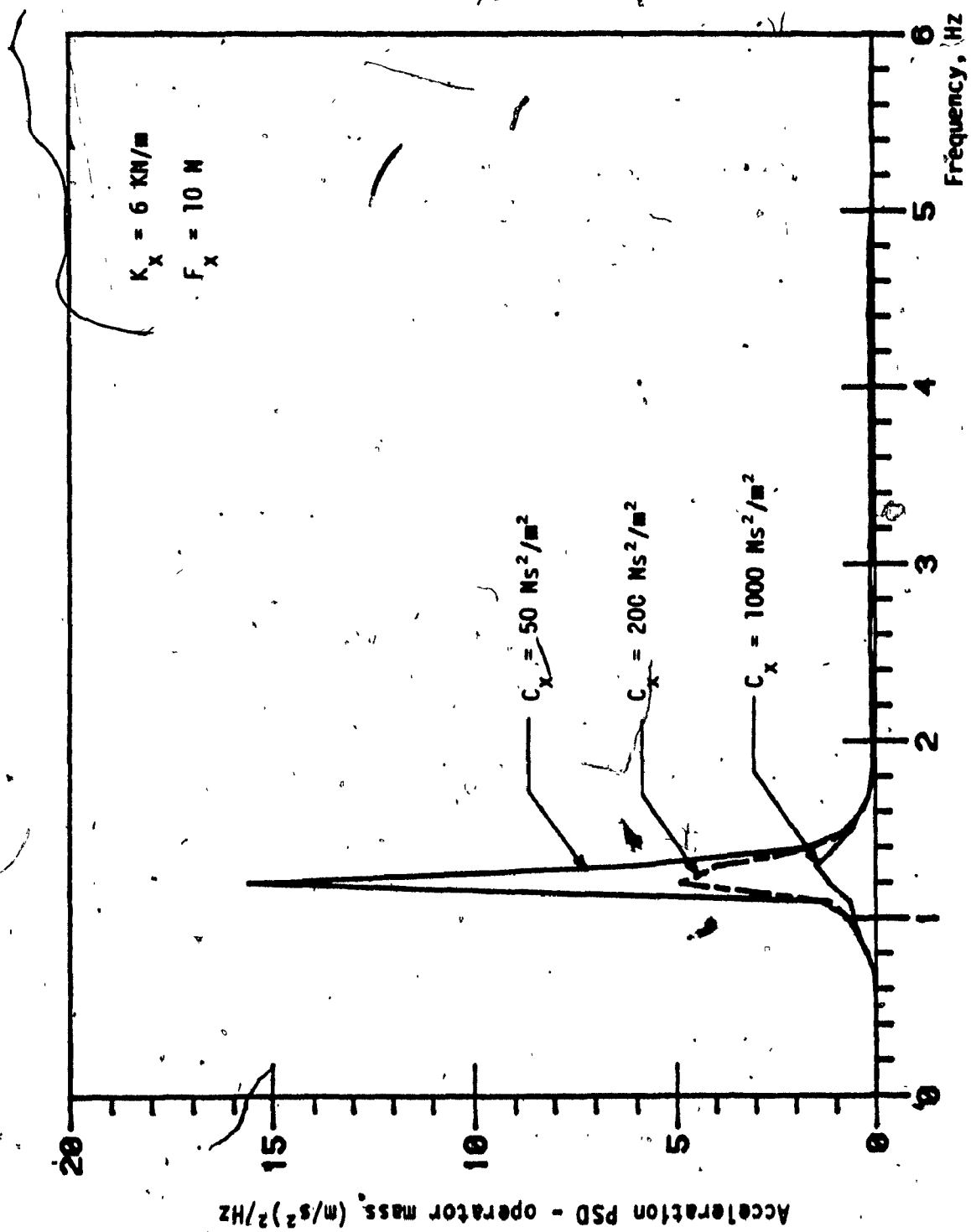

FIGURE 5.7: Influence of shock absorber damping on the performance of longitudinal seat suspension.

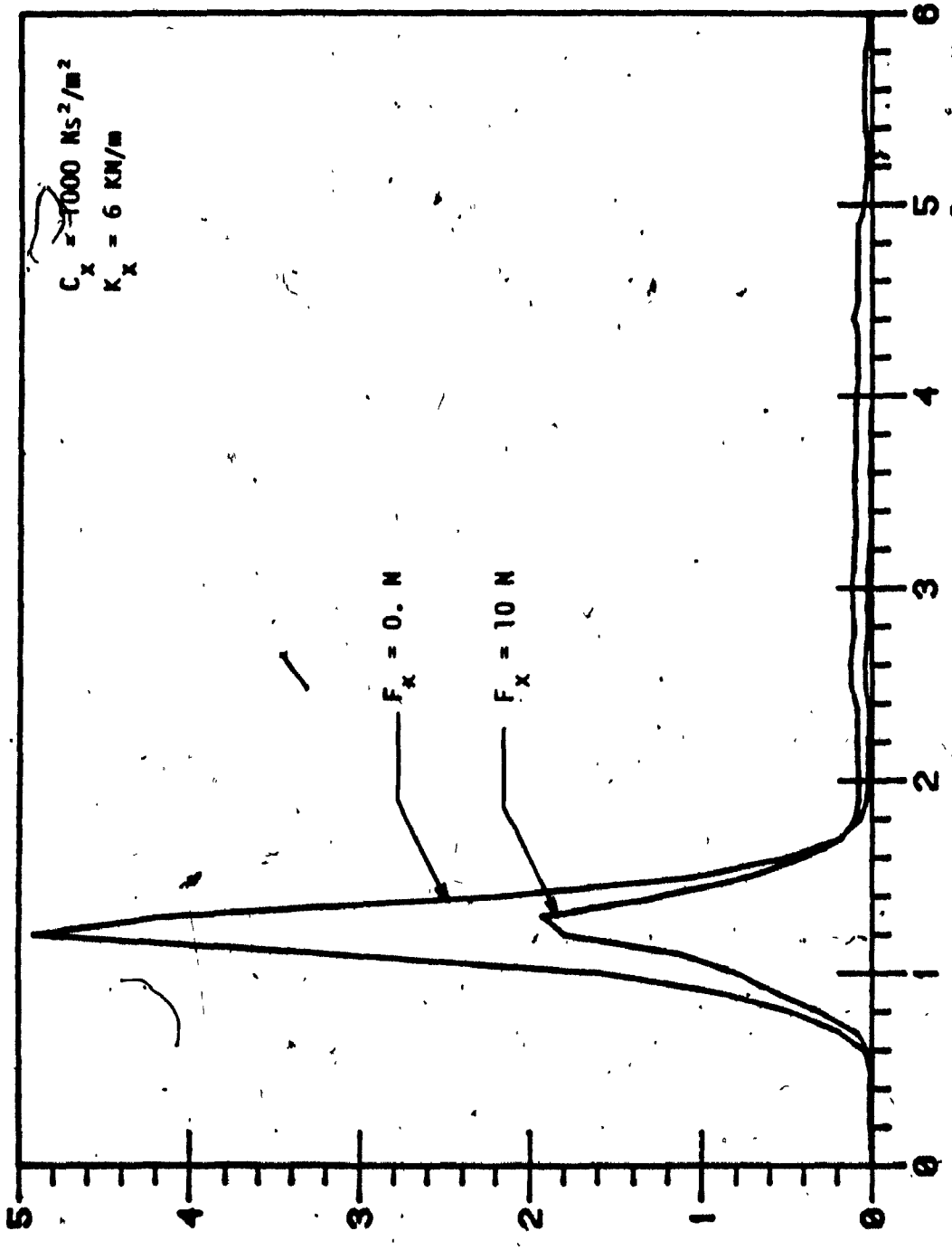

FIGURE 5.8: Influence of Coulomb damping on the performance of longitudinal seat suspension.

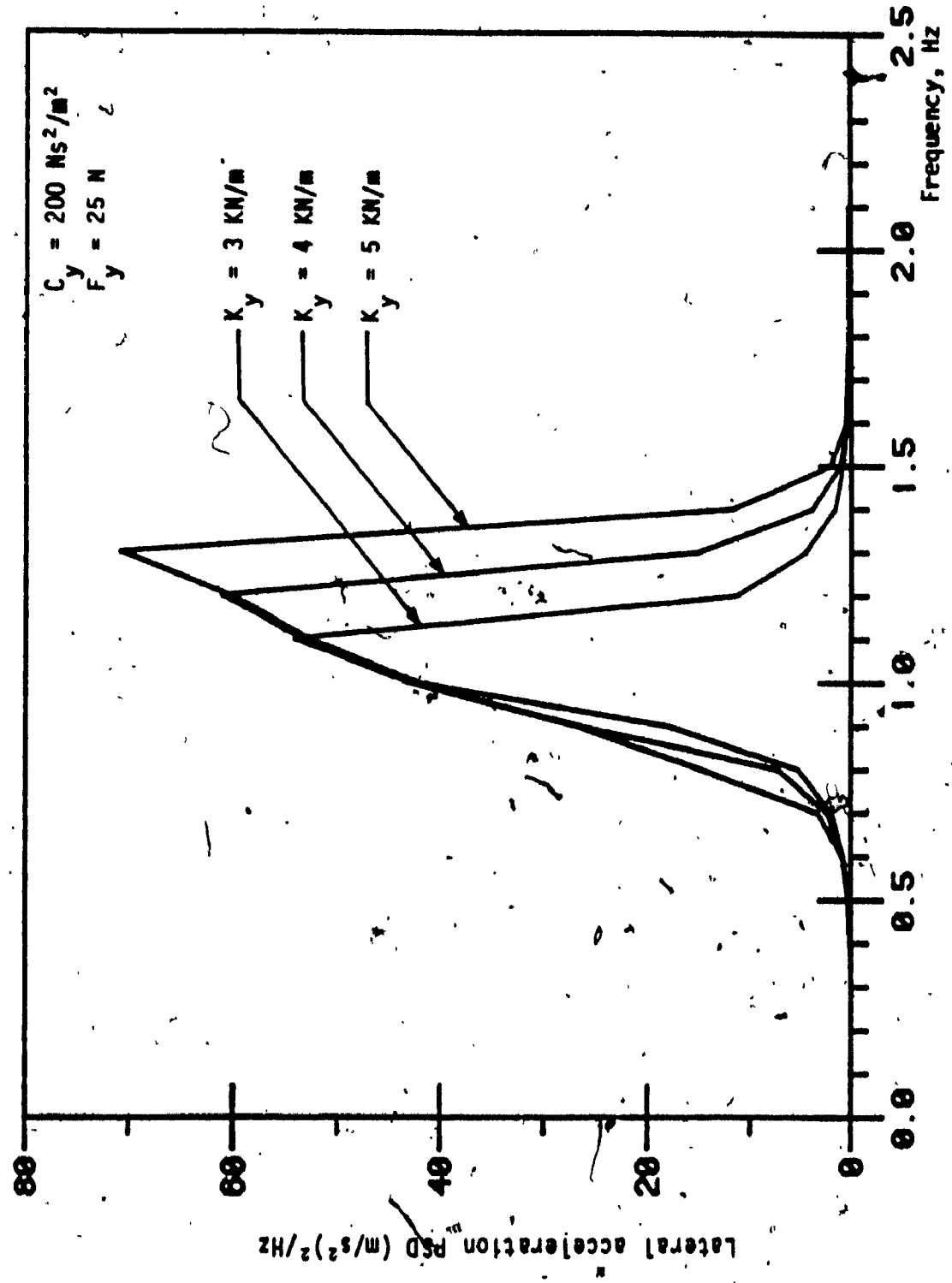

FIGURE 5.9: Influence of variations in suspension stiffness on the acceleration response of the lateral seat isolator.

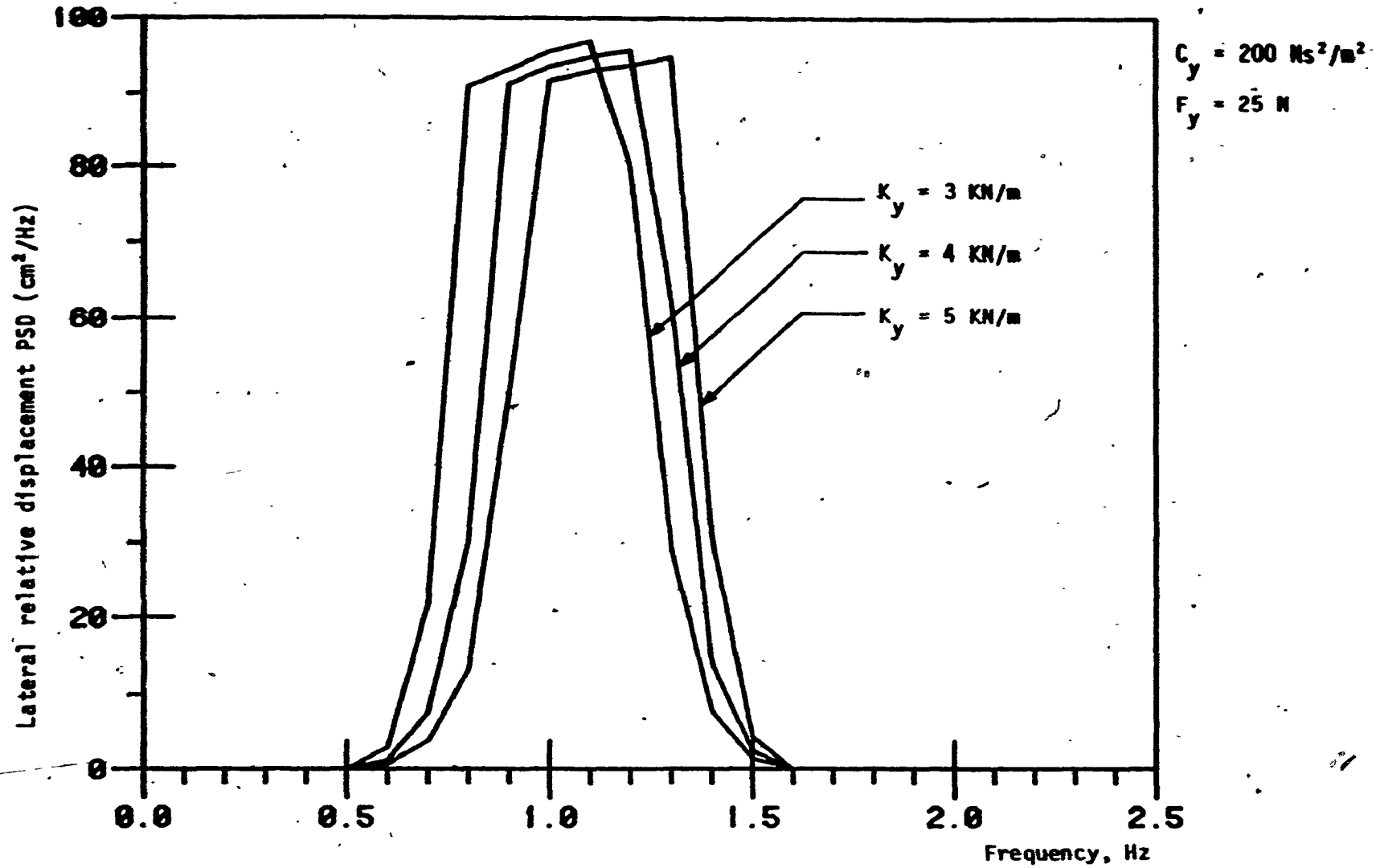

FIGURE 5.10: Influence of variations in suspension stiffness (K_y) on the relative displacement response of the lateral seat isolator.

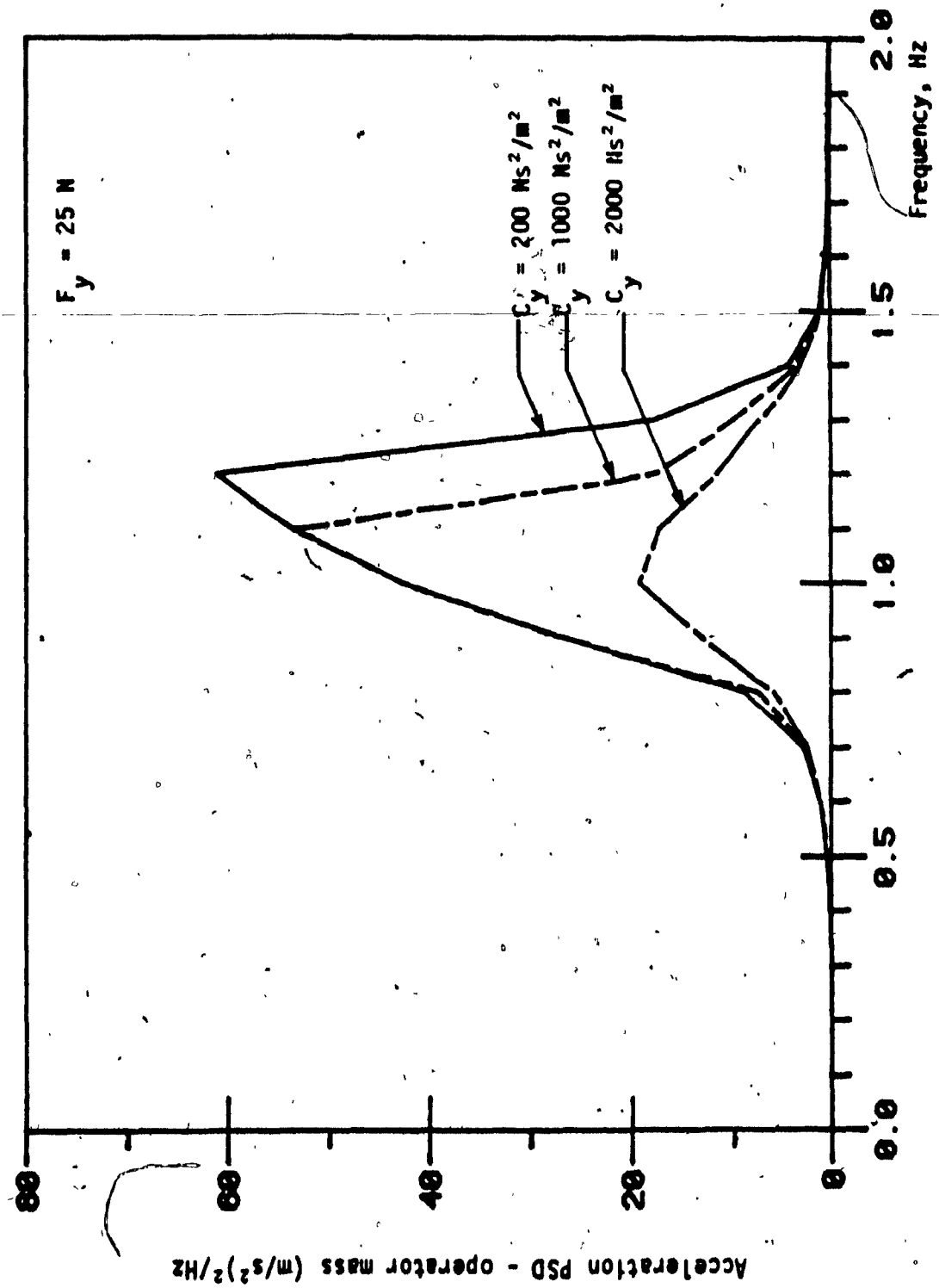

FIGURE 5.11: The influence of lateral damping coefficient on the lateral performance of translational seat suspension model.

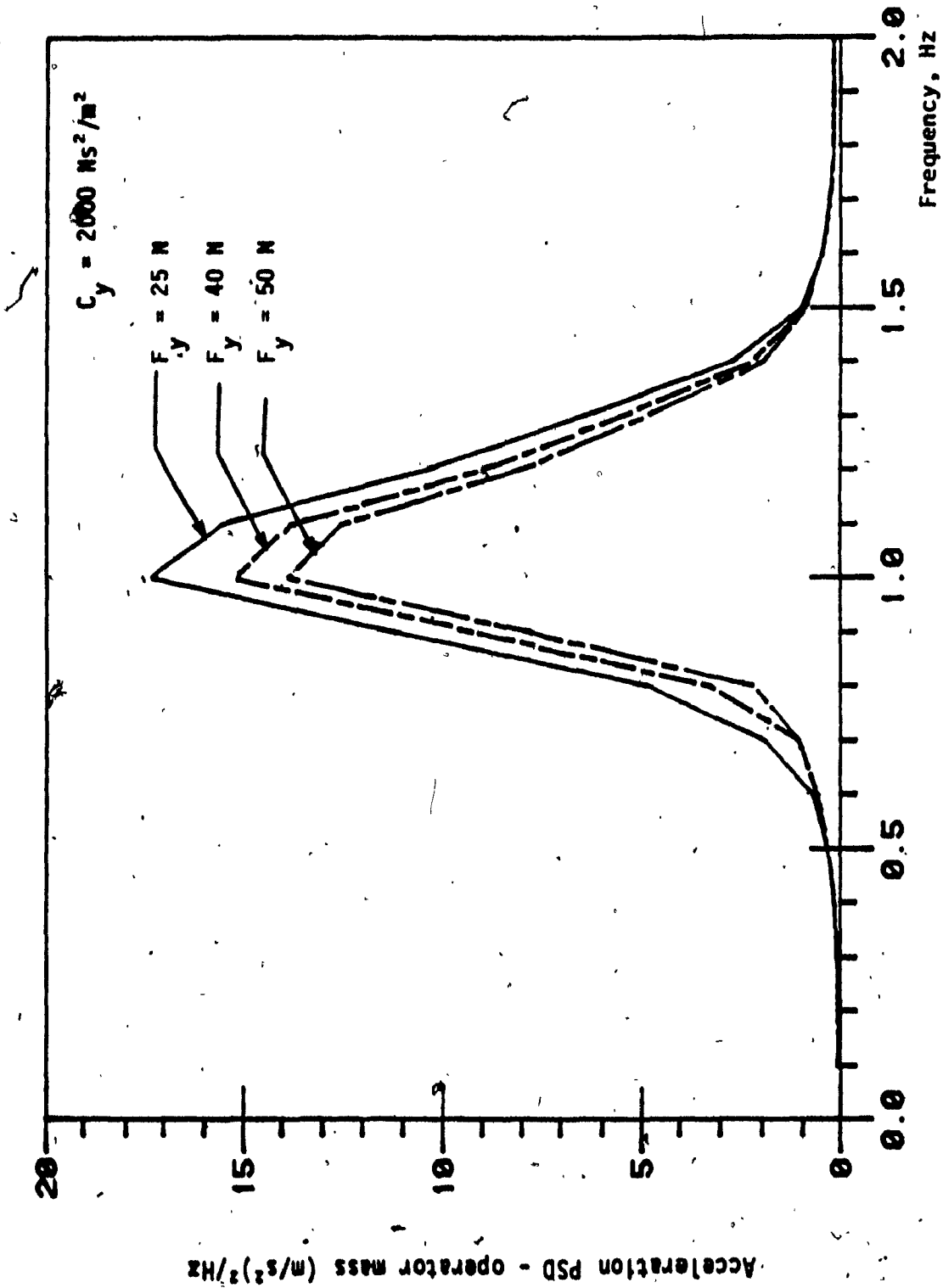

FIGURE 5.12: Influence of Coulomb damping force on the performance of the lateral seat isolators.

The influence of variations in above suspension parameters on the bounce, pitch and roll acceleration responses of the rotational seat isolator is presented in Figures 5.13 through 5.26. Influence of bounce suspension stiffness on bounce and pitch acceleration response is shown in Figures 5.13 and 5.14. The response plots reveal that a softer bounce suspension lowers the bounce resonance frequency with significantly lower bounce aoceleration response at low frequencies. The pitch acceleration response exhibits two peaks corresponding to pitch and bounce resonant frequencies, respectively. The peak pitch acceleration response corresponding to bounce resonant frequency decreases significantly with softer bounce suspension, howeven the pitch response corresponding to the pitch resonant frequency does not change significantly.

Larger value of bounce suspension seat damping provides excellent bounce resonance response (Figure 5.15), and significant improvement in pitch acceleration response corresponding to bounce resonant frequency is achieved as shown in Figure 5.16. However bounce suspension damping has no noticeable influence on the pitch acceleration response corresponding to the pitch resonant frequency of the rotational isolator. The magnitude of Coulomb friction force has significant influence on the bounce and pitch acceleration performance of rotational seat isolator as shown in Figures 5.17 and 5.18. An increase in Coulomb damping force results in excellent bounce and pitch acceleration response corresponding to bounce resonant frequency. However, no significant influence on the pitch acceleration response corresponding to the pitch resonant frequency, is observed. The bounce and pitch acceleration response of the rotational isolator is deteriorated in the isolation region with increase in Coulomb damping.

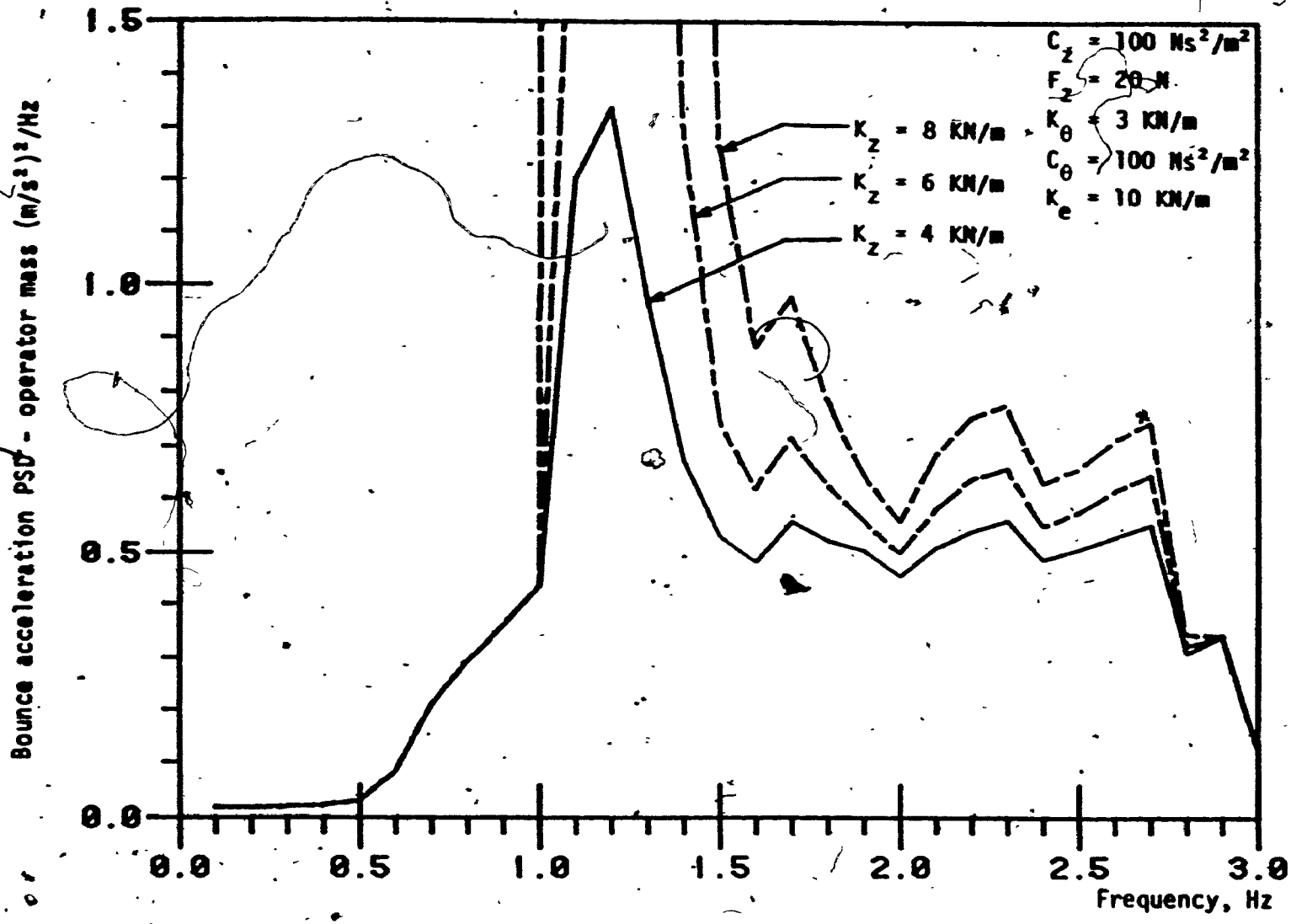

FIGURE 5.15: Influence of variations in bounce suspension stiffness (K_z) on the bounce performance of rotational isolator.

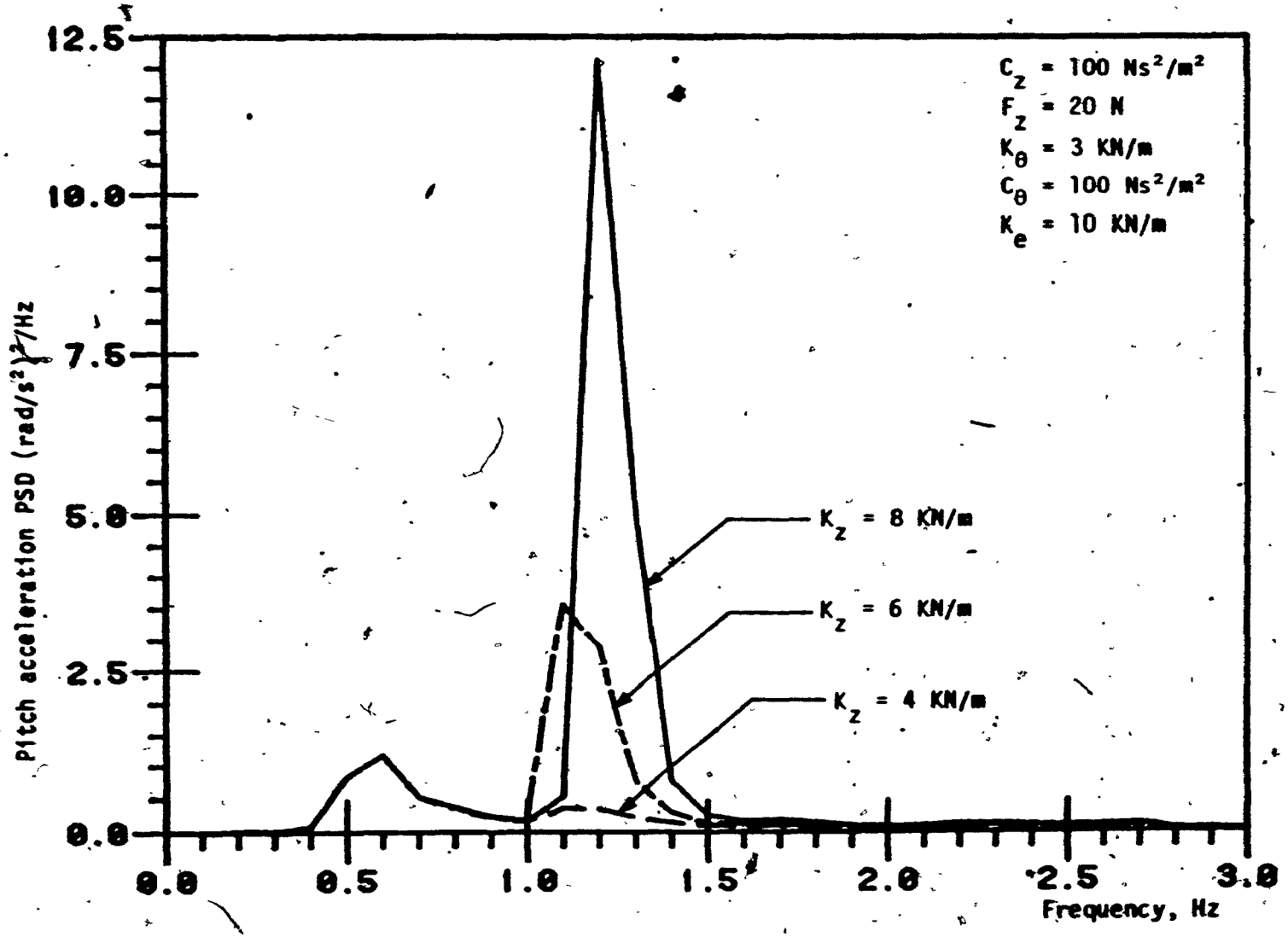

FIGURE 5.14: The influence of variations in bounce suspension stiffness (K_z) on the pitch performance of rotational isolator.

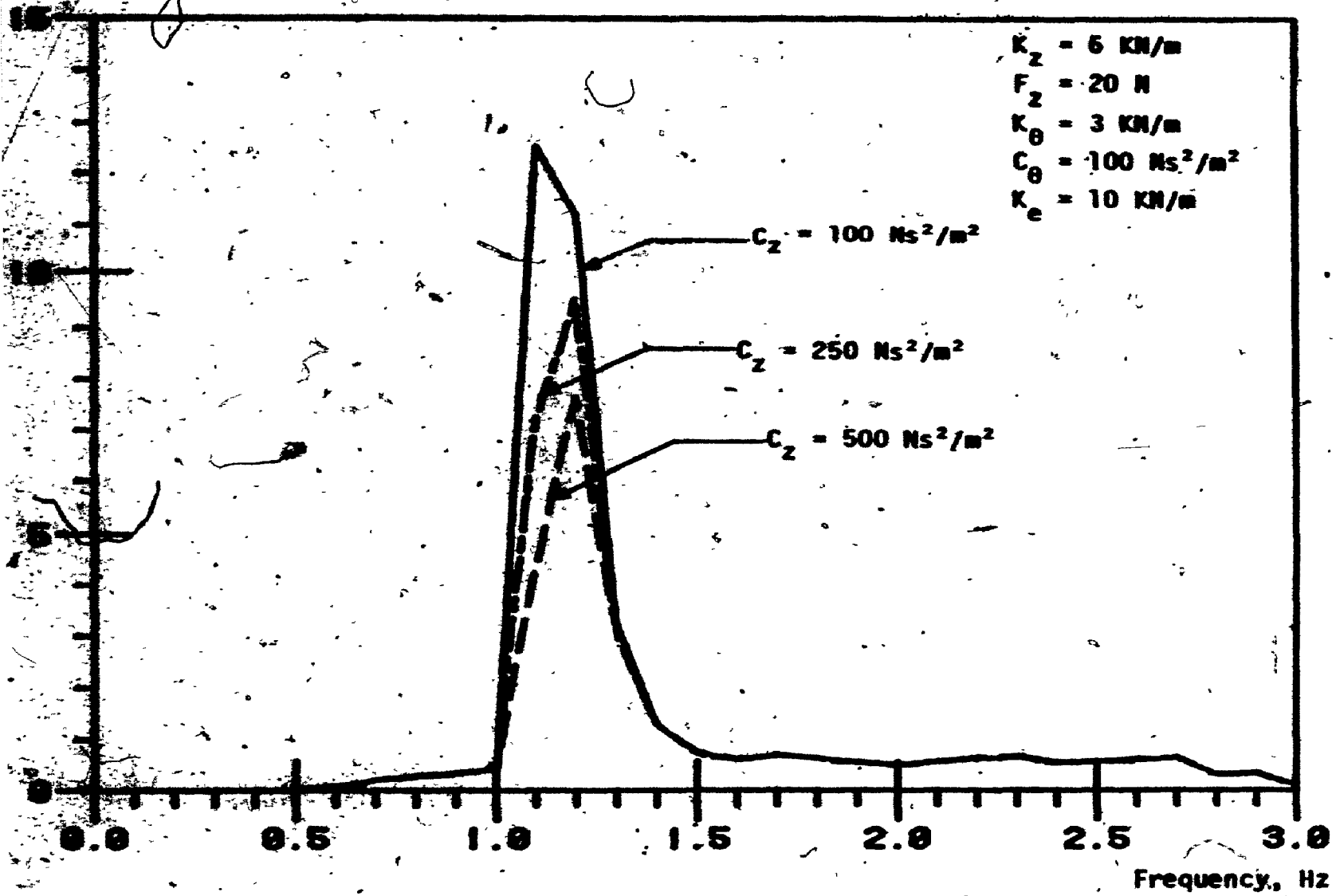

FIGURE 5.15: Sensitivity of rotational isolator's bounce performance to variations in bounce suspension damping coefficient.

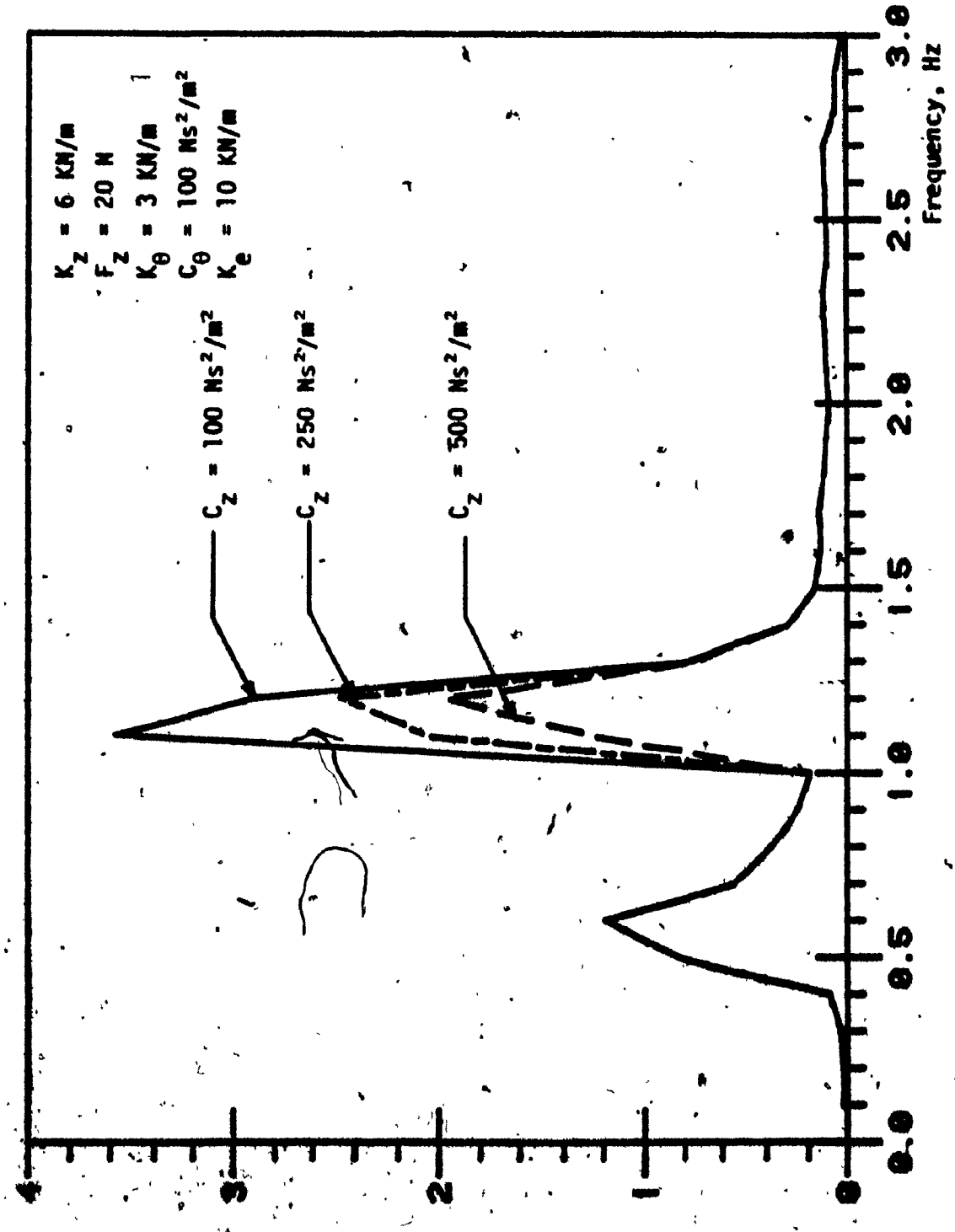

FIGURE 5.16: Sensitivity of rotational isolator's pitch performance to variations in bounce suspension damping coefficient.

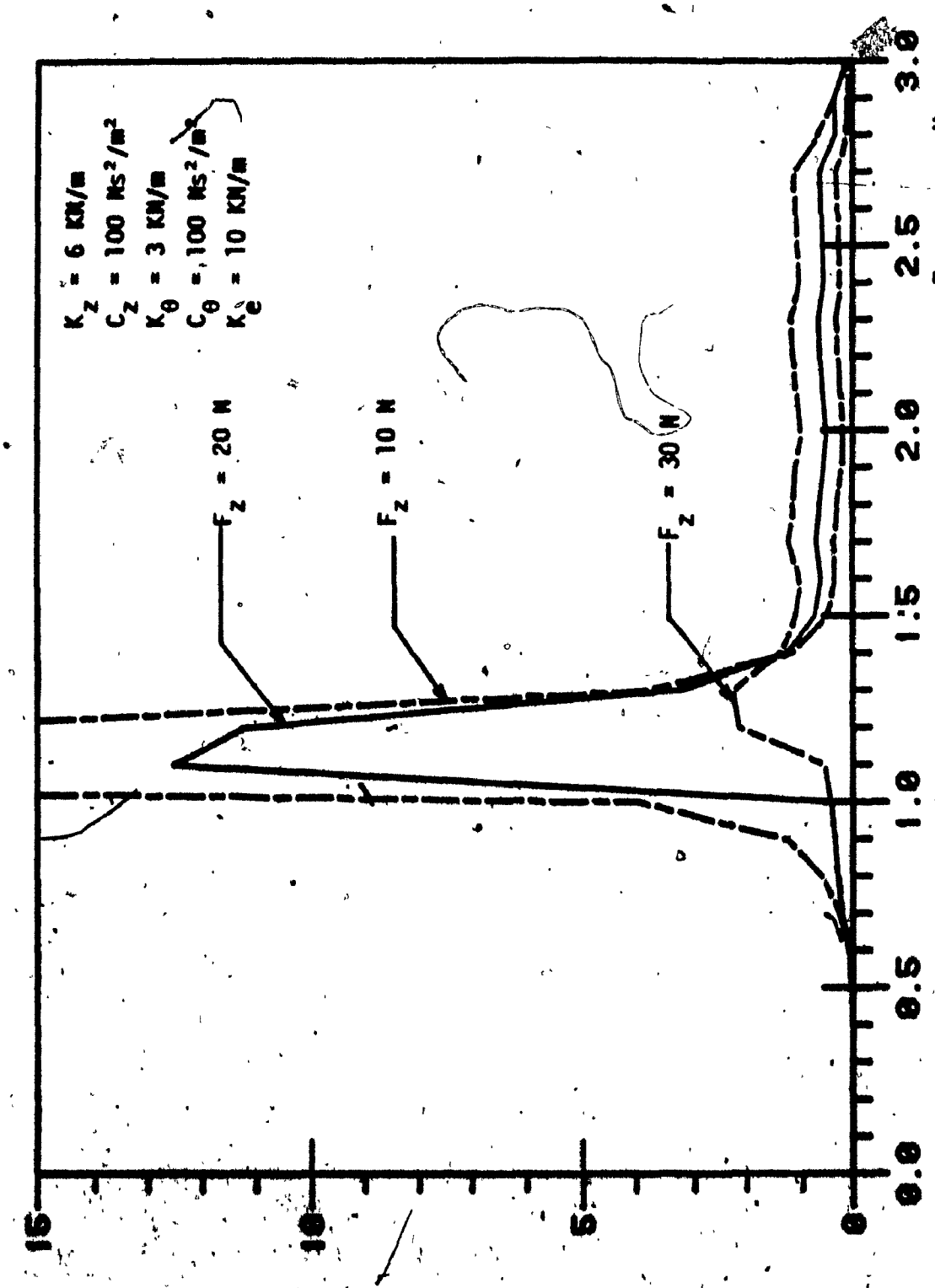

FIGURE 5.17: Influence of Coulomb friction force on the bounce performance of rotational isolators.

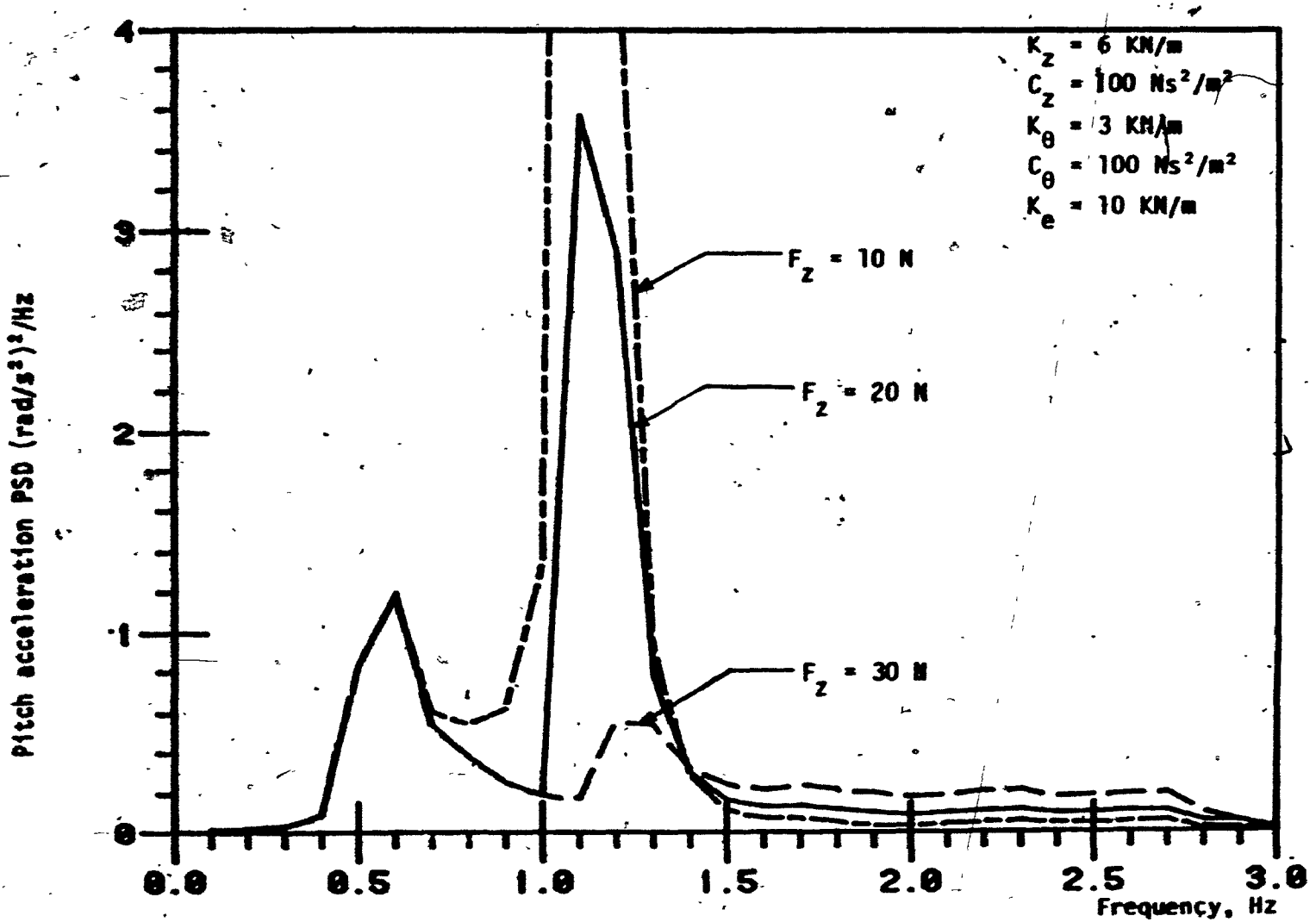

FIGURE 5.18: Influence of Coulomb friction force on the pitch performance of the rotational seat isolator.

The bounce, pitch and roll acceleration response of the rotational seat suspension is observed to be highly sensitive to the stiffness of end supports as shown in Figures 5.19, 5.20 and 5.21. Extremely soft end supports lead to large bounce and pitch acceleration response corresponding to the bounce resonant frequency of the rotational isolator as shown in Figures 5.19 and 5.20, respectively. An increase in the stiffness of end supports increases the bounce resonant frequency with significantly lower bounce and pitch acceleration response. However, a further increase in the stiffness of end supports worsens the bounce and pitch acceleration response corresponding to the bounce resonant frequency. The pitch acceleration response corresponding to the pitch resonant frequency also shows similar behaviour with variations in the stiffness of end supports.

The roll acceleration response, presented in Figure 5.21, reveals that the roll resonant frequency is dominantly influenced by the stiffness of end supports. The torsional stiffness of the shaft has no significant influence on the resonant frequency as shown in Figure 5.22. The roll acceleration response shows large peak with soft end supports, however, a slight increase in the stiffness of end supports lowers the peak roll acceleration significantly. Further increase in the stiffness value of end supports worsens the roll acceleration response (Figure 5.21). Thus, there exists an optimum value for the supports stiffness, that would result in best bounce, pitch and roll acceleration response of the rotational seat isolator.

Influence of pitching suspension parameters on bounce and pitch acceleration response is demonstrated by the response plots presented in Figures 5.23 through 5.26. An increase in stiffness of the pitching suspension unit shows poor resonance response in the bounce mode (Figure 5.23), with a significant increase in pitch acceleration corresponding

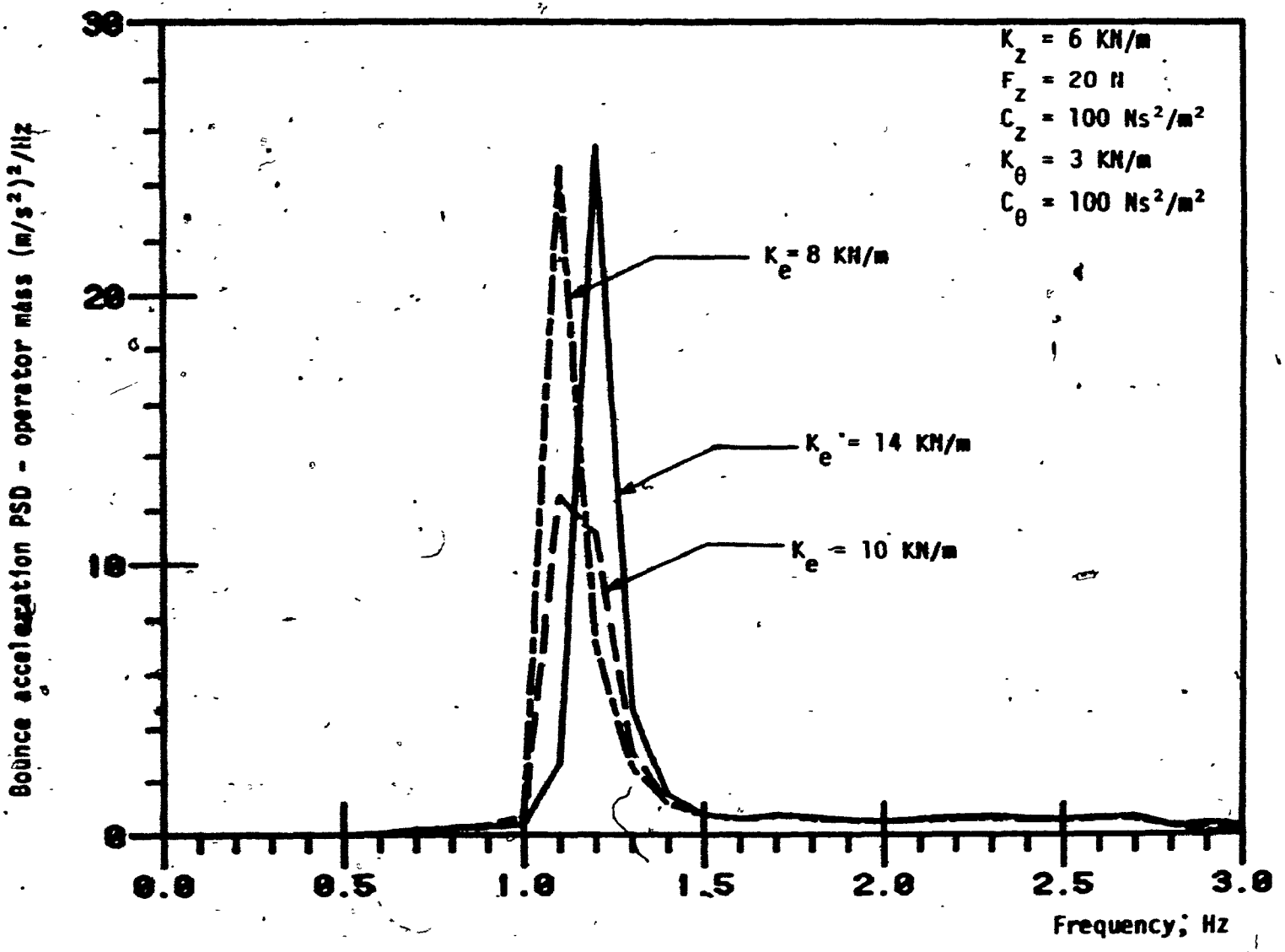

FIGURE 5.19: Sensitivity of bounce performance of the rotational seat isolator due to variations in support stiffness.

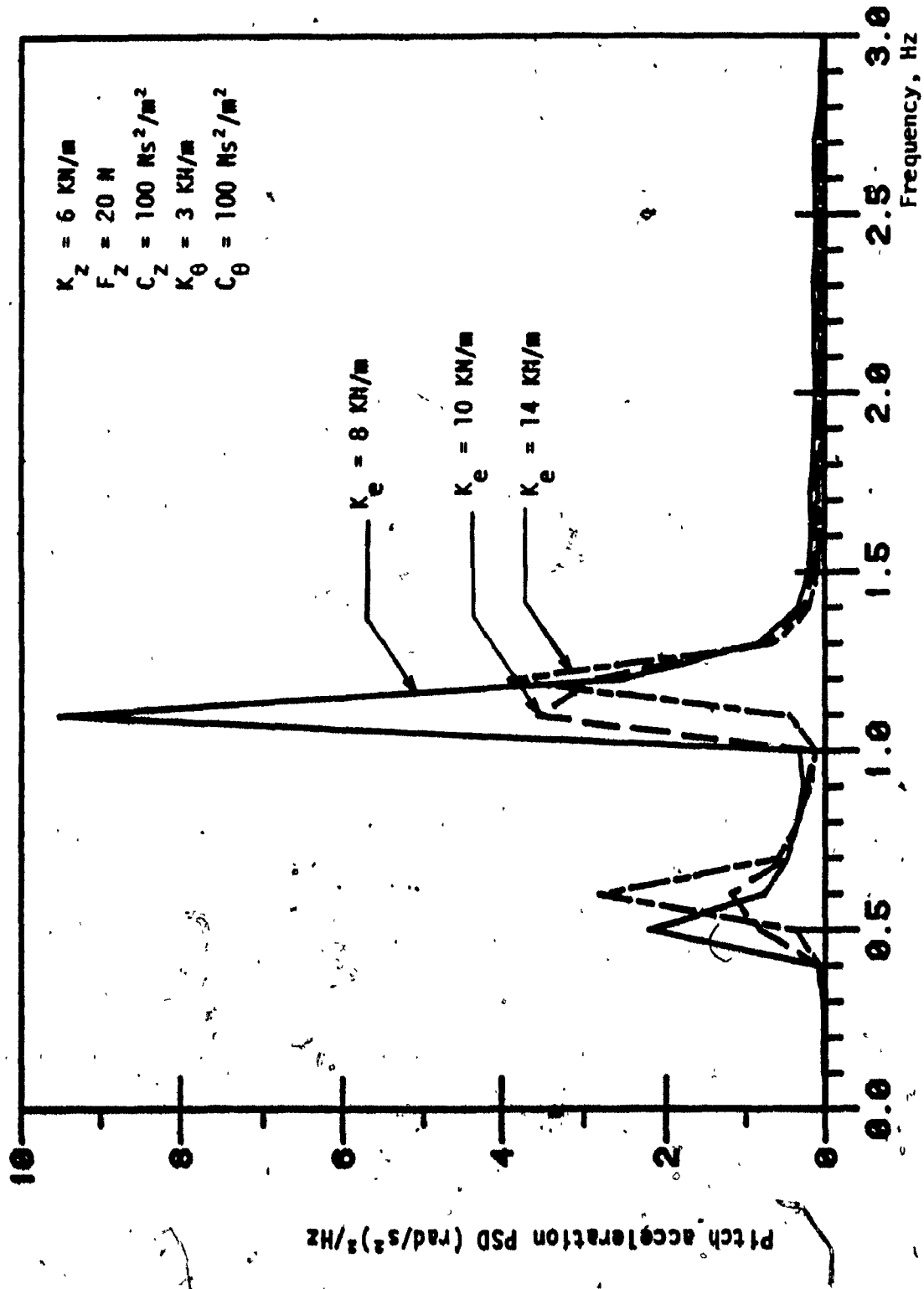

FIGURE 5.20: Pitch performance of the rotational seat isolator with variations in the stiffness of end supports.

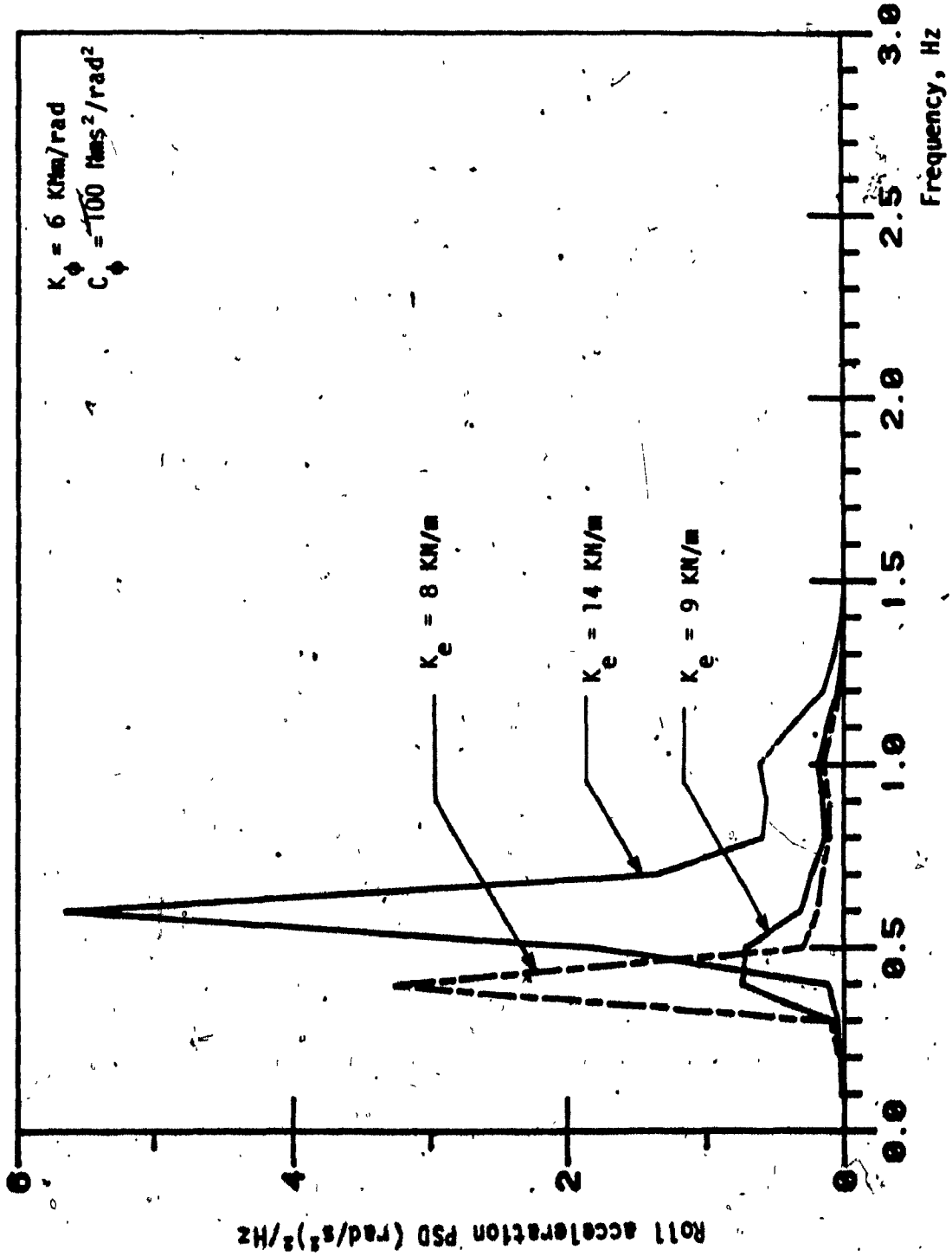

FIGURE 5.21: Influence of end supports stiffness on the roll response of rotational seat isolator.

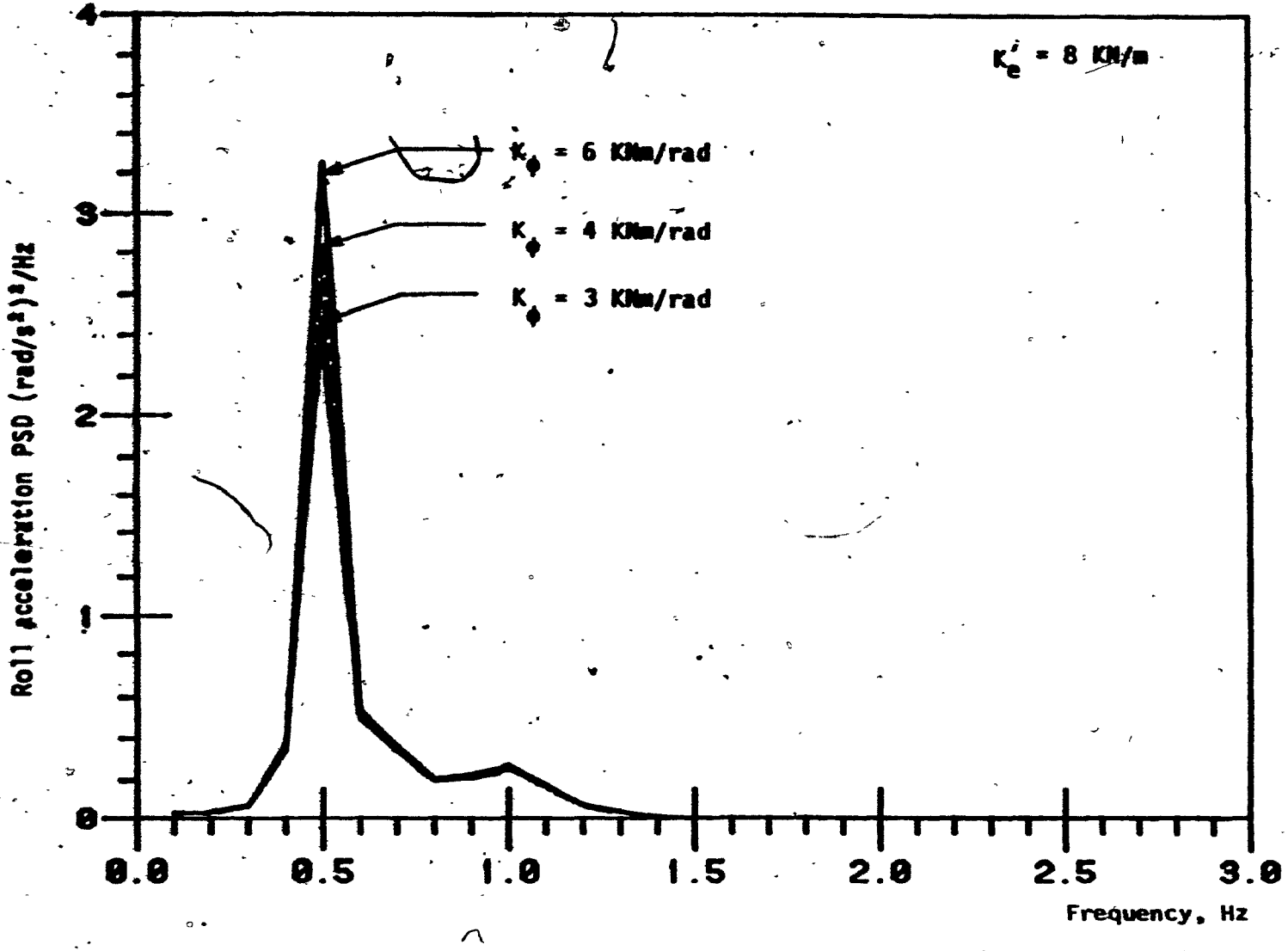

FIGURE 5.22: Influence of variations in torsional stiffness (K_ϕ) on the roll acceleration response of rotational seat isolator.

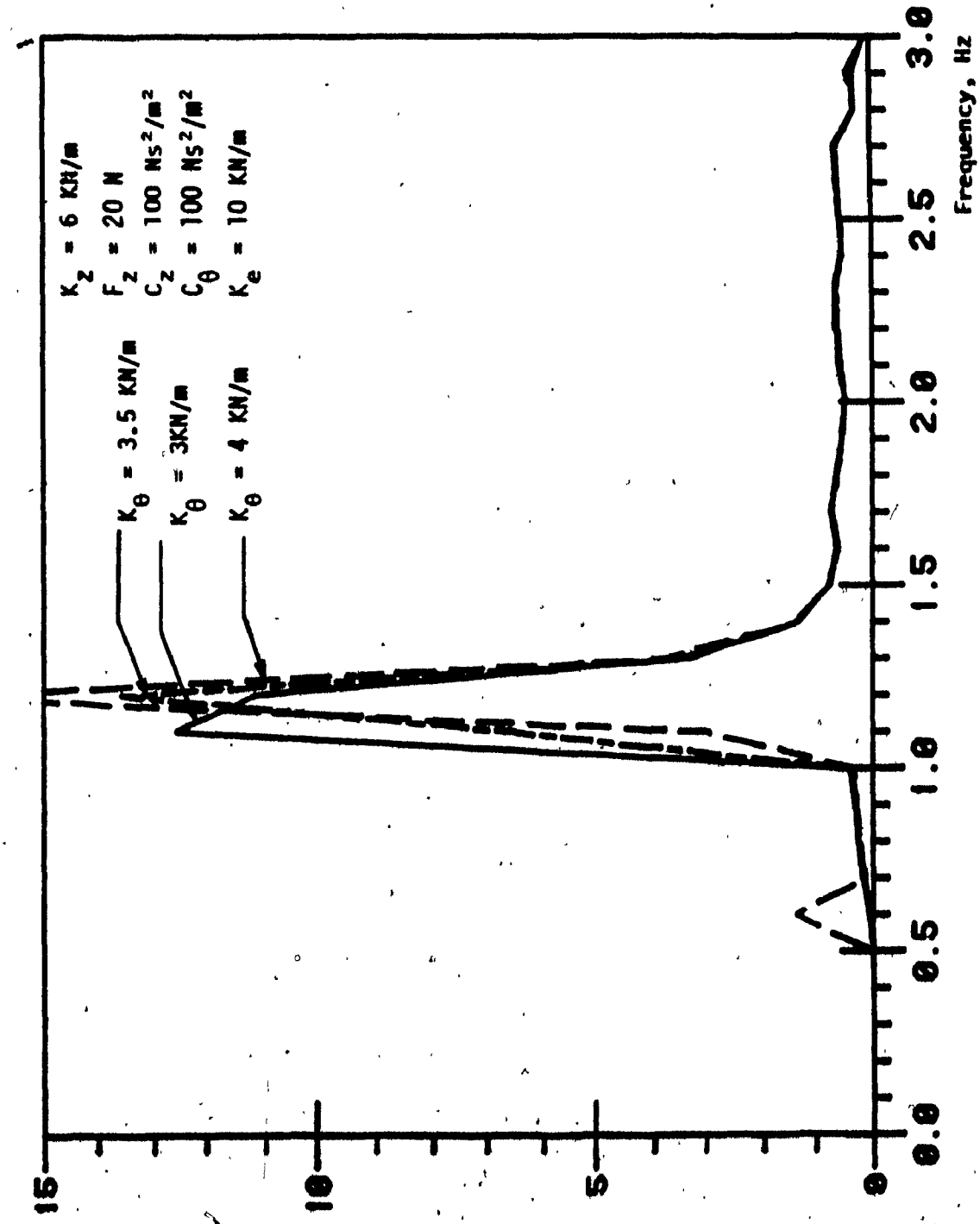

FIGURE 5.23: Influence of variations in the stiffness of pitching suspension (K_θ) on the bounce acceleration response of the rotational seat isolator.

to pitch as well as bounce resonant frequencies of the rotational isolator as shown in Figure 5.24. An increase in the damping coefficient of the pitching suspension improves the bounce as well as pitch acceleration response at bounce resonant frequency only, as indicated by the response acceleration PSD's of Figures 5.25 and 5.26.

5.3.3 INFLUENCE OF SUSPENSION PARAMETERS ON THE PERFORMANCE OF CAB SUSPENSION MODEL

Sensitivity of the cab-suspension performance to variations in suspension parameters is presented in this section. The performance of the cab-suspension model is taken as a measure of: bounce, lateral, longitudinal, roll and pitch accelerations of the cab; lateral and longitudinal accelerations at the cab cg; bounce, longitudinal, and lateral acceleration response at the seat. Sensitivity of suspension performance to variations in parameters of corner mounts, longitudinal isolator and lateral isolator is summarized in the following sections.

1) Influence of Corner Mount's Stiffness

An increase in the value of stiffness of cab mounts causes significantly larger bounce acceleration response of the cab at the vehicle resonance frequency (2.60 Hz) as shown in Figure 5.2.7. However, the stiffer mounts do not reveal a significant influence in lower frequency range. Also the roll and pitch acceleration response of the cab is worsened, specifically at vehicle resonant frequencies, as the stiffness of cab mounts is increased as shown in Figures 5.28 and 5.29. Although softer cab mounts show better bounce, roll and pitch-acceleration response, the relative motion response of the cab with respect to the chassis is increased, as shown in Figures 5.30, 5.31 and 5.32.

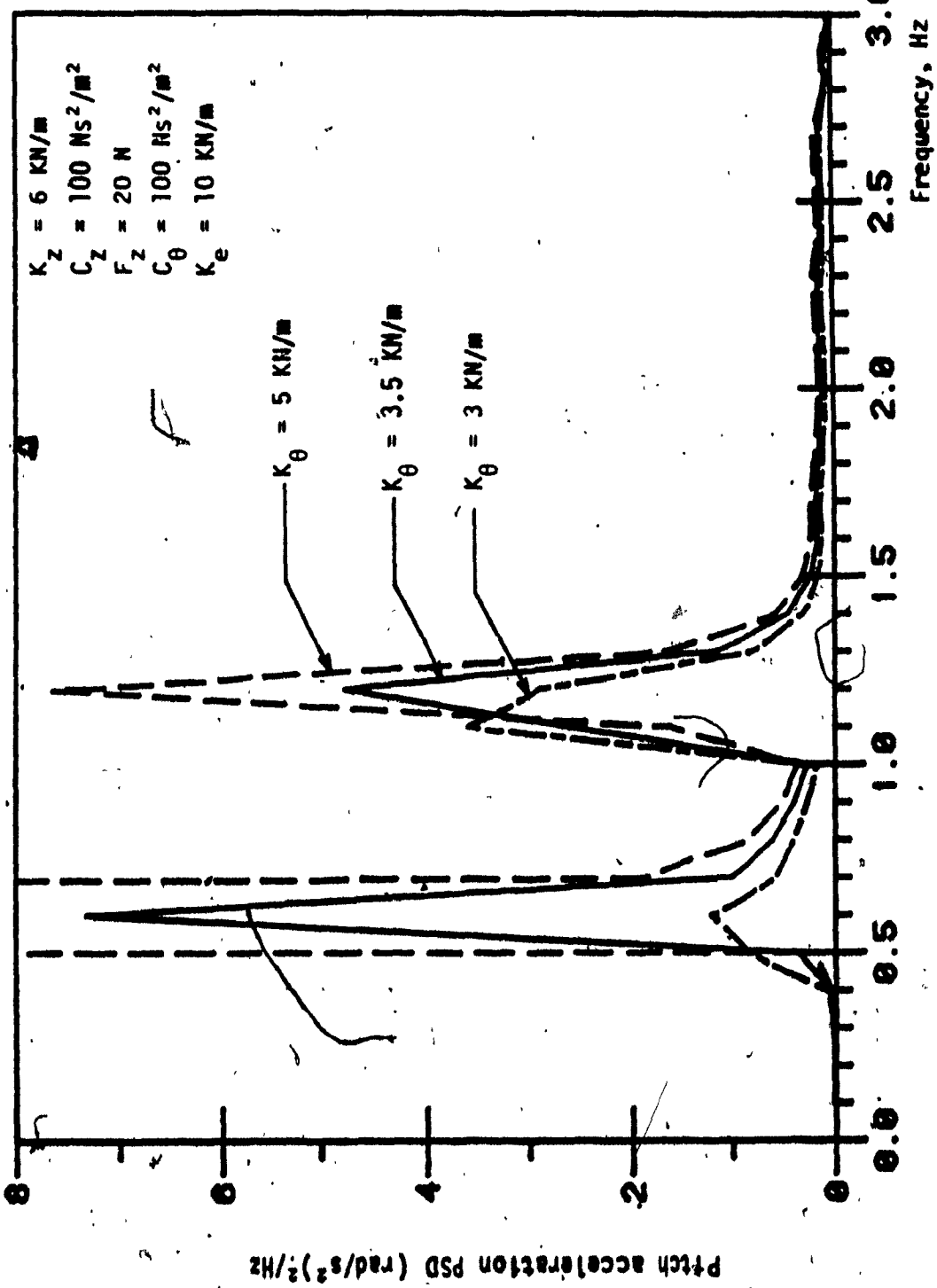

FIGURE 5.24: Pitch acceleration response of rotational seat isolators with variations in the stiffness of pitching suspension (K_θ).

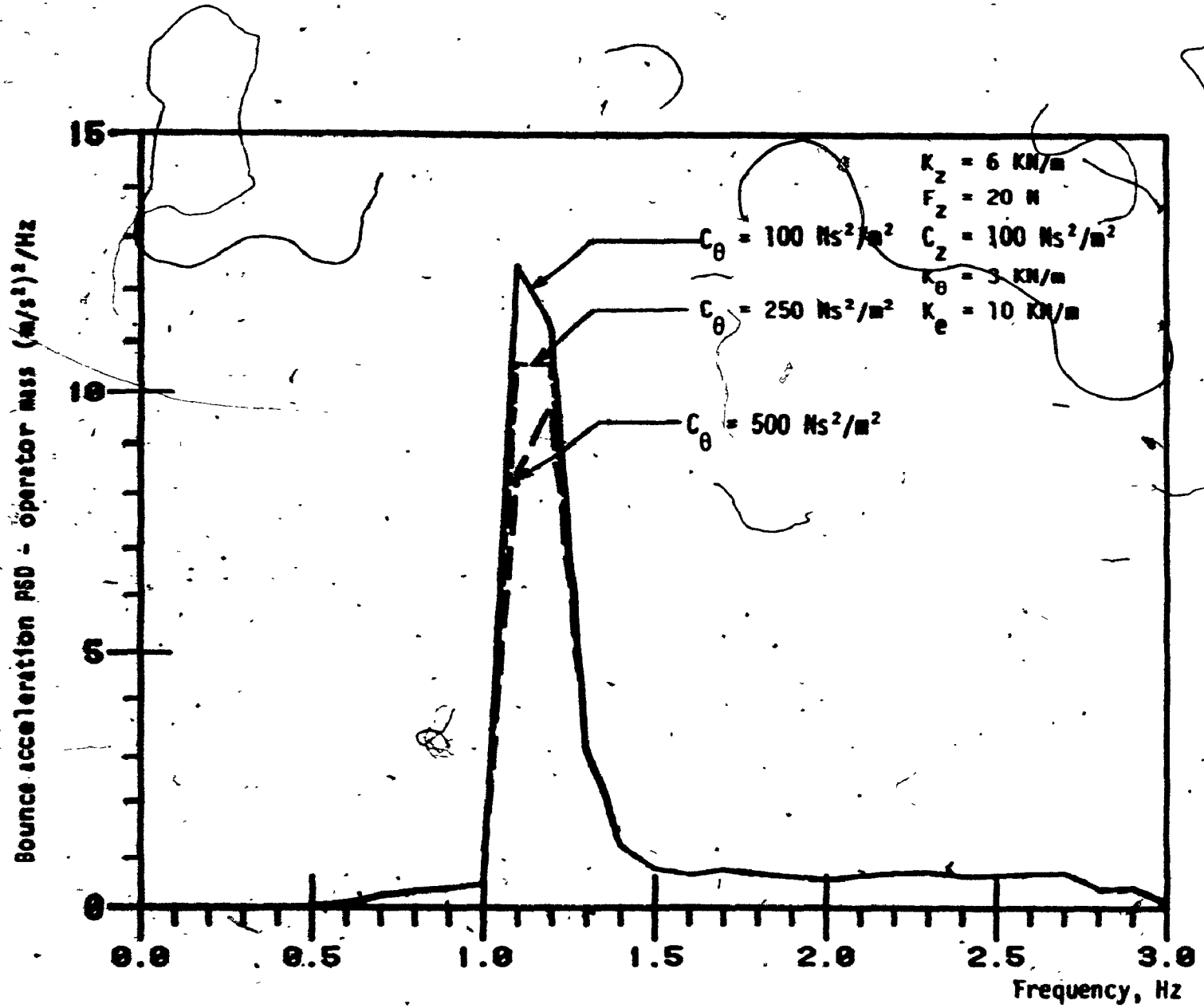

FIGURE 5.25: Bounce acceleration response of rotational seat isolator with variations in pitch suspension damping coefficient (C_θ).

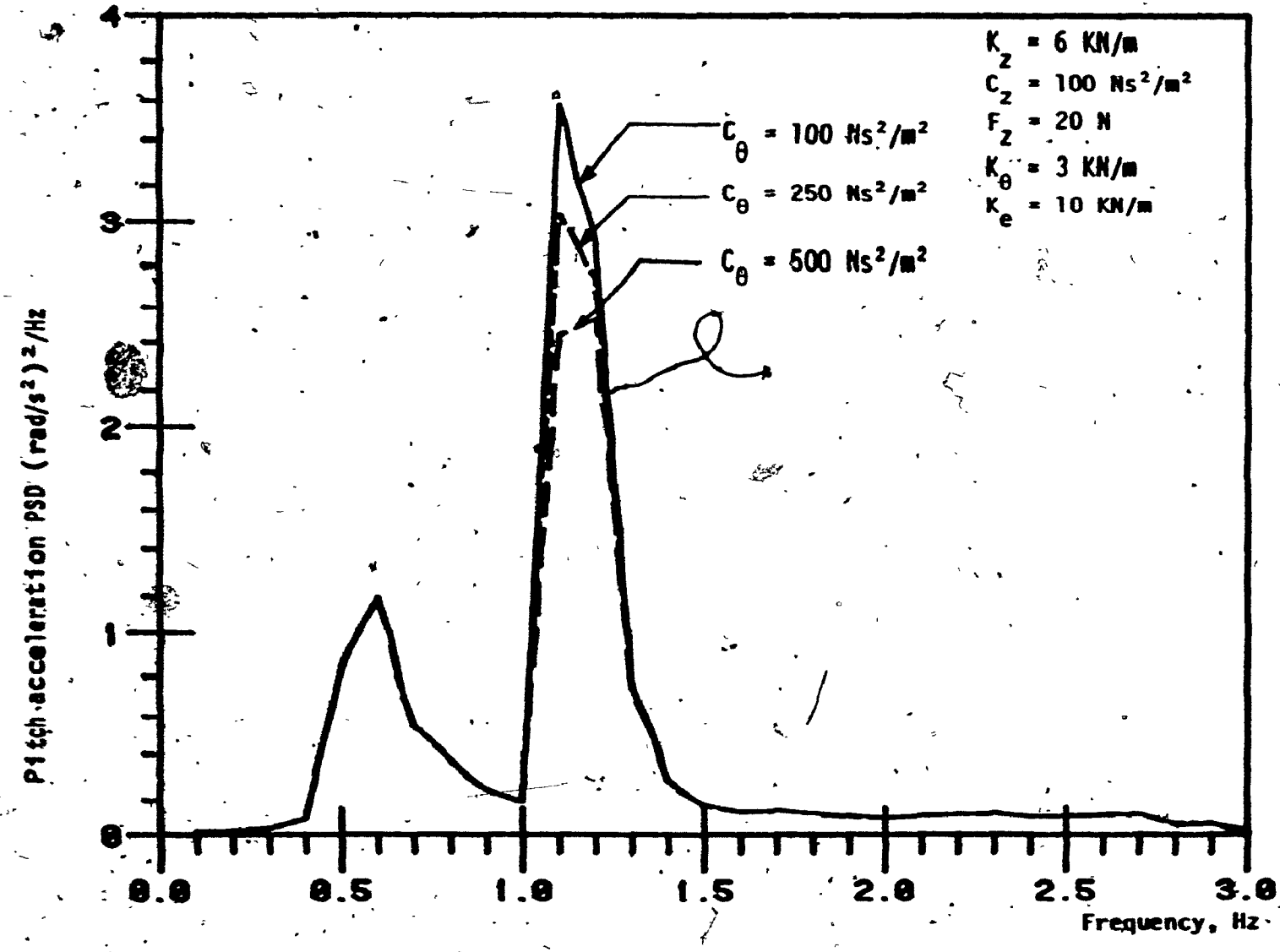

FIGURE 5.26: Influence of variations in the pitch suspension damping coefficient (C_θ) on the pitch acceleration response of rotational seat isolator.

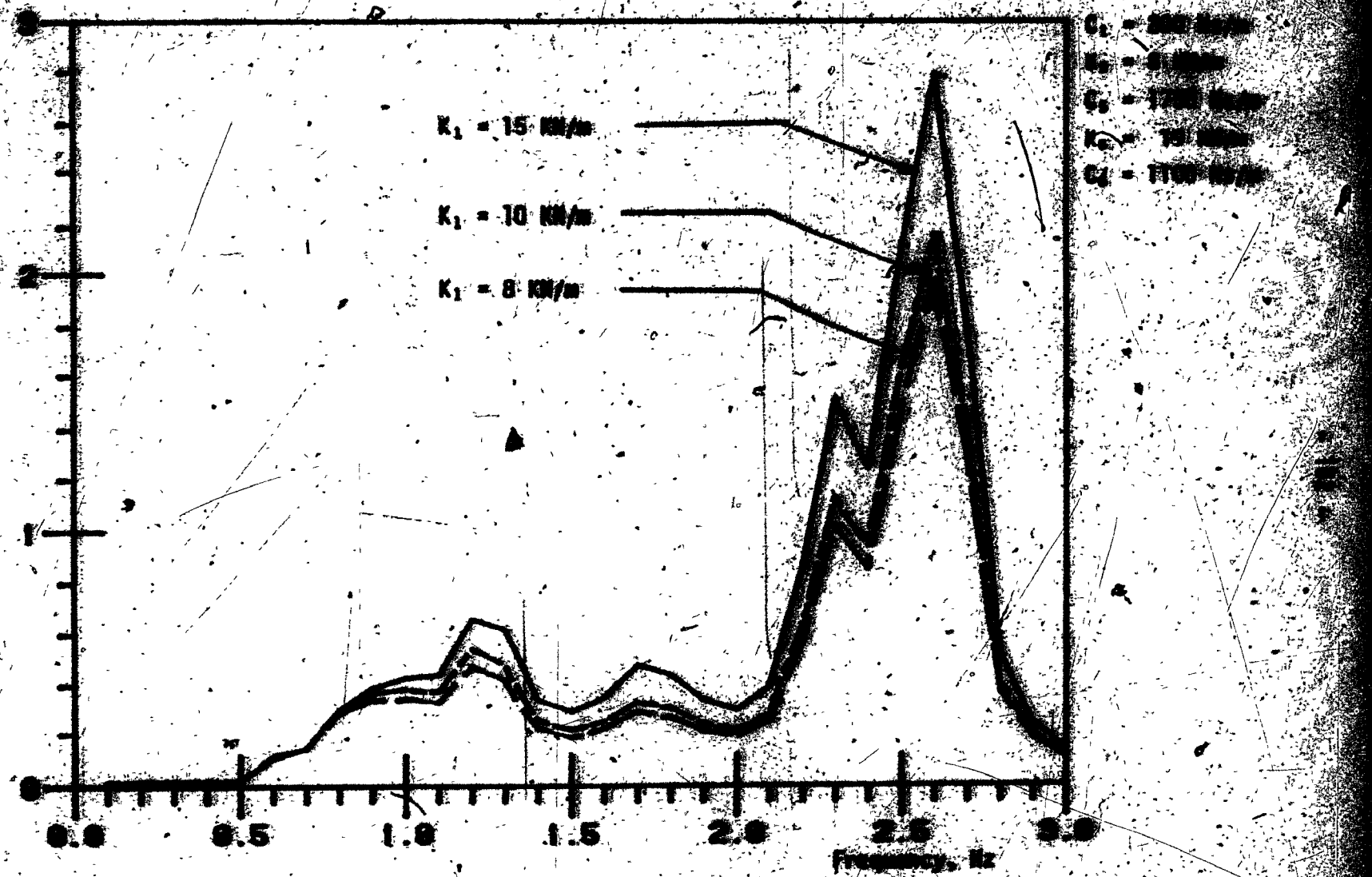

FIGURE 5.27: Bounce acceleration response of 5 D.O.F. cab suspension model.

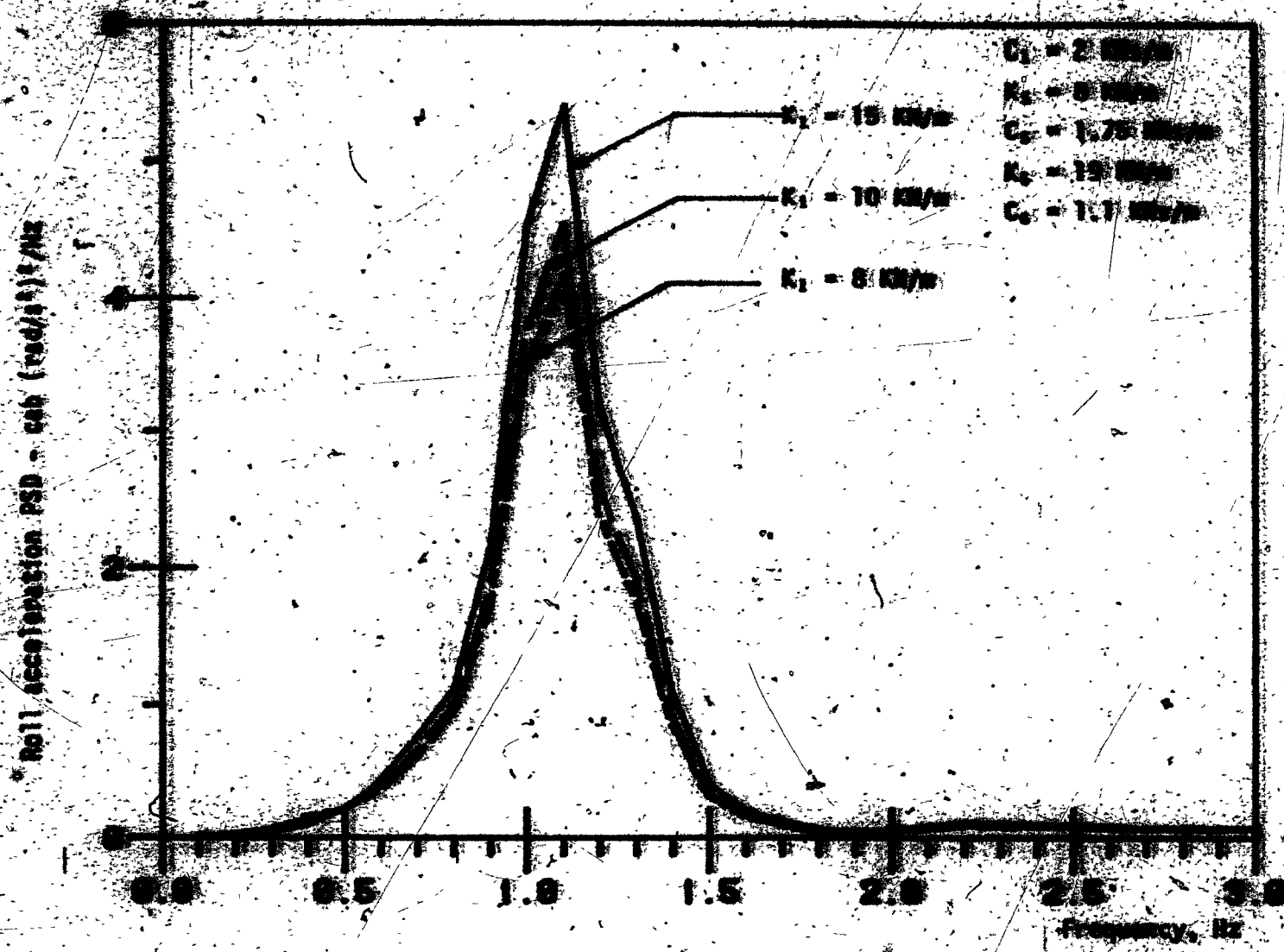

FIGURE 5.28: Roll acceleration response of the 5 D.O.F. cab suspension model.

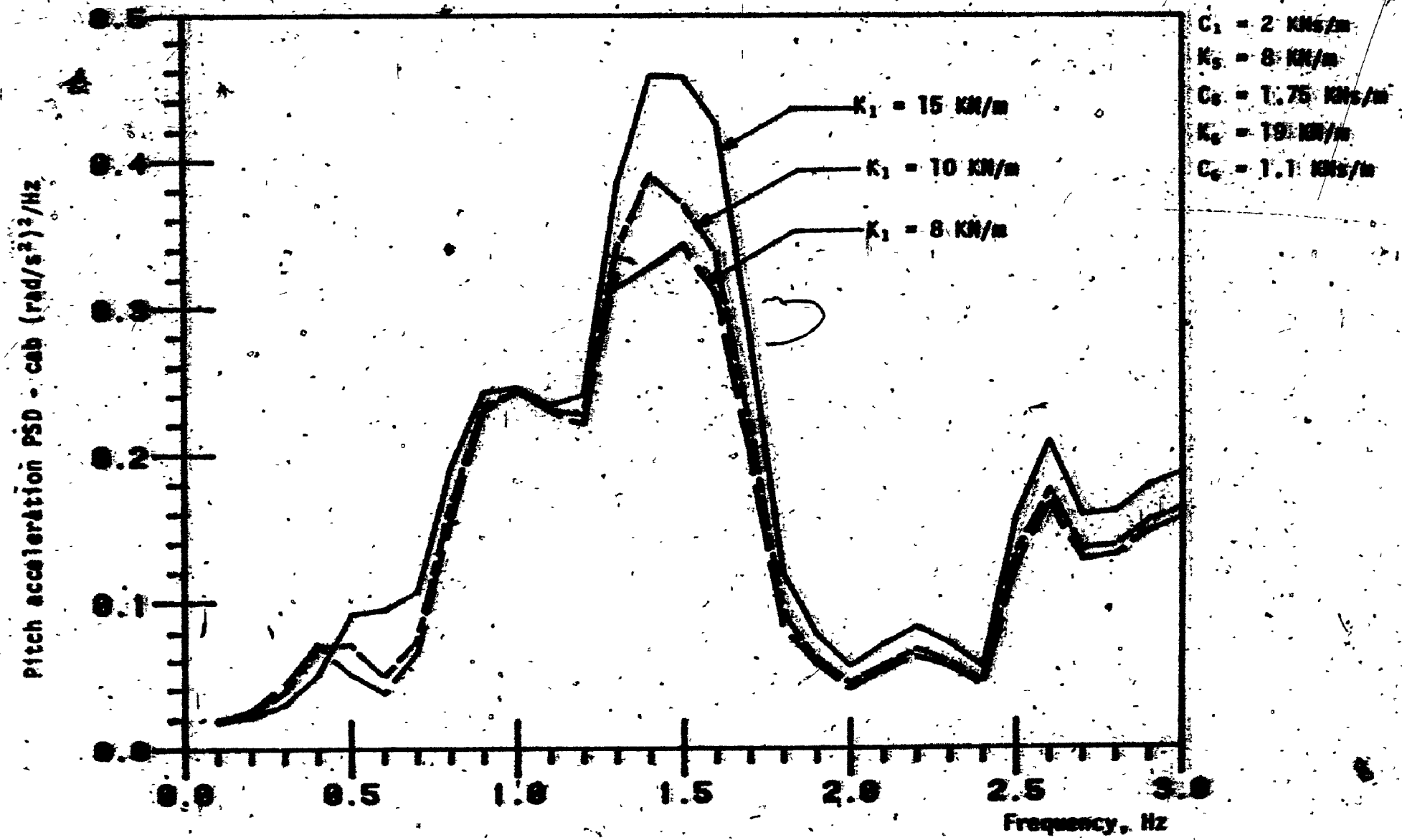

FIGURE 5.29: Pitch acceleration response of 5 D.O.F. cab suspension model.

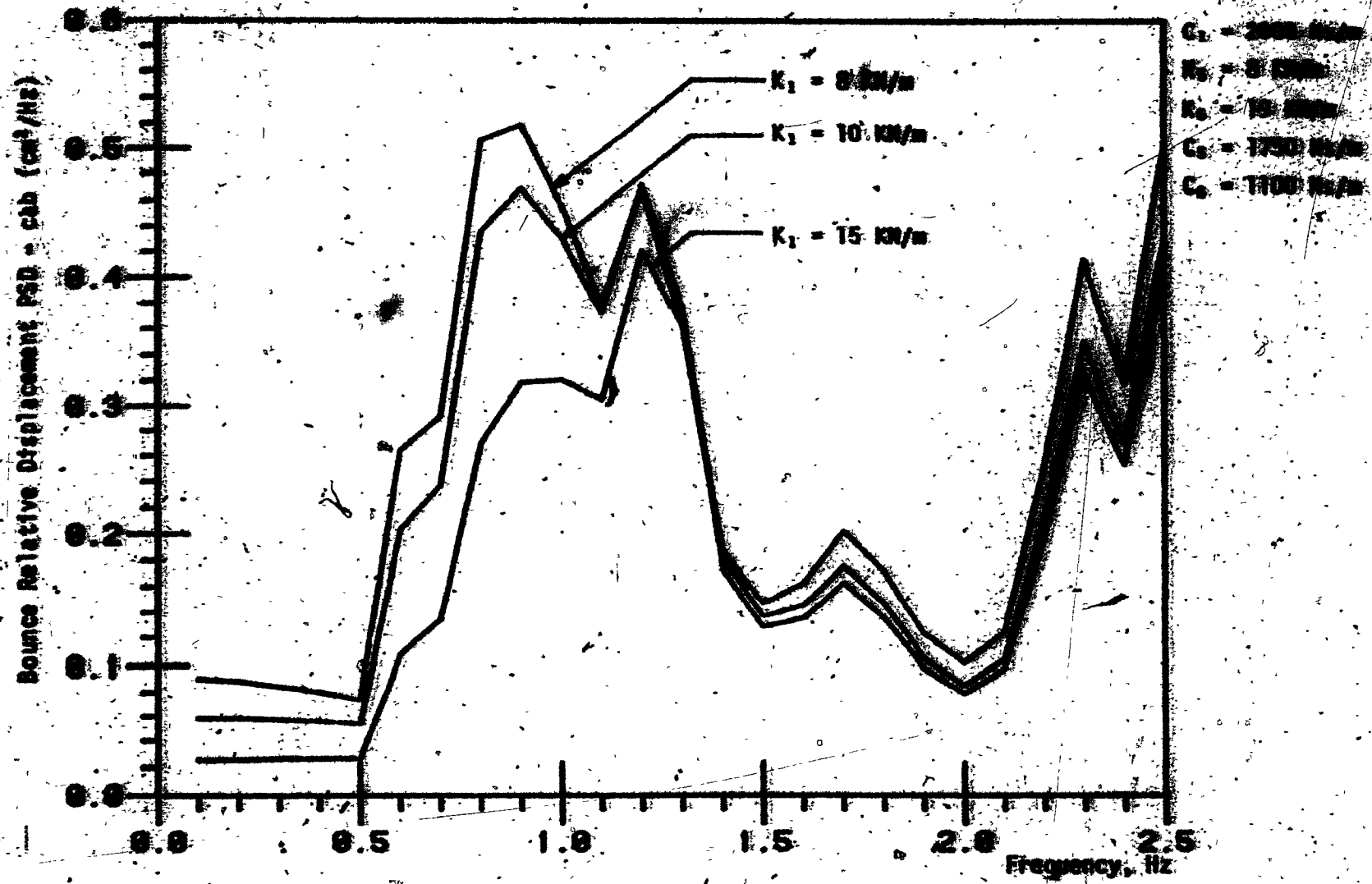

FIGURE 5.30: Influence of variations in the stiffness of corner mounts on the bounce relative displacement response of the 5 DOF cab suspension.

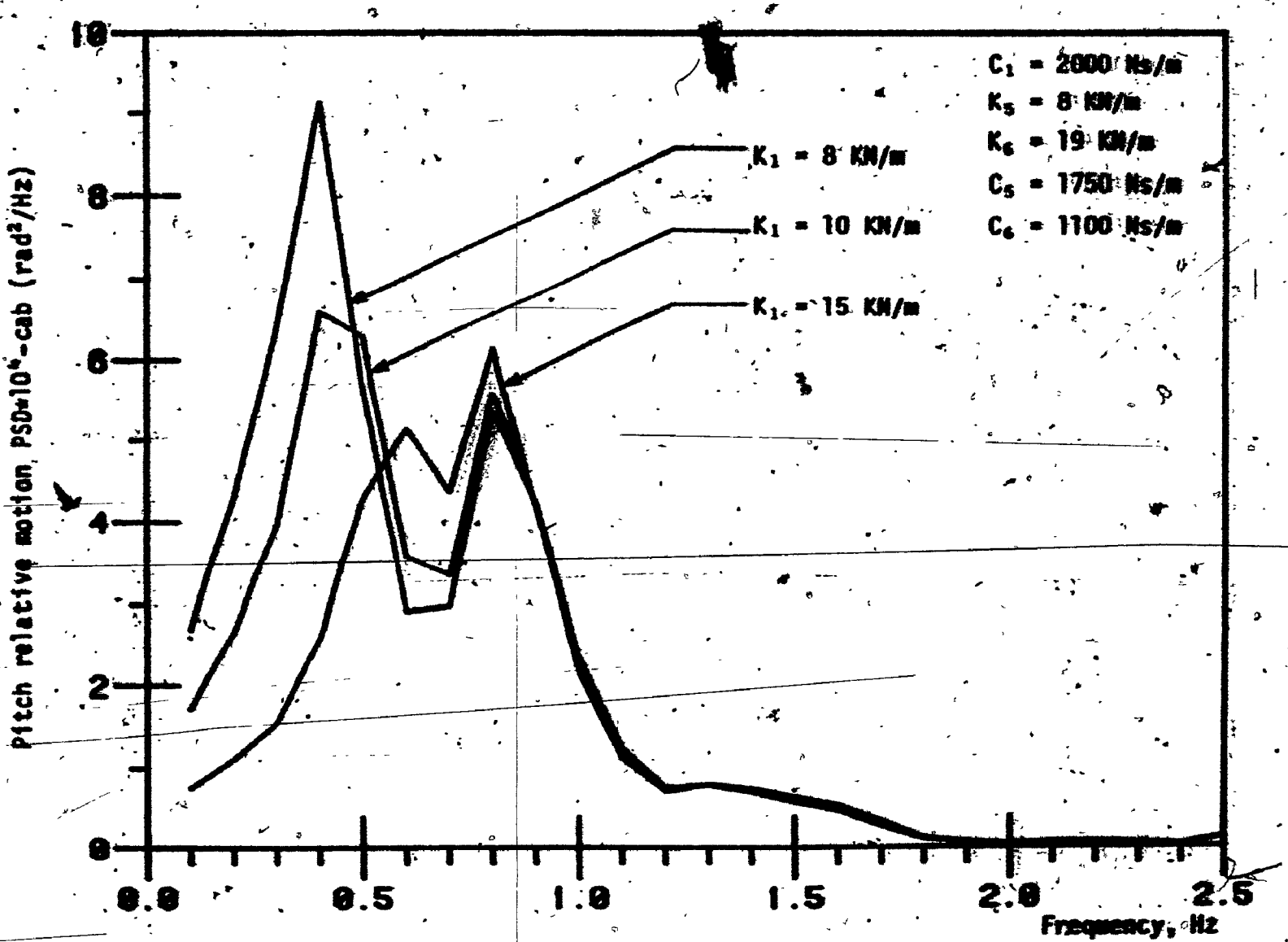

FIGURE 5.31: Influence of variations in the stiffness of corner mounts on the relative motion response of 5 DOF cab suspension.

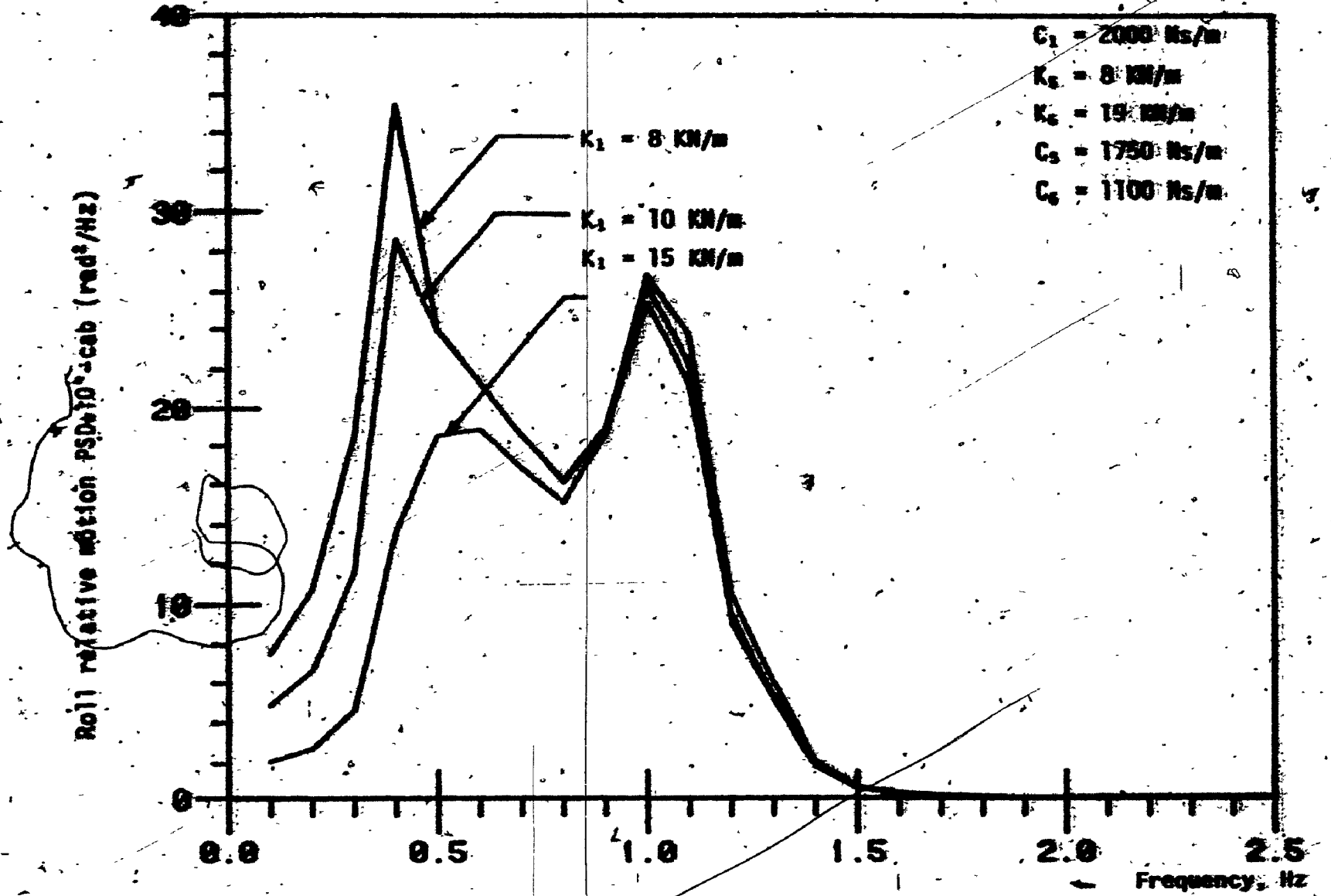

FIGURE 5.32: Influence of variations in the stiffness of corner mounts on the roll relative motion response of 5 DOF cab suspension.

2) Influence of Corner Mounts Damping

Lightly damped cab mounts exhibit superior bounce response corresponding to vehicle resonance, with a significantly large peak occurring at cab suspension resonant frequency as shown in Figure 5.33. The pitch, roll and lateral responses are worsened with lightly damped mounts as presented in Figures 5.34, 5.35 and 5.36. The pitch acceleration response exhibits peaks occurring at pitch and longitudinal resonant frequencies of the cab suspension. The peak response at the two frequencies is worsened with lightly damped cab mounts. The roll and lateral acceleration responses of the cab exhibit large peak corresponding to the lateral resonant frequency of the vehicle. The lateral acceleration at the cab cg improves with lightly dampad cab mounts at the roll resonant frequency of the cab suspension as shown in Figure 5.37. However, heavily damped mounts exhibit superior lateral acceleration response at the cab cg corresponding to lateral resonant frequency of the vehicle.

3) Influence of Lateral Isolator Parameters

Stiffness of the lateral isolator has no influence on the bounce, longitudinal and pitch performance of the 5 D-O-F cab suspension model. Figures 5.38, 5.39 and 5.40 reveal that the softer lateral isolator can provide superior lateral and roll performance of the cab suspension model. However, extremely soft lateral isolator exhibit excessive lateral relative motion of the cab with respect to the chassis as presented in Figures 5.41. The roll relative motion PSD response improves as the stiffness of the lateral isolator is decreased, as shown in Figure 5.42. Figures 5.43, 5.44. and 5.45 indicate that the lateral isolators with large damping results in better lateral and roll acceleration responses.

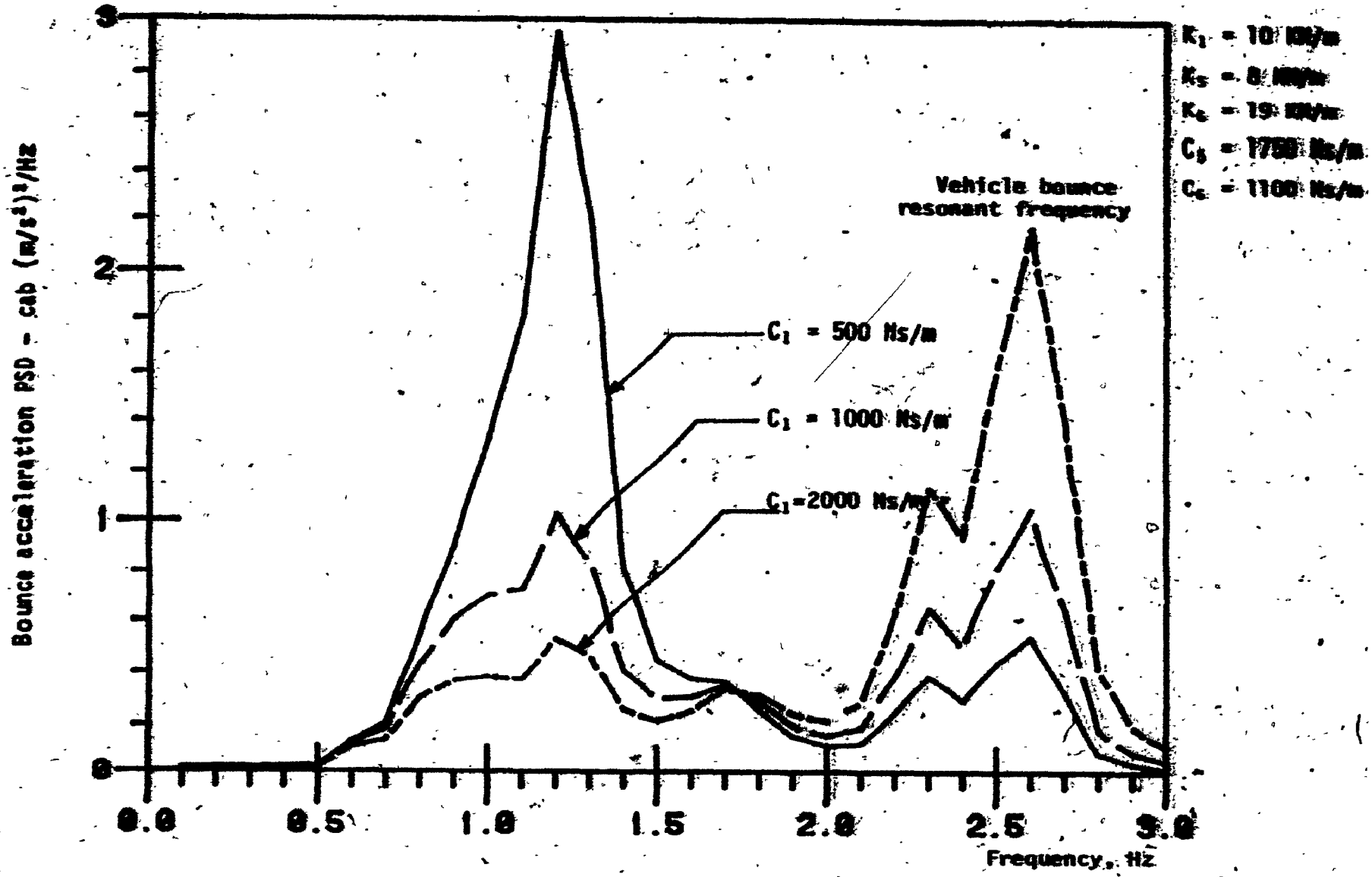

FIGURE 5.33: Sensitivity of bounce acceleration response to variations in corner mounts damping coefficients.

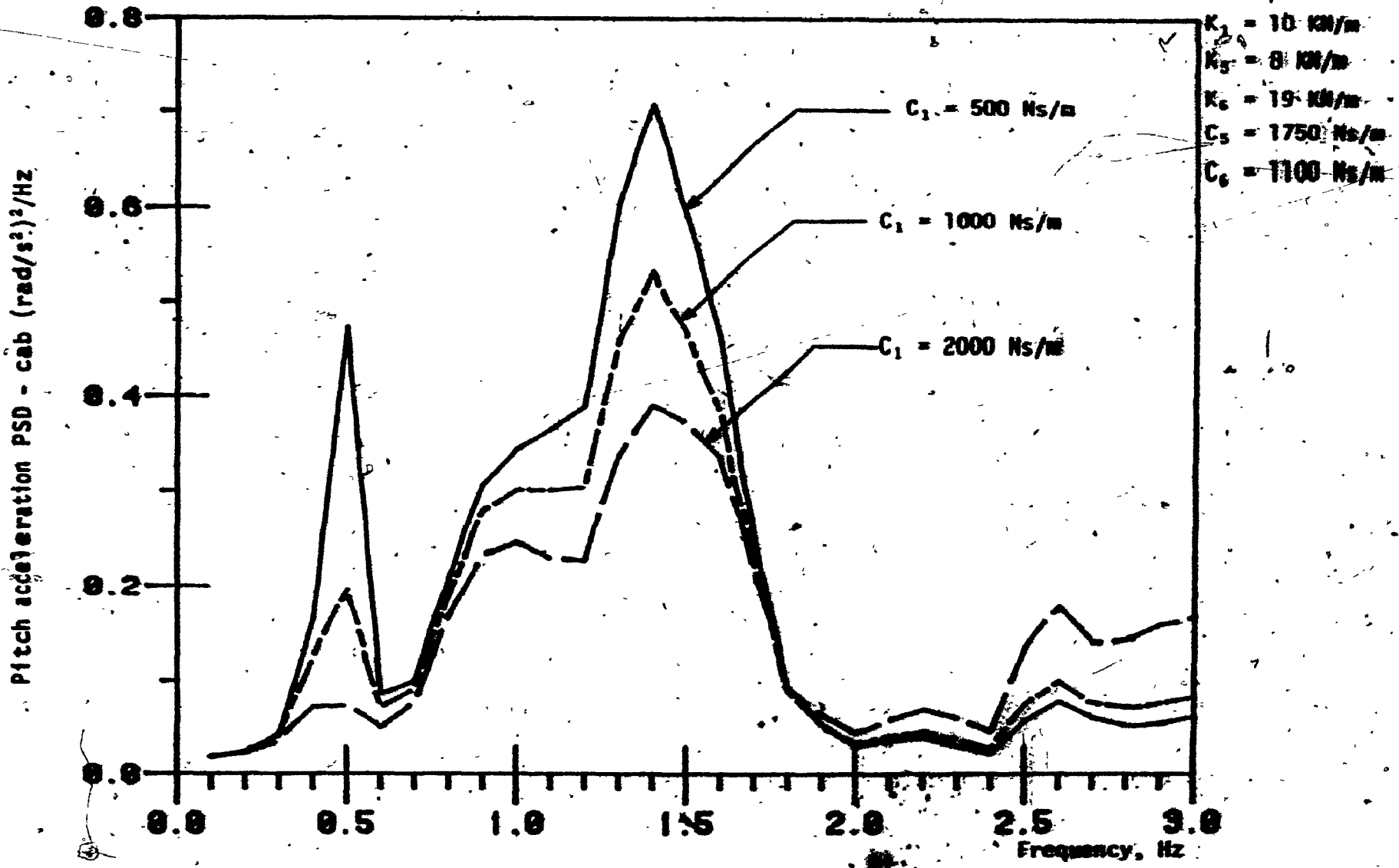

FIGURE 5.34: Influence of corner mounts damping on the pitch acceleration response of 5 DOF cab suspension model.

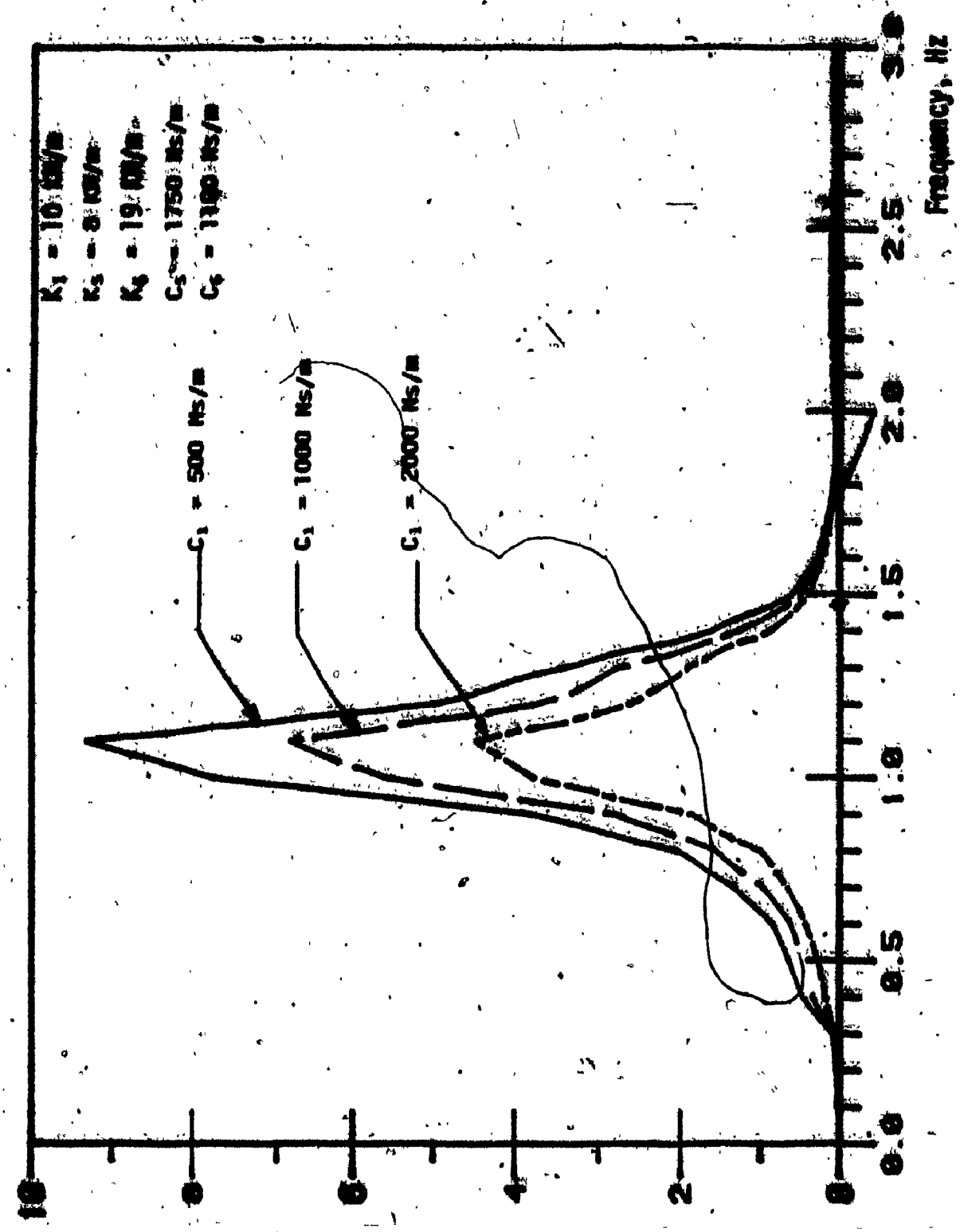

FIGURE 5.35: Influence of corner mounts damping on the roll acceleration response of 5 DOF cab suspension model.

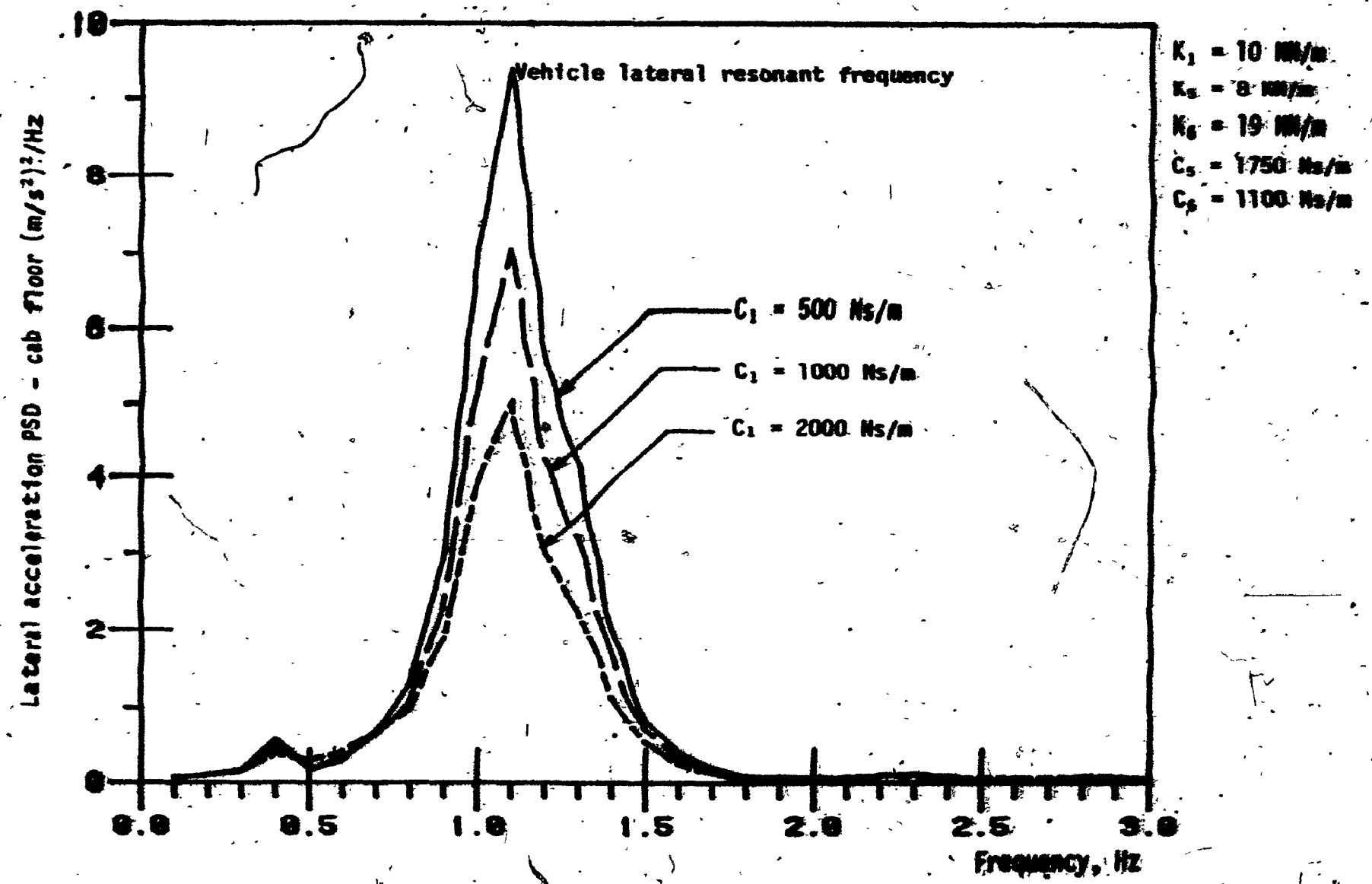

FIGURE 5.36: Lateral acceleration PSD response at the cab floor with variations in corner mounts damping.

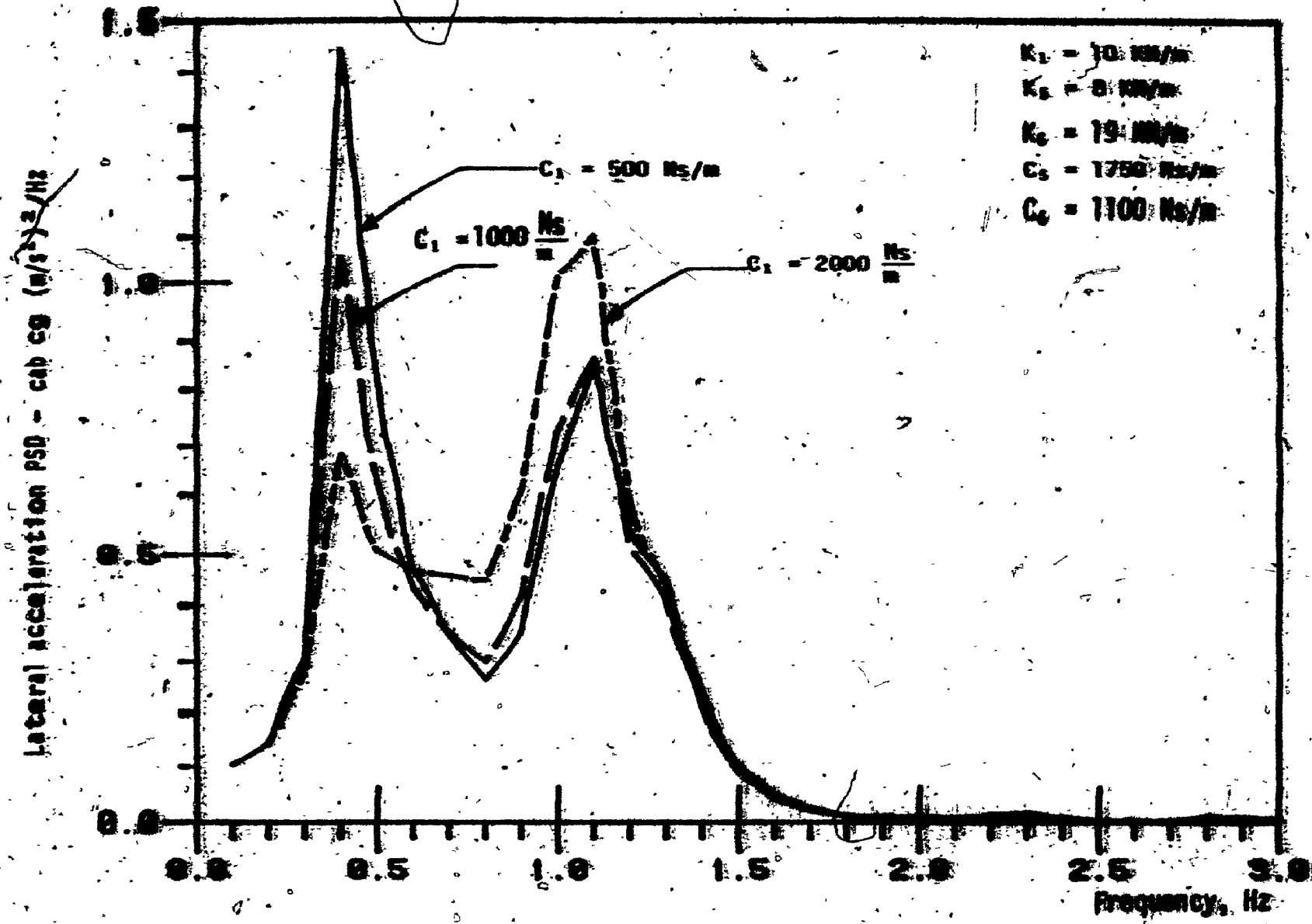

FIGURE 5.37: Influence of corner mounts damping on the cab cg lateral acceleration PSD response of the 5 DOF cab suspension model.

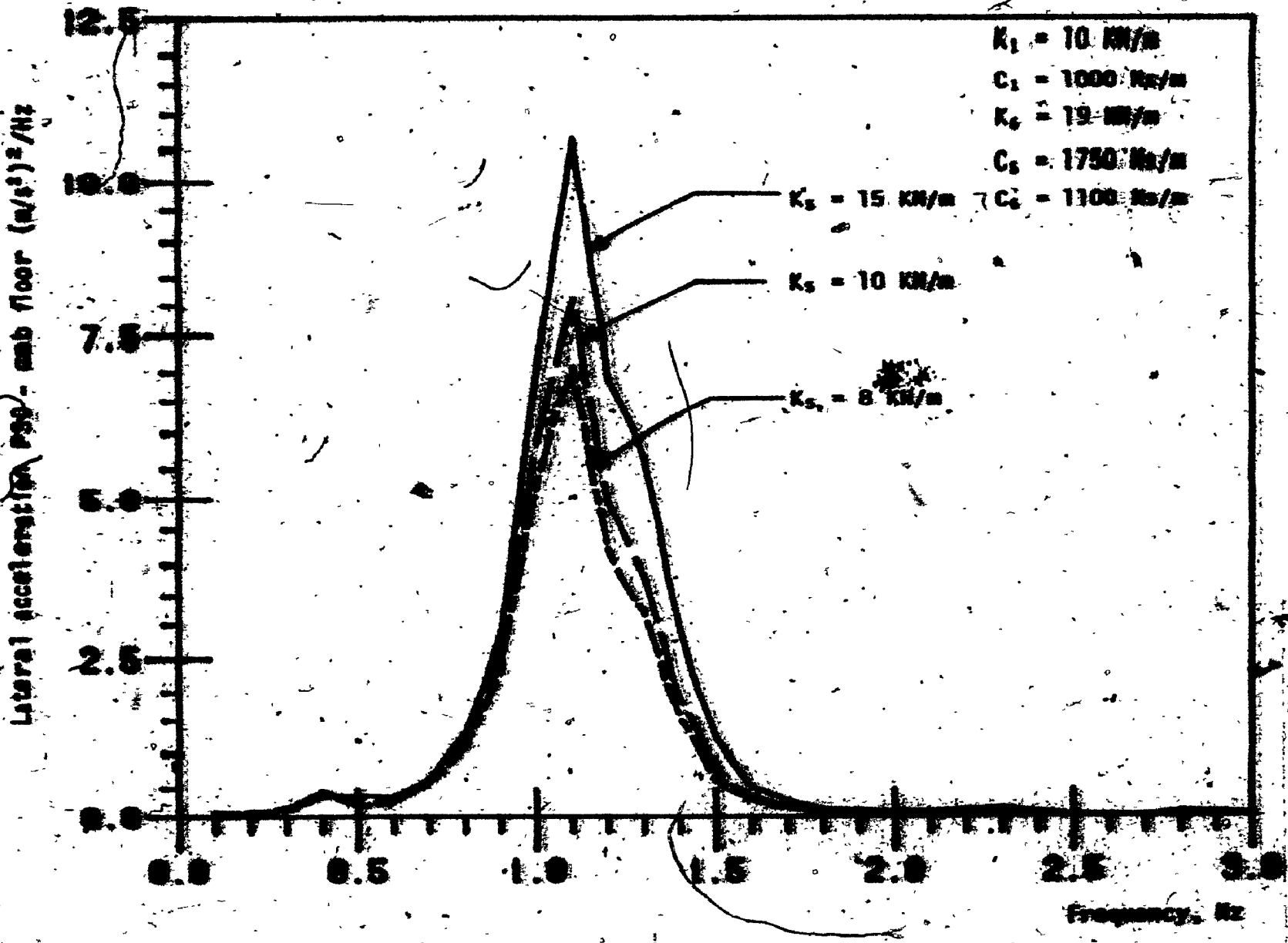

FIGURE 5.38: Influence of variations in lateral isolator stiffness on the lateral acceleration response of 5 DOF cab suspension model.

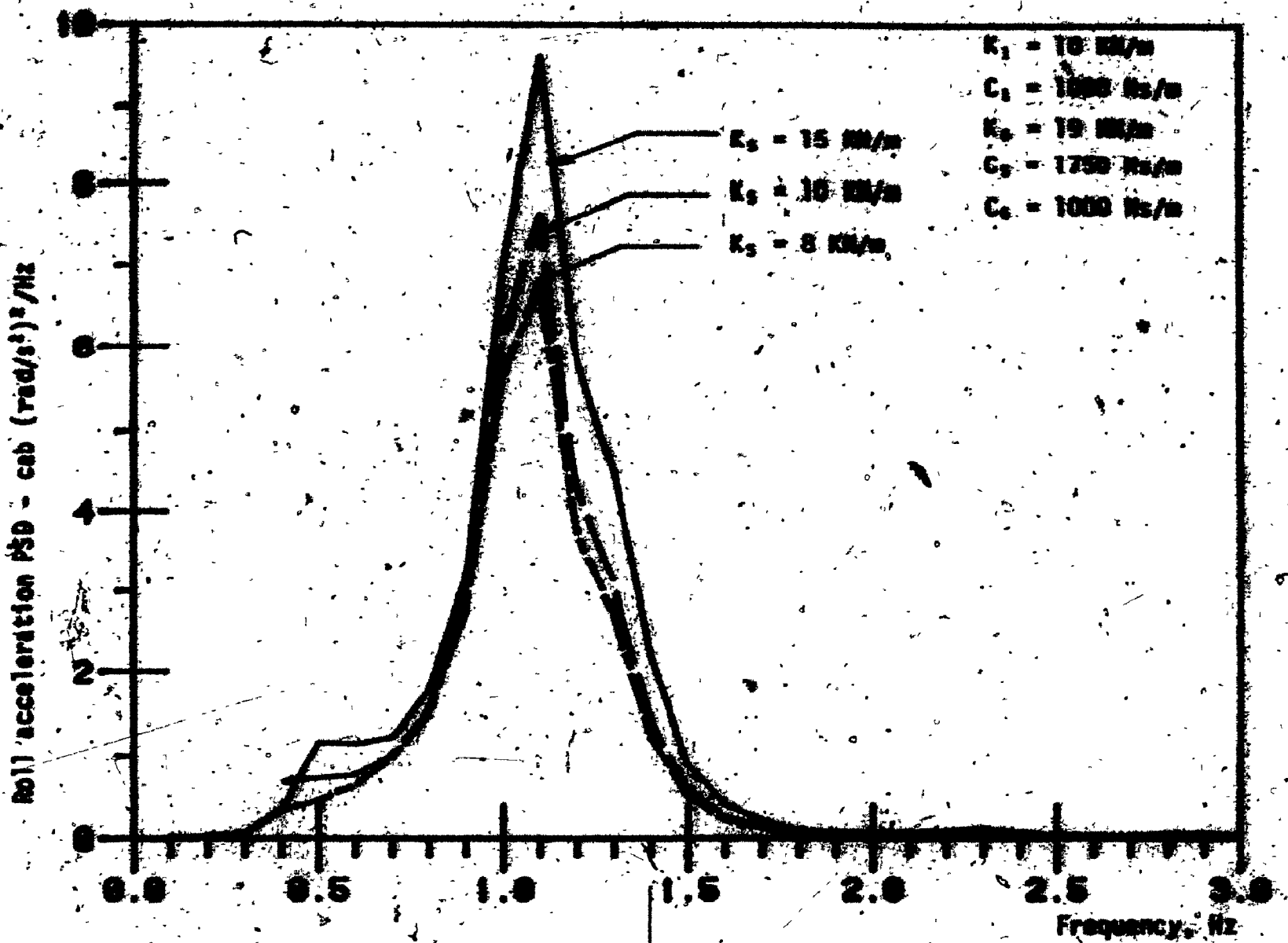

FIGURE 5.39: Influence of variations in lateral isolator stiffness on the roll acceleration response of 5 DOF cab suspension model.

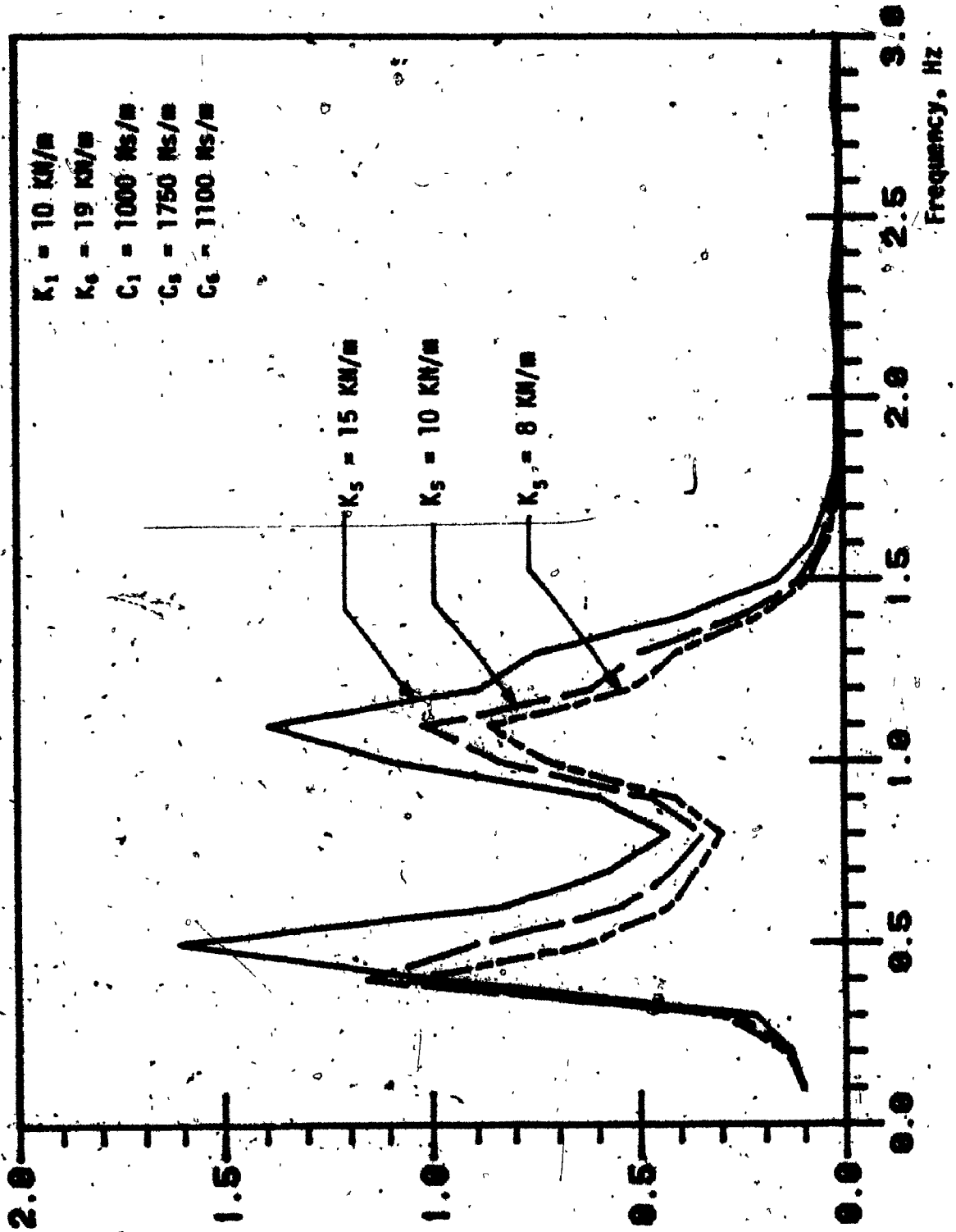

FIGURE 5.40: Influence of variations in lateral isolator stiffness on the lateral acceleration response at cab cg.

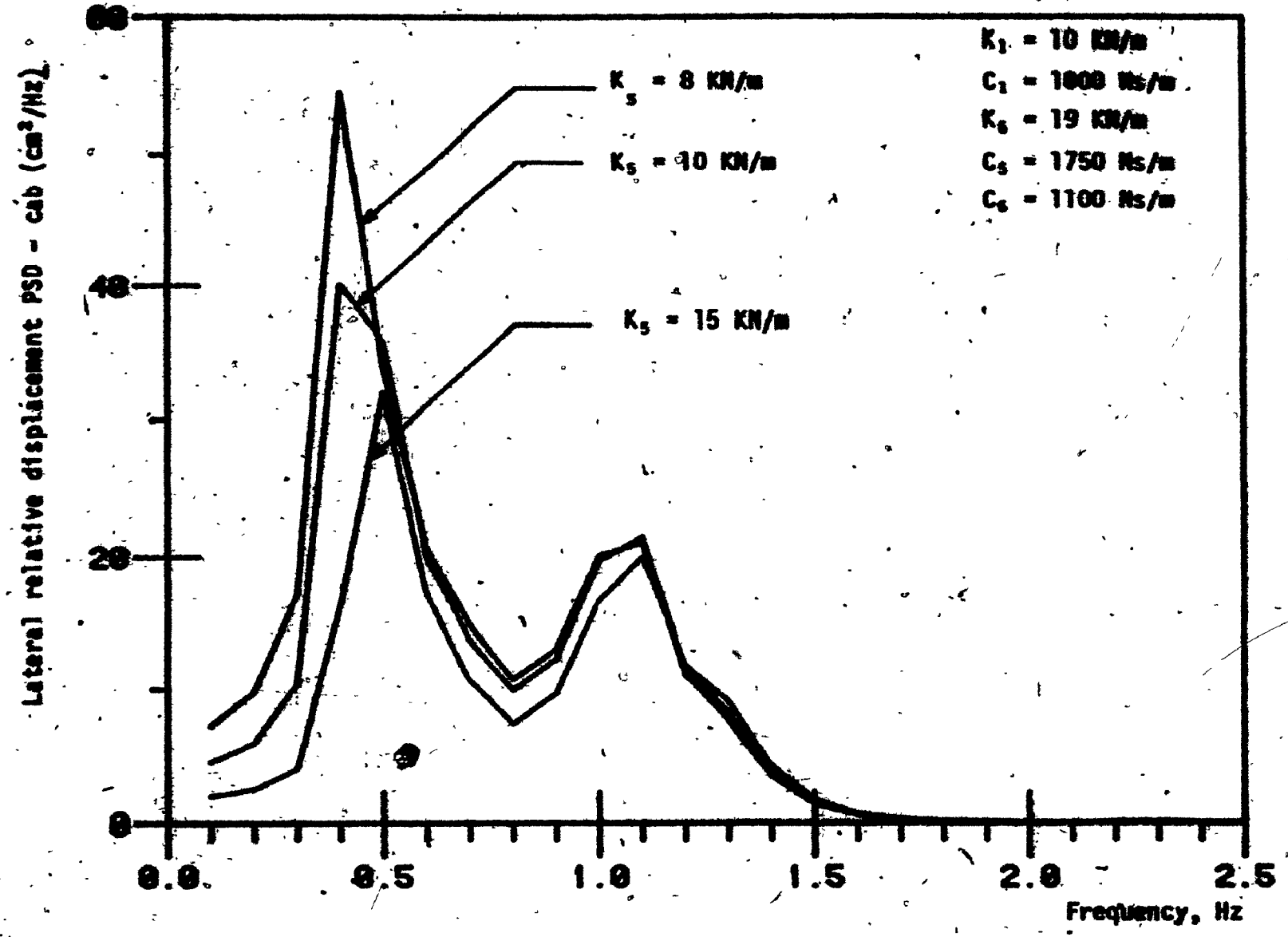

FIGURE 5.41: Influence of variations in the stiffness of lateral isolator (K_s) on the lateral relative displacement response of 5 DOF cab suspension model.

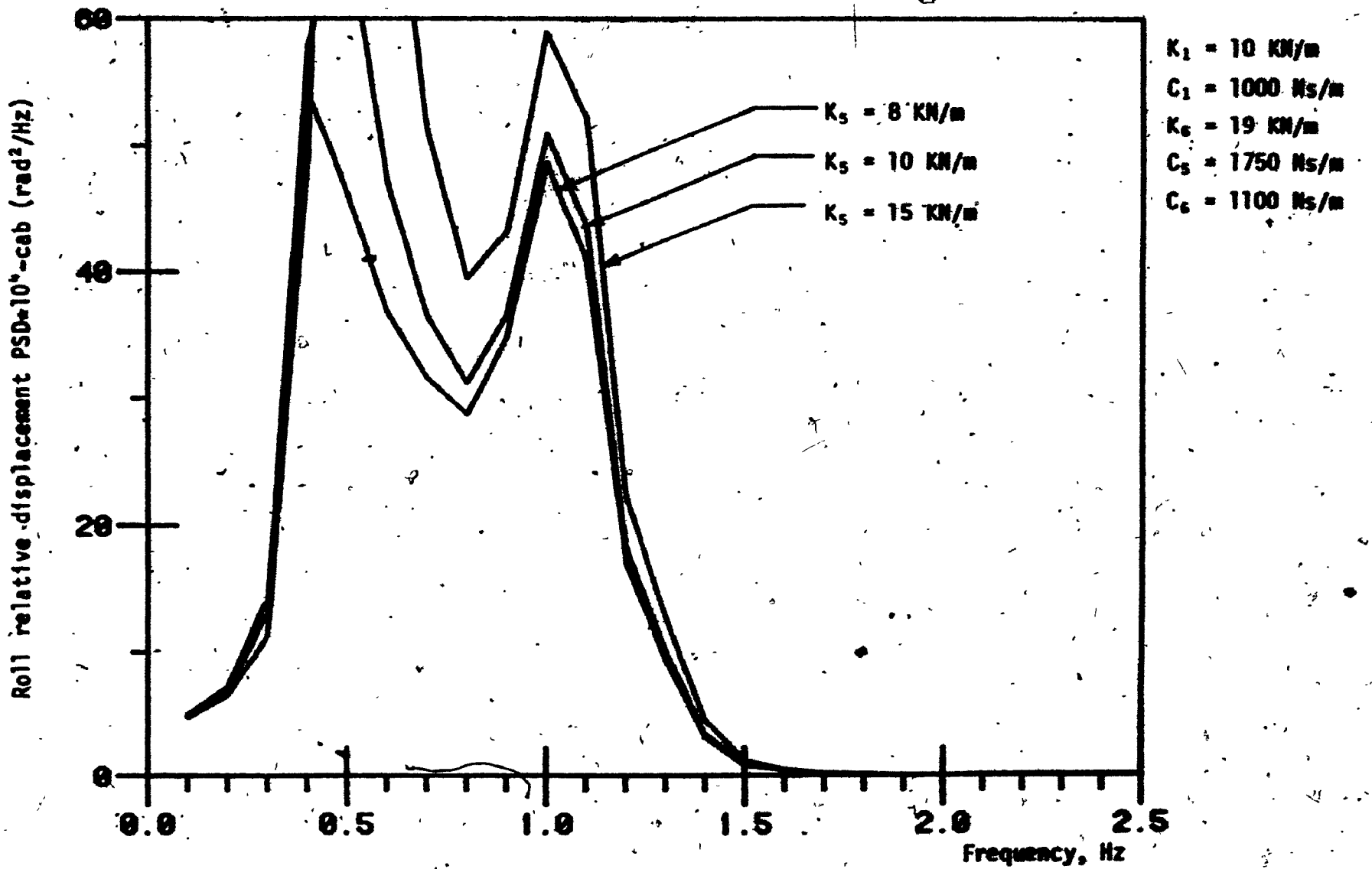

FIGURE 5.42: Influence of variations in the stiffness of lateral isolator (K_5) on the roll displacement response of 5 DOF cab suspension model.

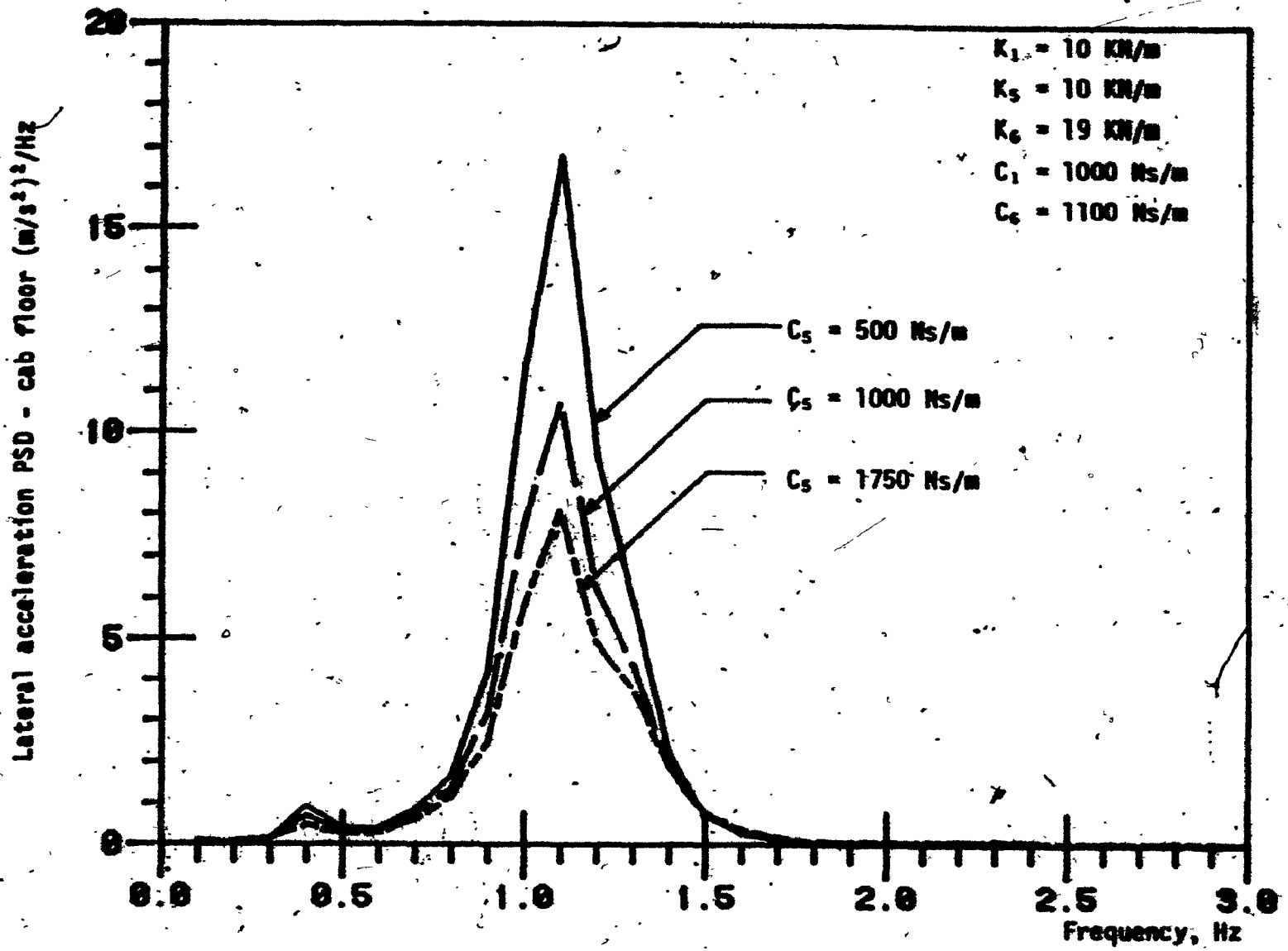

FIGURE 5.43: Influence of variations in lateral isolator damping coefficient on the lateral acceleration response of 5 DOF cab suspension model.

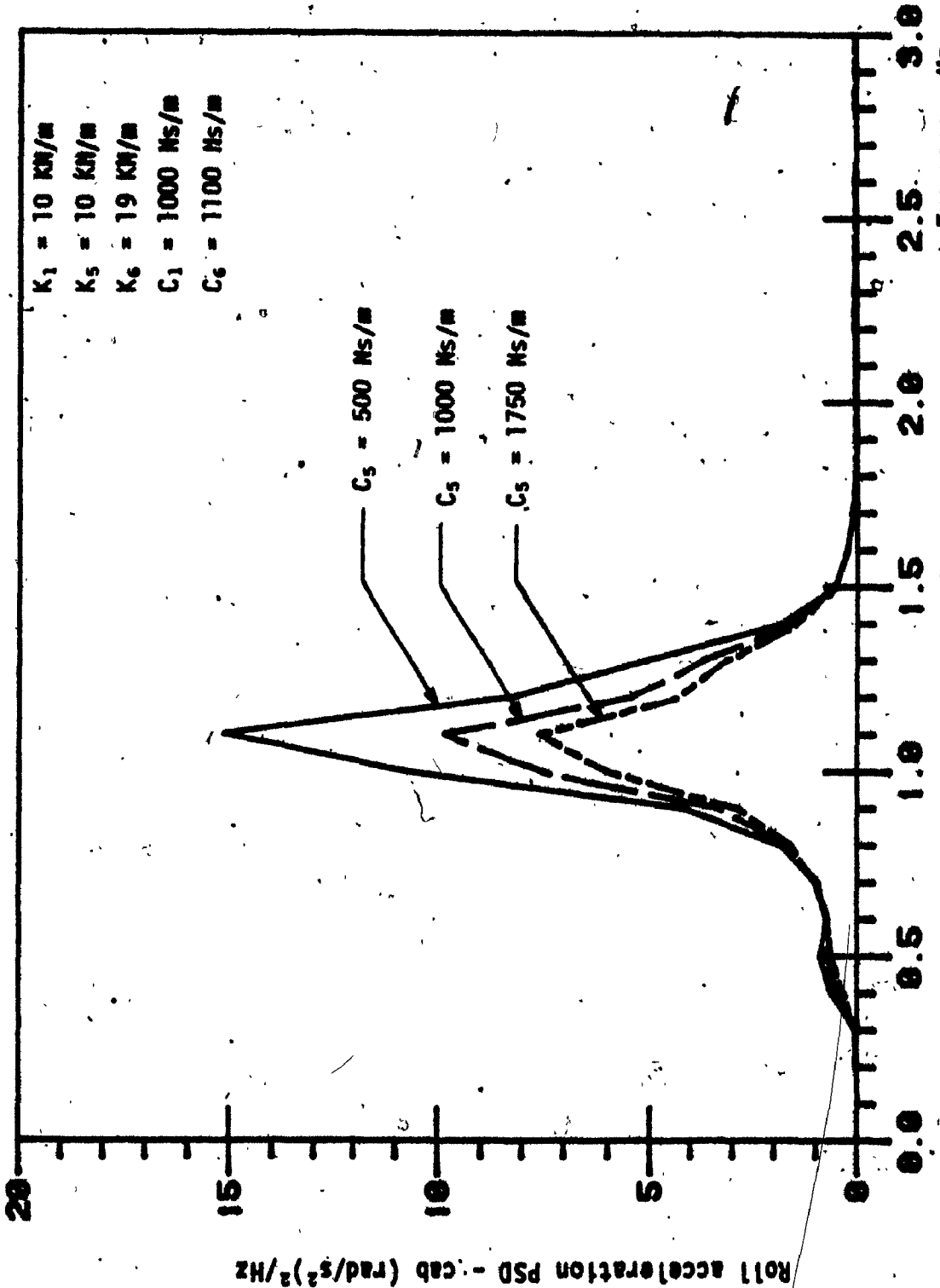

FIGURE 5.44: Influence of variations in lateral isolator damping coefficient on the roll acceleration PSD response of the 5 DOF cab suspension model.

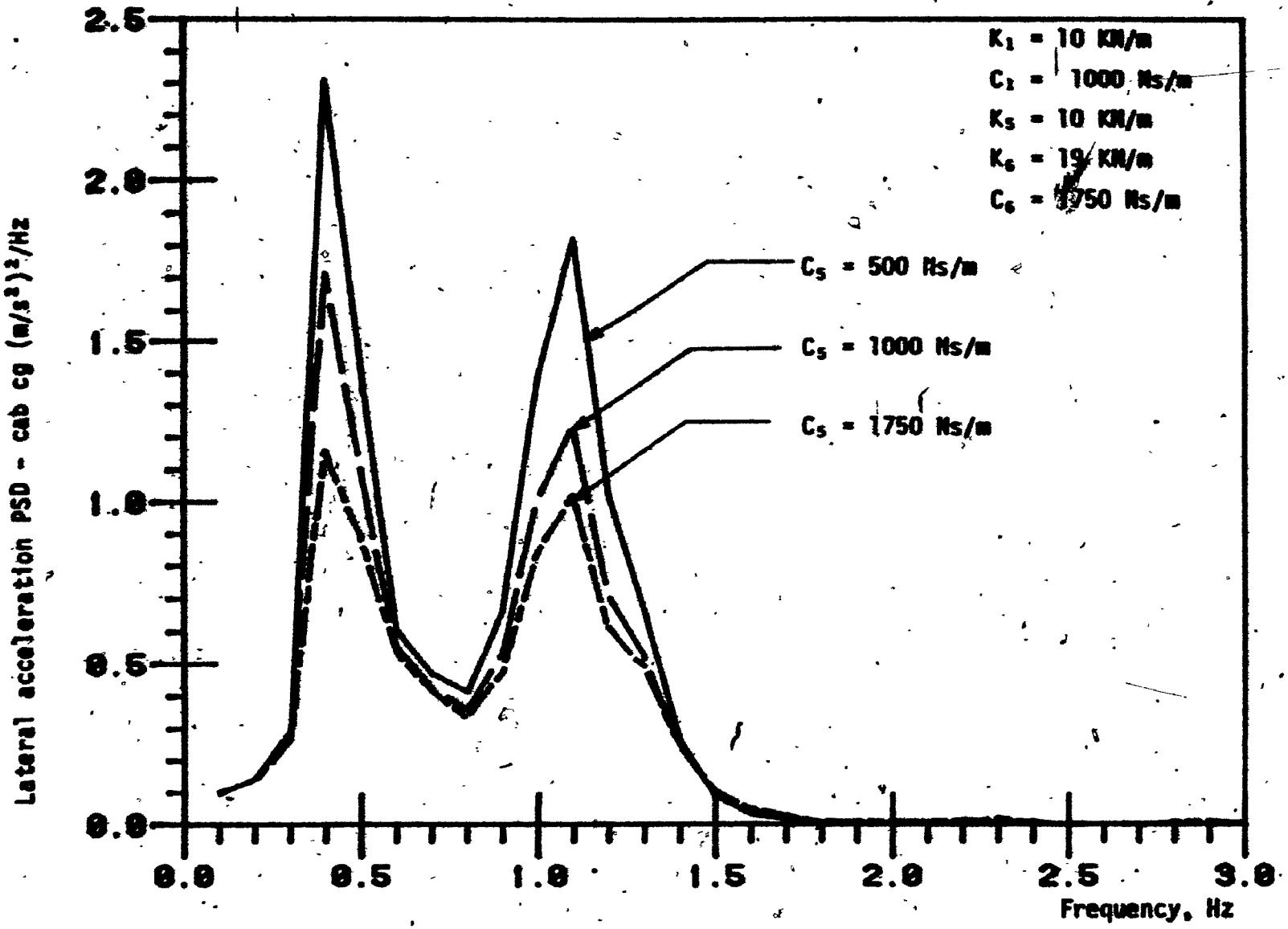

FIGURE 5.46: Influence of variations in lateral isolator damping coefficient on the lateral acceleration response at cab cg.

5.3.4 INFLUENCE OF SUSPENSION PARAMETERS ON THE PERFORMANCE OF CAB AND SEAT SUSPENSION MODELS

Model I: Cab Suspension with Bounce Seat Suspension (6 DOF)

The 6 DOF cab suspension model is an extension of the 5 DOF cab suspension with vertically suspended seat. Addition of vertically suspended seat does not influence longitudinal, pitch, lateral, and roll responses of the cab-suspension model, but the bounce acceleration response of the seat mass is significantly improved, as shown in Figure 5.46. Softer and lightly damped seat suspension exhibits excellent bounce response of the seat mass corresponding to vehicle resonant frequencies as shown in Figures 5.46 and 5.47. Also the influence of parameters, such as seat location, seat height and cab cg height are investigated to find an optimum cab and seat suspension geometry. The parametric study revealed that the location of seat has no significant influence on the bounce response. However, the heights of the seat mass cg and the cab cg have a strong influence on the lateral acceleration response of the seat mass as shown in Figures 5.48, 5.49 and 5.50. The lateral and roll acceleration response of the cab improve significantly, when the location of cab cg height is lowered.

Model II: Cab Suspension with Bounce and Lateral Seat Suspensions

Addition of lateral seat suspension to the six degrees of freedom cab and seat suspension model does not affect the bounce, longitudinal, pitch and roll performance. The lateral seat isolator tends to improve the lateral response slightly at the cab floor as shown in Figures 5.51 and 5.52. However, there exists an optimum value for the stiffness of lateral isolator to achieve the best lateral response of the cab as observed from Figure 5.51. A lightly damped lateral seat isolator provides a significant improvement in the lateral response of the cab floor as

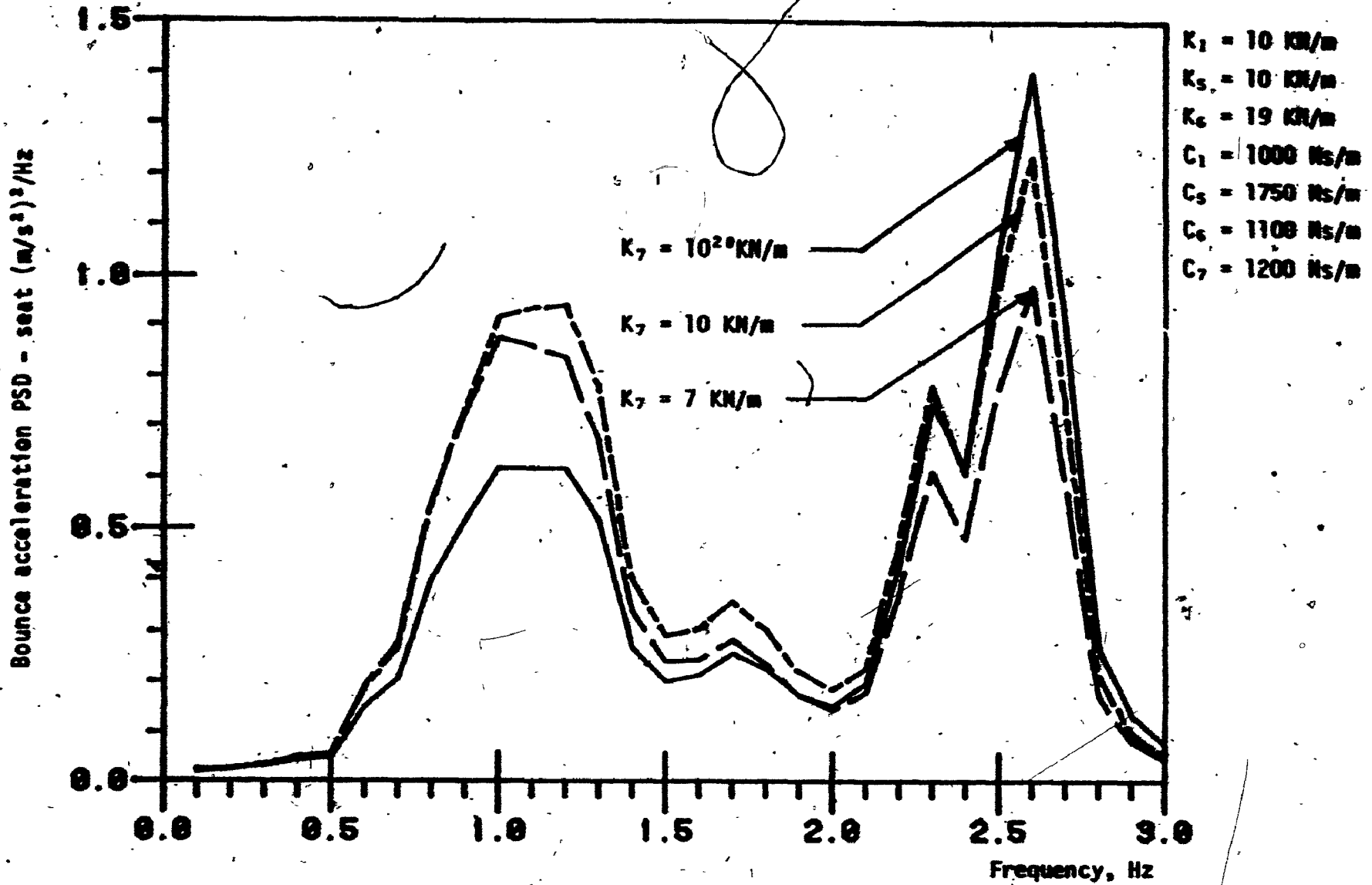

FIGURE 5.46: Sensitivity of the bounce acceleration response of the 6 DOF cab-seat suspension model to variations in bounce seat suspension stiffness (K_7).

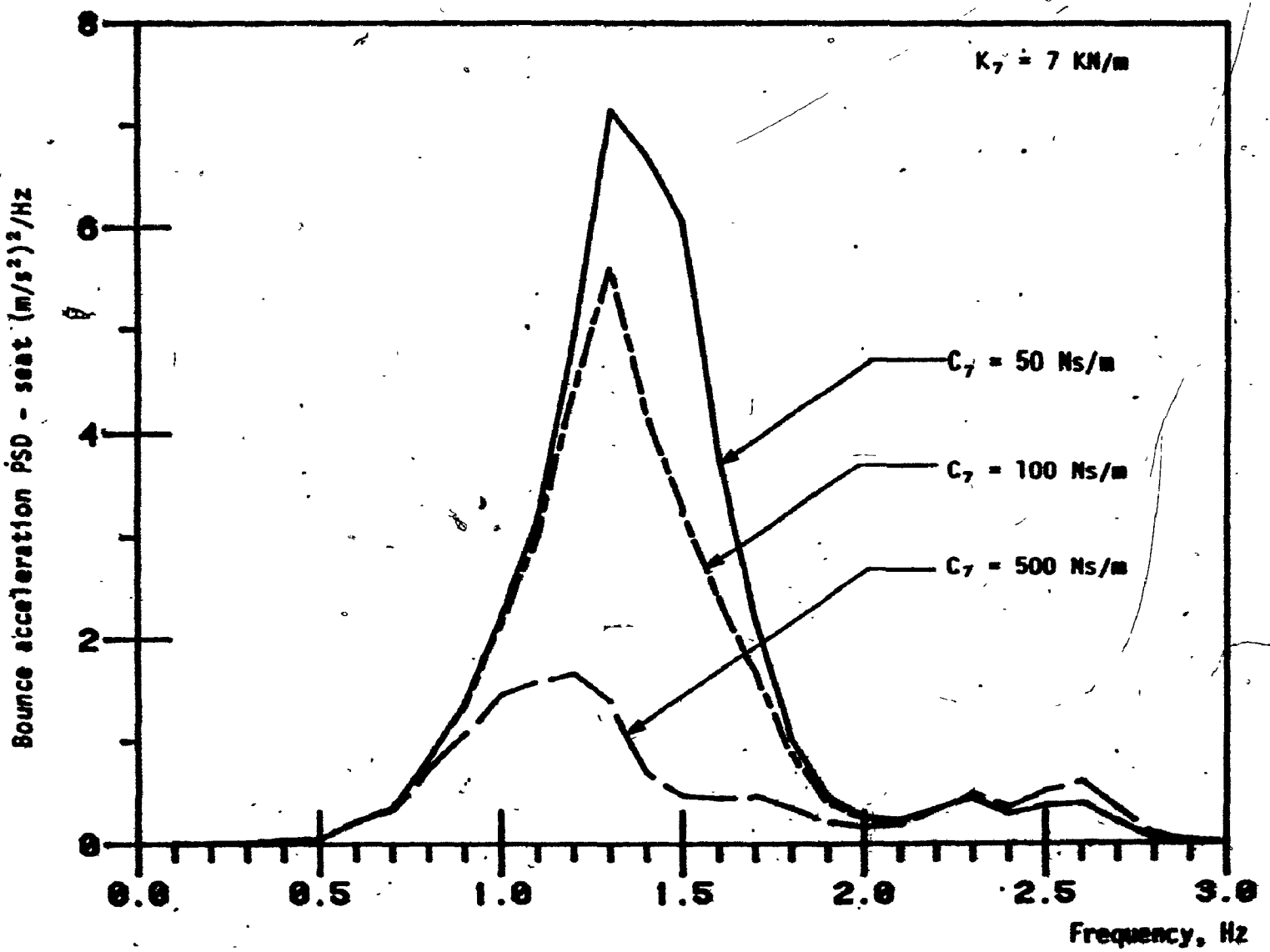

FIGURE 5.47: Sensitivity of bounce acceleration response of 6 DOF cab-seat suspension model to variations in the seat suspension damping.

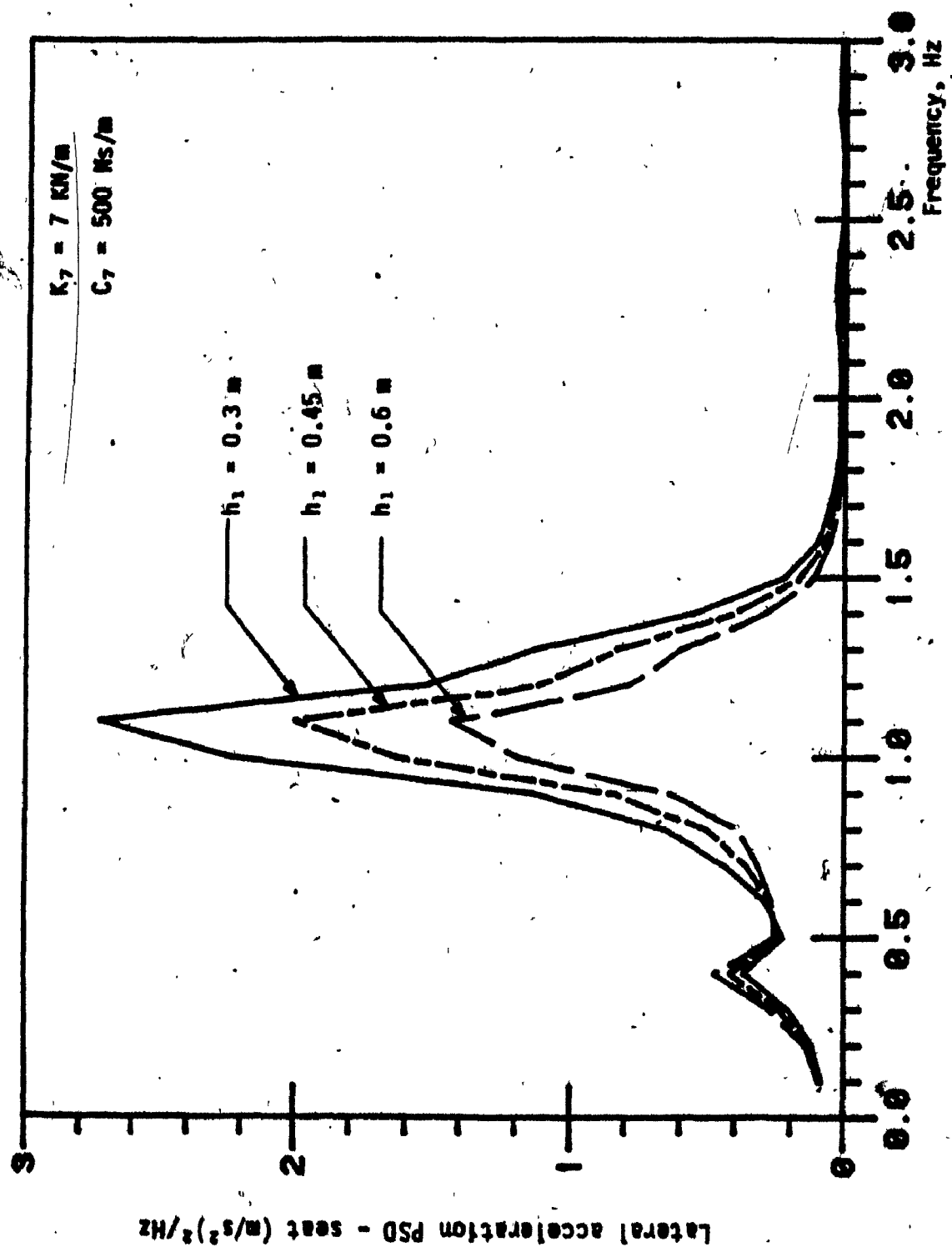

FIGURE 5.48: Influence of seat height on lateral acceleration response at the seat.

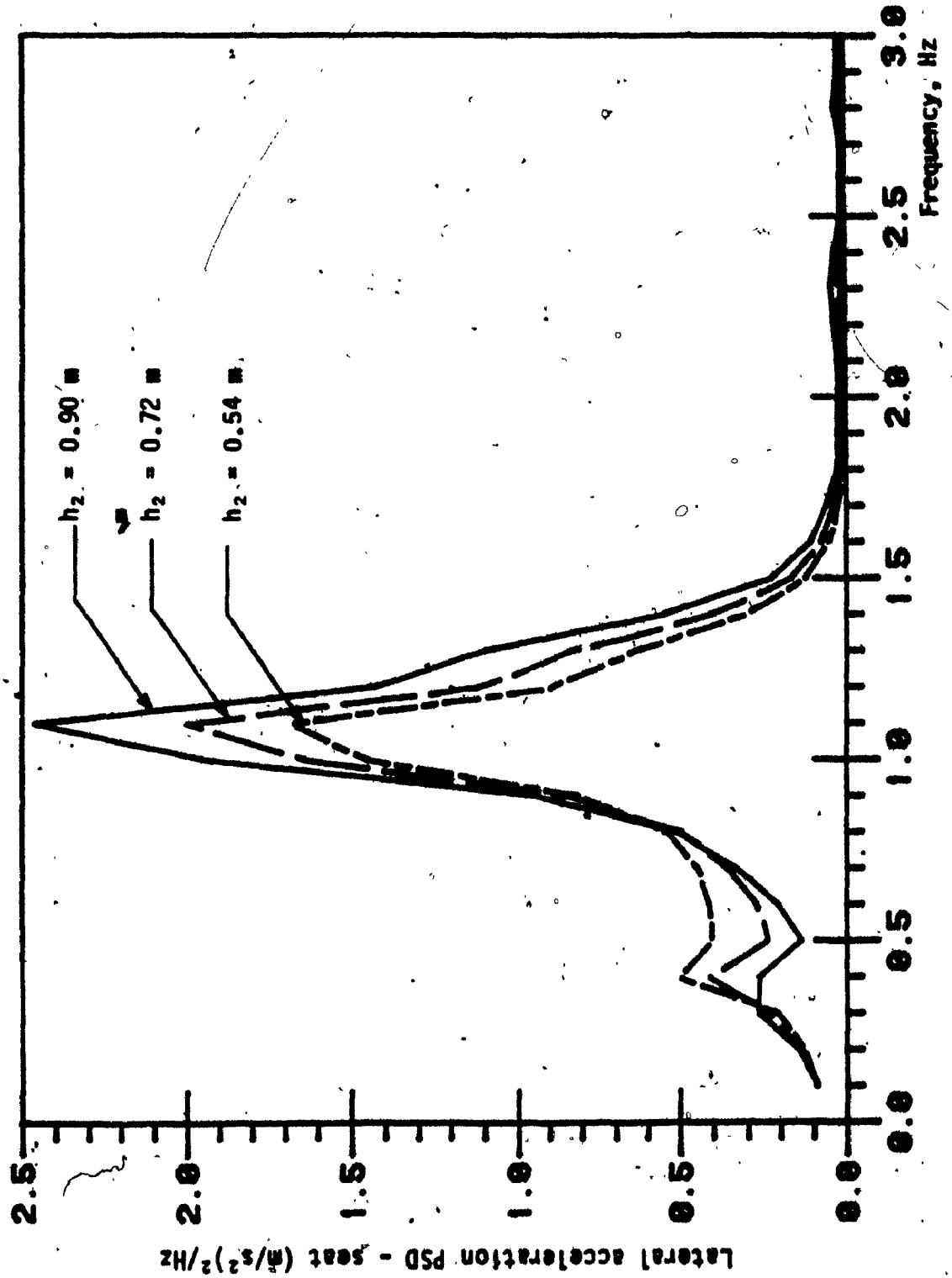

FIGURE 5.49: Influence of cab cg height on the lateral response of seat mass.

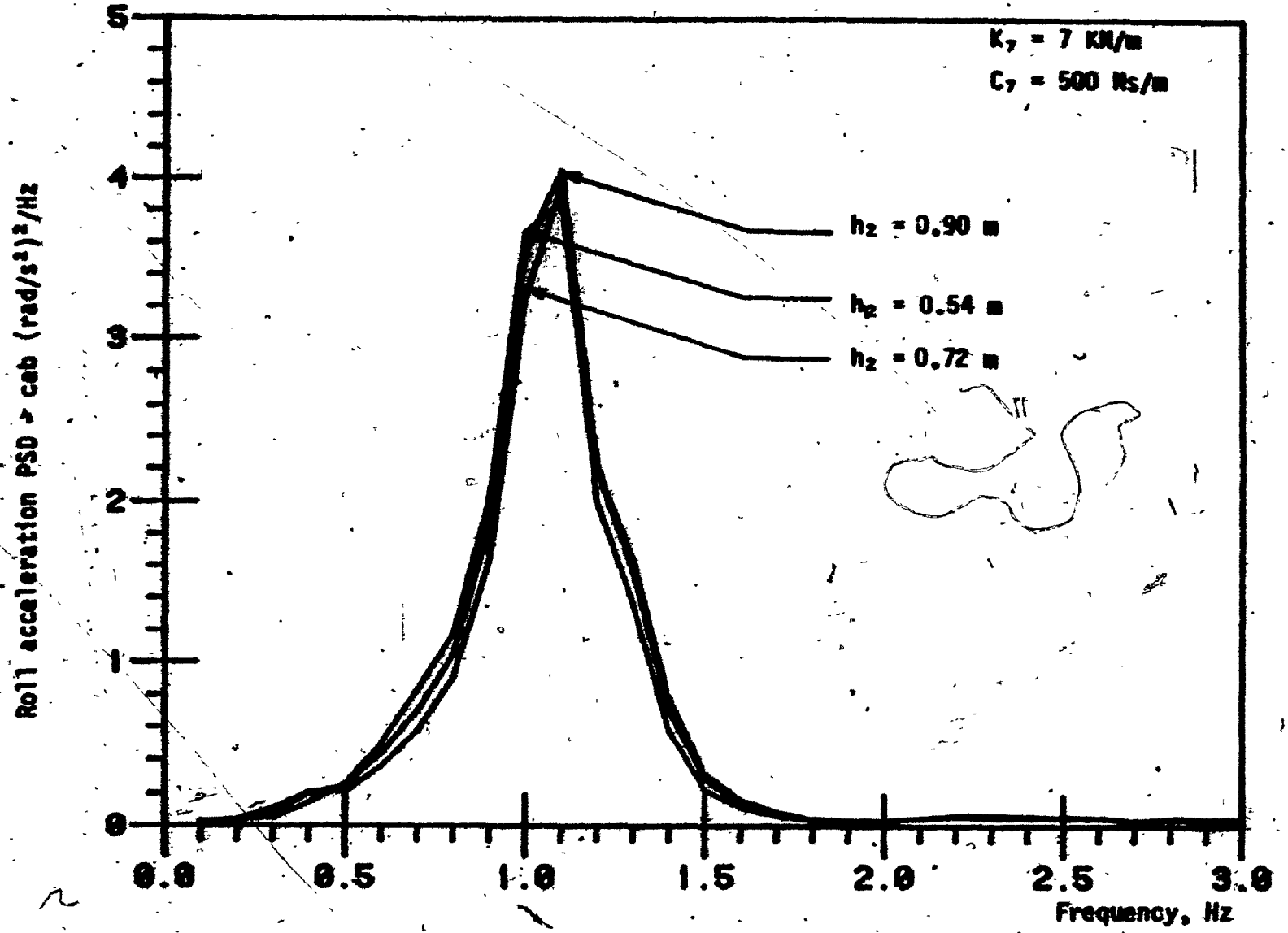

FIGURE 5.50: Influence of cab cg height on the roll acceleration response of cab and bounce seat suspension model.

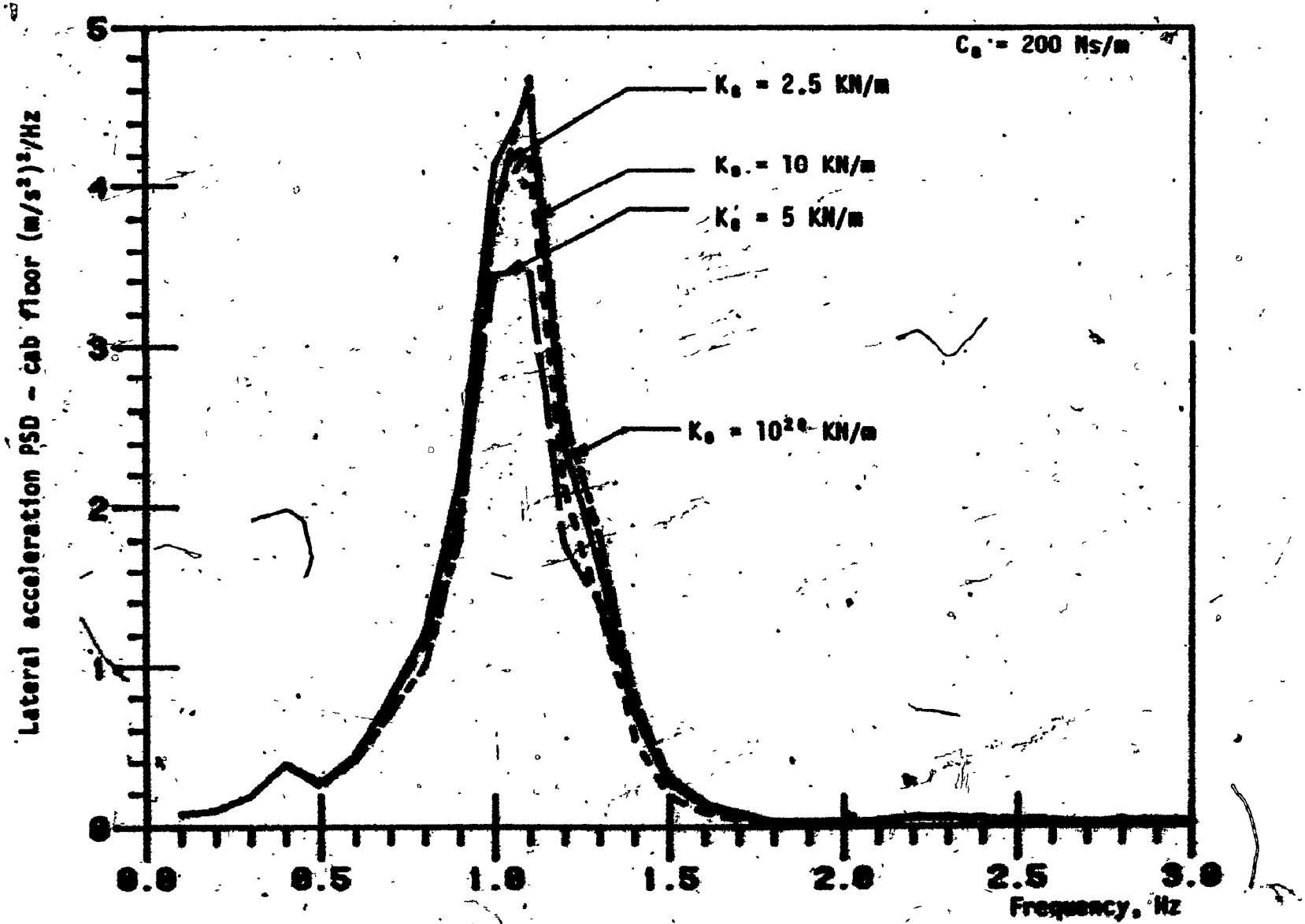

FIGURE 5.51: Lateral acceleration response at the cab floor of the cab with bounce and lateral seat suspension model.

shown in Figure 5.52. Addition of lateral seat isolator may provide improvement to the cab floor lateral response, but it worsens the lateral response of the seat cg as shown in Figures 5.53 and 5.54.

Model III: Cab Suspension with Bounce and Roll Seat Suspension

The addition of roll seat isolator to the 6 DOF cab-seat suspension model exhibits a slight improvement of the roll acceleration response of the seat, whereas the lateral acceleration response of the seat mass is deteriorated. Figures 5.55 and 5.56 reveal that a soft, lightly damped roll seat isolator provides a slightly better roll acceleration response of the seat. The lateral response of the seat mass is worsened with soft and lightly damped roll seat isolator as shown in Figures 5.57and 5.58.

5.4 CONCLUSIONS

The sesnsitivity of passive suspensions performance to variations in suspension parameters is summarized in Tables 5.1 to 5.3. Various conclusions drawn are summarized in the following manner.

5.4.1 TRANSLATIONAL SEAT-SUSPENSION MODEL

(i) Stiffer cushion provides better bounce response of the translational seat-isolator, however, too stiff a cushion may force the bounce resonance of the seat-suspension in the vicinity of vehicle resonance.

(ii) Stiffer bounce suspension leads to significantly lower bounce response at the seat resonant frequency with a poor bounce response in the frequency range, to which human is most sensitive.

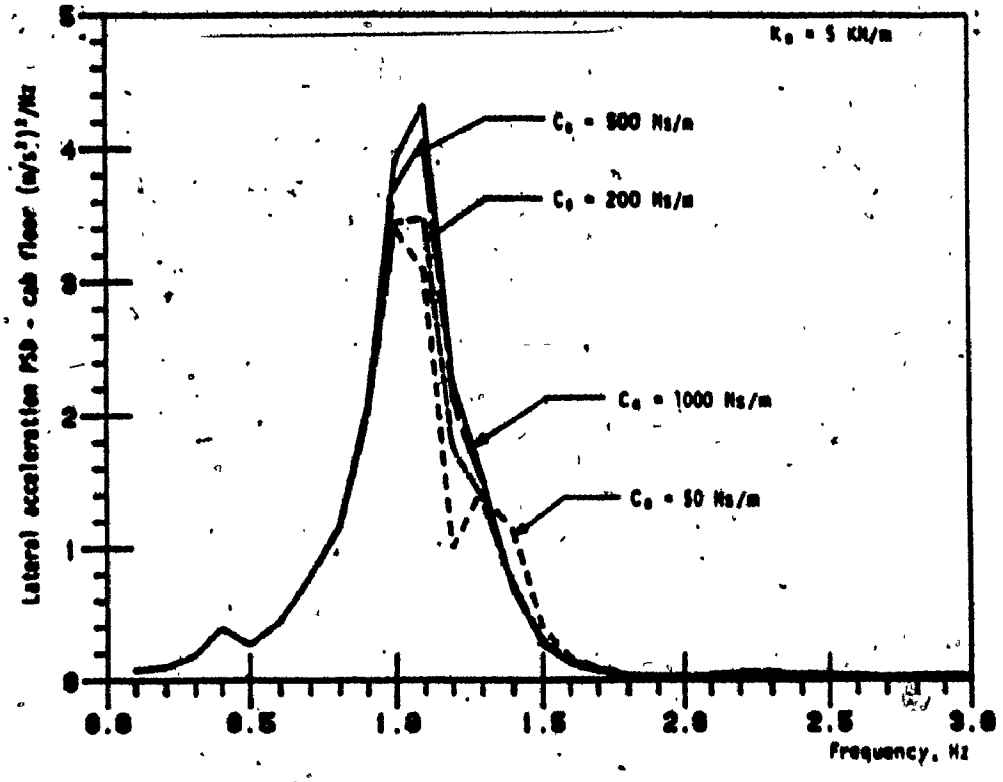

FIGURE 5.52: Influence of variations in the lateral seat isolator damping coefficient on the lateral acceleration response of the cab.

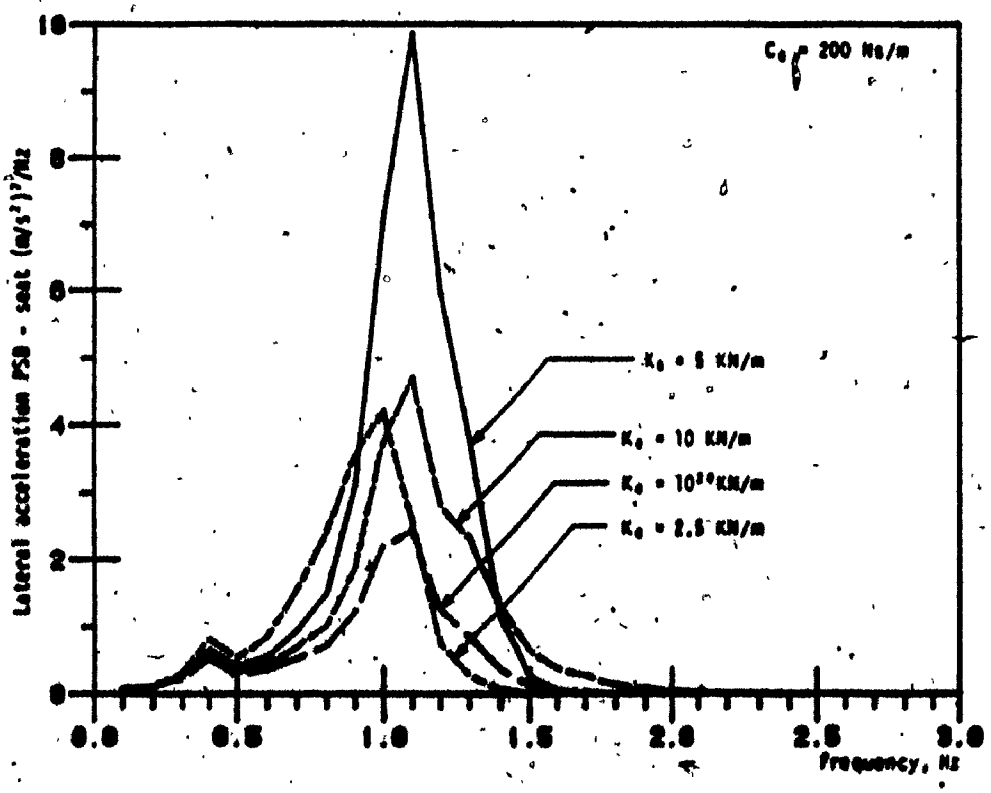

FIGURE 5.53: Sensitivity of seat lateral acceleration response to variations in stiffness of lateral seat isolator.

TABLE 5.1

PARAMETRIC SENSITIVITY OF TRANSLATIONAL SEAT SUSPENSION PERFORMANCE

Suspension parameter	Parameter value	Peak acceleration PSD		
		BOUNCE	LONGITUDINAL	LATERAL
K_c	10. KN/m 30. KN/m	49.0 24.0		
K_z	7. KN/m 8.5 KN/m 10. KN/m	24.1 24.0 19.5		
F_z	10. N 25. N 80. N	24.0 6.5 11.0		
C_z	200. Ns^3/m^3 900. Ns^3/m^3	24.1 11.0		
K_x	4. KN/m 6. KN/m 10. KN/m		5.5 15.5 24.0	
C_x	80. Ns^3/m^3 200. Ns^3/m^3 800. Ns^3/m^3		16.5 4.75 1.5	
K_y	3. KN/m 4. KN/m 5. KN/m			55. 63. 72.
C_y	200. Ns^3/m^3 1000 Ns^3/m^3 2000 Ns^3/m^3			63. 52. 18.
F_y	25. N 40. N 80. N			18. 15. 13.8

TABLE 5.2

PARAMETRIC SENSITIVITY OF ROTATIONAL SEAT SUSPENSION PERFORMANCE

Suspension parameter	Parameter value	Peak Acceleration PSD		
		BOUNCE	PITCH	ROLL
K_z	4. KN/m 6. KN/m 8. KN/m	1.30 5.40 7.40	0.4 3.5 12.0	
C_z	100 Ns^3/m^3 250 Ns^3/m^3 800 Ns^3/m^3	12.5 9.5 7.6	3.6 2.5 1.9	
F_z	20. N 30. N	12.5 2.30	3.6 0.5	
K_θ	8. KN/m 10. KN/m 14. KN/m	24. 12. 26.	9.6 3.5 3.8	3.2 0.75 6.6
K_ϕ	3. KN/m 4. KN/m 6. KN/m			3.2 2.8 2.46
K_θ	3. KN/m 3.8 KN/m 4. KN/m	12.5 13.3 15.8	3.4 4.6 7.5	
C_θ	100 Ns^3/m^3 250 Ns^3/m^3 800 Ns^3/m^3	12.8 10.8 9.8	3.4 2.9 2.6	

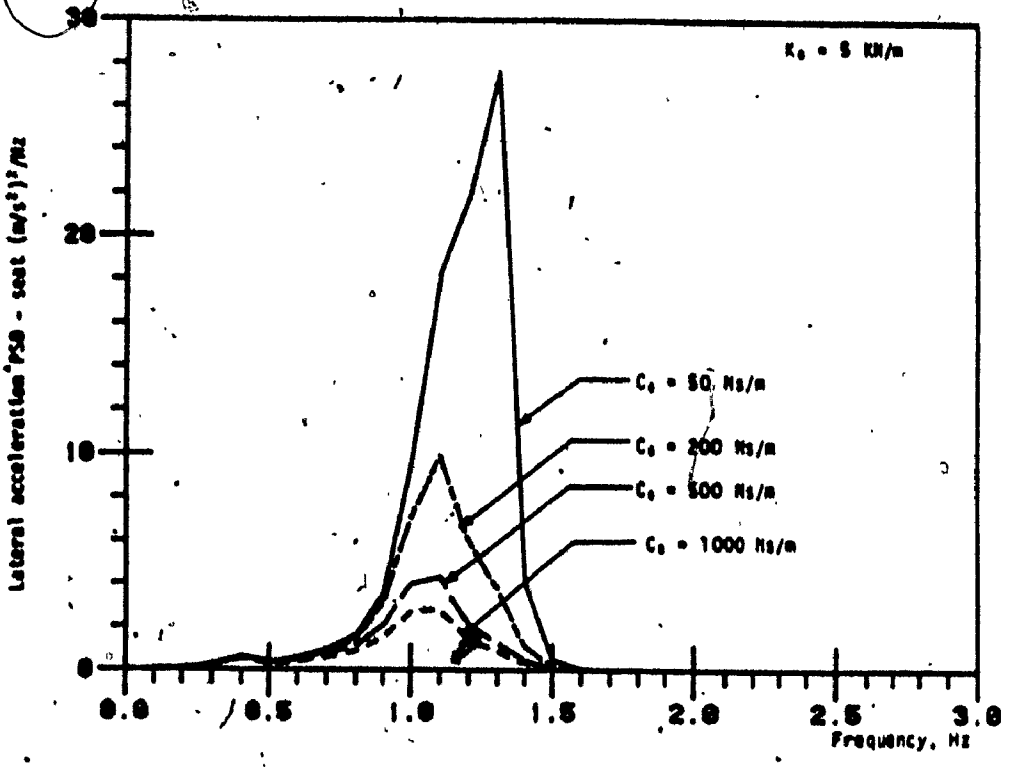

FIGURE 5.54: Sensitivity of the seat lateral acceleration response to variations in the damping coefficient of lateral seat isolator.

TABLE 5.3

PARAMETRIC SENSITIVITY OF CAB SUSPENSION PERFORMANCE

Suspension parameter	Parameter value	Peak Acceleration PSD			
		BOUNCE	LATERAL	ROLL	PITCH
K_1 to K_4	15 KN/m 10 KN/m 8 KN/m	2.7 2.1 1.98		5.40 4.90 4.30	0.46 0.38 0.34
C_1 to C_4	500 Ns/m 1000 Ns/m 2000 Ns/m	0.50 1.0 2.2	9.3 7.1 4.9	9.3 6.7 4.4	0.68 0.51 0.37
K_5	8 KN/m 10 KN/m 15 KN/m		7.0 7.95 10.6	6.7 7.5 9.5	
C_5	500 Ns/m 1000 Ns/m 1780 Ns/m		17.0 10.4 7.95	15.2 9.5 7.1	
K_6	7 KN/m 10 KN/m	0.92 1.25			
C_7	50 Ns/m 100 Ns/m 500 Ns/m	0.60 0.63 0.80			
K_8	2.5 KN/m 5. KN/m 10 KN/m		4.61 3.42 4.10		
C_8	200 Ns/m 500 Ns/m 1000 Ns/m		3.42 3.98 4.21		

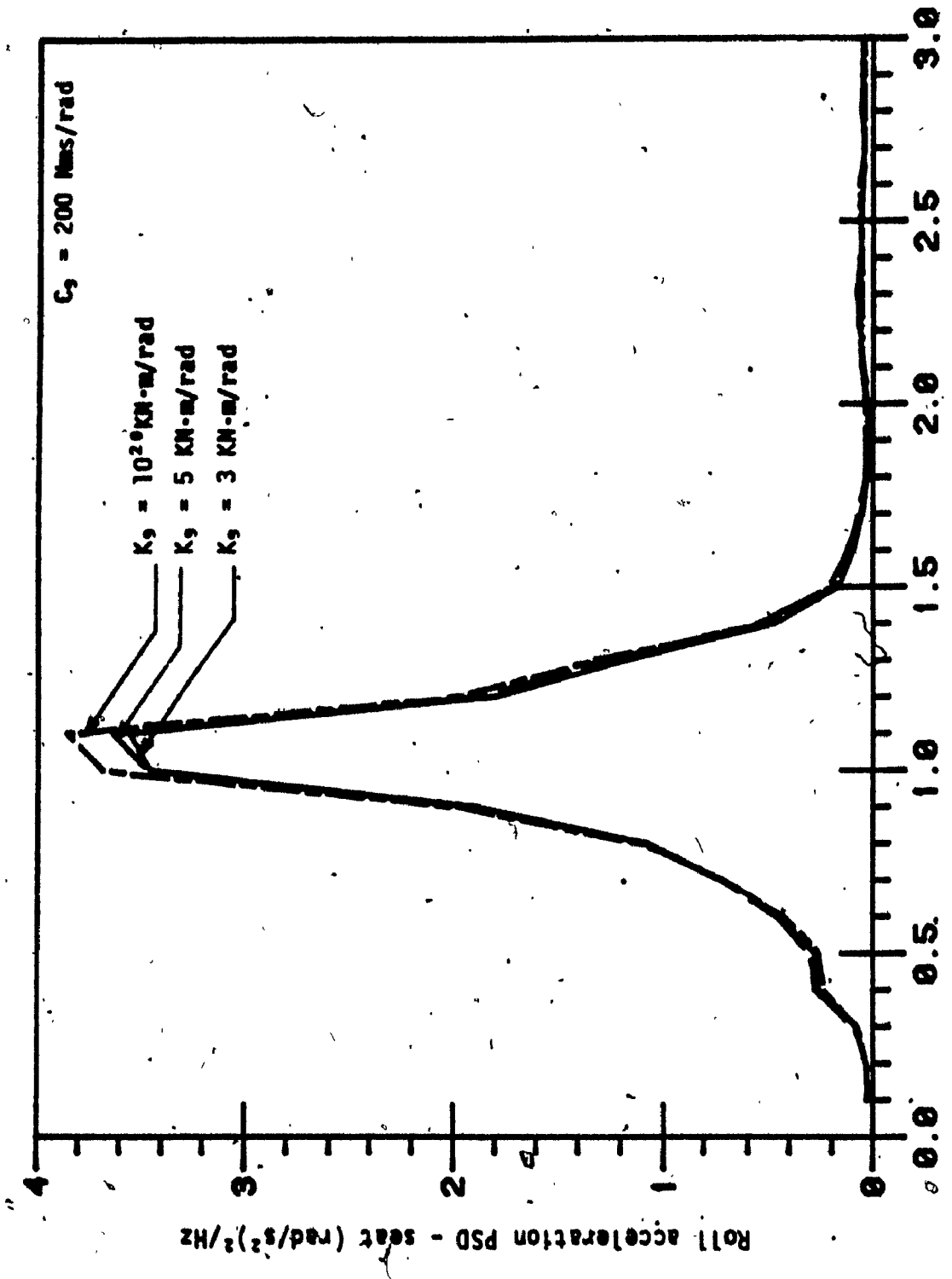

FIGURE 5.55: Sensitivity of seat roll acceleration PSD to variations in the torsional stiffness of the roll seat isolator.

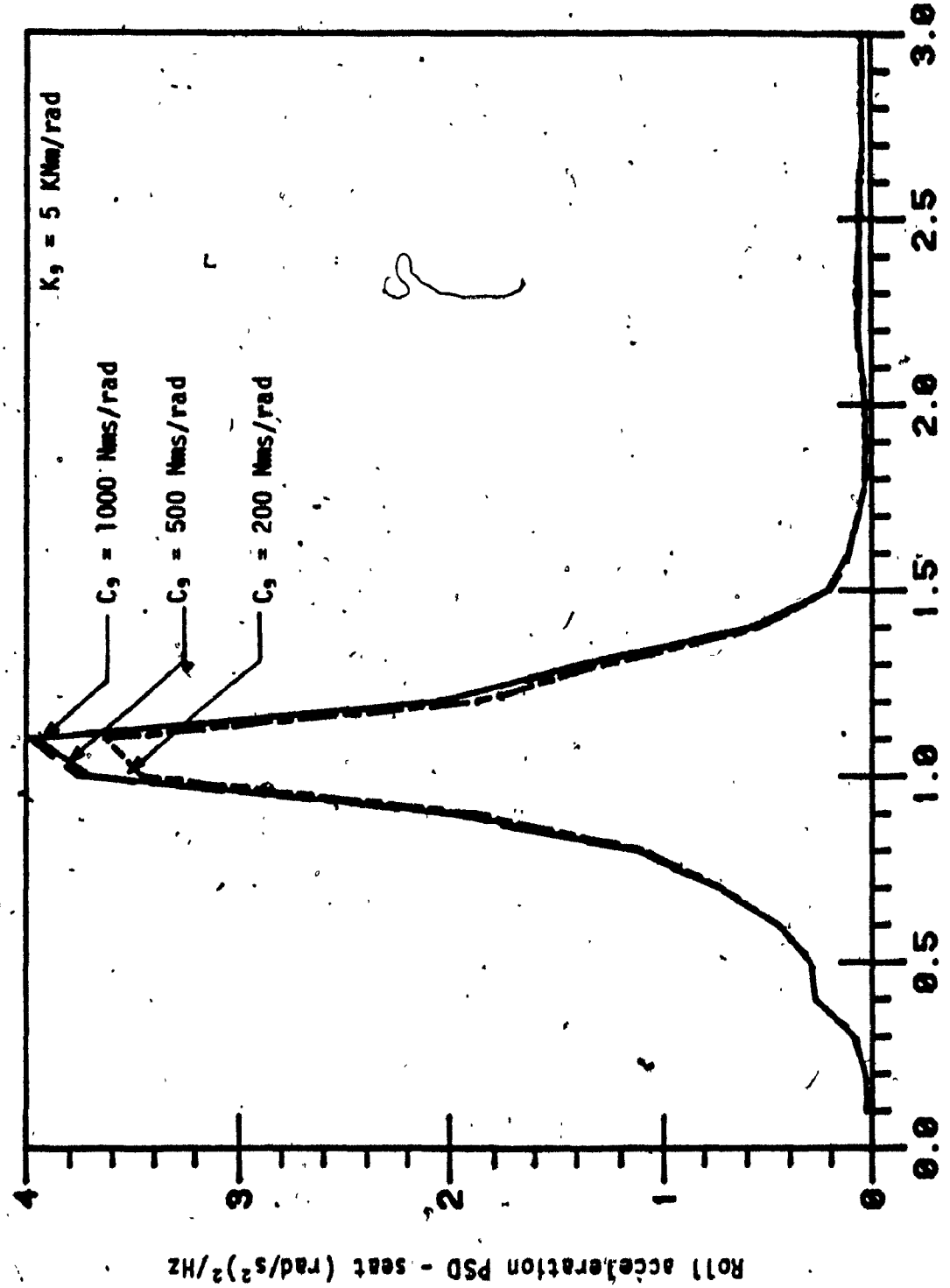

FIGURE 5.56: Influence of variations in roll isolator's damping coefficient on the roll acceleration response of the seat.

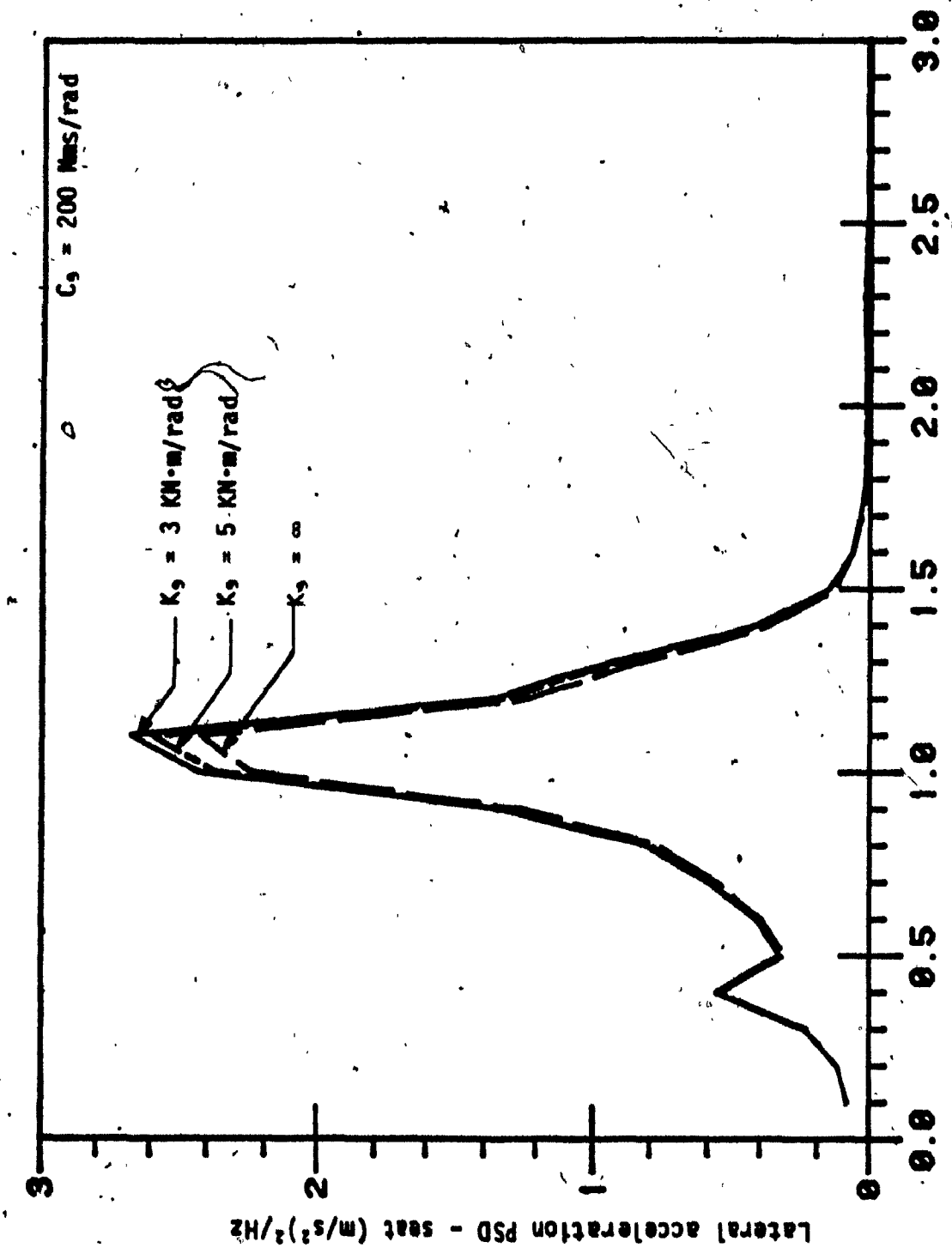

FIGURE 5.57: Sensitivity of the lateral acceleration response at seat to variations in the torsional stiffness of the roll seat isolator.

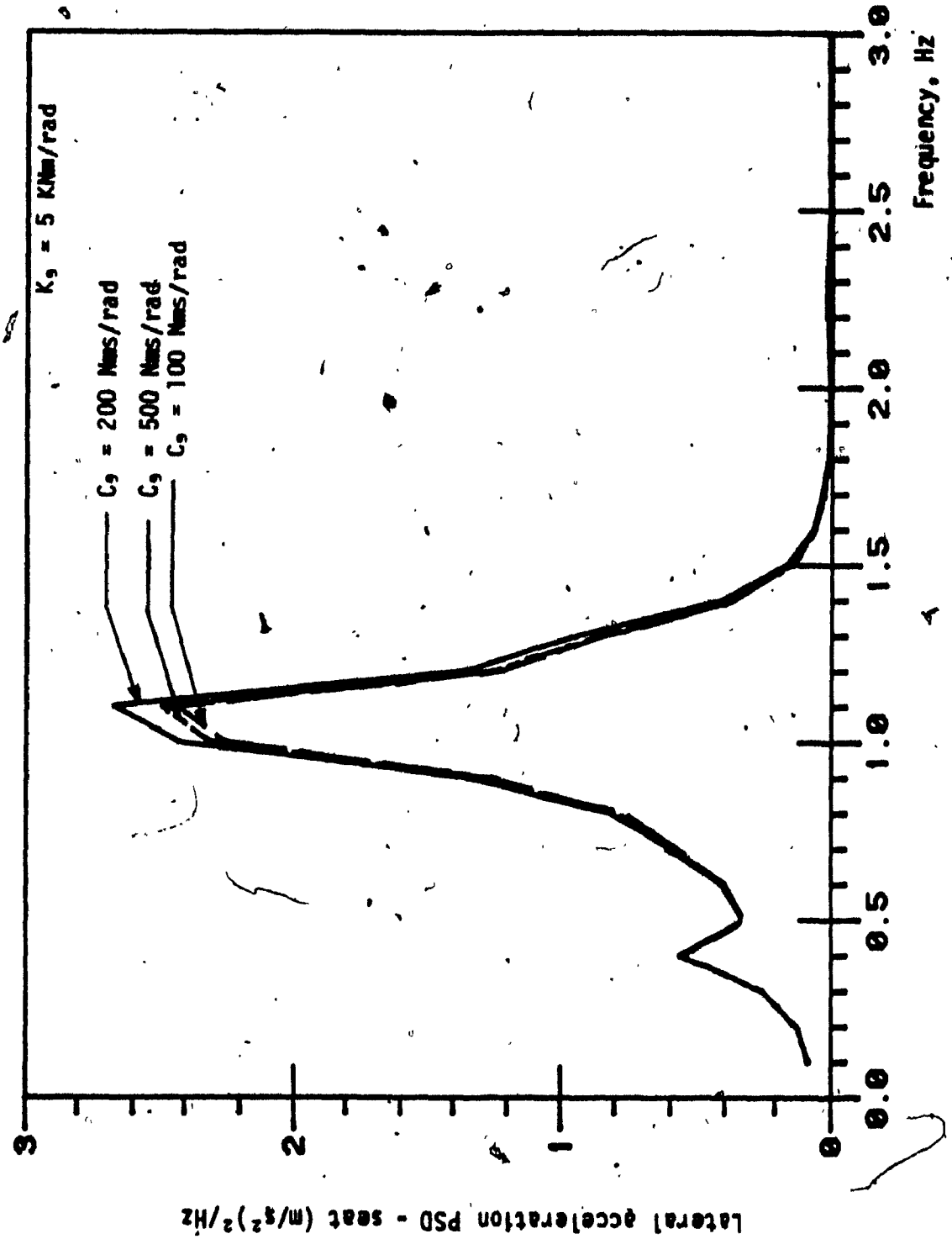

FIGURE 5.58: Lateral acceleration PSD response at the seat due to variations in roll seat isolator damping coefficient.

(iii) Large values of shock absorber and Coulomb damping parameters of seat suspension provide excellent ride performance in the low frequency region. However, too large a value deteriorates the isolation performance.

(iv) Stiffer longitudinal seat isolator causes large acceleration response by forcing the seat isolator's resonance in the region of vehicle resonant frequencies.

(v) Large values of the coefficient of velocity squared damping of the longitudinal seat isolator shows better acceleration as well as relative displacement response.

(vi) Large values of Coulomb friction in the longitudinal seat isolator aid to subside the resonance peak but deteriorate suspension performance in the isolation region.

(vii) Since the lateral resonance of the vehicle occurs around 1 Hz with significantly large acceleration of the cab floor, the lateral seat isolator with low spring rate, and large values of Coulomb and shock absorber damping is desirable. However, an extremely soft isolator will lead to excessive relative motion response.

5.4.2 ROTATIONAL SEAT ISOLATOR

(i) Softer and heavily damped bounce seat suspension subsides the bounce and pitch responses corresponding to the bounce-resonance of the rotational isolator. Large magnitude of Coulomb friction subsides the resonant peaks even further but deteriorates the bounce and pitch performance in the isolation region quite significantly.

(ii) Stiffness of the end supports influences the bounce, pitch and roll performance of the rotational seat isolator significantly. There exists an optimum value for the stiffness of end supports that would lead to the best bounce, pitch and roll acceleration responses of the rotational seat isolator. The response plots indicate that there exists an optimum value for the stiffness of end supports, which shall provide a satisfactory bounce, pitch and roll performance of the isolator.

(iii) Although the torsional stiffness of the shaft has no significant effect on the roll resonant frequency of the rotational isolator, softer torsional shaft provides better roll response.

(iv) Parameters of the pitching suspension do not affect the bounce response of the rotational isolator significantly, but the pitch performance of the isolator is observed to be quite sensitive to the stiffness of the pitching suspension.

5.4.3 CAB SUSPENSION MODEL

(i) Softer corner mounts of the cab suspension exhibit superior bounce, roll and pitch performance of cab suspension model. The stiffness of corner mounts does not influence longitudinal and lateral performance of the cab. However, extremely soft corner mounts lead to large relative motions.

(ii) Large damping values of the cab-mounts show better pitch, roll, and cab floor lateral response of the 5 DOF cab suspension model. The lightly damped cab mounts show superior isolation performance in bounce and lateral (cab cg) modes, in the isolation region, with large resonant peaks in the low frequency region.

(iii) Heavily damped and soft lateral isolator exhibits better roll and lateral acceleration response at the cab, but leads to large lateral relative motion of the cab with with respect to the chassis.

5.4.4 CAB AND SEAT SUSPENSION MODELS

Model I: Cab Suspension with Bounce Seat Suspension

(i) Addition of bounce seat suspension to the 5 DOF cab suspension model shows improved bounce response in the frequency range of vehicle resonance, but causes a larger peak corresponding to the seat resonant frequency. Softer seat suspension leads to larger resonance peak but superior bounce performance in the frequency range, to which human is most sensitive.

(ii) Lightly damped bounce seat suspension shows excessively large resonant peak around 1.25 Hz but excellent bounce acceleration response is observed corresponding to vehicle resonant frequencies.

(iii) Since the lateral acceleration response at the seat is a combination of the roll response and the lateral response at the cab floor, the seat height plays an important part in the lateral acceleration response of the seat mass.

(iv) Higher location of the cg of the cab causes excessively large roll and lateral response of the cab due to large inertias.

Model II: Cab Suspension with Bounce and Lateral Seat Suspensions

Addition of a lateral seat-isolator to the 6 DOF cab suspension model leads to a slight improvement in the lateral response at the cab floor, but worsens the lateral acceleration response of the seat mass.

Model III: Cab Suspension with the Bounce and Roll Seat Suspension

Addition of roll seat isolator to the 6 DOF cab suspension model provides a slight improvement in the roll response of the seat mass, but only at the expense of worse lateral acceleration response at the seat.

5.5 SUMMARY

Parametric study of the suspension models is carried out to establish a better understanding of the sensitivity of suspension performance to variations in suspension parameters. The performance of the suspension model is taken as the acceleration PSD in the frequency range of interest. The conclusions are drawn from the parameter investigation, which will form a basis for carrying out a multivariable optimization in the following chapter.

CHAPTER 6

OPTIMIZATION OF SUSPENSION MODELS

6.1 INTRODUCTION

In Chapter 5, the sensitivity of suspension performance to various suspension variables was presented. The parametric study revealed that in most of the suspension configurations, an optimum set of suspension parameters exist that would provide best suspension performance. In this chapter a performance criterion for each suspension model is formulated along with the constraints on the suspension performance and/or parameters. The problem of finding a set of optimal parameters, that would minimize the performance criterion, is carried out using a non-linear programming technique. The suspension performance is obtained using the optimal suspension parameters and the ride quality of the suspension model is assessed in comparison with the ISO specified *fatigue decreased proficiency* limits.

6.2 SELECTION OF PERFORMANCE CRITERION

The objectives of carrying out the optimization of suspension models is to select the suspension parameters, such that the acceleration response of the human operator (seat-mass) in translational modes does not exceed the ISO specified *fatigue decreased proficiency* limits corresponding to 4 hours exposure time. Also the relative displacement of the seat-mass with respect to the cab floor must be maintained to a minimum possible. In the roll and pitch modes of vibration, since there is no acceptable ride criteria, the peak roll and pitch accelerations and relative rotations shall be maintained to the minimum possible.

The first task is to select the performance criterion and the set of design variables for each suspension model. The constraints on the design variables are selected based on the parametric study carried out in

Chapter 5. The set of design variables chosen for the passive seat suspension and cab suspension models, and the parametric constraints are listed in Tables 6.1 and 6.2. The cab suspension models include the 5 DOF cab suspension model and the 6 DOF cab suspension model (5 DOF cab with bounce seat suspension). No attempts are made to optimize the 7 DOF cab suspension model, since it was concluded from the parameter investigation that addition of roll and lateral seat isolators to the suspended cab does not provide significant improvement in the vehicle ride.

The geometrical parameters of the cab and seat suspension models are not included as design variables in the optimization problem in order to achieve the objectives with existing vehicle configuration.

The optimization functions for each suspension model are formulated in the following sub-sections. The relative displacement response refers to as the relative motion of the operator mass with respect to the cab floor in case of seat suspension models, and as the relative motion of cab mass with respect to the vehicle frame in case of the cab suspension models.

6.2.1 PERFORMANCE CRITERIA FOR TRANSLATIONAL SEAT SUSPENSION MODEL

Due to the uncoupled nature of the translational seat suspension model, the bounce, longitudinal and lateral seat isolators are optimized by formulating independent performance criterion for each mode.

1) BOUNCE PERFORMANCE CRITERION

From the parametric study carried out in Chapter 5, it is observed that the suspension performance is sensitive to variations in stiffness of the cushion, stiffness of the suspension, velocity squared damping coefficient, and the Coulomb damping force. Consequently the design variables include these suspension parameters. The limit constraints imposed on the design variables are as listed in Table 6.1. Since the objective of the optimization is to select a set of optimal parameters, that would result in the suspension performance in accordance to the ISO proposed limits. The performance criterion is formulated as

$$U(\bar{X}) = \text{Minimize } \{\sum_{f} [S_{\ddot{z}}(f) - S_{d}^{\ddot{z}}(f)]^2\}^{1/2} \qquad (6.1)$$

$$\text{for } 1. \leq f \leq 3. \text{Hz}$$

where

$U(\bar{X})$ = The performance criterion as a function of design variables.

$\bar{X}$ = $\{K_c, K_z, C_z, F_z\}^T$, Vector of design variables.

$S_{\ddot{z}}(f)$ = Bounce acceleration PSD at frequency, f.

$S_{d}^{\ddot{z}}(f)$ = The desired acceleration PSD at frequency f, which is derived from the PSD equivalent of the ISO specified *fatigue decreased proficiency* limits for 4 hours exposure time .

TABLE 6.1

DESIGN VARIABLES AND PARAMETRIC CONSTRAINTS

SELECTED FOR OPTIMIZATION OF PASSIVE SEAT SUSPENSION MODELS

Seat Suspension Model	Design Variables	Constraints
Bounce	K_c	$10 \leq K_c \leq 30$, KN/m
	K_z	$5 \leq K_z \leq 12$, KN/m
	F_z	$0. \leq F_z \leq 40$, N
	C_z	$0. \leq C_z \leq 500$, Ns^2/m^2
Longitudinal	K_x	$5 \leq K_x \leq 12$, KN/m
	F_x	$0. \leq F_x \leq 20$, N
	C_x	$0. \leq C_x \leq 500$, Ns^2/m^2
Lateral	F_y	$0 \leq F_y \leq 30$, N
	C_y	$0 \leq C_y \leq 3000$, Ns^2/m^2
	K_y	Opt.1: $1.7 \leq K_y \leq 10$, KN/m
		Opt.2: $1.2 \leq K_y \leq 10$, KN/m
Roll	K_ϕ	$3 \leq K_\theta \leq 10$, KN·m/rad
	K_e	$5 \leq K_e \leq 20$, KN/m
	C_ϕ	$0 \leq C_\phi \leq 500$, $N \cdot ms^2/rad^2$
Pitch and Bounce	K_θ	$3 \leq K_\phi \leq 10$, KN/m
	C_θ	$0. \leq C_\theta \leq 500$ Ns^2/m^2
	K_z	$5 \leq K_z \leq 12$ KN/m
	F_z	$0 \leq F_z \leq 30$ N
	C_z	$0 \leq C_z \leq 500$ Ns^2/m^2
	K_e	$K_e = K_e^*$, the optimum support stiffness value obtained for the roll isolator.

The performance criterion of Equation (6.1) suggests that the root sum square (rss) error between the acceleration PSD response of the bounce suspension model and PSD equivalent of ISO specified limits for 4 hours exposure time is to be minimized, over a pre-selected range of frequencies. The frequency range shall be selected observing the terrain excitations in the bounce mode. Since the bounce acceleration PSD at the vehicles cab-floor is observed to be significant only up to 3 Hz, the sum of errors is evaluated in the frequency range 1 to 3 Hz. However, such an objective function will result in a suspension performance close to the maximum permissible acceleration levels specified by the ISO, but the relative displacement response may be expected to be a minimum possible. Consequently, an additional constraint on the relative displacement is imposed. This implicit constraint is

$$[S_u^z(f)] \leq (S_u^z)_{max} \qquad (6.2)$$

where

$S_u^z(f)$ = Relative displacement PSD response at frequency f.

$(S_u^z)_{max}$ = Maximum permissible bounce relative motion PSD.

2) LONGITUDINAL PERFORMANCE CRITERION

Parametric study of the longitudinal seat isolator revealed that the performance of longitudinal seat suspension is sensitive to the stiffness of the bounce suspension, coefficient of velocity squared damping and Coulomb damping force. Consequently the design variables include all these suspension parameters. The limit constraints imposed on the design variables are presented in Table 6.1. The performance criterion is formulated in an identical manner to the bounce seat suspension. The performance criterion is given by:

$$U(\bar{X}) = \text{Minimize } \{ \sum_f [S_{\ddot{x}}(f) - S_d^{\ddot{x}}(f)]^2 \}^{1/2}$$

$$\text{for } 1 \leq f \leq 3.5 \text{ Hz} \qquad (6.3)$$

Subject to:

$$[S_u^x(f)] \leq (S_u^x)_{max} \qquad (6.4)$$

where,

$\bar{X}$ $= \{K_x, C_x, F_x\}^T$, vector of design variables

$S_{\ddot{x}}(f)$ = Acceleration PSD response in the longitudinal mode at frequency, f.

$S_d^{\ddot{x}}(f)$ = The desired acceleration PSD at frequency f, derived from the PSD equivalent of ISO specified *fatigue decreased proficiency* limits for 4 hours exposure time

$S_u^x(f)$ = Relative displacement PSD response in the longitudinal mode, at frequency f.

$(S_u^x)_{max}$ = Maximum permissible longitudinal relative motion.

3) LATERAL PERFORMANCE CRITERION

Terrain induced lateral vibrations encountered by the tractor-drivers are observed to be of extremely large magnitude occurring around 1 Hz. Attenuation of such low frequency vibration can be achieved only through extremely low natural frequency isolators. However, low natural frequency passive isolators lead to excessive motion of the driver with reference to the vehicle controls. The performance criterion for the lateral ride of translational seat suspension model is formulated such that the undamped natural frequency in the lateral mode is at least equal to a prespecified

value. Moreover, the ISO *fatigue decreased proficiency* limits corresponding to exposure to horizontal vibration have been established for vibrational frequencies greater than 1 Hz, and hence the performance criterion formulated for bounce and longitudinal modes can not be employed. The performance criterion for the lateral mode is then formulated to minimize the peak acceleration response of the seat-mass.

$$U(\bar{X}) = \text{Minimize } \{\text{peak } [S_{\ddot{y}}(f)]\} \quad \text{for } 0 < f \leq 2 \text{ Hz} \tag{6.5}$$

subject to:

$$[S_u^y(f)] \leq (S_u^y)_{max} \tag{6.6}$$

where

$\bar{X}$ = $\{K_y, C_y, F_y\}^T$, vector of design variables

$S_{\ddot{y}}(f)$ = Lateral acceleration PSD response at frequency, f.

$S_u^y(f)$ = PSD of the relative displacement response at frequency, f.

$(S_u^y)_{max}$ = Maximum permissible relative displacement PSD in the lateral mode.

A list of design variables and the limit constraints is presented in Table 6.1. Two lower limits are imposed on the stiffness value of the lateral seat suspension, such that the undamped natural frequency is constrained to be at least 0.7 Hz and 0.6 Hz, respectively. Based on these two different lower limits on the stiffness value, the optimization has been carried out twice.

6.2.2 PERFORMANCE CRITERIA FOR OPTIMIZATION OF ROTATIONAL SEAT ISOLATOR

The design variables in the case of rotational seat isolator include bounce suspension stiffness, Coulomb damping, bounce

suspension damping; pitching suspension stiffness and damping stiffness of end supports; stiffness and damping parameters of roll isolator. The influence of these suspension parameters on the performance of rotational seat isolator has been presented in Chapter 5. Since, it has been established that a completely decoupled roll motion can be obtained by locating the end supports in an equidistant manner, an independent optimization function may be formulated for optimizing the roll response of the isolator. The roll performance criterion is formulated as follows:

$$U(\bar{X}) = \text{Minimize } [\text{peak}\{S_{\ddot{\phi}}(f)\}] \qquad (6.7)$$

$$\text{for } 0 < f \leq 3.5 \text{ Hz}$$

Subject to:

$$[S_u^{\phi}(f)] = (S_u^{\phi})_{max} \qquad (6.8)$$

where

$S_{\ddot{\phi}}(f)$ = PSD of roll acceleration response at frequency, f.

$S_u^{\phi}(f)$ = PSD of roll relative motion response at frequency, f.

$(S_u^{\phi})_{max}$ = Maximum permissible roll relative motion PSD.

A second optimization function may be formulated to optimize the bounce and pitch response of the rotational isolator. Since the ISO specified *fatigue decreased proficiency* limits have been established in the translational modes alone, the performance criteria is formulated as follows:

$$U(\bar{X}) = \text{Minimize } \{\sum_f [S_{\ddot{z}}(f) - S_d^z(f)]^2\}^{1/2} \qquad (6.9)$$

$$\text{for } 1 \leq f \leq 3.0 \text{ Hz}$$

subject to:

$$\left.\begin{aligned} [S_{\ddot{\theta}}(f)] &\leq (S_{\ddot{\theta}})_{max} \\ [S_u^z(f)] &\leq (S_u^z)_{max} \\ [S_u^{\theta}(f)] &\leq (S_u^{\theta})_{max} \end{aligned}\right\} \qquad (6.10)$$

where,

$S_{\ddot{z}}(f)$ = PSD of the bounce acceleration response of the rotational isolator at frequency, f.

$S_{\ddot{\theta}_i}(f)$ = PSD of the pitch acceleration response of the rotational isolator at frequency, f.

$S_u^z(f)$ = Bounce relative motion PSD response at frequency, f.

$S_u^\theta(f)$ = Pitch relative motion PSD response at frequency, f.

$(S_u^\theta)_{max}$ = Maximum permissible pitch relative motion PSD.

Table 6.1 lists the design variables and parametric constraints, employed in carrying out the optimization of rotational isolator. The two performance criteria of Equations (6.7) and (6.9), formulated to optimize roll, and bounce and pitch performance of the rotational isolator, are found sensitive to the stiffness of the end supports. However, the roll performance of the isolator is observed to be extremely sensitive to the stiffness of the end supports (see Chapter 5), thus the optimization of the performance criterion presented in Equation (6.7) is carried out to establish an optimum value for the stiffness of end supports. This optimal value of the end support's stiffness is then used as an equality constraint for the optimization of bounce and pitch response.

6.2.3 PERFORMANCE CRITERIA FOR OPTIMIZING 5 DOF CAB SUSPENSION MODEL

Since the roll and lateral excitations are the most severe ones and occur around 1 Hz, the objectives here are to minimize the roll and lateral acceleration responses, while constraining the bounce and pitch acceleration PSD responses. Since the parametric study of cab-suspension model revealed that the longitudinal isolator has no significant influence on the performance of cab-suspension, the longitudinal isolator's parameters are not included in the formulation of optimization

function. Various suspension parameters considered as design variables and the respective limit constraints are listed in Table 6.2.

Two performance criteria are selected in order to achieve the objectives of minimizing the lateral and roll acceleration responses of the cab suspension model. The performance criteria are listed as follows:

(1) $U(\bar{X})$ = Minimize $[\text{Max}\{S_{\ddot{y}_2}(f)\}]$ (6.11)

for $0. < f \leq 3.$ Hz.

Subject to:

$$[S_{\ddot{z}_2}(f)] \leq (S_{\ddot{z}_2})_{max}$$

$$[S_{\ddot{\phi}_2}(f)] \leq (S_{\ddot{\phi}_2})_{max} \quad (6.12)$$

$$[S_{\ddot{\theta}_2}(f)] \leq (S_{\ddot{\theta}_2})_{max}$$

and

$$[S_u^z(f)] \leq (S_u^z)_{max}$$

$$[S_u^y(f)] \leq (S_u^y)_{max} \quad (6.13)$$

$$[S_u^\theta(f)] \leq (S_u^\theta)_{max}$$

$$[S_u^\phi(f)] \leq (S_u^\phi)_{max}$$

where

$S_{\ddot{y}_2}(f)$ = Lateral acceleration PSD at the cab floor.

$S_{\ddot{z}_2}(f)$ = Bounce acceleration response of the cab.

$S_{\ddot{\theta}_2}(f)$ = Pitch acceleration response of the cab.

$S_{\ddot{\phi}_2}(f)$ = Roll acceleration response of the cab.

TABLE 6.2

DESIGN VARIABLES AND PARAMETRIC CONSTRAINTS

SELECTED FOR OPTIMIZING CAB-SUSPENSION MODELS

Suspension Model	Design Variables	Constraints
5 DOF Cab Suspension Model	K_1, K_2, K_3, K_4, K_5 C_1, C_2, C_3, C_4, C_5	$8 \leq K_1, K_2, K_3, K_4 \leq 20$ KN/m $8 \leq K_5 \leq 20$ KN/m $0 \leq C_1, C_2, C_3, C_4 \leq 2000$ Ns/m $0 \leq C_5 \leq 2000$ Ns/m
6 DOF Cab Suspension Model	K_7 C_7	$5 \leq K_7 \leq 12$ KN/m $0 \leq C_7 \leq 500$ Ns/m

(ii) $U(\bar{X})$ = Minimize [Max $(S_{\ddot{\phi}_2}(f))$] (6.14)

for $0. < f \leq 3.$ Hz

subject to:

$$[S_{\ddot{z}_2}(f)] \leq (S_{\ddot{z}_2})_{max}$$

$$[S_{\ddot{\theta}_2}(f)] \leq (S_{\ddot{\theta}_2})_{max} \quad (6.15)$$

$$[S_{\ddot{y}_2}(f)] \leq (S_{\ddot{y}_2})_{max}$$

and

$$[S_u^z(f)] \leq (S_u^z)_{max}$$

$$[S_u^\theta(f)] \leq (S_u^\theta)_{max}$$

$$[S_u^\phi(f)] \leq (S_u^\phi)_{max} \quad (6.16)$$

$$[S_u^y(f)] \leq (S_u^y)_{max}$$

The optimization of the cab suspension models has been carried out by minimizing the two performance criteria formulated in equations (6.11) and (6.14), independently.

6.2.4 PERFORMANCE CRITERION FOR OPTIMIZING 6 DOF CAB SUSPENSION MODEL

From the parametric study of 6 DOF cab suspension model, it was concluded that addition of bounce seat suspension does not affect the pitch, lateral, and roll acceleration response. Thus the parameters of the cab suspension are chosen as the optimal parameters obtained from the optimization of the 5 DOF cab suspension model. The bounce suspension stiffness and the damping coefficient are selected to be the design variables and the performance criterion is formulated as:

$$U(\bar{X}) = \{\sum_f [S_{\ddot{z}_1}(f) - S_d^z(f)]^2\}^{1/2} \quad (6.17)$$

for $1 \leq f \leq 3$ Hz

Subject to:

$$[S_u^z(f)] \leq (S_u^z)_{max} \tag{6.18}$$

6.3 THE OPTIMIZATION ALGORITHM

The optimization functions formulated in section 6.2 represent constrained nonlinear programming problems. There are many techniques available for the solution of constrained nonlinear programming problems. Of these, the penalty function method is most frequently used due to the sequential nature of the technique. The penalty function methods transform the basic constrained optimization problem into alternative formulations such that the numerical solutions are sought by solving a sequence of unconstrained minimization problems. Let the basic constrained optimization problem be of the form:

$$U(\hat{X}) = U(x_1, x_2, \ldots\ldots, x_n) \tag{6.19}$$

subject to:

$$g_j(\hat{X}) \geq 0., \qquad j = 1, \ldots, q \tag{6.20}$$

where

q = Number of constraint equations

n = Number of design variables

$\hat{X} = \{x_1, x_2, \ldots\ldots, x_n\}^T$, vector of design variables.

The constrained optimization problem is converted into an unconstrained minimization problem by constructing a function of the form:

$$U_m(\hat{X}, r_k) = U(\hat{X}) + r_k \sum_{j=1}^{q} G_j[g_j(\hat{X})] \tag{6.21}$$

where G_j is some function of constraint g_j and r_k is a positive constant known as the penalty parameter. Thus, the convergence to the original constrained problem can be accomplished through minimization of the unconstrained function of equation (6.21).

The penalty function formulations for inequality constraints are achieved by two techniques, *namely*, the interior and the exterior methods. In the interior methods, the unconstrained minima of U_m for all values of r_k lie in the feasible region and converge to the solution of constrained optimization problem of equations (6.19) and (6.20). In the exterior methods, the unconstrained minima of U_m for all values of r_k lie in the infeasible region and converge to the desired solution from the outside as r_k is changed in a specific manner. The two penalty functions are formulated in the following manner.

Interior penalty function:

$$U_m(\hat{X}, r_k) = U(\hat{X}) + r_k \sum_{j=1}^{q} \frac{1}{g_j(\hat{X})} \tag{6.22}$$

Exterior penalty function:

$$U_m(\hat{X}, r_k) = U(\hat{X}) + r_k \sum_{j=1}^{q} \langle g_j(\hat{X}) \rangle^{\ell} \tag{6.23}$$

where,

$$\langle g_j(\hat{X}) \rangle = \max \langle g_j(\hat{X}), 0 \rangle = \begin{cases} g_j(\hat{X}), \text{ if } g_j(\hat{X}) < 0 \\ 0, \text{ if } g_j(\hat{X}) \geq 0 \end{cases} \tag{6.24}$$

From equation (6.22), it is observed that the function U_m will always be greater than the function U for all feasible points ($\hat{X}$). However, the penalty term is not defined for infeasible design vector ($\hat{X}$). This introduces serious shortcoming while using the interior penalty function method. Since the interior penalty function approach does not permit violation of any constraints, it requires a feasible starting point, which may not be readily available in many cases.

In case of exterior penalty function method, the effect of penalty term of equation (6.23) increases in proportion to 2^{th} power of the amount by which the constraints are violated. Thus there will be a penalty for violating the constraints, and the amount of penalty will increase at a

faster rate compared to the amount of violation of a constraint (for $\ell > 1$). Usually, the function $U_m(\hat{X}, r_k)$ possesses a minimum in the infeasible region. The unconstrained minima converges to the optimal solution ($\hat{X}_k^*$) of the original problem as $k \to \infty$ and $r_k \to \infty$. Thus the unconstrained minima approaches the feasible domain gradually and as $k \to \infty$, the ($\hat{X}_k^*$) eventually lies in the feasible region. The penalty function method can be summarized in the following manner.

(i) Start with an initial design vector ($\hat{X}$) and a suitable value of r (set k = 1).

(ii) Find the optimum design vector ($\hat{X}_k^*$) that minimizes the function given by equations (6.22) or (6.23).

(iii) Test whether ($\hat{X}_k$) is the optimum solution and whether it satisfies all the constraints. If ($\hat{X}_k^*$) is feasible and the desired optimum, terminate the procedure. Otherwise continue to step (iv).

(iv) Choose the next value of penalty parameter. In case of an exterior penalty function, select $r_{k+1} > r_k$ and proceed to step (ii). In case of interior penalty function, select $r_{k+1} < \psi r_k$ for $\psi < 1$ and go to step (ii).

Since the interior penalty function method requires a feasible starting point, which may be difficult to determine in many cases, the exterior penalty function method is used to minimize the suspension performance criteria. Also the penalty function approach requires many solutions of the objective function for various values of r_k. Since, the solution of minimization problem is quite demanding on computer time, a constant value of penalty parameter is chosen to formulate the unconstrained objective function.

$$U_m(\hat{X}) = U(\hat{X}) + 10^{20} \sum_{j=1}^{q} \langle g_j(\hat{X}) \rangle \qquad (6.25)$$

where,

$$\langle g_j(\hat{X}) \rangle = \begin{cases} g_j(\hat{X}), \text{ if } g_j(\hat{X}) < 0 \\ 0, \text{ if } g_j(\hat{X}) \geq 0 \end{cases} \qquad (6.26)$$

The minimization of the objective function, equation (6.25), can be carried out using a direct search technique. The direct search technique, proposed by Hooke and Jeeves [76] is used to find the optimal vector of design variables. The technique does not require derivatives and assumes a unimodal function, thus several sets of starting values are recommended to achieve global optimum values of the performance criteria [77,78]. The computer package, SEEK1 developed by McMaster University is used, which utilizes Hooke and Jeeves direct search followed by a random search to achieve the optimal design vector. The routine proceeds as follows:

(i) A base point is selected and the objective function $U_m(\hat{X})$ is evaluated.

(ii) Local searches are made in each direction by stepping x_i a distance δ_i and evaluating the objective function to see if a lower function value is obtained.

(iii) If no improvement in the function value is achieved, the step size is reduced and searches are made from the previous best point.

(iv) If the value of the objective function has decreased, a "temporary head" $x_{i,o}^{(s+1)}$, is located using the two previous base points $x_i^{(s+1)}$ and x_i^s:

$$x_{i,o}^{s+1} = x_i^{s+1} + (AF)*(x_i^{s+1} - x_i^s) \qquad (6.27)$$

where,

i = Variable index, i = 1,2,3,....n

o = Denotes the temporary head

s = Stage index (a stage is the end of n searches)

AF = The acceleration factor.

(v) If the temporary head results in a lower function value, a new local search is performed about the temporary head, a new head is located and the value of optimization function is checked. This expansion continues till the function value decreases.

(vi) If the temporary head does not result in a lower function value, a search is made from the previous best point.

(vii) The procedure terminates when the change in objective function value is found to be less than a prespecified convergence criterion.

6.4 OPTIMIZATION RESULTS AND DISCUSSION

The suspension performance criteria, formulated in the previous sub-sections are minimized using direct search technique. The resulting values of optimal seat and cab suspension parameters are listed in Tables 6.3 and 6.4, respectively. The acceleration and relative displacement PSD response characteristics of the optimal seat and cab suspension models are evaluated. The ride performance characteristics of the passive suspension models are assessed by comparing the acceleration response to the ISO proposed *fatigue decreased proficiency* limits, and are presented in the following sub-sections.

6.4.1 RIDE PERFORMANCE OF OPTIMUM SEAT SUSPENSION

The ride performance characteristics of the optimum seat suspension model as a measure of acceleration and relative displacement response are presented. The ride quality of the suspension models is assessed by comparing the acceleration PSD response of the seat-mass to the ISO *fatigue decreased proficiency* limits. The results are summarized in the following manner.

TABLE 6.3

OPTIMAL SEAT SUSPENSION PARAMETERS

Seat Suspension Model	Suspension Parameters	Parameter Value
Bounce	K_z	7167 N/m
	C_z	400 Ns^2/m^2
	F_z	38 N
	K_c	12000 N/m
Longitudinal	K_x	7517 N/m
	C_x	300 Ns^2/m^2
	F_x	20 N
Lateral Opt. 1	K_y	1700 N/m
	C_y	3000 Ns^2/m^2
	F_y	30 N
Lateral Opt. 2	K_y	1200 N/m
	C_y	563 Ns^2/m^2
	F_y	7.28 N
Roll	K_ϕ	4370 N.m/rad
	C_ϕ	477 N.m s^2/rad^2
	K_e	8974 N/m
Pitch and Bounce	K_z	6023 N/m
	F_z	27.3 N
	C_z	152 Ns^2/m^2
	K_θ	3090 N/m
	C_θ	500 Ns^2/m^2
	K_e	8974 N/m

TABLE 6.4

OPTIMAL CAB SUSPENSION PARAMETERS

Suspension Model	Suspension Parameters	Parameter Value
5 DOF Cab Suspension	K_1, K_2, K_3, K_4,	8000 N/m
	K_5	8000 N/m
	C_1, C_2, C_3, C_4	2000 Ns/m
	C_5	1775
6 DOF Cab Suspension	K_7	8000 N/m
	C_7	200 Ns/m

1) RIDE QUALITY OF OPTIMUM BOUNCE SUSPENSION SEAT

Optimal values for the suspension parameters obtained through minimization of the performance criterion (Equation (6.1)) are listed in Table 6.3. The optimization routine is observed to converge approximately to the upper limit specified for the magnitude of Coulomb damping force, in order to maintain resonant acceleration response within the ISO-FDP (*Fatigue decreased proficiency*) limit. However, the acceleration PSD of the seat-mass exceeds the ISO-FDP limit for 4 hours exposure time corresponding to tractor resonant frequency (2.6 Hz) as shown in Figure 6.1. A reduction in the magnitude of Coulomb damping force can lead to the bounce ride around 2.6 Hz within the 4 hours limit, however the seat resonance acceleration response will be quite large. The relative displacement PSD response of the bounce suspension seat is found to be extremely good, as shown in Figure 6.2. Figure 6.3 presents the ISO-FDP rms acceleration limits for 2.5, 4, and 8 hours exposure. The ride assessment of the bounce suspension seat reveals that an optimum bounce seat can provide a very satisfactory tractor ride for 2.5 hours exposure.

2) RIDE QUALITY OF OPTIMUM LONGITUDINAL SEAT SUSPENSION

The optimal values for the suspension parameters are obtained by minimizing the performance criterion (Equation (6.3)) and are presented in Table 6.3. The optimization routine selects large values for the Coulomb damping in order to subside the resonance response occurring at 1.5 Hz. However, the isolation performance deteriorates beyond 2 Hz as shown in Figure 6.4. The acceleration response of the optimum longitudinal seat suspension is observed

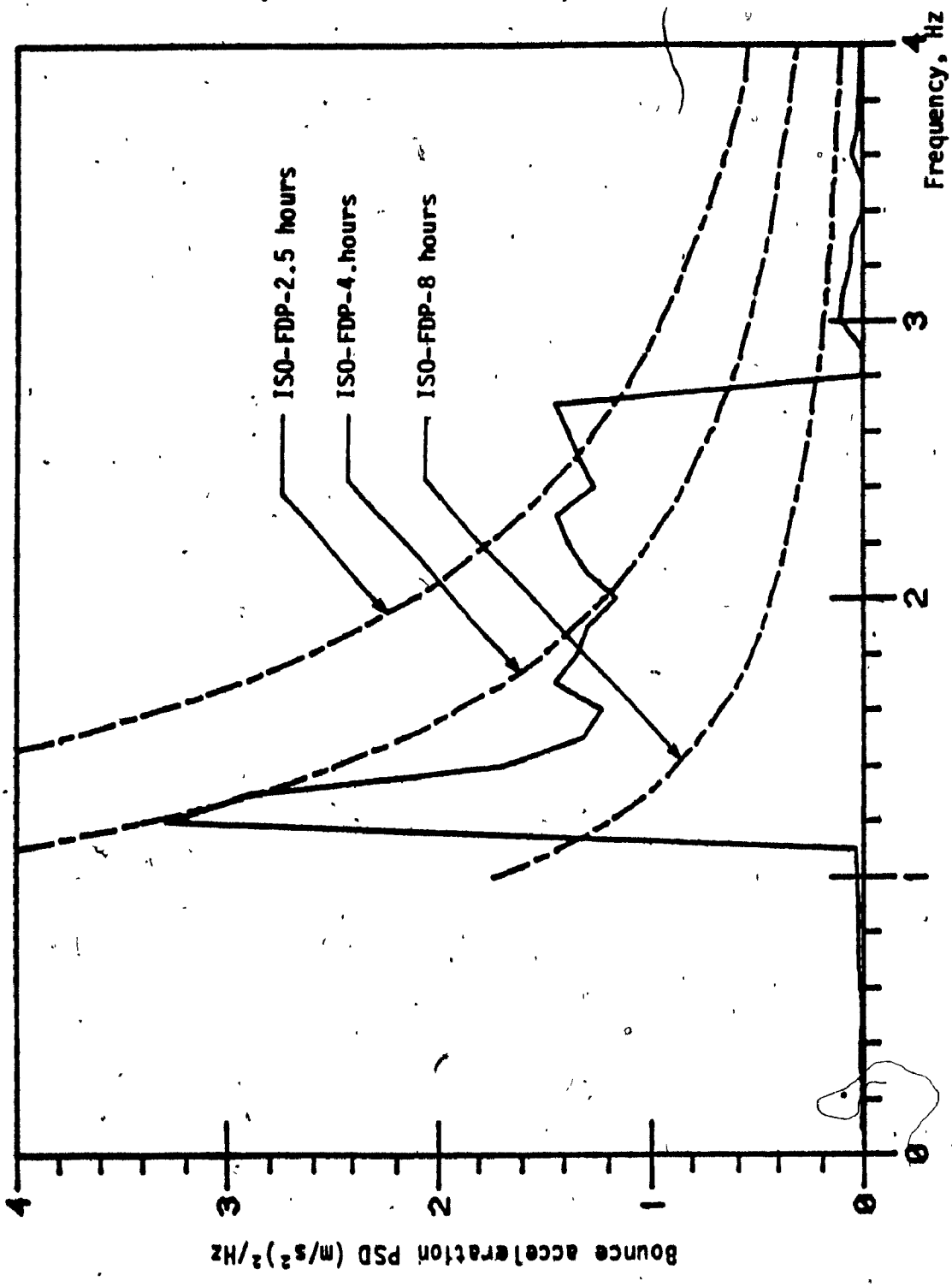

FIGURE 6.1: Bounce acceleration PSD response of the optimum bounce suspension seat.

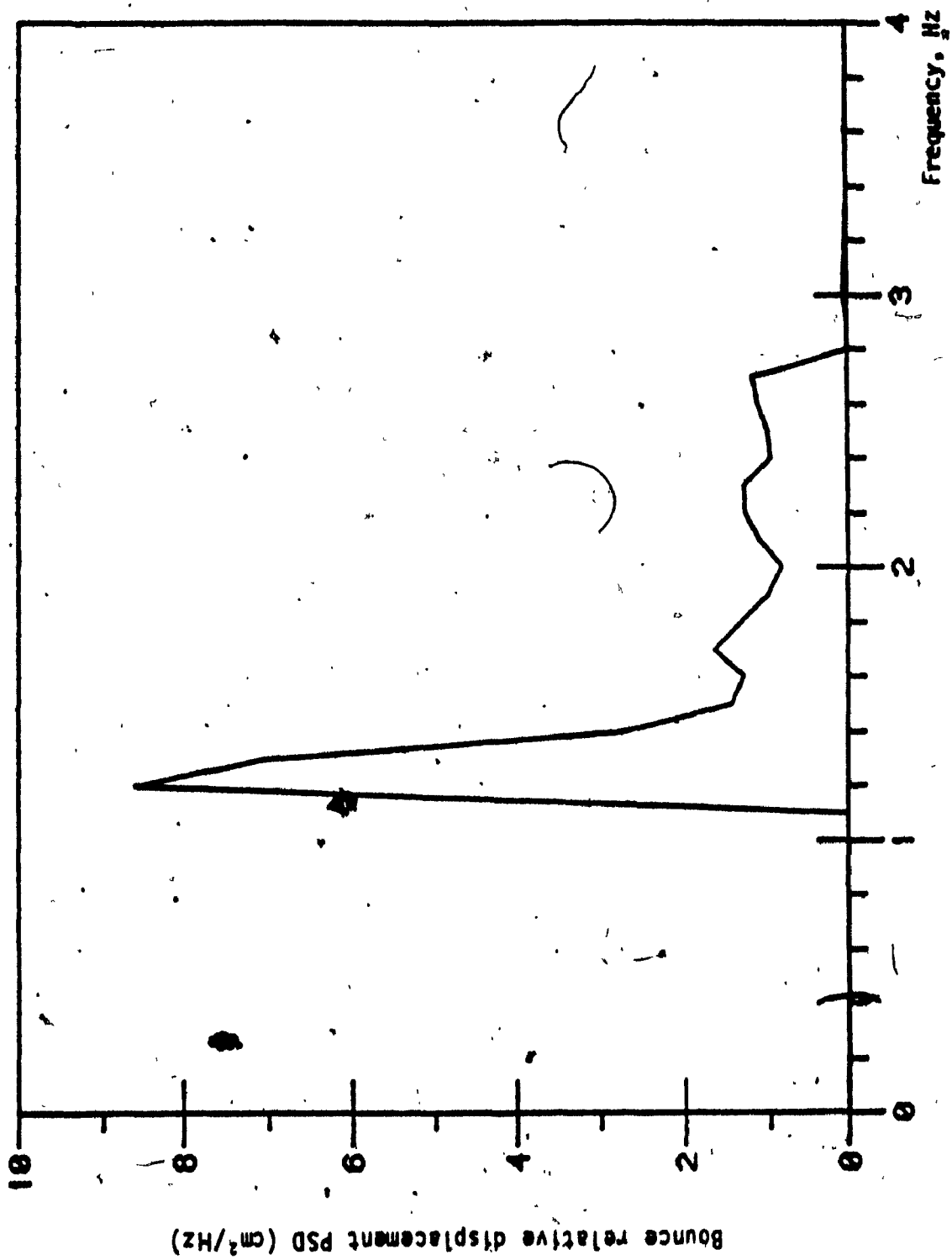

FIGURE 6.2: Relative displacement PSD of an optimum bounce seat suspension.

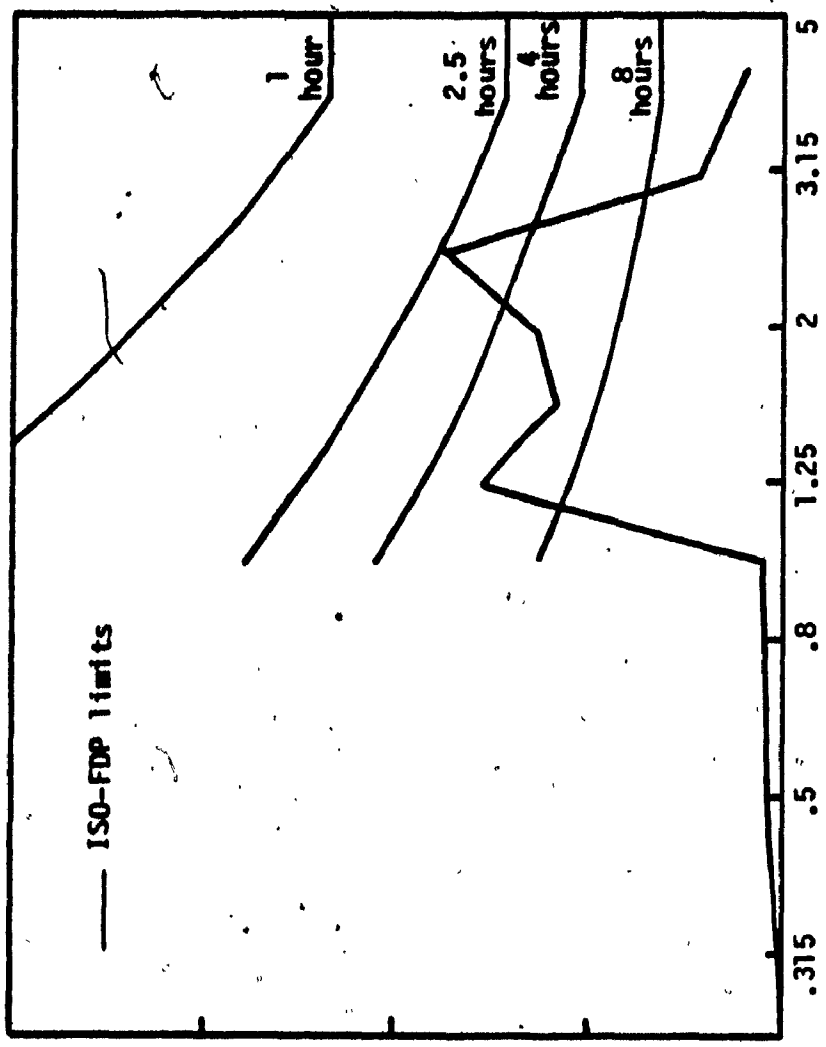

FIGURE 6.3: ISO weighted bounce rms acceleration response of an optimal bounce seat suspension.

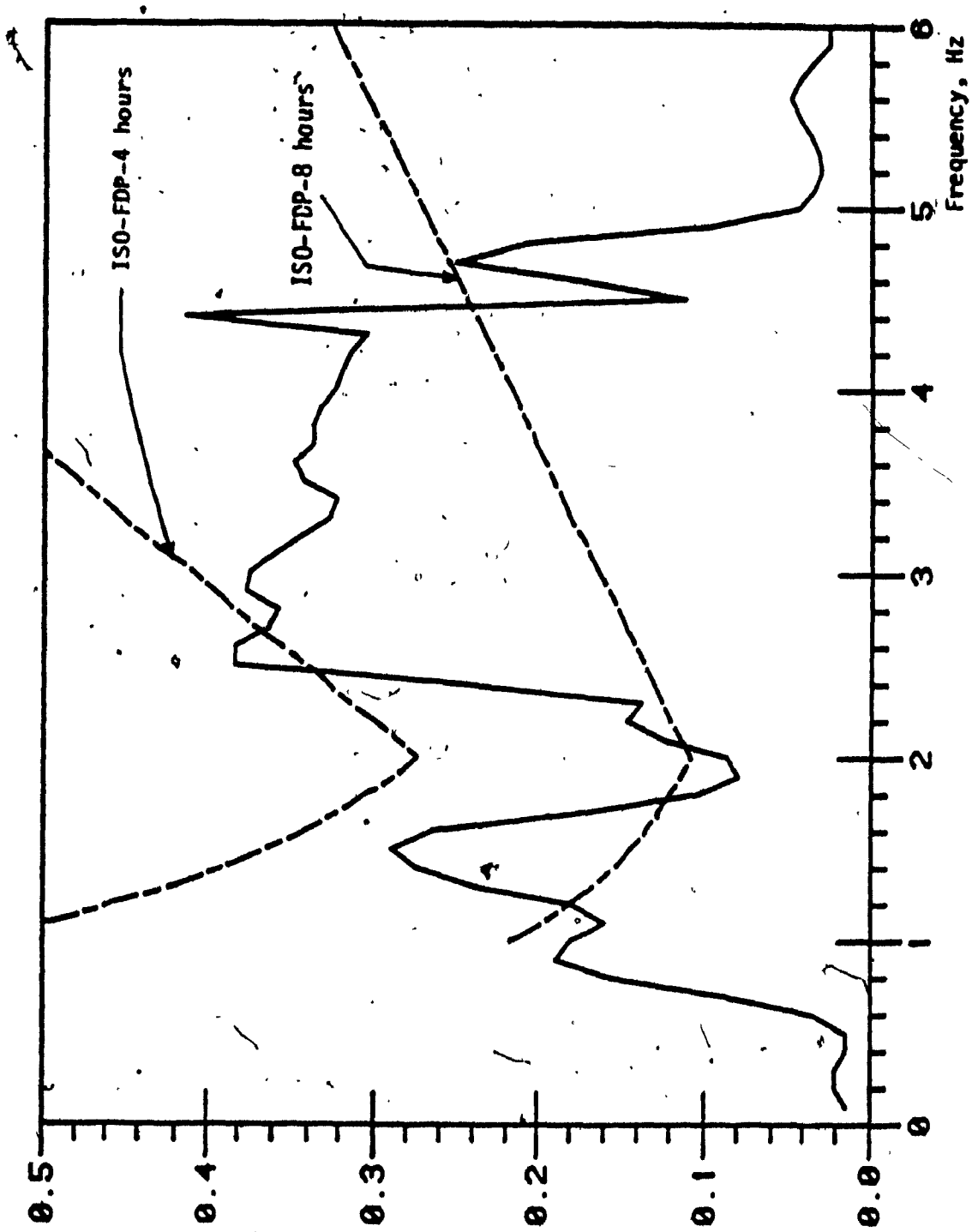

FIGURE 6.4: Longitudinal acceleration PSD response of the optimum longitudinal seat suspension.

to be well within the ISO-FDP limit for 4 hours exposure time. The relative displacement PSD response shows lock up behaviour till 2.4 Hz as shown in Figure 6.5. The relative displacement response peaks in the frequency range 2.5 to 3.0 Hz, but the peak values are of the order 8.5 * 10^{-6} m^2/Hz. The ISO weighted rms acceleration response over the third octave bands is presented in Figure 6.6.

3) RIDE QUALITY OF OPTIMUM LATERAL SEAT SUSPENSION

The lateral seat performance criterion is minimized by constraining the lower limit on suspension stiffness to two different values, namely K_y = 1700 N/m, and K_y = 1200 N/m. The two sets of optimal suspension parameters are obtained as presented in Table 6.3. The direct search routine tends to converge to the lower limit of the suspension stiffness values in both cases. In the former case (K_y = 1700 N/m), the routine converges to the upper limits of velocity squared damping coefficient and Coulomb damping values, in order to minimize the acceleration peak around 1 Hz. However, absolutely no improvement in the lateral ride is obtained, as shown by the acceleration PSD response in Figure 6.7. The relative displacement PSD response is observed to be relatively large compared to other translational modes as shown in Figure 6.8.

A significant improvement in the lateral ride is achieved by imposing lower limit on the suspension stiffness (1200 N/m), such that the undamped natural frequency can be reduced to at least 0.6 Hz. The optimization routine tends to converge to lower limit for the stiffness, and selects low values for Coulomb damping to improve the isolation performance around 1 Hz. The acceleration

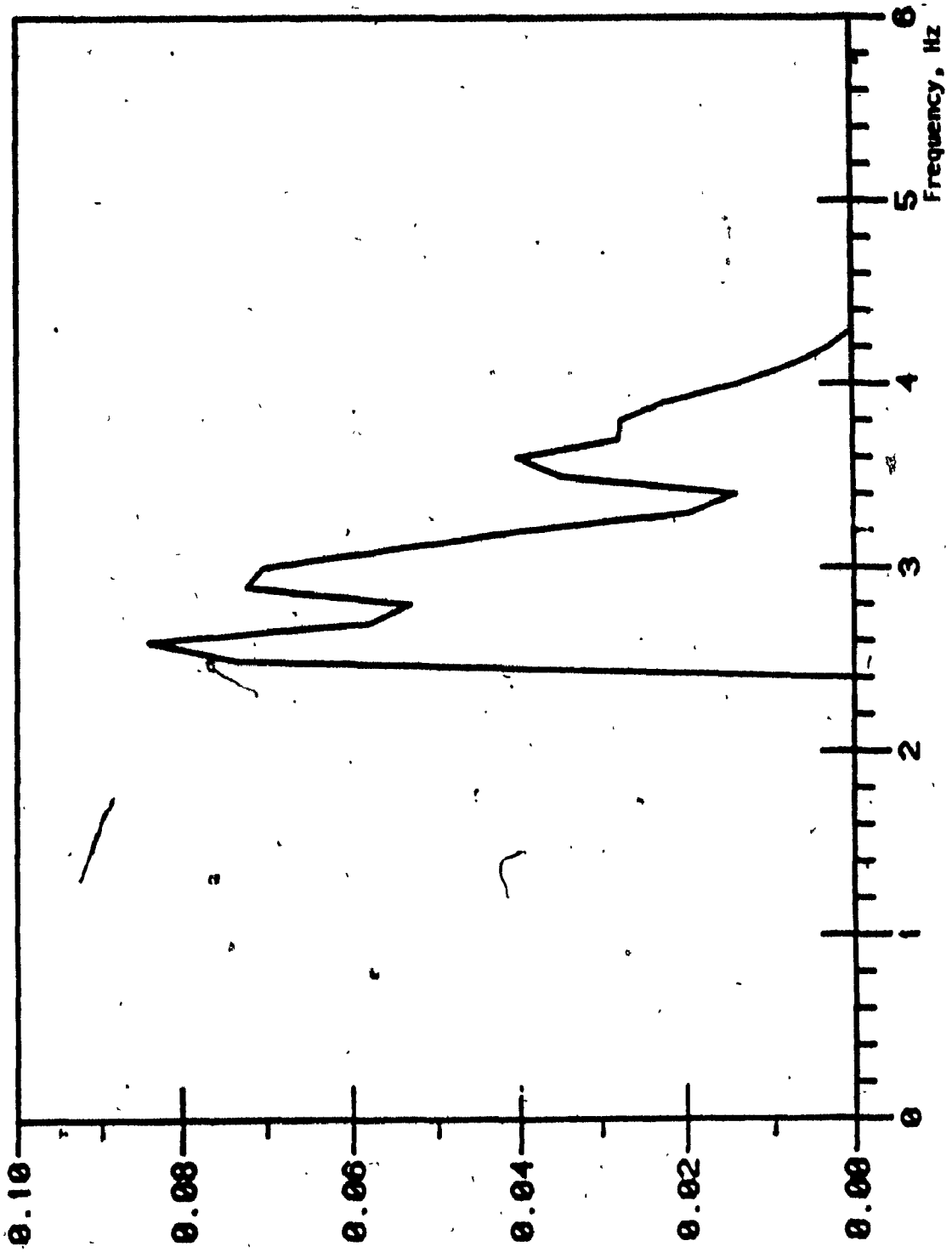

FIGURE 6.5: Relative displacement PSD response of the optimum longitudinal seat suspension.

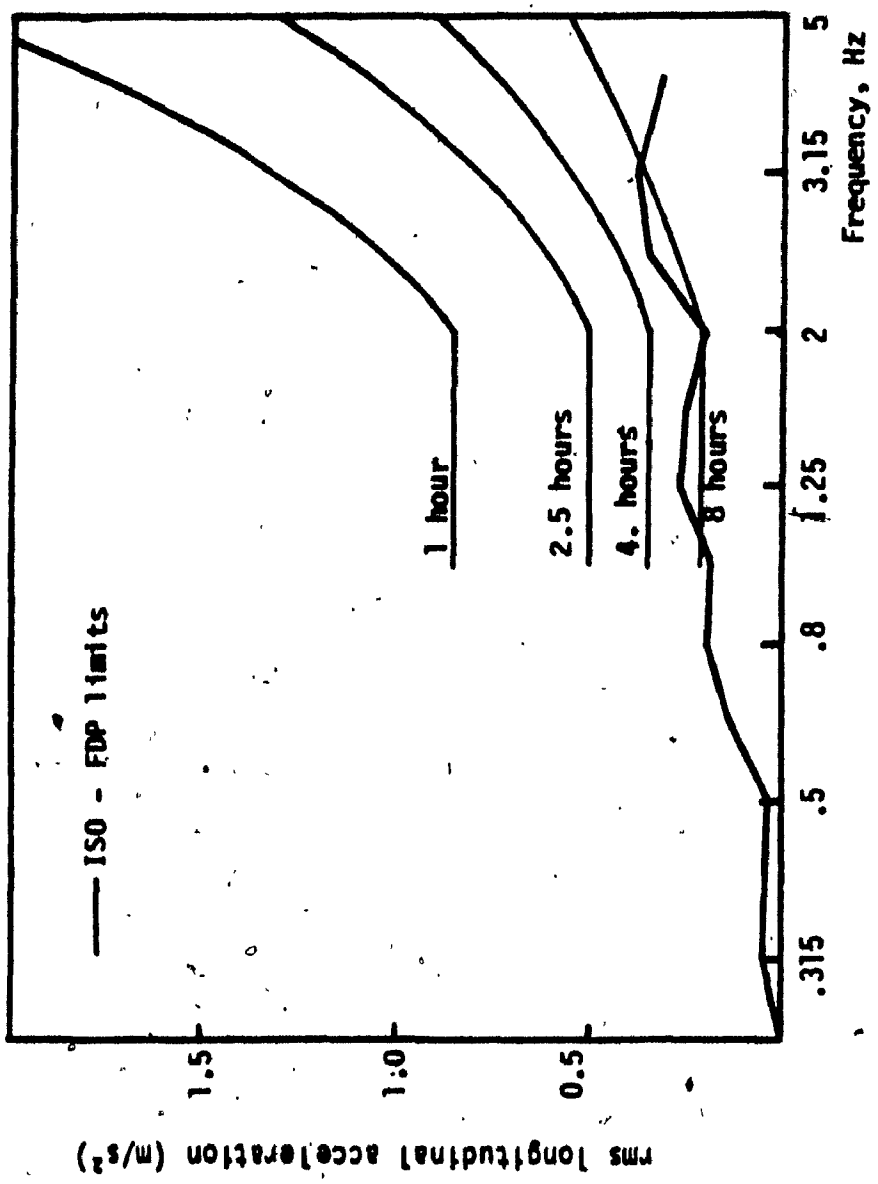

FIGURE 6.6: Longitudinal rms acceleration response of optimal longitudinal seat isolator.

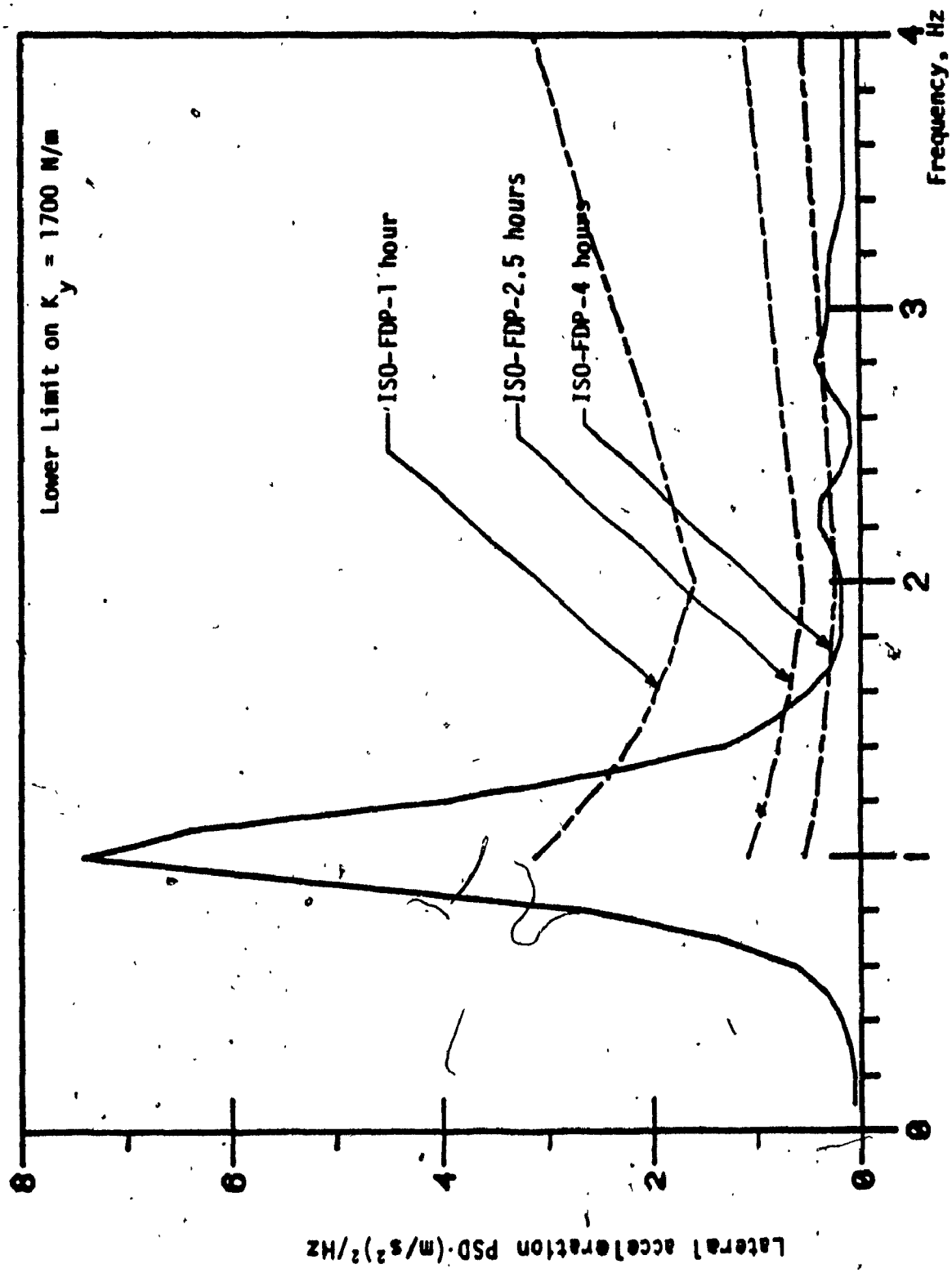

FIGURE 6.7: Lateral acceleration response of the optimum lateral seat suspension.

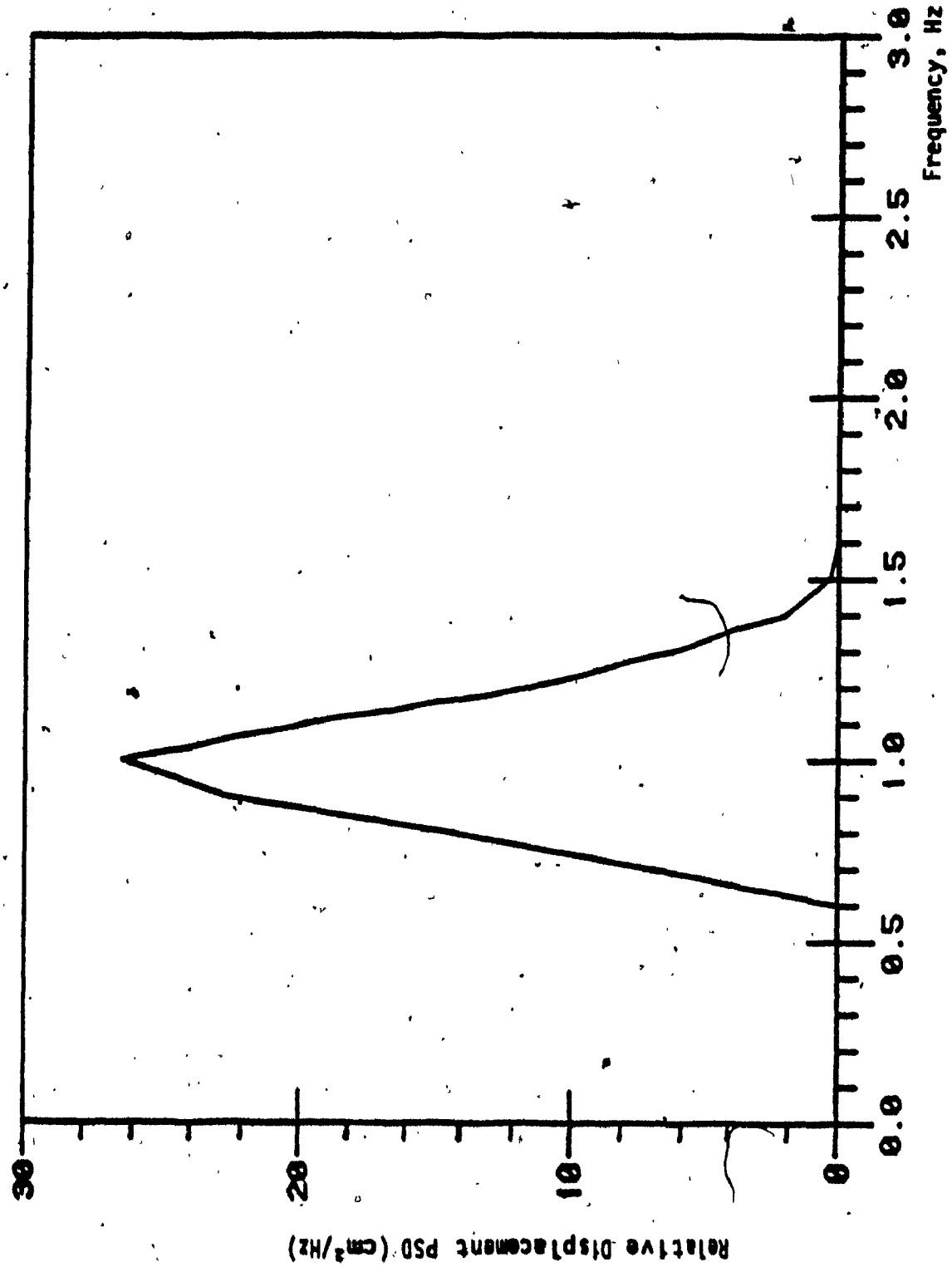

FIGURE 6.8: Lateral relative displacement response of the lateral seat suspension.

and relative displacement PSD responses are presented in Figures 6.9 and 6.10, respectively. The ISO weighted rms acceleration response of lateral seat suspension is shown in Figure 6.11.

4) RIDE QUALITY OF OPTIMUM ROTATIONAL SEAT SUSPENSION.

The parametric optimization of the rotational seat suspension model is carried out by formulating two independent performance criteria. The first criterion is formulated to minimize the peak roll acceleration response of the rotational seat suspension model. A list of optimal parameter values is presented in Table 6.3. The roll acceleration PSD response exhibits a resonance peak at 0.55 Hz as shown in Figure 6.12. The roll excitation peak occurring at 1 Hz is attenuated significantly, whereas the excitation peak corresponding to 3 Hz is entirely eliminated. The relative displacement response PSD in the roll mode exhibits a peak of the order 0.012 rad^2/Hz at frequency 0.55 Hz as shown in Figure 6.13. The rms acceleration response over the third octave bands is obtained assuming the weighting factor to be unity, and is shown in Figure 6.14.

The second optimization criterion was formulated in Equations (6.9) and (6.10) to obtain optimal bounce and pitch performance of the rotational isolator. The resulting values for optimal suspension parameters are listed in Table 6.3. The bounce acceleration PSD response of the frames is presented in Figure 6.15. The response exhibits a large acceleration peak at tractor resonant frequency (2.6 Hz). However, the acceleration PSD response of the seat mass exhibits a resonance peak at 1.2 Hz and the acceleration response in the vicinity of vehicle resonant frequencies is observed to be close to the 4 hours exposure limits as shown in Figure 6.16. The

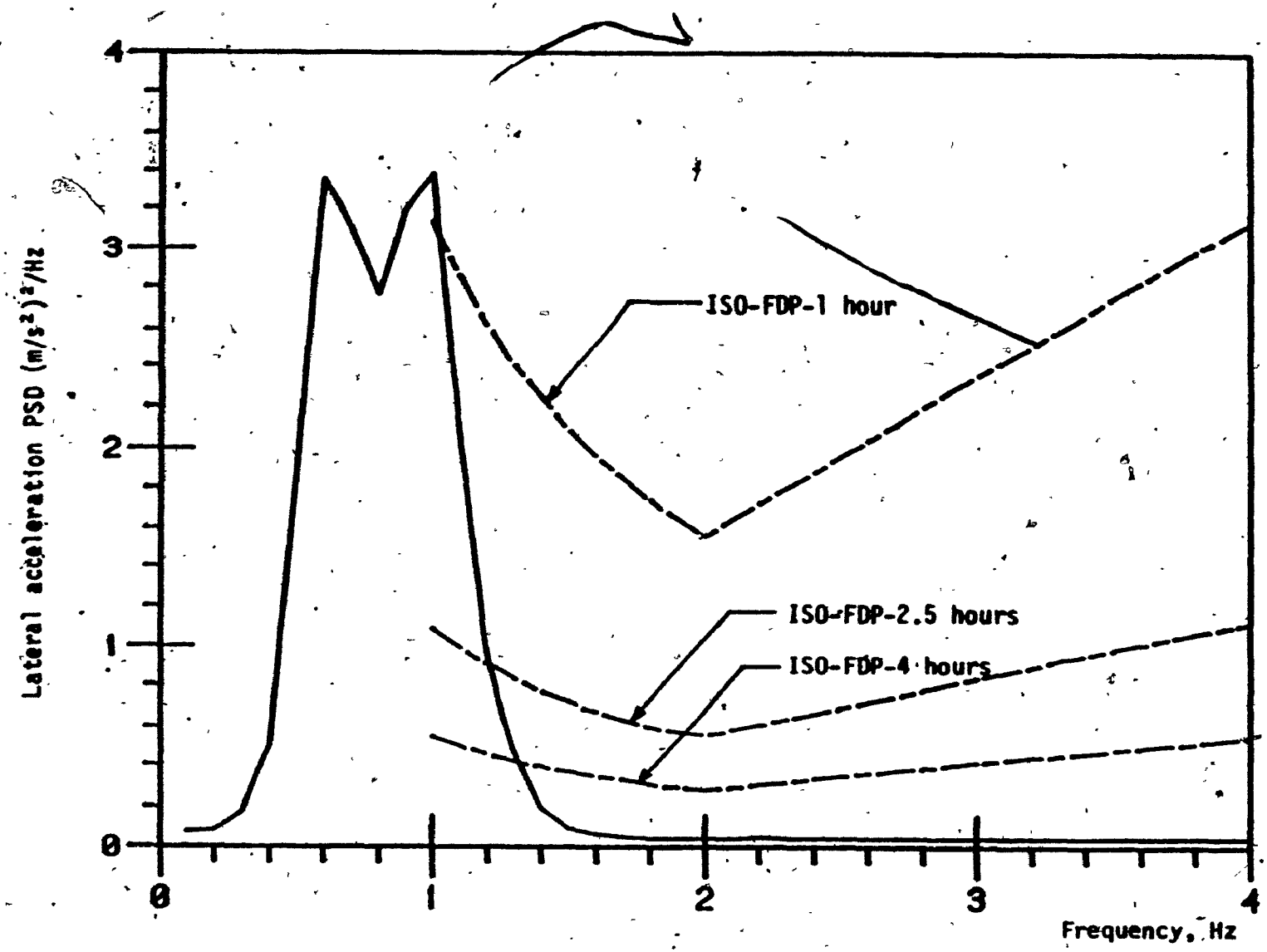

FIGURE 6.9: Lateral acceleration PSD response of the optimum seat suspension.

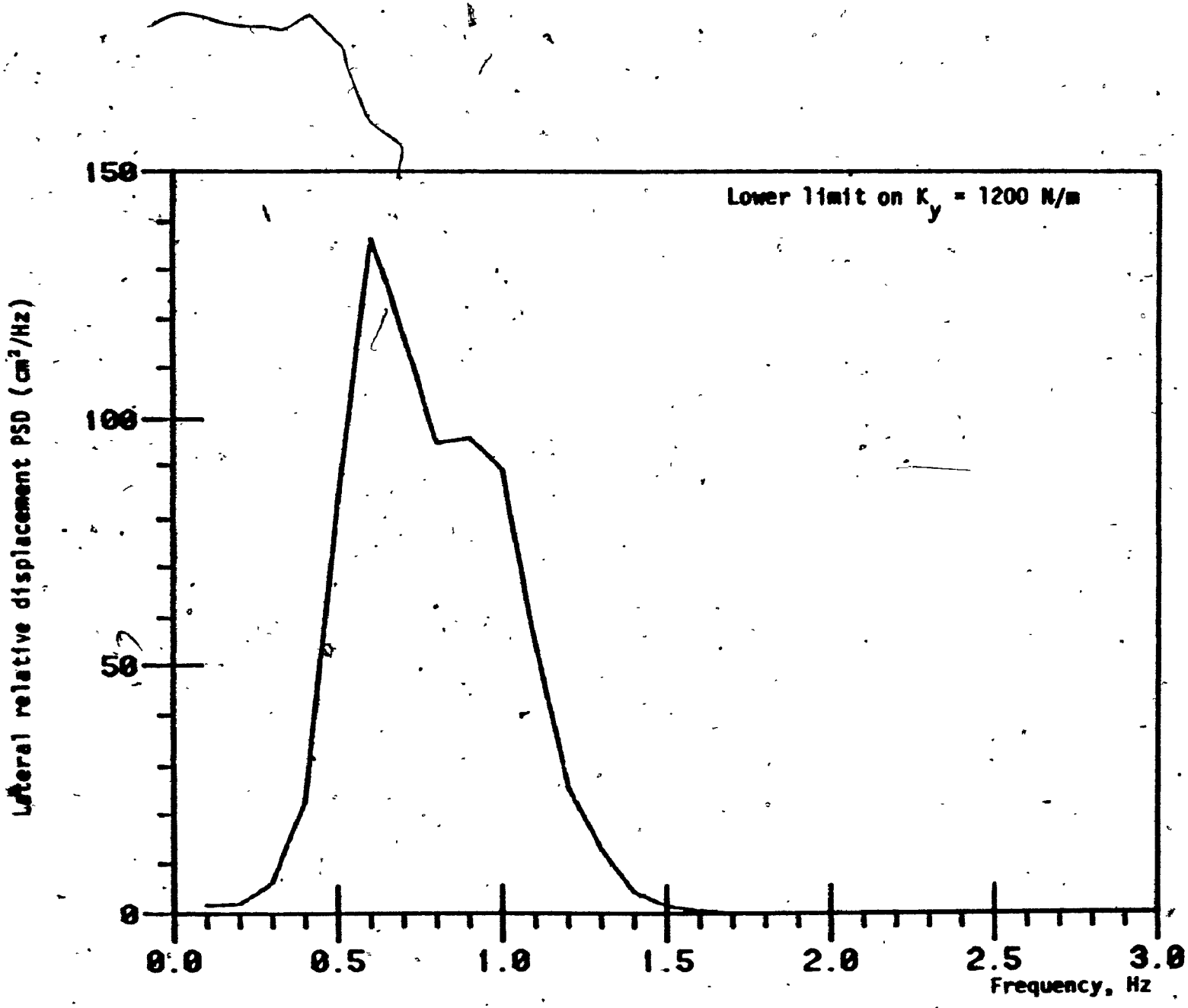

FIGURE 6.10: Lateral relative displacement PSD response of the lateral seat suspension.

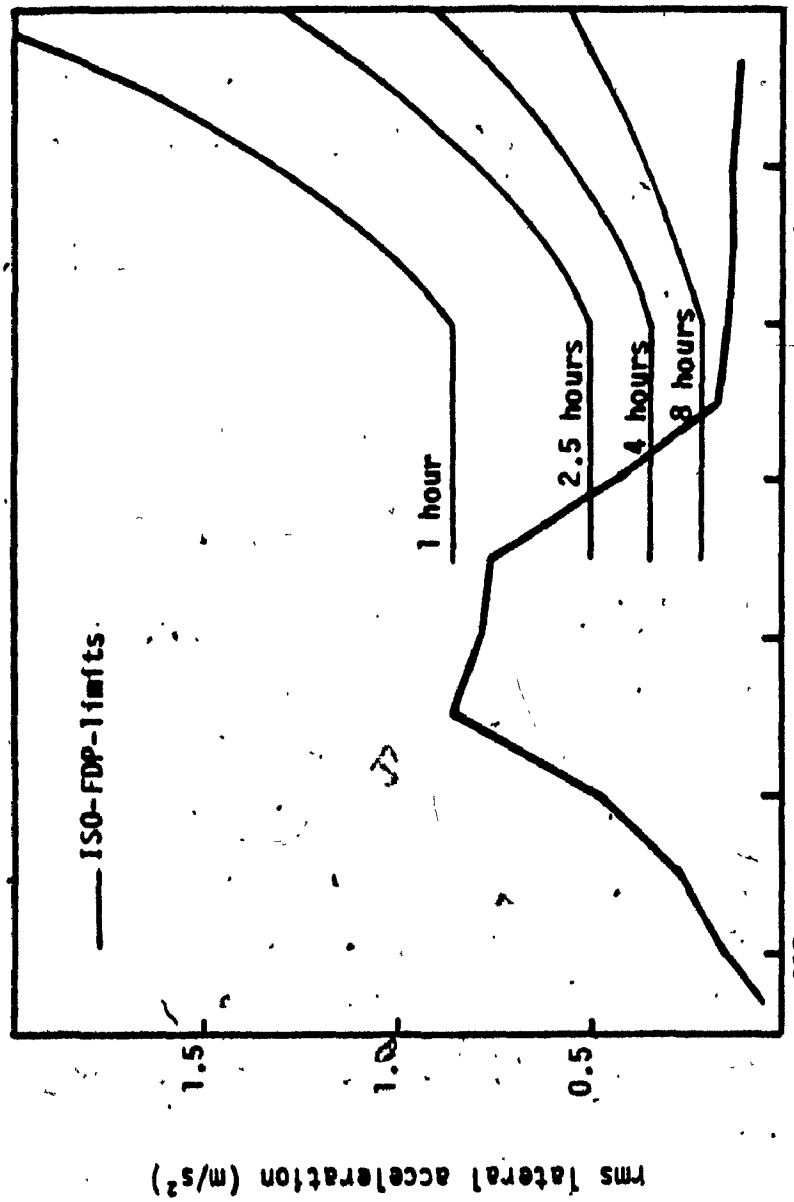

FIGURE 6.11: rms acceleration response of the optimal lateral seat suspension.

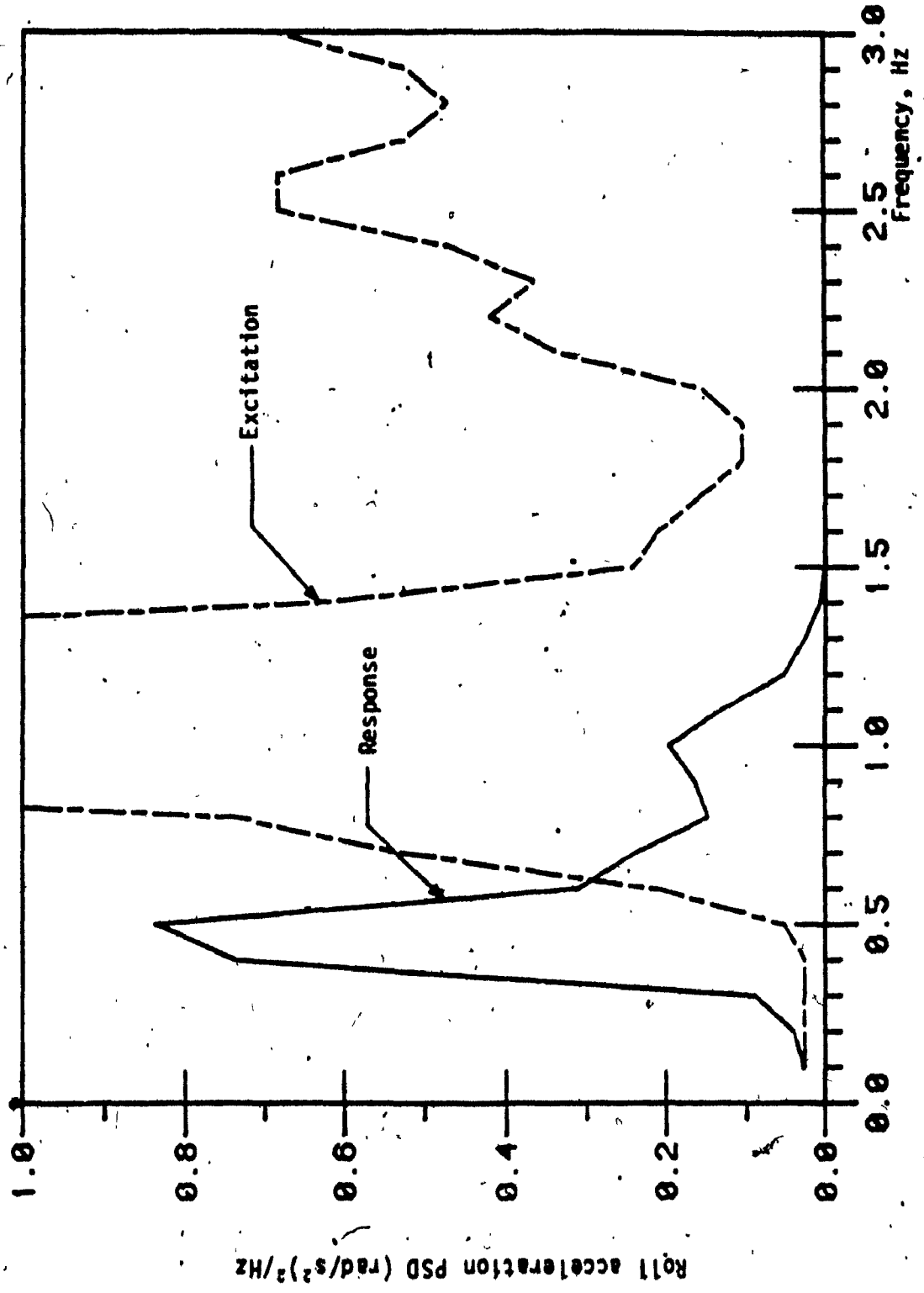

FIGURE 6.12: Roll acceleration PSD response of the optimum rotational isolator.

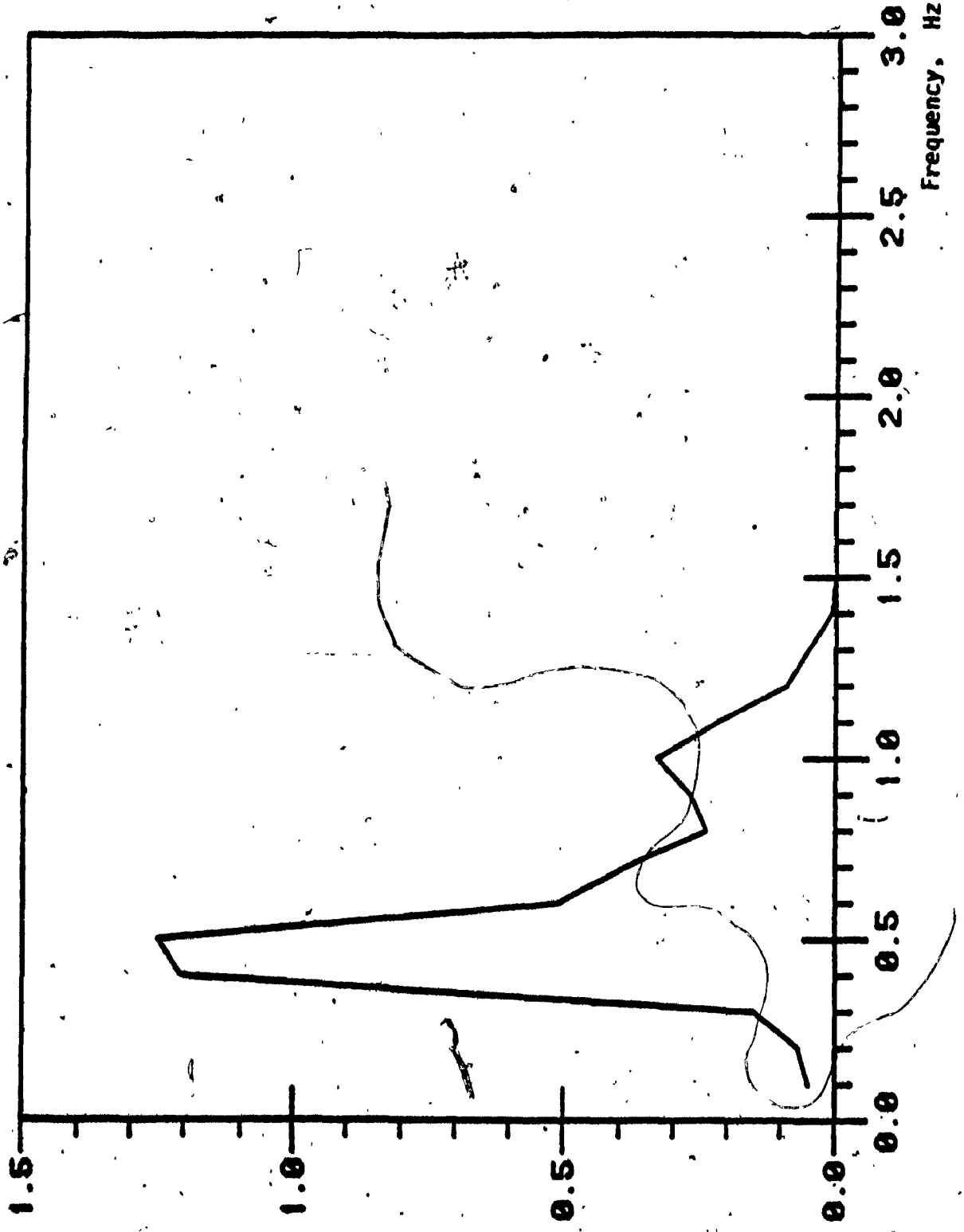

FIGURE 6.13: Roll relative displacement PSD response of optimum rotational seat suspension.

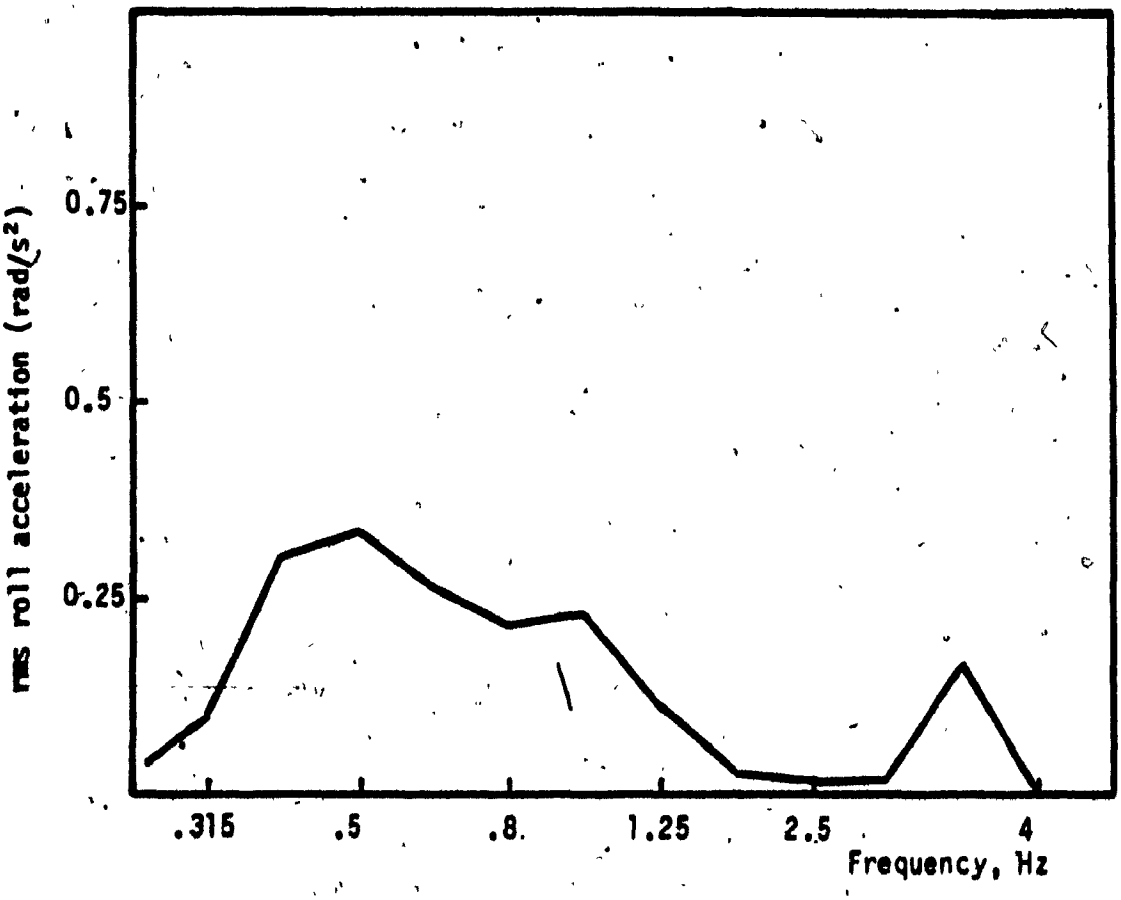

FIGURE 6.14: rms roll acceleration response of optimal rotational seat suspension.

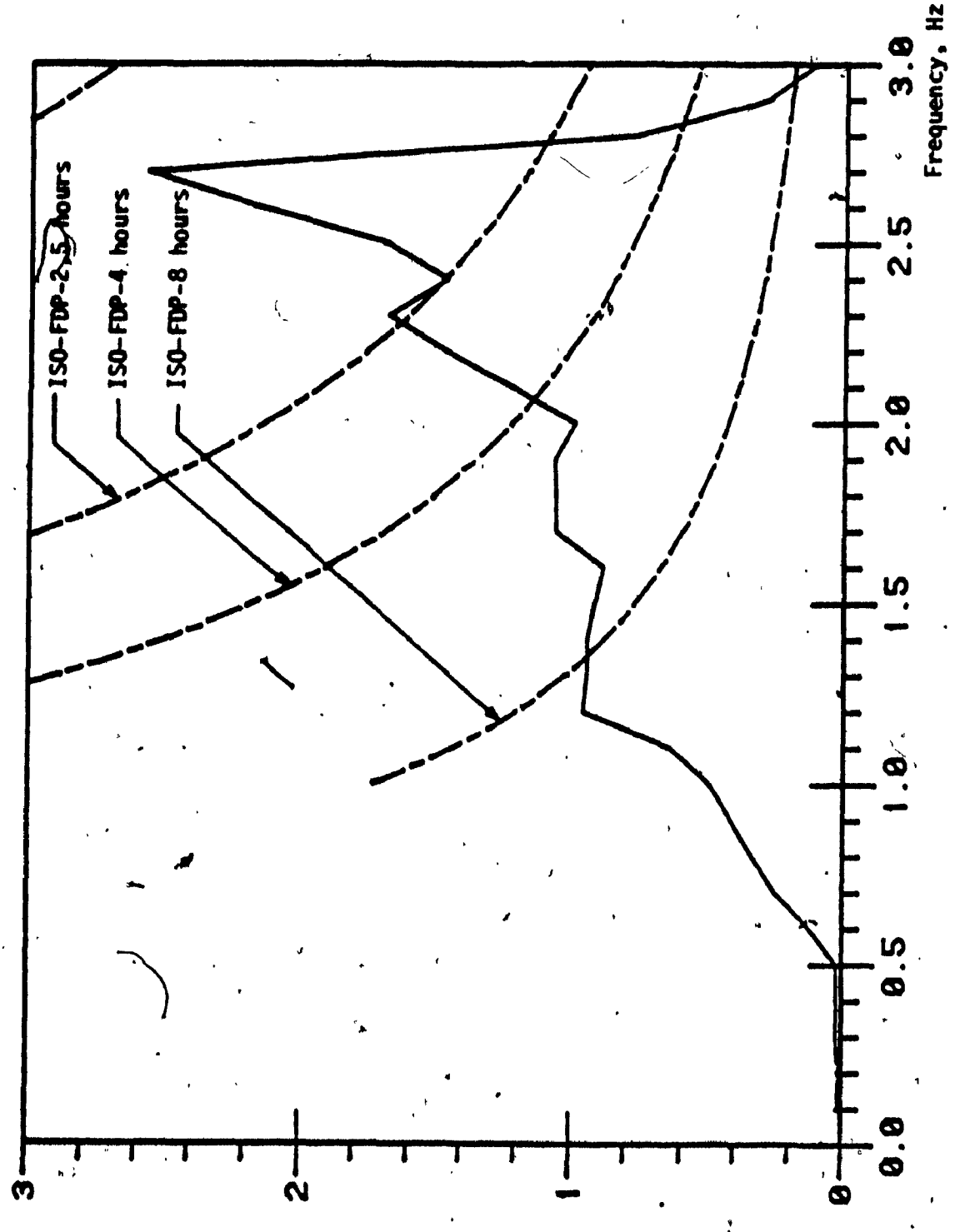

FIGURE 6.15: Bounce acceleration PSD response at the frames of optimum rotational seat suspension.

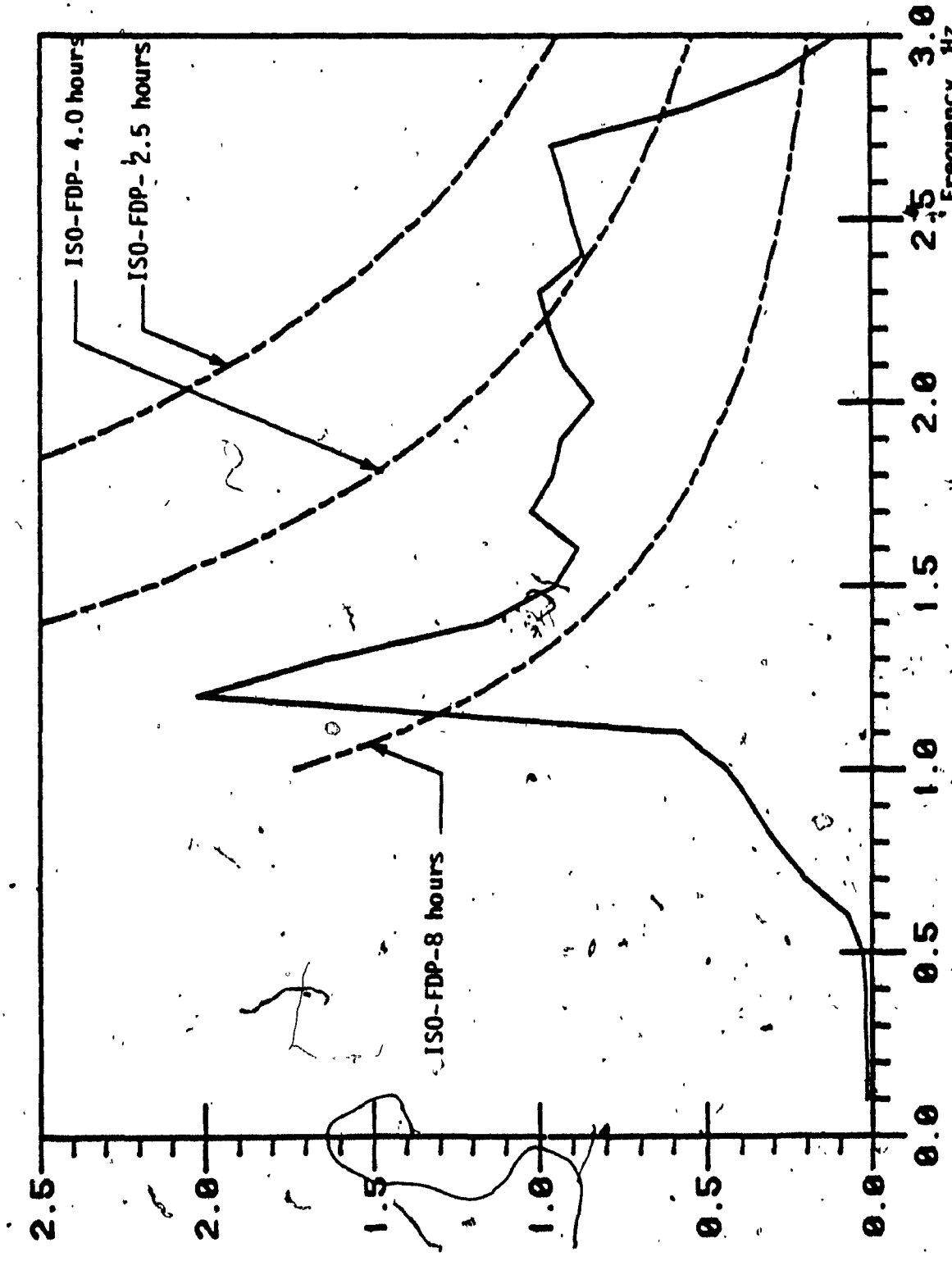

FIGURE 6.16: Bounce acceleration response at the seat mass of the optimum rotational seat suspension.

relative displacement response of the seat mass with respect to the floor is observed to be of the same magnitude as that of a bounce suspension seat alone. The ISO weighted rms acceleration response is presented in Figure 6.17.

The pitch acceleration response of the optimum rotational seat suspension exhibits two peaks corresponding to frequencies 0.65 Hz and 1.2 Hz, respectively as shown in Figure 6.18. The response peak at 0.65 Hz occurs due to the pitch resonance of the rotational seat suspension and peak at 1.2 Hz is attributed to the bounce resonance. The pitch relative motion PSD response of the seat-mass is presented in Figure 6.19. The rms pitch acceleration response over the third octave frequency bands is presented in Figure 6.20.

6.4.2 RIDE PERFORMANCE CHARACTERISTICS OF OPTIMUM CAB SUSPENSION MODEL

The performance criteria listed in section 6.2.3 were formulated to minimize either the lateral acceleration response of the cab or the roll acceleration response of the cab. The optimization has been carried out for the two performance criteria. The minimization of the lateral acceleration PSD response of the cab(performance criteria of Equation (6.11)) leads to good lateral and roll response with poor bounce and pitch response of the cab. However, the optimization carried out to minimize the roll response leads to excellent bounce, roll and pitch ride performance of the cab suspension model with slight deterioration in the lateral ride. The results obtained by minimizing the roll ride of the sprung cab are presented in this section. The optimal suspension parameters obtained are presented in Table 6.4.

The natural frequencies and damping ratios of the cab suspension model employing the optimal suspension parameters are evaluated using

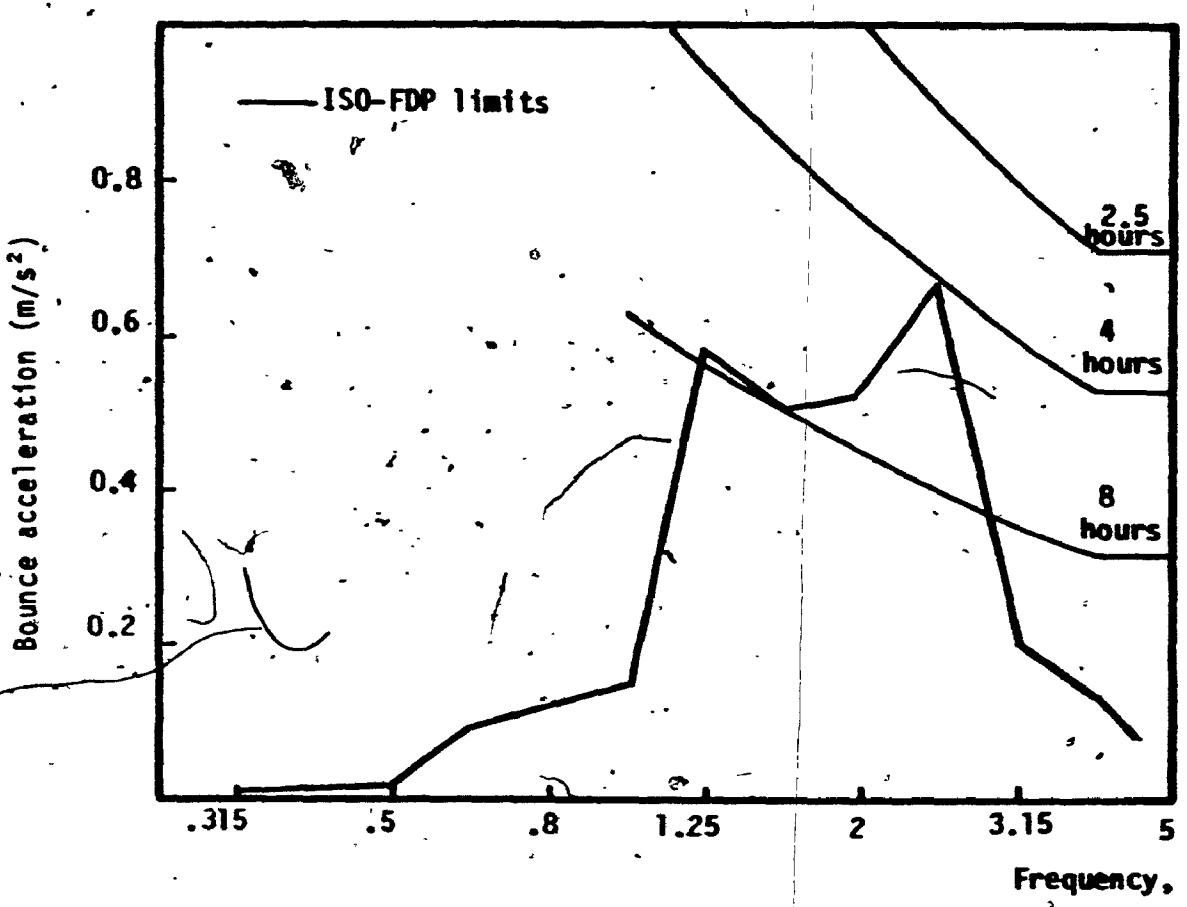

FIGURE 6.17: ISO weighted bounce rms acceleration response of optimal rotational seat isolator.

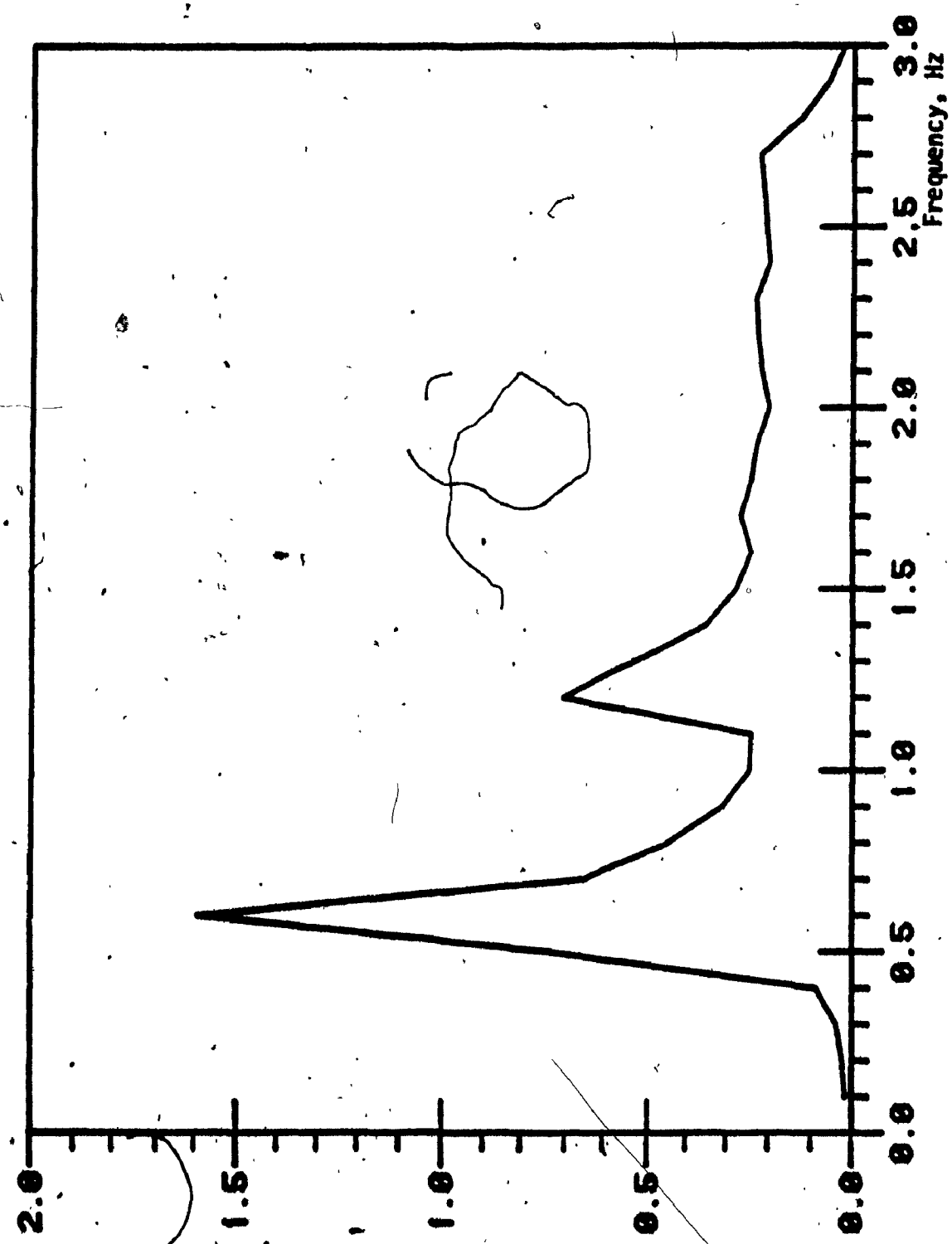

FIGURE 6.18: Pitch acceleration PSD response of the optimal rotational seat suspension.

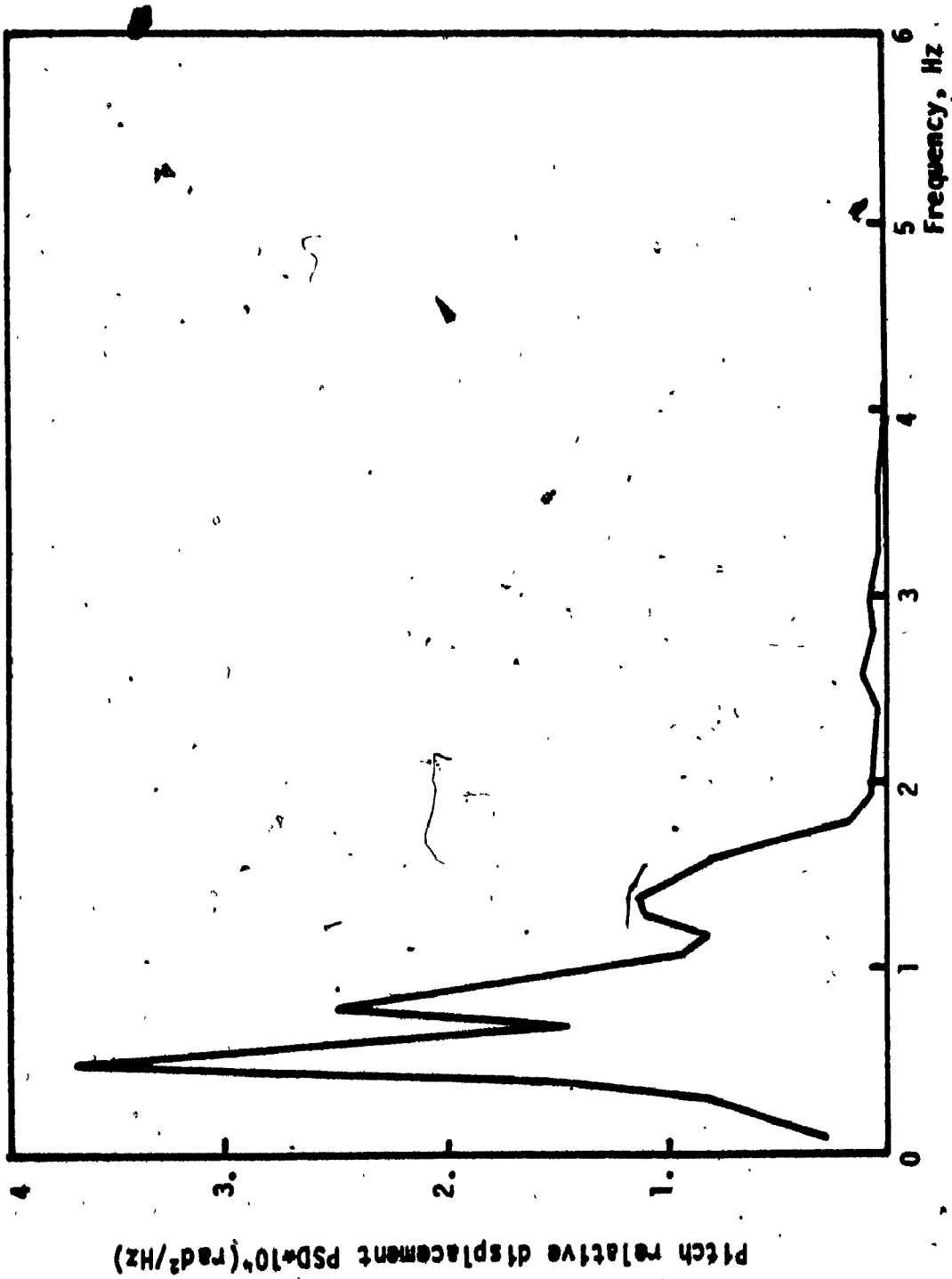

FIGURE 6.19: Pitch relative displacement PSD response of optimal rotational isolator.

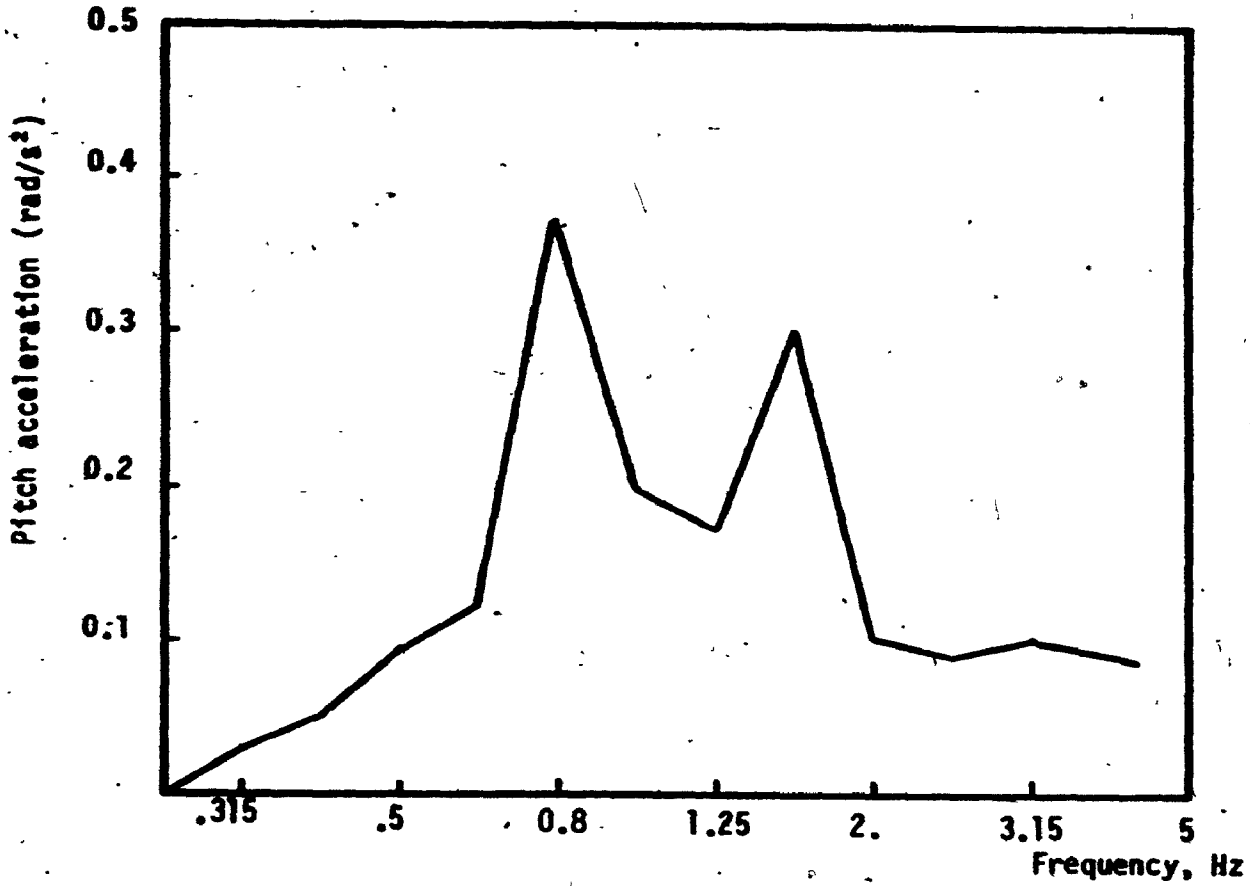

FIGURE 6.20: Pitch rms acceleration response of rotational seat isolator

eigenfunction analysis. Natural frequencies in the bounce, pitch, roll, lateral and longitudinal modes are found to be 1.1, 0.45, 0.4, 1.01 and 1.32 Hz, respectively. The damping ratios in these modes are found to be 0.78, 0.19, 0.30, 0.83 and 0.45, respectively. Variations in the stiffness values of the corner mounts cause significant change in roll and pitch resonant frequencies. However, for the chosen cab geometry, the pitch and roll resonant frequencies are observed to be approximately 45 to 40 percent, of the bounce natural frequency, respectively.

The ride performance characteristics of the optimum 5 DOF cab suspension model are evaluated in the bounce, pitch, roll, lateral, and longitudinal modes. The acceleration PSD, relative displacement PSD, and ISO weighted rms acceleration response plots are presented in Figures 6.21 to 6.36. The PSD of bounce acceleration response of the cab is presented in Figure 6.21. The bounce response exhibits poor performance in the vicinity of vehicle resonant frequency (2.6 Hz). The acceleration response exceeds ISO *fatigue decreased proficiency* (FDP) limits for an exposure time of 2.5 hours. This performance characteristic of the cab suspension model is attributed to the fact that the optimization procedure selects large damping values for corner mounts to isolate low frequency roll excitations. Large damping values of the corner mounts lead to an excellent performance in the low frequency region but poor performance in the region of isolation frequencies. The ISO weighted rms bounce acceleration response and the ISO-FDP rms acceleration limits are presented in Figure 6.22. The bounce relative displacement response of the cab with respect to vehicle frame is observed to be exremely good as shown in Figure 6.23.

The PSD of pitch acceleration response of the cab is shown in Figure 6.24. The pitch response exhibits a peak corresponding to terrain excitations occurring around 1.5 Hz. However, the pitch acceleration

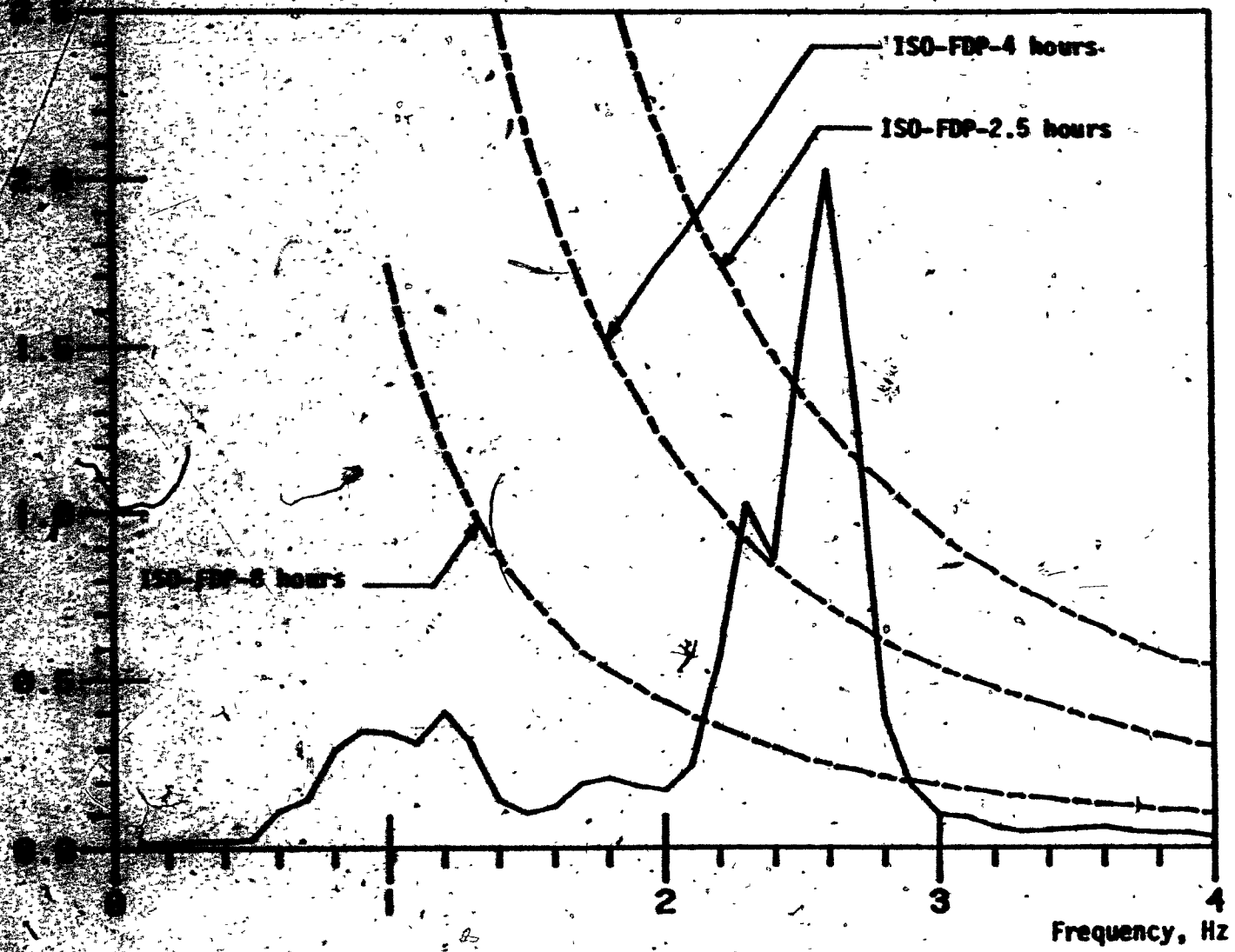

FIGURE 6.21: Bounce acceleration PSD response of the optimum 5 DOF cab suspension model.

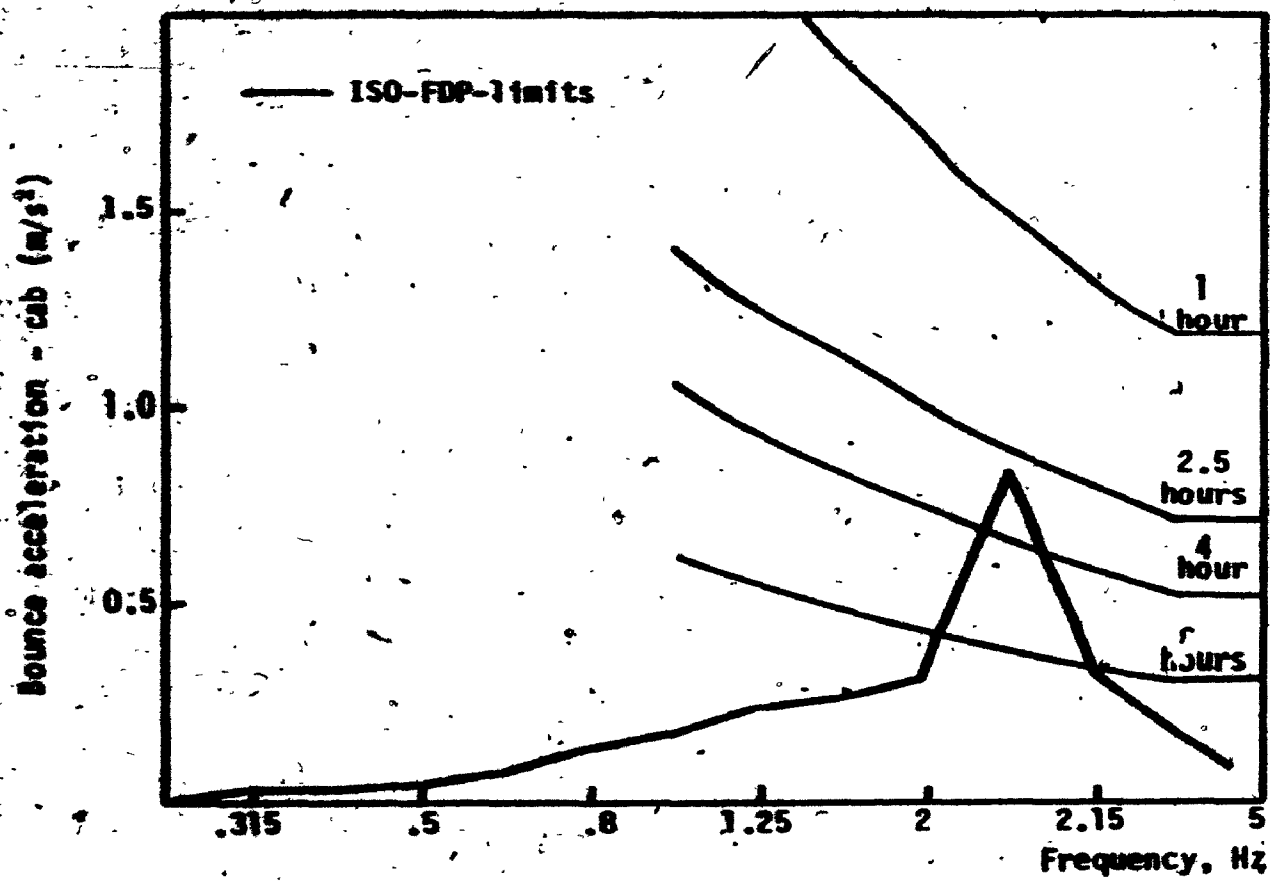

FIGURE 6.22: ISO weighted rms bounce acceleration response of 5 DOF cab suspension.

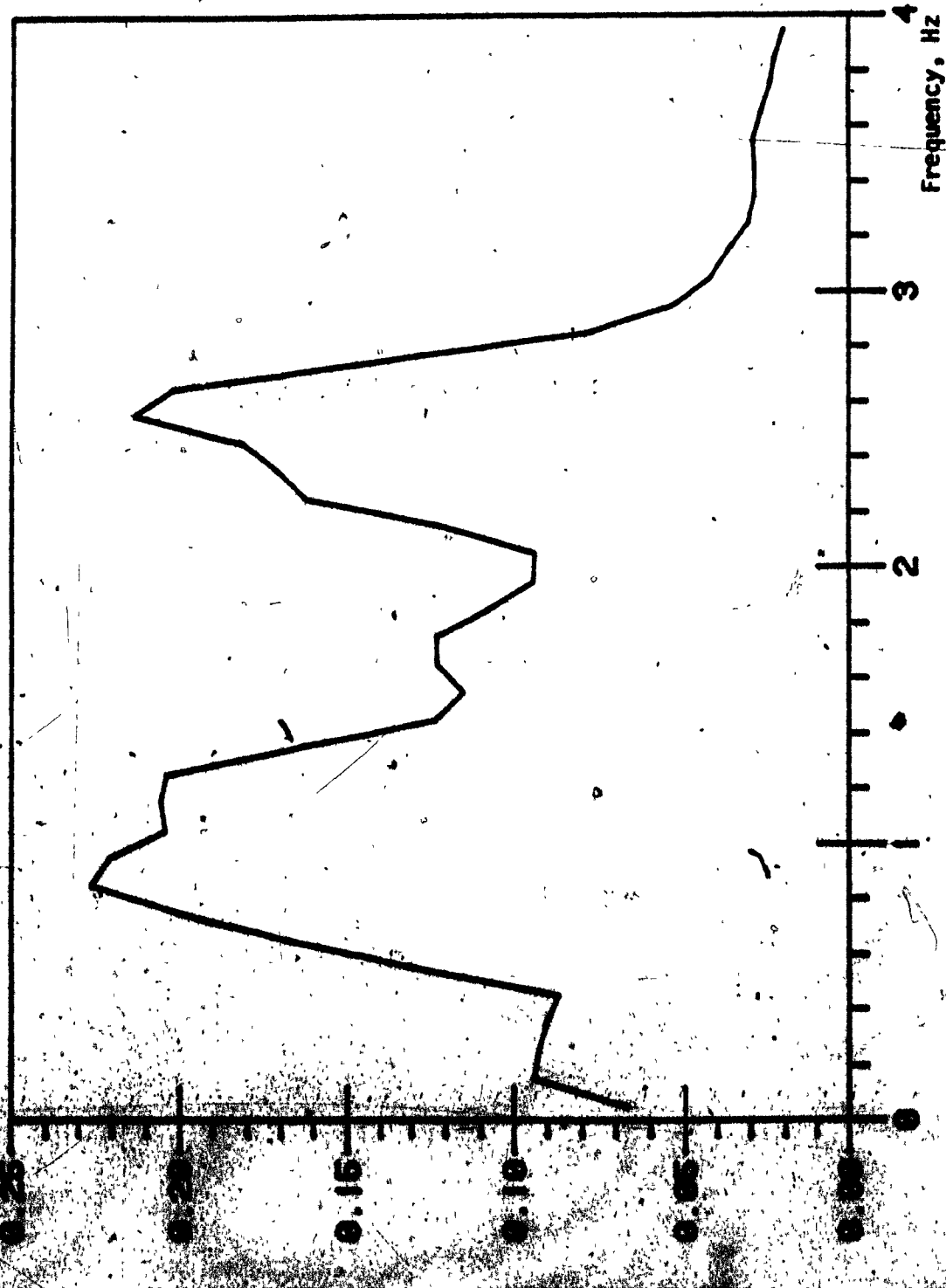

FIGURE 6.23: Bounce relative displacement PSD response of the optimum 5 DOF cab suspension model.

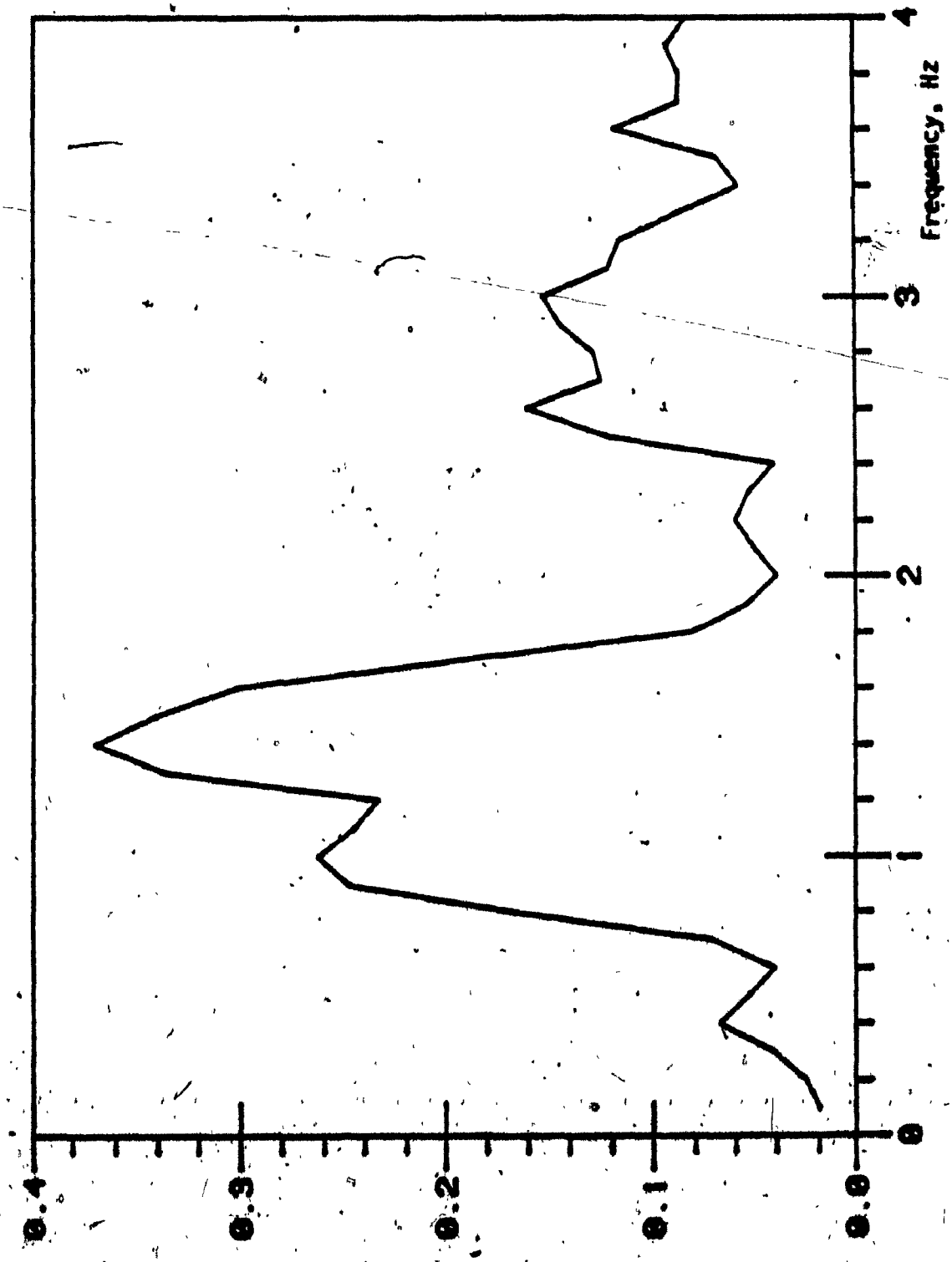

FIGURE 6.24: PSD of the pitch acceleration response of the optimum 5 DOF cab suspension model.

response is found to be excellent in the entire frequency range. The rms acceleration response is obtained over the third octave frequency bands assuming unity weighting factors, as shown in Figure 6.25. The relative displacement PSD response exhibits peak corresponding to the pitch resonance of the cab as shown in Figure 6.26. However, the relative displacement PSD response in the entire frequency range is also quite low.

The roll acceleration PSD response of the 5 DOF optimum cab is shown in Figure 6.27. The response plot reveals an excessively large acceleration peak around the lateral resonant frequency (1.1 Hz) of the tractor. The magnitude of the resonance peak is significantly large due to large values of corner mounts damping selected to subside the bounce, pitch, and roll resonance responses of the cab. The rms acceleration response in the ISO specified third octave bands are evaluated assuming unity weighting factor as shown in Figure 6.28. The roll relative motion response of the cab is observed to be extremely good as shown in Figure 6.29. The roll relative motion response shows two peaks corresponding to roll resonant frequency of the cab and to the lateral resonant frequency of the tractor.

The PSD of lateral acceleration of the cab is shown in Figure 6.30. The acceleration response plot exhibits only a slight improvement in lateral ride of the tractor. The response acceleration exceeds ISO-FDP limits for 1 hour exposure in the vicinity of lateral resonant frequency of the tractor (1.1 Hz). A larger value of lateral isolator damping helps to subside the peak response, but deteriorates the roll performance of the cab suspension. The rms lateral acceleration response, weighted in accordance with ISO is presented in Figure 6.31. The relative displacement response PSD in the lateral mode is observed to be good as shown in Figure 6.32. It may be interesting to observe that the lateral acceleration response at the cab cg is found to be approximately within the ISO-FDP-

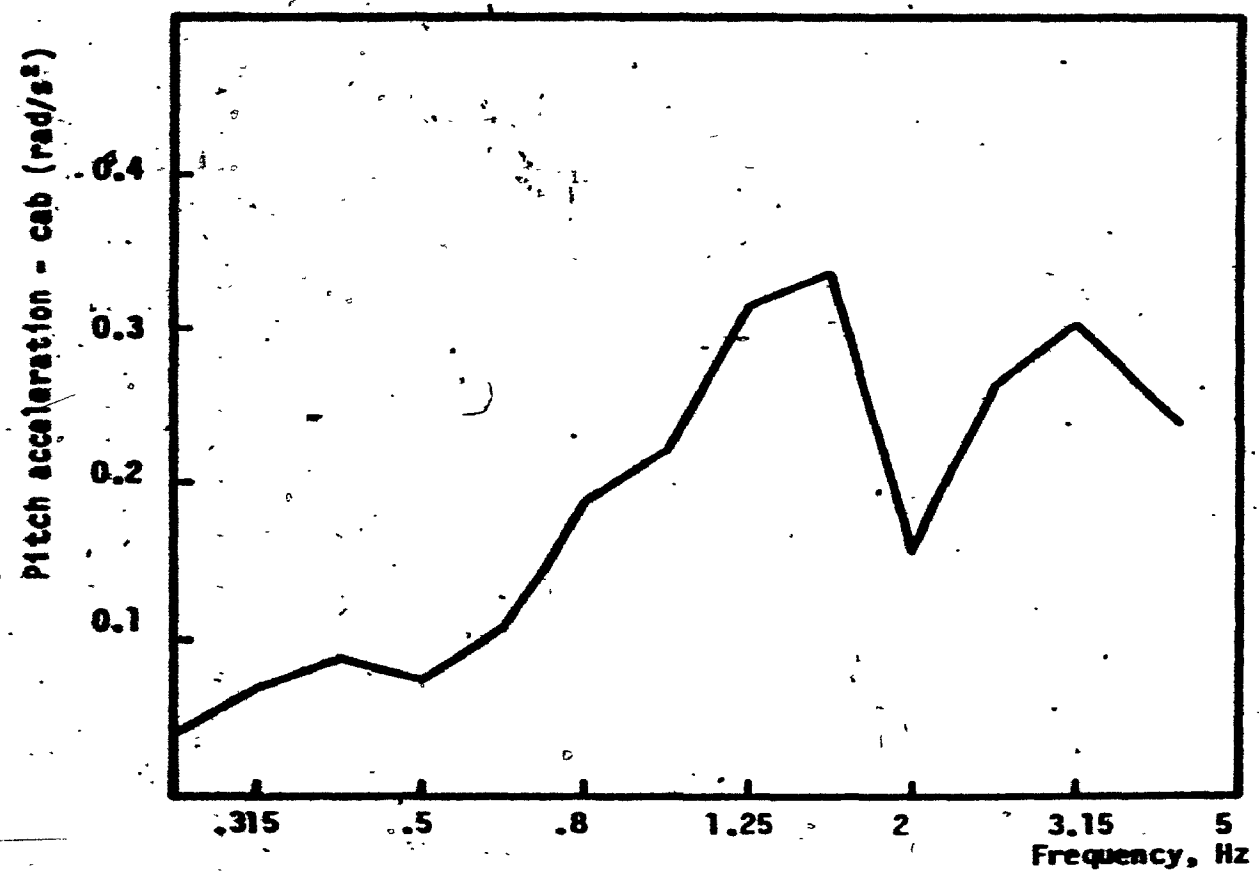

FIGURE 6.25: Pitch acceleration (rms) response of optimal 5 DOF cab suspension model.

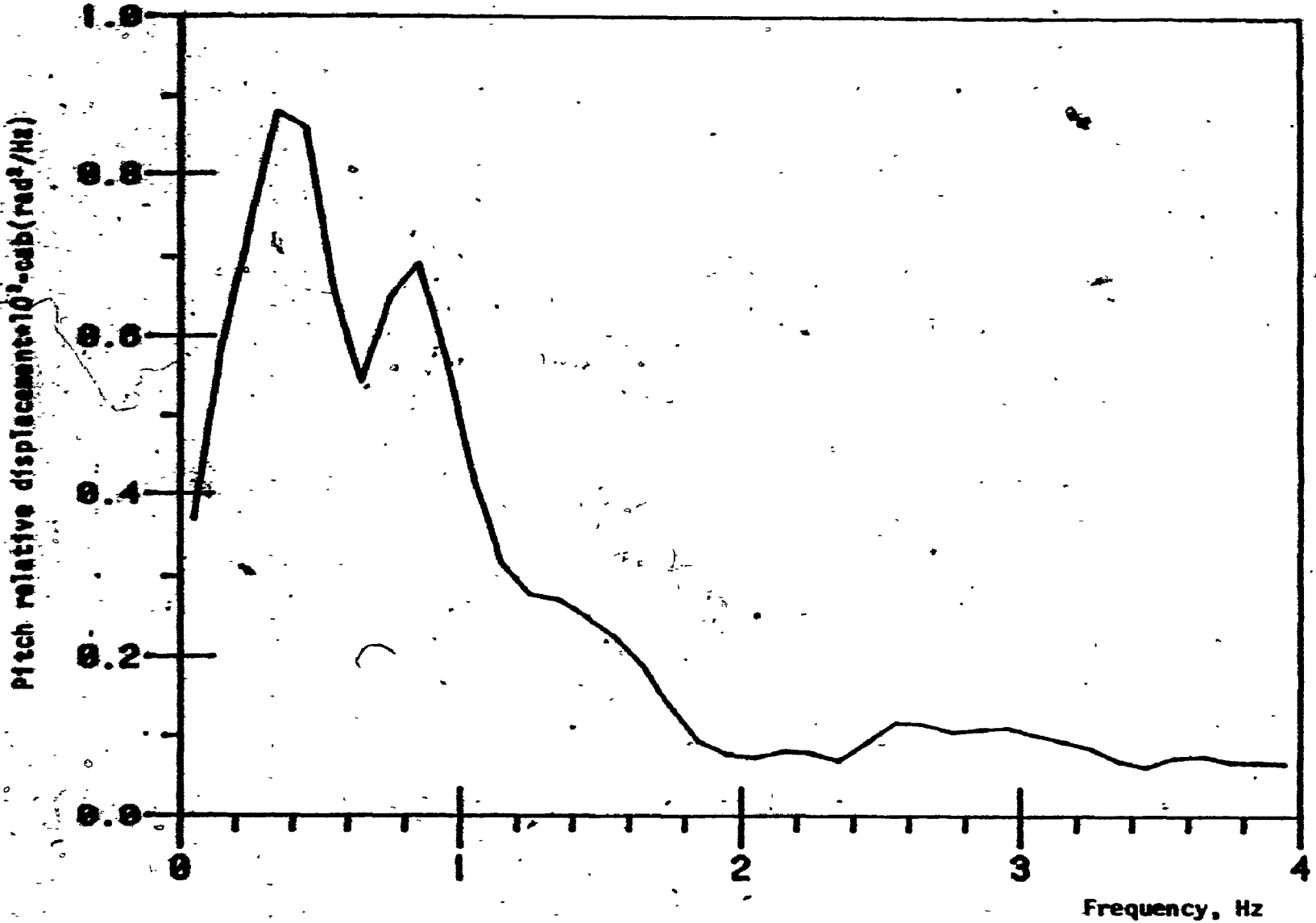

FIGURE 6.26: Pitch relative displacement PSD response of the optimum 5 DOF cab suspension model.

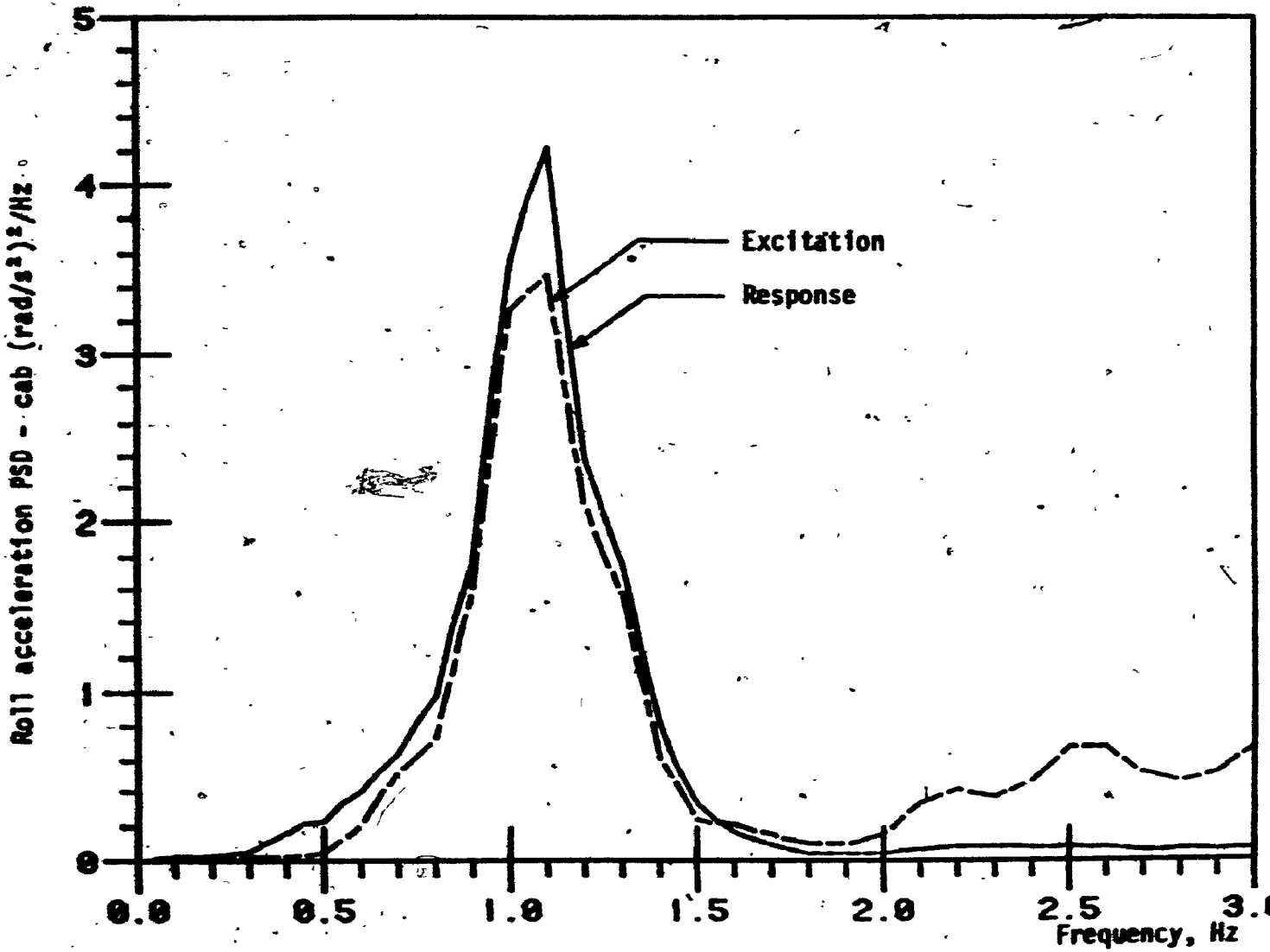

FIGURE 6.27: PSD of the roll acceleration response of 5 DOF optimum cab suspension.

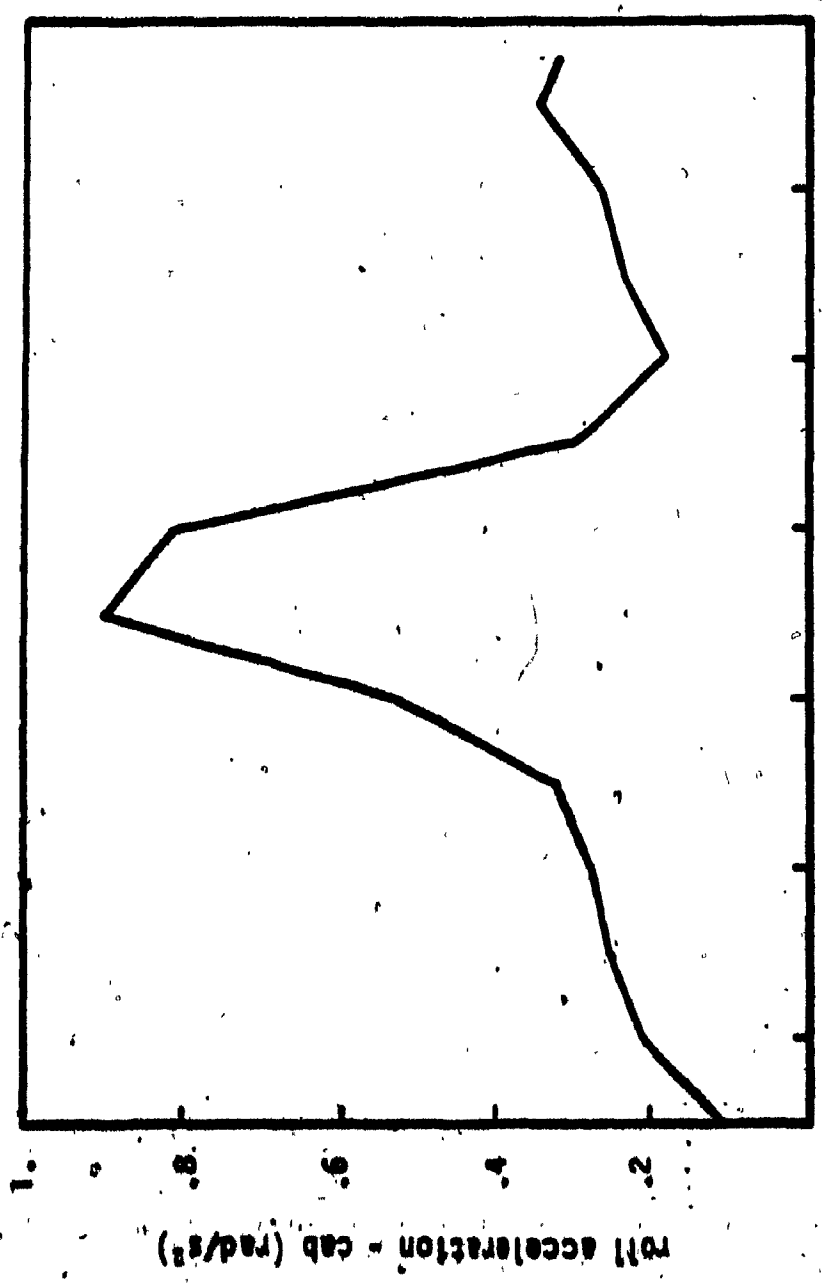

FIGURE 6.28: Roll acceleration (rms) response of optimal 5 DOF cab suspension model.

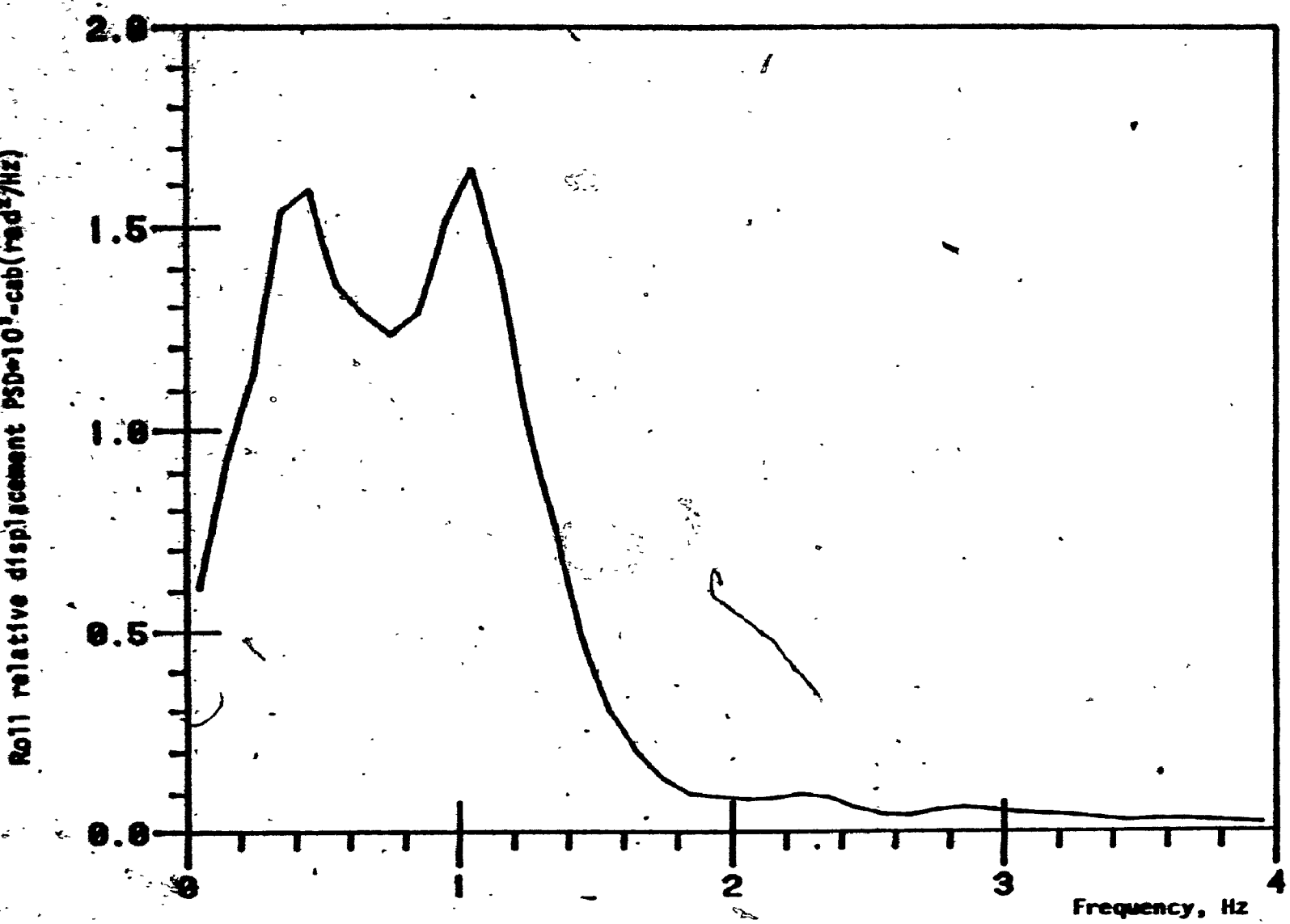

FIGURE 6.29: Roll relative motion response PSD of the optimum 5 DOF cab suspension model.

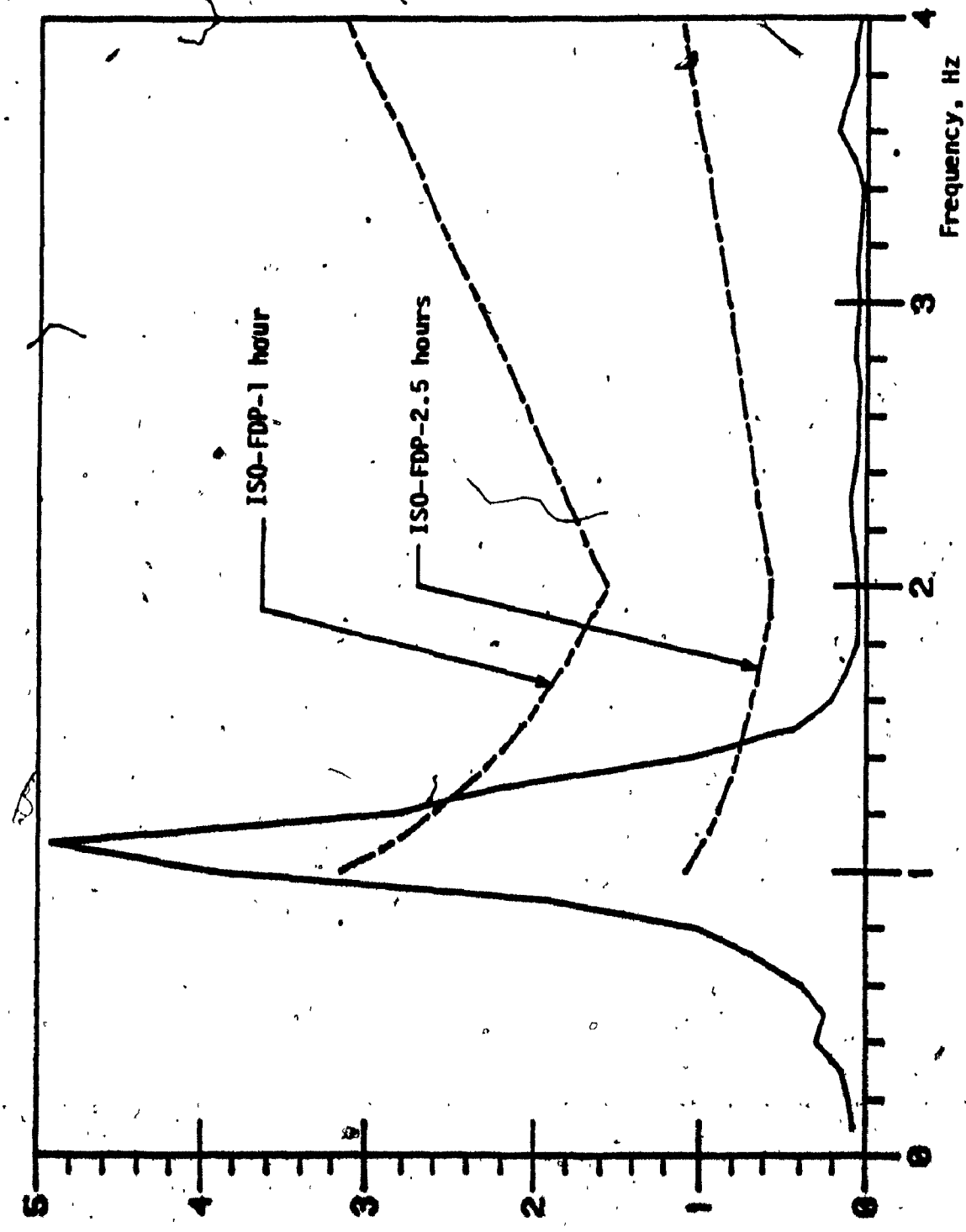

FIGURE 6.30: Lateral acceleration PSD response of the optimum 5 DOF cab suspension model.

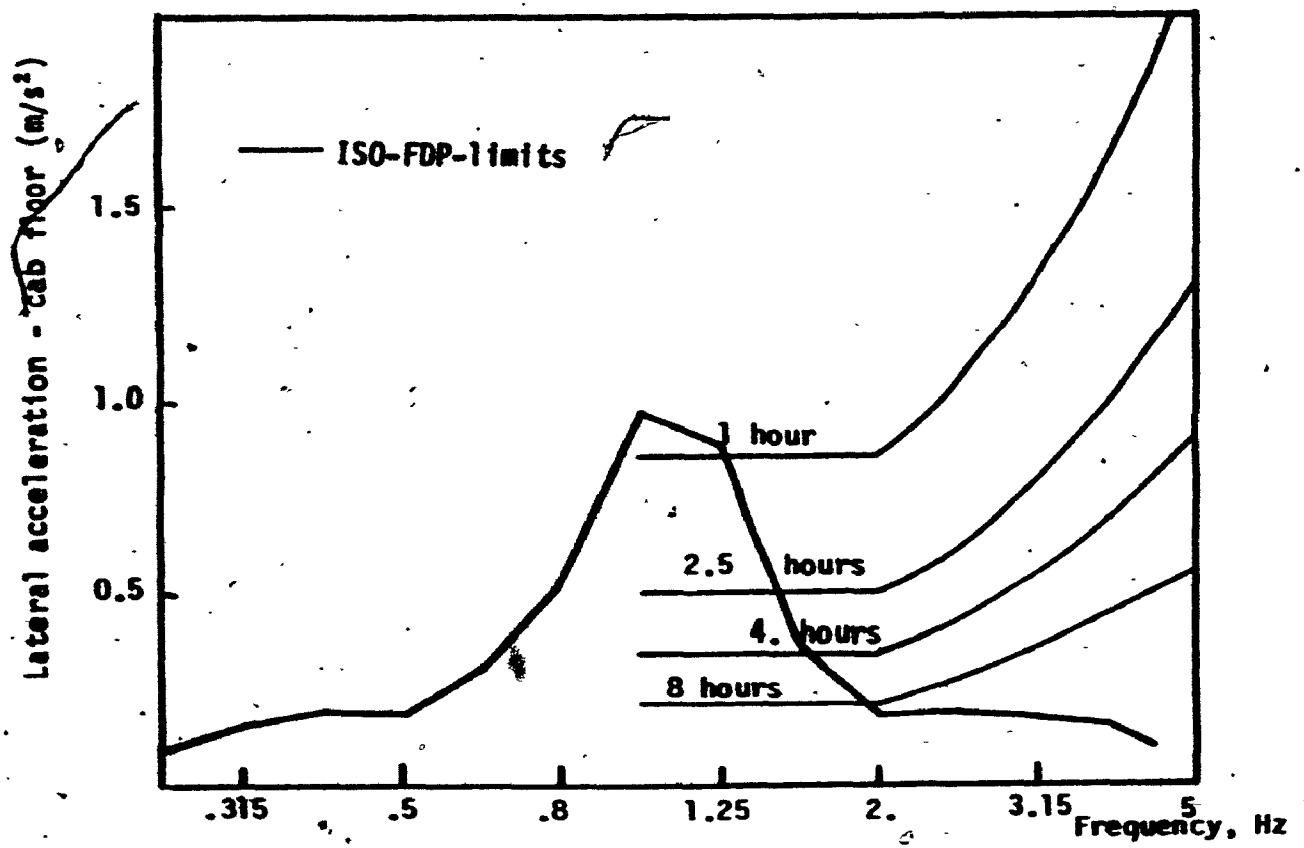

FIGURE 6.31: Lateral acceleration (rms) response of 5 DOF optimal cab suspension.

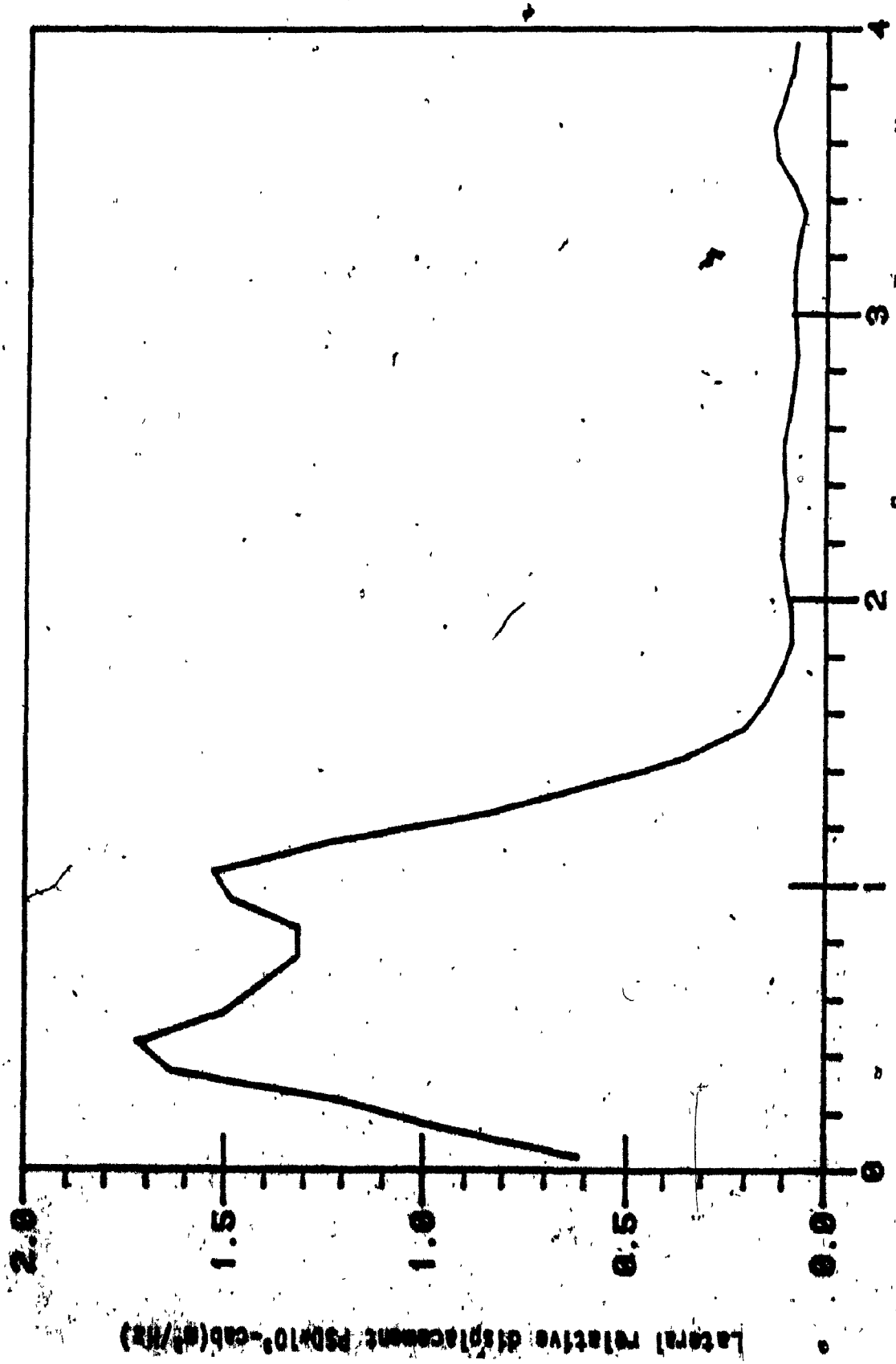

FIGURE 6.32: Lateral relative displacement PSD response of 5 DOF optimum cab suspension model.

2.5 hours limit as shown in Figure 6.33. The lateral acceleration response at the cg is obtained by combining the lateral acceleration at the cab floor and the roll acceleration of the cab. Thus, the response plot exhibits peaks corresponding to roll and lateral resonant frequencies (0.4 and 1.1 Hz), respectively.

The PSD of longitudinal acceleration response of the optimum cab suspension is presented in Figure 6.34. The acceleration response is found to be close to ISO-FDP-4 hours limits. The longitudinal acceleration response exhibits peaks around the resonant frequency 1.3 Hz. The ISO weighted rms acceleration response in the longitudinal mode is presented in Figure 6.35. The relative displacement response of the cab suspension model in the longitudinal mode is found to be extremely good as shown in Figure 6.36.

6.4.3 RIDE PERFORMANCE CHARACTERISTICS OF OPTIMUM CAB AND SEAT SUSPENSION MODEL (6 DOF)

The performance criteria listed in section 6.2.4 was formulated to optimize the bounce performance of the 6 DOF cab and seat suspension model. The optimization was carried out to find the optimal values for the stiffness and damping parameters of the bounce seat suspension. The optimal seat suspension parameters are listed in Table 6.4. The acceleration response characteristics of the optimum cab and seat suspension model are evaluated in the bounce, pitch, roll, lateral, and longitudinal modes. The bounce and pitch acceleration response of the cab remain unchanged, whereas a slight improvement in the lateral and roll acceleration response is observed due to the addition of bounce suspension seat.

The bounce acceleration PSD response of the seat mass is presented in Figure 6.37. The response acceleration plot exhibits a resonance peak

FIGURE 6.33: Lateral acceleration PSD response at

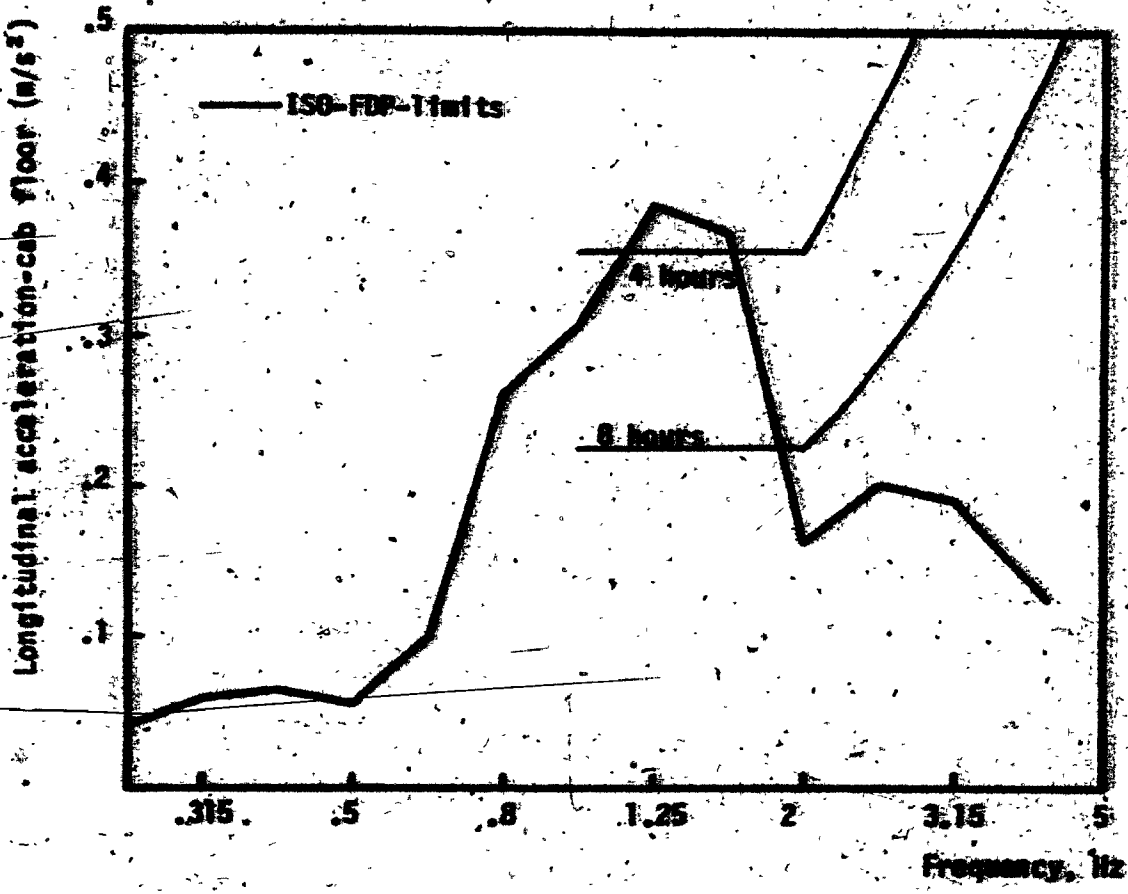

FIGURE 6.35:- Longitudinal acceleration (rms) response of the optimal 5 DOF cab suspension.

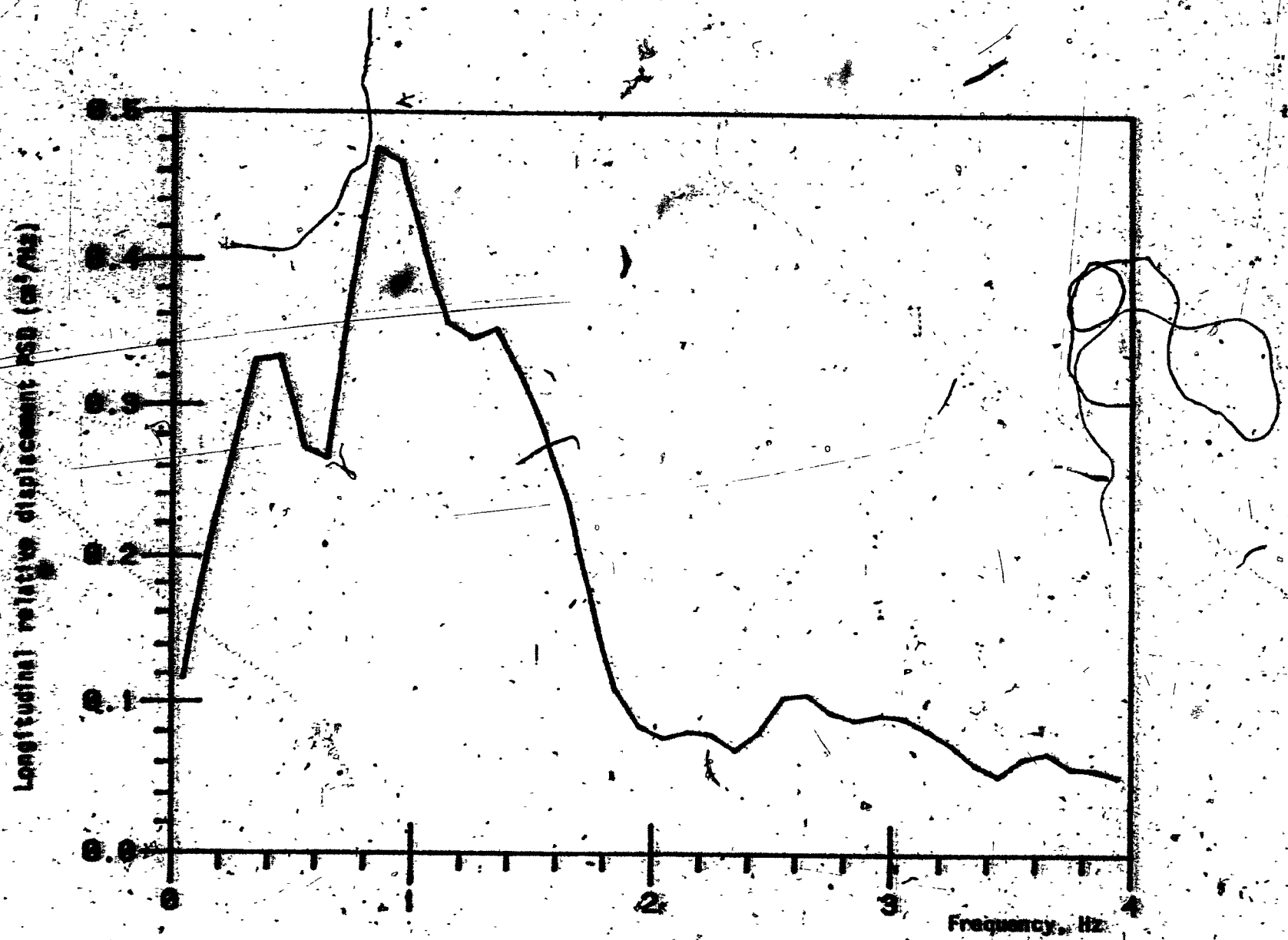

FIGURE 6.36: Longitudinal relative displacement PSD response of optimum 5 DOF cab suspension model.

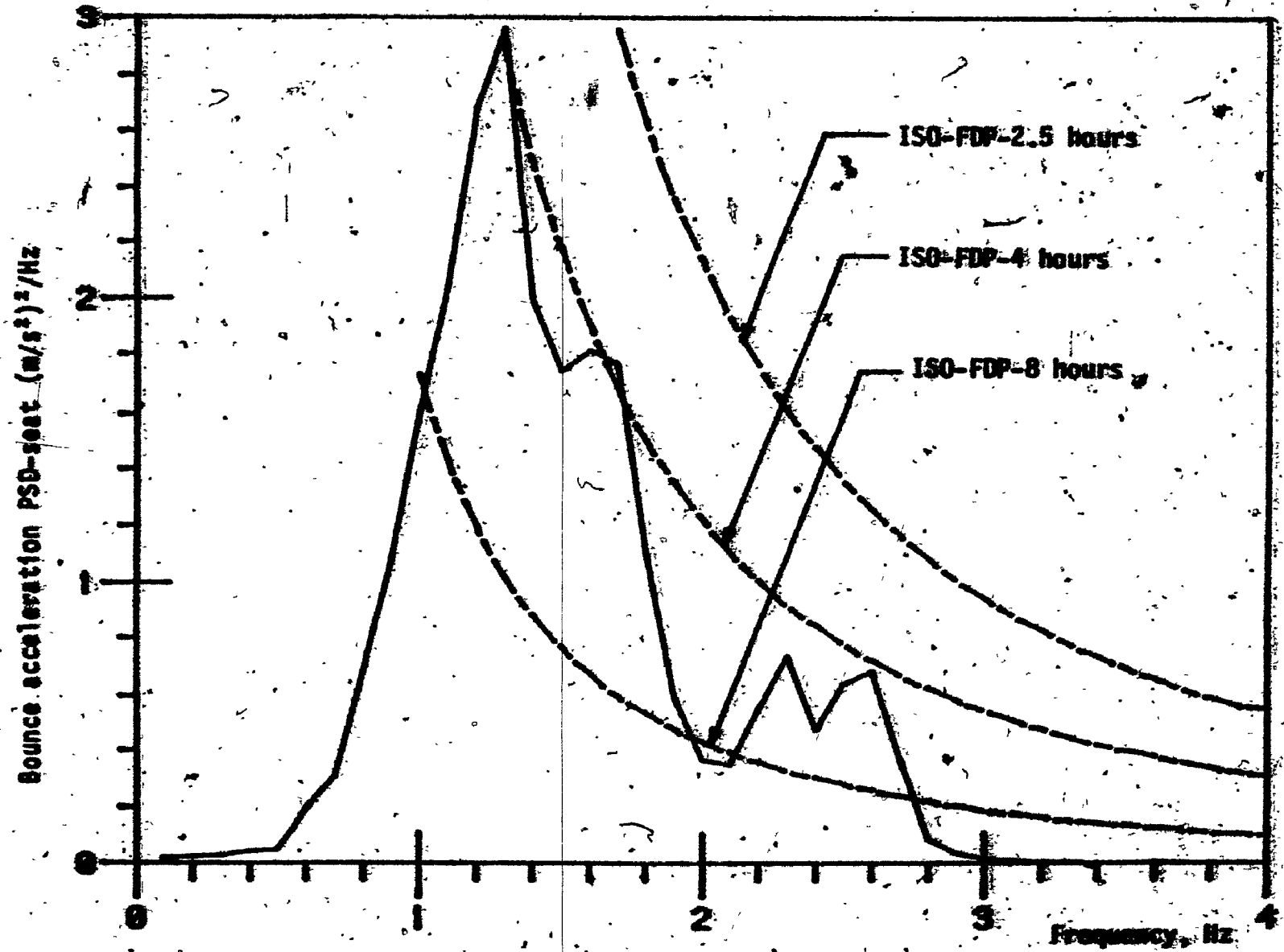

FIGURE 6.37: PSD of the bounce acceleration response at the seat of 6 DOF cab-seat suspension model.

at 1.8 Hz, and the bounce excitations corresponding to tractor resonant frequency (around 2.6 Hz) are attenuated. The acceleration response is found to be well within the ISO-FDP-4 hours exposure limits. The lateral and longitudinal acceleration response at the seat-mass location are evaluated using the kinematic relationship between the translational and rotational acceleration response at the cab. The lateral acceleration response at the seat mass exhibits a large peak (at 1.1Hz) corresponding to lateral resonant frequency of the tractor and a relatively smaller peak (at 0.4 Hz) corresponding to roll resonant frequency of the cab, as shown in Figure 6.38. The lateral acceleration response at the seat-mass is observed to be well within the ISO-FDP-1 hour exposure limit.

The longitudinal acceleration PSD response at the seat-mass is presented in Figure 6.39. The longitudinal acceleration response is observed to be within the ISO-FDP-8 hours exposure limits. The PSD acceleration response at the seat mass in bounce, longitudinal and lateral modes are transformed to weighted rms accelerations in the ISO specified third octave frequency bands. The rms bounce, lateral and longitudinal acceleration response plots are shown in Figures 6.40, 6.41, and 6.42, respectively.

6.5 SUMMARY

In this chapter, the performance criteria are formulated for seat, cab, cab and seat suspension models. The performance criteria are minimized using non-linear programming methods to derive optimal values of suspension parameters, such that the acceleration levels encountered by the driver remain within the ISO-FDP-4 hours limit. Limit constraints are introduced on the values of design variables such that a feasible solution is achieved. The relative displacement response of the suspension

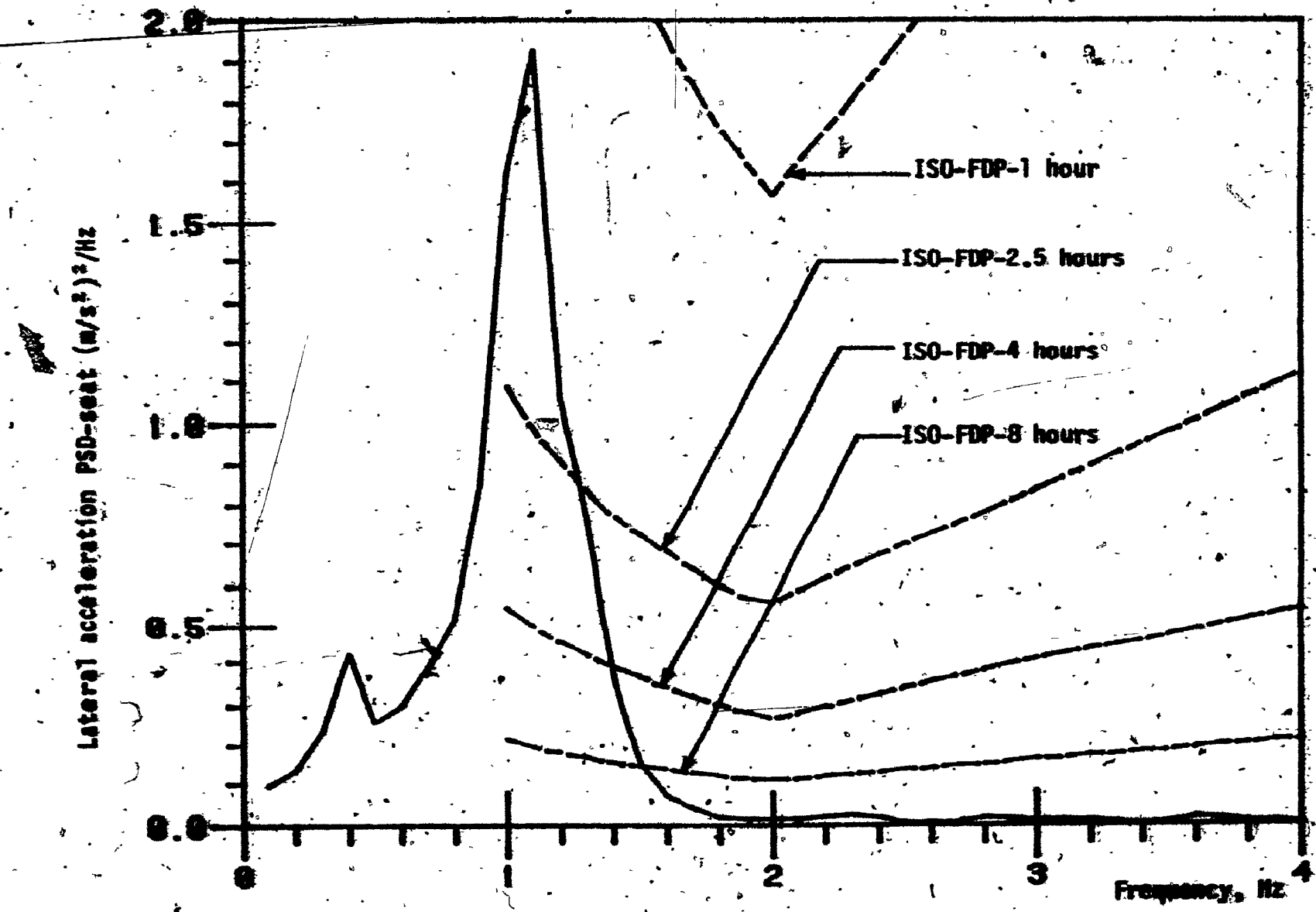

FIGURE 6.38: PSD of the lateral acceleration response at the seat of 6 DOF cab-seat suspension model.

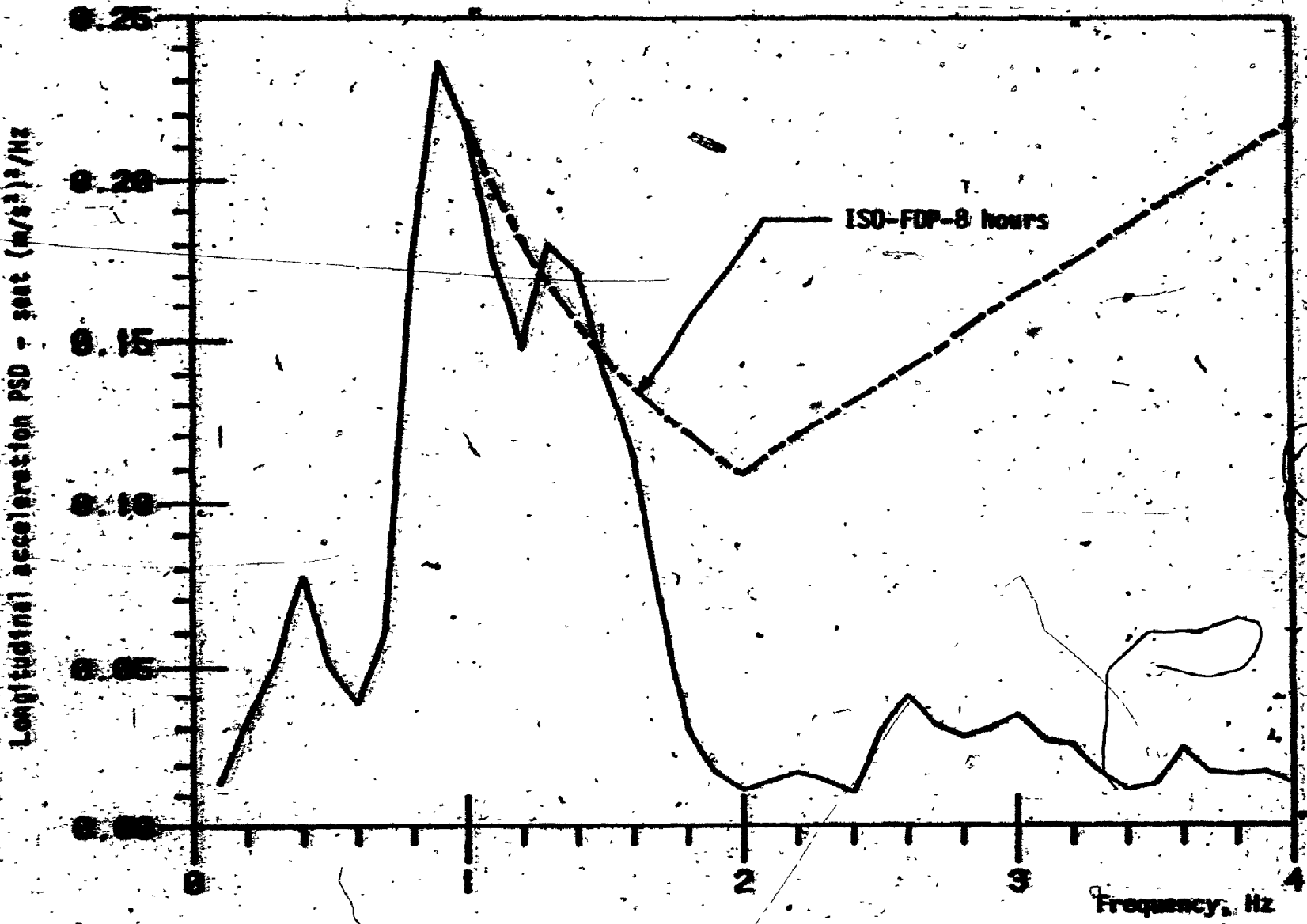

FIGURE 6.39: PSD of the longitudinal acceleration at the seat of optimum 6 DOF cab-seat suspension model.

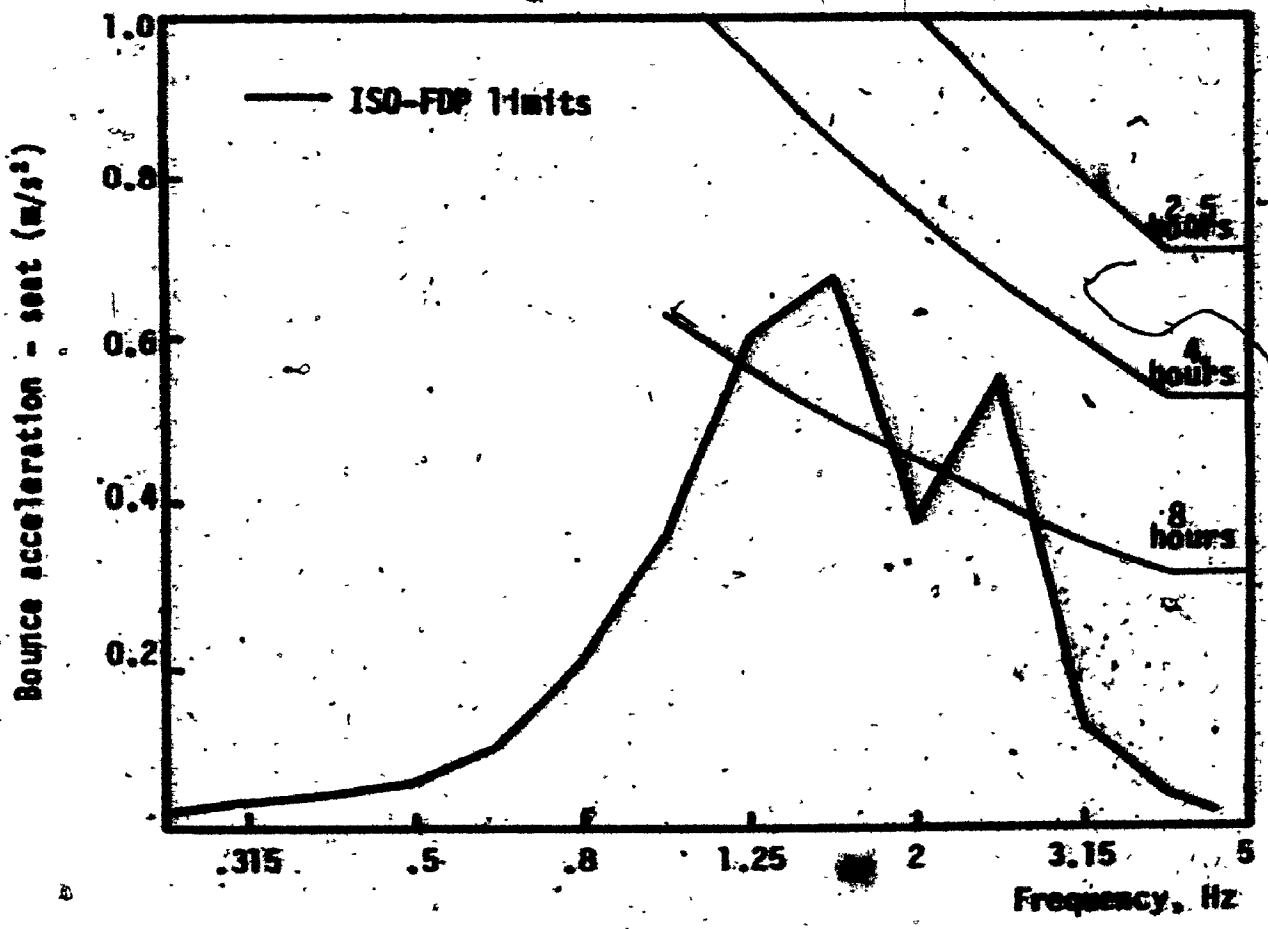

FIGURE 6.40: Bounce acceleration (rms) response at the seat of 6 DOF cab-seat suspension (Model I).

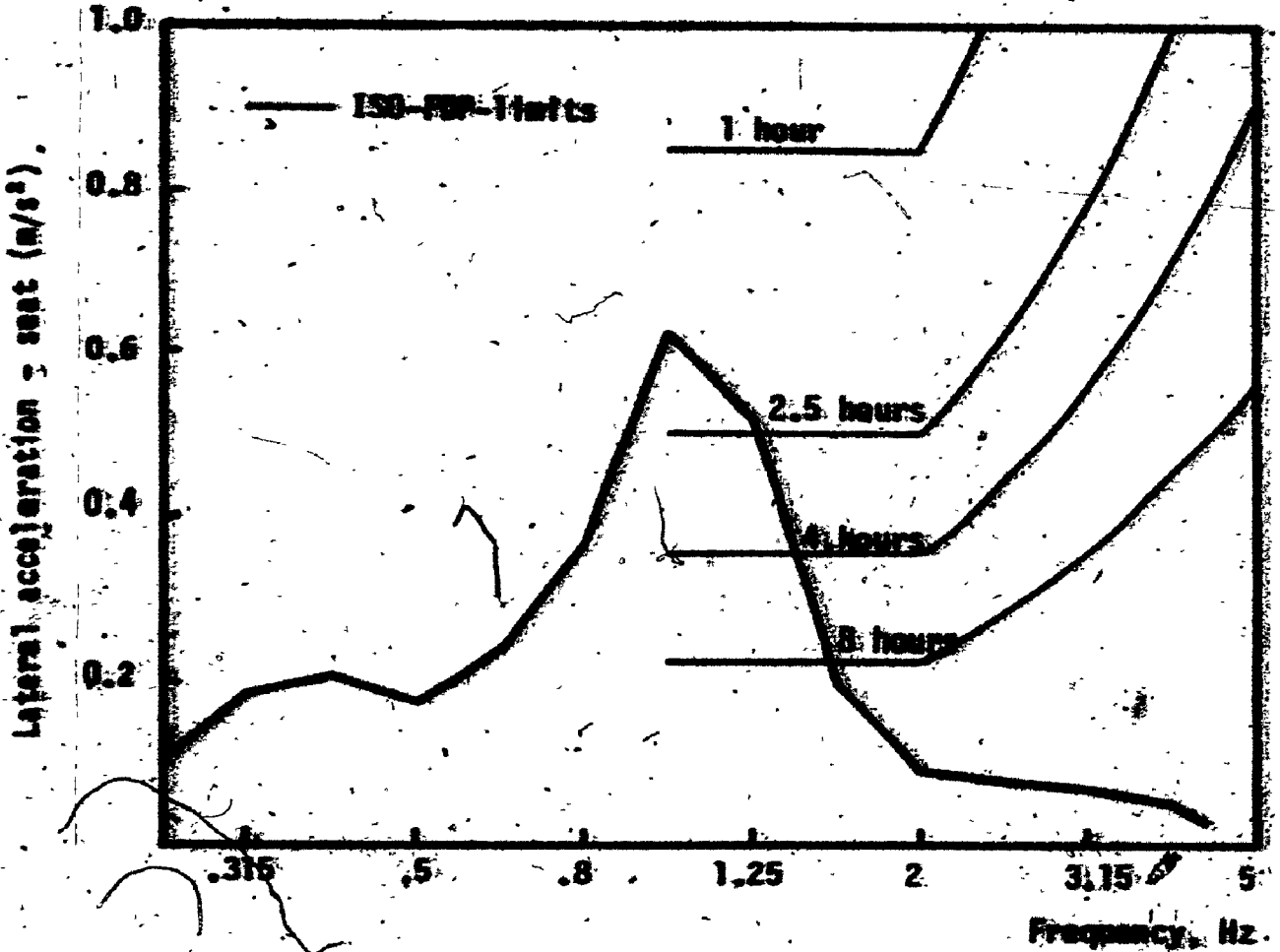

FIGURE 6.41: Lateral acceleration (rms) response at the seat of 6 DOF cab-seat suspension (Model I).

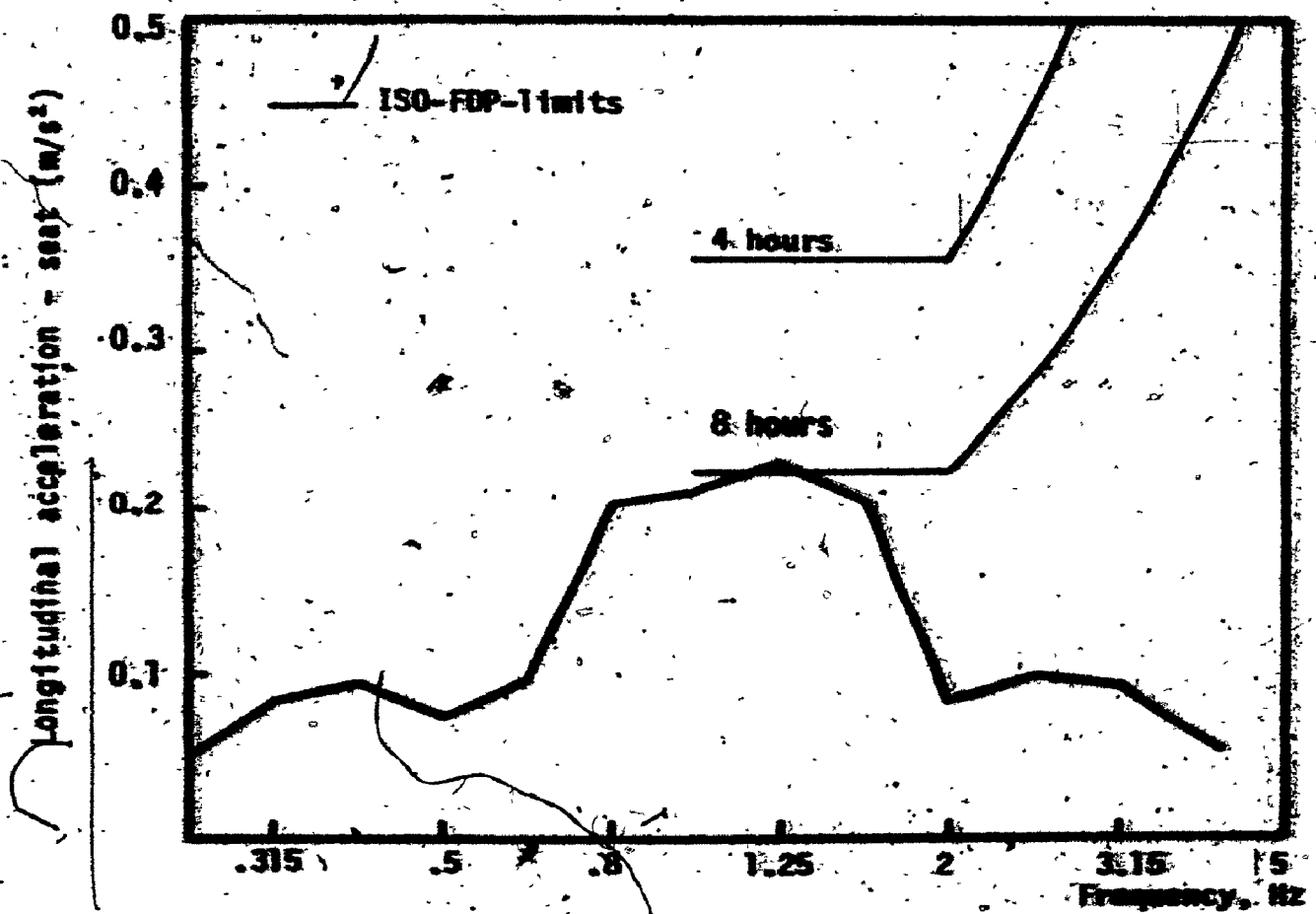

FIGURE 6.42: Longitudinal acceleration (rms) response at the seat of 6 DOF cab-seat suspension model (Model 1)

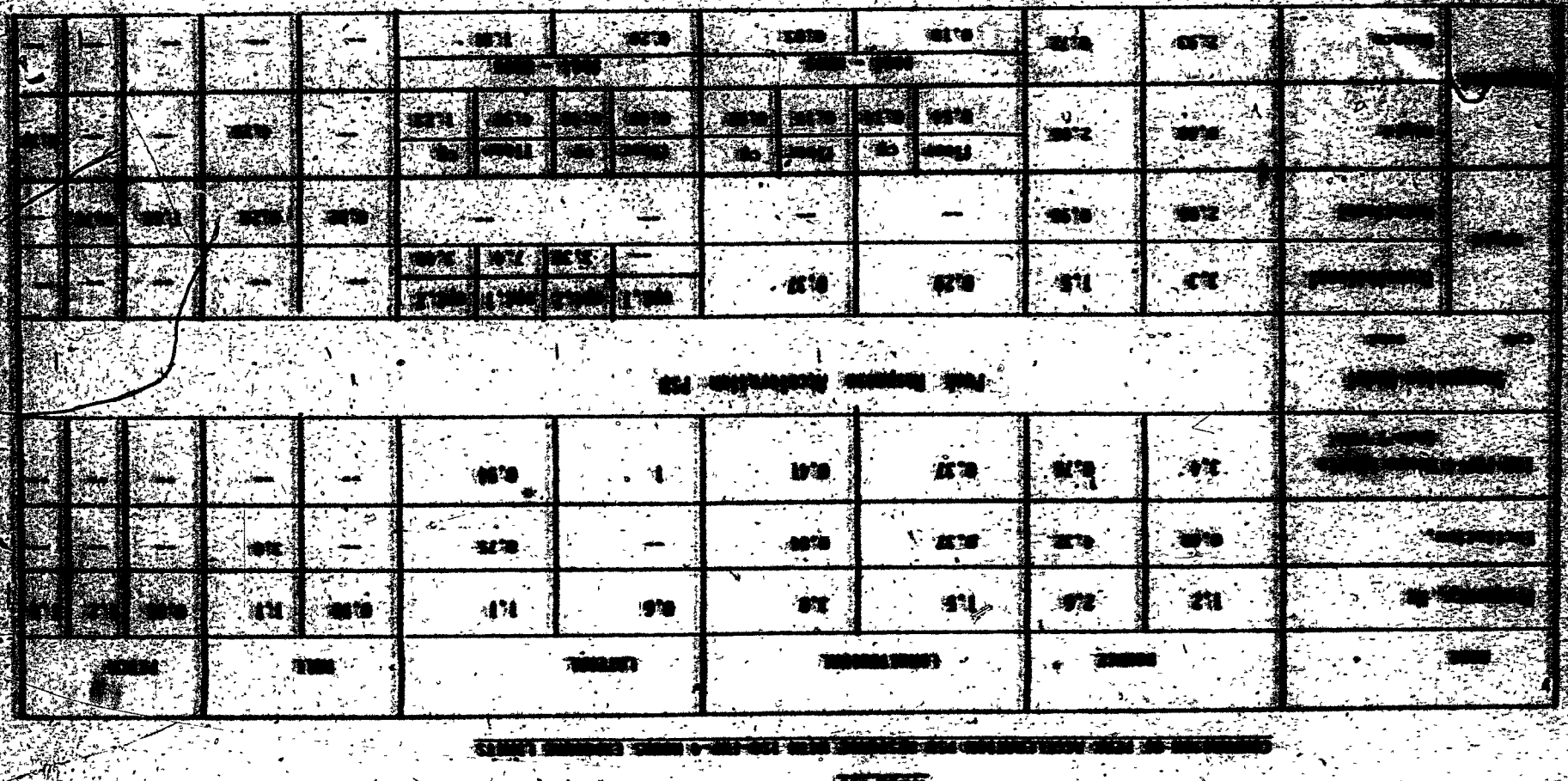

[illegible] the [illegible] of a [illegible] [illegible] [illegible]
the [illegible] [illegible] of the [illegible] [illegible], the [illegible] [illegible]
[illegible] displacement (DD) [illegible] of the [illegible] [illegible] [illegible]
are obtained and the rms quality of the [illegible] will be [illegible]
with reference to the 10-ms time. Table 6.1 compares the rms
acceleration response of the optimum modified suspension result.

CHAPTER 7

PERFORMANCE CHARACTERISTICS OF SEAT SUSPENSION WITH A SEMI-ACTIVE "SKYHOOK" DAMPER

7.1 Introduction

Passive suspension seats are undoubtedly the simplest, inexpensive, and reliable means of vibration isolation, however, there are distinct performance limitations associated with passive devices. The most obvious performance limitation is demonstrated by fixed damping, which suppresses the resonance peak at the expense of deteriorated performance in the isolation region. This phenomenon has been demonstrated in terms of the ride performance of passive suspension models in Chapters 5 and 6. Thus, it is desirable to develop isolation systems with adjustable parameters that could be varied to suit changing excitations or response characteristics. Such adjustable isolation systems can provide better isolation performance than the passive systems with fixed parameters.

Active suspensions can be developed with suspension parameters that change automatically with excitation and response variables. Although active suspensions demonstrate superior performance than the best possible passive system, it is known that the active systems in general are more costly, more complex and therefore, less reliable than passive systems. Thus, the implementation of active means of vibration isolation has been limited to cases, in which the performance gains outweigh the disadvantages of increased cost, complexity, and weight. Recognizing both the performance benefits as well as the limitations of active systems, the concepts of semi-active suspension systems have been developed.

Semi-active isolation systems require only low level electrical power for necessary signal processing, and provide excellent vibration isolation. The concept of semi-active force generators utilizing skyhook damping have been developed [34, 50]. Although the hardware implementation

of the semi-active damper is significantly simpler and less costly than a complex active vibration isolation system with its large power requirement, the cost and complexity of skyhook control may still be prohibitive for general applications. The skyhook damper requires a high bandwidth servo-valve and a microprocessor control system capable of implementing a force feedback loop. In an attempt to simplify the hardware implementations and reduce the cost of active damper to a point where general use is feasible, a simplified "on-off" scheme has been developed [60]. The "on-off" damper operates as a conventional passive damper during a portion of the vibration cycle when the damper force opposes the spring force, but assumes zero damping when a passive damper would normally introduce energy to the system.

In this chapter, an "on-off" skyhook control scheme, proposed by Karnopp [34], is summarized. The same control scheme is adopted to develop an "on-off" damper that operates as a conventional damper during the on-cycle. An alternative control scheme based on directly measurable variables is proposed and its performance is investigated for harmonically excited SDOF seat isolator. The mathematical model of bounce seat suspension employing "on-off" damping is formulated. The ride performance characteristics of the bounce seat suspension with "on-off" damper are compared to that of a passive seat suspension.

7.2 THE CONCEPT

The concept of an "on-off" damper can best be demonstrated through a conventional mass-spring-damper system shown in Figure 7.1. The differential equation of motion for the suspended mass is given by the following expression, assuming linear coefficients:

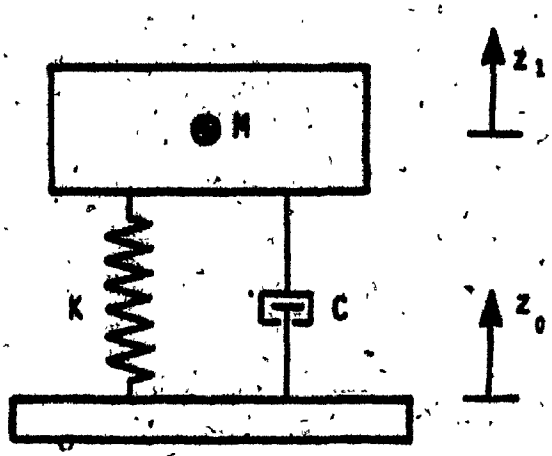

FIGURE 7.1: Conventional spring-mass-damper system.

$$M \ddot{z}_1 = - F_k - F_d \tag{7.1}$$

where

$$F_k = K (z_1 - z_0)$$

$$F_d = C (\dot{z}_1 - \dot{z}_0)$$

Equation (7.1) reveals that during a portion of the cycle, energy is being put into the mass through the damper, resulting in typical damped spring-mass system performance. Poor isolation performance of heavily damped systems is attributed to this phenomenon. Figure 7.2 presents the steady state spring, damper, and inertia force plots of a SDOF system subject to harmonic excitations. It is observed that the magnitude of inertia force:

$$M \ddot{z}_1 = - (|F_k| + |F_d|) \quad \text{for } t_0 < t < t_0 + \frac{\tau}{4}$$

$$= (|F_k| + |F_d|) \quad \text{for } t_0 + \frac{\tau}{2} < t < t_0 + \frac{3\tau}{4} \tag{7.2}$$

$$M \ddot{z}_1 = - (|F_k| - |F_d|) \quad \text{for } t_0 + \frac{\tau}{4} < t < t_0 + \frac{\tau}{2}$$

$$= (|F_k| - |F_d|) \quad \text{for } t_0 + \frac{3\tau}{4} < t < t_0 + \tau \tag{7.3}$$

where

$|F_k|$ = Magnitude of suspension force due to spring, N.

$|F_d|$ = Magnitude of suspension force due to damper, N.

τ = Period of oscillation, s.

Equation 7.2 reflects that the damping force tends to increase the amplitude of mass acceleration during a part of the cycle. Specifically, at high excitation frequencies, when the magnitude of damping force is dominant, the amplitude of mass acceleration due to damping is quite significant. Thus an

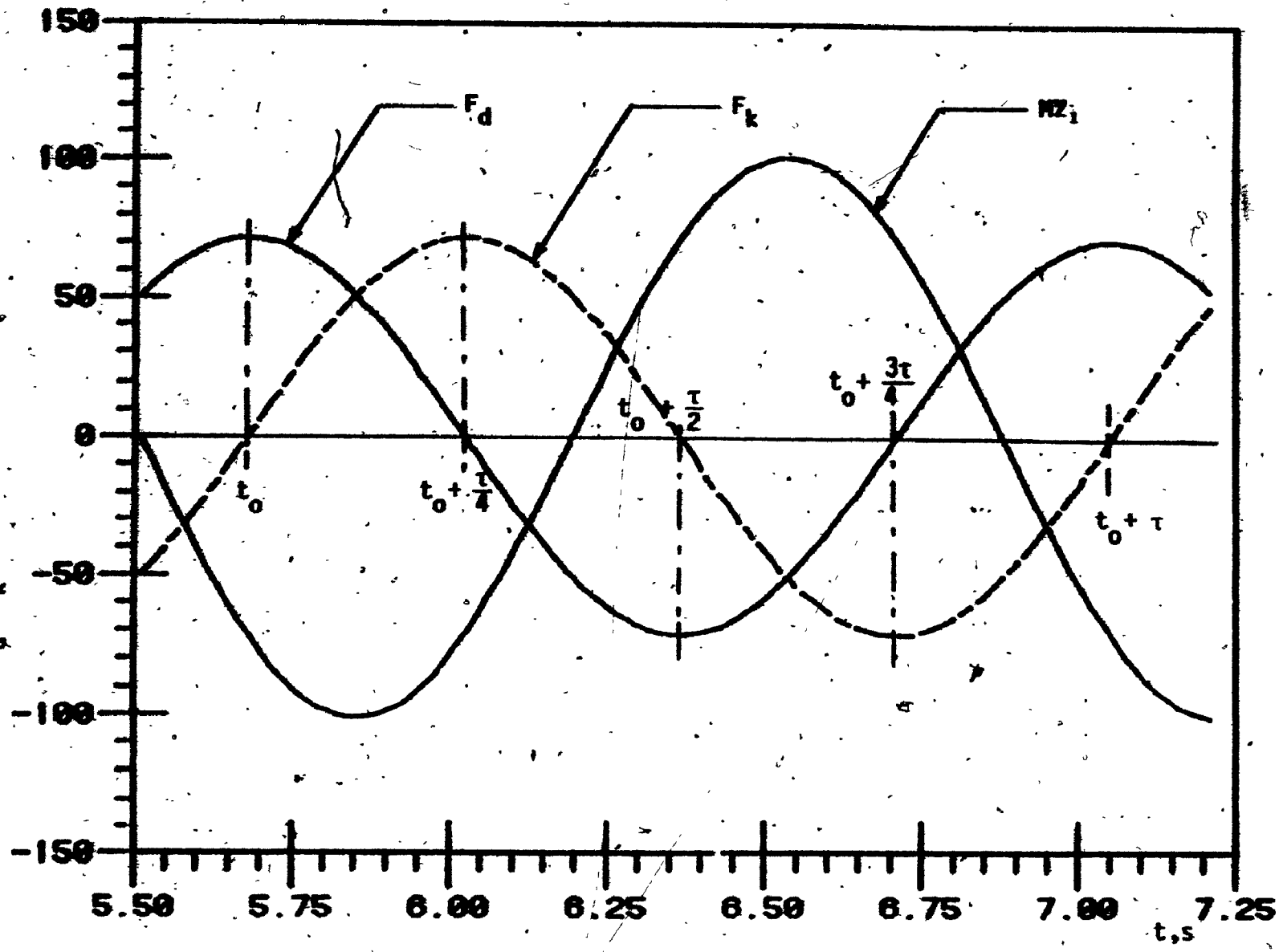

FIGURE 7.2 : Steady state spring, damper and inertial forces of harmonically excited SDOF system.

"on-off" damper can be introduced, which operates as a conventional passive damper, with a constant orifice opening during the part of vibration cycle when it acts to reduce the response acceleration, but assumes a zero damping coefficient during the portion of vibration cycle when a passive damper would normally increase the amplitude of mass acceleration.

Such an "on-off" mechanism can be accomplished by introducing a two position on-off valve to a conventional damper. The on-off valve offers certain orifice restriction during the on-cycle operation of the damper. The orifice size is modulated to its maximum opening during the off-cycle of the damper operation. Realistically, it will assume a small damping coefficient resulting from the orifice modulated to its largest area during the off-cycle. Moreover, the damping force produced by the "on-off" damper is of velocity squared nature due to the orifice restrictions achieved by a simple 2-position on-off valve.

In the following sections, two control schemes are presented in the modeling process of bounce seat suspension with "on-off" velocity squared damper.

7.3 "ON-OFF" DAMPER CONTROL SCHEMES

Karnopp [34] and Krasnicki [35] introduced the concept of skyhook active damper as shown in Figure 7.3. The equation of motion of the "on-off" skyhook damper isolation system is given by the following expression:

$$M \ddot{z}_1 = - (F_k + F_d) \qquad (7.4)$$

where

$$F_d = \begin{cases} C \dot{z}_1, & \text{if } \dot{z}_1 (\dot{z}_1 - \dot{z}_0) > 0 \\ 0, & \text{if } \dot{z}_1 (\dot{z}_1 - \dot{z}_0) < 0 \end{cases} \qquad (7.5)$$

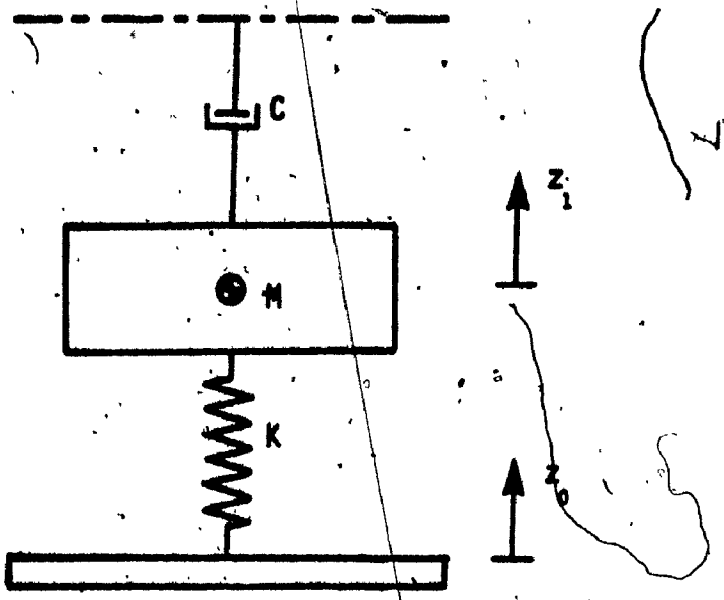

FIGURE 7.3: Semi-active skyhook damper system.

It was established that mass deceleration can be accomplished when the sign of absolute velocity of the mass is the same as that of the relative velocity. Such a skyhook "on-off" semi-active damper is associated with high cost and complexity. In an effort to simplify the complexities and to reduce the cost, a simplified "on-off" damper utilizing the identical scheme with velocity squared damping is developed.

CONTROL SCHEME I

Consider the spring mass damper system of Figure 7.1, where the damper operates as a conventional damper instead of skyhook damper. The equation of motion for velocity squared damping may be written as:

$$M\ddot{z}_1 = -F_k - F_d \tag{7.6}$$

$$F_d = \begin{cases} C_v(\dot{z}_1-\dot{z}_0)|\dot{z}_1-\dot{z}_0| , & \text{if } \dot{z}_1(\dot{z}_1-\dot{z}_0) > 0 \\ C'_v(\dot{z}_1-\dot{z}_0)|\dot{z}_1-\dot{z}_0| , & \text{if } \dot{z}_1(\dot{z}_1-\dot{z}_0) < 0 \end{cases} \tag{7.7}$$

where,

C_v = Coefficient of velocity squared damping due to the smallest orifice opening.

C'_v = Coefficient of velocity squared damping when the orifice is modulated to its maximum opening.

The special cases for the "on-off" damper exist, when the product $\dot{z}(\dot{z}-\dot{z}_0) = 0$. The damper force $F_d = 0$ when $(\dot{z}-\dot{z}_0) = 0$ and $\dot{z} \neq 0$. The damper force is generated in accordance with equation (7.7) when $\dot{z} = 0$ and $(\dot{z}-\dot{z}_0) \neq 0$. This control scheme is quite simple to implement with a two position "on-off" valve. However, the measurement of absolute velocity introduces certain complexities. Specifically, integration of a low frequency acceleration signal imposes significant complexities.

CONTROL SCHEME II

Alternatively, a control scheme based on directly measurable variables is developed. Equations (7.2), (7.3) and Figure 7.2 reveal that amplitude of inertia force approaches the peak value when the suspension forces due to spring and damper possess the same sign. Conversely, the amplitude of inertia force is lowered when the damping force opposes the spring force. The suspension forces due to spring and damper being functions of relative position and relative velocity, respectively, it can be established that inertia force increases whenever the relative velocity and relative position possess the same sign. Thus, "on-off" damper scheme may be established as:

$$F_d = \begin{cases} C_v(\dot{z}_1-\dot{z}_0)|\dot{z}_1-\dot{z}_0|, & \text{if } (\dot{z}_1-\dot{z}_0)(z_1-z_0) \leq 0 \\ C'_v(\dot{z}_1-\dot{z}_0)|\dot{z}_1-\dot{z}_0|, & \text{if } (\dot{z}_1-\dot{z}_0)(z_1-z_0) > 0 \end{cases} \qquad (7.8)$$

The "on-off" damper operating with this control scheme will act as as conventional orifice damper when the relative velocity and relative displacement carry opposite signs. The damper operates as a conventional orifice damper with lower value of damping coefficient due to large orifice opening when the relative velocity and the relative displacement response of the mass possess the same sign.

7.4 DEVELOPMENT OF SEAT SUSPENSION MODEL USING "ON-OFF " DAMPING

In Chapter 6, the direct search optimization was carried out to minimize the bounce seat suspension performance criterion. The optimization routine was observed to converge to approximately the upper limit specified for Coulomb friction, in order to suppress the resonance peak. Although, large Coulomb friction lowers the resonance peak, it also reduces the suspension travel and deteriorates the suspension performance in the isolation region. Alternatively, large value of velocity squared damping

coefficient may be used to lower the resonance response, however, the large value of damping coefficient also leads to deteriorated performance around the vehicle resonant frequency (2.6 Hz). In an attempt to overcome this performance limitation, the "on-off" damper is employed in the bounce seat suspension. The Coulomb friction, elastic limit stops, and cushion stiffness are neglected to simplify the bounce seat suspension model to a SDOF system. The equation of motion of the suspension model with "on-off" damping is given by:

$$M'\ddot{z}_1 + F_d^z + K_z(z_1 - z_0) = 0 \tag{7.9}$$

where

$$M' = M_0 + M_s^z$$

The "on-off" damper operating with control scheme I provides the damping force as:

$$F_d^z = \begin{cases} C_z(\dot{z}_1 - \dot{z}_0)|\dot{z}_1 - \dot{z}_0|, & \text{if } \dot{z}_1(\dot{z}_1 - \dot{z}_0) \geq 0 \\ C_z'(\dot{z}_1 - \dot{z}_0)|\dot{z}_1 - \dot{z}_0|, & \text{if } \dot{z}_1(\dot{z}_1 - \dot{z}_0) < 0 \end{cases} \tag{7.10}$$

The damper operating with control scheme II provides the damping force as:

$$F_d^z = \begin{cases} C_z(\dot{z}_1 - \dot{z}_0)|\dot{z}_1 - \dot{z}_0|, & \text{if } (\dot{z}_1 - \dot{z}_0)(z_1 - z_0) \leq 0 \\ C_z'(\dot{z}_1 - \dot{z}_0)|\dot{z}_1 - \dot{z}_0|, & \text{if } (\dot{z}_1 - \dot{z}_0)(z_1 - z_0) > 0 \end{cases} \tag{7.11}$$

where C_z' is taken as a fraction of C_z.

The performance of bounce seat suspension incorporating "on-off" velocity squared damping is intially investigated for harmonic excitations, in the following section.

7.5 PERFORMANCE CHARACTERISTICS OF BOUNCE SEAT SUSPENSION WITH "ON-OFF" DAMPING

The non-linear differential equation of motion of the bounce seat suspension with "on-off" damping is solved using numerical integration

technique. The differential equation is initially solved for harmonic excitations in order to establish an understanding of the behaviour of "on-off" damper. An attempt is made to establish the transmissibility characteristics from the steady state acceleration response trace of the seat suspension using schemes I and II. The transmissibility characteristics are compared to that of a passive system. The performance of seat suspension is also evaluated for stochastically described excitations measured at the seat attachment point using numerical integration followed by Fast Fourier Transform to generate acceleration PSD estimates. The acceleration PSD response of the seat suspension using "on-off" damper operating with two control schemes is compared to that of a passive system.

7.5.1 HARMONIC EXCITATION

The steady state time trace of inertia force ($M'\ddot{z}_1$), spring force (F_k), and damper force (F_d^z) are obtained for the SDOF bounce seat suspension employing passive and "on-off" damping, when subject to harmonic acceleration excitation. The suspension forces are observed for various frequencies of excitation to establish an understanding of the performance behaviour of "on-off" damper. The time traces of suspension forces are presented in Figures 7.4 to 7.15. The magnitude of damping force in a passive system is observed to be small as compared to spring force, for low frequency excitations ($f/f_n = 0.50$), as shown in Figure 7.4. The amplitude of passive damping force tends to increase as the frequency of excitation is increased as shown in Figure 7.5 ($f/f_n = 0.75$). The dominance of damping forces becomes more significant for even larger frequencies of excitation.

The "on-off" damper operating with control scheme I indicates a short off cycle duration for low frequency excitations as shown in Figure 7.6. However, the off-cycle duration increases as the frequency of excitation

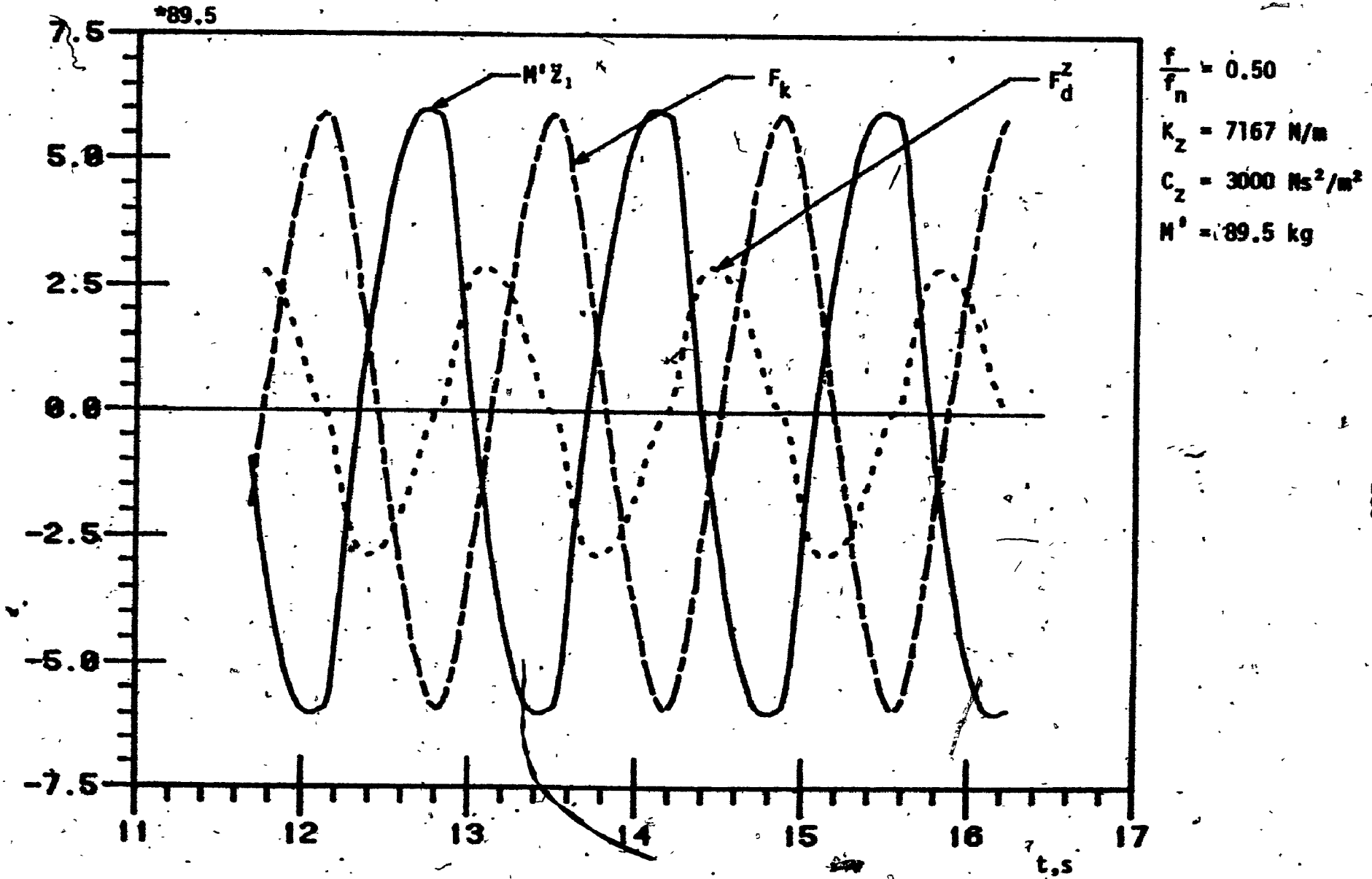

FIGURE 7.4: Inertia, spring, and damper forces of a SDOF passive bounce seat suspension ($f/f_n = 0.5$).

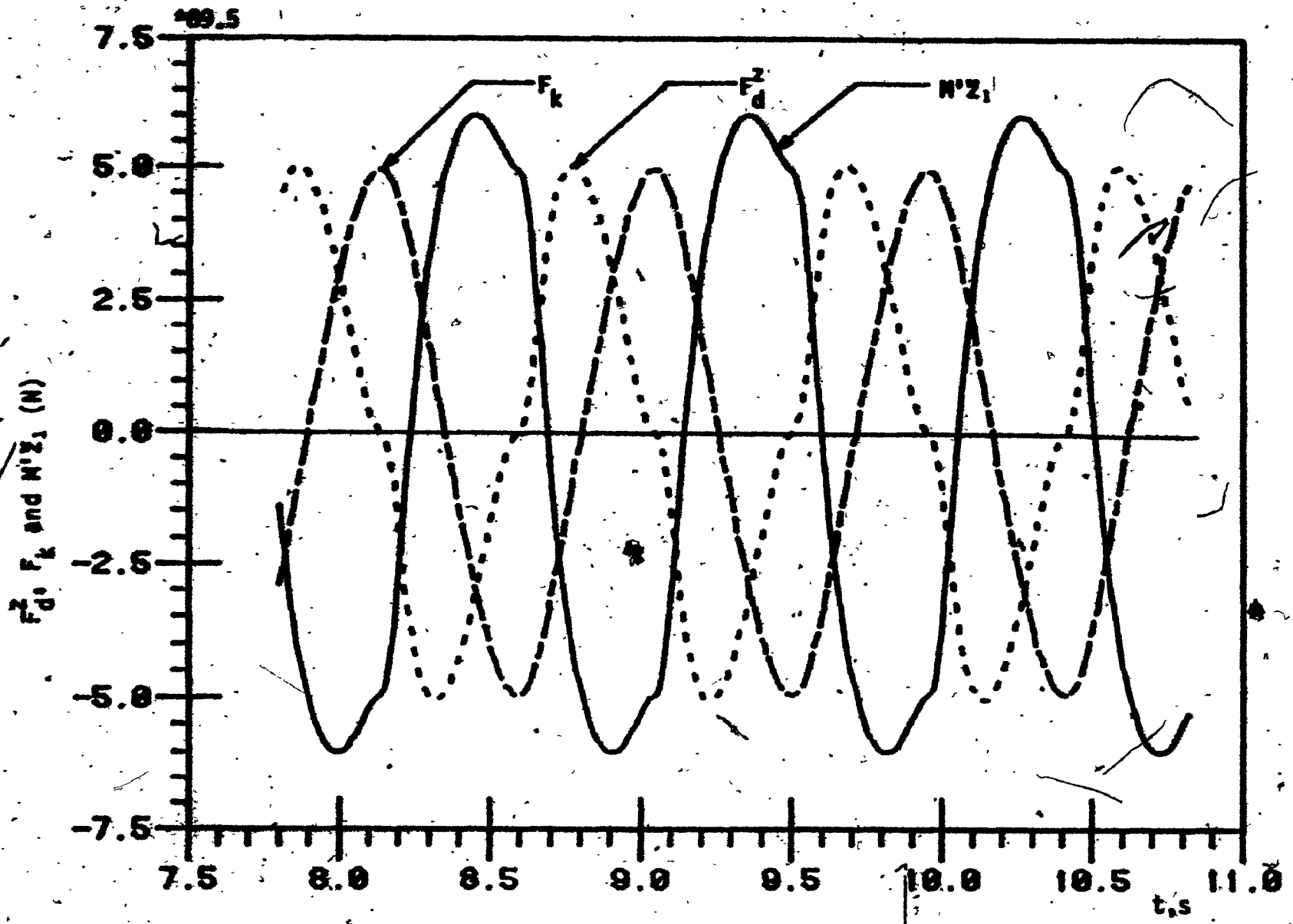

FIGURE 7.5: Inertia, spring, and damper forces of harmonically excited SDOF passive system ($\frac{f}{f_n} = 0.75$)

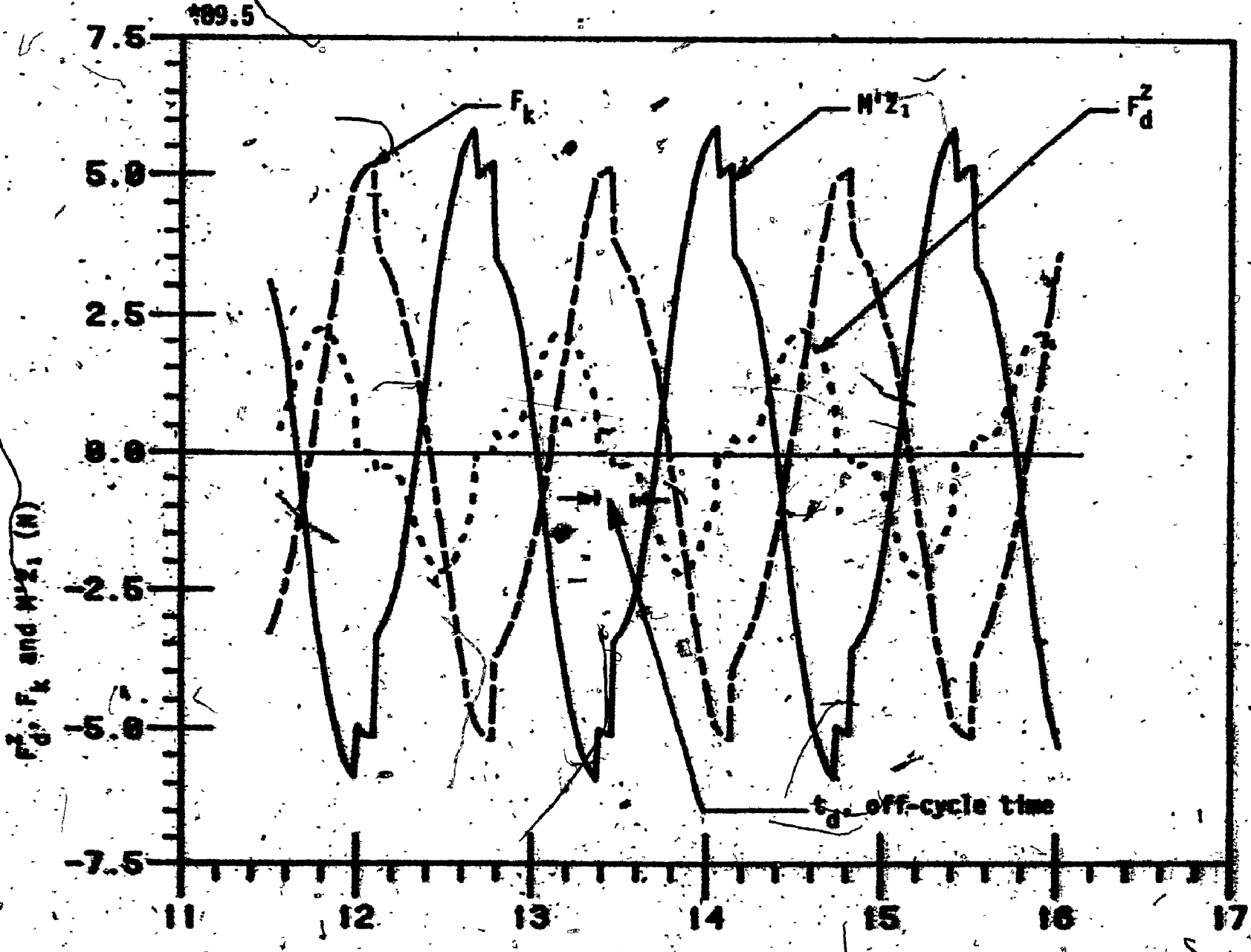

FIGURE 7.6: Inertia, spring and damper forces of semi-active seat suspension using control scheme I ($\frac{f}{f_n} = 0.5$)

is increased as shown in Figures 7.7 to 7.10. The acceleration response consistently reveals two peaks during every operation cycle of the "on-off" damper, irrespective of the frequency of excitation. The acceleration response approaches a peak value during the normal operation of the "on-off" damper. Then as the damper is turned off, the amplitude of acceleration is lowered instantaneously. The acceleration response, then rises to another peak value during the off-cycle operation of the damper (C_2' is assumed to be 5% of C_2). For low frequency excitations, there is no significant difference in amplitudes of the two acceleration peaks occurring during normal and off-cycle operation of the "on-off" damper. This performance behaviour is attributed to two facts, viz., the damper operates as a conventional damper for the major part of the period of oscillation, and the amplitude of damping force is much smaller as compared to the spring force. Thus, the absence of damping force during the off-cycle does not alter the acceleration response for low frequency excitations (Figure 7.6).

As the frequency of excitation is increased, the amplitude of damping force increases considerably as shown in Figure 7.7. During the normal operation of the "on-off" damper, the acceleration peak value is observed to be of the same order as that in case of passive system. However, the second acceleration peak occuring during the off cycle operation of the "on-off" damper ($C_2' = 0.05\ C_2$) is of significantly smaller amplitude as compared to the passive system's response, as shown in Figures (7.8), (7.9) and (7.10).

The "on-off" damper operating with control scheme II operates as a conventional damper for 50% of the period of oscillation and assumes negligible damping coefficient value (C_2') for the remaining off-cycle period, irrespective of the frequency of excitation. During the normal

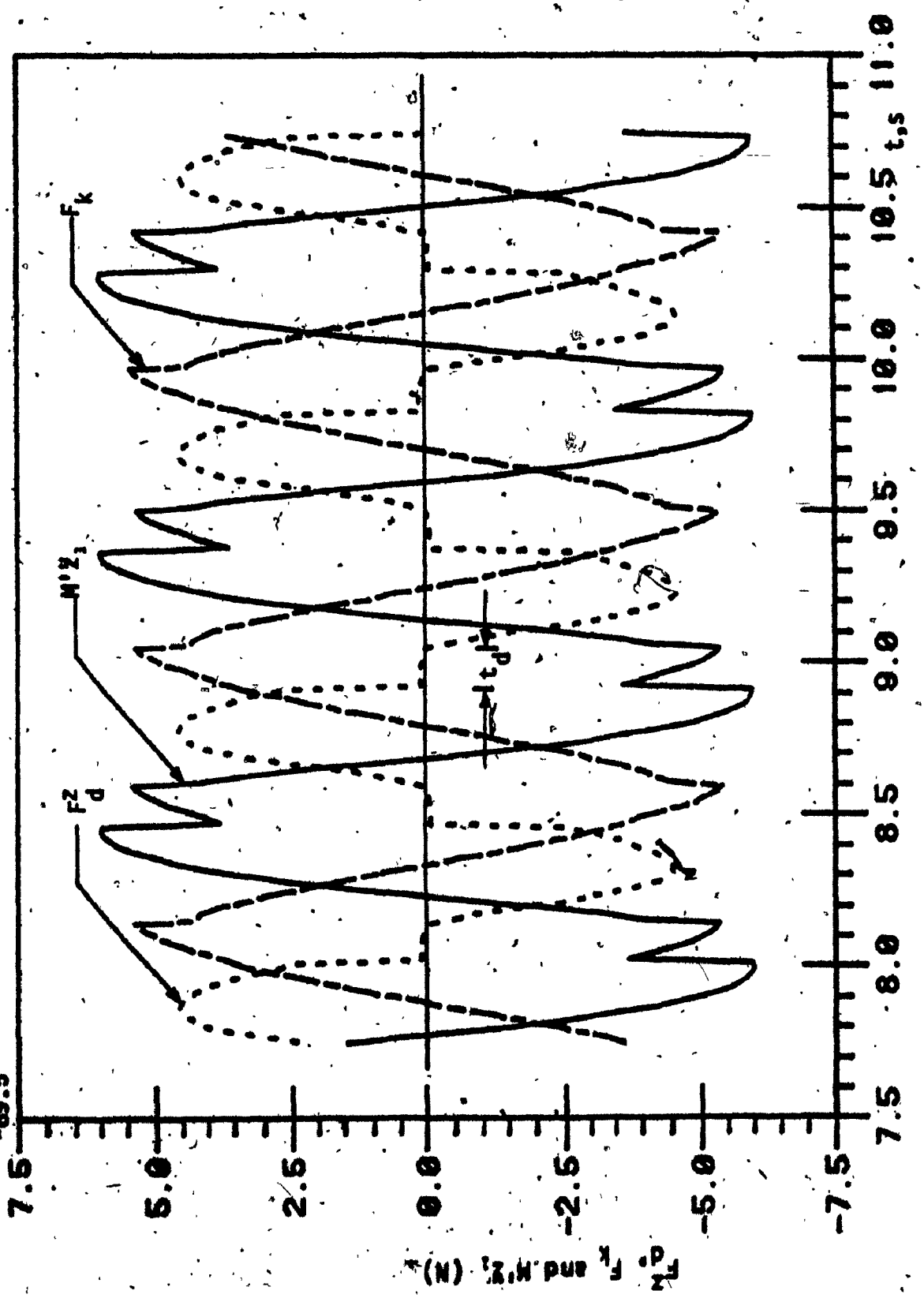

FIGURE 7.7: Inertia, spring and damper forces of semi-active seat suspension using control scheme 1 ($\frac{f}{f_n} \approx 0.75$).

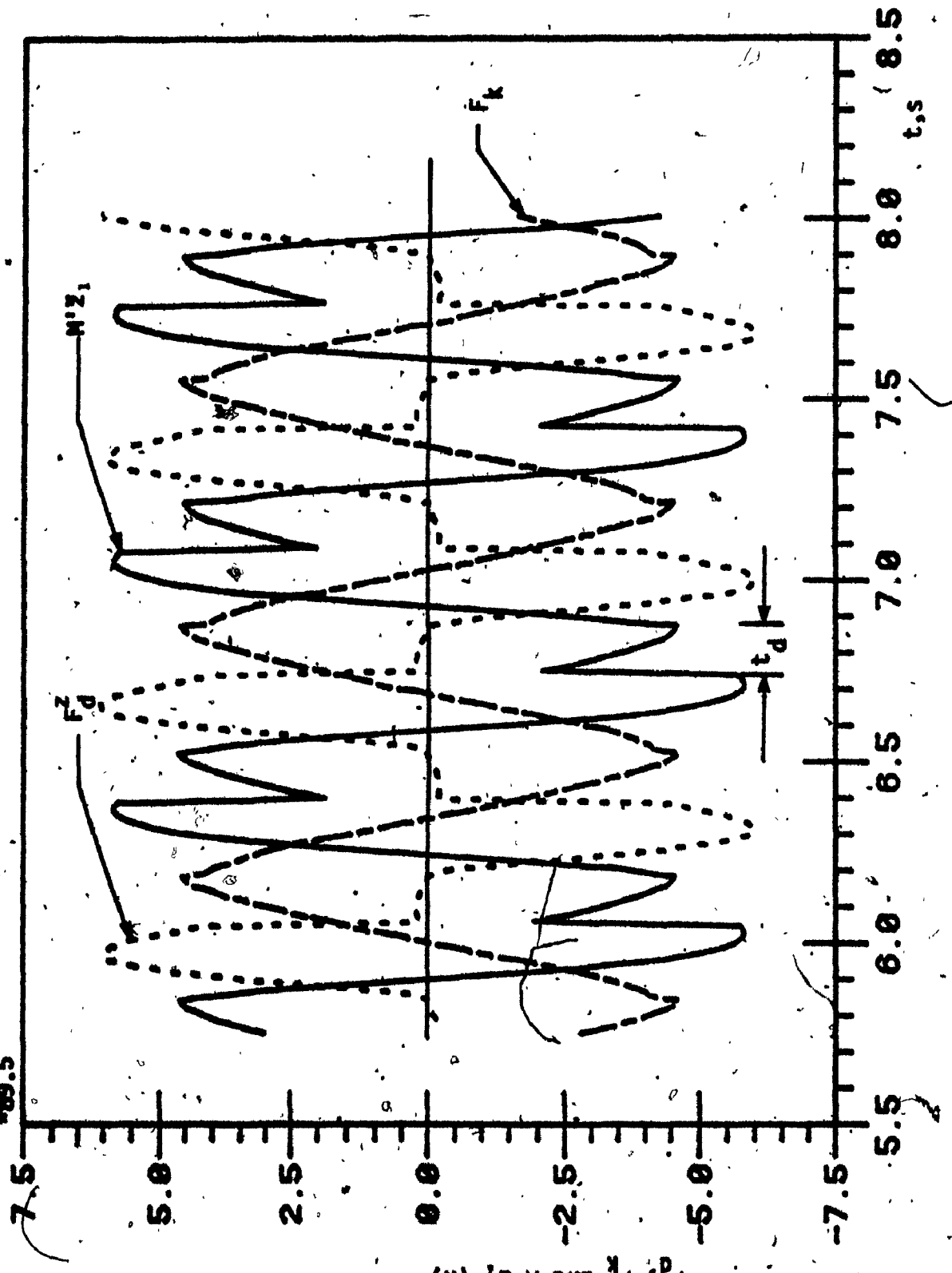

FIGURE 7.8: Spring, damper and inertia forces of semi-active seat suspension operating with scheme I ($\frac{f}{f_n} = \frac{1}{2}$)

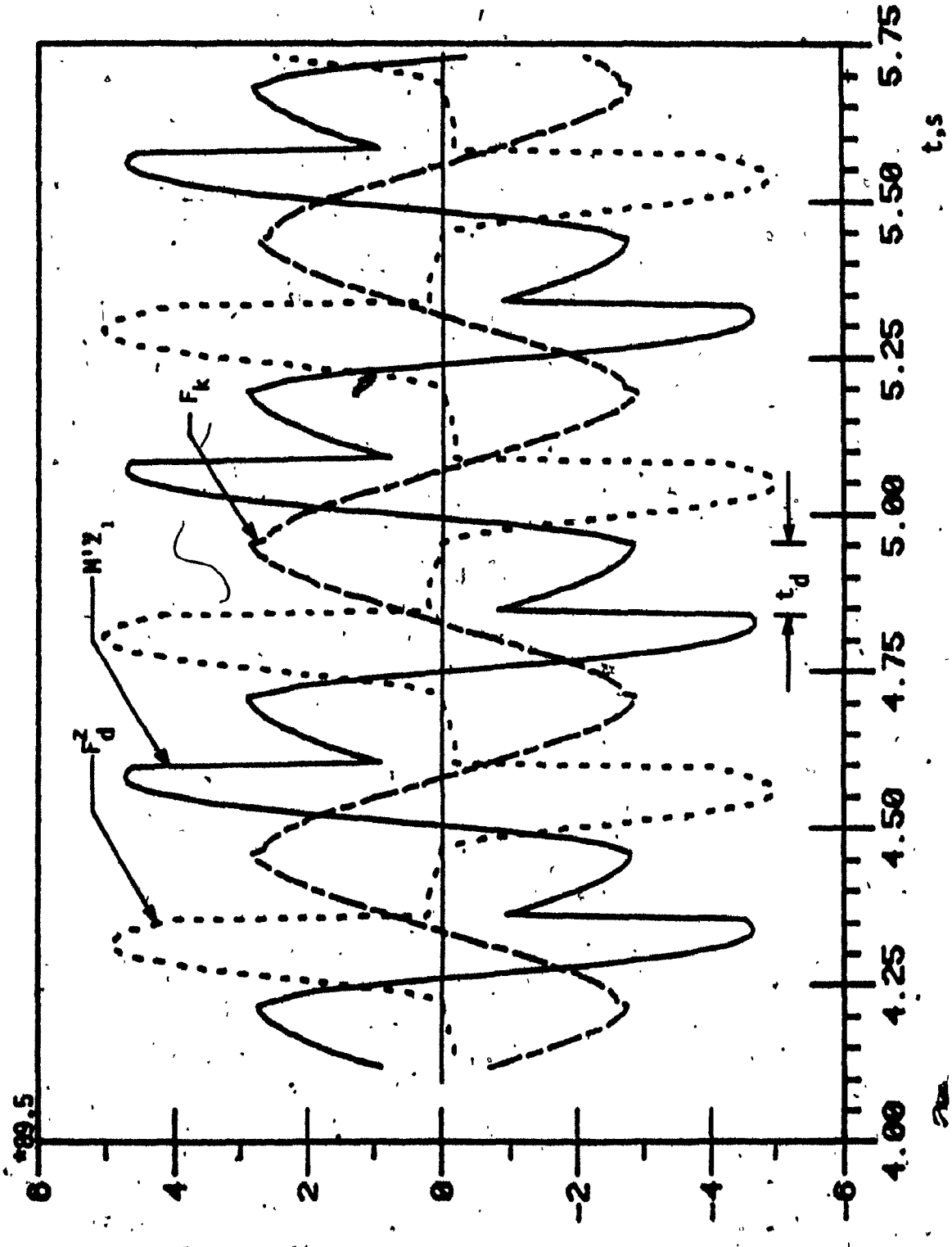

FIGURE 7.9: Inertia, spring and damper forces of semi-active seat suspension using scheme I ($\frac{f}{f_n} = 1.4$)

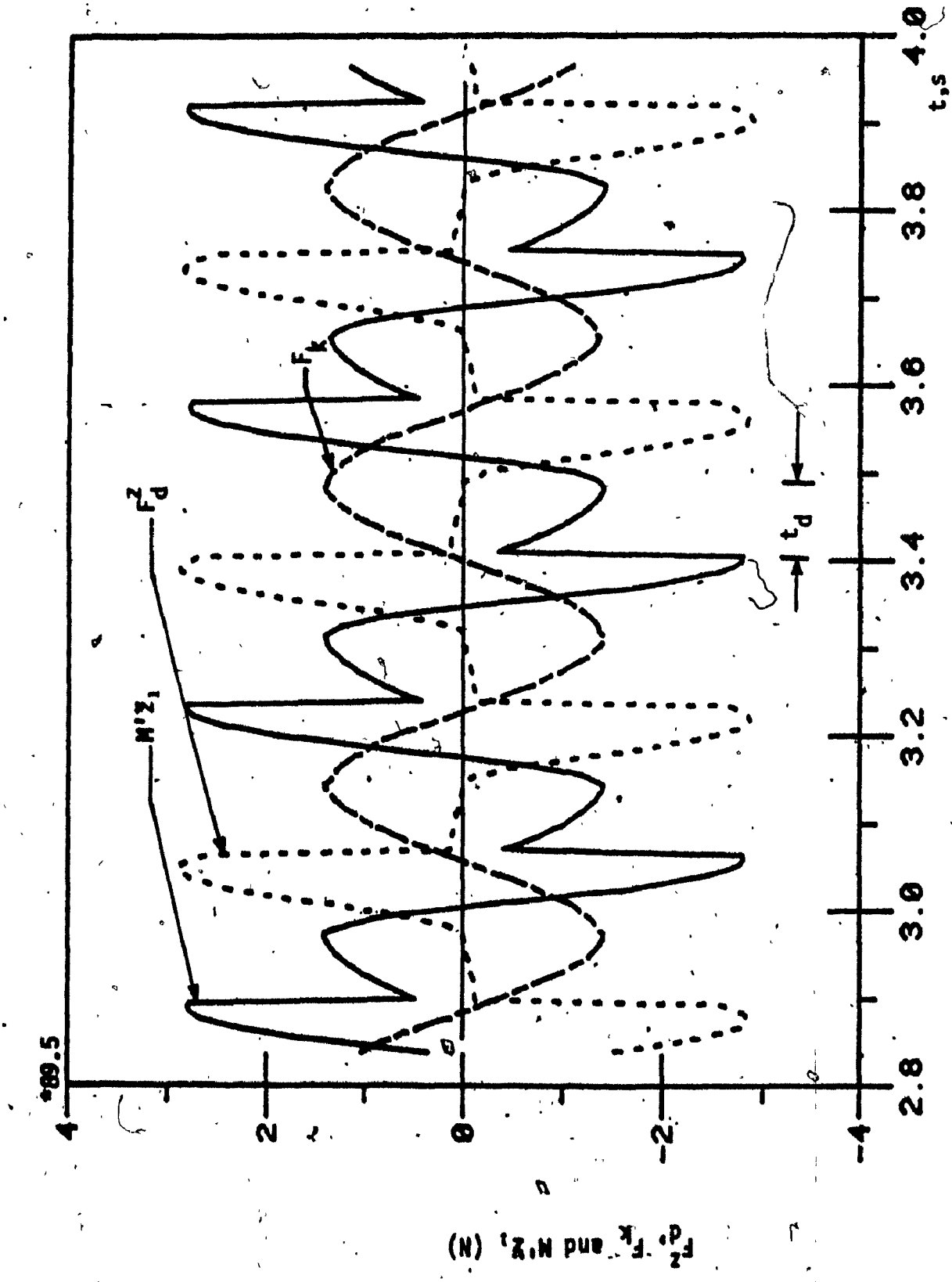

FIGURE 7.10: Inertia, spring and damper force of semi-active seat suspension using control scheme I ($\frac{f}{f_n} = 2.$)

operation of the damper (on-cycle), the damping force opposes the spring force for the entire range of frequencies of excitation as shown in Figures 7.11 to 7.15. The response acceleration exhibits two peaks for every cycle of the damper operation, similar to the control scheme I. The peak acceleration transmissibility characteristics of the suspension seat with "on-off" damper are summarized and compared to the acceleration transmissibility characteristics of a passive suspension system, in Table 7.1.

It is observed that the "on-damper" using control scheme II performs superior to passive as well as the "on-off" damper using control scheme I, during extremely low frequency excitations. However, the control scheme I shows superior acceleration transmissibility for excitation frequencies near the resonant frequency (f_n). The acceleration transmissibility characteristics of "on-off" damper using control scheme I are slightly superior to the transmissibility ratio of "on-off" damper using control scheme II during the on-cycle of the damper. The acceleration response during the damper off-cycle is significantly lower than the acceleration response of the passive system.

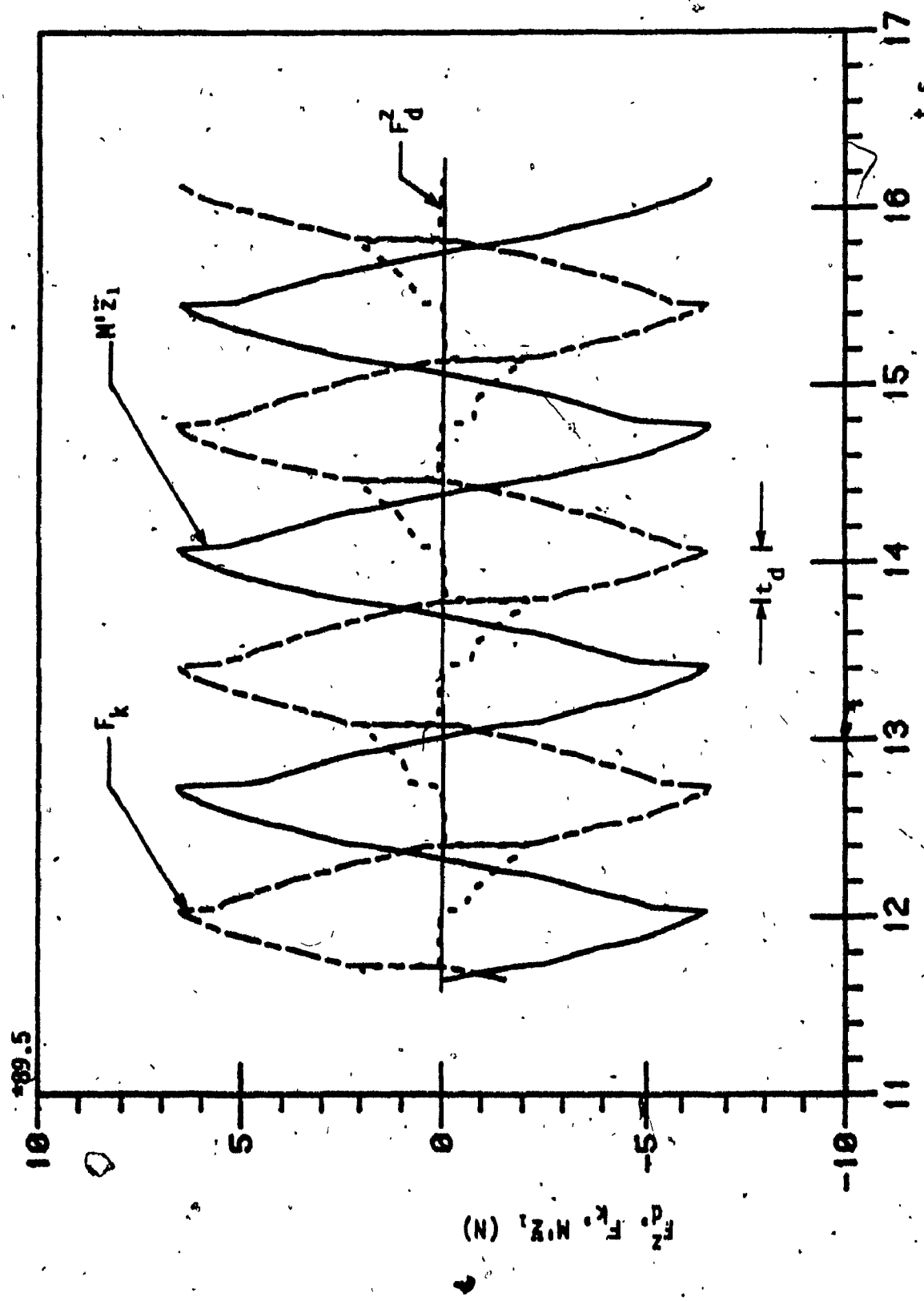

FIGURE 7.11: Inertia, spring and damper force plots of semi-active seat suspension using control scheme II ($f/f_n = 0.5$).

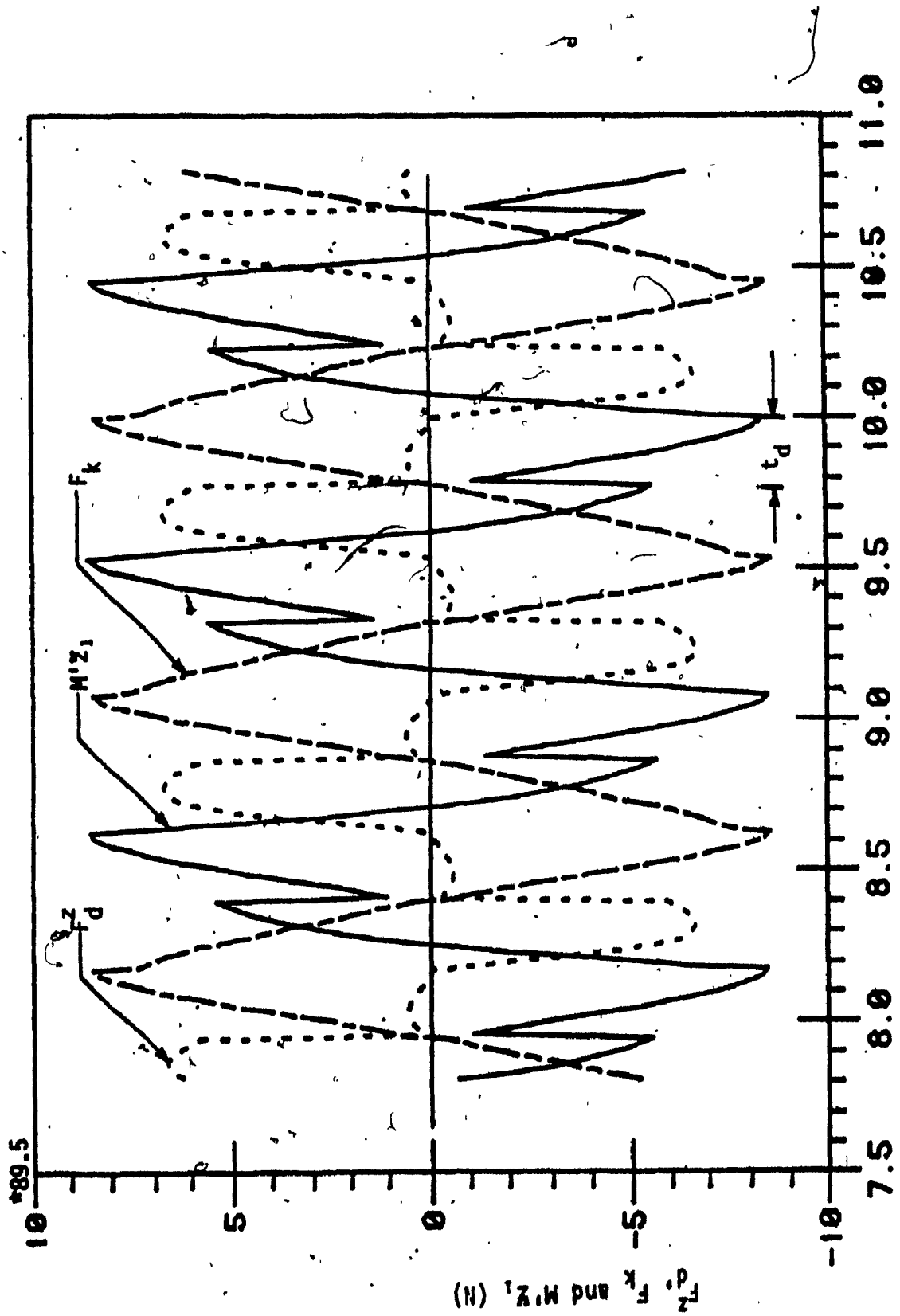

FIGURE 7.12: Inertia, spring and damper force plots of semi-active seat suspension using control scheme II ($\frac{f}{f_n} = 0.75$)

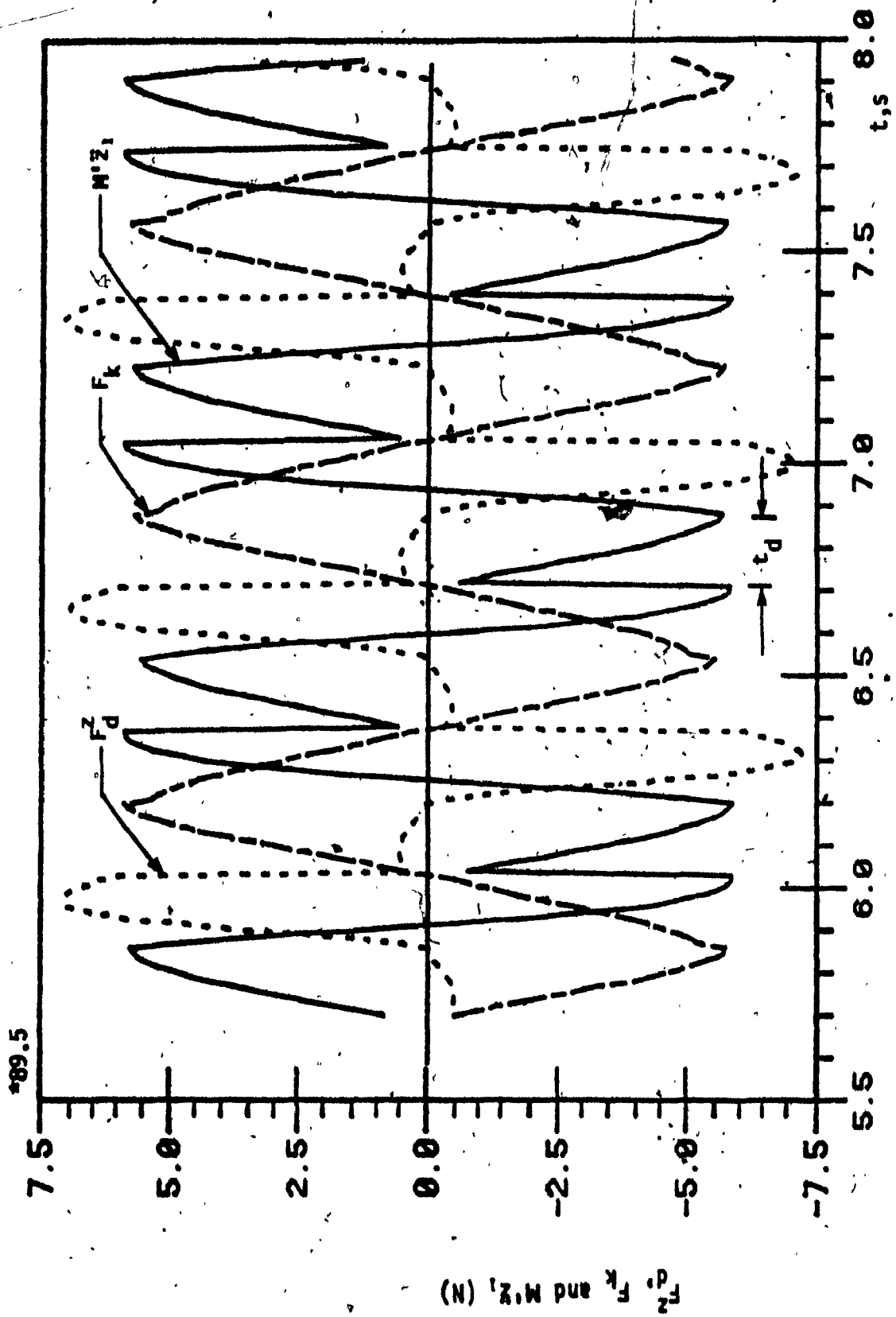

FIGURE 7.13: Inertia, spring and damper force plots of semi-active seat suspension using control scheme II ($\frac{f}{f_n} = 1$).

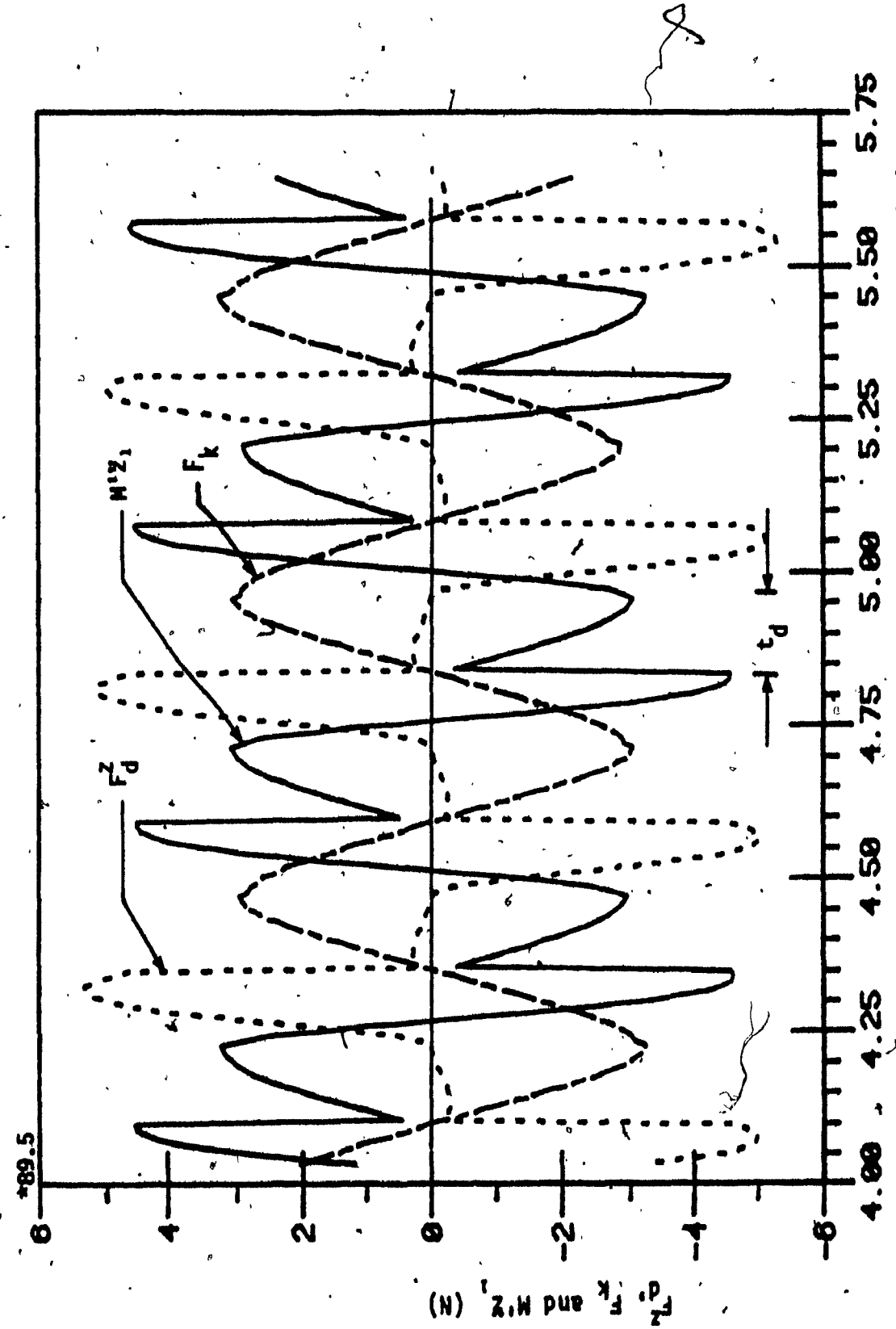

FIGURE 7.14: Inertia, spring and damper force plots of semi-active seat suspension using control scheme II ($\frac{f}{f_n} = 1.4$).

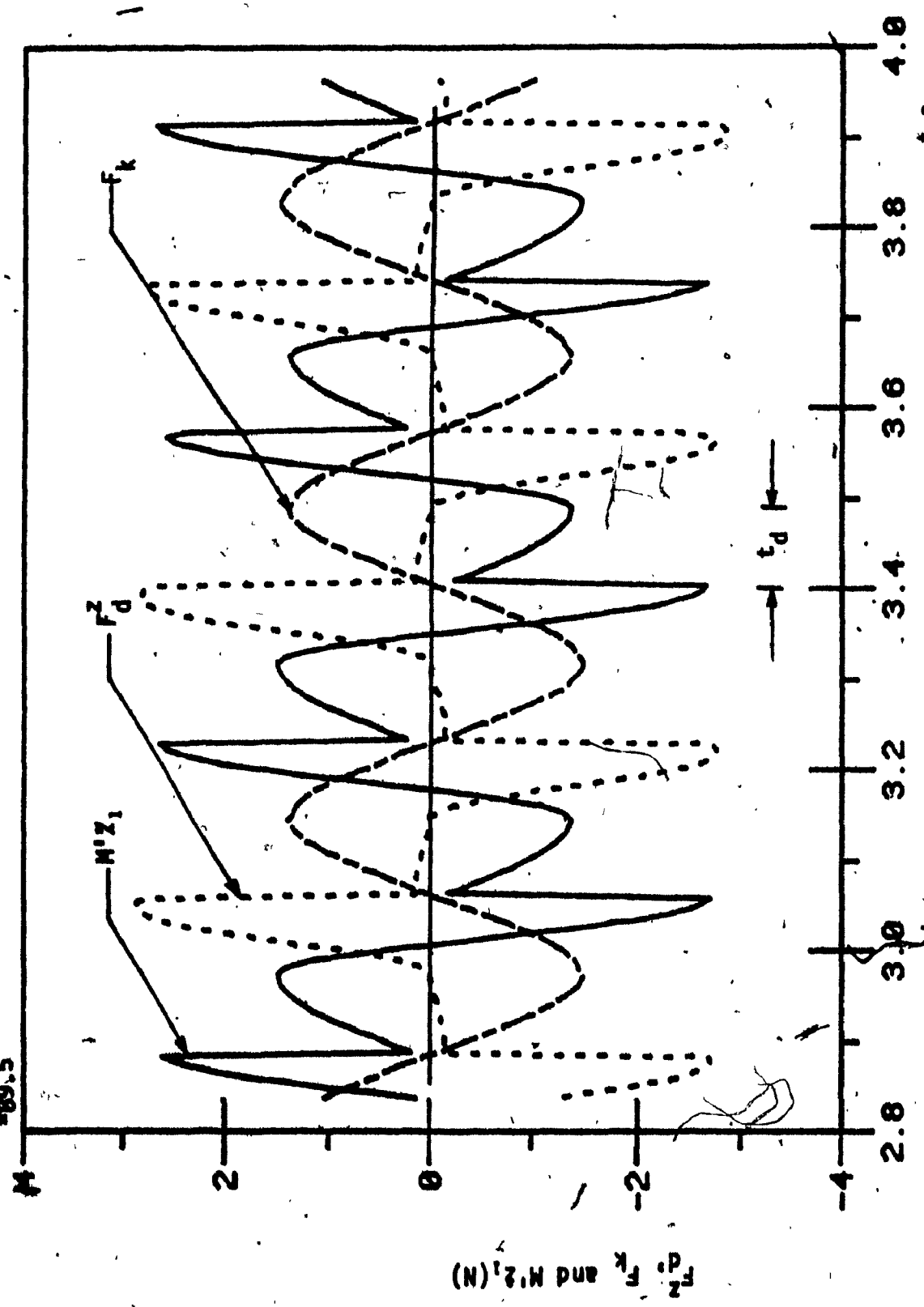

FIGURE 7.15: Inertia, spring and damper force plots of the semi-active seat suspension using scheme II ($\frac{f}{f_n} = 2.$)

TABLE 7.1

ACCELERATION TRANSMISSIBILITY OF BOUNCE SUSPENSION SEAT WITH PASSIVE AND "ON-OFF" DAMPING

Frequency ratio	Acceleration Transmissibility $\lvert \ddot{Z}_1/\ddot{Z}_0 \rvert$				
	Passive damping	"ON-OFF" Damping			
		Control Scheme I		Control Scheme II	
		On-Cycle	Off-Cycle	On-Cycle	Off-Cycle
0.25	1.08	1.12	--	1.04	--
0.40	1.17	1.16	--	1.01	1.03
0.50	1.20	1.07	1.04	--	1.20
0.75	1.22	1.20	1.06	1.08	1.62
1.0	1.16	1.16	0.93	1.16	1.14
1.4	1.02	0.94	0.58	0.91	0.59
1.75	0.78	0.70	0.38	0.65	0.37
2.	0.64	0.56	0.29	0.51	0.30
2.5	0.43	0.37	0.18	0.33	0.19

7.5.2 RIDE PERFORMANCE CHARACTERISTICS OF SUSPENSION SEAT WITH "ON-OFF" DAMPING WHEN SUBJECTED TO STOCHASTICALLY DESCRIBED TERRAIN EXCITATIONS

The ride performance of bounce suspension seat with "on-off" damping is evaluated using stochastically described terrain excitations. The PSD of the measured bounce acceleration at the tractor cab floor is expressed as a summation of sinusoidal components as described in Chapter 3. The differential equation of motion of the bounce suspension seat is solved for the stochastically described excitations represented by summation of sinusoidal components. The acceleration PSD estimates are obtained by performing a Fast Fourier Transform of the response acceleration time history.

The PSD of the response acceleration of bounce suspension seat employing "on-off" damping with the two control schemes are obtained and compared with acceleration PSD response of the passive bounce seat suspension as shown in Figure 7.16. The passive system exhibits a peak corresponding to the seat suspension resonant frequency (around 1.3 Hz) and shows significantly large peak around the vehicle resonant frequency (2.6Hz). The deteriorated performance in the vicinity of vehicle resonant frequency (2.6Hz) is attributed to large value of fixed damping used in the passive system.

The acceleration PSD response of bounce seat suspension employing "on-off" damper, operating with control scheme I, shows a peak corresponding to the resonant frequency of the suspension (aroung 1.3). The amplitude of this resonant peak is observed to be larger when compared to the passive system's acceleration PSD response, by approximately 12%. However, the suspension performance in the vicinity of vehicle resonant frequency improves by approximately 42%. The acceleration PSD performance of the bounce seat suspension employing "on-off" damper operating with control scheme II, also shows an identical peak corresponding to the resonant

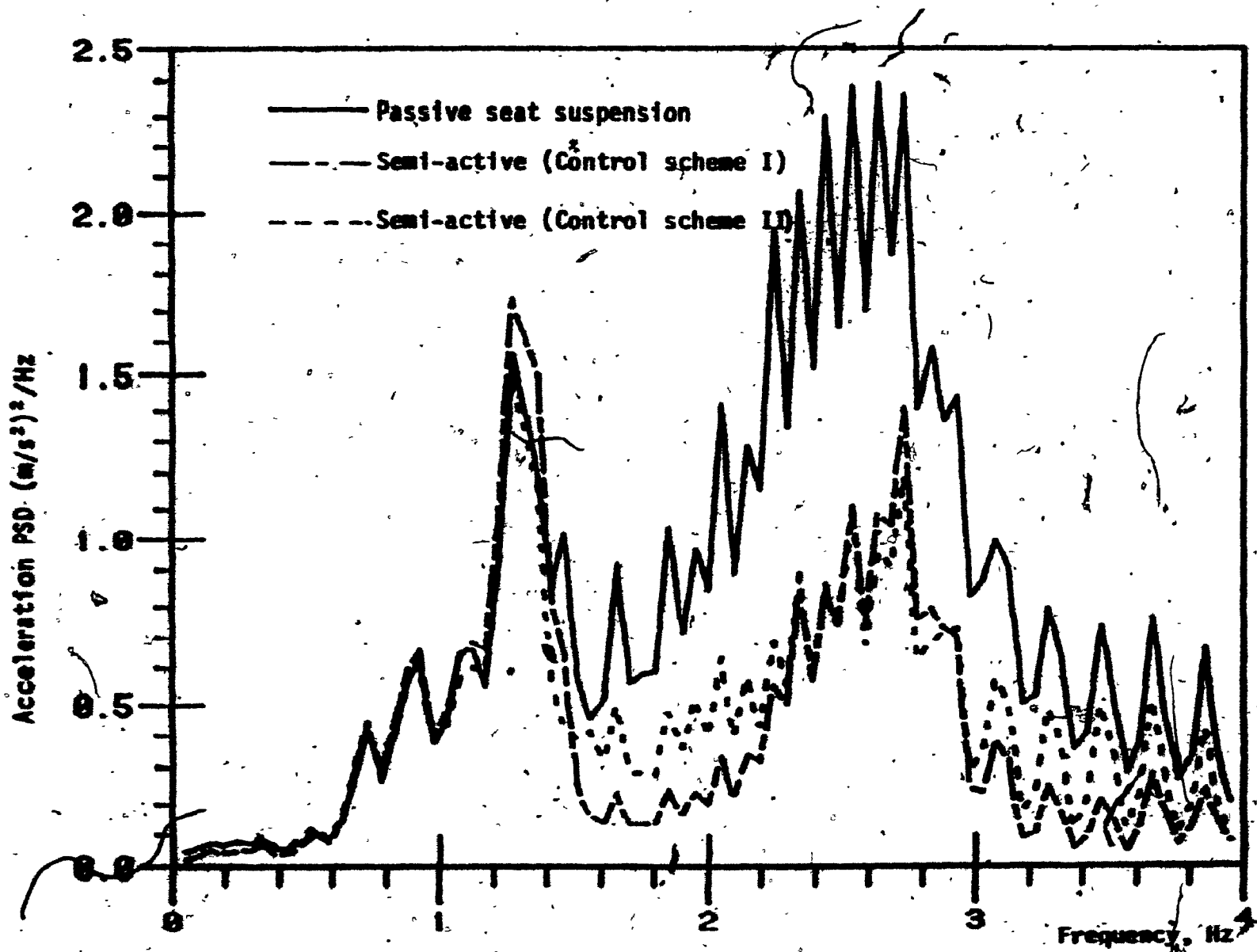

FIGURE 7.16: Acceleration PSD response of passive and semi-active seat suspensions.

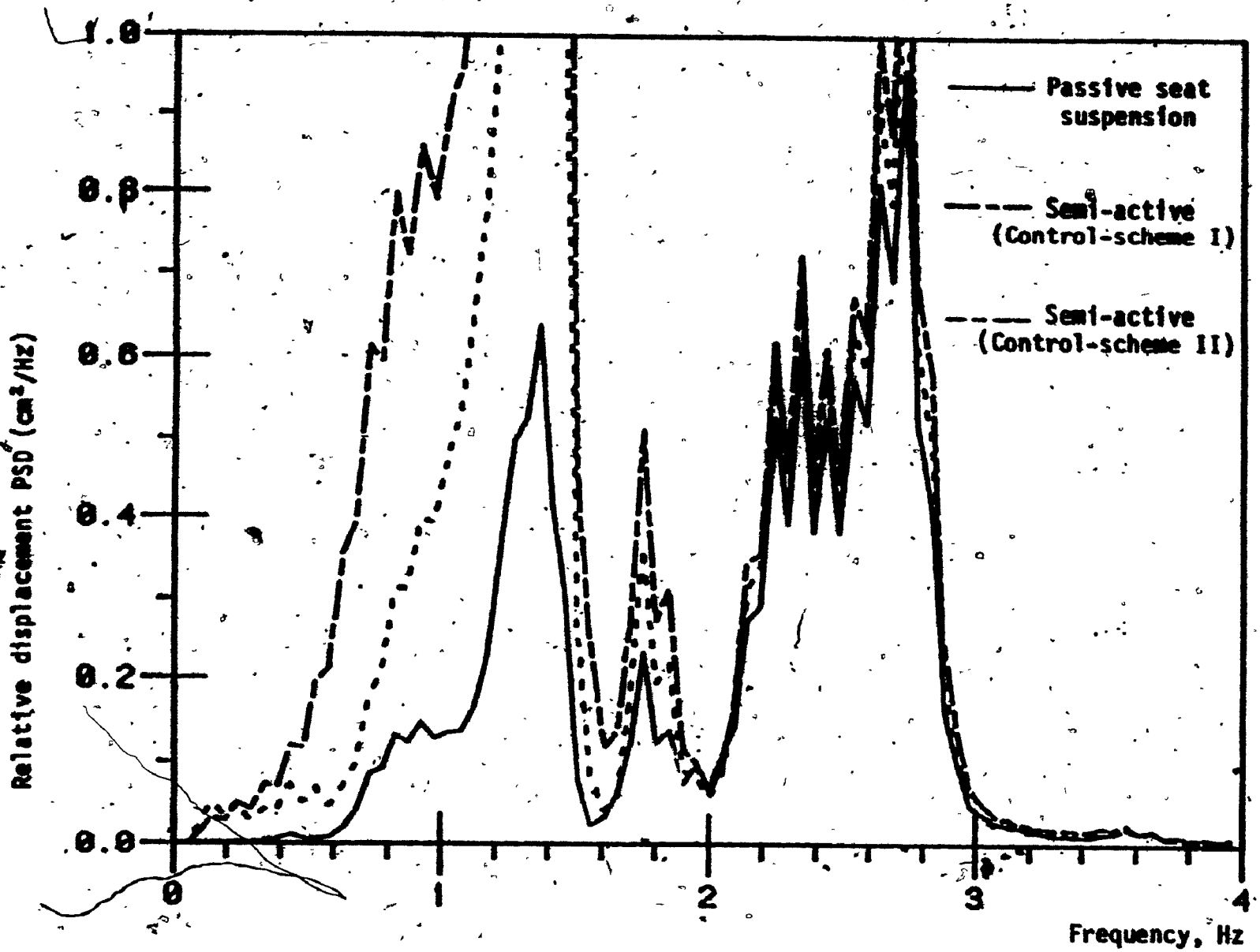

FIGURE 7.17: Relative displacement PSD response of the passive and semi-active seat suspensions.

frequency of the suspension seat. The amplitude of the peak acceleration is of the same order as that of the passive suspension seat. However, the peak acceleration performance in the vicinity of the vehicle resonant frequency is observed to be slightly superior to the peak acceleration PSD performance of the "on-off" damper employing control scheme I. The acceleration performance around 2.6 Hz is improved by approximately 50% over the performance of the passive suspension seat. The PSD estimate of the relative displacement response is presented in Figure 7.17. The "on-off" damper exhibits large relative displacement around the resonant frequency of the seat suspension. However, the relative displacement PSD response in the vicinity of vehicle resonant frequency is of the same order as that of passive seat suspension. Also the "on-off" damper employing control scheme II exhibits relative displacement response superior to the damper employing control scheme I.

7.6 SUMMARY

In this chapter, the concept of a semi-active "on-off" damper, that operates as a conventional passive damper during the part of vibration cycle when damper tends to reduce the acceleration of mass and assumes almost negligible damping when the passive damper would normally introduce energy to the mass, is presented. Two control schemes for operation of "on-off" damper are developed. Transmissibility characteristics of bounce suspension seat with "on-off" damping are evaluated and compared to the transmissibility characteristics of the passive system. The ride performance of bounce seat suspension with "on-off" damping is evaluated when subjected to stochastically described terrain excitations. The acceleration response of semi-active seat suspension is found to be superior to that of a passive seat suspension.

CHAPTER 8

CONCLUSIONS AND RECOMMENDATIONS FOR FUTURE WORK

8.1 GENERAL

In this thesis, two approaches to ride improvement of agricultural tractors are proposed, *namely*, suspension at the seat and suspension at the cab, for their easier adaptability to an existing vehicle. Configurations of longitudinal, lateral, roll, and pitch seat isolators are proposed. Commercially available bounce suspension seat is attached to the longitudinal and lateral seat isolators, and a computer model is developed for the isolator in the translational modes. Computer model is developed for the rotational seat isolator, which is the synthesis of bounce, roll, and pitch isolators. The computer models include non-linearities arising from the coulomb friction, shock absorber damping, and elastic limit stops. Computer models are also developed for the linear cab, and cab-seat suspensions.

A linearization technique, based on the dissipation of energy, is developed to represent the non-linear suspension models by their linear equivalents. The computer models of the seat, cab, and cab-seat suspensions are analyzed in the frequency domain for stochastically described agricultural terrain excitations. The acceleration and relative displacement responses of suspension models are evaluated to establish a measure of suspension performance. The sensitivity of the response of suspension models to variations in suspension parameters is investigated to establish an understanding of the suspension performance characteristics.

Objective functions are formulated for the suspension models, such that the acceleration PSD at the seat remains within ISO recommended *fatigue decreased proficiency* limits for at least 4 hours long exposure

in the bounce, longitudinal, and lateral modes. The objective functions are minimized subject to constraints on the peak relative displacement response, using non-linear programming techniques. The ride performance of optimum passive suspension models is assessed with reference to the ISO recommended *fatigue decreased proficiency* limits.

In the final phase of this investigation, it is demonstrated that fixed damping in a suspension system attenuates only for a part of the vibration cycle and accelerates the mass for the remaining portion of the vibration cycle. Hence, an "on-off" semi-active damper, that operates as a conventional passive damper during the attenuation part of the vibration cycle, and assumes negligible damping when the conventional damper would normally increase the mass acceleration, is developed for the bounce seat suspension. The performance characteristics of the bounce suspension seat with an "on-off" damper are investigated for harmonic as well as stochastically described excitations. The response characteristics are compared to that of a passive suspension seat.

8.2 MAJOR HIGHLIGHTS OF THE INVESTIGATION

The major highlights of this investigation are summarized in the following subsections.

1) Configurations of Passive Seat Suspensions

Commercially available suspension seats isolate the driver only in the bounce mode. Recognizing the severity of terrain induced vibrations in the longitudinal, lateral, roll, and pitch modes, the seat suspensions are configured in these modes. An identical suspension configuration is proposed for longitudinal as well as lateral seat isolators, such that they can be mounted on to each other. Also the commercially available bounce suspension seat can be easily attached on top of either the longitudinal or the lateral isolator to formulate a passive

seat suspension capable of attenuating terrain induced vibrations in all the three translational modes.

The configuration of a rotational isolator is proposed to attenuate terrain induced roll and pitch vibrations. The configuration consists of two gimbal mounted frames linked through a torsional shaft and a torsional damper. The frames are supported on to the springs and a damper. The bounce, longitudinal and/or lateral seat isolators can be attached on top of the frames to formulate a multi-mode passive seat isolation system. The rotational seat suspension model presented in the thesis, however, incorporates the bounce suspension seat alone. The suspension seats are modeled to include non-linearities arising from the shock absorber, coulomb friction, and elastic limit stops.

11) Development of Frequency Dependent Linearization Technique and Response Evaluation of Suspension Models

Equations of motion characterizing linear suspension models are analysed through the frequency domain computations. The equations of motion characterizing non-linear suspension models are solved using numerical integration techniques. However, the simulation of suspension models, subject to random terrain inputs, using numerical integration technique is extremely demanding on computer and human resources. Thus, the computer models developed for non-linear suspension seats are represented by their linear equivalents using a systematic technique based on dissipation of energy.

The systematic linearization technique developed in Chapter 4 establishes an equivalent viscous damping coefficient corr-

esponding to each discrete excitation frequency and amplitude, and hence referred to as "Frequency Dependent Linearization" technique. The linear equivalent damping parameter is obtained by equating the energy dissipated by the non-linear dissipative element to the energy dissipated by a viscous damper, at each discrete frequency. The frequency dependent linearization technique is a step by step iterative procedure and is found to be very simple to implement to solve the non-linear suspension models. The linearization technique has been thoroughly tested for harmonic excitations by comparing the response characteristics of linearized models to the response characteristics of non-linear suspension models obtained from numerical integration techniques. The methodology has been extended for solving the non-linear suspension models subjected to stochastically described excitations. The methodology has been found very accurate and economical with computer time, for example, the solution of SDOF longitudinal/lateral seat isolator requires 0.7 s execution time using the frequency dependent linearization methodology compared to 170 s execution time required by numerical integration technique.

iii) Optimization and Ride Assessment of Suspension Models

The performance criteria, as a function of response accelerations and relative displacements are formulated for the seat, cab, and cab-seat suspension models. These performance criteria are utilized to formulate the objective functions for the suspension models, such that the acceleration levels at the seat remain within the ISO recommended *fatigue decreased proficiency* limits for at least 4 hours long exposure, while the

relative displacements being constrained to a certain permissible value. The limit constraints are imposed on the design variables, depending on the type of suspension system being optimized. The non-linear programming technique is employed to minimize the objective function and the respective optimal suspension parameters are obtained.

The acceleration and relative displacement responses of the optimal suspension models are obtained. The acceleration response in the translational modes are compared to the *fatigue decreased proficiency* limits to assess the ride quality achievable from the optimal suspension models. The relative ride performance of seat and cab suspension models is discussed. The results reveal that passive seat suspension can provide satisfactory ride in the bounce, longitudinal, roll, and pitch modes. Since the lateral resonance of the vehicle occurs around 1.1 Hz, an extremely low natural frequency lateral seat isolator is required. However, the low natural frequency isolator leads to extremely large relative motion response.

The ride performance of optimal cab suspension with rigid seat (5 DOF) is observed to be superior in the longitudinal, lateral, and pitch modes. The roll performance of the 5 DOF cab suspension model is found to be inferior to the roll performance of rotational seat isolator. Addition of bounce suspension seat to the suspended cab revealed significant improvement in the bounce ride, however, no significant ride improvement is accomplished due to addition of lateral or roll seat isolators.

iv) Development of Bounce Seat Suspension Model with Semi-Active "On-Off" Damping

The acceleration response of optimal bounce seat suspension shows a large peak corresponding to its resonant frequency. An increase in the value of damping coefficient suppresses this peak but deteriorates the performance corresponding to the vehicle resonant frequency (around 2.6 Hz). This is attributed to the most obvious performance limitation demonstrated by fixed damping. The fixed damping in a passive isolation system introduces the energy into the mass during a portion of the vibration cycle, hence increases the mass acceleration. Thus, an "on-off" semi-active damper is introduced, which operates as a conventional passive damper with a constant orifice opening during a part of vibration cycle, but assumes negligible damping by modulating the orifice to the maximum opening, during the portion of vibration cycle when a passive damper would normally increase the amplitude of mass acceleration.

Control schemes associated with the operation of "on-off" damper are developed and a bounce suspension seat is modeled with the "on-off" damping. The performance characteristics of the "on-off" suspension model are investigated for harmonic and stochastic excitations. The results reveal that a bounce seat suspension system with an "on-off" damper can provide the resonant response similar to that of a heavily damped system, while the response characteristics in the isolation region are comparable to the response of a lightly damped passive system.

v) Other Applications

In this investigation, the techniques associated with development of suspension configurations, development of suspension models, response evaluation, and ride predictions are fairly general. The techniques can be extended to the ride improvement of a class of off-road vehicles, *namely*, earth-movers, snow-pushers, mining, and other construction vehicles, without any change in the methodology.

8.3 CONCLUSIONS

Based on the studies, the following specific conclusions are drawn:

- Soft seat cushion lowers the natural frequency of bounce suspension seat and increases the resonant response.
- The resonance response of bounce seat suspension decreases and the isolation performance is deteriorated with stiffer bounce suspension.
- Increase in coulomb damping force and velocity squared damping cause lower resonance peak with deteriorated isolation performance of the bounce, longitudinal, and lateral seat isolators.
- The magnitude of resonance response of lateral and longitudinal seat isolators is lowered considerably with lower stiffness values.
- Soft bounce suspension results in superior bounce and pitch performance of the rotational seat isolator.
- The bounce and pitch peak acceleration responses corresponding to the bounce resonant frequency are lowered considerably with increase in the magnitude of coulomb friction and the coefficient of velocity squared damping. However, the bounce and pitch

acceleration response is deteriorated in the isolation region.

- The bounce, pitch, and roll performance of the rotational seat isolator are found to be extremely sensitive to the stiffness of end supports. A suitable value of the stiffness of end supports can lead to improved acceleration response in bounce, pitch, and roll modes.
- The pitch acceleration response corresponding to the pitch and bounce resonant frequencies is significantly lowered with softer pitch suspension (K_θ) of the rotational seat isolator.
- The bounce, pitch, and roll acceleration responses of the 5 DOF cab suspension model (cab suspension with rigid seat), are lowered with decrease in the stiffness of corner mounts.
- Increase in the damping coefficients of the corner mounts cause lower lateral, pitch, and roll acceleration responses but large bounce acceleration response corresponding to the bounce resonant frequency of the vehicle.
- Addition of bounce seat isolator to the 5 DOF cab suspension attenuates the bounce vibrations of the cab corresponding to the bounce resonant frequency of the vehicle, while causing an acceleration peak at lower frequency.
- Soft and heavily damped lateral isolator lowers the peak lateral and roll accelerations at the cab.
- Higher location of the cab cg causes larger lateral and roll accelerations at the cab, however, the increased seat height lowers the lateral acceleration at the seat.
- No significant improvement in the ride is accomplished due to the addition of roll and lateral seat isolators to the suspended cab.

- The optimal bounce suspension seat provides a satisfactory ride for 2.5 hours exposure with reference to the *fatigue decreased proficiency* limit. The bounce ride performance of rotational seat isolator is found to be superior to the bounce ride performance of the bounce suspension seat alone. The bounce acceleration response of optimal 5 DOF cab suspension model exceeds the 2.5 hours limit. However, the bounce ride of cab suspension with bounce suspension seat model is observed to be well within the 4 hours exposure limit.
- Optimal longitudinal seat isolator provides a satisfactory ride with reference to the 4 hours exposure limit. The longitudinal ride performance of the 5 DOF cab suspension model is found to be slightly inferior to the ride performance of seat isolator. The relative displacement response in both cases is extremely small.
- The optimal parameters of the lateral seat isolator obtained by constraining the undamped natural frequency to be at least 0.7 Hz lead to no improvement in the lateral ride. Although, the optimal parameters obtained through constraining the undamped natural frequency to at least 0.6 Hz provided a significant improvement in the lateral ride, the response acceleration exceeds the *fatigue decreased proficiency* limits for even 1 hour exposure. Moreover, the relative displacement response is observed to be quite large. Although, the lateral acceleration response of the optimal 5 DOF cab suspension is quite large, the relative displacement response of the cab with respect to the vehicle frame is found to be excellent.

- The pitch acceleration response of the optimal cab suspension is superior to the pitch response of rotational seat isolator.
- The roll acceleration response of the rotational seat isolator reveals excellent isolation performance of the rotational seat isolator. However, the optimal cab suspension provides extremely poor roll performance.
- The "on-off" damper exhibits the transmissibility characteristics of a passive damper during the on-cycle but significantly lower transmissibility ratio is obtained during the off-cycle operation of the "on-off" damper.
- The acceleration response of the bounce suspension seat with "on-off" damping is identical to that of a passive bounce suspension corresponding to the seat resonant frequency. However, the acceleration response of the suspension seat in the isolation region is significantly lower than the acceleration response of passive suspension seat.

Some of the results of this investigation have been presented and published in journals [81,82,83] .

8.4 RECOMMENDATIONS FOR FURTHER WORK

Mathematical models and computer simulation provide suspension performance projections but physical model agreement is necessary for confidence in the mathematical results. Hence, an attempt should be made to physically substantiate the computer models.

Whole vehicle modeling, to include a particular cab suspension, would provide more exact results for suspension performance coupled with vehicle dynamics.

Although seat suspension provide satisfactory ride, the resulting relative displacement limits the performance rate of the tractor operator. The cab suspension overcomes this performance limitation of seat suspension, but the ride performance of cab suspension in the bounce, longitudinal and roll modes is inferior to the ride performance of seat suspension. Alternatively, the suspension at the axles may be investigated for the ride improvement of agricultural vehicle.

Efforts are needed to integrate this analysis with other design considerations such as location of cab mounts, cab cg height, wheelbase length, and seat location.

Future dynamic studies of cab suspension should include the non-linear characteristics of the suspension elements.

Attempts should be made to develop the physical model of an "on-off" suspension with a two position on-off valve. The influence of valve transients on the performance of "on-off" damper, should also be investigated.

REFERENCES

EFFECTS OF OFF-ROAD VEHICLE VIBRATION

[1] Rosegger, R. and S. Rosegger, 1960. Health Effects of Tractor Driving. J. of Agric. Engng. Res., Vol. 5, No. 3, p. 242.

[2] Reason, J. 1978. Motion Sickness: Some Theoretical and Practical Considerations. Applied Ergonomics, Vol. 9, No. 3, p. 167.

[3] Radke, A.O., 1957. Vehicle Vibration-Man's New Environment. ASME Paper No. 57-A, 54: pp. 1-8.

[4] Pisbien, W., and L.C. Salter, 1950. The Relation Between Truck and Tractor Driving and Disorders of the Spine and Supporting Structures. Ind. Med. Surv., Vol. 19, p. 444.

[5] Dupuis, H., and W. Christ, 1966. Study of the Risk of Spinal Damage to Tractor Drivers. Rep. Max Planck Institut Landarb. Landtech., Bad Kreuznach.

[6] Gibbon, J.M. and D.S. Boyse, 1971. Tractor Operators Survey, NIAE Dept. Note, DS/SY/123/1952, July 1971.

[7] Schmitz, M.A., and A.K. Simons, 1959. Man's Response to Low Frequency Vibration. ASME Paper No. 5A-A-200.

[8] Hornick, R.J., 1961. Effects of Tractor Driving on Operators. Agric. Engng., Vol. 42, No. 12, pp. 674-676.

[9] Matthews, J., 1964. Ride Comfort for Tractor Operators. I. Review of Existing Information. J. of Agric. Engng. Res., Vol. 9, No. 1, pp. 3-31.

[10] Müller, E.A., 1938. The Effects of Sinusoidal Vertical Vibrations on a Man in Sitting and Standing Positions. Arb. Physiol. Argew. Ent., Berlin, Vol. 5, p. 459.

[11] Matthews, John, 1973. Measurement of Tractor Ride Comfort, Trans. SAE, Vol. 82, pp. 2712-2727.

[12] Society of Automotive Engineers, 1975. Measurement of Whole Body Vibration of the Seated Operator of Agricultural Equipment. SAE Handbook, J1013.

[13] Van Deusen, B.D., 1968. Human Response to Vehicle Vibration. Trans. SAE, Vol. 77, No. 1, pp. 328-345.

[14] Janeway, R.N., 1948. Passenger Vibration Limits. SAE Journal Vol. 56, No. 8, p. 48.

[15] Goldmann, D.E., 1948. A Review of Subjective Responses to Vibratory Motion of the Human Body in the Frequency Range 1 to 70 cps. Naval Med. Res. Institute, Report No. 4, March 1948.

[16] McCullough, M.L., 1972. Towards the Development of Ratio Scale. Presented at the Human Response Conference, Univ. of Scheffield, U.K.

[17] Oborne, D.J., and D.A. Humphery, 1976. Individual Ability in Human Response to Whole Body Vibration. Ergonomics, Vol. 19, No. 6, pp. 719-726.

[18] International Organization for Standardization, 1974. Guide for Evaluation of Human Exposure to Whole Body Vibration. ISO 2631, 1974(E).

[19] Verein Deutscher Ingenieure. 1963. Assessing the Effects of Vibration on Human Beings. VDI-2057. Translated and Published by Peter Peregrinus Ltd., Stevenge, Herts, U.K.

[20] Lee, R.A. and F. Pradko, 1968. Analytical Analysis of Human Vibrations. Trans. SAE, Vol. 77, No. 1, pp. 346-370.

[21] De Longchamp, J.H., 1973. Operator Seat Design Problems in Reference to Theoretical Vibration Isolation and Practical European Recommendations. SAE Paper No. 730824.

[22] Stikeleather, L.F., 1976. Review of Ride Vibration Standards and Tolerance Criteria. Trans. SAE Vol. 85, pp. 1460-1467.

MODELLING OF HUMAN BODY

[23] Coermann, R.R., and A.L. Whittwer, 1960. The Passive Dynamic Mechanical Properties of the Human Thorax Abdomen System and of the Whole Body System. Aerospace Med. Vol. 31, No. 6, p. 443.

[24] Griffin, M.J., 1981. Biodynamic Response to Whole Body Vibration. Shock and Vibration Digest, Vol. 13, No. 8, pp. 3-12, Aug. 1981.

[25] Suggs, C.W., L.F. Stikeleather, J.Y. Harrison and R.E. Young, 1970. Application of Dynamic Simulator in Seat Testing. Trans. ASAE, Vol. 13, No. 3, pp. 378-381.

[26] Park, W.H., and J.C. Wambold, 1975. A Human Model for Measuring Objective Ride Quality. ASME Paper No. 75-DET-6. Presented at Design Engineering Technical Conference, Washington, D.C., Sept. 17-19, 1975.

[27] Patil, M.K., M.S. Palanichamy and D.N. Ghista, 1980. Response of Human Body to Tractor Vibration and its Minimization by Provision of Relaxation Suspension to Both Wheels and Seat at the Plane of Centre of Gravity. Medical and Biological Engineering & Computing, Vol. 18, pp. 554-562.

TRACTOR RIDE IMPROVEMENT

[28] Matthews, J., 1964. Ride Comfort for Tractor Operators, II. Analysis of Ride Vibrations on Pneumatic Tyred Tractors. J. Agric. Engng. Res. Vol. 11, No. 1, pp. 147-158.

[29] Claar II, P.W., W.F. Buchele, S.J. Marley, and P.N. Seth, 1980. Agricultural Tractor Chassis Suspension System for Improved Ride Comfort. SAE Paper No. 80T020. Presented at Int. Off-Highway Meet. and Expo., MECCA, Milwaukee, Sept. 8-11, 1980.

[30] Claar II, P.W., W.F. Buchele, S.J. Marley, and P.N. Seth, 1980. Off-Road Vehicle Ride: Review of Concepts and Design Evaluation with Computer Simulation. SAE Paper No. 801023. Presented at Int. Off-Highway Meet. and Expo., MECCA, Milwaukee, Sept. 8-11, 1980.

[31] Matthews, J. and J.D.C. Talamo, 1965. Ride Comfort for Tractor Operators, III. Investigation of Tractor Dynamics by Analogue Computer Simulation. J. Agric. Engng. Res. Vol. 10, No. 1, pp. 93-108.

[32] Patil, M.K., M.S. Palanichamy and D.N. Ghista, 1977. Dynamic Response of Human Body Seated on a Tractor and Effectiveness of Suspension Systems. SAE Paper No. 7709322. Trans. SAE Vol. 86, pp. 3221-3236.

[33] Bender, E.K., 1968. Some Fundamental Limitations of Active and Passive Vehicle Suspensions. Trans. SAE Vol. 77, No. 4, pp. 2910-2915.

[34] Karnopp, D.C., M.J. Crosby and R.A. Harwood, 1974. Vibration Control Using Semi-Active Force Generator. Trans. ASME. J. of Engineering for Industry. Vol. 98, Ser. B, pp. 914-918.

[35] Kransnicki, E.J., 1979. Comparison of Analytical and Experimental Results for a Semi-Active Vibration Isolator. Proc. of the 50th Shock and Vibration Symposium, Colorado Springs, Colorado.

[36] Lowe, D.G., 1974. Practical Aspects of Suspension Seat Designs. Bostrom (UK) Report.

[37] Varterasian, J.H. and R.R. Thompson, 1977. Dynamic Characteristics of Seats with Human Occupants. SAE Paper No. 770249, 12 p.

[38] Rosso, G., 1969. Study of Seat Suspension for the Off the Road Wheeled Vehicles. Centro Studi Motorizzazione Agricola (CESMA) del C.N.R. Torino, Italy. Int. Soc. for Terrain-Vehicle Systems,

Inc., Proc. of the 3rd Int. Conf., July 1969, Essen, West Germany.

[39] Zach, D.J., 1971. The Development of a Seat Suspension for Mobile Construction Equipment. SAE Paper No. 710515.

[40] Koutsky, J.L., 1978. Development of a Suspension Seat for Earthmoving Vehicles. SAE Paper No. 780474.

[41] Stikeleather, L.F., 1973. Evaluating the Vibration and Shock Isolation Qualities of Operator Seats for Construction Machinery. Trans. SAE, Vol. 82, pp. 1460-1467.

[42] Haack, M., 1955, Tractor Seat Suspension for Easy Riding. Trans. SAE, Vol. 63, pp. 435-470.

[43] Matthews, J., 1966. Ride Comfort for Tractor Operators. IV Assessment of the Ride Quality of Seats. J. Agric. Engng. Res. Vol. 11, No. 1, pp. 44-57.

[44] Thompson, J.E. 1977. Tractor Ride Comfort Package. SAE Paper No. 770705.

[45] Stikeleather, L.F., and C.W. Suggs, 1968. The Development of an Active Seat Suspension for Off-Road Vehicles. ASAE Paper No. 68-632, Presented at ASAE Winter Annual Meeting, 1968.

[46] Suggs, C.W., L.F. Stikeleather and C.F. Abrams Jr., 1970. Field Tests of an Active Seat Suspension for Off-Road Vehicles. Trans. ASAE Vol. 13, NO. 4, pp. 608-611.

[47] Grimm, E.A., G.T.H. Huff and J.N. Wilson, 1977. An Active Seat Suspension for Off-Road Vehicles. University of Saskatchewan, Saskatoon.

[48] Young, R.E. and C.W. Suggs, 1973. Active Seat Suspension for Isolation of Roll and Pitch in Off-Road Vehicles. ASAE Paper No. 73-156. Univ. of Kentucky, June 1973.

[49] Kim, K., 1981. Ride Simulation of Passive, Active, and Semi-Active Seat Suspension for Off-Road Vehicles. Ph.D. Thesis. Univ. of Illinois at Urbana-Champain.

[50] Crosby, M.J. and D.C. Karnopp, 1973. The Active Damper - A New Concept for Shock and Vibration Control. The Shock and Vibration Bulletin, No. 43.

[51] Karnopp, D.C., 1978. Are Active Suspensions Necessary? ASME Paper No. 78-WA-12. Presented at the ASME Winter Annual Meeting, San Francisco, Calif. Dec. 10-15, 1978.

[52] Stayner, R.M. 1974. Vibration and the Tractor Driver. N.I.A.E. Paper No. 74-V-404.

[53] Suggs, C.W. and B.K. Huang, 1969. Tractor Cab Suspension Design and Scale Model Simulation. Trans. ASAE, Vol. 12, No. 3, pp. 283-285.

[54] Hilton, D.J., and P. Moran, 1975. Experiments in Improving Tractor Operator Ride by Means of Cab Suspension. J. Agric. Engng. Res., Vol. 20, pp. 433-448.

[55] Roley, D.G., 1975. Tractor Cab Suspension Performance Modeling. Ph.D. Thesis Univ. of California, Davis.

[56] Foster, A.W., 1978. Truck Cab Suspension SAE Paper No. 780408.

[57] Wallace, Flower, 1978. Front and Rear Cab Isolation. SAE Paper No. 780411.

[58] Crosby, M.J. and R.E. Allen, 1974. Cab Isolation and Ride Quality. SAE Paper No. 740294.

[59] Horvat, D., and D.L. Margolis, 1981. An Experimental Comparison between semi-active and passive suspension for air-cushion vehicles. Int. J. of Vehicle Design, Vol. 2, No. 3, pp. 308-321.

[60] Karnopp, D., and Ross. R. Allen, 1976. Semi-active Control of Multimode Vibratory Systems Using the ILSM Concept. Trans. ASME. of Engineering for Industry, pp. 914-918.

ANALYTICAL TECHNIQUES

[61] Greenwood, Donald T., 1977. Classical Dynamics, Prentice-Hall, Inc., Englewood Cliffs, N.J.

[62] I.S.O., 1980. Agricultural Wheeled Tractors-Operator Seat-Measurement of Transmitted Vibrations. ISO/TR. 5007-1980 (E).

[63] Bendat, J.S., and A.G. Piersol, 1971. Random Data: Analysis and Measurement Procedures. John Wiley and Sons Inc., New York.

[64] Levy, S., and J.P.D. Wilkinson, 1975. Generation of Artificial Time Histories Rich in All Frequencies from Given Response Spectra. Joint Automatic Control Conf. of the American Auto. Control Council, Paper No. K1/7.

[65] Hullender, D.A., 1979. Generation of a Random Time series with a Specified Spectral Density Function. Proc. Joint Automatic Control Conference, Denver, Colo, June 17-21. Publ. by AICHE, New York, N.Y., 1979, pp. 532-535.

[66] Tsai, Nien-Chien, 1972. Spectrum Compatible Motions for Design Pruposes. Journal of Engng. Mechanics, Proc. ASCE, April 1972.

[67] Caughy, T.K. 1963. Derivation and Application of the Fokker Planck Equation to Discrete Non-Linear Dynamic Systems Subject to White Random Excitation. The J. of the Acoustical Soc. of America, Vol. 35, No. 11. pp. 1683-1692.

[68] Ariaratnam, S.T., 1960. Random Response of Non-linear Suspensions, J. of Mech. Engng. Sc., Vol. 2, No. 3, pp. 195-201.

[69] Roberts, J.B., 1981. Response of Non-Linear Mechanical Systems to Random Excitations. Part 2: Equivalent Linearization and Other Methods, Shock and Vibration Digest, Vol. 13, No. 5, May, 1981, pp. 15-29.

[70] Crandall, S.H., 1963. Perturbation Techniques for Random Vibration of Non-Linear Systems. The J. of the Acoustical Soc. of America, Vol. 35, No. 11, pp. 1700-1705.

[71] Caughy, T.K., 1963. Equivalent Linearization Techniques. The J. of Acoustical Soc. of America. Vol. 35, No. 11, pp. 1706-1711.

[72] Iwan, W.D. and I-Min Yang, 1972. Application of Statistical Linearization Techniques of Non-Linear Multidegree-of-Freedom Systems. J. of App. Mech., Trans. of ASME, June 1972, pp. 545-550.

[73] Bandstra, J., 1981. Comparison of Equivalent Viscous Damping and Non-Linear Discrete and Continuous Vibrating Systems. ASME Paper No. 81-DET-89. Presented at the 8th ASME Design Engineering Conference, Hartford, Conn., Sept. 20-23, 1981.

[74] Hobbs, G.K., 1971, Methods of Modeling and Analyzing Viscoelastically damped structures. Proc. of the ASME, Design Engineering Div. Vibrations Conference and the International Design Automation Conference, Toronto, September 1971, p. 8.

[75] Scanlan, R.H., 1970. Linear Damping Models and Casuality in Vibrations - Letters to the Editor. J. of Sound and Vibrations. Vol. 13, no. 4, pp. 449-509.

OPTIMIZATION

[76] Wolkovitch, Julian, 1968. Techniques for Optimizing the Response of Mechanical Systems to Shock and Vibration. SAE Trans., Vol. 77, pp. 2887-2898, No. 680748.

[77] Hooke, R., and T.A. Jeeves, 1961. Direct Search Solution of Numerical and Statistical Problems. J. Assoc. Comp. Mach., Vol. 8, pp. 212-229.

[78] Himmelblau, David M., 1972. Applied Non-Linear Programming, McGraw-Hill Book Company, New York.

[79] Kuester, James L., and Joe H. Mize, 1973. Optimization Techniques with Fortran, McGraw Hill Book Company N.Y.

[80] Beveridge, Gordon, S.G., and Robert S. Schechter, 1970. Optimization: Theory and Practive, McGraw-Hill, Kogakusha, Ltd. Tokyo.

[81] Rakheja, S., and S. Sankar, 1982. An Optimum Seat-Suspension for Off-Road Vehicles. Presented at 53rd Shock and Vibration Symposium, Oct. 26-28, 1982, Danvers, Mass., and published in the Bulletin of Shock and Vibration, Part 3. May 1983.

[82] Rakheja, S., and S. Sankar, 1983. Improved Off-Road Tractor Ride via Passive Cab and Seat Suspensions. Presented at the Design and Production Engineering Technical Conference, Dearborn, Michigan, and accepted for publication in J. Vibration, Acoustics, Stress and Reliability Design.

[83] Rakheja, S., and S. Sankar, 1983. Ride Quality Improvement of Off-Road Vehicles via Optimal Seat Suspension. Presented at CAN/CAM Conference, Saskatoon, Sask., 1983.

APPENDIX I

EXPERIMENTAL VERIFICATION OF THE PASSIVE SEAT SUSPENSION MODEL

A Bostrom seat suspension is tested in the laboratory to verify the mathematical models formulated in Chapter 2. The experimental verification is initiated by identifying and measuring the various suspension components. The bounce suspension system consists of a cross linkage mechanism supported on guided rollers, and an inclined shock absorber. A schematic of the cross linkage mechanism is presented in Figure I.1. The stiffness and hysteretic characteristics of the linkage are measured by gradually loading and unloading the suspension system in the absence of shock absorber. The static characteristics of suspension system subjected to a number of preload settings are presented in Figures I.2. The stiffness coefficient is determined by:

$$K_z = \frac{dF}{dz} \qquad (I.1)$$

and is found to be a constant in the preload range 440 N to 835 N. The static magnitude of coulomb friction is also observed to be constant in the above preload range. The resulting values for stiffness coefficient and static friction are listed in Table I.1. The damping force due to shock absorber is evaluated from the shock absorber geometry presented in Figure I.3. The specifications are listed in Table I.2. The damping force can be evaluated through force balance and flow equations in the following manner [75].

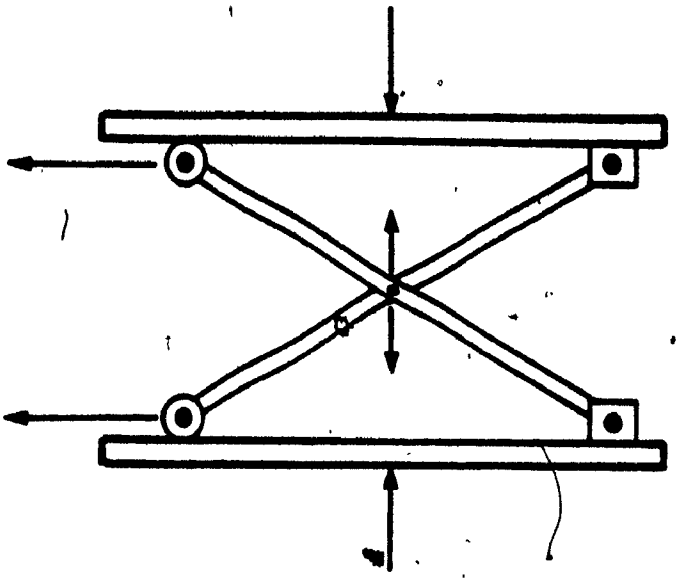

FIGURE I.1: Schematic of the seat suspension linkage mechanism

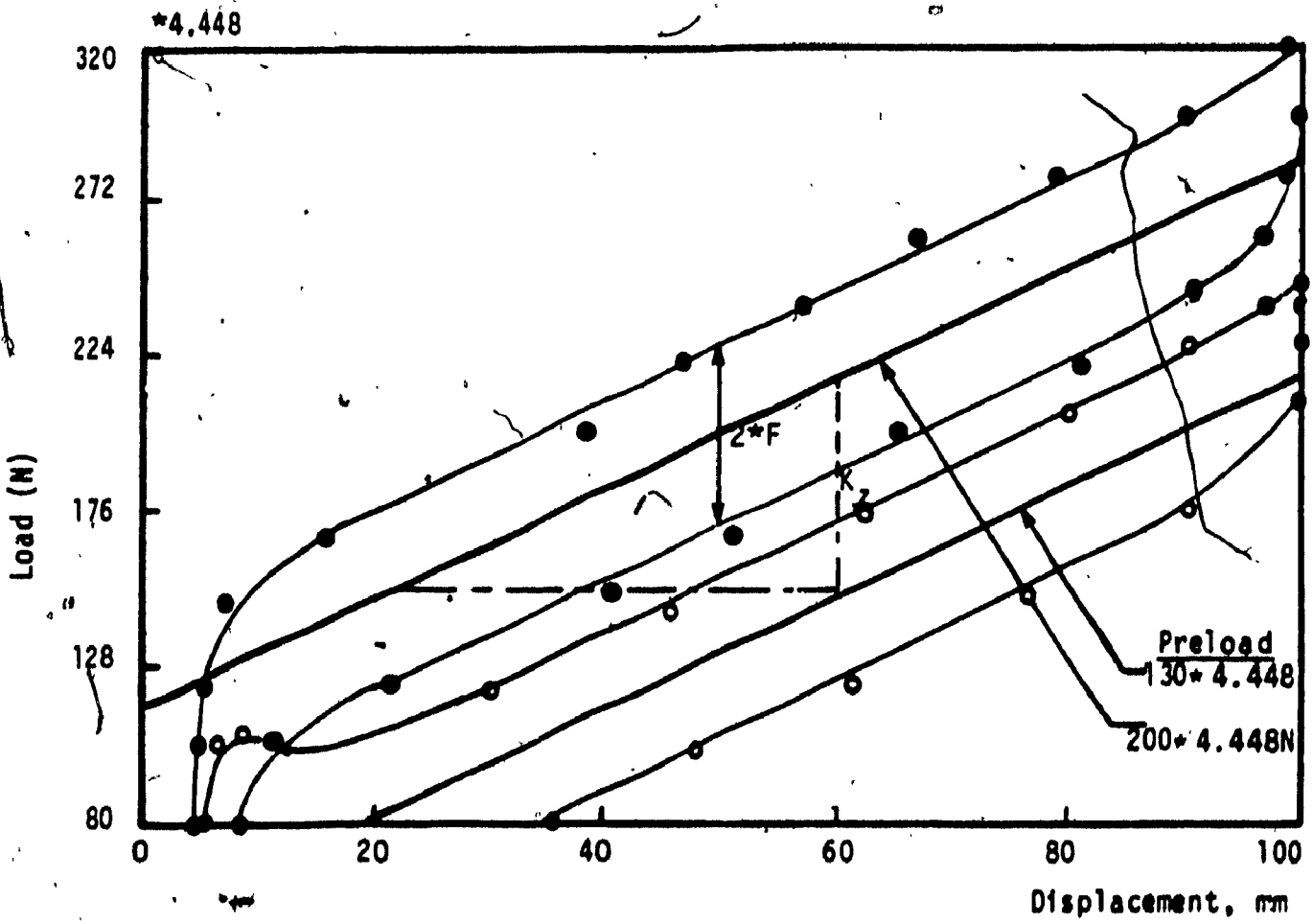

FIGURE I.2: Static characteristics of suspension linkage mechanism

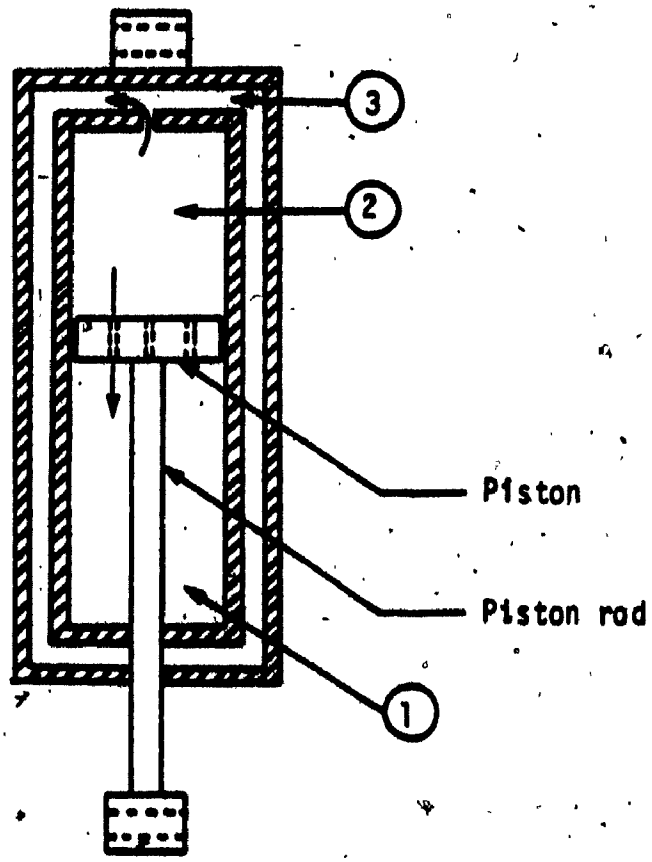

FIGURE I.3: Schematic of the Bostrom shock absorber

TABLE I.1

STATIC CHARACTERISTICS OF SUSPENSION

LINKAGE MECHANISM

Mid-ride Load*.102 (N)	Stiffness constant (N/cm)	Magnitude of static friction (N)
45	85.	97.8
55	87.	111.0
59	87.	115.0
65	87	111.0
75	87	116.0
85	87	116.0

TABLE I.2

GEOMETRIC PARAMETERS OF THE BOSTROM

SHOCK ABSORBER

Piston diameter	2.54 cm
Rod diameter	1.08 cm
Stroke	5.1 cm
Number of orifices on the piston	4
Orifice diameter	0.315 cm
Numer of orifices on the cylinder	1
Orifice diameter	0.3175 cm

Flow equations:

Flow from Chamber (2) to (1) -

$$A_p \dot{u} = 4\, C_{d_1}\, A_{r_1} \sqrt{\frac{2(P_2 - P_1)}{\rho}} \qquad (1)$$

Flow from Chamber (2) to (3)

$$A_R \dot{u} = C_{d_2}\, A_{r_2} \sqrt{\frac{2(P_2 - P_3)}{\rho}} \qquad (2)$$

Force equation:

$$F_d = P_2\, (A_p + A_R) - P_1 A_p \qquad (3)$$

Pressure equation:

Assuming isothermal conditions

$$P_3 V_3 = P_0 V_0 \qquad (4)$$

$$V_3 = V_0 - A_R u \qquad (5)$$

where,

A_p = Area of the piston.

A_R = Area due to piston rod.

A_{r_1} = Area due to orifices on the piston.

A_{r_2} = Area of the cylinder orifice.

C_{d_1}, C_{d_2} = Discharge coefficients due to orifices (1) and (2) respectively.

P_1, P_2 = Pressure of the fluid in chambers (1) and (2), respectively.

P_3 = Gage pressure of the fluid in chamber (3).

ρ = Density of the shock absorber oil.

V_3 = Volume of the inert gas in chamber (3).

P_0, V_0 = Initial absolute pressure, and volume of the inert gas in chamber (3).

F_d = Damping force.

$u, \dot{u}$ = Relative displacement and velocity of the piston.

P_A = Atomospheric pressure.

From equations (1) and (2)

$$P_2 - P_1 = \frac{\rho}{32 C_{d_1}^2} \left(\frac{A_p}{A_{r_1}}\right)^2 \dot{u}^2 \tag{6}$$

$$P_2 - P_3 = \frac{\rho}{2 C_{d_2}^2} \left(\frac{A_R}{A_{r_2}}\right)^2 \dot{u}^2 \tag{7}$$

From equation (5)

$$P_3 = \left[\frac{P_0 V_0}{V_0 - A_R u} - P_A\right] \tag{8}$$

Rewrite force equation (3)

$$F_d = (P_2 - P_1) A_p + (P_2 - P_3) A_R + P_3 A_R \tag{9}$$

Substitute equations (6), (7) and (8) in (9)

$$F_d = \frac{\rho \dot{u}^2}{2} \left[\frac{A_p}{16 C_{d_1}^2} \left(\frac{A_p}{A_{r_1}}\right)^2 + \frac{A_R}{C_{d_2}^2} \left(\frac{A_R}{A_{r_2}}\right)^2\right] + \left[\frac{P_0 V_0}{V_0 - A_R u} - P_A\right] A_R \tag{10}$$

Neglecting the terms due to inert gas column

$$F_d = C_z \dot{u}^2 \tag{11}$$

where,

$$C_z = \frac{\rho}{2} \left[\frac{A_p}{16 C_{d_1}^2} \left(\frac{A_p}{A_{r_1}}\right)^2 + \frac{A_R}{C_{d_2}^2} \left(\frac{A_R}{A_{r_2}}\right)^2\right] \tag{12}$$

The static characteristics of the cushion are measured by gradually loading and unloading the preload seat cushion. The characteristics are shown in Figure I.4. The stiffness coefficient of the cushion is found to be a constant in the range of selected preload.

The suspension transmissibility characteristics are obtained in the laboratory by strapping a wooden torso to the seat cushion. The straps however, introduce a significant stiffness element between the torso and the suspension mass. A dynamic measurement of the strapped cushion in the laboratory indicated an equivalent stiffness 1390 N/cm. in comparison with the cushion stiffness of 148 N/cm. Hence, for the practical purposes, the model may be reduced to a single degree of freedom system, by assuming cushion to be highly stiff. The experimental transmissibility characteristics are presented in Figures I.5 and I.6 along with the transmissibility characteristics obtained from computer simulation of the suspension model. The transmissibility characteristics obtained via experimentation and computer simulation of the formulated model indicate a good agreement.

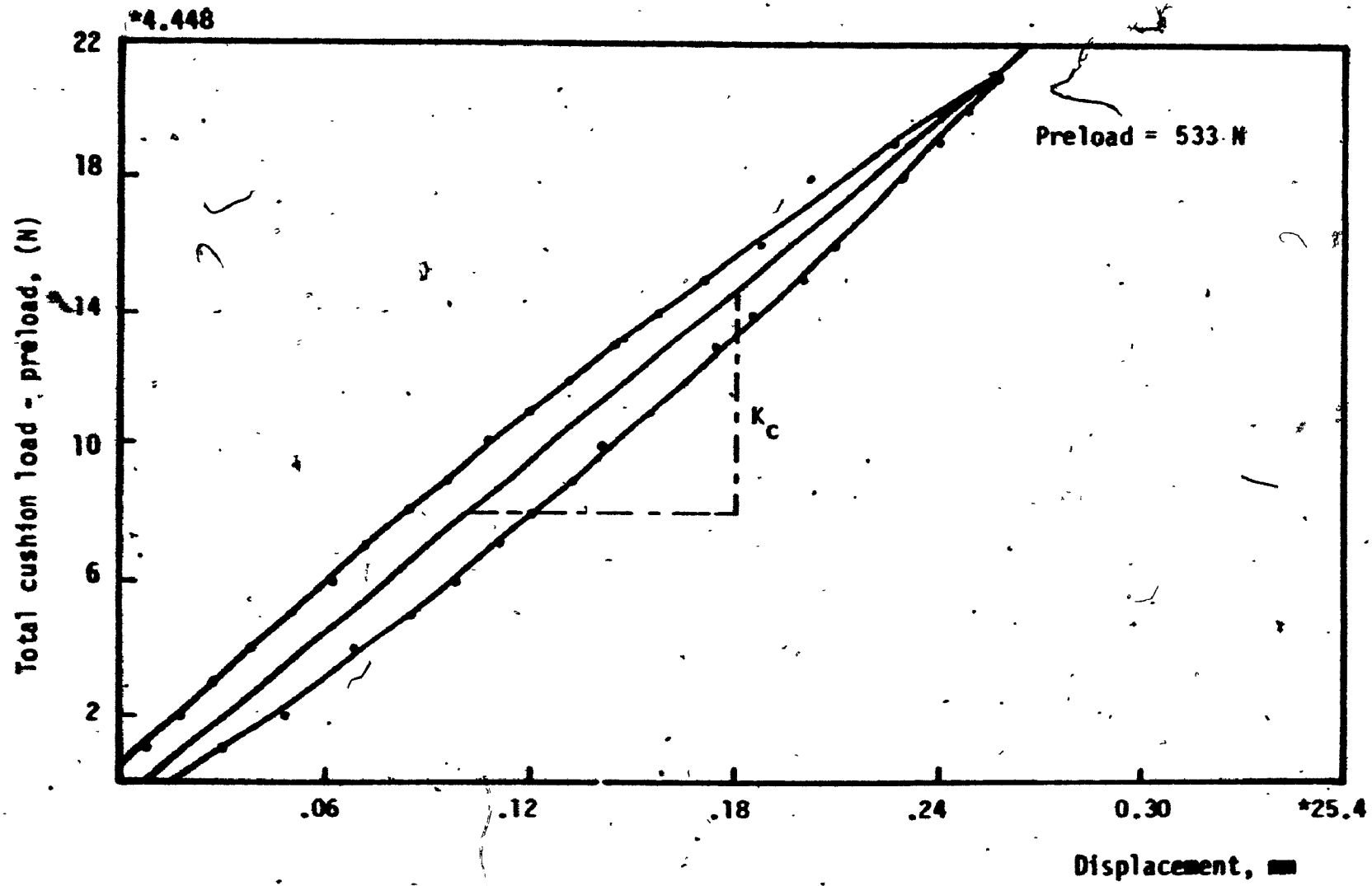

FIGURE I.4: Static characteristics of seat cushion.

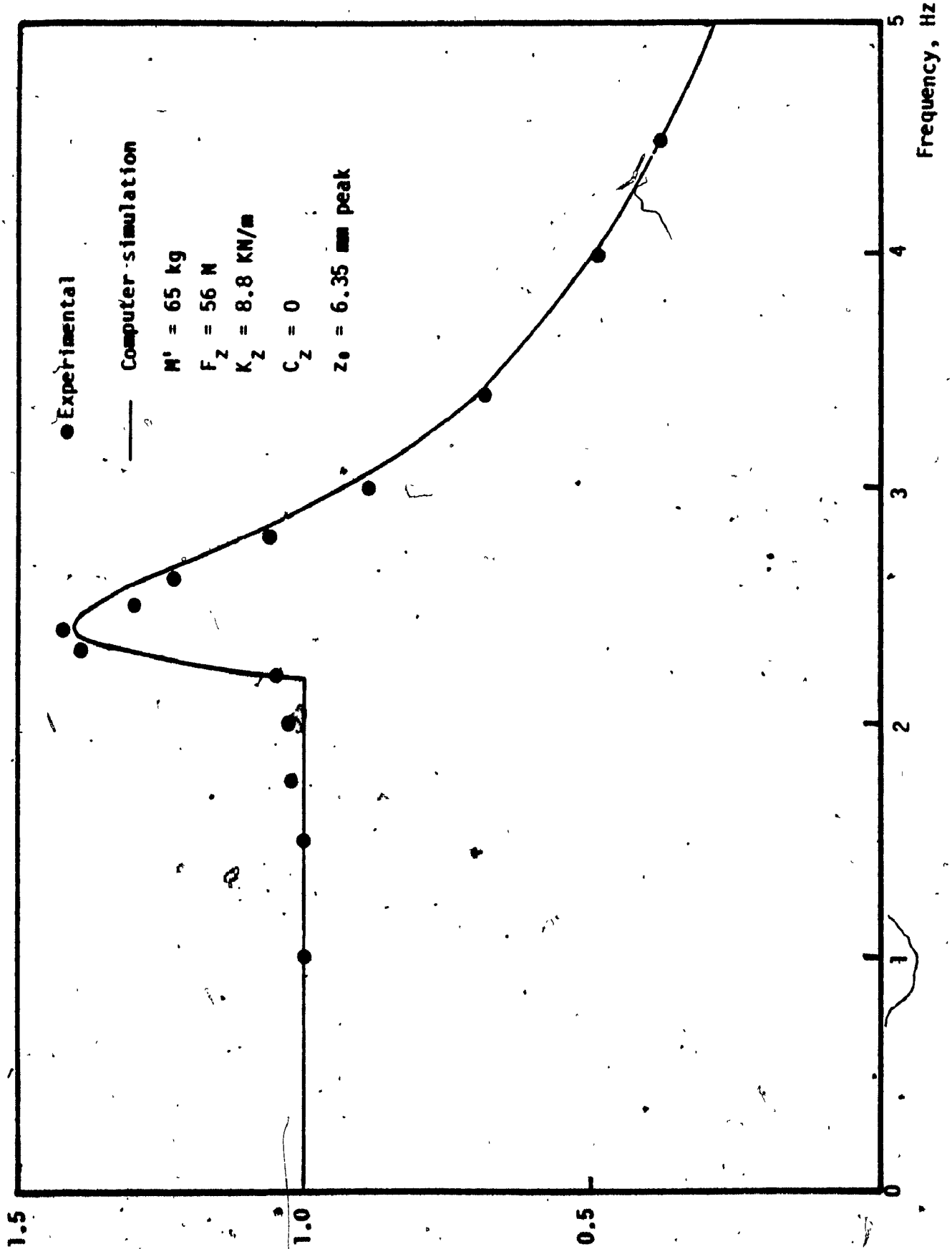

FIGURE I.5: Transmissibility characteristics of bounce seat suspension.

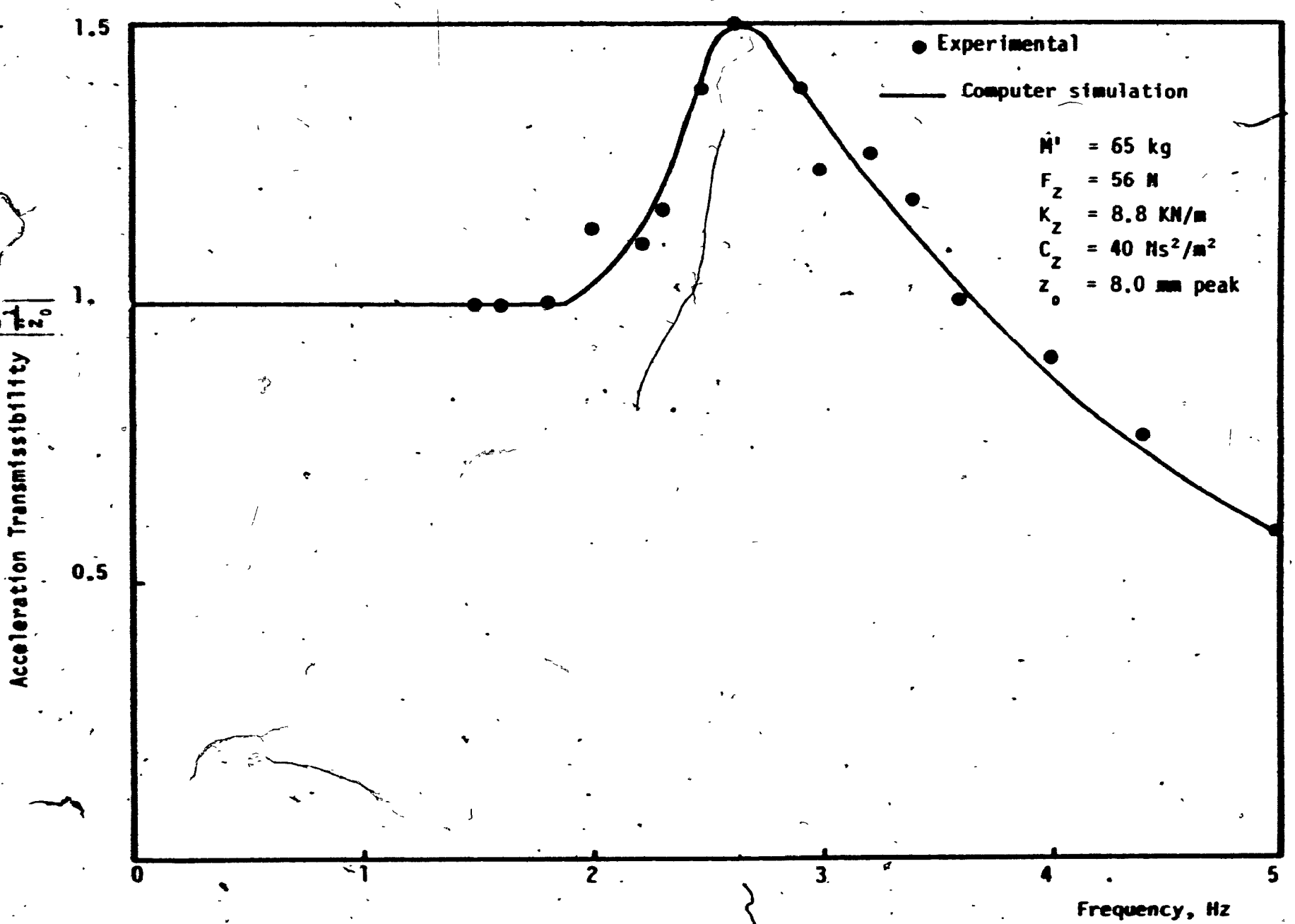

FIGURE I.6: Transmissibility characteristics of bounce seat suspension (assuming constant inclination)

APPENDIX II

MATRICES DESCRIBING EQUATIONS OF MOTION OF CAB AND CAB-SEAT SUSPENSION MODELS

The equations of motion of various cab suspension models presented in Chapter 2 are described by the following matrices.

1) Cab Suspension Model

$$[M] = \begin{bmatrix} M_c & 0 & 0 & 0 & 0 \\ 0 & I^c_{\theta\theta}+M_c h_2^2 & 0 & 0 & M_c h_2 \\ 0 & 0 & I^c_{\phi\phi}+M_c h_2^2 & M_c h_2 & 0 \\ 0 & 0 & M_c h_2 & M_c & 0 \\ 0 & M_c h_2 & 0 & 0 & M_c \end{bmatrix}$$

$$[K]=\begin{bmatrix} K_1+K_2+K_3+K_4 & a_1(K_1+K_4)-a_2(K_2+K_3) & b_1(K_1+K_2)-b_2(K_3+K_4) & 0 & 0 \\ a_1(K_1+K_4)-a_2(K_2+K_3) & a_1^2(K_1+K_4)+a_2^2(K_2+K_3) & b_1(K_1a_1-K_2a_2)+b_2(K_3a_2-K_4a_1) & 0 & 0 \\ b_1(K_1+K_2)-b_2(K_3+K_4) & b_1(K_1a_1-K_2a_2)+b_2(K_3a_2-K_4a_1) & b_1^2(K_1+K_2)+b_2^2(K_3+K_4) & 0 & 0 \\ 0 & 0 & 0 & K_5 & 0 \\ 0 & 0 & 0 & 0 & K_6 \end{bmatrix}$$

$$[C]=\begin{bmatrix} C_1+C_2+C_3+C_4 & a_1(C_1+C_4)-a_2(C_2+C_3) & b_1(C_1+C_2)-b_2(C_3+C_4) & 0 & 0 \\ a_1(C_1+C_4)-a_2(C_2+C_3) & a_1^2(C_1+C_4)+a_2^2(C_2+C_3) & b_1(C_1a_1-C_2a_2)+b_2(C_3a_2-C_4a_1) & 0 & 0 \\ b_1(C_1+C_2)-b_2(C_3+C_4) & b_1(C_1a_1-C_2a_2)+b_2(C_3a_2-C_4a_1) & b_1^2(C_1+C_2)+b_2^2(C_3+C_4) & 0 & 0 \\ 0 & 0 & 0 & C_5 & 0 \\ 0 & 0 & 0 & 0 & C_6 \end{bmatrix}$$

$$[K_f] = [K]$$

$$[C_f] = [C]$$

where, $I^c_{\theta\theta}$ is the pitch moment of inertia of cab about its c.g. ($Kg.m^2$)

$I^c_{\phi\phi}$ is the roll moment of inertia of the cab about its c.g. ($Kg.m^2$)

M_c is the cab mass (Kg).

ii) Model I: Cab Suspension with Bounce Seat Suspension.

$$[M] = \begin{bmatrix} M_c & 0 & 0 & 0 & 0 & 0 \\ 0 & I_{\theta\theta}+M_0h_1^2+M_ch_2^2 & 0 & 0 & M_0h_1+M_ch_2 & 0 \\ 0 & 0 & I_{\phi\phi}+M_0h_1^2+M_ch_2^2 & M_0h_1+M_ch_2 & 0 & 0 \\ 0 & 0 & M_0h_1+M_ch_2 & M_0+M_c & 0 & 0 \\ 0 & M_ch_2+M_0h_1 & 0 & 0 & M_0+M_c & 0 \\ 0 & 0 & 0 & 0 & 0 & M_0 \end{bmatrix}$$

where,

$I_{\theta\theta} = I^c_{\theta\theta} + I^s_{\theta\theta}$

$I_{\phi\phi} = I^c_{\phi\phi} + I^s_{\phi\phi}$

M_0 = Mass of the seated operator (kg)

$I^s_{\theta\theta}$ = Pitch moment of inertia of the seated operator about its cg ($kg \cdot m^2$)

$I^s_{\phi\phi}$ = Roll moment of inertia of the seated operator about its cg ($kg \cdot m^2$)

$$[K] = \begin{bmatrix} K_1+K_2+K_3+K_4+K_7 & a_1(K_1+K_4)-a_2(K_2+K_3)-a_3K_7 & b_1(K_1+K_2)-b_2(K_3+K_4)+b_3K_7 & 0 & 0 & -K_7 \\ a_1(K_1+K_4)-a_2(K_2+K_3) & a_1^2(K_1+K_4)+a_2^2(K_2+K_3) & b_1(K_1a_1-K_2a_2)+b_2(K_3a_2 & 0 & 0 & a_3K_7 \\ -a_3K_7 & +a_3^2K_7 & -K_4a_1)-b_3(a_3K_7) & & & \\ b_1(K_1+K_2)-b_2(K_3+K_4) & b_1(K_1a_1-K_2a_2)+b_2(K_3a_2-K_4a_1) & b_1^2(K_1+K_2)+b_2^2(K_3+K_4) & 0 & 0 & -b_3K_7 \\ +b_3K_7 & -b_3(a_3K_7) & +K_7b_3^2 & & & \\ 0 & 0 & 0 & K_5 & 0 & 0 \\ 0 & 0 & 0 & 0 & K_6 & 0 \\ -K_7 & a_3K_7 & -b_3K_7 & 0 & 0 & K_7 \end{bmatrix}$$

$$[C] = \begin{bmatrix} C_1+C_2+C_3+C_4+C_7 & a_1(C_1+C_4)-a_2(C_2+C_3) & b_1(C_1+C_2)-b_2(C_3+C_4) & 0 & 0 & -C_7 \\ & -a_3C_7 & +b_3K_7 & & & \\ a_1(C_1+C_4)-a_2(C_2+C_3) & a_1^2(C_1+C_4)+a_2^2(C_2+C_3) & b_1(C_1a_1-C_2a_2)+b_2(C_3a_2 & 0 & 0 & a_3C_7 \\ -a_3C_7 & -a_3^2C_7 & -C_4a_1)-b_3(a_3C_7) & & & \\ b_1(C_1+C_2)-b_2(C_3+C_4) & b_1(C_1a_1-C_2a_2)+b_2(C_3a_2 & b_1^2(K_1+K_2)+b_2^2(K_3+K_4) & 0 & 0 & -b_3C_7 \\ +b_3C_7 & -C_4a_1)-b_3(a_3C_7) & +b_3^2K_7 & & & \\ 0 & 0 & 0 & C_5 & 0 & 0 \\ 0 & 0 & 0 & 0 & C_6 & 0 \\ -C_7 & a_3C_7 & -b_3C_7 & 0 & 0 & C_7 \end{bmatrix}$$

Matrices $[K_f]$, and $[C_f]$ are the same as those obtained for the cab-suspension model.

111) Model II: Bounce and Lateral seat suspension with the suspended cab.

$$[M] = \begin{bmatrix} M_c & 0 & 0 & 0 & 0 & 0 & 0 \\ 0 & M_c h_2^2 + M_0 h_1^2 + I_{\theta\theta} & 0 & 0 & M_c h_2 + M_0 h_1 & 0 & 0 \\ 0 & 0 & M_c h_2^2 + I_{\phi\phi} + M_0 h_3^2 & M_c h_2 & 0 & M_0 h_3 & 0 \\ 0 & 0 & M_c h_2 & M_c & 0 & 0 & 0 \\ 0 & M_c h_2 + M_0 h_1 & 0 & 0 & M_c + M_0 & 0 & 0 \\ 0 & 0 & M_0 h_3 & 0 & 0 & M_0 & 0 \\ 0 & 0 & 0 & 0 & 0 & 0 & M_0 \end{bmatrix}$$

$$[C] = \begin{bmatrix}
C_1+C_2+C_3+C_4+C_7 & a_1(C_1+C_4)-a_2(C_2+C_3) & b_1(C_1+C_2)-b_2(C_3+C_4) & 0 & 0 & -C_7 & 0 \\
 & -a_3C_7 & +b_3C_7 & & & & \\
a_1(C_1+C_4)-a_2(C_2+C_3) & a_1^2(C_1+C_4)+a_2^2(C_2+C_3) & b_1(a_1C_1-a_2C_2)+b_2(a_2C_3-a_1C_4) & 0 & 0 & a_3C_7 & 0 \\
-a_3C_7 & +a_3^2C_7 & -a_3b_3C_7 & & & & \\
b_1(C_1+C_2)-b_2(C_3+C_4) & b_1(a_1C_1-a_2C_2)+b_2(a_2C_3-a_1C_4) & b_1^2(C_1+C_2)+b_2^2(C_3+C_4) & h_4C_8 & 0 & -b_3C_7 & -h_4C_8 \\
+b_3C_7 & -a_3b_3C_7 & +b_3^2C_7+h_4^2C_8 & & & & \\
0 & 0 & h_4C_6 & C_5+C_8 & 0 & 0 & -C_8 \\
0 & 0 & 0 & 0 & C_6 & 0 & 0 \\
-C_7 & a_3C_7 & -b_3C_7 & 0 & 0 & C_7 & 0 \\
0 & 0 & -h_4C_8 & -C_8 & 0 & 0 & C_8
\end{bmatrix}$$

$$
[K] = \begin{bmatrix}
K_1+K_2+K_3+K_4+K_7 & a_1(K_1+K_4)-a_2(K_2+K_3) & b_1(K_1+K_2)-b_2(K_3+K_4) & 0 & 0 & -K_7 & 0 \\
 & -a_3K_7 & +b_3K_7 & & & & \\
a_1(K_1+K_4)-a_2(K_2+K_3) & a_1^2(K_1+K_4)+a_2^2(K_2+K_3) & b_1(a_1K_1-a_2K_2) & 0 & 0 & a_3K_7 & 0 \\
-a_3K_7 & +a_3^2K_7 & +b_2(a_2K_3-a_1K_4) & & & & \\
 & & -a_3b_3K_7 & & & & \\
b_1(K_1+K_2)+b_2(K_3+K_4) & b_1(a_1K_1-a_2K_3) & b_1^2(K_1+K_2)+b_2^2(K_3+K_4) & h_4K_8 & 0 & -b_3K_7 & -h_4K_8 \\
+b_3K_7 & +b_2(a_2K_3-a_1K_4) & +b_3^2K_7 & & & & \\
 & -a_3b_3K_7 & +h_4^2K_8 & & & & \\
0 & 0 & h_4K_8 & K_8+K_5 & 0 & 0 & -K_8 \\
0 & 0 & 0 & 0 & K_6 & 0 & 0 \\
-K_7 & a_3K_7 & -b_3K_7 & 0 & 0 & K_7 & 0 \\
0 & 0 & -h_4K_8 & -K_8 & 0 & 0 & K_8
\end{bmatrix}
$$

iv) Model III: Cab Suspension with Bounce and Roll Seat Suspensions

$$[M] = \begin{bmatrix} M_c & 0 & 0 & 0 & 0 & 0 & 0 \\ 0 & M_c h_2^2 + M_0 h_1^2 + I_{\theta\theta} & 0 & 0 & M_c h_2 + M_0 h_1 & 0 & 0 \\ 0 & 0 & M_c h_2^2 + I^c_{\phi\phi} & M_c h_2 & 0 & 0 & 0 \\ 0 & 0 & M_c h_2 & M_0 + M_c & 0 & 0 & M_0 h_4 \\ 0 & M_c h_2 + M_0 h_1 & 0 & 0 & M_0 + M_c & 0 & 0 \\ 0 & 0 & 0 & 0 & 0 & M_0 & 0 \\ 0 & 0 & M_0 h_4 & 0 & 0 & 0 & M_0 h_4^2 + I^s_{\phi\phi} \end{bmatrix}$$

$$
[K]=\begin{bmatrix}
K_1+K_2+K_3+K_4+K_7 & a_1(K_1+K_4)-a_2(K_2+K_3)-a_3K_7 & b_1(K_1+K_2)-b_2(K_3+K_4)\ b_3K_7. & 0 & 0 & -K_7 & 0 \\
a_1(K_1+K_4)-a_2(K_2+K_3)-a_3K_7 & a_1^2(K_1+K_4)+a_2^2(K_2+K_3)+a_3^2K_7 & b_1(a_1K_1-a_2K_2)+b_2(a_2K_3-a_1K_4)-a_3b_3K_7 & 0 & 0 & a_3K_7 & 0 \\
b_1(K_1+K_2)+b_2(K_3+K_4)+b_3K_7 & b_1(a_1K_1-a_2K_2)+b_2(a_2K_3-a_1K_4)-a_3b_3K_7 & b_1^2(K_1+K_2)+b_2^2(K_3+K_4)+b_3^2K_7+K_9 & 0 & 0 & -b_3K_7 & -K_9 \\
0 & 0 & 0 & K_5 & 0 & 0 & 0 \\
0 & 0 & 0 & 0 & K_6 & 0 & 0 \\
-K_7 & a_3K_7 & -b_3K_7 & 0 & 0 & K_7 & 0 \\
0 & 0 & -K_9 & 0 & 0 & 0 & K_9
\end{bmatrix}
$$

$$
[C] = \begin{bmatrix}
C_1+C_2+C_3+C_4+C_7 & a_1(C_1+C_4)-a_2(C_2+C_3) & b_1(C_1+C_2)-b_2(C_3+C_4) & 0 & 0 & -C_7 & 0 \\
 & -a_3C_7 & +b_3C_7 & & & & \\
a_1(C_1+C_4)-a_2(C_2+C_3) & a_1^2(C_1+C_4)+a_2^2(C_2+C_3) & b_1(a_1C_1-a_2C_2) & 0 & 0 & a_3C_7 & 0 \\
-a_3C_7 & +a_3^2C_7 & +b_2(a_2C_3-a_1C_4) & & & & \\
 & & -a_3b_3C_7 & & & & \\
b_1(C_1+C_2)-b_2(C_3+C_4) & b_1(a_1C_1-a_2C_2) & b_1^2(C_1+C_2)+b_2^2(C_3+C_4) & 0 & 0 & -b_3C_7 & -C_9 \\
+b_3C_7 & +b_2(a_2C_3-a_1C_4) & +b_3^2C_7+C_9 & & & & \\
 & -a_3b_3C_7 & & & & & \\
0 & 0 & 0 & C_5 & 0 & 0 & 0 \\
0 & 0 & 0 & 0 & C_6 & 0 & 0 \\
-C_7 & a_3C_7 & -b_3C_7 & 0 & 0 & C_7 & 0 \\
0 & 0 & -C_9 & 0 & 0 & 0 & C_9
\end{bmatrix}
$$

It can be seen that the rotation of cab contributes to the bounce, longitudinal, and lateral motion of the operator. Table I presents expressions relating absolute motion of seated operator to the cab pitch and roll motions.

TABLE II.1

ABSOLUTE TRANSLATIONAL MOTION OF THE SEATED OPERATOR

Suspension Model	Motion at the operator seat		
	Bounce	Longitudinal	Lateral
Cab with rigid seat	$z_1=z_2-a_1\theta_2+b_1\phi_2$	$x_1=x_2+h_1\theta_2$	$y_1=y_2+h_1\phi_2$
Cab with bounce suspension seat	z_1	$x_1=x_2+h_1\theta_2$	$y_1=y_2+h_1\phi_2$
Cab with bounce and lateral seat suspensions	z_1	$x_1=x_2+h_1\theta_2$	y_1
Cab with bounce and roll seat suspension	z_1	$x_1=x_2+h_1\theta_2$	$y_1=y_2+h_1\phi_1$

APPENDIX III

GENERATION OF EQUIVALENT ACCELERATION PSD LIMITS FROM RMS ACCELERATION LIMITS

The International Organization for Standardization has specified rms acceleration limits associated with human operator *fatigue decreased proficiency* [12]. Since the random vehicle vibrations are often characterized by their power spectral density, it is desirable to convert ISO rms acceleration limits to its equivalent power spectral density limits [74]. Since ISO standard assumes averaging over finite bands of one-third octave width, the average PSD can be expressed as

$$\bar{S}(\bar{f}) = \frac{\bar{a}^2(\bar{f})}{\Delta f} \tag{III.1}$$

where $\bar{S}(\bar{f})$ is the average PSD and $\bar{a}(\bar{f})$ is the rms acceleration at center frequency $\bar{f}$ of the frequency band Δf. The bandwidth and the center frequency are related as;

$$\Delta f = f_u - f_\ell$$

and

$$\bar{f} = (f_u + f_\ell)/2. \tag{III.2}$$

where f_1, f_2 are the lower and higher frequency limits, respectively. The definition of a one-third octave band, and equation (III.2) yield;

$$\Delta f = 0.23\,\bar{f} \tag{III.3}$$

Substituting (III.3) into (III.1), the average PSD is expressed as:

$$\bar{S}(\bar{f}) = \frac{\bar{a}^2(\bar{f})}{0.23\bar{f}} \tag{III.4}$$

Consider ISO specified rms acceleration limits in bounce mode shown in Figure 1.5. The rms limits are straight line segments on log-log plots of the form

$$\log \bar{a}(\bar{f}) = m \log \bar{f} + n \tag{III.5}$$

where m_i and b_i are the slope and intercept, respectively, for the i^{th} segment. Taking the logarithm of (III.4) and substituting in (III.5) yields;

$$\log \bar{S}(\bar{f}) = (2m_i - 1) \log \bar{f} + (2 b_i - \log 0.23) \qquad \text{(III.6)}$$

From equation (III.6), it is observed that average PSD equivalent also consists of straight line segments plotted on log-log coordinates. The slope and intercept of the new segment are $(2m_i-1)$, and $(2b_i-\log 0.23)$, respectively. Table III.1 lists the slopes and intercepts for various segments of bounce and horizontal vibration limits. The PSD equivalent limits described by equation (III.6), in the bounce and horizontal modes, are plotted in Figures III.1 and III.2, respectively.

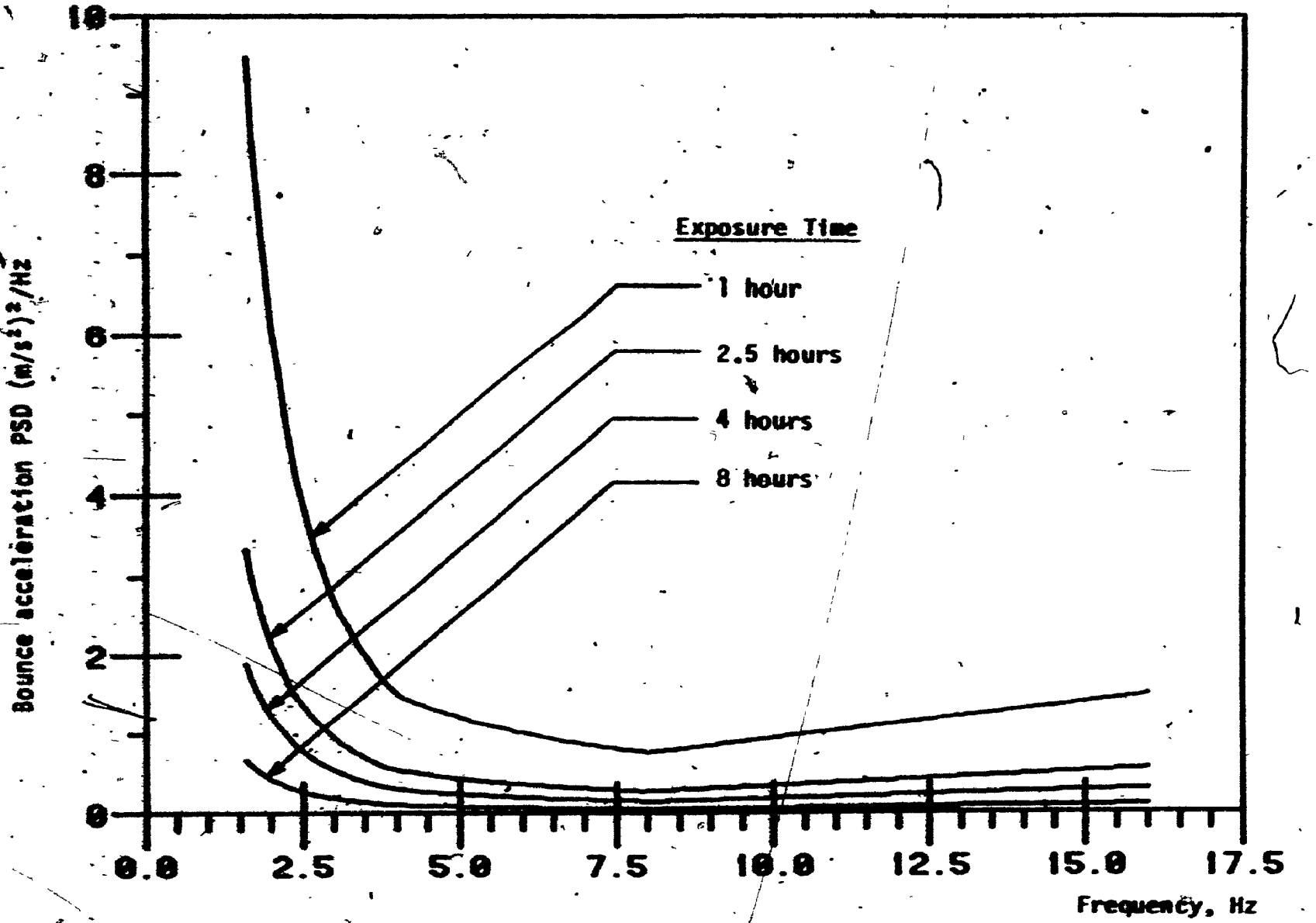

FIGURE IM.1: Equivalent acceleration PSD *fatigue decreased proficiency* boundaries, for exposure to bounce vibrations.

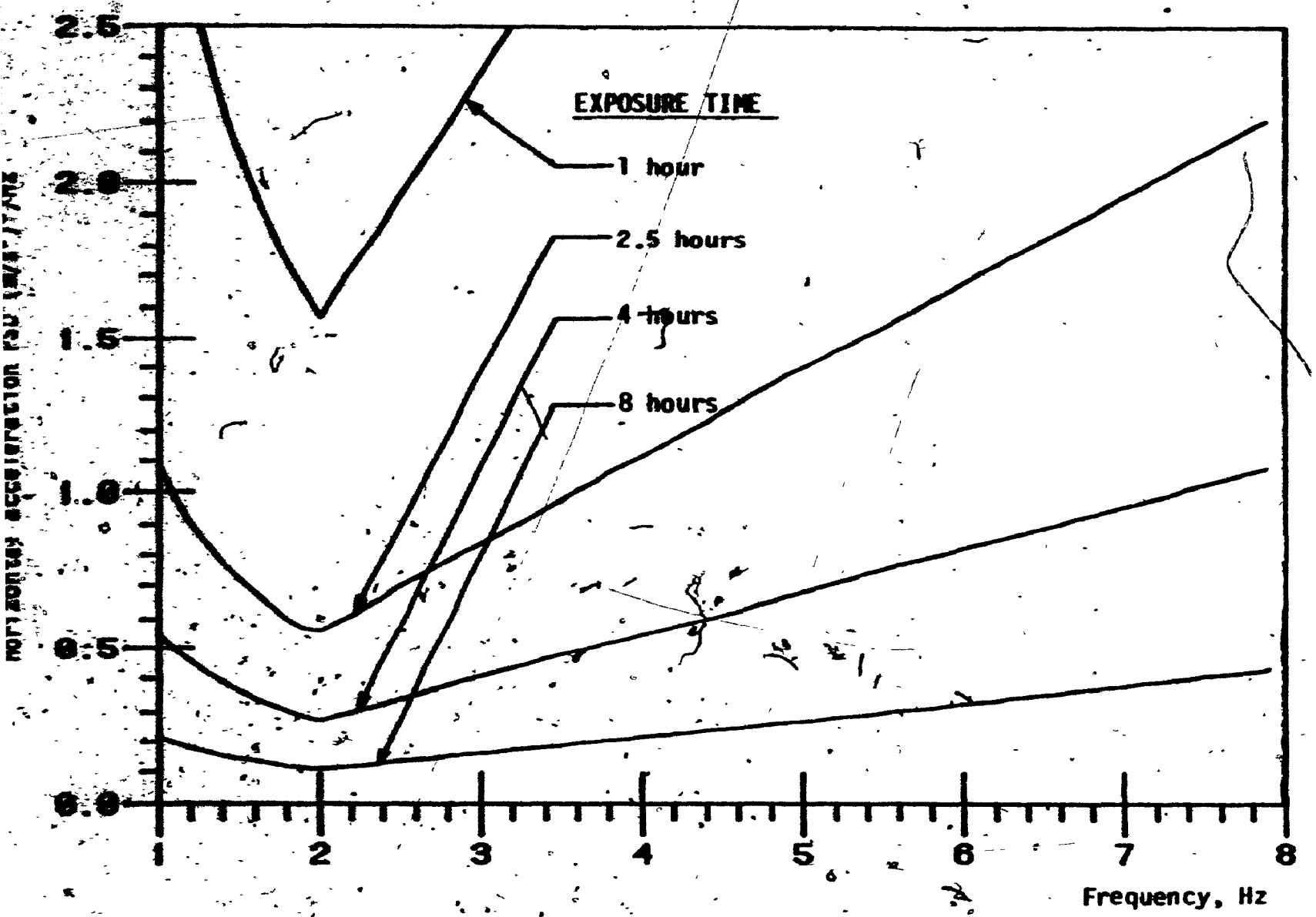

FIGURE III.2: Equivalent acceleration PSD *fatigue decreased proficiency* boundaries, for exposure to horizontal vibrations.

TABLE III.1

SLOPES AND INTERCEPTS OF RMS AND EQUIVALENT PSD LIMITS

(FATIGUE DECREASED PROFICIENCY BOUNDARIES)

Axis	Duration of Exposure hours	Segment	rms		PSD equivalent	
			SLOPE m_1	INTERCEPT b_1	SLOPE $(2m_1-1)$	INTERCEPT $(2b_1-\log 0.23)$
Bounce	1	1	-0.5	0.373	-2.0	1.3843
		2	0.0	0.07188	-1.0	0.782
		3	1.0	-0.8312	1.0	-1.02412
	4	1	-0.5	0.0253	-2.0	0.6889
		2	0.0	-0.2757	-1.0	0.08687
		3	1.0	-1.1788	1.0	-1.7193
	8	1	-0.5	-.20	-2.0	0.2383
		2	0.	-0.5017	-1.0	-0.3651
		3	1.	-1.4048	1.0	-2.1713
Horizontal	1	1	0.0	-0.0706	-1.0	0.497
		2	1.0	-0.3716	1.0	-0.105
	4	1	0.	-0.4498	-1.0	-0.2613
		2	1.0	-0.7508	1.0	-0.8533
	8	1	0.0	-0.65	-1.0	-0.6617
		2	1.0	-0.9507	1.0	-1.2633

APPENDIX IV

TIME SERIES REPRESENTATION OF INPUT SPECTRAL DENSITIES

For the simulation of non-linear system, it is often necessary to specify input random time-histories. The random terrain inputs, which are characterized by spectral densities can be represented by summing sine waves. A number of methods have been devised for generating time-history whose spectra are replicas of some given spectra [64, 65, 66]. Input spectral densities characterizing Silsoe track can be represented by their respective root mean square spectrum. The rms spectrum is computed as

$$\bar{a}(f) = \left[\int_0^f S(f)\, df \right]^{1/2} \qquad (IV.1)$$

where

$\bar{a}(f)$ = rms input spectrum corresponding to frequency f.

$S(f)$ = input power spectral density corresponding to frequency f.

RMS spectrums corresponding to bounce, longitudinal, roll, and pitch excitations have been presented in Figures 3.9 to 3.11. The frequency spectrum can be represented by summation of several harmonics corresponding to discrete frequencies [65]. The acceleration time history of the terrain excitation is expressed by

$$F(t) = \sum_{i=1}^{N} a_i \sin (2\pi f_i t) \qquad (IV.2)$$

where

$F(t)$ = The acceleration time-history.

a_i = Coefficient determined from the frequency spectrum corresponding to frequency f_i.

N = Total number of frequencies required to cover the frequency

The frequencies f_i must have a spacing such that the successive frequencies have overlapping half-power points. Equations (IV.1) and (IV.2) provide an equivalent time series that would be compatible to the spectras specified by the Silsoe track. The validity of equations (IV.1) and (IV.2) is examined by generating the power spectrum of the artificial time-history and comparing it with the Silsoe track spectral densities. The comparison of acceleration PSD's obtained from Silsoe track data and from the sine series is shown in Figures IV.1 to IV.5.

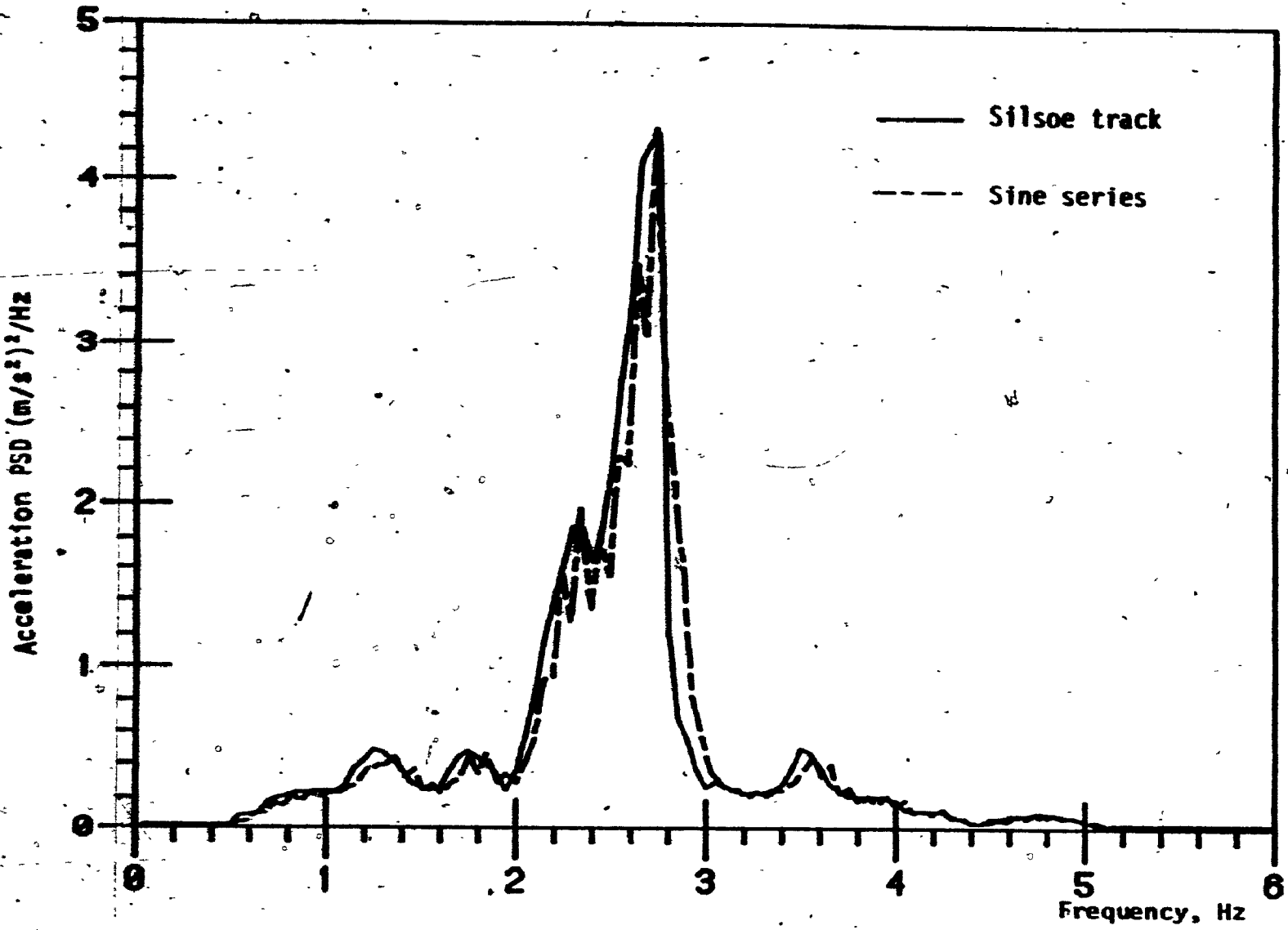

FIGURE IV.1: Bounce Acceleration PSD

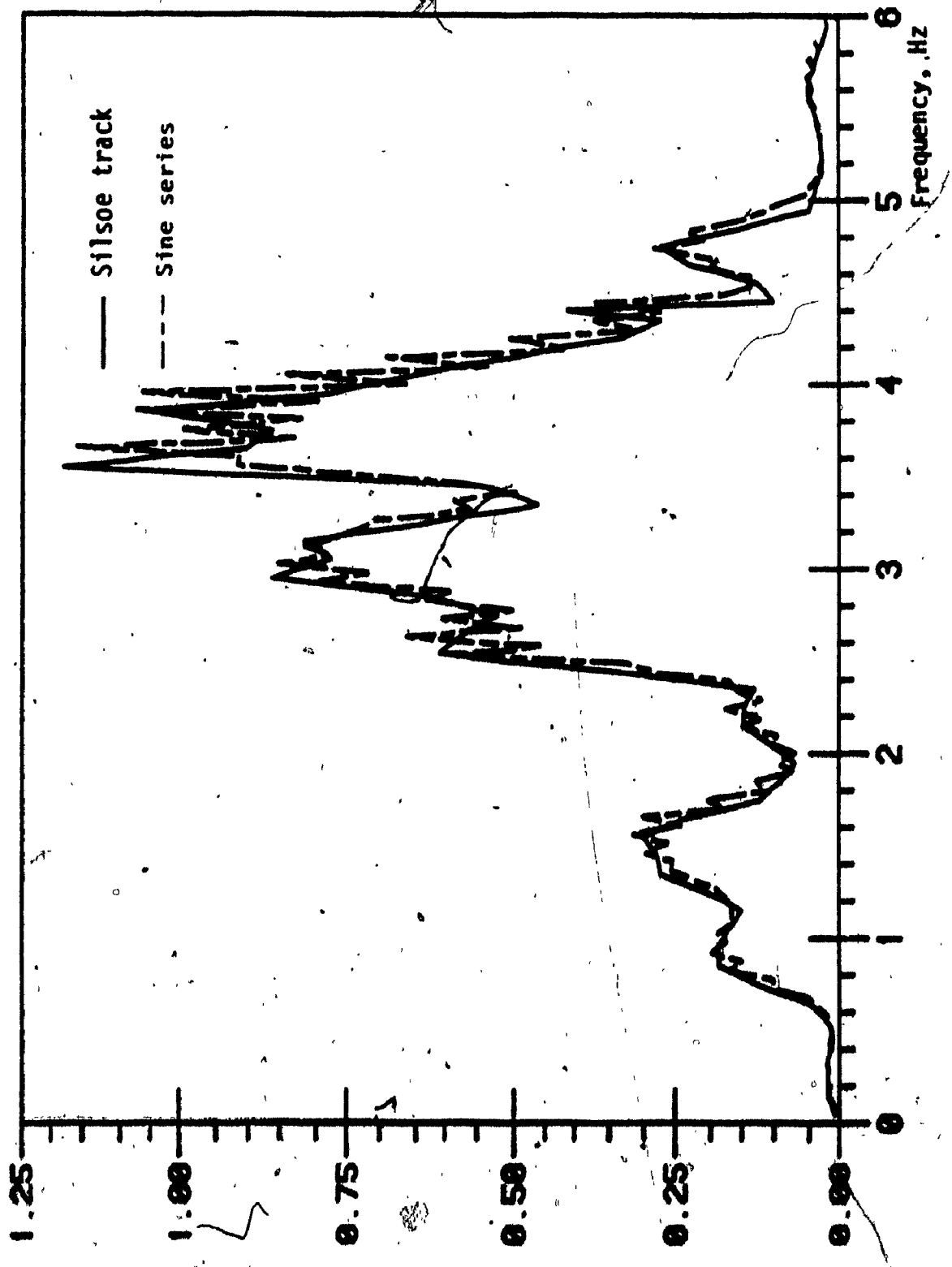

FIGURE IV.2: Longitudinal Acceleration PSD

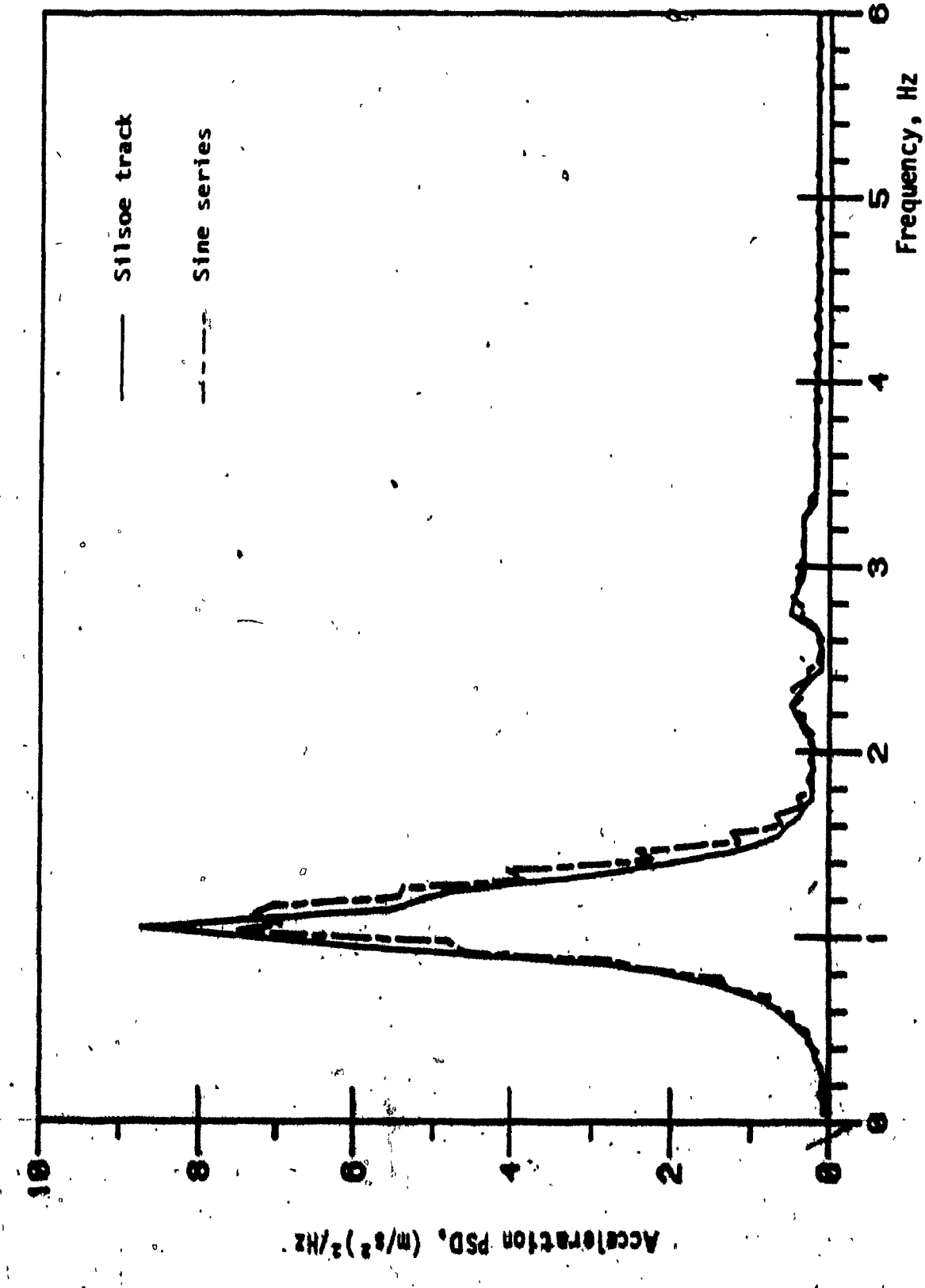

FIGURE IV.3: Lateral acceleration PSD

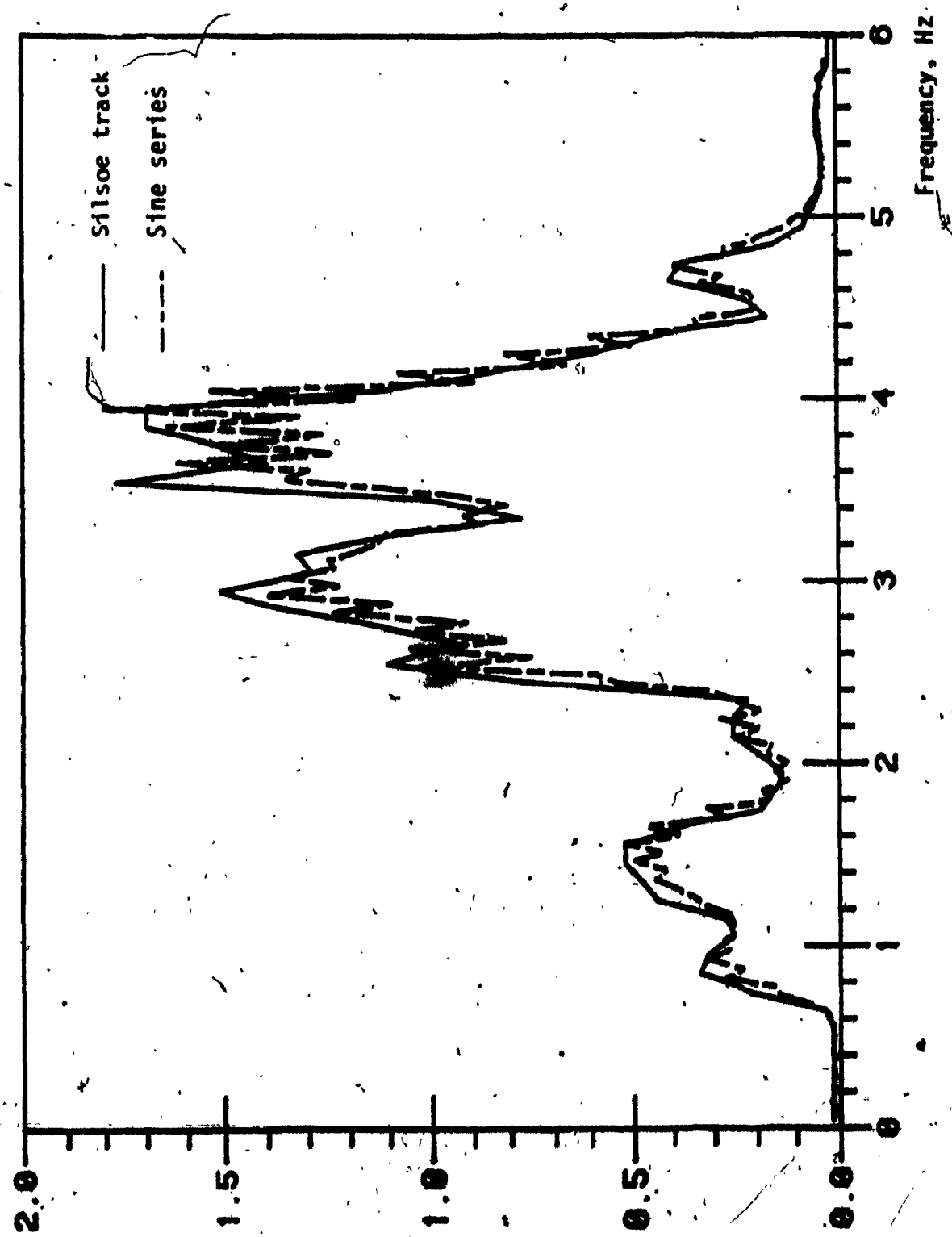

FIGURE IV.4: Pitch acceleration PSD

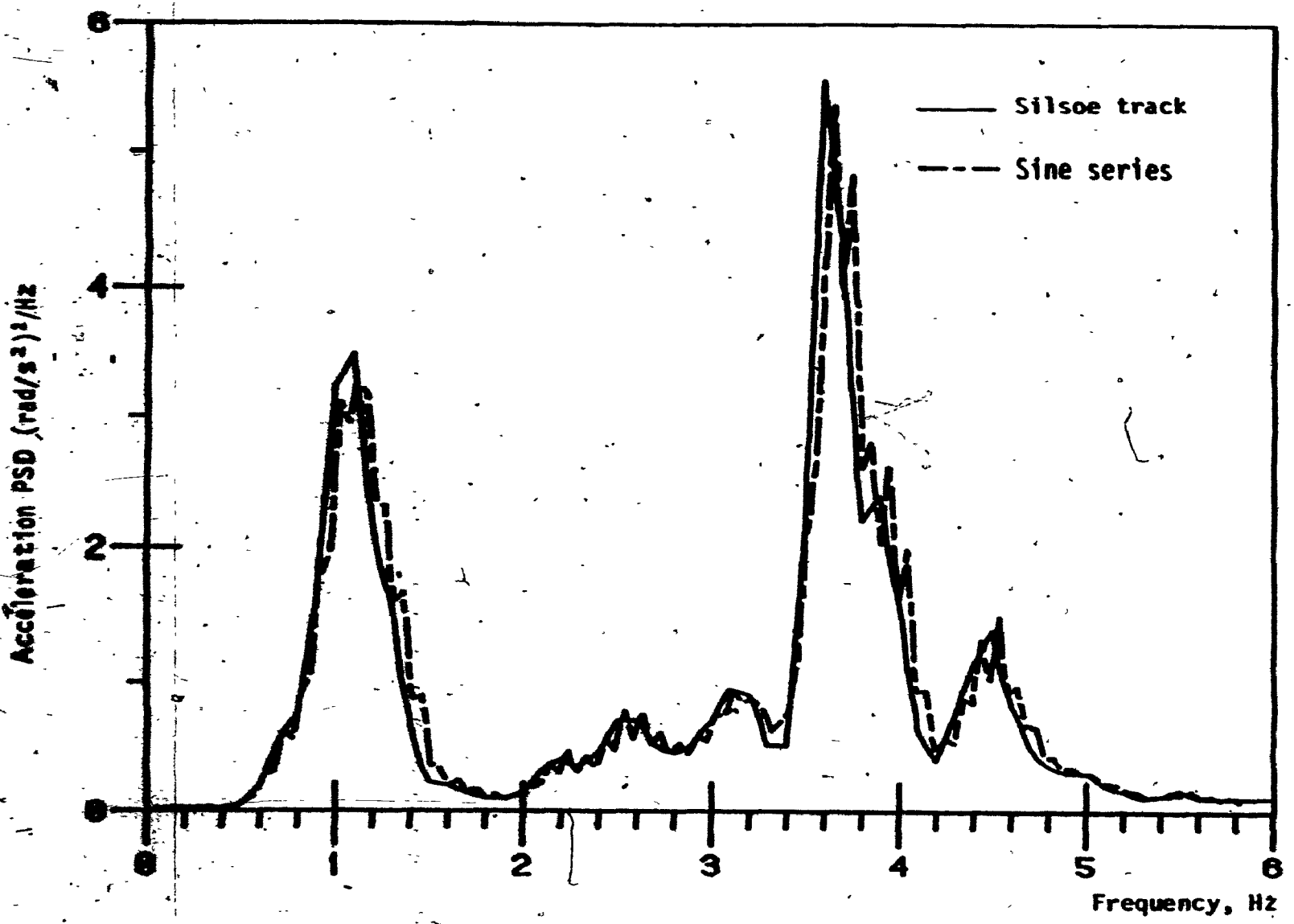

FIGURE IC.5: Roll acceleration PSD.